Springer Proceedings in Mathematics & Statistics

Santiago Ibáñez
Jesús S. Pérez del Río
Antonio Pumariño
J. Ángel Rodríguez *Editors*

Progress and Challenges in Dynamical Systems

Springer

Springer Proceedings in Mathematics & Statistics

Volume 54

For further volumes:
http://www.springer.com/series/10533

Springer Proceedings in Mathematics & Statistics

This book series features volumes composed of selected contributions from workshops and conferences in all areas of current research in mathematics and statistics, including OR and optimization. In addition to an overall evaluation of the interest, scientific quality, and timeliness of each proposal at the hands of the publisher, individual contributions are all refereed to the high quality standards of leading journals in the field. Thus, this series provides the research community with well-edited, authoritative reports on developments in the most exciting areas of mathematical and statistical research today.

Santiago Ibáñez • Jesús S. Pérez del Río
Antonio Pumariño • J. Ángel Rodríguez
Editors

Progress and Challenges in Dynamical Systems

Proceedings of the International Conference Dynamical Systems: 100 Years after Poincaré, September 2012, Gijón, Spain

Springer

Editors
Santiago Ibáñez
Jesús S. Pérez del Río
Antonio Pumariño
J. Ángel Rodríguez
Department of Mathematics
University of Oviedo
Oviedo, Spain

ISSN 2194-1009 ISSN 2194-1017 (electronic)
ISBN 978-3-642-38829-3 ISBN 978-3-642-38830-9 (eBook)
DOI 10.1007/978-3-642-38830-9
Springer Heidelberg New York Dordrecht London

Library of Congress Control Number: 2013947945

Mathematics Subject Classification (2010): 34-XX, 37-XX, 39-XX, 92-XX, 93-XX

Printed on acid-free paper

Springer is part of Springer Science+Business Media (www.springer.com)

It is by logic that we prove, but by intuition that we discover. To know how to criticize is good, to know how to create is better

Henri Poincaré

Foreword

René Thom once said that "what limits the *true* is not the *false*, it is the *insignificant*." He did not mean that writing correct proofs of theorems is not important but that the truth of a statement is not a warrant of its significance. Henri Poincaré's researches were never motivated by academic questions. This is particularly clear in his works on Celestial Mechanics, or on electro-magnetic oscillations, two of the main origins of the realm of *Dynamical Systems*, a realm which he essentially created. Being mostly inspired by "natural" phenomena, this domain of mathematics lacks the unity of other fields: using concepts from geometry, analysis, algebra, probability, and also the full strength of computers, it often looks as the "bricolage" which François Jacob, borrowing the notion from Claude Lévi-Strauss, considered as a fundamental way of natural evolution. Thanks to the *Dynamical Systems Group* of the University of Oviedo who organized such a nice homage to Poincaré, parts of which are featured in this book, we can once more be impressed by the diversity of the legacy of this most remarkable man.

Paris, France
April 2013

Alain Chenciner

Preface

This proceedings volume contains a collection of referred contributions by participants of the international conference *Dynamical Systems: 100 years after Poincaré*, (held in Gijón, Spain, September 3–7, 2012) which commemorated H. Poincaré.

In the exceptional paradise of Asturias, with the sun shining brightly all week over the Cantabrian sea, more than 100 researchers from 20 countries joined together to discuss new trends in Dynamical Systems. In total, 71 talks, including 11 plenary lectures, completed more than 30 h of intensive scientific work as the waves beat against the impressive beach of San Lorenzo.

The name of Poincaré, often considered as the *last universalist*, can be claimed by the majority of mathematicians and a great part of contemporary scientists. His conjecture about the topological characterization of 3-dimensional spheres or his pioneering contributions to the Principles of Relativity interpreting Lorentz's theory are themselves reasons for such general acknowledgement in the worlds of Maths and Theoretical Physics. However, it is the field of Dynamical Systems in which his work reaches our time with the greatest influence and most promising future prospects.

Knowledgeable about the difficulties of solving differential equations, Poincaré understood the need for a new geometrical and qualitative approach. Solutions of differential equations, as particular functions, would no longer be the main interest. Instead, the behaviour of the solutions as a whole, that is, the phase portrait, would be the focus. A vector field on a differentiable manifold defines a partition of such manifold in orbits (trajectories or integral curves); this interpretation later led to the notion of foliation. Topological properties of these curves and their disposal inside the phase space gain a true dynamical significance and become the principal target in the study of differential equations. The functional approach gave way to a novel geometrical view. The analytical properties of the solutions were no longer so relevant and instead the study of invariant sets (their topological properties and their dynamical meaning) became the focus of attention.

But above all, H. Poincaré made it clear that each equation must be understood hereinafter as a whole and, from this new concept, presents the relationship between local and global behaviours, between singularities and closed orbits or

other invariant sets. In any of these respects, all of H. Poincaré's contributions are characterized by an impressive creativity and significance.

Very early, in his doctoral thesis *Sur les propriétés des fonctions définies par les équations aux différences partielles*, he initiated the normal forms theory for singularities of vector fields. These techniques still remain as essential tools when dealing with local bifurcations. As inheritor of Darboux's concerns about the integrability of planar vector fields, Poincaré introduced the notion of remarkable value, bearing in mind the characterization of integrable planar polynomial vector fields. This attempt at relating the nature of a singularity to the global behaviour of a vector field also led him to the notion of index.

In order to study the flows associated with vector fields through the iterations of a diffeomorphism, H. Poincaré introduced what we now know as Poincaré maps, defined at first on transverse sections to a periodic orbit. The understanding of the dynamics around a periodic orbit became dependent on the analysis of the dynamics of a diffeomorphism in the vicinity of a fixed point. It was definitely an innovative idea that moved the world of continuous dynamical systems to the world of discrete dynamical systems. The different aspects of this genius are collected in four articles, published between 1881 and 1886, which completed his work *Sur les courbes définies par une équation différentielle*. This contribution marks a turning point in the way people looked at dynamics. However, an extremely significant boost was just ready to arrive with his work *Sur le probléme des trois corps et les équations de la dynamique*, with which he was awarded a prize granted by King Oscar II of Sweden in 1889.

Considering the equations that model the 3-body problem, he found hyperbolic periodic orbits whose two-dimensional invariant manifolds had non empty intersections and concluded, erroneously, that they should coincide. Hence these invariant manifolds should limit orbits that do not escape to infinity, which implied a false stability in the restricted 3-body problem. After reviewing this mistake, Poincaré introduced the term "homoclinic point" to refer to the points where manifolds intersect. The existence of one of these points implies the presence of many of them, where invariant manifolds intersect but do not coincide, describing a very complex tangle that he himself chose not to draw. Further understanding of the dynamics involved in these homoclinic configurations has led to intense and interesting research throughout the whole twentieth century until the present day, when many interesting open problems are still in need of answers. Thus, with this forcefulness, the prediction that Paul Apell made in 1925 is exceeded: "It is likely that, during the next half-century, this book will be the mine from which more modest researchers will extract their material", and that A. Chenciner reminds us in his contribution "A walk through the *New Methods of Celestial Mechanics*".

It took more than 30 years for a first result, shedding light on the dynamics near a homoclinic point, to arrive. In 1935, G. Birkhoff showed that in general, near a homoclinic point there exists an extremely intrincated set of periodic points, mostly with a very long period.

By the mid-1960s, S. Smale placed his geometrical device, the *Smale horseshoe*, in a neighbourhood of a transversal homoclinic orbit, thus explaining Birkhoff's

result and arranged the complicated dynamics that takes place near such a orbit by means of a conjugation to the shift of Bernouilli. These horseshoe maps were, for the last decades, the most useful tools to classify dynamical systems, understand their transitions and explain chaotic behaviours.

Horseshoes and Anosov diffeomorphisms were the source of inspiration to introduce the notion of axiom-A diffeomorphisms or uniformly hyperbolic containing the open class of structurally stable diffeomorphisms. A mechanism of transition between this set and its complementary is the creation/destruction of horseshoes which takes place when a homoclinic tangency is unfolded. In this scenario, just for 2-dimensional diffeomorphisms, there appear non hyperbolic strange attractors (or repellers) and the Newhouse phenomenon, explaining the persistence of homoclinic tangencies.

For higher dimensional diffeomorphisms, the persistence of non uniformly hyperbolic dynamics is explained with the notion of *blender*, associated to heterodimensional cycles, as introduced by C. Bonatti and L. J. Díaz in 1996. Roughly speaking, a blender can be understood as a sufficiently thick hyperbolic set Γ such that the closure of an invariant manifold of dimension u of a saddle point in Γ contains an invariant manifold of dimension $u + 1$. The most simple scenarios where blenders can be described are the skew products defined on a horseshoe map, where the dynamics on the fibers is given by an iterated system of functions, mostly contractions. In this volume, L. J. Díaz and K. Gelfert show a partially hyperbolic and topologically transitive which they call a porcupine-like horseshoe. Dynamics on this set is given by a skew product over a horseshoe, but the fiber dynamics is given by a one-dimensional genuinely non-contracting iterated function system.The authors explain how the properties of the iterated function system can be translated to topological and ergodic properties of the porcupines.

Ergodic Theory deals with measure preserving processes in a measure space and it appears after the Poincaré recurrence theorem. In particular, it tries to describe the average time spent by typical orbits in different regions of the phase space. According to Birkoff's Ergodic Theorem these times are well defined for almost all points, with respect to any invariant probability measure. However, the notion of typical orbit is usually understood in the sense of volume (Lebesgue measure), which is not always an invariant measure. It is a fundamental open problem to understand under which conditions the behavior of typical (positive Lebesgue measure) orbits is well defined from the statistical point of view. In chaotic dynamical systems this can be precisely formulated by means of Sinai-Ruelle-Bowen (SRB) measures, which were introduced by Sinai for Anosov diffeomorphisms and later extended by Ruelle and Bowen for Axiom A diffeomorphisms and flows. In trying to capture the persistence of the statistical properties of a dynamical system, J. F. Alves and M. Viana proposed the notion of statistical stability, which expresses the continuous variation of SRB measures as a function of the dynamical system. In the contribution by J. F. Alves and M. Soufi some results on the existence and continuous variation of physical measures for families of chaotic dynamical systems are given. In particular, quadratic maps and Lorenz flow are considered in more detail.

Chaotic dynamics, rigourously understood as the existence of strange attractors, is frequent outside the uniformly hyperbolic context. Persistence, in terms of positive probability of existence, of these attractors was proved, with great effort, for the Hénon family, for generic families of diffeomorphisms unfolding homoclinic tangencies and also for families of 3-dimensional vector fields unfolding Shil'nikov homoclinic orbits which are always accompanied by an infinity of horseshoes. In all cases the strange attractors are, as the unstable invariant manifold, of dimension one and therefore they have at most one positive Lyapunv exponent. Proofs are based in unfoldings of unimodal families, whose dynamics were studied along the second half of the past century. In order to prove the existence of persistent non hyperbolic strange attractors with more than one positive Lyapunov exponent it is necessary to consider 3-dimensional diffeomorphisms with homoclinic tangencies involving an unstable invariant manifold with dimension larger than two. There are numerical evidences of the existence of such attractors, but proofs require the study of certain non linear 2-dimensional maps (instead of unimodal maps). They will play the role of limit families that must be unfolded to conclude the existence of a strange attractor in the renormalization neighbourhood of a 3-dimensional homoclinic point.

The contribution by J. C. Tatjer et al. initiates this program with the study of certain piecewise linear maps which generalize in dimension two the tent maps essential in the understanding of the unimodal dynamics. This idea of unfolding lower dimensional dynamics to understand the behaviour in higher dimensions and the use of Poincaré maps defined on crossings sections, sometimes including the hypothesis of invariance for certain foliations on the section, are two routes that justify the study of the iteration of maps on a manifold. The complexity of the dynamics in these maps has been settled down in terms of entropy, either topological or metric, and it has motivated a large number of papers. Two of the contributions featured in this volume are related to such questions. S. Aranzubía and R. Labarca study the continuity of the topological entropy in the Milnor-Thurston World. In the contribution by S. Cánovas the relation between both entropies is considered for the case of a non autonomous discrete system, that is, the ordered iteration $T_n \circ T_{n-1} \circ \cdots \circ T_1(x)$ of a sequence of maps $\{T_j\}_{j\in\mathbb{N}}$ defined on a topological or probabilistic space X.

Homoclinic orbits, or more generally, heteroclinic cycles play a crucial role to explain loss of stability or chaotic behaviour. Nevertheless, finding analytical proofs of the existence of chaos is not at all easy, particularly when the angle of intersection between the invariant manifolds is exponentially small or, for instance, when one wants to prove the existence of Shil'nikov homoclinic orbits. They appear for instance in the unfolding of Bykov cycles, a kind of heteroclinic cycle. In the contribution by I. Laboriau and A.P. Rodrigues, the authors consider an equivariant family of volume-contracting vector fields on the three-dimensional sphere. When part of the symmetry is broken, the vector fields exhibit Bykov cycles and close to the symmetry persistent suspended horseshoes accompanied by attracting periodic trajectories with long periods appear.

Existence of homoclinic and heteroclinic orbits has been commonly argued in the literature, particularly in Celestial Mechanics, taking small perturbations

of hamiltonian vector fields. Regarding this approach one can see the paper by C. Simó and A. Vieiro where 2D diffeomorphisms with a homoclinic figure-eight to a dissipative saddle are perturbed by means of a periodic forcing.

In the more general case, when families of vector fields arise in given applications where the perturbation techniques cannot be applied, one can use numerical methods to prove, for instance, the existence of hypersurfaces of homoclinic bifurcations limiting stability domains in the parameter space or to compute Lyapunov exponents and conclude the existence of strange attractors when one finds any positive. Several contributions included in this volume are closely related to that approach.

The paper by M. Guardia et al. shows the existence of oscillatory motions for any value of the mass ratio in the restricted circular three body problem. The existence of these motions follows from the symbolic dynamics associated to the transversal intersection between the stable and unstable manifolds of infinity, which takes place for any value of the mass ratio and for big values of the Jacobi constant. Since the mass ratio is no longer small, this transversality cannot be checked by means of classical perturbation results.

C. Simó et al. consider again the restricted three-body problem and study the stability around the triangular libration points. The local stability follows from the well known KAM theory and Nekhorosev-like estimates. This paper examines what is the extent of the domains of practical stability. The answer requires the control of the intersection between the invariant manifolds associated to the different transient tori which leads to the arising of Arnold diffusion.

In the paper by L. Benet and A. Jorba, a simple model for the confinement of Saturn's F ring is considered and some preliminary numerical results are discussed. The classical Hindmarsh-Rose neuron model is studied numerically in the paper by M. A. Martínez et al. for certain parameter values where chaotic dynamics exists. The contribution by R. Barrio et al. is also of a computational nature. The authors examine spiral structures in 2-parametric diagrams of dissipative systems with strange attractors. Existence of chaotic dynamics is concluded in the last two mentioned papers by finding attractors with positive Lyapunov exponents. In the paper by R. Barrio et al. a new computational technique is proposed for explorations of parametric chaos in Lorenz like attractor. Numerical analysis of bifurcation diagrams, Lyapunov exponents and stability regions can be found also in the contribution by C. Simó and A. Vieiro, where they study the dynamics of a parametrically driven dissipative pendulum with a magnetic kick force acting on it. P. Benítez et al. study the LiNC/LiCN triatomic molecule vibrational dynamics including all three degrees of freedom by using frequency maps and small alignment index. With these tools they obtain numerical representations of global chaotic dynamics.

From Poincaré on, a vector field was understood as the qualitative picture of all orbits in its phase portrait. First, efforts were addressed to the study of all possible configurations, but bearing in mind vector fields possessing some particular interest. Nowadays, in contrast to such a approach, research is focused on whole sets $\mathscr{X}$ of dynamical systems, either consisting on vector fields or diffeomorphisms, defined on a manifold M. Given a topology and a dynamical equivalence relation,

usually the topological equivalence, defined on $\mathscr{X}$, the first focus of attention is the subset $\Sigma \subset \mathscr{X}$ given by the structurally stable systems, which is obtained by taking the union of the interiors of all equivalence classes. It coincides with the set consisting of all hyperbolic vector fields or diffeomorphisms satisfying the transversality condition. The complement $\mathscr{B}$ of Σ is called the bifurcation set and there one finds those systems whose invariant manifolds are tangent: with non transversal homoclinic points. Homoclinic tangencies are persistent generically on hypersurfaces $\mathscr{H} \subset \mathscr{X}$ of codimension one and just as the existence of a homoclinic point implies the existence of an infinite number of such points, the Newhouse phenomenon, for example, shows that the existence of a hypersurface $\mathscr{H}$ of vector fields or diffeomorphisms with homoclinic tangencies implies the existence of many others arbitrarily close. Hypersurface $\mathscr{H}$ can contain others of higher codimension matching with other dynamical transitions and in between these hypersurfaces there can arise very complicated dynamics which are persistent but not structurally stable (Hénon like strange attractors for instance). All of this shows that $\mathscr{B}$ has a very complex stratification. In order to unravel its structure we can pay attention, emulating Poincaré again, to the simplest elements in $\mathscr{B}$ playing a role in its organization. These elements are those systems with a non hyperbolic equilibrium (or fixed) point and we refer to them as singularities, either thinking in the point or in the system where it appears. The number of strata in $\mathscr{B}$ which are adjacent to a given singularity will depend on its codimension. This approach recalls again Poincaré. On one hand, to understand what happens close to a singularity, we study the singularity itself. In the same way, from the study of the equilibrium points of a vector field (topological index, remarkable values, ...) one can obtain properties of the behaviour in a neighbourhood of the equilibrium point. One of the essential tools when dealing with singularities is the reduction to normal form. This technique was introduced by Poincaré in his thesis and it is based in the use of change of coordinates to obtain simplified expressions of the singularity, where most of the terms in the Taylor expansion are appropriately removed. Since the structure of the bifurcation set is extremely complicated, in order to deal with a given singularity X we consider families of dynamical systems X_μ contained in $\mathscr{X}$ and satisfying $X_0 = X$. These families are called unfoldings of the singularity. The knowledge of the different dynamics present in the families X_μ allows for an understanding of the structure of $\mathscr{B}$ in the vicinity of X. Some examples of unfoldings are considered in the contribution by H. Broer and G. Vegter, which considers the unfolding of some singularities of diffeomorphisms, mainly focusing on the phenomenon of resonance, which is the main concern of this paper. The concept of resonance is discussed and illustrated with a collection of clever examples.

The great variety of feasible dynamics for vector fields in dimension higher that three is not possible in the planar case. The Jordan Curve Lemma permits to prove the Poincaré Bendixson Theorem which characterize the limit sets of orbits in the plane. Thanks to the restrictions stated in that theorem many questions regarding planar flows dynamics have been solved. Nevertheless many other problems remain unsolved, including the integrability, the center-focus problem or the 16th Hilbert problem.

The contribution by A. Gasull and H. Giacomini is related to the 16th Hilbert problem. They use an extension of the Bendixson-Dulac Theorem to control the number and disposal of the limit cycles. The importance of the use of the Bendixson-Dulac results is that in many cases they translate the problem of knowing the number of periodic solutions of a planar polynomial differential equation to a problem of semi-algebraic nature: the control of the sign of a polynomial in a suitable domain.

Questions regarding integrability, limit cycles and center problem can be found in the paper by A. Buică et al., but posed for 3-dimensional vector fields or 2-dimensional non autonomous systems. The principal purpose of this paper is two fold: first to prove the existence and smoothness of inverse Jacobi multiplier V in the region of interest in the phase space and second to show that the invariant set under the flow given by the zero-set of an inverse Jacobi multiplier contains under some assumptions orbits which are relevant in its phase portrait such as periodic orbits, limit cycles, stable, unstable and center manifolds and so on. In the non-autonomous T-periodic case, A. Buică et al. show some relationships between T-periodic orbits and T-periodic inverse Jacobi multipliers.

In the paper by C. Alonso-González et al. an infinitesimal version of the Poincaré-Bendixson problem in dimension three is given. They describe the sets of accumulation of secants for orbits of real analytic vector fields in dimension three with the origin as only ω-limit point. These sets have structure of cyclic graph when the singularities are isolated under one blow-up. If the reduction of singularities is hyperbolic, under conditions of Morse-Smale type, they prove that the accumulation set is a single point or homeomorphic to S^1.

Recently there exist many papers devoted to the study of piecewise linear vector fields. These systems are easily designable using electric circuits and this can motivate the growing interest in their study. From the theoretical point of view researchers are interested in developing a theory which resembles that already known for dynamical systems with higher regularity hypothesis. It was expected that this should be an easy task and also that the main dynamics and transitions already observed in the regular case could be obtained for piecewise linear systems. None of these expectations have been met, but it is true that many of the possible dynamics in regular case can be observed also in this new context.

E. Ponce et al. provide two contributions to this volume. In the first, they consider planar discontinuous piecewise linear systems with two linearity zones, one of them being of focus type. By using an adequate canonical form under certain hypotheses, they characterize the bifurcation of a limit cycle when the focus changes its stability after becoming a linear center. The studied bifurcation appears in real world applications, as shown by the analysis of an electronic Wien bridge oscillator without symmetry. In their second paper, E. Ponce et al. study a possible degeneration of the Hopf-zero bifurcation for a two- parameters family of symmetric three dimensional piecewise linear differential systems with three zones of linearity. Then they show that around the critical point in such parameter plane the unfolding is very similar to the one appearing in the generalized Hopf bifurcation of differentiable dynamics.

E. Freire et al. consider a family of planar piecewise linear systems with a discontinuity line where the crossing set is maximal and it has two dynamics of focus type. Then they give some new results and a survey of known bifurcations for this family.

This volume is completed with four more papers, which also deal with topical issues in dynamical systems. D. Peralta-Salas presents a series of realization problems regarding Foliation Theory which are addressed using the theory of integrable embeddings. This theory is a very rich framework where many classical tools from differential and algebraic topology play a prominent role: Gromov h-principle, Hirch-Smale theory of immersions, complete intersections and obstruction theory. The paper by F. A. Carnicero and F. Sanz deals with real meromorphic linear systems of two ordinary differential equations and studies the asymptotic behaviour of solutions defined either to the left or to the right of 0. In another paper, S. Gefter and T. Stulova present the differential-difference equation $w'(z) = Aw(z-h)+f(z)$, where f is an entire function of zero exponential type and A is a closed linear operator on a complex Banach E space having a bounded inverse operator and whose domain $D(A)$ is not necessarily dense in E. Then they find the explicit formula for zero exponential type entire solutions. Finally, G. de la Vega and S. López de Medrano consider the generalization of the May-Leonard system to the case of a larger number of species.

The Editors of this proceedings volume are senior members of the Group of Dynamical Systems at the University of Oviedo, who are joined by Begoña Alarcón, Pablo G. Barrientos, Fátima Drubi, Belén García and Enrique Vigil. Since the creation of the group, more than 20 years ago, we have received support from many colleagues and research centers. From these pages we want to express our gratitude to all of them. We especially thank the collaboration of the Instituto de Matemática Pura e Aplicada (IMPA) de Rio de Janeiro, the University of Hasselt and all the groups that make up the national network of dynamic systems (DANCE). To a certain extent we have considered that the organization of the meeting was a way to provide feedback to the community for the hospitality that we have enjoyed so many times.

On behalf of the Organizing Committee, in which B. Alarcón, P. G. Barrientos and B. García have also participated, we thank the support of all members of the Scientific Committee: Freddy Dumortier, Marty Golubistky, Ale Jan Homburg, Tere Martínez-Seara, Jacob Palis and Jorge Rocha. We would like to acknowledge the careful work of all the contributors, as well as the anonymous referees and all the participants of the meeting for the excellent scientific level and pleasant atmosphere of this congress. We would also like to thank Springer for this opportunity to show part of the work developed during that marvelous week.

Asturias, Spain
April 2013

Santiago Ibáñez
Jesús S. Pérez del Río
Antonio Pumariño
J. Ángel Rodríguez

Acknowledgements

The International Conference *Dynamical Systems: 100 years after Poincaré* was held with the support of public and academic institutions: Ministry of Economy and Competitiveness, City of Gijón, Real Sociedad Matemática Española, Sociedad Española de Matemática Aplicada and University of Oviedo. We thank all of them for their financial help and also for facilitating the diffusion of the event. We also thank our Department of Mathematics for the financial support but also for helping us with the organization and preparation of the meeting.

Contents

List of Contributors

C. Alonso-González Universidad de Alicante, Alicante, Spain

J. F. Alves Departamento de Matemática, Faculdade de Ciências da Universidade do Porto, Porto, Portugal

Solange Aranzubía Departamento de Matemática y Ciencia de la Computación, Universidad de Santiago de Chile (USACH), Santiago, Chile

Roberto Barrio University of Zaragoza, Zaragoza. Spain

Luis Benet Instituto de Ciencias Físicas, Universidad Nacional Autónoma de México (UNAM), Cuernavaca, Mexico

P. Benítez Grupo de Sistemas Complejos, Departamento de Física y Mecánica, Escuela Técnica Superior de Ingenieros Agrónomos, Universidad Politécnica de Madrid, Madrid, Spain

R.M. Benito Grupo de Sistemas Complejos, Departamento de Física y Mecánica, Escuela Técnica Superior de Ingenieros Agrónomos, Universidad Politécnica de Madrid, Madrid, Spain

Fernando Blesa University of Zaragoza, Zaragoza, Spain

F. Borondo Departamento de Química, Instituto de Ciencias Matemáticas (ICMAT), Universidad Autónoma de Madrid, Madrid, Spain

Henk W. Broer Johann Bernoulli Institute for Mathematics and Computer Science, University of Groningen, Groningen, The Netherlands

Adriana Buică Department of Applied Mathematics, Babeş-Bolyai University, Cluj-Napoca, Romania

F. Cano Universidad de Valladolid, Valladolid, Spain

Jose S. Cánovas Departamento de Matemática Aplicada y Estadística, Universidad Politécnica de Cartagena, Murcia, Spain

Félix Álvaro Carnicero Universidad de Valladolid, Departamento de Álgebra, Análisis Matemático, Geometría y Topología, Facultad de Ciencias, Campus Miguel Delibes, Valladolid, Spain

Alain Chenciner Observatoire de Paris, IMCCE (UMR 8028), Paris, France
Département de mathématique, Université Paris VII, Paris, France

L. J. Díaz Departamento de Matemática, PUC-Rio, Rio de Janeiro, Brazil

Emilio Freire Departamento Matemática Aplicada II, E.T.S. Ingeniería, Sevilla, Spain

Isaac A. García Departament de Matemàtica, Universitat de Lleida, Lleida, Spain

Armengol Gasull Departament de Matemàtiques, Universitat Autònoma de Barcelona, Barcelona, Spain

Sergey Gefter Department of Mechanics and Mathematics, Kharkiv National University, Kharkiv, Ukraine

K. Gelfert Instituto de Matemática Universidade Federal do Rio de Janeiro, Av. Athos da Silveira Ramos 149, Cidade Universitária - Ilha do Fundão, Rio de Janeiro, Brazil

Hector Giacomini Laboratoire de Mathématiques et Physique Théorique, Faculté des Sciences et Techniques, Université de Tours, Tours, France

Marcel Guardia Department of Mathematics, Mathematics Building, University of Maryland, College Park, MD, USA

Angel Jorba Departament de Matemàtica Aplicada i Anàlisi, Universitat de Barcelona, Barcelona, Spain

Rafael Labarca Departamento de Matemática y Ciencia de la Computación, Universidad de Santiago de Chile (USACH), Santiago, Chile

Isabel S. Labouriau Centro de Matemática da Universidade do Porto and Faculdade de Ciências da Universidade do Porto, Porto, Portugal

Santiago López de Medrano Instituto de Matemáticas, UNAM, México, D.F., México

J.C. Losada Grupo de Sistemas Complejos, and Departamento de Física y Mecánica, Escuela Técnica Superior de Ingenieros Agrónomos, Universidad Politécnica de Madrid, Madrid, Spain

Pau Martín Departament de Matemàtica Aplicada IV, Universitat Politècnica de Catalunya, Barcelona, Spain

M. Angeles Martínez Departamento de Matemática Aplicada and IUMA, Universidad de Zaragoza, Zaragoza, Spain

Susanna Maza Departament de Matemàtica, Universitat de Lleida, Lleida, Spain

Daniel Peralta-Salas Instituto de Ciencias Matemáticas (ICMAT), Consejo Superior de Investigaciones Científicas, Madrid, Spain

Enrique Ponce Departamento Matemática Aplicada II, E.T.S. Ingeniería, Sevilla, Spain

A. Pumariño Dept. de Matemáticas, Universidad de Oviedo, Oviedo, Spain

Alexandre A. P. Rodrigues Centro de Matemática da Universidade do Porto and Faculdade de Ciências da Universidade do Porto, Porto, Portugal

J. A. Rodríguez Dept. de Matemáticas, Universidad de Oviedo, Oviedo, Spain

Javier Ros, Departamento Matemática Aplicada II, E.T.S. Ingeniería, Sevilla, Spain

R. Rosas Pontificia Universidad Católica del Perú, San Miguel, Lima, Peru

Fernando Sanz Universidad de Valladolid, Departamento de Álgebra, Análisis Matemático, Geometría y Topología, Facultad de Ciencias, Valladolid, Spain

Tere M. Seara Departament de Matemàtica Aplicada I, Universitat Politècnica de Catalunya, Barcelona, Spain

Sergio Serrano Departamento de Matemática Aplicada and IUMA, Universidad de Zaragoza, Zaragoza, Spain

Andrey Shilnikov Neuroscience Institute and Department of Mathematics and Statistics, Georgia State University, Atlanta, GA, USA

C. Simó Departament de Matemàtica Aplicada i Anàlisi, Universitat de Barcelona, Barcelona, Spain

M. Soufi Departamento de Matemática, Faculdade de Ciências da Universidade do Porto, Porto, Portugal

P. Sousa-Silva Departament de Matemàtica Aplicada i Anàlisi, Universitat de Barcelona, Barcelona, Spain

Tetyana Stulova Department of Mechanics and Mathematics, Kharkiv National University, Kharkiv, Ukraine

J. C. Tatjer Dept. de Matemàtica Aplicada i Anàlisi, Universitat de Barcelona, Barcelona, Spain

M. Terra Instituto Tecnológico de Aeronáutica, São José dos Campos, São Paulo, Brazil

Francisco Torres, Departamento Matemática Aplicada II, E.T.S. Ingeniería, Sevilla, Spain

Genaro de la Vega Instituto de Matemáticas, UNAM and Universidad Nacional Autónoma de México, Area de la Investigación Científica, Circuito Exterior, Cd. Universitaria, México, D.F., México

Gert Vegter Johann Bernoulli Institute for Mathematics and Computer Science, University of Groningen, Groningen, The Netherlands

Elísabet Vela Departamento Matemática Aplicada II, E.T.S. Ingeniería, Sevilla, Spain

A. Vieiro Departament de Matemàtica Aplicada i Anàlisi, Universitat de Barcelona, Barcelona, Spain

E. Vigil Dept. de Matemáticas, Universidad de Oviedo, Oviedo, Spain

Tingli Xing Department of Mathematics and Statistics, Neuroscience Institute, Georgia State University, Atlanta, GA, USA

Secants of Trajectories in Dimension Three

C. Alonso-González, F. Cano, and R. Rosas

Abstract In this paper we give a description of the sets of accumulation of secants for orbits of real analytic vector fields in dimension three with the origin as only ω-limit point. It is an infinitesimal version of the Poincaré-Bendixson problem in dimension three. These sets have structure of cyclic graph when the singularities are isolated under one blow-up. If the reduction of singularities is hyperbolic, under conditions of Morse-Smale type, we prove that the accumulation set is a single point or homeomorphic to $\mathbb{S}^1$.

1 Introduction

Consider ξ a real analytic vector field defined in a neighborhood of the origin of $\mathbb{R}^3$ such that the origin is an isolated singular point. Take now an orbit γ of ξ such that the origin is the only ω-limit point of γ. From the study of the oscillation properties of γ, it arises the question of the existence of the *tangent* of γ at the origin (see [7]). If the *secants* of γ at the origin are the vectors $\gamma(t)/||\gamma(t)|| \in \mathbb{S}^2$, we say that γ has *tangent* at the origin when the limit of secants

$$\lim_{t \mapsto +\infty} \gamma(t)/||\gamma(t)||$$

C. Alonso-González (✉)
Universidad de Alicante, Alicante, Spain
e-mail: clementa.alonso@ua.es

F. Cano
University of Valladolid, Valladolid, Spain
e-mail: fcano@agt.uva.es

R. Rosas
Pontificia Universidad Católica del Perú, San Miguel, Lima, Peru
e-mail: rudy.rosas@pucp.pe

S. Ibáñez et al. (eds.), *Progress and Challenges in Dynamical Systems*,
Springer Proceedings in Mathematics & Statistics 54,
DOI 10.1007/978-3-642-38830-9_1,

exists. Anyway, if the limit above does not exist, a natural question is the description of the set of accumulation of secants

$$\mathrm{Sec}(\gamma) = \bigcap_s \overline{\{\gamma(t)/||\gamma(t)||;\, t \geq s\}} \subset \mathbb{S}^2.$$

As an example, for gradient vector fields, we have that the set $\mathrm{Sec}(\gamma)$ is a single point (see [8]), but in the general case the problem is not yet solved.

To deal with this problem we consider the situation after blowing-up. Hence the transformed trajectory $\tilde{\gamma}$ accumulates to any subset of a two dimensional real analytic manifold, the exceptional divisor D, that is homeomorphic to $\mathbb{S}^2$. The question above is then equivalent to the description of the ω-limit set of $\tilde{\gamma}$. This problem can be regarded as an infinitesimal version of the classical Poincaré-Bendixson Theorem.

In our study, we work with a generic absolutely isolated singularity at the origin. Absolutely isolated singularities of vector fields were introduced in [6]. We have an absolutely isolated singularity if the singularity is isolated and, after any finite sequence of blow-ups with center at singular points, we obtain isolated singular points and the exceptional divisor is invariant. Vector fields with absolutely isolated singularity have always a reduction of singularities after a finite number of blow-ups (see [6]). The generic conditions over the transformed vector field are a three-dimensional version of the classical Morse-Smale conditions (see [9]) and will be explained later on.

For our set of vector fields, we give a precise description of the set of accumulation of secants of any orbit as above.

Theorem 1 ([1]). *Let ξ be a real analytic vector field with a generic absolutely isolated singularity at the origin and γ a trajectory of ξ such that $\lim_{t\to+\infty}\gamma(t) = (0,0,0)$. Then, up to perform finitely many blow-ups, we have one of the following possibilities for the set of accumulation of secants $Sec(\gamma)$:*

1. *A single point.*
2. *A periodic orbit.*
3. *A poly-cycle (i.e. a finite union of singular points p_1, $p_2,\ldots,p_{m+1} = p_1$ and regular orbits $\sigma_1,\sigma_2,\ldots,\sigma_m$ connecting them) homeomorphic to $\mathbb{S}^1$.*

Strategy: We consider the situation after reduction of singularities. To simplify notation, we denote just ξ the transform vector field and γ the orbit of ξ accumulating over the exceptional divisor. Then, we proceed in two steps: First we consider a general absolutely isolated singularity and we show that the ω-limit set of γ is either a periodic orbit or a cyclic graph $\mathscr{C}(\gamma)$: the vertices of $\mathscr{C}(\gamma)$ are singular points of $\xi\mid_D$ and each (oriented) edge of $\mathscr{C}(\gamma)$ is the support of an orbit σ of $\xi\mid_D$ such that the α-limit set $\alpha(\sigma)$ and the ω-limit set $\omega(\sigma)$ are both vertices of $\mathscr{C}(\gamma)$. Secondly we impose our generic conditions (ξ is of Morse-Smale type). Taking into account the possible configurations for $\mathscr{C}(\gamma)$ and by considering suitable *Poincaré-Bendixson traps*, we use Proposition 1 below to show that $\omega(\gamma)$ is either a single point or homeomorphic to $\mathbb{S}^1$.

Without the stated conditions the structure of the ω-limit set $\omega(\gamma)$ it is not yet known. In collaboration with S. Ibáñez we have seen some examples that suggest that it should be possible to get vector fields where $\omega(\gamma)$ does not correspond to the accumulation sets described in the classical Poincaré-Bendixson Theorem. On the other hand, some constructions of Belotto [4] for limits (with respect to the Hausdorff metric) of periodic orbits in families could be adapted to generate examples of accumulation sets $\mathrm{Sec}(\gamma)$ in any real analytic subset of $\mathbb{S}^2$.

2 Morse-Smale Type Conditions

The classical Morse-Smale conditions over two-dimensional dynamical systems establish that all the singularities are hyperbolic and saddle-connections are not allowed (see [9] for details). We impose conditions over the transform vector field restricted to the exceptional divisor $\xi|_D$ similar to these ones. We call them *Morse-Smale type* conditions:

1. The singularities of $\xi|_D$ are all hyperbolic.
2. Two-dimensional saddle-connections between singularities of $\xi|_D$ are not permitted out of the skeleton (i.e. the union of the intersections of divisor components).
3. There are no infinitesimal saddle-connections.

Remark 1. In [2, 3] the reader can find a study of the topological classification of three-dimensional real analytic vector fields whose reduction of singularities is of Morse-Smale type.

We can distinguish the singular points of the transform vector field ξ over the exceptional divisor by the number of irreducible divisor components containing them: *interior singularities* for one component, *skeleton singularities* for two components and *corner singularities* for three. Note that a repeller of ξ could never be in $\omega(\gamma)$. Also, if an attractor p of ξ belongs to $\omega(\gamma)$, then $\omega(\gamma) = \{p\}$. A similar argument works for interior saddles with the two-dimensional variety on D. Then, if $\omega(\gamma)$ is different from just one point or a periodic orbit, we can suppose that the singular points on it are: corners, skeleton singularities or interior saddles whose two-dimensional variety is transversal to the exceptional divisor.

2.1 Two-Dimensional Saddle-Connections

Recall that a two-dimensional saddle-connection appears when two saddles are connected along their unstable-stable varieties. Notice that the second condition we impose means that given a component D_i of the exceptional divisor, there are no two-dimensional saddle-connections of $\xi|_{D_i}$ along unstable-stable varieties

contained exclusively in the component D_i. That is, we allow the existence of two-dimensional saddle-connections of $\xi|_D$ along the skeleton of D. This last situation is rigid in the sense that it is preserved under the usual deformations of the vector field (based on Melnikov's integral) addressed to destroy interior saddle-connections (for details see [5]).

2.2 Infinitesimal Saddle-Connections

To explain the third condition of Morse-Smale type we need to recall some concepts. Suppose that the linear part of a general vector field ξ with a saddle point at p is

$$L\xi = \lambda x \frac{\partial}{\partial x} + \mu y \frac{\partial}{\partial y} + \delta z \frac{\partial}{\partial z}$$

with $\lambda\mu\delta < 0$ and $\mu\delta > 0$. The *intrinsic* (y, z)*-weight* of p is δ/μ (see [2]). Now we describe a process of weights transition $\rho \longrightarrow \rho'$ that has been introduced in [2, 3]. Consider the curve $x = 1, z = y^{\frac{\delta}{\mu}}$. The saturated of this curve by the flow of the vector field accumulates at the invariant variety $x = 0$. If we take a curve $x = 1, z = y^{\rho}$ with $\rho > \delta/\mu$, its saturated accumulates at $\{x = z = 0\}$ and contains the curve $y = 1, z = x^{\rho'}$, where $\rho' = (\delta - \mu\rho)/\lambda$. If $\rho = \delta/\mu$ we say that there is *no transition*; otherwise ρ *transits* to ρ'. The situation is similar if $\rho < \delta/\mu$. By doing the inverse process we have a *weights transition* through the saddle p in the two possible senses.

Now, if we start with the intrinsic weight α of a corner p, by applying this previous rule of weights transition, the value α transits by the flow through connected saddles producing an associated weight at each step. Two situations are possible:

1. The process does not stop at any saddle.
2. There is a saddle q (corner or skeleton singularity) where the transition stops, i.e. the arriving value coincides with the intrinsic weight of q. In this case we say that p and q determine an *infinitesimal saddle-connection* (for details, see [2].)

3 Poincaré-Bendixson Traps

The main technique we use in [1] to proof our result is the construction of the Poincaré-Bendixson traps, that are an adaptation to dimension three of the arguments used in the proof of the classical Poincaré-Bendixson Theorem.

Let $p \in D$ be a non singular point for ξ and σ the orbit of $\xi|_D$ passing through p. Consider now Δ a planar section transversal to σ at p and also Γ an analytic curve $\Gamma \subset \Delta$ passing through p. Taking Δ small enough it can be fully transversal to ξ.

Suppose that we can apply the Poincaré first return over Δ. Denote Γ' the image of Γ by this return. This is an analytic curve and we have three possibilities:

1. Γ' coincides locally with Γ.
2. Γ' intersects Γ locally at the point p.
3. Γ' has no intersection with Γ.

In cases, (2) and (3), we can consider on Δ respectively a triangular small enough region delimited by Γ and Γ' or a rectangular small enough region delimited by Γ, Γ' and D as figure below shows.

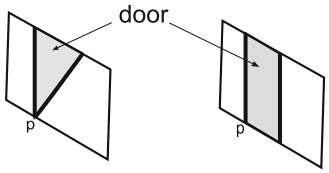

We call *doors* to these regions and *wall* to the saturation of the curve Γ by the vector fields flow from Γ to Γ'. Finally, we can define a *Poincaré-Bendixson trap for* ξ in each case:

1. A Poincaré-Bendixson trap of type (I) is just the wall if the first situation holds (closed trap).
2. A Poincaré-Bendixson trap of type (II) is the union of the wall and the triangular corresponding door in the second situation (semi-open trap).
3. A Poincaré-Bendixson trap of type (III) is the union of the wall and the rectangular corresponding door in the last situation (open trap).

Note that the absence of the Morse-Smale type conditions could be an obstruction for the existence of trapping regions.

In all cases, the intersection of a Poincaré-Bendixson trap with the exceptional divisor D is a Jordan curve C in D and then $D \setminus C$ has exactly two connected components with common frontier C. We have the following result:

Proposition 1. *Let τ be a Poincaré-Bendixson trap for ξ, then the ω-limit set $\omega(\gamma)$ is outside one of the two connected components of $D \setminus (\tau \cap D)$.*

By using this proposition the proof of Theorem 1 follows after partitioning a neighbourhood of the exceptional divisor by means of suitable Poincaré-Bendixson traps.

References

1. Alonso-González, C., Cano, F., Rosas, R.: Infinitesimal Poincaré-Bendixson problem in dimension three. ArXiv:1212.2134 [math.DS]
2. Alonso-González, C., Camacho, M.I., Cano, F.: Topological classification of multiple saddle connections. Discret. Contin. Dyn. Syst. **15**, 395–414 (2006)

3. Alonso-González, C., Camacho, M.I., Cano, F.: Topological invariants for singularities of real vector fields in dimension three. Discret. Contin. Dyn. Syst. **20**, 275–291 (2008)
4. Belotto, A.: Analytic varieties as limit periodic sets. ArXiv: 1109.0877v1 [math.DS]
5. Camacho, M.I.: A contribution to the topological classification of homogeneus vector fields. J. Differ. Equ. **57**, 159–171 (1983)
6. Camacho, C., Cano, F., Sad, P.: Desingularization of absolutely isolated singularities of vector fields. Invent. Math. **98**, 351–369 (1989)
7. Cano, F., Moussu, R., Sanz, F.: Oscillation, spiralement, tourbillonnement. Comment. Math. Helv. **75**, 284–318 (2000)
8. Kurdyka, K., Mostowski, T., Parusinsky, A.: Proof of the gradient conjecture of R. Thom. Ann. Math. **152**(2), 763–792 (2000)
9. Palis, J., de Melo, W.: Geometric Theory of Dynamical Systems. Springer, New York (1982)

Statistical Stability in Chaotic Dynamics

J.F. Alves and M. Soufi

Abstract We present some results on the existence and continuous variation of physical measures for families of chaotic dynamical systems. Quadratic maps and Lorenz flows will be considered in more detail. A brief idea on the proof of a recent theorem in Alves and Soufi (Nonlinearity 25:3527–3552, 2012) on the statistical stability of Lorenz flows will be given.

1 Introduction

The theory of Dynamical Systems started in the work of Poincaré on the three-body problem studies processes which evolve in time. The description of these processes may be given by flows (continuous time) or iterations of maps (discrete time). The main goals of this theory are: to describe the typical behavior of orbits as time goes to infinity; and to understand how this behavior changes under perturbations of the system and to which extent it is stable. In this work we are mostly concerned with the stability of dynamical systems.

Ergodic Theory deals with measure preserving processes in a measure space. In particular, it tries to describe the average time spent by typical orbits in different regions of the phase space. According to Birkoff's Ergodic Theorem, these times are well defined for almost all points, with respect to any invariant probability measure. However, the notion of typical orbit is usually meant in the sense of volume (Lebesgue measure), which is not always an invariant measure.

It is a fundamental open problem to understand under which conditions the behavior of typical (positive Lebesgue measure) orbits is well defined from the

J.F. Alves (✉) · M. Soufi
Departamento de Matemática, Faculdade de Ciências da Universidade do Porto,
Rua do Campo Alegre 687, 4169-007 Porto, Portugal
e-mail: falves@fc.up.pt; msoufin@gmail.com

S. Ibáñez et al. (eds.), *Progress and Challenges in Dynamical Systems*,
Springer Proceedings in Mathematics & Statistics 54,
DOI 10.1007/978-3-642-38830-9_2,

statistical point of view. In chaotic dynamical systems this can be precisely formulated by means of *Sinai-Ruelle-Bowen (SRB) measures*, which were introduced by Sinai for Anosov diffeomorphisms [23] and later extended by Ruelle and Bowen for Axiom A diffeomorphisms [21] and flows [9]. In trying to capture the persistence of the statistical properties of a dynamical system, Alves and Viana [4] proposed the notion of *statistical stability*, which expresses the continuous variation of SRB measures as a function of the dynamical system and is the problem that we address in this work.

2 Physical Measures

Let M be a compact connected Riemannian manifold, $f : M \to M$ a (possibly piecewise) C^k map, for some $k > 1$. We shall denote by λ the Lebesgue measure on the Borel sets of M.

The *basin* of an f-invariant probability measure μ on the Borel sets of M is the set of points $x \in M$ such that

$$\lim_{n\to+\infty} \frac{1}{n} \sum_{j=0}^{n-1} \varphi(f^j(x)) = \int \varphi \, d\mu, \quad \text{for any continuous } \varphi : M \to \mathbb{R}.$$

A probability measure μ is called a *physical measure* if its basin has positive Lebesgue measure.

Example 1. If $p \in M$ has an attracting periodic orbit of period $k \geq 1$, then the average of Dirac measures on the orbit of p,

$$\mu = \frac{1}{k} \left(\delta_p + \cdots + \delta_{f^{k-1}(p)} \right),$$

is a physical measure.

Example 2. It follows from Birkhoff's Ergodic Theorem that any ergodic invariant probability measure which is absolutely continuous with respect to Lebesgue measure is a physical measure. We shall refer to this special case of physical measures as *Sinai-Ruelle-Bowen (SRB) measures*.

A probability measure μ which is invariant under a flow $(X^t)_t$ is called a *physical measure* if the basin of μ, i.e. the set of points x such that

$$\lim_{T\to+\infty} \frac{1}{T} \int_0^T \varphi(X^t(x)) \, dt = \int \varphi \, d\mu, \quad \text{for any continuous } \varphi : M \to \mathbb{R},$$

has positive Lebesgue measure.

We shall refer to *statistical stability* as the continuous variation of the physical measures in the weak* topology as a function of the dynamical system. *Strong statistical stability* means the continuous variation of the densities (if they exist) of the physical measures in the L^1-norm as a function of the dynamical system.

3 Quadratic Maps

In this section we consider some results on the statistical stability of the family of quadratic maps, $f_a : [-1, 1] \to [-1, 1]$, with $a \in [0, 2]$, given for $x \in [-1, 1]$ by

$$f_a(x) = 1 - ax^2.$$

The dynamics of the maps in this family has been exhaustively studied by many authors in the last decades, serving as a model for many important results in the field.

3.1 Physical Measures

The first result on the existence of SRB measures is for parameters for which the critical point is nonrecurrent. Recall that a point is *nonrecurrent* if that point is not accumulated by its orbit.

Theorem 1 (Misiurewicz [19]). *If the orbit of* 0 *is nonrecurrent, then* f_a *has an SRB measure.*

The set $\mathscr{M}$ of *Misiurewicz parameters*, i.e. the set of parameters $a \in [0, 2]$ for which the orbit of 0 under f_a is nonrecurrent, has the cardinality of the continuum but zero Lebesgue measure. As the orbit of 0 is nonrecurrent for f_2, then $2 \in \mathscr{M}$ and f_2 has an SRB measure (f_2 is actually conjugated to the tent map by a diffeomorphism of (−1,1)).

The next result shows that SRB measures appear more generally from a measure theoretical point of view.

Theorem 2 (Jakobson [14]). *There is a positive Lebesgue measure set* $\mathscr{J}$ *of parameters* $a \in [0, 2]$ *for which* f_a *has an SRB measure.*

In particular, for a in the set of Jakobson parameters, f_a has no attracting periodic orbit.

Theorem 3 (Lyubich [17]). *For Lebesgue almost every* $a \in [0, 2]$ *the map* f_a *has either a periodic attracting orbit or an SRB measure.*

Let $\mathscr{P}$ be the set of parameters in $[0, 2]$ which have a physical measure. By Lyubich Theorem, the set $\mathscr{P}$ has full Lebesgue measure in $[0, 2]$.

3.2 Statistical Instability

Now we address ourselves to the statistical stability on the set of parameters whose dynamics has a physical measure. The first result shows that we do not have statistical stability inside that family.

Theorem 4 (Hofbauer-Keller [13]). *The map $\mathscr{P} \ni a \to \mu_a$ is not (weak*) continuous at $a = 2$.*

As mentioned before, f_2 has an SRB measure. On the other hand, Hofbauer and Keller showed that $a = 2$ is accumulated by a sequence of parameters a_n for which f_{a_n} has a physical measure which is a Dirac measure supported on a repelling fixed point.

The next result shows that statistical instability is not a so uncommon phenomenum.

Theorem 5 (Thunberg [24]).

1. *$\mathscr{P} \ni a \mapsto \mu_a$ is not (weak*) continuous at any Misiurewicz parameter;*
2. *$\mathscr{P} \ni a \mapsto \mu_a$ is not (weak*) continuous at any full Lebesgue measure subset of [0,2].*

3.3 Statistical Stability

Here we see some results showing that when restricted to some special sets of parameters we can have statistical stability, even in a strong sense. The first result is for Misiurewicz parameters.

Theorem 6 (Rychlik-Sorets [22]). *The map $\mathscr{M} \ni a \to \mu_a$ is (strongly) continuous.*

The next result shows that we can have a similar result in a wider context.

Theorem 7 (Tsujii [25]). *There is $\mathscr{T} \subset [0,2]$ with positive Lebesgue measure and positive density at 2 such that $\mathscr{T} \ni a \to \mu_a$ is (weak*) continuous.*

For the proof of the next result, Benedicks and Carleson developed a strategy that enabled them to extend some results on the chaotic behavior of many parameters (positive Lebesgue measure) in the quadratic family to the family of two-dimensional Hènon diffeomorphisms; see [6].

Theorem 8 (Benedicks-Carleson [6]). *There is $\mathscr{BC} \subset [0,2]$ with positive Lebesgue measure and positive density at 2 and constants $c, \alpha > 0$ such that for each $a \in \mathscr{BC}$*

1. $|(f_a^n)'(f_a(0))| \geq e^{cn}, \quad \forall n \in \mathbb{N}$;
2. $|f_a^n(0) - 0| \geq e^{-\alpha n}, \quad \forall n \in \mathbb{N}$.

The proof on the existence of SRB measures for these parameters is stated in the next result.

Theorem 9 (Benedicks-Young [7]). *For each $a \in \mathscr{BC}$, the map f_a has a unique SRB measure.*

However, we do not have statistical stability for the parameters $\mathscr{BC}$ when we consider the full set of parameters $\mathscr{P}$ which have a physical measure.

Theorem 10 (Thunberg [24]). *The map $\mathscr{P} \ni a \to \mu_a$ is not (weak*) continuous at any $a \in \mathscr{BC}$.*

On the other hand, the next shows that restricting ourselves to the $\mathscr{BC}$ parameters we do have statistical stability.

Theorem 11 (Freitas [11]). *The map $\mathscr{BC} \ni a \to \mu_a$ is (strongly) continuous.*

In order to prove this result, Freitas showed that, for each $a \in \mathscr{BC}$, the expansion and slow recurrence conditions stated by Benedicks and Carleson Theorem for the critical orbit hold for Lebesgue almost every point in the phase space:

1. f_a is *nonuniformly expanding*:

$$\liminf_{n\to\infty} \frac{1}{n} \sum_{i=0}^{n-1} \log(f_a'(f_a^i(x))) > c, \quad \text{Lebesgue a.e. } x$$

2. f_a has *slow recurrence to the critical set*: for each $\epsilon > 0$ there is $\delta > 0$ such that

$$\liminf_{n\to\infty} \frac{1}{n} \sum_{i=0}^{n-1} \log d_\delta(f_a^i(x), 0) > -\epsilon, \quad \text{Lebesgue a.e. } x$$

where d_δ is the δ-truncated distance, defined as

$$d_\delta(x, y) = \begin{cases} |x - y| & \text{if} \quad |x - y| \le \delta, \\ 1 & \text{if} \quad |x - y| > \delta. \end{cases}$$

This allows us to introduce the *expansion time*

$$E_a(x) = \min \left\{ N \ge 1 : \frac{1}{n} \sum_{i=0}^{n-1} \log f_a'(f_a^i(x)) > c, \forall n \ge N \right\},$$

the *recurrence time*

$$R_a(x) = \min \left\{ N \ge 1 : \frac{1}{n} \sum_{i=0}^{n-1} \log d_\delta(f_a^i(x), 0) > -\epsilon, \forall n \ge N \right\},$$

and the *tail set* (at time n)

$$\Gamma_a^n = \left\{x \in I : E_a(x) > n \quad \text{or} \quad R_a(x) > n\right\}.$$

Freitas [11] proved that there are $C, \gamma > 0$ such that $|\Gamma_a^n| \leq Ce^{-\gamma n}$ for all $n \geq 1$ and $a \in \mathscr{BC}$, which together with the following result gives the conclusion of Theorem 11.

Theorem 12 (Alves [1]). *Let $\mathscr{A}$ be a set of parameters for which there are $C > 0$ and $\gamma > 1$ with $|\Gamma_a^n| \leq Cn^{-\gamma}$, for all $n \geq 1$ and all $a \in \mathscr{A}$. Then each f_a with $a \in \mathscr{A}$ has an SRB measure μ_a and $\mathscr{A} \ni a \longmapsto d\mu_a/d\lambda$ is continuous.*

4 Lorenz Flow

Lorenz [16] studied numerically the vector field X defined by

$$\begin{cases} \dot{x} = a(y - x), \\ \dot{y} = bx - y - xz, \\ \dot{z} = xy - cz, \end{cases}$$

for the parameters $a = 10$, $b = 28$ and $c = 8/3$. The following properties are well known for this vector field:

1. X has a *singularity* at the origin with eigenvalues
$$0 < -\lambda_3 \approx 2.6 < \lambda_1 \approx 11.83 < -\lambda_2 \approx 22.83;$$
2. There is *trapping region* U such that $\Lambda = \cap_{t>0} X^t(U)$ is an attractor and the origin is the unique singularity contained in U;
3. The divergence of X is negative:
$$\text{div}X = \partial\dot{x}/dx + \partial\dot{y}/dy + \partial\dot{z}/dz = -(a + 1 + c) < 0,$$

Thus X contracts volume, and in particular Λ has zero volume.

In experimental computations, Lorenz realized that the flow has *sensitivity to the initial conditions*, i.e. even a small initial error lead to enormous differences in the outcome.

4.1 Geometric Model

In the 1970s, Guckenheimer and Williams [12] introduced a *geometric model* for the Lorenz flow. The vector field X is linear in a neighborhood of the singularity $(0, 0, 0)$ whose eigenvalues satisfy

$$0 < -\lambda_3 < \lambda_1 < -\lambda_2.$$

Fig. 1 The cross-section

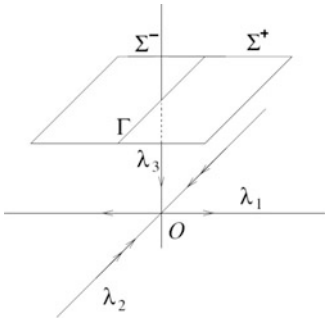

X has a cross-section $\Sigma = \{z = 1, |x| \leq 1/2, |y| \leq 1/2\}$ intersecting the (two-dimensional) stable manifold of the singularity 0 along a curve Γ which divides Σ into two regions Σ^+ and Σ^- (Fig. 1).

An easy calculation shows that the time needed to go from $\Sigma^\pm$ to $S^\pm = \{x = \pm 1, |y| \leq 1, 0 \leq z \leq 1\}$ is given by

$$\tau_0(x, y, 1) = -\frac{1}{\lambda_1} \log |x|.$$

To complete the geometric model of Lorenz flow, it is assumed that the flow from $S^\pm$ reaches Σ in finite time T_0. Hence, the return time from Σ to itself is

$$\tau_0(x, y, 1) = -\frac{1}{\lambda_1} \log |x| + T_0.$$

Poincaré Return Map

The return map $P : \Sigma \setminus \Gamma \to \Sigma$ admits a *stable foliation* $\mathscr{F}$ on Σ with the following properties (Fig. 2):

- *Invariant:* the image under P of a stable leaf ξ (distinct from Γ) is contained in another stable leaf;
- *Contracting:* the diameter of $P^n(\xi)$ goes to zero when $n \to \infty$, uniformly over all leaves;
- *Quotient map:* P induces a map f on the quotient space $\Sigma/\mathscr{F} \sim [-1/2, 1/2] = I$.

Assuming *the strong dissipative condition* at the singularity

$$-\frac{\lambda_2}{\lambda_1} > -\frac{\lambda_3}{\lambda_1} + 2,$$

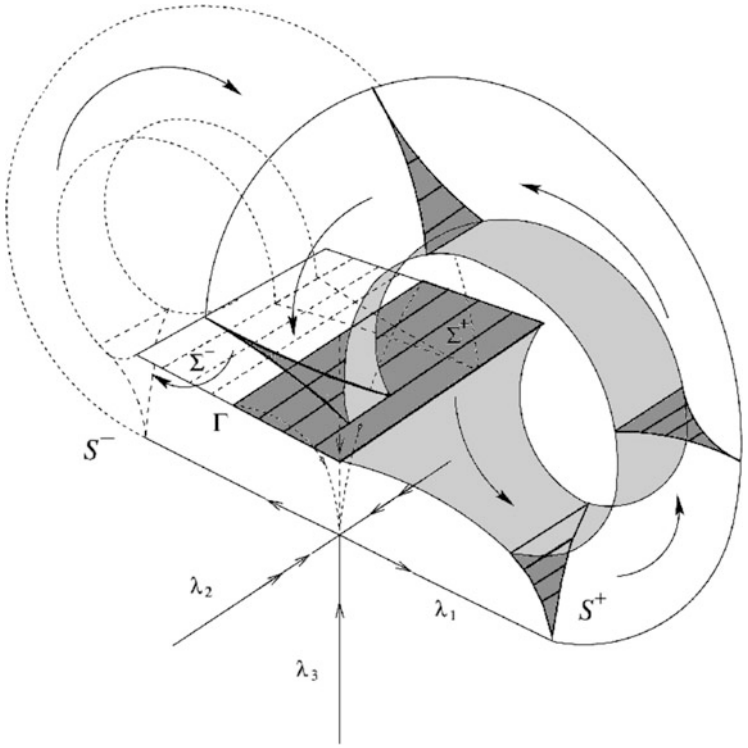

Fig. 2 The return map

the foliation $\mathscr{F}$ is C^2, and the one-dimensional quotient map f is C^2 away from the singularity. The map f has the following properties:

1. f is discontinuous at $x = 0$: $\lim_{x\to 0^+} f(x) = -1/2$ and $\lim_{x\to 0^-} f(x) = 1/2$;
2. f is differentiable on $I \setminus \{0\}$ and $f'(x) > \sqrt{2}$ for all $x \in I \setminus \{0\}$;
3. $\lim_{x\to 0^+} f'(x) = \lim_{x\to 0^-} f'(x) = +\infty$ (Fig. 3).

Attractor

The geometric model X admits a *strange attractor*, i.e. there is a compact set Λ such that:

1. Λ is invariant under the flow;
2. Λ contains a dense orbit;
3. Λ contains the singularity O;
4. There is an open neighborhood U of Λ such that $\Lambda = \cap_{t>0} X_t(U)$;
5. The flow has sensitive dependence on the initial conditions in U.

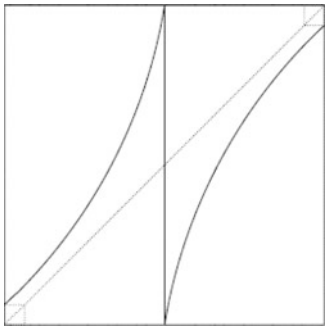

Fig. 3 The one-dimensional map

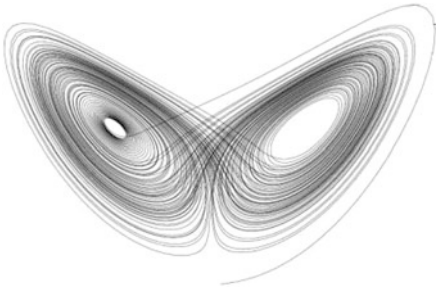

Fig. 4 Lorenz attractor

The next result shows that the classical values of Lorenz equations do indeed support a strange attractor (Fig. 4).

Theorem 13 (Tucker [26]). *For the classical parameter values, Lorenz equations support a robust strange attractor.*

Robustness

Observe that all the properties in the geometric model for the Lorenz flow remain valid under small perturbations. We consider a *family* $\mathscr{L}$ *of Lorenz flows* as a C^2 neighborhood of X such that for each $Y \in \mathscr{L}$:

1. The maximal forward invariant set Λ_Y inside U is an attractor containing a hyperbolic singularity;
2. Σ is a cross-section for the flow with a return time τ_Y and a Poincaré map P_Y;
3. P_Y admits a C^2 uniformly contracting invariant foliation $\mathscr{F}_Y$ on Σ with projection along the leaves of $\mathscr{F}_Y$ onto I given by a map π_Y;
4. The quotient map f_Y on I is a C^2 piecewise expanding with two branches; moreover, $f_Y' > \sqrt{2}$ except at the unique discontinuity point c_Y and $\lim_{x \to c_Y^{\pm}} f_Y'(x) = +\infty$;
5. There is some constant $C > 0$ such that for each $Y \in \mathscr{L}$

$$\tau_Y(x) \leq -C \log |\pi_Y(x) - c_Y|.$$

4.2 Physical Measures

It is well know that a one-dimensional map with the properties of f_Y above, for $Y \in \mathscr{L}$, has some SRB measure. Actually, we have the following folklore result; see e.g. [27].

Theorem 14. *For each $Y \in \mathscr{L}$, the map f_Y has a unique ergodic acip $\bar{\mu}_Y$ whose density (wrt Lebesgue measure) has bounded variation.*

The statistical stability for the maps f_Y with $Y \in \mathscr{L}$ was proved by Keller.

Theorem 15 (Keller [15]). *For each $Y \in \mathscr{L}$, the map f_Y is strongly statistically stable.*

It actually follows from the proof of this last result that the densities of the SRB measures are uniformly bounded: there is $C > 0$ such that for any $Y \in \mathscr{L}$

$$\left\| \frac{d\bar{\mu}_Y}{d\lambda} \right\|_\infty \leq C.$$

Given $Y \in \mathscr{L}$, let $P_Y : \Sigma \setminus \Gamma_Y \to \Sigma$ be its Poincaré map and $\bar{\mu}_Y$ be the physical measure for the quotient map. Given a bounded function $\varphi : \Sigma \to \mathbb{R}$, define

$$\varphi_+(x) := \sup_{y \in \xi(x)} \varphi(y) \qquad \text{and} \qquad \varphi_-(x) := \inf_{y \in \xi(x)} \varphi(y),$$

where $\xi(x)$ is the leaf in the foliation $\mathscr{F}_Y$ which contains x. The proof of the next lemma follows standard arguments in hyperbolic dynamics; see e.g. [8].

Lemma 1. *Given any continuous function $\varphi : \Sigma \to \mathbb{R}$, both limits*

$$\lim_{n\to\infty} \int (\varphi \circ P_Y^n)_- d\bar{\mu}_Y \qquad \text{and} \qquad \lim_{n\to\infty} \int (\varphi \circ P_Y^n)_+ d\bar{\mu}_Y$$

exist and they coincide.

Using Riesz-Markov Representation Theorem we easily deduce the next result.

Corollary 1. *There is a P_Y-invariant probability measure $\tilde{\mu}_Y$ on Σ such that*

$$\int \varphi \, d\tilde{\mu}_Y = \lim_{n\to\infty} \int (\varphi \circ P_Y^n)_- d\bar{\mu}_Y = \lim_{n\to\infty} \int (\varphi \circ P_Y^n)_+ d\bar{\mu}_Y,$$

for each continuous function $\varphi : \Sigma \to \mathbb{R}$.

One can check that $\tilde{\mu}_Y$ is a physical measure for the Poincaré map P_Y and using more or less standard arguments we build a measure for Y; see e.g. [5].

Theorem 16. *For $Y \in \mathscr{L}$, the physical measure μ of Y on U is given by*

$$\int \varphi \, d\mu = \frac{1}{\int \tau \, d\tilde{\mu}} \int \int_0^{\tau(x)} \varphi(X(x,t)) dt \, d\tilde{\mu}(x)$$

for any continuous $\varphi : U \to \mathbb{R}$. The measure μ_Y is a unique physical measure supported on the attractor Λ_Y.

The next result gives the statistical stability of Lorenz flows.

Theorem 17 (Alves-Soufi [3]). *Each $Y \in \mathscr{L}$ is statistically stable.*

Our goal in the subsections below is to give a brief idea about the proof of this theorem.

Remark 1. As the physical measure is supported on attractor Λ_Y, which has zero Lebesgue measure, it makes no sense to talk about strong statistical stability. In the sections below we shall give an idea of the proof of this last result.

4.3 Statistical Stability

Let $X_n \in \mathscr{L}$ is a sequence converging to $X_0 \in \mathscr{L}$ in the C^2 topology. We shall simplify our notations and write $\tilde{\mu}_n = \tilde{\mu}_{X_n}$ and $\mu_n = \mu_{X_n}$ for all $n \geq 0$. We also let λ denote Lebesgue measure.

The next result gives the statistical stability of the Poincaré maps.

Proposition 1. *$\tilde{\mu}_n \longrightarrow \tilde{\mu}_0$ as $n \to \infty$ in the weak* topology.*

Proof. We need to show that for any continuous $\varphi : \Sigma \to \mathbb{R}$ we have

$$\lim_{n\to\infty} \int \varphi d\,\tilde{\mu}_n = \int \varphi d\,\tilde{\mu}_0.$$

By definition

$$\lim_{n\to\infty} \int \varphi d\,\tilde{\mu}_n = \lim_{n\to\infty} \lim_{m\to\infty} \int (\varphi \circ P_n^m)_- \, d\,\bar{\mu}_n.$$

We have

$$\left| \int (\varphi \circ P_n^m)_- d\,\bar{\mu}_n - \int (\varphi \circ P_0^m)_- d\,\bar{\mu}_0 \right| \leq$$

$$\left| \int (\varphi \circ P_n^m)_- d\,\bar{\mu}_n - \int (\varphi \circ P_0^m)_- d\,\bar{\mu}_n \right|$$

$$+ \left| \int (\varphi \circ P_0^m)_- d\,\bar{\mu}_n - \int (\varphi \circ P_0^m)_- d\,\bar{\mu}_0 \right|.$$

The second term tends to zero since it is less that $\|\varphi\|_\infty \|d\bar{\mu}_n/d\lambda - d\bar{\mu}_0/d\lambda\|_1$ and

$$d\bar{\mu}_n/d\lambda \xrightarrow{L^1} \bar{\mu}_0/d\lambda, \quad \text{as } n \to \infty.$$

We are left to prove that the first term converges to zero when $n \to \infty$.

$$\begin{aligned}
&\left| \int (\varphi \circ P_n^m)_- d\bar{\mu}_n - \int (\varphi \circ P_0^m)_- d\bar{\mu}_n \right| \\
&\quad = \left| \int (\varphi \circ P_n^m)_- \frac{d\bar{\mu}_n}{d\lambda} d\lambda - \int (\varphi \circ P_0^m)_- \frac{d\bar{\mu}_n}{d\lambda} d\lambda \right| \\
&\quad \leq \int |(\varphi \circ P_n^m)_- - (\varphi \circ P_0^m)_-| \left| \frac{d\bar{\mu}_n}{d\lambda} \right| d\lambda \\
&\quad \leq C \int |(\varphi \circ P_n^m)_- - (\varphi \circ P_0^m)_-| d\lambda
\end{aligned}$$

The contraction factor on the stable leaves of the cross-section Σ can be taken the same for all vector fields in $\mathscr{L}$. So, the last expression can be made uniformly small. □

Proposition 2. *$\mu_n \longrightarrow \mu_0$ as $n \to \infty$ in the weak* topology.*

To prove this result we need to show that for any uniformly continuous and bounded function $\varphi : U \to \mathbb{R}$,

$$\left| \int \varphi \, d\mu_n - \int \varphi \, d\mu_0 \right| \tag{1}$$

can be made small when we take large n. Observe that (1) is bounded by the sum of the terms

$$\left| \frac{1}{\int \tau_n d\tilde{\mu}_n} - \frac{1}{\int \tau_0 d\tilde{\mu}_0} \right| \int \int_0^{\tau_0(x)} |\varphi(X_0(x,t))| dt \, d\tilde{\mu}_0(x), \tag{*}$$

and

$$\frac{1}{\int \tau_n d\tilde{\mu}_n} \left| \int \int_0^{\tau_n(x)} \varphi(X_n(x,t)) dt \, d\tilde{\mu}_n - \int \int_0^{\tau_0(x)} \varphi(X_0(x,t)) dt \, d\tilde{\mu}_0 \right| \tag{**}$$

Lemma 2. $\lim_{n\to\infty} \int \tau_n \, d\tilde{\mu}_n = \int \tau_0 \, d\tilde{\mu}_0.$

Proof. Let A be a small rectangle containing the singular curve of τ_0 and τ_n. Observe that

$$\left|\int \tau_n \, d\tilde{\mu}_n - \int \tau_0 \, d\tilde{\mu}_0\right| = \left|\int_A \tau_n \, d\tilde{\mu}_n - \int_A \tau_0 \, d\tilde{\mu}_0\right| + \left|\int_{A^c} \tau_n \, d\tilde{\mu}_n - \int_{A^c} \tau_0 \, d\tilde{\mu}_0\right|.$$

Since τ_0 and τ_n are both integrable, then first term can be made small by taking A small enough. The second term is bounded by

$$\left|\int_{A^c} \tau_n \, d\tilde{\mu}_n - \int_{A^c} \tau_0 \, d\tilde{\mu}_n\right| + \left|\int_{A^c} \tau_0 \, d\tilde{\mu}_n - \int_{A^c} \tau_0 \, d\tilde{\mu}_0\right|.$$

In A^c we have bounded return time and so $|\tau_n - \tau_0|$ can be made arbitrarily small by taking n large enough. The second term converges to zero as n goes to ∞, because $\tilde{\mu}_n \xrightarrow{\text{w}^*} \tilde{\mu}_0$. □

The previous lemma gives the convergence of (*) to zero as $n \to \infty$:

$$\left|\frac{1}{\int \tau_n \, d\tilde{\mu}_n} - \frac{1}{\int \tau_0 \, d\tilde{\mu}_0}\right| \iint_0^{\tau_0(\xi)} |\varphi(X_0(x,t))| dt \, d\tilde{\mu}_0(x)$$
$$\leq \left|\frac{1}{\int \tau_n \, d\tilde{\mu}_n} - \frac{1}{\int \tau_0 \, d\tilde{\mu}_0}\right| \|\varphi\|_\infty \int \tau_0 \, d\tilde{\mu}_0.$$

For (**) we use the next result.

Lemma 3. $$\lim_{n\to+\infty} \iint_0^{\tau_n(x)} \varphi(X_n(x,t)) dt \, d\tilde{\mu}_n(x) = \iint_0^{\tau_0(x)} \varphi(X_0(x,t)) dt \, d\tilde{\mu}_0(x).$$

Proof. Again let A be a small rectangle containing the singular curve of τ_0 and τ_n. The difference

$$\left|\int \int_0^{\tau_n(x)} \varphi(X_n(x,t)) dt \, d\tilde{\mu}_n(x) - \int \int_0^{\tau_0(x)} \varphi(X_0(x,t)) dt \, d\tilde{\mu}_0(x)\right|$$

is bounded by the sum of

$$\left|\int_A \int_0^{\tau_n(x)} \varphi(X_n(x,t)) dt \, d\tilde{\mu}_n(x) - \int_A \int_0^{\tau_0(x)} \varphi(X_0(x,t)) dt \, d\tilde{\mu}_0(x)\right|, \quad (2)$$

and

$$\left|\int_{A^c} \int_0^{\tau_n(x)} \varphi(X_n(x,t)) dt \, d\tilde{\mu}_n(x) - \int_{A^c} \int_0^{\tau_0(x)} \varphi(X_0(x,t)) dt \, d\tilde{\mu}_0(x)\right|. \quad (3)$$

Since $\int_0^{\tau_n(x)} \varphi(X_n(x,t))dt$ and $\int_0^{\tau_0(x)} \varphi(X_0(x,t))dt$ are respectively $\tilde{\mu}_n$ and $\tilde{\mu}_0$ integrable, (2) can be made arbitrarily small by taking A small enough. Observe that (3) is bounded by the sum of

$$\int_{A^c} \left| \int_0^{\tau_n(x)} \varphi(X_n(x,t))dt - \int_0^{\tau_0(x)} \varphi(X_0(x,t))dt \right| d\tilde{\mu}_n(x),$$

and

$$\left| \int_{A^c} \int_0^{\tau_0(x)} \varphi(X_0(x,t))dt\, d\tilde{\mu}_n(x) - \int_{A^c} \int_0^{\tau_0(x)} \varphi(X_0(x,t))dt\, d\tilde{\mu}(x) \right|.$$

As the return times are bounded on A^c, by the continuous variation of trajectories in finite periods of time, we can make the integrand in the first term small for large n. The second term converges to zero as n goes to ∞, because $\tilde{\mu}_n \xrightarrow{\text{W}^*} \tilde{\mu}_0$.

□

This completes the proof of Proposition 2.

Remark 2. The previous lemmas are essentially consequence of the following two key ingredients:

1. $\tau_n(x, y, 1) \sim -\log|x - c_n| \in L^1(\lambda)$, where the c_n is the discontinuity point of the quotient map f_{X_n}; and
2. There exists $C > 0$ such that $d\bar{\mu}_n/d\lambda \leq C$ for all n.

This implies that

$$\int \tau_n d\bar{\mu}_n$$

uniformly bounded. By Hölder Inequality, the same arguments can be carried out under the assumption that $d\bar{\mu}_n/d\lambda$ is uniformly bounded in $L^p(\lambda)$, for some $p < \infty$, as long as we have $\tau_n \in L^q(\lambda)$ for all $q > 1$.

5 Contracting Lorenz Flow

Now we consider a geometric Lorenz vector field X_0 where replace the usual *expanding condition* $\lambda_3 + \lambda_1 > 0$ in the Lorenz vector field by the *contracting condition*

$$\lambda_3 + \lambda_1 < 0.$$

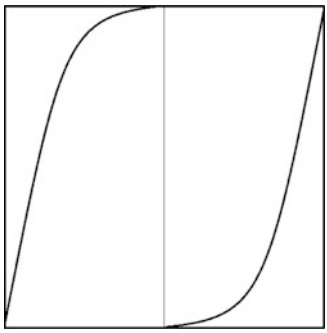

Fig. 5 The map f_0

Under these conditions there is still a trapping region U for X_0 on which

$$\Lambda = \cap_{t\geq 0} X_0^t(U)$$

is a singular-hyperbolic attractor (*Rovella attractor*).

Rovella attractor is not robust. However, Rovella proved in [20] that the chaotic attractor persists in a measure theoretical sense: there exists a one parameter family $(X_a)_{a\in[0,1]}$ of C^3 close vector fields to X_0 which have a transitive non-hyperbolic attractor.

5.1 Rovella Maps

As in the classical Lorenz flow, there is a Poincaré section for X_0 whose return map preserves a stable foliation. Under reasonable conditions, Rovella shows that the quotient map $f_0 : I \setminus \{0\} \to I$ satisfies (Fig. 5):

1. $\lim_{x\to 0^{\pm}} f_0(x) = \mp 1$;
2. ± 1 are pre-periodic and repelling;
3. f_0 is C^3 on $I \setminus \{0\}$ with negative Schwarzian derivative.

The next result shows that for many parameters in the family $(X_a)_a$ the corresponding one-dimensional quotient map behaves as the quadratic maps for the parameters in the set $\mathscr{BC}$.

Theorem 18 (Rovella [20]). *There is a set $\mathscr{R} \subseteq [0, 1]$ with full density at 0 such that:*

1. For all $a \in \mathscr{R}$, f_a is C^3 on $I \setminus \{0\}$ and satisfies

$$K_2|x|^{s-1} \leq f_a'(x) \leq K_1|x|^{s-1};$$

2. *There exists* $c > 0$ *such that for all* $a \in \mathscr{R}$

$$(f_a^n)'(\pm 1) > e^{cn}, \quad \text{for all } n \geq 0;$$

3. *There is* $\alpha > 0$ *such that for all* $a \in \mathscr{R}$

$$|f_a^{n-1}(\pm 1)| > e^{-\alpha n}, \quad \text{for all } n \geq 1.$$

The existence of physical measures for the one-dimensional Rovella maps can also be proved in this case.

Theorem 19 (Metzger [18]). *For each* $a \in \mathscr{R}$*, the map* f_a *admits a unique SRB measure* μ_a*.*

We have statistical stability when restricted to set of Rovella parameters.

Theorem 20 (Alves-Soufi [2]). *Rovella maps are nonuniformly expanding with slow recurrence to the critical point. Moreover, there are constants* $C, \tau > 0$ *such that for all* $n \in \mathbb{N}$ *and* $a \in \mathscr{R}$*,*

$$\left|\Gamma_a^n\right| \leq Ce^{-\tau n}.$$

The next corollary follows immediately from Theorems 12 and 20.

Corollary 2. *The map* $\mathscr{R} \ni a \longmapsto d\mu_a/d\lambda$ *is (strongly) continuous.*

5.2 A Final Remark

We obtain physical measures for the Rovella flows exactly as in the classical case. However, the statistical stability for the Rovella flows is still an open problem. We believe that at least when restricted to those flows corresponding to Rovella parameters we have statistical stability. Comparing to the classical case, the main difficulty lies in the fact that the density $d\mu_a/d\lambda$ is no longer (uniformly) bounded. In this direction, the following result has been obtained recently.

Theorem 21 (Cui-Ding [10]). *For* $a \in \mathscr{R}$*, the density of* μ_a *with respect to the Lebesgue measure belongs to some* $L^p(\lambda)$ *with* $p > 1$*, where* p *depends only on the (side) orders of the critical point.*

As observed in Remark 2, statistical stability for the contracting Lorenz flows in the Rovella parameters can be deduced, once we can show that $d\mu_a/d\lambda$ is uniformly bounded in $L^p(\lambda)$, for some $p > 1$. That is an interesting open problem.

Acknowledgements The authors were partially supported by Fundação Calouste Gulbenkian, by CMUP, by the European Regional Development Fund through the Programme COMPETE and by FCT under the projects PTDC/MAT/099493/2008 and PEst-C/MAT/UI0144/2011.

References

1. Alves, J.F.: Strong statistical stability of non-uniformly expanding maps. Nonlinearity **17**(4), 1193–1215 (2004)
2. Alves, J.F., Soufi, M.: Statistical stability and limit laws for Rovella maps. Nonlinearity **25**, 3527–3552 (2012)
3. Alves, J.F., Soufi, M.: Statistical stability of Lorenz attractors (2012, preprint)
4. Alves, J.F., Viana, M.: Statistical stability for robust classes of maps with non-uniform expansion. Ergod. Theory Dyn. Syst. **22**(1), 1–32 (2002)
5. Araujo, V., Pacifico, M.J., Pujals, E.R., Viana, M.: Singular-hyperbolic attractors are chaotic. Trans. Am. Math. Soc. **361**(5), 2431–2485 (2009)
6. Benedicks, M., Carleson, L.: The dynamics of the hénon map. Ann. Math. (2) **133**(1), 73–169 (1991)
7. Benedicks, M., Young, L.-S.: Absolutely continuous invariant measures and random perturbations for certain one-dimensional maps. Ergod. Theory Dyn. Syst. **12**(1), 13–37 (1992)
8. Bowen, R.: Equilibrium States and the Ergodic Theory of Anosov Diffeomorphisms. Lecture Notes in Mathematics, vol. 470. Springer, Berlin (1975)
9. Bowen, R., Ruelle, D.: The ergodic theory of Axiom A flows. Invent. Math. **29**(3), 181–202 (1975)
10. Cui, H., Ding, Y.: Invariant measures for interval maps with different one-side orders. Ergod. Theory Dyn. Syst. (to appear). doi:10.1017/etds.2013.62
11. Freitas, J.M.: Continuity of SRB measure and entropy for Benedicks-Carleson quadratic maps. Nonlinearity **18**(2), 831–854 (2005)
12. Guckenheimer, J., Williams, R.F.: Structural stability of Lorenz attractors. Inst. Hautes Études Sci. Publ. Math. **50**, 59–72 (1979)
13. Hofbauer, F., Keller, G.: Quadratic maps without asymptotic measure. Commun. Math. Phys. **127**(2), 319–337 (1990)
14. Jakobson, M.V.: Absolutely continuous invariant measures for one-parameter families of one-dimensional maps. Commun. Math. Phys. **81**(1), 39–88 (1981)
15. Keller, G.: Stochastic stability in some chaotic dynamical systems. Monatsh. Math. **94**(4), 313–333 (1982)
16. Lorenz, E.N.: Deterministic non-periodic flow. J. Atmos. Sci. **20**, 130–141 (1963)
17. Lyubich, M.: Almost every real quadratic map is either regular or stochastic. Ann. Math. (2) **156**(1), 1–78 (2002)
18. Metzger, R.J.: Sinai-Ruelle-Bowen measures for contracting Lorenz maps and flows. Ann. Inst. Henri Poincaré Anal. Non Linéaire **17**(2), 247–276 (2000)
19. Misiurewicz, M.: Absolutely continuous measures for certain maps of an interval. Inst. Hautes Études Sci. Publ. Math. **53**, 17–51 (1981)
20. Rovella, A.: The dynamics of perturbations of the contracting Lorenz attractor. Bol. Soc. Brasil. Mat. (N.S.) **24**(2), 233–259 (1993)
21. Ruelle, D.: A measure associated with Axiom-A attractors. Am. J. Math. **98**(3), 619–654 (1976)
22. Rychlik, M., Sorets, E.: Regularity and other properties of absolutely continuous invariant measures for the quadratic family. Commun. Math. Phys. **150**(2), 217–236 (1992)
23. Sinai, J.G.: Gibbs measures in ergodic theory. Uspehi Mat. Nauk **27**(4), 21–64 (1972)
24. Thunberg, H.: Unfolding of chaotic unimodal maps and the parameter dependence of natural measures. Nonlinearity **14**(2), 323–337 (2001)

25. Tsujii, M.: On continuity of Bowen-Ruelle-Sinai measures in families of one-dimensional maps. Commun. Math. Phys. **177**(1), 1–11 (1996)
26. Tucker, W.: The Lorenz attractor exists. C. R. Acad. Sci. Paris Sér. I Math. **328**(12), 1197–1202 (1999)
27. Viana, M.: Stochastic dynamics of deterministic systems. Publicações Matemáticas do IMPA. [IMPA Mathematical Publications]. Instituto de Matemática Pura e Aplicada (IMPA), Rio de Janeiro (1997). 22o Colóquio Brasileiro de Matemática. (22th Brazilian Mathematics Colloquium)

Combinatorial Dynamics and an Elementary Proof of the Continuity of the Topological Entropy at $\theta = \underline{101}$, in the Milnor Thurston World

Solange Aranzubía and Rafael Labarca

Abstract In the present paper we deal with the Milnor-Thurston world and we present elementary proofs of some results by combining dynamics, combinatory, linear algebra and entropy.

1 Introduction and Statements of the Results

The term combinatorial dynamics have been used by several authors in different contexts, see for instance [1, 4, 6, 8, 24]. Here, we use the term properly in the sense of the line of research presented by Labarca et al. in [2, 13–21]; which is near to the one posed by Alseda, Llibre and Misiurewicz mainly in [1].

It is well know that one of the purpose of the topological theory of dynamical systems is to find universal models describing the topological dynamics of a large class of systems (see for instance [1, 5]).

One of these universal models is the shift on n-symbols (Σ_n, d, σ) where Σ_n is the set of sequences $\{\theta : \mathbb{N}_0 \to \{0, 1, 2, \ldots, n-1\}\}$ endowed with certain metric, d, and $\sigma : \Sigma_n \to \Sigma_n$ is the shift map defined by $(\sigma(\theta))(i) = \theta(i+1)$. This model has been introduced to model one dimensional dynamics, by Metropolis, Stein, Stein at [22] and [23] (actually, for $n = 2$ with a different (said "naive") presentation) and eventually stated formally by J. Milnor and W. Thurston at [25], where the notion of a signed order in the shift space (Σ_n, d, σ) was also defined. In fact, several signed orders can be defined in Σ_n in a different way (see for instance [21]).

These models has been extensively used to obtain a great amount of information about maps defined in an interval (see for instances [1, 5, 10, 13–16, 26]); vector

S. Aranzubía (✉) · R. Labarca
Departamento de Matemática y Ciencia de la Computación, Universidad de Santiago de Chile (USACH), Santiago, Chile
e-mail: solange.aranzubia@usach.cl; rafael.labarca@usach.cl

S. Ibáñez et al. (eds.), *Progress and Challenges in Dynamical Systems*,
Springer Proceedings in Mathematics & Statistics 54,
DOI 10.1007/978-3-642-38830-9_3,

fields on three dimensional manifolds (see for instance [3,7,9,11,17]) among other kinds of dynamical systems.

In the special case of one dimensional dynamics, the shift of two symbols may be used to study increasing (decreasing) map with one discontinuity like the Lorenz maps, unimodal maps like the quadratic family or increasing-decreasing (decreasing-increasing) maps with one discontinuity. Namely, for $n = 2$ the ordered metric compact space $(\Sigma_2, \tau_T, \leq_T)$ corresponding to the increasing-increasing map T is known as the lexicographical space which generates the lexicographical world (see for instances [2,13–16,18,19]) which is denoted LW.

The ordered compact metric space corresponding to the map $T : I_0 \cup I_1 \to I$ which is increasing-decreasing is called the Milnor-Thurston space (see [20,21]) which generates the Milnor-Thurston world which is denoted MTW.

In the present paper we deal with the Milnor Thurston world and we present elementary proofs of some results by combining dynamics, combinatory, linear algebra and entropy. As far as we known, the technical lemma is new and the method of proving the continuity of the topological entropy, at a given point, also is new.

Let us now state our results.

Consider the symbolic space of Milnor-Thurton $(\Sigma_2, \tau, \leq)$ (see Sect. 2.1) and the shift map $\sigma : \Sigma_2 \to \Sigma_2$. A sequence $\alpha \in \Sigma_0 = \{\theta \in \Sigma_2; \theta_0 = 0\}$ is called *minimal* if $\sigma^i(\alpha) \geq \alpha$ for all $i \in \mathbb{N}_0 = \mathbb{N} \cup \{0\}$. A sequence $\beta \in \Sigma_1 = \{\theta \in \Sigma_2; \theta_0 = 1\}$ is called *maximal* if $\sigma^i(\beta) \leq \beta$ for all $i \in \mathbb{N}_0$. Let Min_2 (Max_2) denote the set of minimal (resp. maximal) sequences.

For $\alpha \in \Sigma_0$ and $\beta \in \Sigma_1$ let $\Sigma[\alpha, \beta] = \{\theta \in \Sigma_2; \alpha \leq \sigma^i(\theta) \leq \beta \text{ for any } i \in \mathbb{N}_0\} = \bigcap_{j=0}^{\infty} \sigma^{-j}([\alpha, \beta])$ (where $[\alpha, \beta] = \{\theta \in \Sigma_2; \alpha \leq \theta \leq \beta\}$).

The *Milnor Thurston world* is the set of pairs $(\alpha, \beta) \in Min_2 \times Max_2$ such that $\{\alpha, \beta\} \subset \Sigma[\alpha, \beta]$. Let MTW denote the Milnor Thurston world.

Let $H : MTW \to [0, \log 2]$ denote the map $H(\alpha, \beta) = h_{top}(\sigma|_{\Sigma[\alpha,\beta]}) =$ topological entropy of the map $\sigma|_{\Sigma[\alpha,\beta]} : \Sigma[\alpha, \beta] \to \Sigma[\alpha, \beta]$. Recently, in [21] it is proved that the map $H(\alpha, \beta)$ is continuous. Nevertheless, the proof is not elementary. We recall that a periodic orbit of *period prime* N, for the map σ is a sequence $\theta \in \Sigma_2$ such that $\sigma^i(\theta) \neq \theta$ for $1 \leq i \leq N - 1$ and $\sigma^N(\theta) = \theta$.

In the way of proving this continuity by elementary methods one can consider $\theta \in Max_2$ and the map $h(\theta) = h_{top}(\sigma|_{\Sigma[\sigma(\theta),\theta]})$.

The graph of the map $\{(\theta, h(\theta)); \theta \in \Sigma_1\} \subset \Sigma_1 \times [0, \log 2]$ is a devil's staircase and since the periodic orbits are dense in Max_2 its seems relevant to consider $\theta \in Max_2$ a periodic orbit and to prove that h is continuous at θ. To do this we have to prove that h is continuous from the right and from the left of θ.

Our first result implies that the proof of the continuity is guarantee from one side. In fact: for $\theta \in \Sigma_2, \theta = \underline{\theta_0\theta_1 \dots \theta_n}$; let $\theta^* = \underline{\theta_0\theta_1 \dots \theta_n^*}$ be the sequence defined by $\theta_n^* = 0$ if $\theta_n = 1$ and $\theta_n^* = 1$ if $\theta_n = 0$.

Theorem A. *For $\theta \in Max_2$ we have that $\theta^* \in Max_2$ and if $I(\theta, \theta^*)$ denote $[\theta, \theta^*]$ for $\theta < \theta^*$ or $[\theta^*, \theta]$ for $\theta^* < \theta$ then $h(\alpha) = h(\theta)$ for any $\alpha \in I(\theta, \theta^*)$.*

This results imply the continuity of h from one side. To prove the continuity for any $\theta \in Max_2 \cap Per(\sigma)$ from the remaining side, by elementary methods, is not easy. Any way, we have developed a method by using the entropy associated to graphs with dynamical meaning that is able to apply for specific elements in $Max_2 \cap Per(\sigma)$.

In this paper we prove the continuity of the map h at $\theta = \underline{101}$. Specifically we prove:

Theorem B. *The map h is continuous at* $\theta = \underline{101}$ *from the left.*

To do so, we will construct a sequence $\theta_n = \underline{(101)^n 111}$ which satisfy

(a) $\theta_1 < \theta_2 < \theta_3 < \ldots < \underline{101}$
(b) $\lim_{n\to\infty} \theta_n = \underline{101}$ and
(c) $h(\theta_n) \to h(\theta)$ as $n \to \infty$

Now, let us consider the renormalization operator

$$H_{11,10} : \Sigma_2 \to \Sigma_2, H_{11,10}(\theta_0, \theta_1, \ldots) = \widetilde{\theta_1}\widetilde{\theta_2}\widetilde{\theta_3}\ldots,$$

where $\widetilde{\theta_i} = 11$ if $\theta_i = 0$ and $\widetilde{\theta_i} = 10$ if $\theta_i = 1$. Let $\alpha_k = H^k_{11,10}(\underline{101})$ we have:

Corollary 1. *The map h is continuous at any* $\alpha_k \in Max_2, k \in \mathbb{N}$

Corollary 2. *Let* $\alpha_\infty = \lim_{k\to\infty} \alpha_k$. *Then* $h(\alpha_\infty) = 0$ *and h is continuous at* α_∞.

The sequence $\alpha_\infty \in Max_2$ corresponds to the limit of the period doubling sequences (see [23]).

Our method implies, in particular, the following results: Let us consider the sequence of square matrix $(M_{3k+2})_{k=1}^{\infty}$ given by

$$M_5 = \begin{bmatrix} 1&1&0&0&0 \\ 0&0&1&0&0 \\ 0&0&0&1&0 \\ 0&0&0&0&1 \\ 0&1&0&1&0 \end{bmatrix}_{5\times 5}$$

$$M_8 = \begin{bmatrix} 1&1&0&0&0&0&0&0 \\ 0&0&1&0&0&1&0&0 \\ 0&0&0&1&0&0&0&0 \\ 0&0&0&0&1&0&0&0 \\ 0&1&0&1&0&0&1&0 \\ 0&0&0&0&0&0&1&0 \\ 0&0&0&0&0&0&0&1 \\ 1&0&1&0&0&0&0&0 \end{bmatrix}_{8\times 8}$$

$$M_{11} = \left[\begin{array}{cccccccc|ccc} 1&1&0&0&0&0&0&0&0&0&0 \\ 0&0&1&0&0&1&0&0&1&0&0 \\ 0&0&0&1&0&0&0&0&0&0&0 \\ 0&0&0&0&1&0&0&0&0&0&0 \\ 0&1&0&1&0&0&1&0&0&1&0 \\ 0&0&0&0&0&0&0&1&0&0&0 \\ 0&0&0&0&0&0&0&0&1&0&0 \\ 1&0&1&0&0&0&0&0&0&0&0 \\ 0&0&0&0&0&0&0&0&0&1&0 \\ 0&0&0&0&0&0&0&0&0&0&1 \\ 0&0&0&0&0&1&0&0&0&0&0 \end{array}\right]_{11\times 11}$$

and for $k \geq 3$,

$$M_{3\cdot(k+1)+2} = \begin{bmatrix} M_{3k+2} & A_{3k+2} \\ C_{3k+2} & B_{3\times 3} \end{bmatrix}$$

where,

$$A_{3k+2} = \begin{bmatrix} 0\,0\,0 \\ 1\,0\,0 \\ 0\,0\,0 \\ 0\,0\,0 \\ 0\,1\,0 \\ 0\,0\,0 \\ 0\,0\,0 \\ \vdots \\ 0\,0\,0 \end{bmatrix}_{(3k+2)\times 3} \qquad B_{3\times 3} = \begin{bmatrix} 0\,1\,0 \\ 1\,0\,1 \\ 0\,0\,0 \end{bmatrix}$$

$$C_{3k+2} = \begin{bmatrix} 0\,0\,0\,0\,0\,0\,0\,0\,\ldots\,0 \\ 0\,0\,0\,0\,0\,0\,0\,0\,\ldots\,0 \\ 0\,0\,0\,0\,0\,1\,0\,0\,\ldots\,0 \end{bmatrix}_{3\times(3k+2)}$$

Let $p_k(x) = \det(M_{3k+2} - xI)$ be the characteristic polynomial associated to M_{3k+2}. Then $p_{k+1}(x) = (-1)^{k+1}x^{3(k+1)}(x^2 - x - 1) - p_k(x)$ and the sequence of spectral radio's $(r_k)_{k\geq 1}$ associated to $(M_{3k+2})_{k\geq 1}$, satisfy $1 < r_1 < r_2 < r_3 < \ldots < r_k < r_{k+1} < \ldots < \overline{r}$ where $1 < \overline{r} < 2$ is the root of the polynomial $x^2 - x - 1 = 0$. Moreover $\lim_{k\to\infty} r_k = \overline{r}$.

This paper is organized as follows: Sect. 1 contains the previous elements; Sect. 2 contains the proof of the technical Lemma and Sect. 3 contains the proof of the continuity of the topological entropy at $\theta = \underline{101}$ and applications of this results.

2 A Technical Lemma

2.1 Maximal Neighbors Periodic Orbits

Let $\theta = \underline{10^{k_1}1^{k_2}0^{k_3}1^{k_4}\ldots 0^{k_{2p-1}}1^{k_{2p}}}$ be a maximal periodic orbit of period prime $N = 1 + k_1 + k_2 + \ldots + k_{2p}$ and $\tilde{\theta} = \underline{10^{k_1}1^{k_2}0^{k_3}1^{k_4}\ldots 0^{k_{2p-1}}1^{k_{2p-1}}0}$. We note that if $k_2 + k_4 + \ldots + k_{2p}$ is even then $\tilde{\theta} < \theta$ (in fact θ and $\tilde{\theta}$ coincides in $1 + k_2 + \ldots + k_{2p} - 1 = k_2 + \ldots k_{2p}$ ones, thus both sequences coincides in a even number of ones and then $\tilde{\theta} < \theta$). In a similar way if $k_2 + k_4 + \ldots + k_{2p}$ is odd we conclude that $\theta < \tilde{\theta}$.

Proposition 1. *The sequence $\tilde{\theta}$ is a maximal periodic orbit.*

Proof. Here we prove that $\sigma^j(\tilde{\theta}) < \tilde{\theta}$, for each $j = 1, 2, \ldots, N-1$. Clearly, if the sequence $\sigma^j(\tilde{\theta})$ begin with a zero then $\sigma^j(\tilde{\theta}) < \tilde{\theta}$. Also, if $\sigma^j(\tilde{\theta})$ begins with two

ones then $\sigma^j(\tilde{\theta}) < \tilde{\theta}$. So, the result is relevant only when $\sigma^j(\tilde{\theta})$ is an iterated that start with a one followed by zeros.

Consider $j = k_1 + k_2$, for this case:

$$\sigma^{k_1+k_2}(\tilde{\theta}) = \underline{10^{k_3}1^{k_4}\ldots 0^{k_{2p-1}}1^{k_{2p}-1}010^{k_1}1^{k_2-1}}.$$

If $k_3 > k_1$, then θ is not a maximal sequence, so $k_3 \leq k_1$. If $k_3 < k_1$, then $\sigma^{k_1+k_2}(\tilde{\theta}) < \tilde{\theta}$.

So, we assume that $k_3 = k_1$ and $\tilde{\theta} = \underline{10^{k_1}1^{k_2}0^{k_1}1^{k_4}0^{k_5}\ldots 0^{k_{2p-1}}1^{k_{2p}-1}0}$, hence $\sigma^{k_1+k_2}(\tilde{\theta}) = \underline{10^{k_1}1^{k_4}0^{k_5}\ldots 0^{k_{2p-1}}1^{k_{2p}-1}010^{k_1}1^{k_2-1}}$. If $k_4 \neq k_2$, the maximality condition of θ implies that $\sigma^{k_1+k_2}(\tilde{\theta}) < \tilde{\theta}$.

So assuming $k_2 = k_4$ we have $\tilde{\theta} = \underline{10^{k_1}1^{k_2}0^{k_1}1^{k_2}0^{k_5}1^{k_6}\ldots 0^{k_{2p-1}}1^{k_{2p}-1}0}$ and $\sigma^{k_1+k_2}(\tilde{\theta}) = \underline{10^{k_1}1^{k_2}0^{k_5}1^{k_6}\ldots 0^{k_{2p-1}}1^{k_{2p}-1}010^{k_1}1^{k_2-1}}$. If $k_1 \neq k_5$, then maximality of θ implies that $\sigma^{k_1+k_2}(\tilde{\theta}) < \tilde{\theta}$. If $k_1 = k_5$ we have

$$\tilde{\theta} = \underline{10^{k_1}1^{k_2}0^{k_1}1^{k_2}0^{k_1}1^{k_6}0^{k_7}\ldots 0^{k_{2p-1}}1^{k_{2p}-1}0}.$$

Successively $k_6 = k_2, k_7 = k_1, k_8 = k_2, k_9 = k_1, \ldots, k_{2p-2} = k_2, k_{2p-1} = k_1$ and $\tilde{\theta} = \underline{10^{k_1}1^{k_2}0^{k_1}1^{k_2}0^{k_1}\ldots 1^{k_2}0^{k_1}1^{k_{2p}-1}0}$. This implies that

$$\theta = \underline{10^{k_1}1^{k_2}0^{k_1}1^{k_2}0^{k_1}1^{k_2}\ldots 1^{k_2}0^{k_1}1^{k_{2p}}}$$

and $\sigma^{k_1+k_2}(\theta) = \underline{10^{k_1}1^{k_2}0^{k_1}1^{k_2}0^{k_1}1^{k_2}\ldots 1^{k_2}0^{k_1}1^{k_{2p}}10^{k_1}1^{k_2-1}}$. If $k_2 = k_{2p}+1$, then $k_2 - 1 = k_{2p}$ and $\theta = \underline{10^{k_1}1^{k_2}0^{k_1}1^{k_2}0^{k_1}1^{k_2}\ldots 1^{k_2}0^{k_1}1^{k_2}0^{k_1}1^{k_2-1}}$,

$$\sigma^{k_1+k_2}(\theta) = \underline{10^{k_1}1^{k_2}0^{k_1}1^{k_2}0^{k_1}1^{k_2}\ldots 1^{k_2}0^{k_1}1^{k_2}0^{k_1}1^{k_2-1}}.$$

Thus $\sigma^{k_1+k_2}(\theta) = \theta$, therefore $\theta = \underline{10^{k_1}1^{k_2-1}} = \underline{10^{k_1}1^{k_2}}$. In this case $\tilde{\theta} = \underline{10^{k_1}1^{k_2-1}0}$ and it is easy to verify that $\sigma^s(\tilde{\theta}) < \tilde{\theta}$, for all $1 \leq s \leq k_1 + k_2$. So assume that $k_2 \neq k_{2p} + 1$. Let us assume that $k_2 < k_{2p} + 1$. In this case there is $s \in \mathbb{N}$ for which $k_2 + s = k_{2p} + 1$. If occur that $s = 1$, then $k_2 = k_{2p}$ and we have $\theta = \underline{10^{k_1}1^{k_2}0^{k_1}1^{k_2}\ldots 1^{k_2}0^{k_1}1^{k_2}0^{k_1}1^{k_2}}$, and

$$\sigma^{k_1+k_2}(\theta) = \underline{10^{k_1}1^{k_2}0^{k_1}1^{k_2}0^{k_1}1^{k_2}\ldots 1^{k_2}0^{k_1}1^{k_2}10^{k_1}1^{k_2-1}}.$$

In this case there is an odd number of ones in the places where θ and $\sigma^{k_1+k_2}(\theta)$ coincides. Hence, for $\tilde{\theta}$ we have: $\tilde{\theta} = \underline{10^{k_1}1^{k_2}0^{k_1}1^{k_2}0^{k_1}1^{k_2}\ldots 1^{k_2}0^{k_1}1^{k_2}0^{k_1}1^{k_2-1}0}$, and $\sigma^{k_1+k_2}(\tilde{\theta}) = \underline{10^{k_1}1^{k_2}0^{k_1}1^{k_2}0^{k_1}1^{k_2}\ldots 1^{k_2}0^{k_1}1^{k_2-1}010^{k_1}1^{k_2-1}}$. We conclude that the places where $\tilde{\theta}$ and $\sigma^{k_1+k_2}(\tilde{\theta})$ coincides there is an 1 less than the number of ones where θ and $\sigma^{k_1+k_2}(\theta)$ coincides. In the first place where the two sequences do not match, $\tilde{\theta}$ has a one and $\sigma^{k_1+k_2}(\tilde{\theta})$ has a zero, therefore $\sigma^{k_1+k_2}(\tilde{\theta}) < \tilde{\theta}$ and we are done. Let us assume that $s > 1$. In this case $k_{2p} = k_2 + s - 1$, $\theta = \underline{10^{k_1}1^{k_2}0^{k_1}1^{k_2}0^{k_1}1^{k_2}\ldots 1^{k_2}0^{k_1}1^{k_2}0^{k_1}1^{k_2+s-1}}$, and

$$\sigma^{k_1+k_2}(\theta) = \underline{10^{k_1}1^{k_2}0^{k_1}1^{k_2}0^{k_1}1^{k_2}\ldots 1^{k_2}0^{k_1}1^{k_2}1^{s}0^{k_1}1^{k_2-1}}.$$

For $\tilde{\theta}$ we have: $\tilde{\theta} = \underline{10^{k_1}1^{k_2}0^{k_1}1^{k_2}0^{k_1}1^{k_2}\ldots 1^{k_2}0^{k_1}1^{k_2}0^{k_1}1^{k_2+s-2}0}$, and $\sigma^{k_1+k_2}(\tilde{\theta}) = \underline{10^{k_1}1^{k_2}0^{k_1}1^{k_2}0^{k_1}1^{k_2}\ldots 1^{k_2}0^{k_1}1^{k_2}1^{s-2}010^{k_1}1^{k_2-1}}$. If $s > 2$, then the number of ones where $\tilde{\theta}$ and $\sigma^{k_1+k_2}(\tilde{\theta})$ coincides match the number of ones where θ and $\sigma^{k_1+k_2}(\theta)$ coincides, therefore $\sigma^{k_1+k_2}(\tilde{\theta}) < \tilde{\theta}$. If $s = 2$, then

$$\tilde{\theta} = \underline{10^{k_1}1^{k_2}0^{k_1}1^{k_2}0^{k_1}1^{k_2}\ldots 1^{k_2}0^{k_1}1^{k_2}0^{k_1}1^{k_2}0},$$

and $\sigma^{k_1+k_2}(\tilde{\theta}) = \underline{10^{k_1}1^{k_2}0^{k_1}1^{k_2}0^{k_1}1^{k_2}\ldots 1^{k_2}0^{k_1}1^{k_2}010^{k_1}1^{k_2-1}}$. If it happens that $k_1 \geq 2$, then $\tilde{\theta}$ and $\sigma^{k_1+k_2}(\tilde{\theta})$ coincides in as many 1's as θ and $\sigma^{k_1+k_2}(\theta)$ coincides, therefore $\sigma^{k_1+k_2}(\tilde{\theta}) < \tilde{\theta}$. So, let us assume that $k_1 = 1$, in this case $\tilde{\theta} = \underline{101^{k_2}01^{k_2}01^{k_2}\ldots 1^{k_2}01^{k_2}01^{k_2}0}$, and $\sigma^{k_1+k_2}(\tilde{\theta}) = \underline{101^{k_2}01^{k_2}01^{k_2}\ldots 1^{k_2}01^{k_2}0101^{k_2-1}}$. If $k_2 = 1$, then we should have $\theta = \underline{1010101\ldots101011}$ and $\tilde{\theta} = \underline{10}$, which is a maximal sequence. If $k_2 \geq 2$, then the number of ones where $\tilde{\theta}$ and $\sigma^{k_1+k_2}(\tilde{\theta})$ coincides, is the same as the number of 1's where θ and $\sigma^{k_1+k_2}(\theta)$ coincide plus one. Due to the fact that first symbol of the sequence $\tilde{\theta}$ which is different from the sequence $\sigma^{k_1+k_2}(\tilde{\theta})$ is a 1 then we have $\sigma^{k_1+k_2}(\tilde{\theta}) < \tilde{\theta}$. The case $k_2 > k_{2p} + 1$ can be done in a similar way as we did in the case $k_2 < k_{2p} + 1$. This concludes the proof that $\sigma^{k_1+k_2}(\tilde{\theta}) < \tilde{\theta}$ in all the cases. The proof that $\sigma^{k_1+k_2+k_3+k_4+\ldots+k_{2s+1}+k_{2s}}(\tilde{\theta}) < \tilde{\theta}$, for $s = 2, 3, \ldots, p$; can be done in a similar way as in the case $s = 1$. □

Examples.

1. $\theta = \underline{101}$, $\tilde{\theta} = \underline{100}$, $\theta < \tilde{\theta}$.

2. $\theta = \underline{1011}$, $\tilde{\theta} = \underline{1010} = \underline{10}$, $\tilde{\theta} < \theta$.

Remark 1. Note that if $\theta_k = \underline{(10)^k11}$ with $k \geq 2$ then θ is not maximal. In fact, for $k = 2$, we have $\theta = \underline{101011} < \underline{101110} = \sigma^2(\theta)$. If $k = 3$, then $\theta = \underline{10101011} < \underline{10111010} = \sigma^4(\theta)$. In general $\theta = \underline{(10)^k11} < \underline{1011(10)^{k-1}} = \sigma^{2(k-1)}(\theta)$.

The converse of the previous proposition is also true. That is:

Proposition 2. *If $\tilde{\theta} = \underline{10^{k_1}1^{k_2}0^{k_3}\ldots 0^{k_{2p-1}}1^{k_{2p}-1}0}$ with prime period $N = 1 + k_1+k_2+\ldots+k_{2p-1}+k_{2p}$ is a maximal sequence, then $\theta = \underline{10^{k_1}1^{k_2}0^{k_3}\ldots 0^{k_{2p-1}}1^{k_{2p}}}$ of prime period N is a maximal sequence.*

Remark 2. Note, in any case, that θ and $\tilde{\theta}$ are consecutive periodic orbits with the same period (maximal or not).

2.2 The Permutation Map

Assume now that $\theta = \underline{10^{k_1}1^{k_2}0^{k_3}\ldots 0^{k_{2p-1}}1^{k_{2p}}}$ and $\tilde{\theta} = \underline{10^{k_1}1^{k_2}0^{k_3}\ldots 0^{k_{2p-1}}1^{k_{2p}-1}0}$ are maximal sequences of period prime N and let $\alpha_{N-1} = \underline{10^{k_1}1^{k_2}0^{k_3}\ldots 0^{k_{2p-1}}1^{k_{2p}-1}}$

be the word of length $k_1 + k_2 + \ldots + k_{2p}$ which is a root of θ and $\tilde{\theta}$. Here *root* means the following:

Definition 1. A finite word α is called a *root* of $\theta \in \Sigma_2$ if $\theta \in C(\alpha)$, where $C(\alpha) = \{\eta \in \Sigma_2; \eta_i = \alpha_i, i = 0, 1, \ldots, \text{length}(\alpha) - 1\}$.

We have $\theta, \tilde{\theta} \in C(\alpha_{N-1})$ (here any set as $C(\alpha)$ will be called a cylinder). The amount of ones in α_{N-1} is $\mathbf{1}(\alpha_{N-1}) = 1 + k_2 + k_4 + \ldots + k_{2p} - 1 = k_2 + k_4 + \ldots + k_{2p}$.

1. If $\mathbf{1}(\alpha_{N-1})$ is even, then $\tilde{\theta} < \theta$ and are located in the following way in the cylinder $C(\alpha_{N-1})$.

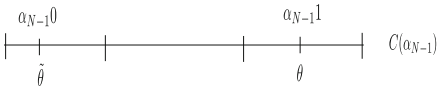

2. If $\mathbf{1}(\alpha_{N-1})$ is odd, then $\theta < \tilde{\theta}$ and are located in the following way in the cylinder $C(\alpha_{N-1})$.

Without loss of generality, we assume that we are in case 1. In this case:

$$\sigma(\theta) = \underline{0^{k_1}1^{k_2}0^{k_3}\ldots 1^{k_{2p}-1}11} < \sigma(\tilde{\theta}) = \underline{0^{k_1}1^{k_2}0^{k_3}\ldots 1^{k_{2p}-1}01}.$$

$$\sigma^2(\theta) = \underline{0^{k_1-1}1^{k_2}0^{k_3}\ldots 1^{k_{2p}-1}110} < \sigma^2(\tilde{\theta}) = \underline{0^{k_1-1}1^{k_2}0^{k_3}\ldots 1^{k_{2p}-1}010}.$$

$$\vdots$$

$$\sigma^{1+k_1}(\theta) = \underline{1^{k_2}0^{k_3}\ldots 1^{k_{2p}-1}110^{k_1}} < \sigma^{1+k_1}(\tilde{\theta}) = \underline{1^{k_2}0^{k_3}\ldots 1^{k_{2p}-1}010^{k_1}}.$$

We note that both iterations $\sigma^{1+k_1}(\theta)$ and $\sigma^{1+k_1}(\tilde{\theta})$ are in the same side of $\underline{1}$.

If k_2 is even, then $1\underline{10} \leq \sigma^{1+k_1}(\theta) < \sigma^{1+k_1}(\tilde{\theta}) < \underline{1}$, and if k_2 is odd, then $\underline{1} < \sigma^{1+k_1}(\theta) < \sigma^{1+k_1}(\tilde{\theta}) < 1\underline{0}$.

(A) $k_2 = 2a_2$ is even, then:

$$\sigma^{1+k_1+2a_2}(\theta) = \underline{0^{k_3}1^{k_4}\ldots 1^{k_{2p}-1}110^{k_1}1^{2a_2}} <$$

$$\sigma^{1+k_1+2a_2}(\tilde{\theta}) = \underline{0^{k_3}1^{k_4}\ldots 1^{k_{2p}-1}010^{k_1}1^{2a_2}}.$$

(B) $k_2 = 2a_2 + 1$ is odd, then:

$$\sigma^{1+k_1+2a_2+1}(\tilde{\theta}) = \underline{0^{k_3}1^{k_4}\ldots 1^{k_{2p}-1}010^{k_1}1^{2a_2}} <$$
$$\sigma^{1+k_1+2a_2+1}(\tilde{\theta}) = \underline{0^{k_3}1^{k_4}\ldots 1^{k_{2p}-1}110^{k_1}1^{2a_2}}.$$

The following picture shows the evolution of the iterations of θ and $\tilde{\theta}$ in the case A.

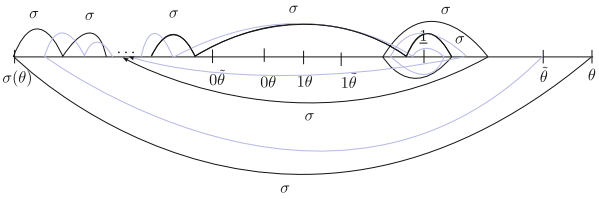

We ordered the iterations of θ in the form

$$\theta_1 = \sigma(\theta) < \theta_2 < \ldots < \theta_{N-1} < \theta_N = \theta_0 = \theta.$$

for each of the following index $i = 0, 1, 2, \ldots, N-1$, there is $l_i \in \{0, 1, 2, \ldots, N-1\}$ such that $\theta_i = \sigma^{l_i}(\theta)$. If we denote $l_i = P(\theta)(i)$ then we define a permutation:

$$P(\theta) : \{0, 1, 2, \ldots, N-1\} \to \{0, 1, 2, \ldots, N-1\},$$

given by: $P(\theta)(i) = j$ if and only if $\theta_i = \sigma^j(\theta)$. Note that we have $\theta_0 = \sigma^0(\theta) = \theta$, $P(\theta)(0) = 0$, $\theta_1 = \sigma^1(\theta)$ and then $P(\theta)(1) = 1$. Thus the equation that satisfies $P(\theta)(i)$ is: $\theta_i = \sigma^{P(\theta)(i)}(\theta)$, $i = 0, 1, \ldots, N-1$.

Proposition 3. *If* $\theta = \underline{10^{k_1}1^{k_2}0^{k_3}\ldots 0^{k_{2p-1}}1^{k_{2p}}}$ *is a maximal sequence of period prime* $N = 1 + k_1 + k_2 + \ldots + k_{2p}$ *and* $\tilde{\theta} = \underline{10^{k_1}1^{k_2}0^{k_3}\ldots 0^{k_{2p-1}}1^{k_{2p}-1}0}$*, then* $P(\theta) = P(\tilde{\theta})$.

Proof. Consider the iterated $\sigma(\theta) = \theta_1, \sigma^2(\theta), \ldots, \sigma^{k_1}(\theta)$ we have:

$$\theta_1 < \sigma^2(\theta) < \sigma^3(\theta) < \ldots < \sigma^{k_1}(\theta) = \underline{01^{k_2}0^{k_3}\ldots 0^{k_{2p-1}}1^{k_{2p}}0^{k_1-1}}.$$

If it happens that k_2 is even, then:

$$\sigma^{1+k_1}(\theta) \in [1\theta = \sigma^{N-1}(\theta), \underline{1}[, \text{ then}$$
$$\sigma^{k_1+2}(\theta) \in]\underline{1}, \theta], \ \sigma^{k_1+3}(\theta) \in [1\theta, \sigma^{k_1+1}(\theta)], \sigma^{k_1+4}(\theta) \in [\sigma^{k_1+2}(\theta), \theta],$$
$$\sigma^{k_1+5}(\theta) \in [1\theta, \sigma^{k_1+3}(\theta)], \ \sigma^{k_1+6}(\theta) \in [\sigma^{k_1+4}(\theta), \theta],$$

and in general $\sigma^{k_1+1+2s}(\theta) \in [1\theta,\ \sigma^{k_1+1+2s-1}(\theta)]$; $\sigma^{k_1+1+2s+1}(\theta) \in [\sigma^{k_1+2s}(\theta), \theta]$ to $s = 1, , \ldots , \dfrac{k_2}{2} - 1$.

For $s = \dfrac{k_2}{2} - 1$ we have:

$$\sigma^{k_1+1+2\cdot(\frac{k_2}{2}-1)+1}(\theta) = \sigma^{k_1+k_2}(\theta)$$
$$= \underline{10^{k_3}1^{k_4}\ldots 0^{k_{2p-1}}1^{k_{2p}}10^{k_1}1^{k_2-1}} \in [\sigma^{k_1+k_2-2}(\theta),\ \theta]$$

and $\sigma^{k_1+k_2+1}(\theta) = \underline{0^{k_3}1^{k_4}\ldots 0^{k_{2p-1}}1^{k_{2p}}10^{k_1}1^{k_2}} \in [\sigma^{i}(\theta), \sigma^{i+1}(\theta)]$ for some $1 \leq i \leq k_1 - 1$. So $\sigma^{k_1+k_2+1+j}(\theta) \in [\sigma^{i+j}(\theta), \sigma^{i+1+j}(\theta)] \subset \Sigma_0$, for $j = 0, 1, \ldots, k_1 - i - 1$.

We have

$$\sigma^{k_1+k_2+1+k_1-i-1}(\theta) \in [\sigma^{i+k_1-i-1}(\theta), \sigma^{i+1+k_1-i-1}(\theta)] = [\sigma^{k_1-1}(\theta), \sigma^{k_1}(\theta)]$$

and $\sigma^{k_1+k_2+1+k_1-i}(\theta) \in [\sigma^{k_1}(\theta), \sigma^{k_1+1}(\theta)]$. From this point, it may occurs:

(i) $\sigma^{k_1+k_2+1+k_1-i}(\theta) \in [\sigma^{k_1}(\theta), 0\theta]$, or (ii) $\sigma^{k_1+k_2+1+k_1-i}(\theta) \in [1\theta, \sigma^{k_1+1}(\theta)]$.

In the first case $\sigma^{k_1+k_2+1+k_1-i}(\theta) = \underline{01^{k_4}0^{k_5}\ldots 0^{k_{2p-1}}1^{k_{2p}}10^{k_1}1^{k_2}0^{k_3-1}}$ and $k_1 - i = k_3 - 1$ thus $i = k_1 + 1 - k_3$. In the second case

$$\sigma^{k_1+k_2+1+k_1-i-1}(\theta) = \underline{01^{k_4}0^{k_5}\ldots 0^{k_{2p-1}}1^{k_{2p}}10^{k_1}1^{k_2}0^{k_3-1}}$$

and $k_1 - i - 1 = k_3 - 1$ thus $i = k_1 - k_3$. In the first case we have $\sigma^{k_1+k_2+k_3+1}(\theta) \in [\sigma^{k_1+1}(\theta), \theta]$. In the second case $\sigma^{k_1+k_2+k_3+1}(\theta) \in [1\theta,\ \sigma^{k_1+1}(\theta)]$. Now

$$\sigma^{k_1+k_2+k_3+1}(\theta) = \underline{1^{k_4}0^{k_5}\ldots 0^{k_{2p-1}}1^{k_{2p}}10^{k_1}1^{k_2}0^{k_3}}.$$

Assume that k_4 is even, then $\sigma^{k_1+k_2+k_3+1}(\theta) < \underline{1}$. If $k_4 > k_2$ then only the first case occurs, in fact: $1\theta \leq \sigma^{k_1+k_2+k_3+1}(\theta) < \sigma^{k_1+1}(\theta)$ and therefore $\sigma^{k_1+2}(\theta) < \sigma^{k_1+k_2+k_3+1+1}(\theta) \leq \theta$, $1\theta \leq \sigma^{k_1+k_2+k_3+1+2}(\theta) < \sigma^{k_1+1+2}(\theta) < \sigma^{k_1+1}(\theta)$. Successively $\sigma^{k_1+k_2+k_3+1+1+k_2}(\theta) \in \Sigma_0$ and this cannot happens because $k_2 < k_4$. Thus only can occur the first case. In this situation, the iterations $\sigma^{k_1+k_2+k_3+1+i}(\theta)$, $i = 1, 2, \ldots, k_4 - k_2$ are in $[\sigma^{k_1+1}(\theta),\ \underline{1}]$ or in $[\underline{1},\ \sigma^{k_1+2}(\theta)]$. The next iterations follows the iterations of the sequence $\sigma^{k_1+2}(\theta)$. If $k_4 < k_2$ then only occurs the second case, otherwise $\sigma^{k_1+k_2+k_3+1}(\theta)$ doesn't reach Σ_0 after k_4 iterations. If $k_4 = k_2$ it may occur any case and $\sigma^{k_1+k_2+k_3+1}(\theta)$ reach Σ_0 in k_2 iterations (in a similar way as $\sigma^{k_1+1}(\theta)$). Analogously we see that it is possible to analyze the case that k_4 is odd (in such case it must be that $\sigma^{k_1+k_2+k_3+1}(\theta) \in [\underline{1}, \theta]$ and then $\sigma^{k_1+k_2+k_3+1}(\theta) \in [\underline{1},\ \sigma^{k_1+2}(\theta)]$ or exists t such that $\sigma^{k_1+k_2+k_3+1}(\theta) \in [\sigma^{k_1+2+2t}(\theta),\ \sigma^{k_1+2+2t+2}(\theta)]$ or $\sigma^{k_1+k_2+k_3+1}(\theta) \in [\sigma^{k_1+k_2-2}(\theta),\ \theta]$). By making the analysis case by case we establishes the way in

which the iterations $\theta, \sigma(\theta), \sigma^2(\theta), \ldots, \sigma^{N-2}(\theta), \sigma^{N-1}(\theta) = 1\theta$ are distributed in the interval.

For $\tilde{\theta}$ occurs a similar distribution with its iterations and it differs from those of θ in the iterated $\sigma^{N-1}(\tilde{\theta}) = 0\tilde{\theta}$. Since, between 0θ and 1θ, there is not iterations of θ and between $0\tilde{\theta}$ and $1\tilde{\theta}$ there in not iterations of $\tilde{\theta}$ we conclude that the distribution of iterations of θ and $\tilde{\theta}$ is the same, that is, $P(\theta) = P(\tilde{\theta})$, as we announce. □

Next, we associated to $\theta = \underline{10^{k_1}1^{k_2}0^{k_3}\ldots 0^{k_{2p-1}}1^{k_{2p}}}$ a piecewise linear application $f_\theta : \bigcup_{i=1}^{N-1} I_i \to [0,1]$ defined in the following way: We suppose that:

$$\sigma(\theta) = \theta_1 < \theta_2 < \ldots < \theta_k < 0\theta < 1\theta = \sigma^{N-1}(\theta) = \theta_{k+1} < \theta_{k+2} < \ldots < \theta_{k+N-k} = \theta$$

is the ordered orbit of θ. Let $I_i = [\sigma^{P(\theta)(i)}(\theta), \sigma^{P(\theta)(i+1)}(\theta)]$, $i = 1, 2, \ldots k-1$, $I_k = [\theta_k, 0\theta]$; $I_{k+1} = [1\theta, \sigma^{P(\theta)(k+2)}(\theta)], \ldots, I_{N-1} = [\sigma^{P(\theta)(N-1)}(\theta), \sigma^{P(\theta)(N)}(\theta)]$. $f|_{I_j}$ is defined linearly satisfying that: $f \circ \sigma^i(\theta) = \sigma^{i+1}(\theta)$. Thus $f(\sigma(\theta)) = f(\theta_1) = \sigma(\theta_1), \ldots, f(\theta_{k-1}) = \sigma(\theta_{k-1}), f(\theta_k) = \sigma(\theta_k) = \theta_{N-1}, f(0\theta) = \theta, f(1\theta) = \theta$ and successively.

Example 1. Let us make the previous construction for $\theta = \underline{100010011}$.

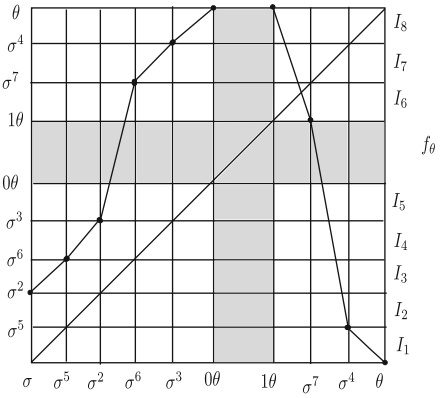

Associated to f_θ we have the A-graph:

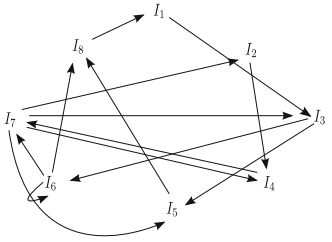

Associated to the A-graph we have the incidence matrix $M(\theta)$ and associated to the matrix $M(\theta)$ we have the greatest real value $1 \leq \lambda(\theta) \leq 2$, for which we obtain that $h_{top}(\theta) = \log(\lambda(\theta))$ (see [12]). We note that the incidence matrix $M(\theta)$ is given by:

$$M(\theta) = \begin{bmatrix} 0&0&1&0&0&0&0&0 \\ 0&0&0&1&0&0&0&0 \\ 0&0&0&0&1&1&0&0 \\ 0&0&0&0&0&0&1&0 \\ 0&0&0&0&0&0&0&1 \\ 0&0&0&0&0&1&1&1 \\ 0&1&1&1&1&0&0&0 \\ 1&0&0&0&0&0&0&0 \end{bmatrix}$$

Now, we present the graph for $f_{\tilde{\theta}}$ where $\tilde{\theta} = \underline{100010010}$.

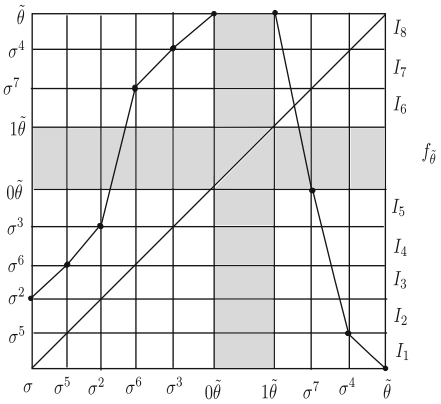

Associated to $f_{\tilde{\theta}}$ we have the A-graph:

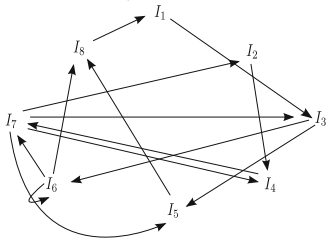

We observe that this A-graph is the same as the A-graph associated to f_θ and hence $M(\tilde{\theta}) = M(\theta)$ and therefore $h(\tilde{\theta}) = h(\theta)$.

Thus we conclude the following proposition (the proof follows from the technical lemma and the construction above).

Proposition 4. *If* $\theta = \underline{10^{k_1}1^{k_2}0^{k_3}1^{k_4}\ldots 0^{k_{2p-1}}1^{k_{2p}}}$ *is a maximal periodic orbit, then for* $\tilde{\theta} = \underline{10^{k_1}1^{k_2}0^{k_3}1^{k_4}\ldots 0^{k_{2p-1}}1^{k_{2p}-1}0}$ *we have* $h(\theta) = h(\tilde{\theta})$, *where* $h(\theta) = h_{top}(\sigma|_{\Lambda(\theta)}), h(\tilde{\theta}) = h_{top}(\sigma|_{\Lambda(\tilde{\theta})})$.

Moreover, we have the following:

Corollary 3. *If* $I(\theta, \tilde{\theta})$ *is the interval* $[\theta, \tilde{\theta}]$ *(case* $\theta < \tilde{\theta}$*) or* $[\tilde{\theta}, \theta]$ *(case* $\tilde{\theta} < \theta$*), then for all* $\alpha \in I(\theta, \tilde{\theta})$ *we have* $h(\alpha) = h(\theta)$.

Proof. In fact, since $h(\theta) \leq h(\alpha) \leq h(\tilde{\theta})$ if $(\theta < \tilde{\theta})$ or $h(\tilde{\theta}) \leq h(\alpha) \leq h(\theta)$ if $(\tilde{\theta} < \theta)$, and $h(\theta) = h(\tilde{\theta})$, we conclude the result. □

Corollary 4. *(a) If occur* $\theta < \tilde{\theta}$ *then* $h(\beta)$ *it is continuous to the right of* θ *and to the left of* $\tilde{\theta}$.
(b) If $\tilde{\theta} < \theta$ *then* $h(\beta)$ *is continuous to the left of* θ *and to the right of* $\tilde{\theta}$.

Then we conclude that to prove that the map $h(\beta)$ is continuous at θ it is enough to prove that the map is continuous to the left of θ if $\theta < \tilde{\theta}$ and to the right of θ if $\tilde{\theta} < \theta$.

3 Proof of the Continuity of the Map $h(\theta)$ at $\theta = \underline{101}$

In this section we will prove the continuity of the map $h(\theta)$ at $\theta = \underline{101}$. To do this, we consider the sequence: $\theta_n = \underline{(101)^n 111}$, $n = 1, 2, 3, \ldots$, we observe that $\theta_1 = \underline{101111} < \theta_2 = \underline{101101111} < \theta_3 = \underline{101101101111} < \ldots < \theta_n < \ldots < \theta$ and $\lim_{n\to\infty} \theta_n = \theta = \underline{101}$.

To prove the continuity at $\theta = \underline{101}$, it is sufficiently to compute $h(\theta_n)$ and to prove that $h(\theta_n) \to h(\theta)$. With this, and the previous Corollary 4, we will conclude the continuity of $h(\theta)$ at $\theta = \underline{101}$.

Hence, see [12,21], it is enough to compute f_{θ_n}; the A-graph of f_{θ_n}; its incidence matrix $M(\theta_n)$ (or a rome $R(\theta_n)$ and its incidence matrix $A(\theta_n)$) and to prove that $\lambda(\theta_n) \to \lambda(\theta)$, (here $\lambda(\rho)$ is the greatest real eigenvalue of the incidence matrix $M(\rho)$). The rest of this section is devoted to compute all of these elements.

1. Initially we compute $h_{top}(\underline{101})$. To do so, $\theta = \underline{101}$, $\sigma(\theta) = \underline{011}$ and $\sigma^2(\theta) = \underline{110}$. We have $0\theta = 0\underline{101}$, $1\theta = 1\underline{101} = \underline{110} = \sigma^2(\theta)$ and $\sigma(\theta) < 0\theta < 1\theta = \sigma^2(\theta) < \theta$. The f-map associated to θ is:

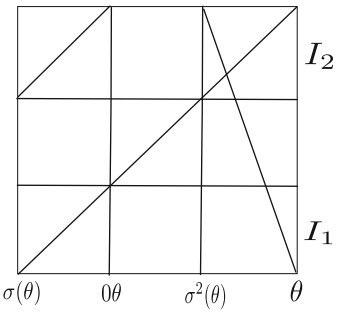

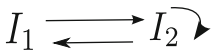

The matrix $M(\theta)$ is

$$\begin{vmatrix} 0 & 1 \\ 1 & 1 \end{vmatrix}$$

whose characteristic polynomial is $p(\theta) = \det(M(\theta) - xI) = x^2 - x - 1$. The maximal root of the characteristic equation is $\overline{x} = \dfrac{1+\sqrt{5}}{2}$. Hence $h_{top}(\underline{101}) = \log(\dfrac{1+\sqrt{5}}{2})$ (see [12,21]).

2. $\theta_1 = \underline{101111}$, $\sigma(\theta_1) = \underline{011111}$, $\sigma^2(\theta_1) = \underline{111110}$, $\sigma^3(\theta_1) = \underline{111101}$, $\sigma^4(\theta_1) = \underline{111011}$, $\sigma^5(\theta_1) = \underline{110111}$.

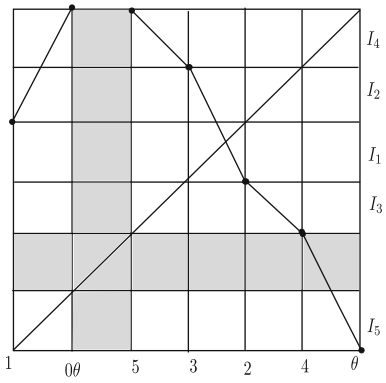

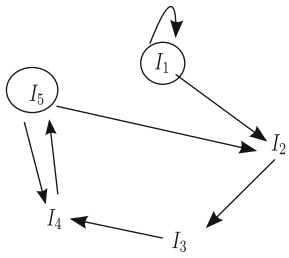

We use the rome $R = \{I_1,\ I_5\}$ to compute the matrix $A(x)$:

$$\begin{array}{cc} a_{11} = x^{-1} & a_{15} = x^{-4} \\ (1,1). & (1,2,3,4,5). \\ a_{51} = 0 & a_{55} = x^{-2} + x^{-4} \\ & (5,4,5),\ (5,2,3,4,5). \end{array}$$

$$(-1)^{5-2}x^5 \begin{vmatrix} x^{-1}-1 & x^{-4} \\ 0 & x^{-2}+x^{-4}-1 \end{vmatrix} = -x^3(x^2-x-1) - x^2 + x - 1.$$

Then $p(\underline{101111})(\overline{x}) = -x^3 p(\underline{101})(x) - x^2 + x - 1$. If $\overline{x}$ is such that $p(\underline{101})(\overline{x}) = 0$, then $p(\underline{101111})(\overline{x}) = -\overline{x}^2 + \overline{x} - 1$. Now $p(\underline{101})(x) = x^2 - x - 1 = 0$ if and only if $x = \frac{1\pm\sqrt{1+4}}{2}, \overline{x} = \frac{1+\sqrt{5}}{2}$.

$$p(\underline{101111})(\overline{x}) = -\frac{1}{2}(3+\sqrt{5}) + \frac{1}{2}(1+\sqrt{5}) - 1 = -2 < 0.$$

$$p(\underline{101111})(1) = 0,\ p(\underline{101111})'(x) = -5x^4 + 4x^3 + 3x^2 - 2x + 1.$$

$$p(\underline{101111})'(1) = -5 + 4 + 3 - 2 + 1 = 1 > 0.$$

Therefore, there exists $x_1 \in]1, \overline{x}[$ such that $p(\underline{101111})(x_1) = 0$. We have $1 < x_1 < \overline{x}$ and $h_{top}(\theta_1) = \log(x_1)$.

3. $\theta_2 = \underline{101101111}$.

$$\begin{array}{l} \sigma(\theta_2) = \underline{011011111},\ \sigma^2(\theta_2) = \underline{110111110},\ \sigma^3(\theta_2) = \underline{101111101}, \\ \sigma^4(\theta_2) = \underline{011111011},\ \sigma^5(\theta_2) = \underline{111110110},\ \sigma^6(\theta_2) = \underline{111101101}, \\ \sigma^7(\theta_2) = \underline{111011011},\ \sigma^8(\theta_2) = \underline{110110111}. \end{array}$$

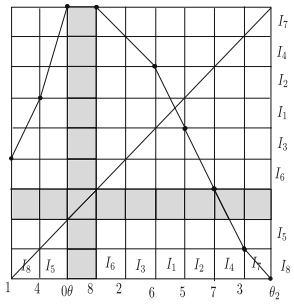

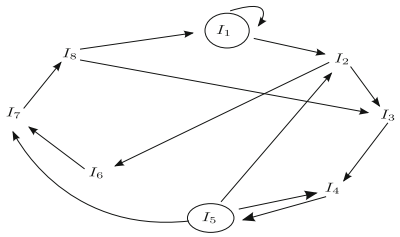

We use the rome $R = \{I_1,\ I_5\}$ to compute the matrix $A(x)$:

$$\begin{array}{ll} a_{11} = x^{-1} + x^{-5} & a_{15} = x^{-4} + x^{-7} \\ (1,1),\ (1,2,6,7,8,1) & (1,2,3,4,5),\ (1,2,6,7,8,3,4,5) \\ a_{51} = x^{-3} + x^{-5} & x_{55} = x^{-2} + x^{-4} + x^{-5} + x^{-7} \\ (5,7,8,1),\ (5,2,6,7,8,1) & (5,4,5),\ (5,2,3,4,5),\ (5,7,8,3,4,5), \\ & (5,2,6,7,8,3,4,5) \end{array}$$

$$(-1)^{8-2}x^8 \begin{vmatrix} x^{-1} + x^{-5} - 1 & x^{-4} + x^{-7} \\ x^{-3} + x^{-5} & x^{-2} + x^{-4} + x^{-5} + x^{-7} - 1 \end{vmatrix}$$

$$= x^8 - x^7 - x^6 + x^5 - x^4 - x^3 + x^2 - x + 1$$

$$= x^8 - x^7 - x^6 - p(\underline{101111})(x)$$

$$= x^6 p(\underline{101})(x) - p(\underline{101111})(x) = p(\underline{101101111})(x).$$

$$p(\underline{101101111})(x_1) = x_2^6 p(\underline{101})(x_1) < 0.$$

$$p(\underline{101101111})(\overline{x}) = -p(\underline{101111})(\overline{x}) > 0.$$

Therefore, there exists x_2; $x_1 < x_2 < \overline{x}$ such that $p(\underline{101101111})(x_2) = 0$ and $h_{top}(\underline{101101111}) = \log(x_2)$.

4. $\theta_3 = \underline{101101101111}$.

$$\begin{array}{l} \sigma(\theta_3) = \underline{011011011111},\ \ \sigma^2(\theta_3) = \underline{110110111110},\ \sigma^3(\theta_3) = \underline{101101111101}, \\ \sigma^4(\theta_3) = \underline{011011111011},\ \sigma^5(\theta_3) = \underline{110111110110},\ \sigma^6(\theta_3) = \underline{101111101101}, \\ \sigma^7(\theta_3) = \underline{011111011011},\ \sigma^8(\theta_3) = \underline{111110110110},\ \sigma^9(\theta_3) = \underline{111101101101}, \\ \sigma^{10}(\theta_3) = \underline{111011011011},\ \sigma^{11}(\theta_3) = \underline{110110110111}. \end{array}$$

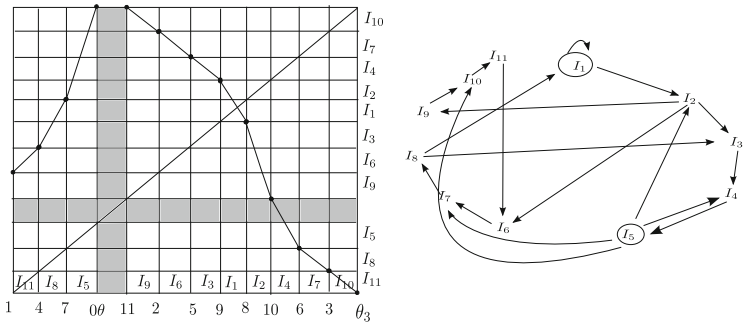

We use the rome $R = \{I_1,\ I_5\}$ to compute the matrix $A(x)$:

$a_{11} = x^{-1} + x^{-5} + x^{-8}$ $\quad$ $a_{15} = x^{-4} + x^{-7} + x^{-10}$
$(1,1),\ (1,2,6,7,8,1),$ $\quad$ $(1,2,3,4,5),\ (1,2,6,7,8,3,4,5),$
$(1,2,9,1,11,6,7,8,1).$ $\quad$ $(1,2,9,10,11,6,7,8,3,4,5).$
$a_{51} = x^{-3} + x^{-5} + x^{-6} + x^{-8}$ $\quad$ $a_{55} = x^{-2} + x^{-4} + x^{-5} + x^{-7} + x^{-8} + x^{-10}$
$(5,7,8,1),\ (5,2,6,7,8,1),$ $\quad$ $(5,4,5),\ (5,2,3,4,5),\ (5,7,8,3,4,5),$
$(5,10,11,6,7,8,1),$ $\quad$ $(5,2,6,7,8,3,4,5),\ (5,10,11,6,7,8,3,4,5),$
$(5,2,9,10,11,6,7,8,1).$ $\quad$ $(5,2,9,10,11,6,7,8,3,4,5).$

We have:

$$(-1)^{11-2}x^{11}\begin{vmatrix} x^{-1}+x^{-5}+x^{-8}-1 & x^{-4}+x^{-7}+x^{-10} \\ x^{-3}+x^{-5}+x^{-6}+x^{-8} & x^{-2}+x^{-4}+x^{-5}+x^{-7}+x^{-8}+x^{-10}-1 \end{vmatrix}$$

$$= -x^{11} + x^{10} + x^9 - x^8 + x^7 + x^6 - x^5 + x^4 + x^3 - x^2 + x - 1$$
$$= -x^9(x^2 - x - 1) - [x^8 - x^7 - x^6 + x^5 - x^4 - x^3 + x^2 - x + 1]$$
$$= -x^9 p(\underline{101})(x) - p(\underline{(101)^2 111})(x) = p(\underline{(101)^3 111})(x).$$

We have:

$p(\underline{(101)^3 111})(x_2) = x^{-9} p(\underline{101})(x_2) > 0.$

$p(\underline{(101)^3 111})(\overline{x}) = -p(\underline{(101)^2 111})(\overline{x}) < 0.$

Therefore there exists $x_3;\ \ x_1 < x_2 < x_3 < \overline{x}$ such that $p(\underline{(101)^3 111})(x_3) = 0$ and $h_{top}(\underline{(101)^3 111}) = \log(x_3)$.

Therefore the expression:

$$p(\underline{(101)^k 111})(x) = (-1)^k x^{3k}(x^2 - x - 1) - p(\underline{(101)^{k-1} 111})(x),$$

holds for $k = 2$ and 3. Inductively, we will assume that the previous expression are true for $k = 2, 3, 4, \ldots, n$ and that there are sequence $x_n;\ \ x_1 < x_2 < \ldots < x_n < \overline{x}$ such that $p(\underline{(101)^n 111})(x_n) = 0$ and it is the unique solution in $[x_{n-1}, \overline{x}]$ with $p(\underline{(101)^n 111})(x_{n-1}) \cdot p(\underline{(101)^n 111})(\overline{x}) < 0$. Also, by the inductive process, we may

suppose that:

$$A_k(x) - I = \begin{bmatrix} A_k & D_k \\ C_k & B_k \end{bmatrix}, k = 1, 2, 3, \ldots, n$$

where
$A_1 = x^{-1} - 1$, $A_2 = x^{-1} + x^{-5} - 1$, $A_3 = x^{-1} + x^{-5} + x^{-8} - 1$, and in general,

$$A_k = x^{-1} + \sum_{i=1}^{k-1} x^{-(3i+2)} - 1, k \geq 2.$$

$D_1 = x^{-4}$, $D_2 = x^{-4} + x^{-7}$, $D_3 = x^{-4} + x^{-7} + x^{-10}$, and in general,

$$D_k = \sum_{i=1}^{k} x^{-(3i+1)}, \ k \geq 2.$$

$C_1 = 0$, $C_2 = x^{-3} + x^{-5}$, $C_3 = x^{-3} + x^{-5} + x^{-6} + x^{-8}$, and in general,

$$C_k = \sum_{i=1}^{k-1} x^{-3i}(1 + x^{-2}), \ k \geq 2.$$

$B_1 = x^{-2} + x^{-4} - 1$, $B_2 = x^{-2} + x^{-4} + x^{-5} + x^{-7} - 1$, and in general,

$$B_k = \sum_{i=1}^{k} x^{-(3i-1)}(1 + x^{-2}) - 1, \ k \geq 2.$$

Writing $A_k = a_{11}^k - 1$, $D_k = a_{15}^k$, $C_k = a_{51}^k$, $B_k = a_{55}^k - 1$, where the a_{ij}^k are coefficients associated to the matrix $A_k(x)$ defined by the rome $R = \{I_1, I_5\}$ from the restriction of the shift to $[\sigma(\underline{(101)^k 111}), \underline{(101)^k 111}]$ and whose A-graph for the partition $A = \{I_1, I_2, \ldots I_{3k+2}\}$, where $\overline{[I_{3k+2} I_{3k-1} \ldots I_{11} I_8 I_5 \ I_{3k} I_{3(k-1)} \ldots I_3 I_1 I_2 I_4 I_7 \ldots I_{3k+1}]} = [\sigma(\underline{(101)^k 111}), \underline{(101)^k 111}]$ is:

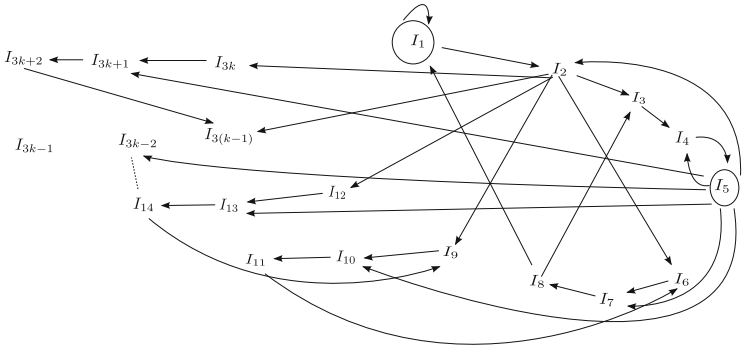

The related interval map is defined by:

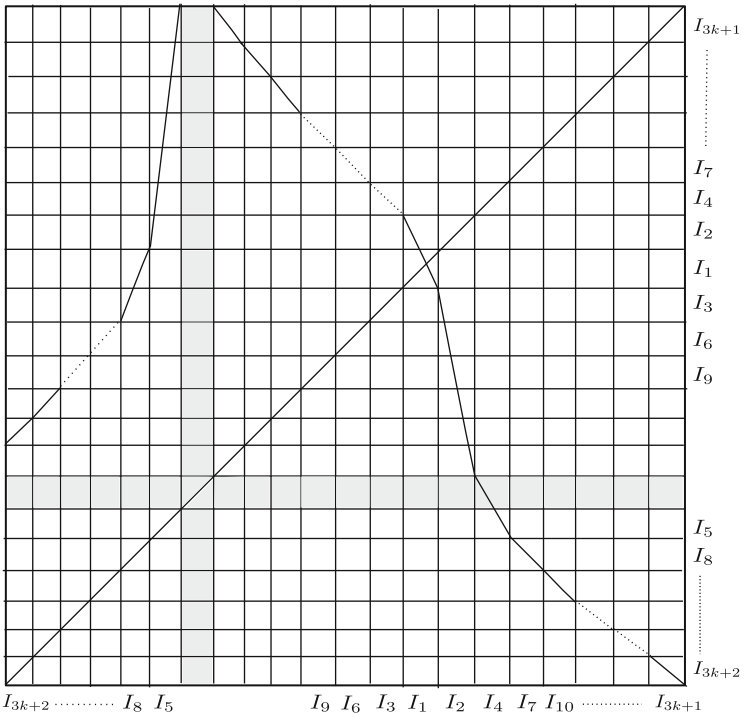

This is the graph of the restriction of the map σ to $[\sigma(\underline{(101)^k 111}), \underline{(101)^k 111}]$.

We consider now the case of $\theta_{k+1} = \underline{(101)^{k+1}111}$.

The first step is to write the iterations of θ_{k+1}.

(1) $\theta_{k+1} = P_1 = \underline{(101)^{k+1}111} = \underline{1(011)^{k+1}11}$.

(2) $P_2 = \sigma(P_1) = \underline{(011)^{k+1}111} = \underline{0(110)^k 11111}$.

(3) $P_3 = \sigma(P_2) = \underline{(110)^k 111(110)} = \underline{1(101)^k 11110}$.

(4) $P_4 = \sigma(P_3) = \underline{(101)^k 111(101)} = \underline{1(011)^k 11101}$.

$\vdots$

(3j) $P_{3j} = \sigma(P_{3j-1}) = \underline{(110)^{k+1-j}111(110)^j}$, $j = 3, 4, \ldots k$.

(3j + 1) $P_{3j+1} = \sigma(P_{3j}) = \underline{(101)^{k+1-j}111(101)^j}$.

(3j + 2) $P_{3j+2} = \sigma(P_{3j+1}) = \underline{(011)^{k+1-j}111(011)^j}$.

$\vdots$

(3k) $P_{3k} = \sigma(P_{3k-1}) = \underline{(110)111(110)^k}$.

(3k + 1) $P_{3k+1} = \sigma(P_{3k}) = \underline{(101)111(101)^k}$.

(3k + 2) $P_{3k+2} = \sigma(P_{3k+1}) = \underline{(011)111(011)^k}$.

(3(k + 1)) $P_{3(k+1)} = \sigma(P_{3k+2}) = \underline{111(110)^{k+1}}$.

(3(k + 1) + 1) $P_{3k+4} = \sigma(P_{3k+3}) = \underline{11(110)^{k+1}1} = \underline{111(101)^{k+1}}$.
(3(k + 1) + 2) $P_{3k+5} = \sigma(P_{3k+4}) = \underline{11(101)^{k+1}1} = \underline{111(011)^{k+1}}$.
(3(k + 1) + 3) $P_{3k+6} = \sigma(P_{3k+5}) = \underline{(110)^{k+1}111}$.

Ordering the points $P_1, P_2, \ldots, P_{3k+6}$ in the interval we have:

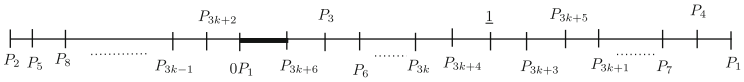

We make the corresponding graph for the restriction of σ to the interval $[\sigma(\underline{(101)^{k+1}111}), \underline{(101)^{k+1}111}]$.

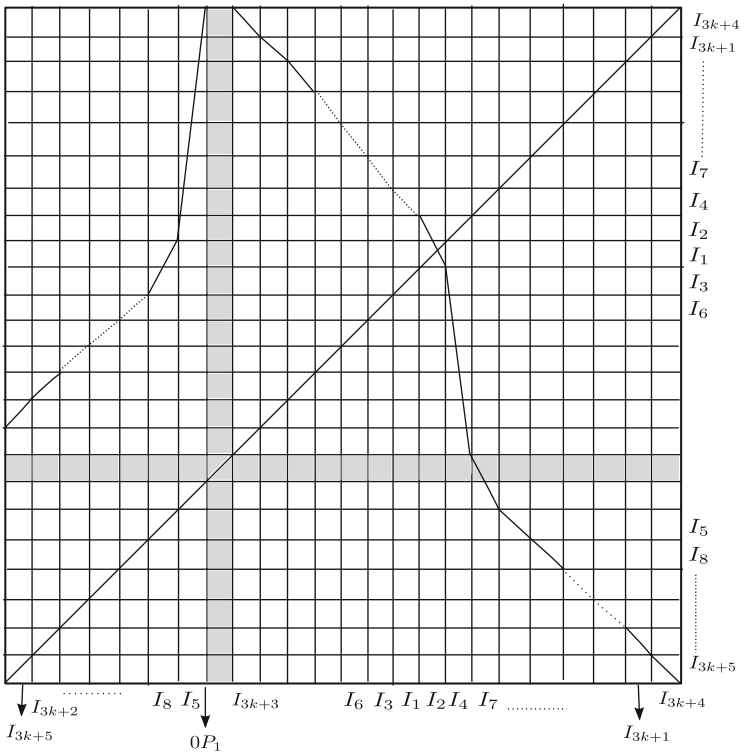

This graph is obtained joining linearly the points $(P_i, \sigma(P_i))$.
We consider the partition:

$$A(k+1) = \{I_{3k+5}, I_{3k+2}, \ldots, I_8, I_5, I_{3k+3}, I_{3k}, \ldots, I_6, I_3, I_1, I_2, I_4, I_7, \ldots, I_{3k+1}, I_{3k+4}\}.$$

The A-graph associated to this map is:

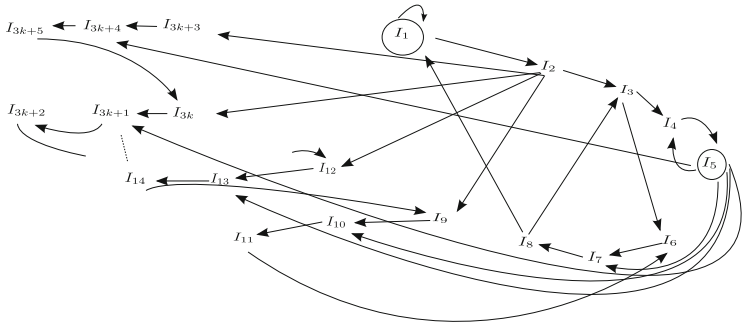

We observe that this A-graph is like the A-graph of the restriction of σ to $[\sigma(\underline{(101)^k 111}), \underline{(101)^k 111}]$ where we have add the following (red) arrows:

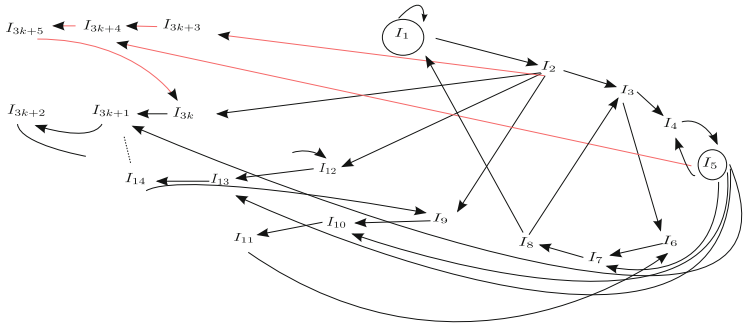

This will imply that

$$a_{11}^{k+1} = a_{11}^k + x^{-(3k+2)}, \qquad a_{15}^{k+1} = a_{15}^k + x^{-(3k+4)},$$
$$a_{51}^{k+1} = a_{51}^k + x^{-3k}(1 + x^{-2}), \; a_{55}^{k+1} = a_{55}^k + x^{-(3k+2)}(1 + x^{-2}).$$

That is:
$A_{k+1} = A_k + x^{-(3k+2)}$, $D_{k+1} = D_k + x^{-(3k+4)}$, $C_{k+1} = C_k + x^{-3k}(1 + x^{-2})$,
$B_{k+1} = B_k + x^{-(3k+2)}(1 + x^{-2})$.
Here we have denoted:

$$A_k(x) - I = \begin{bmatrix} A_k(x) & D_k(x) \\ C_k(x) & B_k(x) \end{bmatrix} \text{ and } A_{k+1}(x) - I = \begin{bmatrix} A_{k+1}(x) & D_{k+1}(x) \\ C_{k+1}(x) & B_{k+1}(x) \end{bmatrix}$$

Thus

$$\begin{aligned}
&A_{k+1}\cdot B_{k+1}-C_{k+1}\cdot D_{k+1}\\
&=(A_k+x^{-(3k+2)})\cdot(B_k+x^{-(3k+2)}(1+x^{-2}))\\
&\quad -(C_k+x^{-3k}(1+x^{-2}))(D_k+x^{-(3k+4)})\\
&=A_kB_k+A_kx^{-(3k+2)}(1+x^{-2})+B_kx^{-(3k+2)}+x^{-6k-4}(1+x^{-2})\\
&\quad -C_kD_k-C_kx^{-(3k+4)}-D_kx^{-3k}(1+x^{-2})-x^{-6k-4}(1+x^{-2})\\
&=A_kB_k-C_kD_k+A_kx^{-(3k+2)}(1+x^{-2})+B_kx^{-3k-2}-C_kx^{-3k-4}-D_kx^{-3k}(1+x^{-2}).
\end{aligned}$$

We have:

$$x^{-3k-2}(1+x^{-2})A_k=x^{-3k-2}(1+x^{-2})(x^{-1}-1)+\sum_{i=1}^{k-1}x^{-3i-3k-4}(1+x^{-2}),$$

$$x^{-3k-2}B_k=(1+x^{-2})\sum_{i=1}^{k}x^{-3i-3k-1}-x^{-3k-2}.$$

$$-x^{-3k-4}C_k=-(1+x^{-2})\sum_{i=1}^{k-1}x^{-3i-3k-4}.$$

$$-x^{-3k}(1+x^{-2})D_k=-(1+x^{-2})\sum_{i=1}^{k}x^{-3i-3k-1}.$$

Therefore:

$$\begin{aligned}
A_{k+1}B_{k+1}-C_{k+1}D_{k+1}&=A_kB_k-C_kD_k+x^{-3k-2}(x^{-1}-1+x^{-3}-x^{-2})-x^{-3k-2}\\
&=A_kB_k-C_kD_k-2x^{-3k-2}+x^{-3k-3}-x^{-3k-4}+x^{-3k-5}.
\end{aligned}$$

Making $(-1)^{3k+5-2}x^{3k+5}\det(A_{k+1}(x)-I)$, that is the characteristic polynomial of the matrix associated to the graph of $\sigma|_{[\sigma(\underline{(101)^{k+1}111}),\,\underline{(101)^{k+1}111}]}$, we have:

$$\begin{aligned}
&(-1)^{3k+3}x^{3k+5}(A_kB_k-C_kD_k+x^{-3k-3}-2x^{-3k-2}+x^{-3k-5}-x^{-3k-4})\\
&=(-1)^{3k+1}(x^{3k+5}(A_kB_k-C_kD_k)+x^2-2x^3+1-x)\\
&=(-1)^{3k+1}(x^3x^{3k+2}(A_kB_k-C_kD_k)-2x^3+x^2-x+1).
\end{aligned}$$

Since, $p(\underline{(101)^k111})(x)=(-1)^{3k+2-2}x^{3k+2-2}\det(A_k-I)=(-1)^{3k}x^{3k+2}(A_kB_k-C_kD_k)$. We have: $x^{3k+2}(A_kB_k-C_kD_k)=(-1)^{3k}p(\underline{(101)^k111})(x)$, and hence

$$\begin{aligned}
p(\underline{(101)^{k+1}111})(x)&=(-1)^{3k+1}[x^3(-1)^{3k}p(\underline{(101)^k111})(x)-2x^3+x^2-x+1]\\
&=-x^3p(\underline{(101)^k111})(x)+(-1)^{3k+1}(-2x^3+x^2-x+1).
\end{aligned}$$

Using the induction hypothesis over $p(\underline{(101)^k 111})(x)$, namely $p(\underline{(101)^k 111})(x) = (-1)^k x^{3k} p(\underline{101})(x) - p(\underline{(101)^{k-1} 111})(x)$, we have:

$$\begin{aligned}
&p(\underline{(101)^{k+1} 111})(x)\\
&= -x^3((-1)^k x^{3k} p(\underline{101})(x) - p(\underline{(101)^{k-1} 111})(x))\\
&\quad +(-1)^{3k+1}(-2x^3 + x^2 - x + 1)\\
&= (-1)^{k+1} x^{3k+3} p(\underline{101})(x) + x^3 p(\underline{(101)^{k-1} 111})(x)\\
&\quad +(-1)^{3k} 2x^3 + (-1)^{k+1}(x^2 - x + 1)\\
&= (-1)^{k+1} x^{3(k+1)} p(\underline{101})(x) + x^3((-1)^{k-1} x^{3(k-1)} p(\underline{101})(x)\\
&\quad -p(\underline{(101)^{k-2} 111})(x)) + (-1)^k 2x^3 + (-1)^{k+1}(x^2 - x + 1)\\
&= (-1)^{k+1} x^{3(k+1)} p(\underline{101})(x) + (-1)^{k+1} x^{3k} p(\underline{101})(x)\\
&\quad -x^3 p(\underline{(101)^{k-2} 111})(x) + (-1)^k 2x^3 + (-1)^{k+1}(x^2 - x + 1)\\
&= (-1)^{k+1}(x^{3(k+1)} + x^{3k}) p(\underline{101})(x) + (-1)^3 x^3 p(\underline{(101)^{k-2} 111})(x)\\
&\quad +(-1)^{k+1}(-2x^3 + x^2 - x + 1)
\end{aligned}$$

Successively

$$\begin{aligned}
&= (-1)^{k+1}(x^{3(k+1)} + x^{3k} + x^{3(k-1)} + \ldots + x^{3\cdot 4} + x^{3\cdot 3}) p(\underline{101})(x) +\\
&\quad + (-1)^k x^3 p(\underline{101111})(x) + (-1)^{k+1}(-2x^3 + x^2 - x + 1)\\
&= (-1)^{k+1} p(\underline{101})(x) \cdot \sum_{i=3}^{k+1} x^{3i} + (-1)^k x^3(-x^5 + x^4 + x^3 - x^2 + x - 1) +\\
&\quad + (-1)^{k+1}(-2x^3 + x^2 - x + 1)\\
&= (-1)^{k+1} p(\underline{101})(x) \cdot \sum_{i=3}^{k+1} x^{3i} + (-1)^{k+1} x^{3\cdot 2}(x^2 - x - 1) + (-1)^{k+1} x^5 + (-1)^k x^4 +\\
&\quad + (-1)^{k+1} x^3 + (-1)^{k+2} 2x^3 + (-1)^{k+1}(x^2 - x + 1)\\
&= (-1)^{k+1} p(\underline{101})(x) \cdot \sum_{i=2}^{k+1} x^{3i} + (-1)^{k+1} x^3(x^2 - x - 1) + (-1)^{k+1}(x^2 - x + 1)\\
&= (-1)^{k+1} p(\underline{101})(x) \cdot \sum_{i=1}^{k+1} x^{3i} + (-1)^{k+1}(x^2 - x + 1)
\end{aligned}$$

$$\begin{aligned}
&= (-1)^{k+1} x^{3(k+1)} p(\underline{101})(x)\\
&\quad +(-1)^{k+1}(x^2 - x - 1) \cdot \sum_{i=1}^{k} x^{3i} + (-1)^{k+1}(x^2 - x + 1).
\end{aligned} \tag{1}$$

Thus we have obtained that, $p(\underline{(101)^{k+1}111})(x) = (-1)^{k+1}x^{3(k+1)}p(\underline{101})(x) + (-1)^{k+1}(x^2 - x - 1) \cdot \sum_{i=1}^{k} x^{3i} + (-1)^{k+1}(x^2 - x + 1)$. Let us now compute the polynomial expansion of $p(\underline{(101)^k 111})$.

$$
\begin{aligned}
&p(\underline{(101)^k 111}) = \\
&= (-1)^k x^{3k} p(\underline{101})(x) - p(\underline{(101)^{k-1}111})(x) \\
&= (-1)^k x^{3k} p(\underline{101})(x) - ((-1)^{k-1}x^{3(k-1)} p(\underline{101})(x) - p(\underline{(101)^{k-2}111})(x)) \\
&= (-1)^k x^{3k} p(\underline{101})(x) + (-1)^k x^{3(k-1)} p(\underline{101})(x) + p(\underline{(101)^{k-2}111})(x) \\
&= (-1)^k p(\underline{101})(x)(x^{3k} + x^{3(k-1)}) + p(\underline{(101)^{k-2}111})(x) \\
&= (-1)^k p(\underline{101})(x)(x^{3k} + x^{3(k-1)}) + (-1)^{k-2}x^{3(k-2)} p(\underline{101}) + \\
&\quad (-1)^3 p(\underline{(101)^{k-3}111})(x) \\
&= (-1)^k p(\underline{101})(x)(x^{3k} + x^{3(k-1)} + x^{3(k-2)}) + (-1)^3 p(\underline{(101)^{k-3}111})(x).
\end{aligned}
$$

Successively

$$
\begin{aligned}
&= (-1)^k p(\underline{101})(x)(x^{3k} + x^{3(k-1)} + \ldots + x^{3\cdot 2}) + (-1)^{k-1} p(\underline{101111})(x) \\
&= (-1)^k p(\underline{101})(x)(x^{3k} + x^{3(k-1)} + \ldots + x^{3\cdot 2}) + (-1)^{k-1}(-x^5 + x^4 + x^3 - x^2 + \\
&\quad + x - 1) \\
&= (-1)^k p(\underline{101})(x)(x^{3k} + x^{3(k-1)} + \ldots + x^{3\cdot 2}) + (-1)^k x^3(x^2 - x - 1) + \\
&\quad (-1)^{k-1}(-x^2 + x - 1) \\
&= (-1)^k p(\underline{101})(x)(x^{3k} + x^{3(k-1)} + \ldots + x^{3\cdot 2} + x^3) + (-1)^{k-1}(-1)(x^2 - x + 1) \\
&= (-1)^k p(\underline{101})(x)\sum_{i=1}^{k} x^{3i} + (-1)^k(x^2 - x + 1).
\end{aligned}
$$

Therefore,

$$
- p(\underline{(101)^k 111})(x) = (-1)^k p(\underline{101})(x)\sum_{i=1}^{k} x^{3i} + (-1)^k(x^2 - x + 1). \quad (2)
$$

Replacing (2) in (1) we have:

$$
p(\underline{(101)^{k+1}111})(x) = (-1)^{k+1}x^{3(k+1)} p(\underline{101})(x) - p(\underline{(101)^k 111})(x),
$$

as we want to prove.

Now, $p(\underline{(101)^{n+1}111})(\overline{x}) = -p(\underline{(101)^n 111})(\overline{x})$ and $p(\underline{(101)^{n+1}111})(x_n) = (-1)^{n+1} x_n^{3(n+1)} \cdot p(\underline{101})(x_n)$.

$$(-1)^n p(\underline{(101)^{n+1}111})(\overline{x}) = (-1)^{n+1} p(\underline{(101)^n 111})(\overline{x}) = (-1)^{n-1} p(\underline{(101)^n 111})(\overline{x}) < 0.$$

$$(-1)^n p(\underline{(101)^{n+1}111})(x_n) = (-1)^{2n+1} x^{3(n+1)} p(\underline{101})(x_n) = -x_n^{3(n+1)} p(\underline{101})(x_n).$$

Since $p(\underline{101})(x_n) < 0$, then $(-1)^n p(\underline{(101)^{n+1}111})(x_n) > 0$. Thus $p(\underline{(101)^{n+1}111})(\overline{x})$ and $p(\underline{(101)^{n+1}111})(x_n)$ have different signs. Thus there exists x_{n+1}; $x_1 < x_2 < \ldots < x_n < x_{n+1} < \overline{x}$ such that $p(\underline{(101)^{n+1}111})(x_{n+1}) = 0$.

Let us now to prove that

$$\lim_{n\to\infty} x_n = \overline{x}. \tag{3}$$

If (3) is true hence, taking into account that $h_{top}(\underline{(101)^n 111}) = \log x_n$, we have that $h_{top}(\underline{(101)^n 111}) \to h_{top}(\underline{101}) = \log \overline{x}$. That is h_{top} is continuous at $\theta = \underline{101}$. In fact: we know that h_{top} is increasing; $h_{top}(\theta) = h_{top}(\underline{101})$ for each $\theta \in [\underline{101}, \underline{100}]$. If $\xi_n < \underline{101}$ is any sequence such that $\xi_n \to \theta = \underline{101}$ then for each n there exists $m(n) \in \mathbb{N}$ such that $\underline{(101)^{m(n)}111} \le \xi_n < \underline{(101)^{m(n)+1}111}$ and $m(n) \to \infty$ if $n \to \infty$ therefore

$$h_{top}(\underline{(101)^{m(n)}111}) \le h_{top}(\xi_n) < h_{top}(\underline{(101)^{m(n)+1}111}).$$

Thus

$$\lim_{n\to\infty} h_{top}(\xi_n) = h_{top}(\underline{101}).$$

Therefore h_{top} is continuous at $\theta = \underline{101}$. Now we will prove (3) ($\lim_{n\to\infty} x_n = \overline{x}$).

$$\begin{aligned}
&p(\underline{(101)^{k+1}111})(x) = (-1)^{k+1} x^{3(k+1)} p(\underline{101})(x) - p(\underline{(101)^k 111})(x)\\
&= (-1)^{k+1} x^{3(k+1)} p(\underline{101})(x) - [(-1)^k x^{3k} p(\underline{101})(x) - p(\underline{(101)^{k-1}111})(x)]\\
&= (-1)^{k+1} x^{3(k+1)} p(\underline{101})(x) + (-1)^{k+1} x^{3k} p(\underline{101})(x) + (-1)^2 p(\underline{(101)^{k-1}111})(x)\\
&= (-1)^{k+1} p(\underline{101})(x)(x^{3(k+1)} + x^{3k}) + (-1)^2 p(\underline{(101)^{k-1}111})(x)]\\
&= (-1)^{k+1} p(\underline{101})(x)(x^{3(k+1)} + x^{3k}) + (-1)^2 [(-1)^{k-1} x^{3(k-1)} p(\underline{101})(x) -\\
&\quad p(\underline{(101)^{k-2}111})(x)]\\
&= (-1)^{k+1} p(\underline{101})(x)(x^{3(k+1)} + x^{3k} + x^{3(k-1)}) + (-1)^3 p(\underline{(101)^{k-2}111})(x)\\
&= (-1)^{k+1} p(\underline{101})(x)(x^{3(k+1)} + x^{3k} + \ldots + x^{3\cdot 2}) + (-1)^k p(\underline{101111})(x)
\end{aligned}$$

$$
\begin{aligned}
&= (-1)^{k+1} p(\underline{101})(x)(x^{3(k+1)} + \ldots + x^{3\cdot 2}) + (-1)^k[-x^5 + x^4 + x^3 - x^2 + x - 1] \\
&= (-1)^{k+1} p(\underline{101})(x)(x^{3(k+1)} + \ldots + x^{3\cdot 2}) + (-1)^k x^3(-x^2 + x + 1) + \\
&\quad + (-1)^k(-x^2 + x - 1) \\
&= (-1)^{k+1} p(\underline{101})(x)(x^{3(k+1)} + \ldots + x^{3\cdot 2}) + (-1)^{k+1} x^3(x^2 - x - 1) + \\
&\quad + (-1)^k(-x^2 + x - 1) \\
&= (-1)^{k+1} p(\underline{101})(x)\left[\sum_{i=1}^{k+1} x^{3i}\right] + (-1)^k(-x^2 + x - 1). \\
&= (-1)^{k+1} p(\underline{101})(x) \cdot x^3\left[\sum_{i=0}^{k} x^{3i}\right] + (-1)^k(-x^2 + x - 1).
\end{aligned}
$$

From $p(\underline{(101)^{k+1}111})(x_{k+1}) = 0$, we obtain:

$$
(-1)^{k+1} p(\underline{101})(x_{k+1}) \cdot x_{k+1}^3\left[\sum_{i=0}^{k} x_{k+1}^{3i}\right] = (-1)^{k+1}(-x_{k+1}^2 + x_{k+1} - 1).
$$

i.e.

$$
p(\underline{101})(x_{k+1}) \cdot x_{k+1}^3 \cdot \frac{x_{k+1}^{3(k+1)} - 1}{x_{k+1}^3 - 1} = -x_{k+1}^2 + x_{k+1} - 1
$$

$$
p(\underline{101})(x_{k+1}) \cdot x_{k+1}^3(x_{k+1}^{3(k+1)} - 1) = (x_{k+1}^3 - 1) \cdot (-x_{k+1}^2 + x_{k+1} - 1).
$$

Dividing by x_{k+1}^3,

$$
p(\underline{101})(x_{k+1}) \cdot (x_{k+1}^{3(k+1)} - 1) = \left(1 - \frac{1}{x_{k+1}^3}\right) \cdot (-x_{k+1}^2 + x_{k+1} - 1).
$$

Dividing by $x_{k+1}^{3(k+1)}$, we have

$$
p(\underline{101})(x_{k+1}) \cdot \left(1 - \frac{1}{x_{k+1}^{3(k+1)}}\right) = \frac{1}{x_{k+1}^{3(k+1)}} \cdot \left(1 - \frac{1}{x_{k+1}^3}\right) \cdot (-x_{k+1}^2 + x_{k+1} - 1).
$$

Since $1 < x_1 < x_2 < \ldots < x_{k+1} < \overline{x}$, we conclude that,

$$
\lim_{k\to\infty} x_{k+1}^{3(k+1)} = \infty.
$$

Therefore

$$\lim_{k\to\infty} p(\underline{101})(x_{k+1}) = 0.$$

The only way that this happens is that $\lim_{k\to\infty} x_{k+1} = \overline{x}$. □

So, we have proved:

Proposition 5. *The map* $h_{top}(\theta) = h_{top}(\sigma|_{\Sigma[\sigma(\theta),\,\theta]})$ *is continuous at* $\theta = \underline{101}$.

We can think all of these "dynamical" computations from the linear algebra point of view, in the following way:
We consider the sequence of quadratic matrix

$$M_5 = M_{3\cdot 1+2} = \begin{bmatrix} 1&1&0&0&0\\ 0&0&1&0&0\\ 0&0&0&1&0\\ 0&0&0&0&1\\ 0&1&0&1&0 \end{bmatrix}_{5\times 5}$$

$$M_{3\cdot 2+2} = \begin{bmatrix} 1&1&0&0&0&0&0&0\\ 0&0&1&0&0&1&0&0\\ 0&0&0&1&0&0&0&0\\ 0&0&0&0&1&0&0&0\\ 0&1&0&1&0&0&1&0\\ 0&0&0&0&0&0&1&0\\ 0&0&0&0&0&0&0&1\\ 1&0&1&0&0&0&0&0 \end{bmatrix}_{8\times 8}$$

$$M_{3\cdot 3+2} = \left[\begin{array}{cccccccc|ccc} 1&1&0&0&0&0&0&0&0&0&0\\ 0&0&1&0&0&1&0&0&1&0&0\\ 0&0&0&1&0&0&0&0&0&0&0\\ 0&0&0&0&1&0&0&0&0&0&0\\ 0&1&0&1&0&0&1&0&0&1&0\\ 0&0&0&0&0&0&1&0&0&0&0\\ 0&0&0&0&0&0&0&1&0&0&0\\ \underline{1}&\underline{0}&\underline{1}&\underline{0}&\underline{0}&\underline{0}&\underline{0}&\underline{0}&\underline{0}&\underline{0}&\underline{0}\\ \hline 0&0&0&0&0&0&0&0&0&1&0\\ 0&0&0&0&0&0&0&0&0&0&1\\ 0&0&0&0&0&1&0&0&0&0&0 \end{array}\right]_{11\times 11}$$

And in general for $k \geq 3$,

$$M_{3\cdot(k+1)+2} = \begin{bmatrix} M_{3k+2} & A_{3k+2} \\ C_{3k+2} & B_{3\times 3} \end{bmatrix}$$

where,

$$A_{3k+2} = \begin{bmatrix} 0\,0\,0 \\ 1\,0\,0 \\ 0\,0\,0 \\ 0\,0\,0 \\ 0\,1\,0 \\ 0\,0\,0 \\ 0\,0\,0 \\ \vdots \\ 0\,0\,0 \end{bmatrix}_{(3k+2)\times 3} \qquad B_{3\times 3} = \begin{bmatrix} 0\,1\,0 \\ 1\,0\,1 \\ 0\,0\,0 \end{bmatrix}$$

$$C_{3k+2} = \begin{bmatrix} 0\,0\,0\,0\,0\,0\,0\,0\,\ldots\,0 \\ 0\,0\,0\,0\,0\,0\,0\,0\,\ldots\,0 \\ 0\,0\,0\,0\,0\,1\,0\,0\,\ldots\,0 \end{bmatrix}_{3\times(3k+2)}$$

If $p_k(x) = \det(M_{3k+2} - xI)$, is the characteristic polynomial, then we have that

$$p_{k+1}(x) = (-1)^{k+1}x^{3(k+1)}(x^2 - x - 1) - p_k(x);$$

and the sequences of spectral radios r_k of M_{3k+2} satisfy $1 < r_1 < r_2 < r_3 < \ldots < r_k < \overline{r}$, where $\overline{r}$ is the root $1 < \overline{r} < 2$ of $x^2 - x - 1 = 0$. Moreover $\lim_{k\to\infty} r_k = \overline{r}$.

3.1 Continuity of the Map $h_{top}(\theta)$ at $\theta_k = H^k_{11,10}(\underline{101})$, $k = 1, 2, 3, \ldots$

For $a = 11, b = 10$ we denote by $\Sigma_{a,b}$ the set of sequences $\theta : \mathbb{N}_0 \to \{a, b\}$. In the same way, as we did with $(\Sigma_2, \tau, \leq_T)$, we can obtain a topology $\tau_{a,b}$ for $\Sigma_{a,b}$ and we can induce a total order, $\leq_{a,b}$, between its elements. In fact, we replace I_0 by I_{11} and I_1 by I_{10} in the construction of the map $T : I_{11} \cup I_{10} \to [0, 1]$ and we proceed as in the previous case.

Let $\sigma_{a,b} : \Sigma_{a,b} \to \Sigma_{a,b}$ be the shift map. Let $H_{a,b} : \Sigma_2 \to \Sigma_{a,b}$ be the map: $H_{a,b}(\theta_0, \theta_1, \theta_2, \ldots) = (\widetilde{\theta_0}, \widetilde{\theta_1}, \widetilde{\theta_2}, \ldots)$ where $\widetilde{\theta_i} = a$ si $\theta_i = 0$ and $\widetilde{\theta_i} = b$ si $\theta_i = 1$. We call $H_{a,b}$ the *renormalization* map.

It is easy to verify that $H_{11,10}$ is an homeomorphism between Σ_2 and $\Sigma_{a,b}$.

Using the previous result and the continuity result of $h_{top}(\theta)$ for $\theta = \underline{101}$ it is possible to conclude the continuity of $h_{top}(\theta_k)$ for $\theta_k = H^k_{11,10}(\underline{101})$ (see for instance [20]).

Here

$$\theta_1 = H_{11,10}(\underline{101}) = \underline{101110}$$

$$\theta_2 = H^2_{11,10}(\underline{101}) = H_{11,10}(\underline{101110}) = \underline{101110101011}$$

$$\theta_3 = H^3_{11,10}(\underline{101}) = \underline{101110101011101110111010}$$

$$\theta_4 = H^4_{11,10}(\underline{101}) = \underline{101110101011101110111010101110101011101010111011},$$

and so on.

Acknowledgements Part of this paper is an outgrowth of research during a visit of the authors to IMPA (Brazil). The authors were partially supported by DICYT – USACH (Chile), PCI – IMPA (Brazil) and by the Dirección de Graduados of the USACH. We thanks IMPA and USACH for its support while preparing the present paper.

References

1. Alseda, L., Llibre, J., Misiurewicz, M.: Combinatorial Dynamics and Entropy in Dimension One. Advenced Series in Nonlinear Dynamics, vol. 5, 2nd edn, pp. xvi + 15. World Scientific, River Edge (2000). ISBN:981-02-4053-8
2. Aranzubía, S., Labarca, R.: On the existence of bubbles of constant entropy in the lexicographical world. prepint (2012)
3. Bamón, R., Labarca, R., Pacifico, M.J., Mañé, R.: The explosion of singular cycles. Publ. Math. IHES **78**, 207–232 (1993)
4. Cooper, R.D., Hoare, M.R.: Distributive processes and combinatorial dynamics. J. Stat. Phys. **20**(6), 597–628 (1979)
5. de Melo, W., Van Strien, S.: One-Dimensional Dynamics. Ergebnisse der Mathematik und ihrer Grenzgebiete (3) [Results in Mathematics and Related Areas (3)], vol. 25. Springer, Berlin/New York (1993)
6. Field, M.: Combinatorial dynamics. Dyn. Syst. **19**(3), 217–243 (2004)
7. Guckenheimer, J., Williams, R.F.: Structured stability of Lorenz attractors. Publ. Math IHES **50**, 59–72 (1979)
8. Kauffman, S., Smolin, L.: Combinatorial dynamics and time in quantum gravity. In: Kowalski-Glikman, J. (ed.) Towards Quantum Gravity: Proceedings of the XXXV International Winter School on Theoretical Physics (Polanica, 1999). Lecture Notes in Physics, vol. 541, pp. 101–129. Springer, Berlin (2000)
9. Labarca, R.: Bifurcation of contracting singular cycles. Ann. Scient. Ec. Norm. Sup. 4 Serie t. **28**, 705–745 (1993)
10. Labarca, R.: A note on the topological classification of Lorenz maps on the interval. In: Blanchard, F., Maass, A., Nogueira, A. (eds.) Topics in Symbolic Dynamics and Applications. London Mathematical Society Lecture Note Series, vol. 279, pp. 229–245. Cambridge University Press (2000)
11. Labarca, R.: Unfolding singular cycles. Notas Soc. Mat. Chile (NS) **1**, 38–71 (2001)
12. Labarca, R.: La Entropía Topológica, Propiedades Generales y algunos cálculos en el caso de Milnor-Thurston. XXIV Escuela Venezolana de Matemáticas. EMALCA-Venezuela 2011. Ediciones IVIC (2011)
13. Labarca, R., Moreira, C.: Bifurcation of the essential dynamics of Lorenz maps of the real line and the bifurcation scenario of the linear family. Sci. Sci. A Math. Sci. (NS) **7**, 13–29 (2001)
14. Labarca, R., Moreira, C.: Bifurcations of the essential dynamics of Lorenz maps and applications to Lorenz like flows: contributions to the study of the expanding case. Bol. Soc. Bras. Mat. (NS) **32**, 107–144 (2001)
15. Labarca, R., Moreira, C.: Essential dynamics for Lorenz maps on the real line and the lexicographical world. Annales de L'Institut H. Poncaré Analyse non Linéaire **23**, 683–694 (2006)
16. Labarca, R., Moreira, C.: Bifurcations of the essential dynamics of Lorenz maps on the real line and the bifurcation scenario for Lorenz like flows: the contracting case. Proyecciones **29**(3), 247–293 (2010)
17. Labarca, R., Plaza, S.: Bifurcation of discontinuous maps of the interval and palindromic numbers. Bol. Soc. Mat. Mex. (3) **7**(1), 99–116 (2001)
18. Labarca, R., Vásquez L.: On the characterization of the kneading sequences associated to injective Lorenz maps of the interval and to orientation preserving homeomorphism of the circle. Bol. Soc. Mat. Mex. 3a Ser. **16**(2), 101–116 (2010)

19. Labarca, R., Vásquez, L.: On the characterization of the kneading sequences associated to Lorenz maps of the interval. Bol. Soc. Bras. Mat. (NS) **43**(2), 221–245 (2012)
20. Labarca, R., Pumariño, A., Rodriguez, J.A.: On the boundary of topological chaos for the Milnor-Thurston world. Commun. Contemp. Math. **11**(9), 1049–1066 (2009)
21. Labarca, R., Moreira, C., Pumariño, A., Rodriguez, J.A.: On bifurcation set for symbolic dynamics in the Milnor-Thurston world. Commun. Contemp. Math. **14**(4), 1250024 1–16 (2012)
22. Metropolis, N., Stein, M.L., Stein, P.R.: Stabe states of a nonlinear transformation. Numer. Math. **10**, 1–19 (1967)
23. Metropolis, N., Stein, M.L., Stein, P.R.: On finite limit sets for transformations on the unit interval. J. Comb. Theory (A) **15**, 25–44 (1973)
24. Mielnik, B.: Combinatorial dynamics. In: Proccedings of the 14th ICGTMP (Seoul, 1985), pp. 265–267. World Scientific, Singapore, (1986). 81B05
25. Milnor, J., Thurston, W.: On iterated maps on the interval. In: Alexander, J.C. (ed.) Dynamical Systems. Lecture Notes in Mathematics, vol. 1342, pp 465–563. Springer, Berlin (1988)
26. Moreira, C.: Maximal invariant sets for restriction of tent and unimodal maps. Anal. Theory Dyn. Syst. **2**(2), 385–398 (2001)

Homoclinic Spirals: Theory and Numerics

Roberto Barrio, Fernando Blesa, Sergio Serrano, Tingli Xing, and Andrey Shilnikov

Abstract In this paper we examine spiral structures in bi-parametric diagrams of dissipative systems with strange attractors. First, we show that the organizing center for spiral structures in a model with the Shilnikov saddle-focus is related to the change of the structure of the attractor transitioning between the spiral and screw-like types located at the turning point of a homoclinic bifurcation curve. Then, a new computational technique based on the symbolic description utilizing kneading invariants is proposed for explorations of parametric chaos in Lorenz like attractors. The technique allows for uncovering the stunning complexity and universality of the patterns discovered in the bi-parametric scans of the given models and detects their organizing centers – codimension-two T-points and separating saddles.

1 Introduction

Several analytic and experimental studies, including modeling simulations, have focused on the identification of key signatures to serve as structural invariants. Invariants would allow dynamically similar nonlinear systems with chaotic dynamics from diverse origins to be united into a single class. Among these key structures are various homoclinic and heteroclinic bifurcations of low codimensions that are the heart of the understanding of complex behaviors because of their roles as organizing centers of dynamics in parameterized dynamical systems.

R. Barrio (✉) · F. Blesa · S. Serrano
IUMA, University of Zaragoza, E-50009 Zaragoza, Spain
e-mail: rbarrio@unizar.es

T. Xing · A. Shilnikov
Department of Mathematics and Statistics, Neuroscience Institute, Georgia State University, Atlanta, 30303 GA, USA

S. Ibáñez et al. (eds.), *Progress and Challenges in Dynamical Systems*,
Springer Proceedings in Mathematics & Statistics 54,
DOI 10.1007/978-3-642-38830-9_4,

One computationally justified approach for studying complex dynamics capitalizes on the sensitivity of deterministic chaos. Sensitivity of chaotic trajectories can be quantified in terms of the divergence rate evaluated through the largest Lyapunov characteristic exponent. In several low-order dissipative systems, like the Rössler model, the computational technique based on the largest Lyapunov characteristic exponent reveals that they possess common, easily recognizable patterns involving spiral structures in bi-parametric planes [1,2]. Such patterns have turned out to be ubiquitously in various discrete and continuous-time systems [3], and they are easily located, as spiral patterns have regular and chaotic spiral "arms" in the systems with the Shilnikov saddle-focus [4–6].

Application of the Lyapunov exponents technique fails, in general, to reveal fine structures embedded in the bi-parametric scans of Lorenz-like systems. This implies that the instability of the Lorenz attractors does not vary noticeably as control parameters of the system are varied. This holds true when one attempts to find the presence of characteristic spiral structures that are known to theoretically exist in Lorenz-like systems [7], identified using accurate bifurcation continuation approaches [8, 9]. Such spirals in a bi-parametric parameter plane of a Lorenz-like system are organized around the T[erminal]-points; corresponding to codimension-two, closed heteroclinic connections involving two saddle-foci and a saddle at the origin, see Fig. 6. Such T-points have been located in various models of diverse origins including electronic oscillators and nonlinear optics.

Despite the overwhelming number of studies reporting the occurrence of spiral structures, there is still little known about the fine construction details and underlying bifurcation scenarios for these patterns. In this paper we study the genesis of the spiral structures in several low order systems and reveal the generality of underlying global bifurcations. We will start with the Rössler model and demonstrate that such parametric patterns are the key feature of systems with homoclinic connections involving saddle-foci meeting a single Shilnikov condition [10, 11]. The occurrence of this bifurcation causing complex dynamics is common for a plethora of dissipative systems, describing (electro)chemical reactions [12], population dynamics [13], electronic circuits [3, 14]. The other group is made of models with the Lorenz attractor. Here we present a computational toolkit capitalizing on the symbolic representation for the dynamics of Lorenz-like systems that employ kneading invariants [15, 16].

2 Spiral Structures: Homoclinic Loop

One of the most paradigmatic examples of low-dimensional deterministic chaos is the canonical Rössler system [17]:

$$\dot{x} = -(y + z), \quad \dot{y} = x + ay, \quad \dot{z} = b + z(x - c),$$

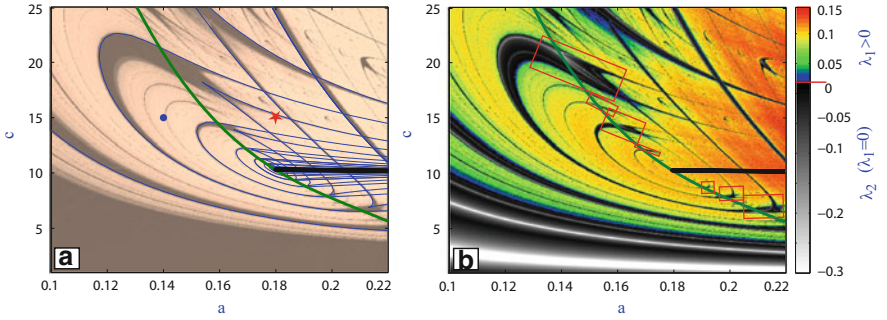

Fig. 1 Spirals and "shrimps" in the 1,000 × 1,000 grid biparametric bifurcation diagrams for the Rössler model. The F-point of the hub is located at $(a, c) = (0.1798, 10.3084)$. The color bars for the Lyapunov exponent range identify the regions of chaotic and regular dynamics. *Left* monochrome panels are superimposed with bifurcation curves: *thin blue* for saddle-nodes, and *thick black* for homoclinic bifurcations of saddle-foci. The *medium-thick green* boundary determines a change in the topological structure of chaotic attractors from spiral (at •) to screw-shaped (at ⋆)

with two bifurcation parameters a and c (we fix $b = 0.2$). For $c^2 > 4ab$ the model has two equilibrium states, $P_{1,2}(ap_{\pm}, -p_{\pm}, p_{\pm})$, where $p_{\pm} = (c \pm \sqrt{c^2 - 4ab})/2a$. This classical model exhibits the spiral and screw chaotic attractors after a period doubling cascade followed by the Shilnikov bifurcations of the saddle-focus P_2.

Bi-parametric screening of the Rössler model unveils a stunning universality of the periodicity hubs in the bifurcation diagrams shown in Fig. 1 [5]. The diagram is built on a dense grid of $1{,}000 \times 1{,}000$ points in the $(a\, c)$-parameter plane. Solutions of the model were integrated using the high precision ODE solver TIDES [18]. The color is related with the Lyapunov exponents, where dark and light colors discriminate between the regions of regular and chaotic dynamics corresponding to a zero and positive maximal Lyapunov exponent λ_1, respectively. The figure reveals the characteristic spiral patterns due to variations of the Lyapunov exponents.

The chaotic-regular regions spiral around a F[ocal] point [3] located at $(a, c) = (0.1798, 10.3084)$. This F-point terminates the bifurcation curve (black) corresponding to the formation of a homoclinic loop of the saddle-focus, P_2, in the phase space of the Rössler model [2]. Another curve (medium green) passes through the F-point: crossing it rightward the chaotic attractor in the phase space of the model changes the topological structure from spiral to screw-shaped.

The dark bifurcation curve in Fig. 1 corresponds to a formation of the homoclinic orbits to the saddle-focus, P_2, of topological type (1,2), i.e. with 1D stable and 2D unstable manifolds, in the Rössler model. Depending on the magnitudes of the characteristic exponents of the saddle-focus, the homoclinic bifurcation can give rise to the onset of either rich complex or trivial dynamics in the system [10, 11, 19]. The cases under considerations meet the Shilnikov conditions and hence the existence of a single homoclinic orbit implies chaotic dynamics in the models within the parameter range in the presented diagrams. We remark that the homoclinic

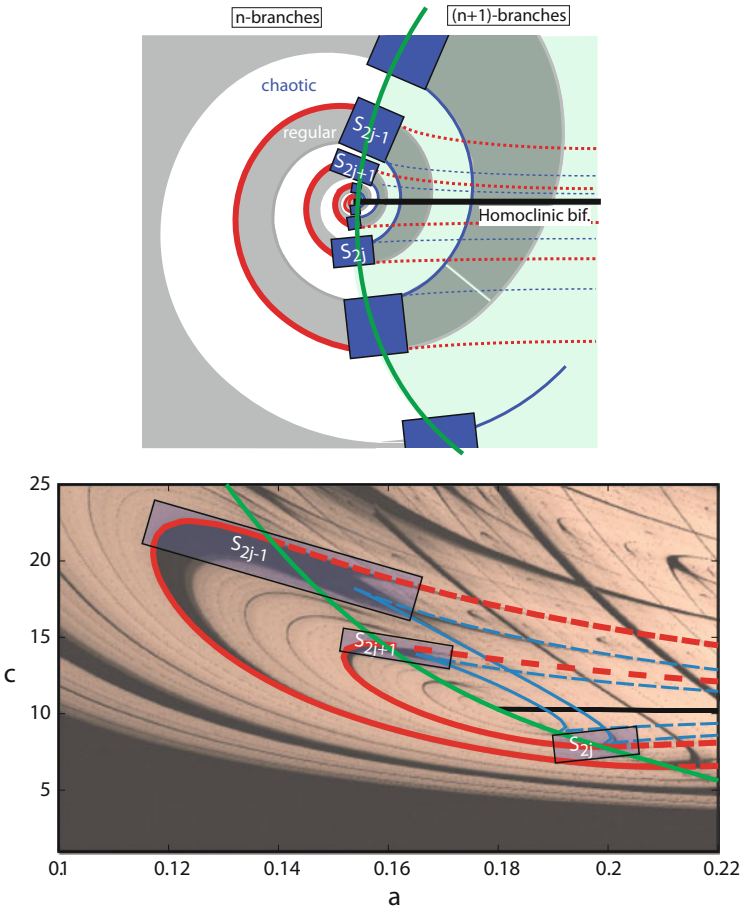

Fig. 2 Outline of the spiral structures: (*Top*) phenomenological sketch of the spiral hub formed by the "shrimps." (*Bottom*) Magnification of the bifurcation portrait of the spiral hub, overlaid with principal folded (*thick red*) and cusp-shaped (*thin blue*) bifurcation curves setting the boundaries for largest "shrimps" in the Rössler model

bifurcation curve in the diagram (Fig. 1) has actually two branches, although very close each other. This curve has a U-shape with the turn at the F-point.

Figure 2 outlines the structure of the bifurcation unfolding around the spiral hub [2, 5]. The picture depicts a number of the identified folded and cusp-shaped saddle-node bifurcation curves of periodic orbits, toward the spiral hub in the (a, c)-parameter plane for the Rössler model. Note that none of these curves is actually a spiral – the overall spiral structure must be supported by homoclinic bifurcations. At this B-point, the saddle with real characteristic exponents becomes a saddle-focus for smaller values of the parameter a.

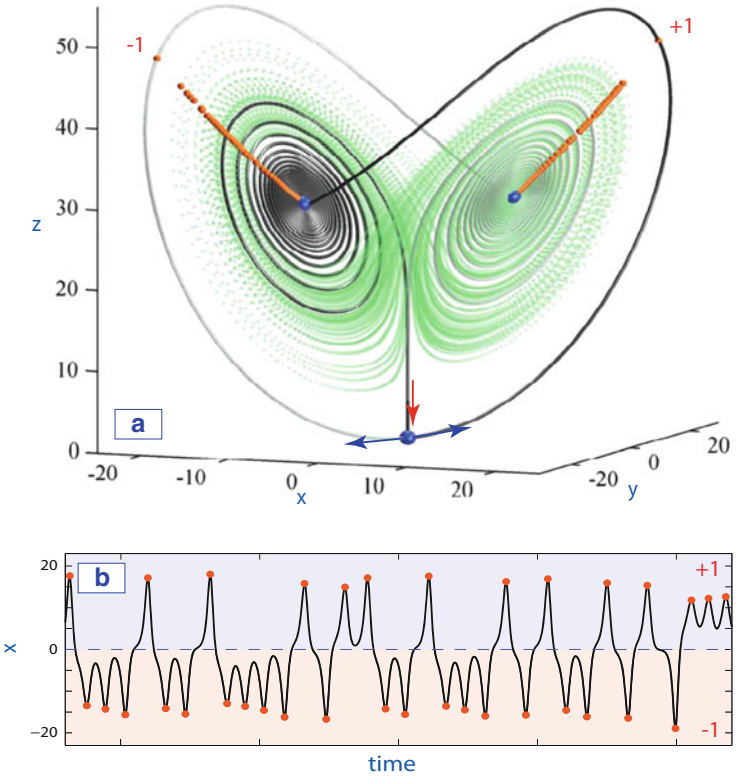

Fig. 3 (**a**) Heteroclinic connection (in *dark color*) between the saddle at the origin and two saddle-foci (*blue spheres*) being overlaid with the strange attractor (*green light color*) on the background at the primary T-point ($r = 30.38$, $\sigma = 10.2$) in the Lorenz model. *Orange spheres* on the butterfly wings indicating the turning points around the *right* and *left* saddle-foci define the kneading sequence entries, $\{\pm 1\}$, respectively. (**b**) A typical time evolution of either symmetric coordinate of the *right* separatrix of the saddle

3 Homoclinic Spirals: Kneading Invariants for Lorenz Like Systems

Chaos can be quantified by several means. One customary way is through the evaluation of topological entropy. The greater the value of topological entropy, the more developed and unpredictable the chaotic dynamics become. Another practical approach for measuring chaos in simulations capitalizes on evaluations of the largest (positive) Lyapunov exponent of a long yet finite-time transient on the chaotic attractor.

A trademark of any Lorenz-like system is the strange attractor of the iconic butterfly shape, such as shown in Fig. 3. The "wings" of the butterfly are marked with two symmetric "eyes" containing equilibrium states, stable or not, isolated from the

trajectories of the Lorenz attractor. This attractor is structurally unstable [20, 21] as it bifurcates constantly as the parameters are varied. The primary cause of structural and dynamic instability of chaos in the Lorenz equations and similar models is the singularity at the origin – a saddle with two one-dimensional outgoing separatrices. Both separatrices densely fill the two spatially symmetric wings of the Lorenz attractor in the phase space. The Lorenz attractor undergoes a homoclinic bifurcation when the separatrices of the saddle change the alternating pattern of switching between the butterfly wings centered around the saddle-foci. At such a change, the separatrices comes back to the saddle thereby causing a homoclinic explosions in phase space [22, 23]. Other important points, that act as organizing centers, are the codimension-two T-points and separating saddles, but these points cannot be detected by using Lyapunov exponents as we can see in Fig. 4, where on the top we show the maximum Lyapunov exponent that cannot reveal the hidden structures inside the chaotic region. Among these structures is a T-point, that form a "kind" of "diamonds-mine" (middle pic) formed by homoclinic spirals as it can be shown by detailed bifurcation analysis (bottom pic). Therefore, we focus on presenting a new computational tool that locates automatically "all" the T-points.

The time progression of the "right" (or symmetrical "left") separatrix of the origin can be described geometrically and categorized in terms of the number of alternations around the nonzero equilibrium states in the phase space of the Lorenz-like system (Fig. 3). Alternatively, the description can be reduced to the time-evolution of a coordinate of the separatrix, as shown in panel b of Fig. 3. The sign-alternation of the x-coordinate suggests the introduction of a $\{\pm 1\}$-based alphabet for the symbolic description of the separatrix. Namely, whenever the right separatrix turns around O_1 or O_2, we record $+1$ or -1, respectively. For example, the time series shown in panel b generates the following kneading sequence starting with $\{+1, -1, -1, -1, +1, -1, -1, +1, -1, \ldots\}$.

We introduce and demonstrate a new computational toolkit for the analysis of chaos in the Lorenz-like models. The toolkit is inspired by the idea of kneading invariants introduced in [15]. A kneading invariant is a quantity that is intended to uniquely describe the complex dynamics of the system that admit a symbolic description using two symbols, here $+1$ and -1.

The kneading invariant for either separatrix of the saddle equilibrium state of the Lorenz attractor can be defined in the form of a formal power series:

$$P(q) = \sum_{n=0}^{\infty} \kappa_n \, q^n. \tag{1}$$

Letting $q \in (0, 1)$ guarantees the series is convergent. The smallest zero, q^*, if any, of the graph of (1) in the interval $q \in (0, 1)$ yields the topological entropy, $h(T) = \ln(1/q^*)$.

The kneading sequence $\{\kappa_n\}$ composed of only $+1$s corresponds to the "right" separatrix of the saddle converging to an ω-limit set with $x(t) > 0$, such as a stable focus or stable periodic orbit. The corresponding kneading invariant is maximized

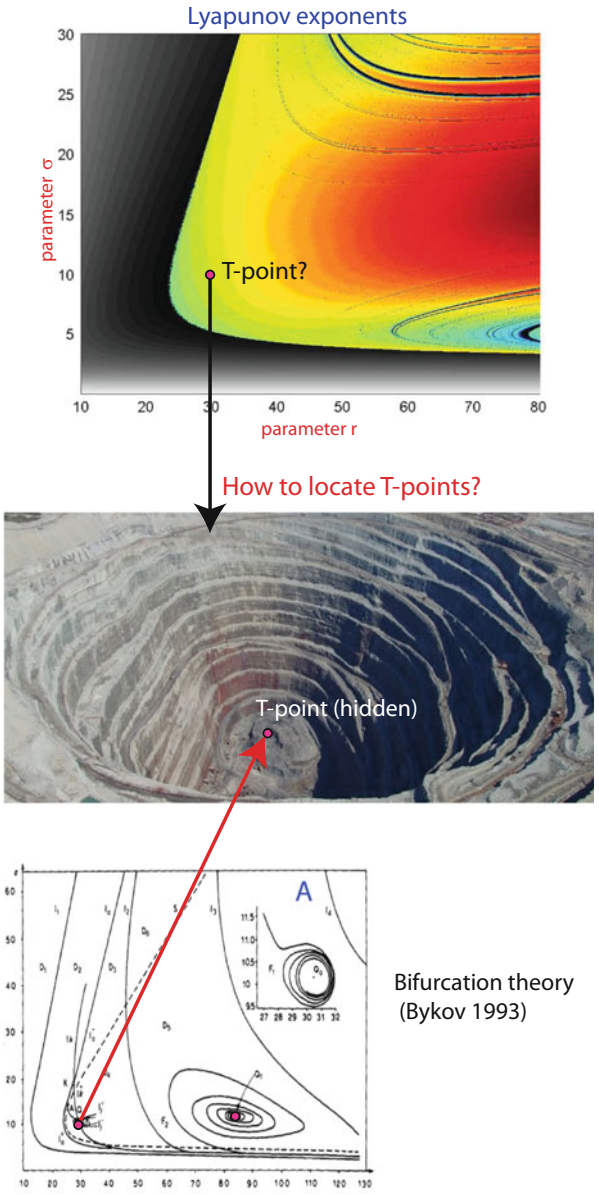

Fig. 4 (*Top*) Finite-time largest-Lyapunov exponent, $L_{\max}$, scan of the Lorenz equation showing no sign of spiral structures in the (r, σ)-parameter plane. The *dark region* corresponds to trivial attractors, where $L_{\max} \leq 0$, while the *red color* indicates $L_{\max} > 0$ in chaotic regions. The *red dot* points out the position of the primary T-point. (*Bottom*) Original bifurcation diagram of the Lorenz equation depicting the two detected T-points and primary homoclinic bifurcation curves from [7]

at $\{P_{\max}(q)\} = 1/(1-q)$. When the right separatrix converges to an attractor with $x(t) < 0$, then the kneading invariant is given by $\{P_{\min}(q)\} = 1 - q/(1-q)$ because the first entry $+1$ in the kneading sequence is followed by infinite -1s. Thus, $[\{P_{\min}(q)\}, \{P_{\max}(q)\}]$ yield the range of the kneading invariant values; for instance $[\{P_{\min}(1/2)\} = 0, \{P_{\max}(1/2)\} = 2]$.

In computational studies of the models below, we will consider a partial kneading power series truncated to the first 20 entries: $P_{20}(q) = \sum_{n=0}^{20} \kappa_n q^n$. The choice of the number of entries is not motivated by numerical precision, but by simplicity, as well as by resolution of the bitmap mappings for the bi-parametric scans of the models. One has also to determine the proper value of q: setting it too small makes the convergence fast so that the tail of the series has a little significance and hence does not differentiate the fine dynamics of the Lorenz equation for longer kneading sequences.

At the first stage of the routine, we perform a bi-parametric scan of the model within a specific range in the parameter plane. The resolution of scans is set by using mesh grids of [1,000 × 1,000] equally distanced points. Next by integrating the same separatrix of the saddle point we identify and record the sequences $\{\kappa_n\}_{20}$ for each point of the grid in the parameter plane. The mapping is then colorized in Matlab by using various built-in functions ranging between to $P_{20}^{\min}$ and $P_{20}^{\max}$, respectively. In the mapping, a particular color in the spectrum is associated with a persistent value of the kneading invariant on a level curve. Such level curves densely foliate the bi-parametric scans. Now, we repeat the study for the Lorenz model with the new technique in Fig. 5. Now we can observe that the T-points are revealed automatically.

Besides, we examine the kneading-based bi-parametric scanning of the Shimizu-Morioka model [8,24]:

$$\dot{x} = y, \quad \dot{y} = x - \lambda y - xz, \quad \dot{z} = -\alpha z + x^2; \tag{2}$$

with α and λ being positive bifurcation parameters. The Z_2-symmetric model has three equilibrium states: a simple saddle, with one-dimensional separatrices, at the origin, and two symmetric stable-foci which can become saddle-foci through a supercritical Andronov-Hopf bifurcation.

This model was originally introduced to examine a pitch-fork bifurcation of the stable figure-8 periodic orbit that gives rise to multiple cascades of period doubling bifurcations in the Lorenz equation at large values of the Reynolds number. It was proved in [9] that the Eqs. (2) would be a universal normal form for several codimension-three bifurcations of equilibria and periodic orbits on Z_2-central manifolds. The model turned out to be very rich dynamically: it exhibits various interesting global bifurcations [25] including T-points for heteroclinic connections.

The structure of the bifurcation set of the Shimizu-Morioka is very complex. The detailed bifurcation diagram is shown in the top-left panel of Fig. 6. It reveals several T-points, and multiples curves corresponding to an Andronov-Hopf (AH), pitch-fork (PF), period doubling (PD) and homoclinic (H) bifurcations that shape the existence region of the Lorenz attractor in the model. The detailed description of the bifurcation structure of the Shimizu-Morioka model is out of scope of this paper. The reader can find a wealth of information on bifurcations of the Lorenz attractor in the original papers [9,25].

The panels b and c of Fig. 6 is a de-facto proof of the new kneading invariant mapping technique. The panel represents the color bi-parametric scan of the dynamics of the Shimizu-Morioka model that is based on the evaluation of the first

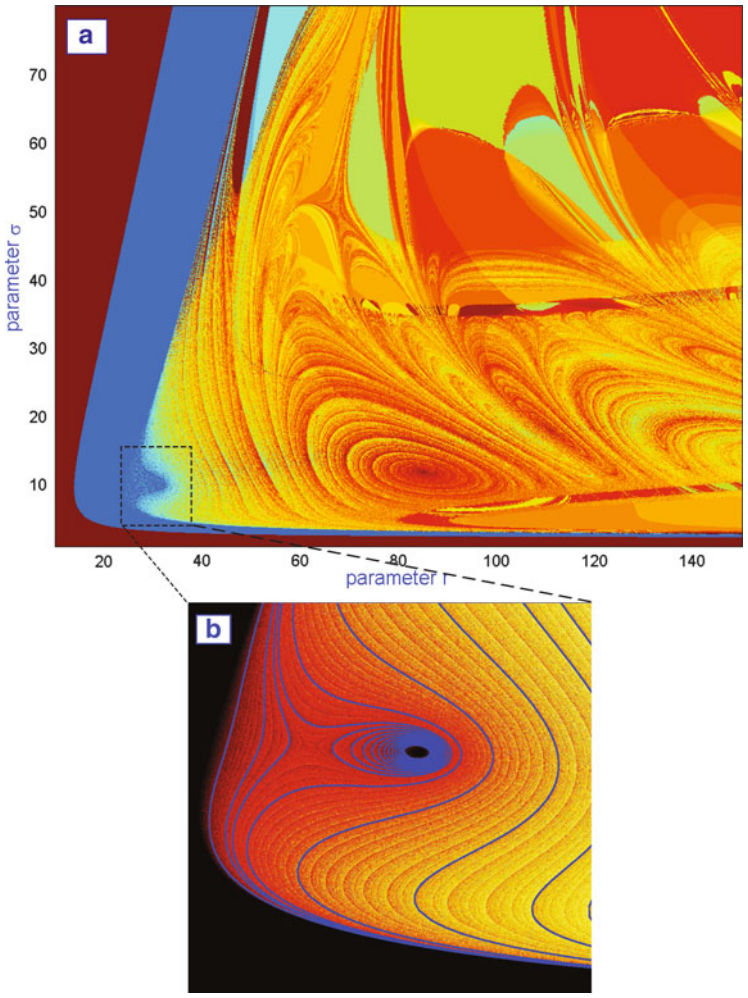

Fig. 5 (**a**) Kneading-based biparametric scan revealing multiple T-points and saddles that organize globally complex chaotic dynamics of the Lorenz equation in the (r, σ) parameter plane. *Solid-color regions* associated with constant values of the kneading invariant correspond to simple dynamics dominated by stable equilibria or stable periodic orbits. The border line between the *brown* and *blue region* corresponds to the bifurcation curve of the homoclinic butterfly. The border line between the *blue* and *yellow-reddish* region corresponds to the formation of the Lorenz attractor (below $\sigma \simeq 50$). (**b**) Zoom of the vicinity of the primary T-point at $(r = 30.4, \sigma = 10.2)$ to which a homoclinic bifurcation curve spirals onto (Data for the homoclinic curves (in *blue*) are courtesy of Yu. Kuznetsov)

20 kneadings of the separatrix of the saddle on the grid of 1,000 × 1,000 points in the (α, λ)-parameter region. Getting the mapping took a few hours on a high-end workstation without any parallelization efforts. The color scan reveals a plethora of primary, large, and small scale T-points as well as the saddles separating spiral structures.

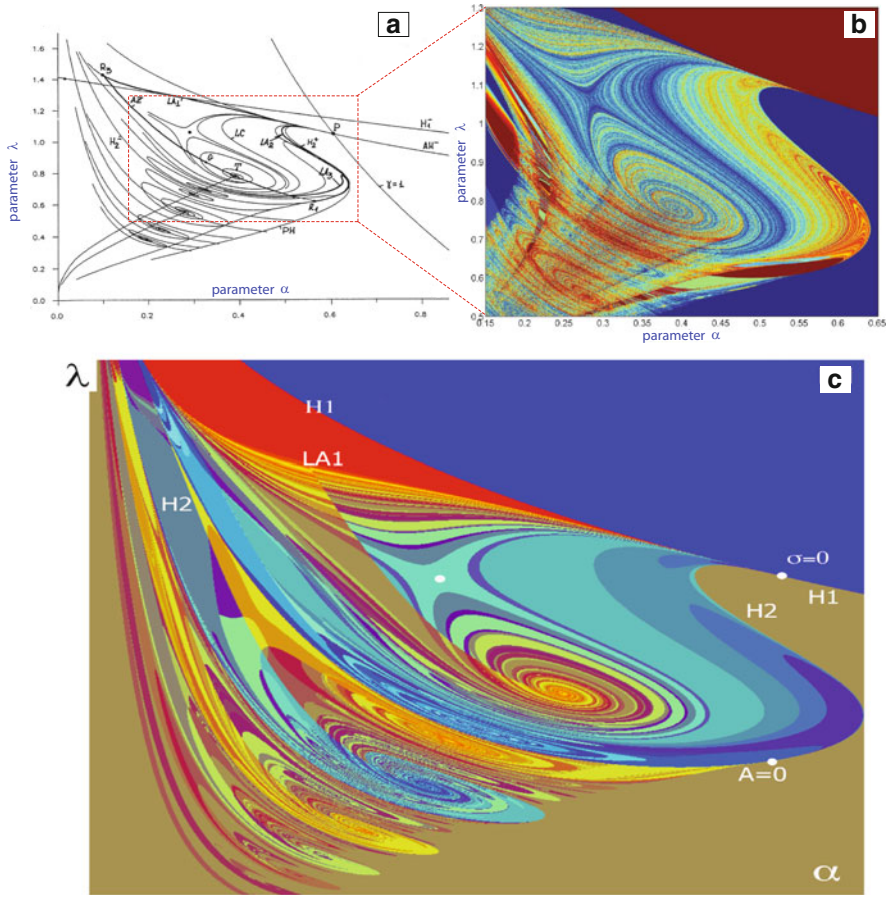

Fig. 6 (*Top-left*) Detailed (α, λ)-parameter plane of the Shimizu-Morioka model obtained by the parameter continuation method (Courtesy of [9]). Legend: AH stands for a supercritical Andronov-Hopf bifurcation, H_1 stands for the homoclinic butterfly made of two separatrix loops; the codimension-two points corresponding to the resonant saddle P on H_1 organizes the bifurcation unfolding of the model; cod-2 point $R_1 0$ stands for an orbit-flip bifurcation for the double-loop homoclinics on H_2. The *thick line* demarcates, with good precision, the existence region of the Lorenz attractor bounded by LA_1 and LA_2. (*Top-right* and *bottom*) Two kenading scans revealing multiple T-points and saddles that globally organize complex chaotic dynamics of the Shimizu-Morioka model. *Solid-color regions* associated with constant values of the kneading invariant correspond to simple dynamics dominated by stable equilibria (*brown*) or stable periodic orbits (*blue*). The border between the *brown* and *blue regions* corresponds to the bifurcation curve of the homoclinic butterfly

The solid-color zones in the mapping correspond to simple dynamics in the model. Such dynamics are due to either the separatrix converging to the stable equilibria or periodic orbits with the same kneading invariant (blue region), or to the symmetric and asymmetric stable figure-8 periodic orbits (brown region).

The borderlines between the simple and complex dynamics in the Shimizu-Morioka model are clearly demarcated. On the top is the curve, LA_1, (see the top-left panel of Fig. 6). The transition from the stable 8-shaped periodic orbits to the Lorenz attractor (through the boundary, LA_2) is similar though more complicated as it involves a pitch-fork bifurcation and bifurcations of double-pulsed homoclinics, see [9,25] for details.

One can clearly see the evident resemblance between both diagrams found using the bifurcationaly exact numerical methods and by scanning the dynamics of the model using the proposed kneading invariant technique. The latter reveals a richer structure providing finer details. The structure can be enhanced further by examining longer tails of the kneading sequences. This allows for the detection of smaller-scale spiral structures within scrolls of the primary T-vortices, as predicted by the theory.

4 Conclusions

We have examined two formation mechanisms of spiral structures in biparametric mappings of systems with the Shilnikov saddle-focus and with the Lorenz attractor. The feature of the spiral hubs in the Rössler model is that the F[ocal]-point gives rise to the alternation of the topological structure of the chaotic attractor transitioning between the spiral and screw-like types, as well as terminates the primary homoclinic curves of the saddle-focus equilibrium state influencing the forward-time dynamics of the model. The findings let us hypothesize about universality of the structure of the spiral hubs in similar systems with chaotic attractors due to homoclinics of the Shilnikov saddle-focus.

We have demonstrated a new computational toolkit for thorough explorations of chaotic dynamics in models with the Lorenz attractor. The algorithmically simple yet powerful toolkit is based on the scanning technique that maps the dynamics of the system onto the bi-parametric plane. The core of the approach is the evaluation of the kneading invariants for regularly or chaotically varying alternating patterns of a single trajectory – the separatrix of the saddle singularity in the system. In the theory, the approach allows two systems with structurally unstable Lorenz attractors to be conjugated with a single number – the kneading invariant. The kneading scans unambiguously reveal the key features in Lorenz-like systems such as a plethora of underlying spiral structures around T-points, separating saddles in intrinsically fractal regions corresponding to complex chaotic dynamics. We point out that no other techniques, including approaches based on the Lyapunov exponents, can reveal the discovered parametric chaos with such stunning clarity and beauty.

The method should be beneficial for detailed studies of other systems admitting a reasonable symbolic description.

Acknowledgements This work is supported by the Spanish Research project MTM2012-31883 (to R.B. and S.S.), and by NSF grant DMS-1009591, RFFI Grant No. 08-01-00083, and MESRF project 14.740.11.0919 (to A.S).

References

1. Gaspard, P., Kapral, R., Nicolis, G.: Bifurcation phenomena near homoclinic systems: a two-parameter analysis. J. Stat. Phys. **35**, 697–727 (1984)
2. Barrio, R., Blesa, F., Serrano, S.: Qualitative analysis of the Rössler equations: bifurcations of limit cycles and chaotic attractors. Phys. D **238**, 1087–1100 (2009)
3. Bonatto, C., Gallas, J.A.C.: Periodicity hub and nested spirals in the phase diagram of a simple resistive circuit. Phys. Rev. Lett. **101**, 054101 (2008)
4. Shilnikov, L., Shilnikov, A.: Shilnikov bifurcation. Scholarpedia **2**(8), 1891 (2007)
5. Barrio, R., Blesa, F., Serrano, S., Shilnikov, A.: Global organization of spiral structures in biparameter space of dissipative systems with Shilnikov saddle-foci. Phys. Rev. E **84**, 035201 (2011)
6. Barrio, R., Blesa, F., Serrano, S.: Topological changes in periodicity hubs of dissipative systems. Phys. Rev. Lett. **108**, 214102 (2012)
7. Bykov, V.V.: The bifurcations of separatrix contours and chaos. Phys. D **62**, 290–299 (1993)
8. Shilnikov, A.: Bifurcation and chaos in the Morioka-Shimizu system. Sel. Math. Sov. **10**(2), 105–117 (1991)
9. Shilnikov, A.L., Shilnikov, L.P., Turaev, D.V.: Normal forms and Lorenz attractors. Int. J. Bifurc. Chaos Appl. Sci. Eng. **3**, 1123–1139 (1993)
10. Shilnikov, L.P.: A case of the existence of a countable number of periodic motions. Sov. Math. Dokl. **6**, 163 (1965)
11. Shilnikov, L.P., Shilnikov, A.L., Turaev, D., Chua, L.O.: Methods of Qualitative Theory in Nonlinear Dynamics. Part II. World Scientific Series on Nonlinear Science. Series A: Monographs and Treatises, vol. 5, pp. i–xxiv and 393–957. World Scientific, River Edge (2001)
12. Nascimento, M.A., Gallas, J.A.C., Varela, H.: Self-organized distribution of periodicity and chaos in an electrochemical oscillator. Phys. Chem. Chem. Phys. **13**, 441–446 (2011)
13. Hastings, A., Powell, T.: Chaos in a three-species food chain. Ecology **72**, 896–903 (1991)
14. Shilnikov, L.: Chua's circuit: rigorous results and future problems. J. Bifurc. Chaos **4**(3), 489–518 (1994)
15. Milnor, J., Thurston, W.: On iterated maps of the interval. Lect. Notes Math. **1342**, 465–563 (1988)
16. Barrio, R., Shilnikov, A., Shilnikov, L.: Kneadings, symbolic dynamics and painting Lorenz chaos. Int. J. Bifur. Chaos Appl. Sci. Eng. **22**, 1230016, 24 (2012)
17. Rössler, O.E.: An equation for continuous chaos. Phys. Lett. A **57**, 397–398 (1976)
18. Abad, A., Barrio, R., Blesa, F., Rodríguez, M.: Algorithm 924: TIDES, a Taylor series integrator for differential equations. ACM T. Math. Softw. **39**, 5:1–5:28 (2012)
19. Gaspard, P., Nicolis, G.: What can we learn from homoclinic orbits in chaotic dynamics? J. Stat. Phys. **31**, 499–518 (1983)
20. Guckenheimer, J., Williams, R.F.: Structural stability of Lorenz attractors. Inst. Hautes Études Sci. Publ. Math. **50**, 59–72 (1979)
21. Afraimovic, V., Bykov, V.V., Shilnikov, L.P.: On structurally unstable attracting limit sets of Lorenz attractor type. Trans. Mosc. Math. Soc. **44**, 153–216 (1983)
22. Afraimovic, V., Bykov, V.V., Shilnikov, L.P.: The origin and structure of the Lorenz attractor. Sov. Phys. Dokl. **22**, 253–255 (1977)
23. Kaplan, J.L., Yorke, J.A.: Preturbulence: a regime observed in a fluid flow model of Lorenz. Commun. Math. Phys. **67**, 93–108 (1979)
24. Shimizu, T., Morioka, N.: On the bifurcation of a symmetric limit cycle to an asymmetric one in a simple model. Phys. Lett. A **76**, 201–204 (1980)
25. Shilnikov, A.: On bifurcations of the Lorenz attractor in the Shimizu-Morioka model. Phys. D **62**(1–4), 338–346 (1993)

Numerical Results on a Simple Model for the Confinement of Saturn's F Ring

Luis Benet and Àngel Jorba

Abstract In this paper we discuss a simple model for the confinement of Saturn's F ring and present some preliminary numerical results. The model involves the gravitational interaction of independent test particles with Saturn, including its second zonal harmonic, the shepherd moons Prometheus and Pandora, and Titan, the largest of Saturn's satellites. We perform accurate long-time integrations (3.2×10^6 revolutions of Prometheus) to check if the particle has escaped or remains trapped in the region between the shepherds. A particle escapes if its orbit crosses the region between the shepherds, or if it displays a physical collisions (lies with Hill's region) with them. We find a wide region of initial conditions of the test particle that remain confined. We carry out a frequency analysis and use the ratio of the standard deviation over the average main frequencies as stability index. This indicator separates clearly the set of trapped initial conditions of the test particles, displaying some localised structures for the most stable ones. Retaining only those particles which are more stable according to our indicator, we obtain a narrow elliptic ring displaying sharp edges which agrees with the nominal location of Saturn's F ring.

L. Benet (✉)
Instituto de Ciencias Físicas, Universidad Nacional Autónoma de México (UNAM),
Apdo. Postal 48–3, 62251-Cuernavaca, Mexico
e-mail: benet@fis.unam.mx

À. Jorba
Departament de Matemàtica Aplicada i Anàlisi, Universitat de Barcelona, Gran Via 585,
08007 Barcelona, Spain
e-mail: angel@maia.ub.es

S. Ibáñez et al. (eds.), *Progress and Challenges in Dynamical Systems*,
Springer Proceedings in Mathematics & Statistics 54,
DOI 10.1007/978-3-642-38830-9_5, © Springer-Verlag Berlin Heidelberg 2013

1 Introduction

Saturn's F ring is a fascinating narrow eccentric ring with a very rich and dynamical structure: beside its non-zero eccentricity and sharp-edges, it has multiple components entangled in a complicated way which show a variety of short-time features [2, 3]. This ring is located just outside the main rings of Saturn, close to Roche's limit for ice, and it is believed to be the result of the action of accretion and disruptive process [2]. Aside from the difficult questions related to its origin and evolution, its location and its highly dynamical structural properties pose interesting questions. The current understanding on the confinement of narrow planetary rings is based on the shepherd theory, introduced by Goldreich and Tremaine [5]. In its original form, the shepherd theory postulates the existence of two moons orbiting the central planet, the shepherd moons. These moons repel away the ring particles through gravitational angular-momentum exchange mechanisms, and induce ring-particle eccentric orbits which are circularised by mutual ring-particle collisions. The ring is confined between the shepherd moons where the angular-momentum torques balance, or by mean-motion resonances. While the shepherd theory is successful for the ϵ ring of Uranus, its application to Saturn's F ring is not so straightforward, since there is no mean-motion resonance that confines the ring, the masses of the shepherds moons Prometheus and Pandora are too small, and the angular momentum torques are not balanced at the actual location of the ring (see e.g. [3]). In addition, the eccentricity of the ring and its sharp edges pose further questions. The confinement of Saturn's F-ring remains unexplained.

In this paper we discuss a model to understand from a dynamical point of view the confinement of Saturn's F ring. We argue that a minimal model for Saturn's F ring needs to include at least the gravitational interactions of Saturn (we also include corrections due to its flattening), the shepherd moons, and Saturn's most massive moon, Titan. We follow the scattering approach to narrow rings [13] where ring particles are treated within a particle-independent model, i.e., ring particle collisions are neglected. In this approach, the location and structure of the ring follows from an ensemble of ring particles that remains trapped despite the existence of escaping and leaking mechanisms in the system, which in the present case are mainly physical collisions with the shepherd moons. We compute the orbits of an ensemble of non-interacting test particles during 3.2×10^6 periods of the innermost shepherd moon, Prometheus. Test particles that remain trapped between the orbits of the shepherds are filtered with respect to a dimensionless stability index which we use as a dynamical indicator for the possibility of escape. After this filtering, we obtain a narrow eccentric ring that displays sharp edges, located close to the nominal observations for Saturn's F ring.

The paper is organized as follows: In Sect. 2 we introduce and motivate the $(4 + 1)$-body problem considered as a model for the F ring of Saturn. Section 3 describes some of our numerical simulations, including the definition of the stability index and the motivation for filtering out the particles whose associated dynamical indicator is too large. Finally, Sect. 4 summarizes the main results of the paper.

2 A 'Minimalist' Model for Saturn's F Ring

A complete description of the dynamics of Saturn's F ring includes the gravitational interactions of Saturn with its flattening, its major moons including the influence of the shepherd moons Prometheus and Pandora, and the interactions among the ring particles themselves. The latter involves non-trivial processes associated to physical collisions among the particles of the ring, such as accretion and fragmentation processes. Clearly, the understanding of such a system is a monumental task. Here we shall thus address a simpler problem which is the understanding of a possible mechanism for confinement of Saturn's F ring and, once this is settled, we shall consider the structural properties of the resulting confined ring.

The starting point of our model is the assumption that the F ring consists of an ensemble of non-interacting test particles, which are dynamically trapped by their interactions with Saturn and its major moons. We study the dynamics of an ensemble of test particles defined by its initial conditions in phase space; their time evolution determines whether a test particle remains dynamically trapped and hence belongs to the ring, or if it simply escapes. This is the framework of the so-called scattering approach to narrow rings [1, 13]. The crude assumption of considering non-interacting test particles allows us to treat each particle independently. This assumption is therefore equivalent to disregard any effects related to collisions among the ring particles and the dynamical effects related to their actual shape and size, processes that are important for the detailed understanding of the fine structure and life-time of the ring [2, 14, 16]. In addition, we shall neglect the influence of the whole ring in the motion of any of the major bodies considered or of the particles of the ring; this is tantamount of having massless test particles. We shall assume for simplicity that the motion of all bodies takes place on the equatorial plane of Saturn. These assumptions allow us to consider a planar restricted $(N+1)$-body problem, where one test particle is influenced by the motion of N massive bodies including Saturn and its flattening, but does not influence the motion of the latter.

Our model is naturally divided into two parts. First, the motion of the N-interacting massive bodies is given in an inertial frame by the many-body Hamiltonian

$$\mathscr{H}_N = \sum_{i=0}^{N-1} \frac{1}{2m_i}(P_{x_i}^2 + P_{y_i}^2) - \sum_{i=1}^{N-1} \frac{\mathscr{G}m_0 m_i}{R_{i,0}}\left(1 + \frac{J_2}{2}\frac{R_S^2}{R_{i,0}^2}\right) - \sum_{1\le i<j}^{N-1} \frac{\mathscr{G}m_i m_j}{R_{i,j}}. \quad (1)$$

Here, $\mathscr{G}$ denotes the gravitational constant, $m_0 = M_S = 5.68319 \times 10^{26}$ kg [7] is Saturn's mass, $R_S = 60{,}268.0$ km [17] denotes its equatorial radius, and $J_2 = 16{,}290.71 \times 10^{-6}$ is the value of first zonal gravitational coefficient [7]. The latter is included since we are interested in somewhat long-time integrations; higher-order terms related to the flattening are ignored since they do not provide further physical insight and simply slow down significantly the numerical calculations. The mass of the i-th body is denoted by m_i, its position from the origin (which is the center of

mass of N-body problem) by $\mathbf{R}_i$, and its momentum by $\mathbf{P}_i$. Then, $R_{i,j} = |\mathbf{R}_i - \mathbf{R}_j|$ denotes the distance between the i-th and the j-th bodies, with the convention that $i = 0$ represents Saturn, and the moons included in the model are ordered increasingly with respect to their semi-major axis.

The second part of the model is related to the motion of the test particles, whose Hamiltonian reads

$$\mathscr{H}_{\text{rp}}(t) = \frac{1}{2}(p_x^2 + p_y^2) - \frac{\mathscr{G}m_0}{r_0(t)}\left(1 + \frac{J_2}{2}\frac{R_S^2}{r_0^2(t)}\right) - \sum_{i=1}^{N-1}\frac{\mathscr{G}m_i}{r_i(t)}, \tag{2}$$

where $r_i(t) = |\mathbf{r} - \mathbf{R}_i(t)|$ denotes the distance from the test particle to the i-th massive object, $\mathbf{r}$ denotes the position of the ring particle and $\mathbf{p}$ its momentum. Notice the explicit appearance of time in the test-particle Hamiltonian through the positions $\mathbf{R}_i(t)$; hence, the energy of the test particle is not a constant of motion.

What massive bodies shall we include in a simple model for the F ring? Clearly, we must include the shepherd moons Prometheus and Pandora ($m_1 = 2.4 \times 10^{-10}\, M_S$, $a_1 = 2.312\, R_S$, $e_1 = 0.0024$; $m_2 = 2.3 \times 10^{-10}\, M_S$, $a_2 = 2.352\, R_S$, $e_2 = 0.0042$), which are known to influence the dynamics of the ring, though they do not confine it completely (see [3]). The resulting $(3 + 1)$-body model defined by Saturn, the shepherd moons and the test particle, yields a broad ring instead of a narrow one, which spans essentially all the available initial condition space between the orbits of the shepherd moons. This follows from the fact that the masses of shepherd moons are exceedingly small, so their influence on the test particles is essentially local: Test particles either collide with them, or essentially do not feel their influence at all; their motion is a precessing Kepler ellipse which is too weakly perturbed by the shepherds. Therefore, our minimalist model must include at least another moon, thus becoming a planar restricted $(4 + 1)$-body problem .

There is no obvious choice for such a third moon in the model, since there is no resonance that actually confines the ring [3]. Two possible options are Titan and Mimas: Titan is the most massive moon of Saturn's satellite system ($M_{\text{Titan}} = 2.3669 \times 10^{-4}\, M_S$), with a nominal eccentricity of $e_{\text{Titan}} = 0.0288$, but it is located rather far away from the ring, $a_{\text{Titan}} = 20.27\, R_S$. In turn, Mimas is the major moon of Saturn closest to the F ring ($a_{\text{Mimas}} = 3.076\, R_S$) and may play an important role, since Pandora is close to a $3 : 2$ co-rotation eccentric resonance with Mimas [4]. Yet, the mass of Mimas is comparatively small, $M_{\text{Mimas}} = 6.6 \times 10^{-8}\, M_S$. We notice that the ratio of the force exerted by Titan on a test particle at the nominal semi-major axis of the F ring ($a_{\text{Fring}} = 2.324\, R_S$) is $\sim$4 times larger than the force exerted by Mimas, when Titan is at its furthest location from the particle and Mimas is at the closest one. For this reason we shall consider in our model the influence of Titan on a precessing Kepler elliptic orbit. Finally, due to the small mass ratio between Titan and Saturn and the shepherds and Titan, we simplify the numerics by computing the precessing Kepler motion of Titan due to the gravitational attraction of Saturn and its J_2 coefficient, and for the shepherds we include the additional perturbations by Titan; we further consider that Saturn remains at the origin.

We are interested in the existence of regions of trapped motion between the orbits of the two shepherd moons. Note that our model can be seen as a central field (with a central oblate mass) under a time dependent perturbation coming from the motion of the moons and Saturn. If the motion of these bodies (described by Hamiltonian (1)) is quasi-periodic, then the time dependent perturbation that appears in Hamiltonian (2) is also quasi-periodic. This means that, if all these peturbations are small enough and some generic conditions hold, a version of the KAM theorem [8, 9] can be used to ensure the existence of plenty of quasi-periodic motions for a particle between the two shepherd moons. As these conditions are very difficult to check in this model, we will use numerical simulations to study the dynamics of a test particle.

Therefore, let us define the conditions for escape: We consider that a test particle escapes if it leaves the region defined by the orbits of the shepherds, i.e., if it is not located within the region defined by innermost radial position of Prometheus' orbit and the outermost of Pandora's. In addition, a test particle is said to collide if it is located within Hill's radius of a shepherd moon, that is, $r_i < R_{H_i} = a_i (m_i/3m_0)^{1/3}$ (with $i = 1, 2$ for Prometheus and Pandora respectively). In this case, the test particle will be treated as an escaping particle, since such an event corresponds to a physical collision with one of the shepherds [15]. In either case, the integration of the orbit shall be terminated and the test particle is disregarded. On the other hand, if the test particle does not fulfill any of these requirements before the end of the numerical integration at t_{end}, the test particle is considered to be trapped and, in that sense, a particle of the ring. We shall see below that an additional criterion related to the stability properties of the orbits and the possibility to escape must be imposed.

In the following, mass units shall be expressed in terms of Saturn's mass M_S, distances in terms Saturn's equatorial radius R_S, and time is given in terms of $T_{\text{Prom}} = T_1 = 2\pi$, which corresponds to a full Kepler period of Prometheus.

3 Numerical Results

A dynamical problem is fully defined once the initial conditions are set. Since we are interested in the dynamics of the test particles, we shall fix the initial conditions of the massive bodies, and consider a region of the phase space for the test particles; different initial conditions correspond to independent test particles. The initial conditions of the test particles are defined by the initial semi-major axis a, the eccentricity e, and two angles defining the initial orientation of the instantaneous precessing ellipse ω, the argument of pericenter, and the position along the ellipse ϕ, the true anomaly. In the following we shall focus in the phase-space region defined by $a \in [2.318\, R_S, 2.345\, R_S]$, $e \in [0, 0.00145]$ and $\phi, \omega \in [-\pi, \pi]$. We note that this region in phase space, after projection into the coordinate space, spans the (planar) region between the orbits of Prometheus and Pandora. Therefore, this region includes the orbital elements compatible to particles belonging to Saturn's F ring, but is not restricted to those orbital elements only.

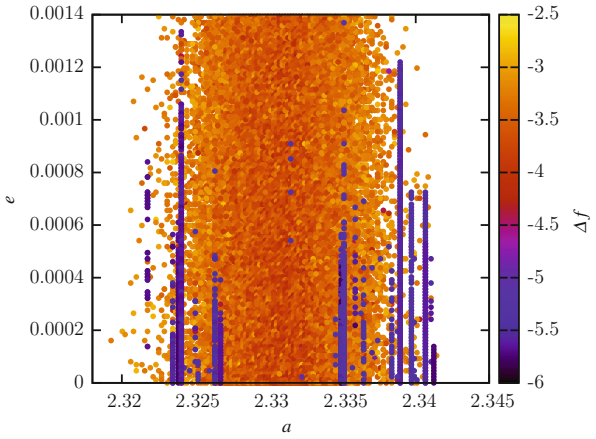

Fig. 1 Projection into the semi-major axis vs eccentricity plane of the initial conditions of test particles that remain trapped at least for $t_{\text{end}} = 2.4 \times 10^6 T_1$. The color code is the stability index Δf in logarithmic scale associated to the mean motion. Notice that there are two localized regions where the particles exhibit an enhancement of the stability index (*blue stripes*)

The numerical results presented below have been computed using a high-order Taylor's method (maximum order of the Taylor expansion is 28) for the numerical integration; see [10] for details on the method. The accuracy of the integrations is such that the energy and the angular momentum of Titan's Kepler motion is conserved to machine precision throughout the integration.

Figure 1 shows the projection into the initial semi-major axis a and eccentricity e plane of test particles that remain trapped at least for $t_{\text{end}} = 2.4 \times 10^6$ periods of Prometheus. In these simulations, the orientation of the initial Kepler ellipses was varied considering 10 equally spaced values, while the true anomaly was set to 0; the semi-major axis and the eccentricity were set on a grid of 256 points for each value of ω. The results in Fig. 1 show that the particles that remain trapped still form a wide and seemingly connected region of both a and e. The result seems deceiving: While the inclusion of Titan in the model foments further collisions with the shepherds, it does not yield a narrow ring that could be compared with the observations, at least after the end of the integration considered. However, contrary to the $(3 + 1)$-body model (the shepherd moons and Saturn), in the present case the trapped test particles do not a priori move along essentially stable precessing Kepler ellipses, due to the presence of Titan. Indeed, since the motion of Titan is eccentric, there is no conserved quantity similar to the Jacobi integral in the circular restricted three-body problem. Then, the eccentric motion of Titan allows test particles to explore radially more extended regions, and thus allows them to fulfill one of the conditions to escape. As we shall see below, some test particles happen to explore radially more extended regions than others; we shall argue that these are particles that eventually escape.

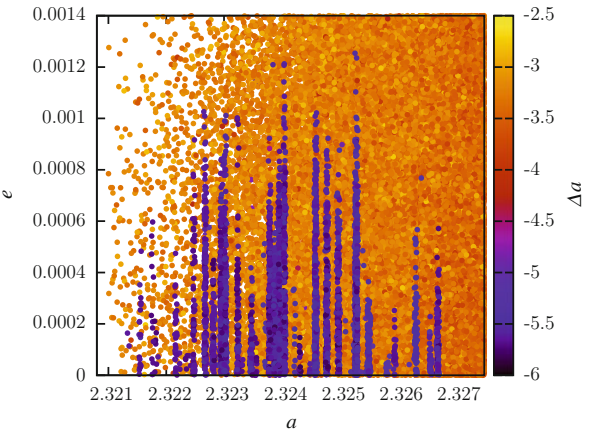

Fig. 2 Same as Fig. 1 for test particles that remain trapped at least for $t_{\text{end}} = 3.2 \times 10^6 T_1$ close to the observed semi-major axis for Saturn's F ring. In this case, the color code corresponds to base-10 logarithm of the stability index Δa constructed with respect to the mean semi-major axis

It is in this sense that we address the stability properties of the test particles that remain trapped, and consider a frequency type analysis [11, 12]. More specifically, motivated from the fact that the motion of the test particle is a small perturbation from an integrable system (the Kepler problem with flattening), we study the stability index defined by the ratio of the standard deviation of a frequency and its average value, computed along the whole trajectory; in particular, we consider the stability index associated to the mean motion $\Delta f = \sigma_f / \overline{f}$. In terms of Δf, quasi-periodic motion yields $\Delta f = 0$; hence, non-zero values of Δf indicate a departure from stable (quasi-periodic) motion.

From the numerical integration of the orbits, we compute the main frequencies of the motion every 200 revolutions of Prometheus using a collocation method [6], from which $\overline{f}$ and σ_f are calculated whenever the test particle remains trapped. The color code in Fig. 1 is based on $\log_{10}(\Delta f)$. Figure 1 displays some vertical blue-violet stripes localized around $a \sim 2.324$ and $a \sim 2.340$, where the particles exhibit an enhancement of the stability index ($\Delta f \sim 10^{-5}$) in comparison to the rest of the trapped particles, i.e. roughly two orders of magnitude. Interestingly, the first group of blue-violet stripes quoted above lies close to the nominal semi-major axis of Saturn's F ring; Fig. 2 displays more extended ($t_{\text{end}} = 3.2 \times 10^6 T_1$) and detailed simulations focusing on this region, where the initial angles of the test particles are chosen at random. The logarithmic color code in Fig. 2 is defined now through the stability index Δa associated to the mean semi-major axis of the orbit (during 200 revolutions of Prometheus), which is a measure of the radial excursion performed by test particles up to t_{end}.

Groups of localized (blue-violet) stripes can again be distinguished in Fig. 2 among the trapped orbits; our simulations suggest that there is no particular, or only a weak dependence, on the initial angles for these test particles. We observe

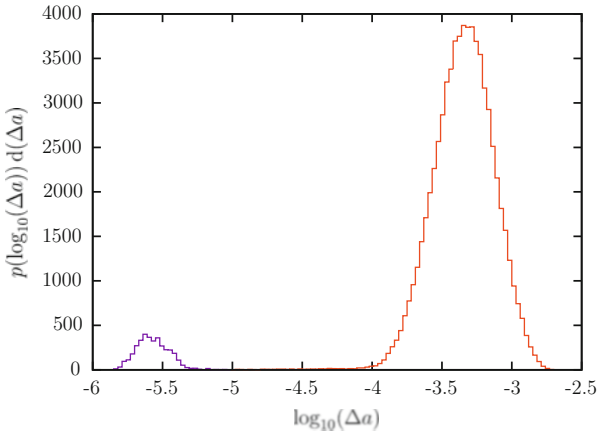

Fig. 3 Frequency histogram of $\log_{10}(\Delta a)$ for the data used for Fig. 2; the normalization corresponds to the total number of trapped test particles. Note that Δa is clearly separated in two disjoint ranges

that according to the stability index Δa, the trapped test particles display two well-separated scales, which correspond to radial excursions of few kilometers and few hundreds of kilometers. This is illustrated in Fig. 3 where we show the frequency histogram of $\log_{10}(\Delta a)$ for the data used in Fig. 2.

We interpret the results of Fig. 3 as follows: A test particle moves along a perturbed precessing ellipse; the orbit displays an additional but quite limited radial excursion due to Titan's interaction. Titan's eccentric orbit may create conditions which permit, in a rather short-time scale, an abrupt change in the semi-major axis and eccentricity, which in turn results in more extended radial excursion of the orbit. This increment of the radial excursion may provide eventually the conditions for the escape of the test particle; in our simulations, this corresponds typically to a collision with one of the shepherd moons. Test particles that experience these events but are still trapped at time t_{end} are those that correspond to the orange–yellow points in Figs. 1 and 2. The blue-violet dots correspond to test particles that may have experienced very few or even none abrupt changes in their semi-major and eccentricity values; therefore, the associated value of Δa is very small.

According to this interpretation, it is a question of time that the test particles belonging to the orange–yellow region will eventually escape. Note that this does not exclude that test particles with very small values of Δa finally escape, but suggests that the time required may be comparatively longer. The structure of Fig. 3 suggests to filter the trapped test particles according to the stability index, and retain only those particles whose stability index is small enough. In particular, we shall consider as ring particles those that satisfy the criterion $\Delta a < 10^{-5}$.

Using this filtering, we present in Fig. 4 a snapshot of the ring obtained close to the nominal location of Saturn's F ring. The ring is clearly narrow, eccentric and displays sharp edges. Fitting a Keplerian ellipse to the data used in Fig. 4

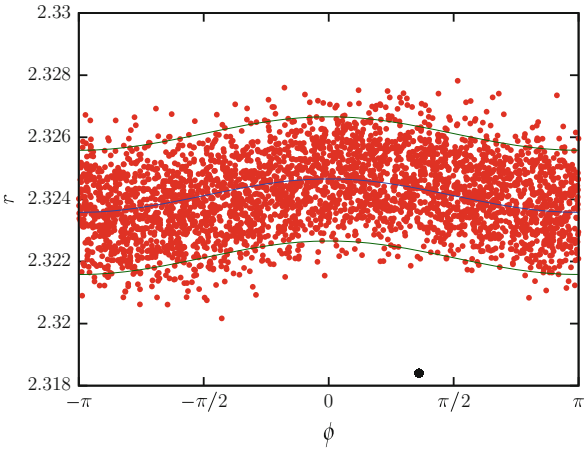

Fig. 4 Snapshot of the ring particles after filtering near the end of our simulations. The x-axis is the azimuthal angle, and the y-axis is the radial location. The *blue middle line* represents the best-fit of the particles of the ring to a Keplerian ellipse; the *outer lines* correspond the same ellipse shifted upwards or downwards by 0.002 R_S and serve to obtain a rough estimate of the width of the ring. The *black dot* close to the *bottom-right* of the figure is Prometheus

we obtain estimates for the semi-major axis $a_{\text{fit}} \approx 2.3241\, R_S$ and the eccentricity $e_{\text{fit}} \approx 2.32 \times 10^{-4}$. A rough estimate for the width of the ring is obtained by shifting radially this Keplerian ellipse; we obtain that within a width $\delta r \lesssim 0.005\, R_S \approx$ 300 km contains more than 90 % of the ring particles. There is indeed a remarkable correspondence of these values with the observations for Saturn's F ring. Yet, we must emphasize that this a posteriori consistency check of comparing our results with the observational data is not a proof of the dynamical consistency of the filtering; only longer numerical integrations, which are quite time consuming, can prove or disprove if the filtered test particles indeed escape. With this proviso, the result is quite rewarding.

4 Discussion

In this paper, we have introduced a simple (4 + 1)-body model for Saturn's F ring, consisting of four bodies (Saturn, Prometheus, Pandora and Titan) which influence the dynamics of a massless test-particle. The model includes the flattening of Saturn through its second zonal coefficient J_2. We argue that a realistic model for the understanding of the confinement and stability of Saturn's F ring requires at least to include these interactions. We found that after long integration times ($t_{\text{end}} = 3.2 \times 10^6 T_1$) there is a wide region in the initial conditions plane (a vs e, essentially independent of the initial angles) which remain trapped. These test particles show a separation of scales (about two orders of magnitude) with respect to a stability index defined as the ratio Δf of the standard deviation of the mean-motion frequency to its average value; the frequencies are computed during a fixed interval of time $200 T_1$ and the average is performed including all the orbital data. Similar results are obtained for a related indicator Δa, defined on the mean semi-major axis, which is a measure of the radial excursion of the orbit of the test

particle during the integration time. In the initial condition plane, the regions of enhanced stability appear as localized stripes immersed in a wide region of trapped test particles.

We have argued that test particles with larger values of Δf or Δa eventually escape from the neighborhood of the ring, or simply collide with one of the shepherds. By filtering out those test particles which are not too stable according to the stability index, we end up with a set of particles that form a narrow ring in the vicinity of the observed Saturn's F ring. Beside being narrow, the ring obtained is eccentric and displays sharp edges. Our estimates for the semi-major axis, eccentricity and width of the ring agree with the observational data. Although the filtering has to be further validated by longer integrations of the orbits, we claim that this model including the stability with respect to escapes may help to understand the confinement of Saturn's F ring as well as some of its structural properties. The basic dynamical mechanism is related to the existence of invariant structures of the dynamics which build transport barriers that effectively trap and confine the particles of the ring; test particles that in our simulations remain trapped but do not survive the filtering procedure, are particles whose dynamics is very slowly drifting away by exploring radially more extended regions, until they eventually collide with one of the shepherd moons. Note that this mechanism explains dynamically the confinement of Saturn's F ring: the organizing object which gives rise to the confining invariant structures explains the observed semi-major axis and eccentricity; the invariant structures which are barriers for the ring particles explain the sharp edges observed in the ring.

Acknowledgements This work was initiated during LB's sabbatical year at the Universitat de Barcelona, which was partially supported by DGAPA (UNAM) and Min. Educación (SAB2010-0123, Spain). We acknowledge financial support provided by the projects IN–110110 (DGAPA–UNAM), 79988 and 144684 (CONACyT), 334309729-9729-4-9 (Min. Ciencia e Innovación), MTM2009-09723 (Min. Ciencia e Innovación) and 2009 SGR 67 (Generalitat de Catalunya). It is a pleasure to thank Carles Simó for his encouragement, valuable comments, questions and discussions.

References

1. Benet, L., Seligman, T.H.: Generic occurrence of rings in rotating scattering systems. Phys. Lett. A **273**, 331–337 (2000)
2. Charnoz, S., Dones, L., Esposito, L.W., Estrada, P.R., Hedman, M.M.: Origin and evolution of Saturn's ring system. In: Dougherty, M.K., Esposito, L.W., Krimigis, S.M. (eds.) Saturn from Cassini-Huygens, pp. 537–575. Springer, Dordrecht (2009)
3. Esposito, L.W.: Planetary Rings. Cambridge University Press, Cambridge (2006)
4. French, R.G., McGhee, C.A., Dones, L., Lissauer, J.J.: Saturn's wayward shepherds: the peregrinations of Prometheus and Pandora. Icarus **162**, 143–160 (2003)
5. Goldreich, P., Tremaine, S.D.: Towards a theory for the Uranian rings. Nature **277**, 97–99 (1979)
6. Gómez, G., Mondelo, J.M., Simó, C.: A collocation method for the numerical Fourier analysis of quasiperiodic functions I: numerical tests and examples. DCDS Ser. B **14**, 41–74 (2010)

7. Jacobson, R.A., et al.: The gravity field of the Saturnian system from satellite observations and spacecraft tracking data. Astron. J. **132**, 2520 (2006)
8. Jorba, À., Simó, C.: On quasiperiodic perturbations of elliptic equilibrium points. SIAM J. Math. Anal. **27**, 1704–1737 (1996)
9. Jorba, À., Villanueva, J.: On the persistence of lower dimensional invariant tori under quasi-periodic perturbations. J. Nonlinear Sci. **7**, 427–473 (1997)
10. Jorba, À., Zou, M.: A software package for the numerical integration of ODE by means of high-order Taylor methods. Exp. Math. **14**, 99–117 (2005)
11. Laskar, J.: The chaotic behavior of the solar system: a numerical estimate of the chaotic zones. Icarus **88**, 266–291 (1992)
12. Laskar, J.: Introduction to frequency map analysis. In: Simó, C. (ed) Hamiltonian Systems with Three or More Degrees of Freedom. NATO Advanced Science Institutes Series C: Mathematical and Physical Sciences, vol. 533, pp. 134–150. Kluwer, Dordrecht (1999)
13. Merlo, O., Benet, L.: Strands and braids in narrow planetary rings: a scattering system approach. Celest. Mech. Dyn. Astron. **97**, 49–72 (2007)
14. Murray, C.D., Beurle, K., Cooper, N.J., Evans, M.W., Williams G.A., Charnoz, S.: The determination of the structure of Saturn's F ring by neraby moonlets. Nature **453**, 739–744 (2008)
15. Ohtsuki, K.: Capture probability of colliding planetesimals – dynamical constraints on accretion of planets, satellites, and ring particles. Icarus **106**, 228–246 (1993)
16. Poulet, F., Sicardy, B., Nicholson, P.D., Karkoschka, E., Caldwell, J.: Saturn's ring-plane crossings of August and November 1995: a model for the new F-ring objects. Icarus **144**, 135–148 (2000)
17. Seidelmann, P.K., et al.: Report of the IAU/IAG working group on cartographic coordinates and rotational elements: 2006. Celest. Mech. Dyn. Astron. **98**, 155–180 (2007)

Analysis of the Full Vibrational Dynamics of the LiNC/LiCN Molecular System

P. Benítez, J.C. Losada, R.M. Benito, and F. Borondo

Abstract A study of the LiNC/LiCN triatomic molecule vibrational dynamics including all three degrees of freedom (dof) using Frequency Map and Small Alignment Index (SALI) analysis is presented. SALI maps are computed as two-dimensional phase space representations, where its asymptotic values are represented in a color scale. These maps provide full information on the dynamical phase space structure of the system, regardless of its dimensionality. SALI results for the 3dof LiNC/LiCN are compared with 2dof results previously reported for this molecule by our group. A representation of the SALI values on the frequency space, that allows a deeper analysis of the dynamics of the system, is also studied.

1 Introduction

The vibrational dynamic processes that occur in single isolated, usually gas phase, molecules are critical to determine their reactivity, which is the ultimate goal of Chemistry. Identifying the vibrational modes that are coupled in an efficient manner, typically through Fermi resonances, and how energy flows through them, is a central problem in Molecular Dynamics [1].

P. Benítez (✉) · J.C. Losada · R.M. Benito
Grupo de Sistemas Complejos, and Departamento de Física y Mecánica, Escuela Técnica Superior de Ingenieros Agrónomos, Universidad Politécnica de Madrid, E-28040 Madrid, Spain
e-mail: pbenitezgamero@gmail.com; juancarlos.losada@upm.es; rosamaria.benito@upm.es

F. Borondo
Departamento de Química, and Instituto de Ciencias Matemáticas (ICMAT), Universidad Autónoma de Madrid, Cantoblanco, E-28049 Madrid, Spain
e-mail: f.borondo@uam.es

S. Ibáñez et al. (eds.), *Progress and Challenges in Dynamical Systems*,
Springer Proceedings in Mathematics & Statistics 54,
DOI 10.1007/978-3-642-38830-9_6,

For 2dof systems, there are well established mathematical tools to study the underlying dynamics. Poincaré surfaces of Sections (SOS) is probably the most straightforward and informative one, although there are other equally good possibilities, such as local Lyapunov exponents, Kolmogorov entropies, etc., to obtain a complete picture of the associated dynamics.

On the other hand, when the system has more than 2dof, the SOS is not longer a computationally feasible possibility, and other more powerful methods [2], such as the Frequency Map (FM) analysis [3] or the Small Alignment Index (SALI) method [4,5] should be used instead. In recent years, atomic and molecular systems with 3dof have been successfully studied by FM [6, 7]. The FM is able to easily distinguish the regular and chaotic areas of phase space, and indications of diffusion on the web formed by resonance lines in the frequency space can also be seen. A complementary study based on the idea of analyzing the separation of nearby orbits, is the calculation of SALIs, which rely on the study the behavior of the associated vectors, that can be easily calculated from the (numerical) integration of Hamilton's equations, regardless of the number of dimensions involved. The SALI value tends rapidly to zero with time (actually $SALI(t) \sim e^{\alpha t}$ with $\alpha < 0$) when the trajectory is chaotic.

In this contribution, we present a study of the vibrational dynamics for the LiNC/LiCN molecular system with 3dof, using FM and SALI as dynamical indicators.

The organization of this chapter is as follows. In Sect. 2, we briefly present the model used to describe LiNC/LiCN. In Sect. 3, we review the calculational procedure involved in the SALI and FM analysis. The results obtained in our study are presented and discussed in Sect. 4. Finally, in Sect. 5 we summarize the main conclusions obtained in this work.

2 The LiNC/LiCN Molecular System

The LiNC/LiCN isomerizing system presents two stable isomers at the linear configurations: Li–N–C and Li–C–N, which are separated by a relatively modest energy barrier of only 0.0157376 a.u. (3,434.0 cm^{-1}). The motion in the bending coordinate is very floppy, and then the Li atom can easily explore ample, yet anharmonic, regions of the potential energy surface, even rotating around the C–N fragment. In this way, chaos sets in at low values of the excitation energy.

Using scattering or Jacobi coordinates (R, r, θ), where R is the distance from the Li atom to the center of mass of the CN fragment, r the C–N distance, and θ the angle formed by these two vectors, the corresponding classical vibrational ($J = 0$) Hamiltonian is given by

$$H = \frac{P_R^2}{2\mu_{Li-CN}} + \frac{P_r^2}{2\mu_{C-N}} + \frac{1}{2}\left(\frac{1}{\mu_{Li-CN}R^2} + \frac{1}{\mu_{C-N}r^2}\right)P_\theta^2 + V(R, r, \theta). \tag{1}$$

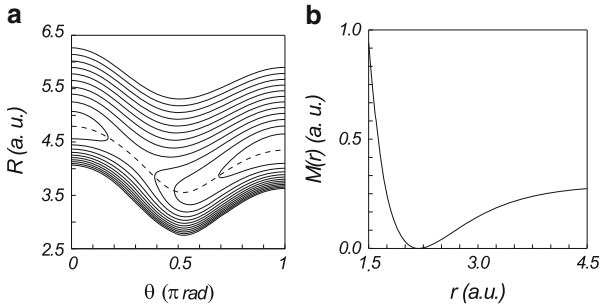

Fig. 1 Potential energy surface, $V(R, r, \theta) = v(R, \theta) + M(r)$, for the LiNC/LiCN isomerizing system: (**a**) Contours plot of $v(R, \theta)$. The minimum energy path, $R_e(\theta)$, connecting the two stable isomers, LiCN ($\theta = 0$) and LiNC ($\theta = \pi$ rad), is shown as a *dashed line*. (**b**) The Morse function, $M(r)$, corresponding to the CN contribution to the potential energy

The vibrational frequency of the C–N motion is very high, and then this mode is not highly coupled with the other vibrations in the molecule. Furthermore, the corresponding potential energy surface can be written in the form

$$V(R, r, \theta) = v(R, \theta) + M(r), \tag{2}$$

where $v(R, \theta)$ represents the potential interaction of the molecule for a fixed value of the r coordinate, and $M(r)$ is the interaction of the C–N fragment. In our case, we take the $v(R, \theta)$ contribution from the literature [8], where it has been reported as an analytical expansion in terms of Legendre polynomials,

$$v(R, \theta) = \sum_{\lambda=1}^{9} a_\lambda(R) P_\lambda(\theta), \tag{3}$$

whose coefficients were fitted to ab initio quantum mechanical calculations performed with the CN distance frozen at its equilibrium value, $r_e = 2.186$ a.u. This function has two wells at the linear configurations, $\theta = 0$ for Li–CN and $\theta = \pi$ for Li–NC, being the latter the most stable one. It is presented in Fig. 1a in the form of a contours plot, along with the minimum energy path (MEP), $R_e(\theta)$, connecting the two isomer wells. To describe the C–N interaction, the Morse function,

$$M(r) = D\{1 - \exp[-\beta(r - r_e)]\}^2, \tag{4}$$

is used in Eq. (2) to account for the r dependence of the potential function (see Fig. 1b). The parameters $D = 0.29135$ a.u. and $\beta = 1.4988$ a.u.$^{-1}$ are directly related to the depth and width of the CN potential well.

3 Computational Procedure

3.1 Trajectory Calculations and Frequency Analysis

Classical trajectories for our system are calculated by numerical integration of the Hamilton's equations of motion corresponding to Eq. (1), getting in this way the time series: $r(t)$, $P_r(t)$, $\theta(t)$, $P_\theta(t)$, $R(t)$, and $P_R(t)$. The vibrational dynamics associated with the isomerization LiNC⇌LiCN process can be adequately followed by monitoring the motion along the angular θ coordinate.

For comparison and to deeply understand the performance of the SALI method in the study of the molecular system, we will also use (in the 2dof model) the more established procedure of Poincaré SOS, and also to select initial conditions in the phase space. The simpler dimensionality reduced 2dof model, where the C–N as distance is kept frozen at its equilibrium value, $r = r_e$, has been extensively considered in the literature [9–11]. In it, Poincaré SOSs were used to extract the dynamical information of the system. For each trajectory a SOS is computed by taking the sectioning coordinate to lie along the minimum energy path connecting the two isomers,

$$\begin{aligned} R_e(\theta) = & \, 4.1159 + 0.25510 \, \cos\theta + 0.49830 \, \cos 2\theta \\ & + 0.053427 \, \cos 3\theta - 0.068124 \, \cos 4\theta \\ & + 0.020578 \, \cos 5\theta \end{aligned} \tag{5}$$

in atomic units. In order to make the SOS an area preserving map, the following canonical transformation [10] is performed

$$\begin{aligned} \rho &= R - R_e(\theta), \\ \psi &= \theta, \\ P_\rho &= P_R, \\ P_\psi &= P_\theta + \left(\frac{\mathrm{d}R_e}{\mathrm{d}\theta} \right)_{\theta=\psi} P_R. \end{aligned} \tag{6}$$

The fundamental frequencies of the system (ν_r, ν_R, ν_ψ) have also been obtained by the application of the FA, as implemented by Laskar [3], to the complex functions

$$\begin{aligned} f_R(t) &= R(t) + \mathrm{i} \, P_R(t), \\ f_r(t) &= r(t) + \mathrm{i} \, P_r(t), \\ f_\theta(t) &= \theta(t) + \mathrm{i} \, P_\theta(t), \end{aligned} \tag{7}$$

and choosing the frequency with biggest amplitude for each function. The FM is then defined as

$$\begin{aligned} \mathbf{FM} : B \in \mathbb{R}^6 & \longrightarrow \Omega \in \mathbb{R}^2 \\ \left(R^0, r^0, \psi^0, P_R^0, P_r^0, P_\psi^0 \right) & \longrightarrow \left(\frac{\nu_\psi}{\nu_R}, \frac{\nu_r}{\nu_R} \right), \end{aligned} \tag{8}$$

where B is the domain of initial conditions, and Ω are the frequencies obtained by FA. Here, we select the initial conditions on the section plane of the Poincaré SOS of the 2D system (P_ψ, ψ), i.e.:

$$\begin{aligned} \psi(0) &= \psi, \\ r(0) &= r_e, \\ R(0) &= R_e(\theta), \\ P_\psi(0) &= P_\psi, \\ P_r(0) &= 0, \\ P_R(0) &= g(E, \psi, r, R, P_\psi, P_r), \end{aligned} \tag{9}$$

where E is the total vibrational energy of the system.

This method has been used successfully before in our group for the study of the vibrational dynamics of triatomic molecules [6, 7, 12–14].

3.2 SALI Calculation

Given a reference trajectory, the SALI is an index able to study the behavior of the nearby trajectories associated vectors, that can indeed be easily calculated after results simply obtained from trajectory propagation. As indicated before it can be used in any system to ascertain its dynamical characteristics, regardless of the involved number of dimensions [4, 5].

The procedure is as follows. For each trajectory, we compute the deviation vectors with two nearby trajectories, and their corresponding unit vectors, in the following way.

Let us define $\mathbf{z} = (q_1, \ldots, q_N, p_1, \ldots, p_N)$ as one trajectory in an otherwise generic Hamiltonian of N dimensions. The corresponding Hamilton's equations of motion are written in symplectic form as

$$\dot{\mathbf{z}} = J \frac{\partial H}{\partial \mathbf{z}} = J \nabla H \tag{10}$$

where the matrix J is given by

$$J = \begin{bmatrix} 0_N & I_N \\ -I_N & 0_N \end{bmatrix} \tag{11}$$

Let us consider now two nearby trajectories $\mathbf{z}_{1,2}$, as shown in Fig. 2. The time evolution of the corresponding deviation vectors, $\mathbf{v}_{1,2} = \mathbf{z}_{1,2} - \mathbf{z}$, can then be calculated using the equations of motion, (Eq. (10)), of the two vectors $\mathbf{z}_{1,2}$

$$\dot{\mathbf{z}}_{1,2} \equiv \frac{d(\mathbf{z} + \mathbf{v})}{dt} = J \frac{\partial H(\mathbf{z} + \mathbf{v})}{\partial \mathbf{z}}. \tag{12}$$

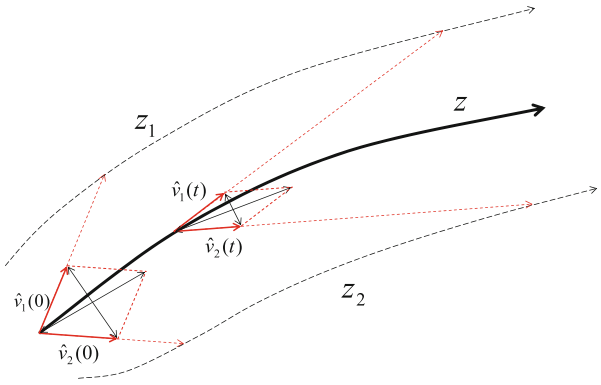

Fig. 2 Graphical illustration on how the sum and difference of two vectors nearby a reference trajectory are calculated

Now by Taylor expanding H up to first order (then assuming $\mathbf{v}$ small)

$$\dot{\mathbf{z}} + \dot{\mathbf{v}} = J \frac{\partial}{\partial \mathbf{z}} \left[H + \frac{\partial H}{\partial \mathbf{z}} \mathbf{v} \right], \tag{13}$$

and taking Eq. (10) into account, one obtains

$$\dot{\mathbf{v}} = J \frac{\partial^2 H}{\partial \mathbf{z}^2} \mathbf{v} = J \nabla^2 H \mathbf{v}. \tag{14}$$

Then by simultaneously (numerically) solving Eqs. (10) and (14) for a given set of initials conditions, both the reference trajectory and the associated values of the deviation vectors of the two nearby orbits are obtained. As can be seen in Fig. 2, the romboid formed by the two deviation vectors changes form with time, in such a way that when there exists an exponential separation in the trajectories, i.e. there is chaos, one of the axis quickly goes to zero.

The SALI indicator is then defined, as

$$SALI(t) = \min \left(|\hat{\mathbf{v}}_1 + \hat{\mathbf{v}}_2| , |\hat{\mathbf{v}}_1 - \hat{\mathbf{v}}_2| \right) \tag{15}$$

where $\hat{\mathbf{v}}$ is the unit vector in the direction of vector $\mathbf{v}$. In Ref. [4] it is shown how expression (15) evolves as $SALI(t) \sim e^{\alpha t}$ with $\alpha < 0$ if the reference trajectory is chaotic, while it oscillates around a constant value if it is regular. Accordingly, by taking a sufficiently long evolution time t, the value of the SALI can be taken as a good indicator of the dynamical character of the reference trajectory.

Some typical results for the 2dof model of LiNC/LiCN are shown in Fig. 3. In it, we present the trajectories in the $R - \theta$ configuration space (left), the corresponding (ψ, P_ψ) SOS (center), and the time evolution of the SALI indicators (right) for three different types of orbits – resonant (top), quasiperiodic (middle), and chaotic

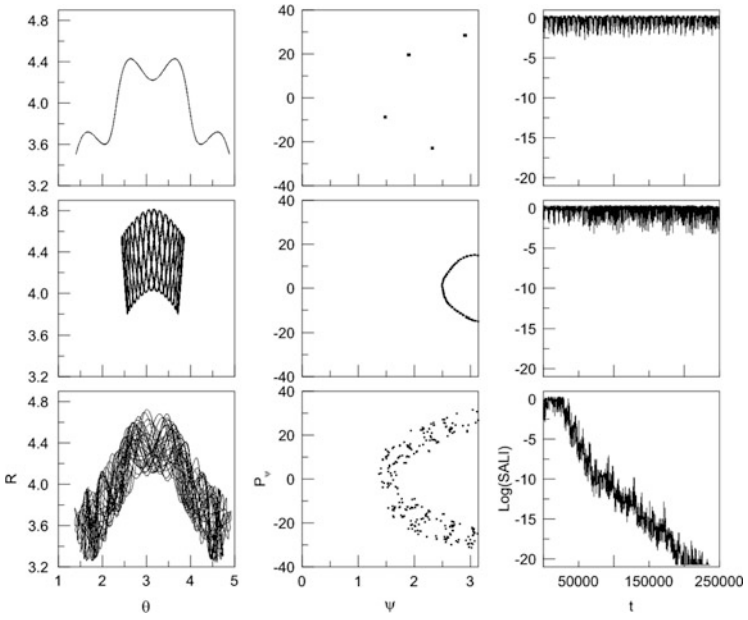

Fig. 3 Trajectories (*left column*), (ψ, P_ψ) Poincaré surfaces of section (*center column*) computed by taking the sectioning coordinate to lie along the minimum energy path, and time evolutions of the SALI (*right column*) for three different types of orbits – resonant (*top*), quasiperiodic (*middle*), and chaotic (*bottom*) – for the 2dof model for LiNC/LiCN described in Sect. 2 at an excitation energy of $E = 2{,}549.2\,\mathrm{cm}^{-1}$. The corresponding initial conditions, that have been taken on the surface of section, are: $(\psi, P_\psi) = (2.9, 28.15)$, $(2.5, 0.0)$, and $(2.3, 15.0)$ in (rad, a.u.) for the resonant, quasiperiodic, and chaotic cases, respectively

(bottom) – at an excitation energy of $E = 2{,}549.2\,\mathrm{cm}^{-1}$. As can be seen, the SALI decays much faster (between 15 to 20 orders of magnitude for the time span considered in the calculation) for the chaotic trajectory as compared to the other regular ones. Also, it is apparent that the SALI decay is (slightly) larger in the quasiperiodic case than for the resonant motion.

4 Results and Discussion

4.1 SALI Maps for the 2dof LiNC/LiCN Model

In Fig. 4 some results for the vibrational dynamics of the 2dof LiNC/LiCN model described in Sect. 2 are shown in the form of SALI maps (right column). They consist of 2D representations of the phase space where the asymptotic value of the SALI is represented with a scale of greys (depicted in the lower right part of the

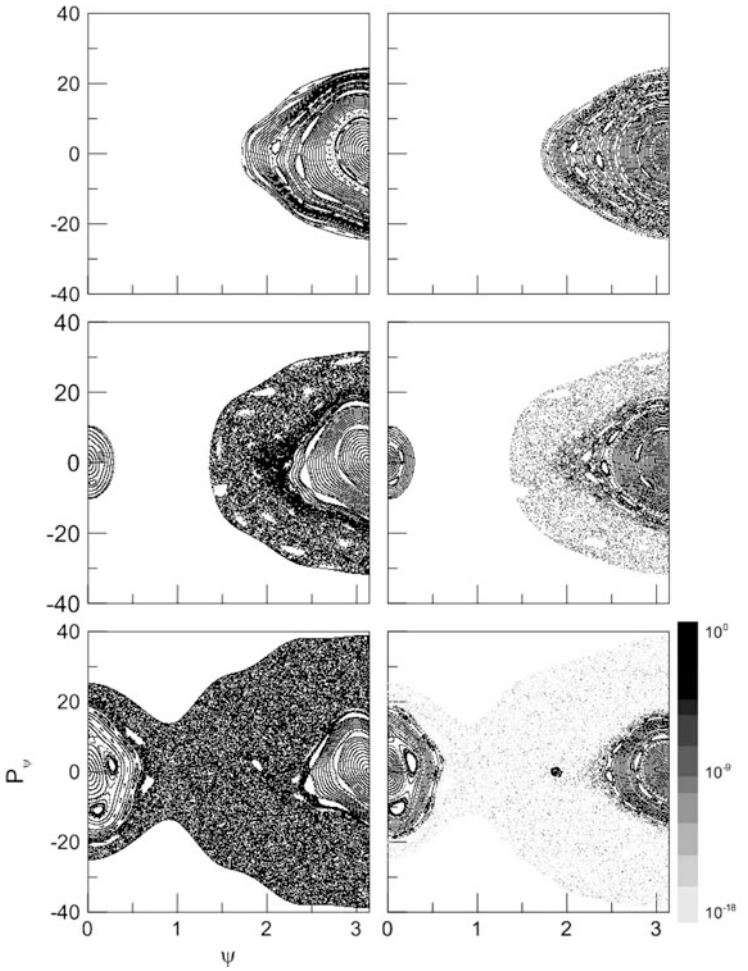

Fig. 4 (ψ, P_ψ) Poincaré surfaces of section computed by taking the sectioning coordinate to lie along the minimum energy path (*left column*), and SALI map (*right column*) at different values of the vibrational energy: $E = 1{,}510.5$ (*top*), 2,964.7 (*middle*), and 3,823.8 cm^{-1} (*bottom*). In the SALI map a logarithmic scale of greys (also shown in the lower right part of the plots) has been used

plot), ranging from black and dark grey for the most regular areas to light grey for the chaotic. To help in the discussion, we also show (left column) the corresponding (ψ, P_ψ) Poincaré SOS computed at the same energy. Trajectories are started over a fine mesh of initial conditions on the SOS and propagated for the same lapse of time, at three different values of the excitation energy. The first one, $E = 1{,}510.5\,\mathrm{cm}^{-1}$, is relatively low and, as can be seen in the SOS, most of the dynamics are regular, taking place around the well corresponding to the (LiNC) most stable isomer. In the middle row, some results for a much larger value of the energy, $E = 2{,}964.7\,\mathrm{cm}^{-1}$,

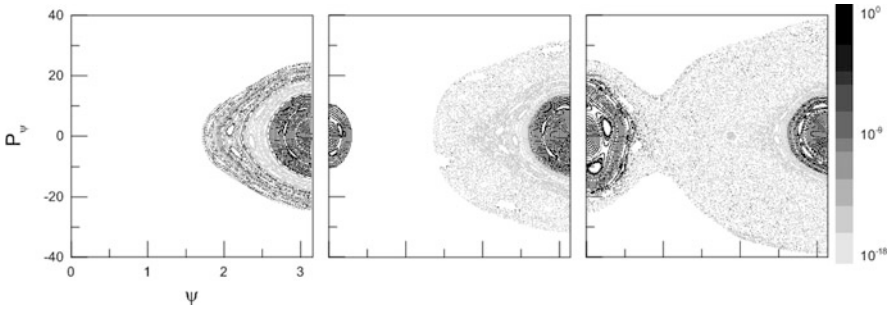

Fig. 5 SALI map for the 3dof model of LiNC/LiCN isomerizing system computed for a set of initial conditions on the 2dof Poincaré surface of section and $r = r_e$, $P_r = 0$, for three different values of the vibrational energy: $E = 1{,}510.5$ (*top*), 2,964.7 (*middle*), and 3,823.8 cm^{-1} (*bottom*). The scale of greys used is shown in the right part of the plot

are shown. Here, motion in the less stable isomer, LiCN, is classically accessible, and there are large regions of the phase space corresponding to the LiNC well, in which chaotic motions take place. Finally, in the bottom panel, an even larger energy of 3,823.8 cm^{-1} is considered. Here, the dynamics become more chaotic and isomerizing/rotating orbits, in which the Li atom rotates around the CN fragment connecting the two potential wells, do exist. The results obtained with the SALI provide essentially the same information. At the wells the darker color indicates that the dynamics are regular. As energy increases more lighter grey areas are visible indicating a fast decrease in the SALI associated with chaotic motions. Even the small island of regularity in the middle of the chaotic sea at $E = 3{,}823.8\,\text{cm}^{-1}$ is visible as a dark area in the SALI map.

4.2 SALI Maps for the Full Dimensional Vibrational Dynamics of the LiNC/LiCN Molecule

In Fig. 5 we present the SALI maps at the same vibrational energies considered in the previous section for the full 3dof dynamics of LiNC/LiCN. Also, a grid of initial conditions consistent with that study has been computed with the aid of Eqs. (9). In this way, we can observe how the structure of the phase space changes with the inclusion of the extra vibrational dof.

The 3dof SALI maps, when compared with those presented in the previous section for the 2dof case, show that the dynamics is now, in general, more chaotic, i.e., the motion in the extra coordinate makes it more unstable. This is specially clear in the first two plots (lowest energies considered). The most interesting result appears at the lowest energy (left plot), where a conspicuous band of lighter color is visible in the middle of the regular area. The corresponding SALI values are not as low as in the fully chaotic case, but are nevertheless much smaller than those found

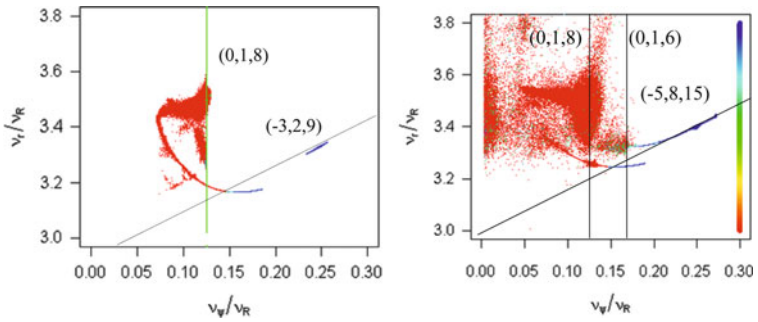

Fig. 6 SALI frequency map for the 3dof model of LiNC/LiCN for a grid of initial conditions chosen in the Poincaré surface of section and $r = r_e, P_r = 0$, at two values of the vibrational energy: $E = 2{,}964.7$ (*left*), and $3{,}823.8\,\mathrm{cm}^{-1}$ (*right*). The color scale, ranging from *red* (chaotic) to *blue* (regular) is shown at the *right*

in the surrounding regular areas of phase space. The reason for the existence of this more irregular motion must be a resonance with the Morse natural frequency in the motion along the r coordinate. This resonance has not been identified at present but certainly deserves further investigation.

4.3 SALI Frequency Maps

Let us now consider the SALI frequency maps corresponding to a representation of SALI values, in color scale, done on the frequency space obtained by the FM. This combines the advantages of both methods, since the FM allows the complementary information involved in the Arnold web formed by the resonant lines of the system. In this way the regular and chaotic regions of phase space are much better defined. Moreover, when a uniform grid of initial conditions is used, any discontinuity of the corresponding phase space image in the frequency space is an indicator that chaotic motion is taking place.

In Fig. 6 we show the SALI frequency map for the 3dof model of LiNC/LiCN at the two highest values of the vibrational energy considered in the previous sections. In this case a color scale for the SALI, ranging from red (chaotic) to blue (regular) is used.

At the lowest energy considered (left plot) two blue lines, corresponding to regular motion, are observed. The rightmost one corresponds to the LiCN well while the other one represents motion of the LiNC isomer. This line (smoothly) turns red just before hitting the $\nu_r, \nu_R, \nu_\psi = (0, 1, 8)$ resonance, point at which ν_r raises considerably. This seems to indicate that the associated chaos is due to the r motion. At the highest energy considered (right plot) similar blue lines are observed, with a much widespread chaos, which evidently in this case involve motion in all coordinates.

5 Summary

To summarize, in this paper we have studied the vibrational dynamics of the LiNC/LiCN taking into account all vibrational dimensions of the system using the SALI indicator. To make this method more powerful we have combined it with the results of the FM analysis.

Our study shows that this method is able to discern when the motion is chaotic, even if this is not visible in the FM analysis. (In the latter, it is not always easy to detect discontinuities.) Moreover, the combination of the two techniques helps a lot to discern the role played by the motion in each coordinate in the global dynamics. The SALI alone is only able to tell, at most, that the motion is globally chaotic, without giving any further insight into this assertion.

Acknowledgements Support from MICINN-Spain under contract No. MTM2012-39101 is gratefully acknowledged.

References

1. Zewail, A. (ed.): The Chemical Bond: Structure and Dynamics. Academic, San Diego (1992)
2. Simó, C. (ed.): Hamiltonian Systems with Three or More Degrees of Freedom. NATO ASI Series C. Kluwer, Dordrecht (1999)
3. Laskar, J.: Frequency analysis for multi-dimensional systems. Global dynamics and diffusion. Phys. D **67**, 257 (1993)
4. Skokos, C., Antonopoulos, C., Bountis, T.C., Vrahatis, M.N.: Detecting order and chaos in Hamiltonian systems by the SALI method. J. Phys. A Math. Gen. **37**, 6269 (2004)
5. Skokos, C., Bountis, T.C., Antonopoulos, C.: Geometrical properties of local dynamics in Hamiltonian systems: the Generalized Alignment Index (GALI) method. Phys. D **231**, 30 (2007)
6. Losada, J.C., Giralda, C.G., Benito, R.M., Borondo, F.: Global dynamics of nonrigid triatomic molecular systems of three degrees of freedom. AIP Proc. **905**, 249 (2007)
7. Losada, J.C., Benito, R.M., Borondo, F.: Frequency map analysis of the 3D vibrational dynamics of the LiNC/LiCN molecular system. Eur. Phys. J. Spec. Top. **165**, 183 (2008)
8. Essers, R., Tennyson, J., Wormer, P.E.S.: An SCF potential energy surface for Lithium Cyanide. Chem. Phys. Lett. **89**, 223 (1982)
9. Henderson, J.R., Tennyson, J.: Very highly excited states of LiCN using a discrete variable representation. Mol. Phys. **69**, 639 (1990); Borondo, F., Gomez–Llorente, J.M., Benito, R.M.: Theoretical methods for the analysis of spectra of highly vibrationally excited polyatomic molecules. Laser Chem. **12**, 85 (1992); Borondo, F., Benito, R.M.: Dynamics and spectroscopy of highly excited molecules. In: Yurtsever, E. (ed.) Frontiers of Chemical Dynamics. NATO ASI Series C. Kluwer, Dordrecht, 1995; Prosmiti, R., Farantos, S.C., Guantes, R., Borondo, F., Benito, R.M.: A periodic orbit analysis od the vibrationally highly excited LiNC/LiCN: a comparison with quantum mechanics. J. Chem. Phys. **104**, 2921 (1996); Arranz, F.J., Borondo, F., Benito, R.M.: Transition from order to chaos in molecular wave functions and spectra. J. Chem. Phys. **104**, 6401 (1996); Arranz, F.J., Borondo, F., Benito, R.M.: Avoided crossings, scars and the transition to chaos. ibid. **107**, 2395 (1997); Probability density distributions in phase space. J. Mol. Struct. (Theochem) **426**, 87 (1998); Borondo, F., Zembekov, A.A., Benito, R.M.: Quantum manifestations of saddle node bifurcations.

Chem. Phys. Lett. **246**, 421 (1995); Saddle node bifurcations in the LiNC/LiCN molecular system. Classical aspects and quantum manifestations. J. Chem. Phys. **105**, 5068 (1996); Semiclassical quantization of fragmented tori: application to saddle-node states of LiNC/LiCN. ibid. **107**, 7934 (1997); Benito, R.M., Borondo, F.: Periodic orbits and quantum mechanics of molecular Hamiltonian systems. In: Simó, C. (ed.): Hamiltonian Systems with Three or More Degrees of Freedom. NATO ASI Series C, pp. 310–313. Kluwer, Dordrecht (1999); Borondo, F., Vergini, E.W., Zembekov, A.A., Benito, R.M.: Homoclinic motions in the vibrational spectra of floppy systems: the LiCN molecule. J. Chem. Phys. **122**, 11101 (2005)

10. Benito, R.M., Borondo, F., Kim, J.H., Sumpter, B.G., Ezra, G.S.: Comparison of classical and quantum phase space structure of non-rigid molecules: LiCN. Chem. Phys. Lett. **161**, 60 (1989)
11. Arranz, F.J., Borondo, F., Benito, R.M.: Scar formation at the edge of the chaotic region. Phys. Rev. Lett. **80**, 944 (1998)
12. Losada, J.C., Estebaranz, J.M., Benito, R.M., Borondo, F.: Local frequency analysis and the structure of classical phase space of the LiNC/LiCN molecular system. J. Chem. Phys. **108**, 63 (1998)
13. Safi, Z.S., Losada, J.C., Benito, R.M., Borondo, F.: Frequency analysis of the molecular vibrations of HCP. J. Chem. Phys. **129**, 164316 (2008)
14. Arranz, F.J., Seidel, L., Giralda, C.G., Benito, R.M., Borondo, F.: Zeros of the Husimi function and quantum numbers in the HCP molecule. Phys. Rev. E **82**(2), 026201 (2010)

Resonance and Singularities

Henk W. Broer and Gert Vegter

Abstract The phenomenon of resonance will be dealt with from the viewpoint of dynamical systems depending on parameters and their bifurcations. Resonance phenomena are associated to open subsets in the parameter space, while their complement corresponds to quasi-periodicity and chaos. The latter phenomena occur for parameter values in fractal sets of positive measure. We describe a universal phenomenon that plays an important role in modelling. This paper gives a summary of the background theory, veined by examples.

1 What Is Resonance?

A heuristic definition of resonance considers a dynamical system, usually depending on parameters, with several oscillatory subsystems having a rational ratio of frequencies and a resulting combined and compatible motion that may be amplified as well. Often the latter motion is also periodic, but it can be more complicated as will be shown below. We shall take a rather eclectic point of view, discussing several examples first. Later we shall turn to a number of universal cases, these are context-free models that occur generically in any system of sufficiently high-dimensional state and parameter space. Part of these results were announced in [14].

Among the examples are the famous problem of Huygens's synchronizing clocks and that of the Botafumeiro in the Cathedral of Santiago de Compostela, but also we briefly touch on tidal resonances in the planetary system. As universal models we shall deal with the Hopf–Neĭmark–Sacker bifurcation and the Hopf saddle-node bifurcation for mappings. The latter two examples form 'next cases' in the

H.W. Broer (✉) · G. Vegter
Johann Bernoulli Institute for Mathematics and Computer Science, University of Groningen,
PO Box 407, 9700 AK Groningen, The Netherlands
e-mail: h.w.broer@rug.nl

S. Ibáñez et al. (eds.), *Progress and Challenges in Dynamical Systems*,
Springer Proceedings in Mathematics & Statistics 54,
DOI 10.1007/978-3-642-38830-9_7,

development of generic bifurcation theory. The term *universal* refers to the context independence of their occurrence: in any with certain generic specifications these bifurcations occur in a persistent way. We witness an increase in complexity in the sense that in the parameter space the resonant phenomena correspond to an open & dense subset union of tongues, while in the complement of this a nowhere dense set of positive measure exists, corresponding to multi- or quasi-periodic dynamics. This nowhere dense set has a fractal geometry in a sense that will be explained later. From the above it follows that this global array of resonance tongues and fractal geometry has a universal character. As we shall see, both locally and globally Singularity Theory can give organizing principles. It should be noted at once that next to periodic and quasi-periodic dynamics also forms of chaotic dynamics will show up.

Remark 1. In many cases the resonant bifurcations are repeated at ever smaller scales inside the tongues, leading to an infinite regress. Then we have to extend the notion of open & dense to *residual* and that of nowhere dense to *meagre*. Here a residual set contains a countable intersection of open & dense sets, while a meagre set is a countable union of nowhere dense sets. One sometimes also speaks in terms of G_δ– or F_σ–sets, respectively [74].

1.1 Periodically Driven Oscillators

Many of the resonant phenomena of interest to us are modelled by periodically driven or coupled oscillators. To fix thoughts we now present two examples, namely the harmonic and the Duffing oscillator subjected to periodic forcing.

The Driven Harmonic Oscillator

One of the simplest class-room examples of resonance occurs in the harmonic oscillator with periodic forcing

$$\ddot{x} = -\alpha^2 x - c\dot{x} + \varepsilon \sin(\omega t) \tag{1}$$

with $x, t \in \mathbb{R}$, where $c > 0$ is the damping and where $\varepsilon \geq 0$ controls the size of the forcing. The forcing has frequency $\omega > 0$ and therefore has period $T = 2\pi/\omega$. The 'response' solution is periodic

$$x(t) = R \sin(\omega t + \phi)$$

with this same frequency. Its amplitude and phase are given by

$$r = \frac{\varepsilon}{\sqrt{(\omega^2 - \alpha^2)^2 + c^2\omega^2}} \quad \text{and} \quad \tan\phi = \frac{c\,\omega}{\omega^2 - \alpha^2}.$$

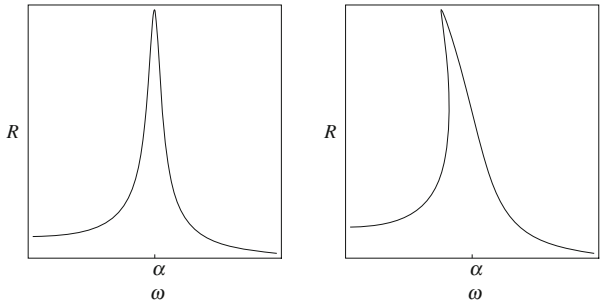

Fig. 1 Amplitude-response diagrams in the (ω, R)–plane. *Left*: the periodically driven harmonic oscillator (1) and *right*: the driven Duffing oscillator (2)

Fixing α, c and ε we consider R as a function of ω, see the amplitude-response diagram in Fig. 1 (left) where the response amplitude R is plotted as a function of ω.

The Driven Duffing Oscillator

As a non-linear variation on the above we consider the Duffing equation with periodic forcing

$$\ddot{x} = -\alpha^2 x - c\dot{x} - \delta x^3 + \varepsilon \sin(\omega t), \tag{2}$$

where $\alpha, \omega, c, \varepsilon$ and are positive and where δ with $0 < \delta \ll 1$ is considered as a perturbation parameter. Fixing α, c and ε as before, by successive approximation of a solution

$$x(t) = R \sin(\omega t + \phi),$$

we obtain the following relation between ε and R:

$$\varepsilon^2 = \left((\omega^2 - \alpha^2)^2 + c^2\omega^2\right) R^2 + \tfrac{3}{2}\delta(\omega^2 - \alpha^2)R^4 + \tfrac{9}{16}\delta^2 R^6 + O(\delta^3),$$

as $\delta \downarrow 0$, with a similar approximation for the phase ϕ, compare with Stoker [83], also see [45]. In Fig. 1 (right) we depict the corresponding curve in the (ω, R)–plane, which now no longer is a graph.

Remarks

– One of the exciting things about resonance concerns the peaks of the amplitude R that can be quite high, even where ε is still moderate. Systems like (1) and (2) form models or *metaphors* for various resonance phenomena in daily life. In many cases high resonance peaks one needs to 'detune' away from the resonance

value corresponding to the peak, think of a marching platoon of soldiers that have to go out of pace when crossing a bridge.
– In other cases, like when 'tuning' the radio receiver to a certain channel, one takes advantage of the peak.
– It should be noted that the nonlinear (2) dynamically is far richer than the linear case (1), e.g., see [59] and references therein.

Geometrical Considerations

In both cases of the driven oscillators witnessed above the state space is $\mathbb{R}^2 \times \mathbb{T}^1 = \{x, y, z\}$, where

$$\begin{aligned} \dot{x} &= y \\ \dot{y} &= a(x, y, \delta) + \varepsilon \sin z \\ \dot{z} &= \omega, \end{aligned}$$

with $a(x, y, \delta) = -\alpha^2 x - cy - \delta x^3$, where $\delta = 0$ in the harmonic example. The second factor is the circle $\mathbb{T}^1 = \mathbb{R}/(2\pi\mathbb{Z})$ which takes into account the periodicity of the systems in z. The response motion of the form $x(t) = R\sin(\omega t + \phi)$ then corresponds to a closed curve

$$\begin{pmatrix} x \\ y \\ z \end{pmatrix}(t) = \begin{pmatrix} R\sin(\omega t + \phi) \\ \omega R\cos(\omega t + \phi) \\ \omega t + \phi \end{pmatrix}. \tag{3}$$

This closed curve, when projected onto the (x, y)–plane, exactly forms an ellipse.

We now can describe this motion in terms of a 2–dimensional torus $\mathbb{T}^2 = \mathbb{T}^1 \times \mathbb{T}^1$, parametrized by two variables φ_1 and φ_2 in a system of differential equations of the format

$$\begin{aligned} \dot{\varphi}_1 &= \omega_1 \\ \dot{\varphi}_2 &= \omega_2, \end{aligned} \tag{4}$$

where $\varphi_1 = z$ and $\omega_1 = \omega$ and where for φ_2 we take the phase of the motion on the ellipse. Thus φ_2 exactly is the time parametrization of this motion, scaled to the period 2π: in this case $\omega_2 = \omega_1 = \omega$. Therefore in this way, the curve (3) can be seen as a 1:1 torus knot.

To view resonant motion in terms of torus dynamics turns out to be extremely useful and this can also be applied to coupled oscillators. Here a classical example is given by Christiaan Huygens [62], who in 1665 observed the following phenomenon, see Fig. 2. Two nearly identical pendulum clocks mounted on a not completely rigid horizontal beam tend to synchronize. Moreover, when the

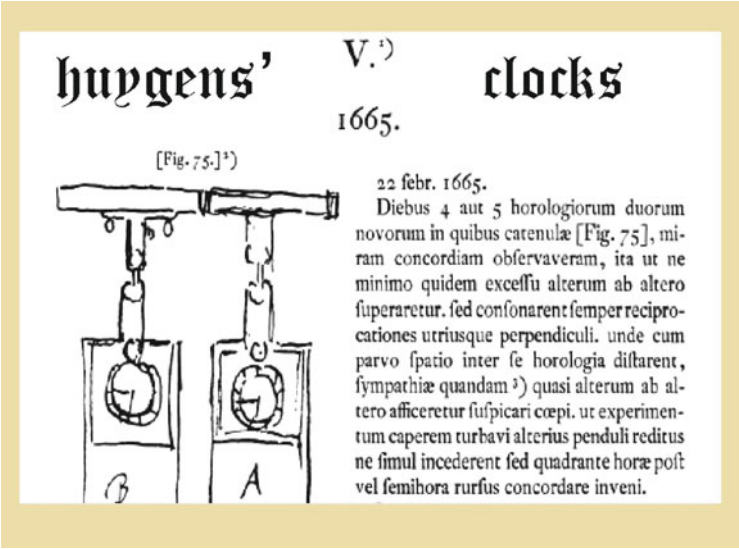

Fig. 2 Huygens's synchronizing clocks [62]

pendula both move in the vertical plane through the beam, they have a tendency to synchronize in anti-phase motion. A simple model describes this system in the format (4), where the angles φ_1 and φ_2 are the phases of the two oscillators and where again $\omega_1 = \omega_2$. Later on we will come back to this and other examples where we will also see other frequency ratios $\omega_1{:}\omega_2$.

1.2 Torus Flows and Circle Mappings

In this section we turn to the dynamics on the 2–dimensional torus $\mathbb{T}^2$ from section "Geometrical Considerations" for its own sake, introducing the weakly coupled system

$$\begin{aligned} \dot{\varphi}_1 &= \omega_1 + \varepsilon f_1(\varphi_1, \varphi_2) \\ \dot{\varphi}_2 &= \omega_2 + \varepsilon f_2(\varphi_1, \varphi_2). \end{aligned} \tag{5}$$

Here f_1 and f_2 are 2π–periodic functions in both variables. Also we use a parameter ε to control the strength of the coupling. For $\varepsilon = 0$ we retrieve the format (4). If T_1 and T_2 are the respective periods of oscillation, then $\omega_1 = 2\pi/T_1$ and $\omega_2 = 2\pi/T_2$. We first define the Poincaré mapping from the circle $\mathbb{T}^1$ to itself and then introduce the rotation number.

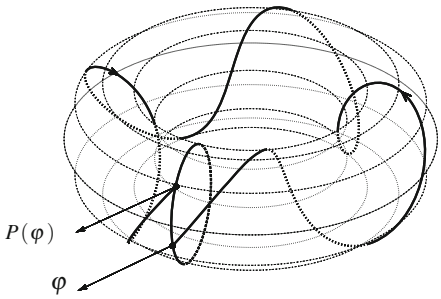

Fig. 3 Poincaré mapping of a torus flow [20]

The Poincaré Mapping

If in (5) the size $|\varepsilon|$ of the coupling is not too large, a first-return Poincaré mapping

$$P : \mathbb{T}^1 \longrightarrow \mathbb{T}^1 \tag{6}$$

is defined, as we shall explain now, also see Fig. 3. Without restricting generality we can take the generating circle to be $\mathbb{T}^1 \times \{0\}$. Baptising $\varphi = \varphi_1$ for simplicity, we follow the integral curve from the initial state $(\varphi_1, \varphi_2) = (\varphi, 0)$ until $(\varphi_1, \varphi_2) = (P(\varphi), 0)$, counting mod $2\pi\mathbb{Z}$. It is easy to see that $P - \mathrm{Id}$ should be a periodic function in φ, which gives P the general form

$$P : \varphi \mapsto \varphi + 2\pi\alpha + \varepsilon f(\varphi), \tag{7}$$

where $\alpha = \omega_2/\omega_1$ and where f is a 2π–periodic function.

Consideration of the $\mathbb{T}^1$–dynamics generated by iteration of P gives a lot of information about the original $\mathbb{T}^2$–flow, in particular its asymptotic properties as $t \to \infty$. For instance, a fixed point attractor of P corresponds to an attracting periodic orbit of the flow which forms a 1:1 torus knot as we saw at the end of Sect. 1.1. Similarly a periodic attractor of P of period q corresponds to an attracting periodic orbit of the flow. In general, periodicity will be related to resonance, but to explain this further we need the notion of rotation number.

Rotation Number

For orientation-preserving homeomorphisms $P : \mathbb{T}^1 \longrightarrow \mathbb{T}^1$ Poincaré has left us the extremely useful concept of *rotation number* $\varrho(P)$, which describes the average amount of rotation as follows:

$$\varrho(P) = \frac{1}{2\pi} \lim_{n\to\infty} \frac{1}{n} (\tilde{P})^n(\varphi) \bmod \mathbb{Z}. \tag{8}$$

Here $\tilde{P} : \mathbb{R} \longrightarrow \mathbb{R}$ is a (non-unique) lift of P which makes the diagram

$$\begin{array}{ccc} \mathbb{R} & \xrightarrow{\tilde{P}} & \mathbb{R} \\ {\scriptstyle \mathrm{pr}}\downarrow & & \downarrow{\scriptstyle \mathrm{pr}} \\ \mathbb{T}^1 & \xrightarrow{P} & \mathbb{T}^1 \end{array}$$

commute, where $\mathrm{pr} : \mathbb{R} \longrightarrow \mathbb{T}^1$ is the natural projection $\varphi \mapsto \mathrm{e}^{\mathrm{i}\varphi}$. This means that in the formula (8) we do not count modulo 2π, but keep counting in $\mathbb{R}$.

From [54, 73] we quote a number of properties of $\varrho(P)$:

1. $\varrho(P)$ depends neither on the choice of the lift $\tilde{P}$ nor on the choice of φ;
2. $\varrho(P)$ is invariant under topological conjugation. This means that if $h : \mathbb{T}^1 \longrightarrow \mathbb{T}^1$ is another orientation-preserving homeomorphism, then
$$\varrho(hPh^{-1}) = \varrho(P);$$
3. If $P : \varphi \mapsto \varphi + 2\pi\alpha$ is a rigid rotation then $\varrho(P) = \alpha \bmod \mathbb{Z}$.
4. $\varrho(P) \in \mathbb{Q}$ precisely when P has a periodic point. Moreover, $\varrho(P) = p/q$ with p and q relatively prime corresponds to a p:q torus knot.
5. If P is of class C^2 and $\varrho(P) = \alpha$ for $\alpha \in \mathbb{R} \setminus \mathbb{Q}$, then, by a result of Denjoy, the mapping P is topologically conjugated to the rigid rotation $\varphi \mapsto \varphi + 2\pi\alpha$.

   Recall that in that case any orbit $\{P^n(\varphi)\}_{n\in\mathbb{Z}}$ forms a dense subset of $\mathbb{T}^1$. The corresponding dynamics is called *quasi-periodic*.
6. If P depends continuously on a parameter, then so does $\varrho(P)$.

The Arnold Family of Circle Mappings

A famous example of maps exhibiting resonance is formed by the Arnold family

$$\mathbb{A}_{\alpha,\varepsilon} : \varphi \mapsto \varphi + 2\pi\alpha + \varepsilon \sin\varphi \tag{9}$$

of circle mappings. So this is the general format (7) where we chose $f(\varphi) = \sin\varphi$.[1]

Periodicity. It is instructive to consider the fixed points of (9), given by the equation

$$\mathbb{A}_{\alpha,\varepsilon}(\varphi) = \varphi,$$

[1]For simplicity we take $|\varepsilon| < 1$ which ensures that (9) is a circle diffeomorphism; for $|\varepsilon| \geq 1$ the mapping becomes a circle *endomorphism* and the current approach breaks down.

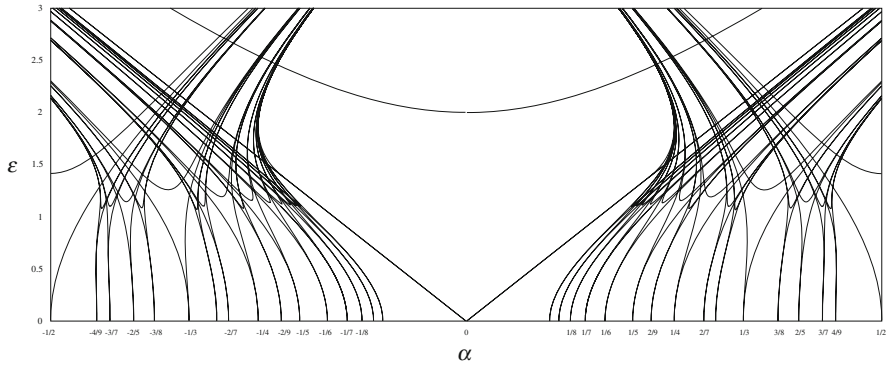

Fig. 4 Resonance tongues in the Arnold family (9)

or, equivalently,

$$\sin\varphi = -\frac{2\pi\alpha}{\varepsilon}.$$

A brief graphical inspection reveals that $\bmod 2\pi\mathbb{Z}$ this equation has exactly two solutions for

$$|\varepsilon| > 2\pi|\alpha|.$$

In Fig. 4 this region, bounded by the two straight lines $\varepsilon = \pm 2\pi\alpha$, is depicted for $\varepsilon > 0$. It is not hard to see that one of the fixed points is attracting and the other repelling. At the boundary $|\varepsilon| = 2\pi|\alpha|$ these annihilate one another in a saddle-node bifurcation. For the entire region $|\varepsilon| \geq 2\pi|\alpha|$ one has $\varrho(\mathbb{A}_{\alpha,\varepsilon}) = 0 \bmod \mathbb{Z}$. This region is called the Arnold tongue of rotation number 0.

From the properties of section "Rotation Number" it follows that, for $(\alpha, \varepsilon) = (p/q, 0)$ with p and q relatively prime, one has $\varrho(\mathbb{A}_{\alpha,\varepsilon}) = p/q$. One can show that from each $(\alpha, \varepsilon) = (p/q, 0)$ an Arnold tongue emanates, in which for all the parameter points (α, ε) one has $\varrho(\mathbb{A}_{\alpha,\varepsilon}) = p/q$, see Fig. 4. The 'sharpness', i.e., the order of contact of the boundaries of the p/q–tongue at $(\alpha, \varepsilon) = (p/q, 0)$ exactly is of order q, see [1, 3, 25].

Fixing $\varepsilon = \varepsilon_0 > 0$ small, we consider the graph of $\alpha \mapsto \varrho(\mathbb{A}_{\alpha,\varepsilon_0})$. By another general property of section "Rotation Number", this function is continuous. Moreover, for every rational value p/q it is constant on some plateau, corresponding to the p/q–tongue, see Fig. 4. The total result is a devil's staircase as depicted in Fig. 5.

Quasi-periodicity. In between the tongues the rotation number $\varrho(\mathbb{A}_{\alpha,\varepsilon})$ is irrational and by the properties of section "Rotation Number" we know that the corresponding iteration dynamics of $\mathbb{A}$ is quasi-periodic and that each individual orbits densely fills $\mathbb{T}^1$.

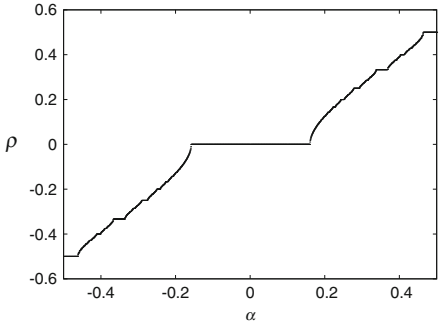

Fig. 5 Devil's staircase related to the Arnold family (9). For small $\varepsilon_0 > 0$ the rotation number $\varrho(\mathbb{A}_{\alpha,\varepsilon_0})$ is depicted as a graph of $\alpha \in [0, 1]$

Open & dense versus nowhere dense. In general the (α, ε)–plane of parameters contains a catalogue of the circle dynamics. Again fixing $\varepsilon = \varepsilon_0 > 0$ small, consider the corresponding horizontal line in the (α, ε)–plane of parameters. We witness the following, also see Fig. 5 and compare with [25] and references therein. The periodic case corresponds to an open & dense subset of the line, and the quasi-periodic case to a nowhere dense subset, which in the 1–dimensional situation is a Cantor set.

Diophantic rotation numbers. Quasi-periodicity corresponds to $\varrho = \varrho(P_{\alpha,\varepsilon_0}) \notin \mathbb{Q}$. If we restrict even further to Diophantine ϱ by requiring that for constants $\tau > 2$ and $\gamma > 0$, for all rationals p/q

$$\left|\varrho - \frac{p}{q}\right| \geq \frac{\gamma}{|q|^\tau}, \tag{10}$$

the conjugations of P_{α,ε_0} with the rigid rotation $\varphi \mapsto \varphi + 2\pi\varrho$ can be taken smooth [1, 20]. The rotation numbers ϱ satisfying (10) form a Cantor subset of the former, which has positive Lebesgue measure, which, by choosing $\gamma = \gamma(\varepsilon_0) = \mathcal{O}(\varepsilon_0)$, can be shown to tend to full measure as $\varepsilon_0 \to 0$. A fortiori this holds for the original Cantor set given by $\varrho(P_{\alpha,\varepsilon_0}) \notin \mathbb{Q}$.

Fractal geometry. The Cantor sets under consideration, since they have positive Lebesgue measure, have Hausdorff dimension equal to 1. Moreover Cantor sets have topological dimension 0, since they are totally disconnected: every point has arbitrarily small neighbourhoods with empty boundary. The fact that the Hausdorff dimension strictly exceeds the topological dimension is a characterisation of fractals, see page 15 of [68]. So our Cantor sets are fractals. They also show a lot of self-similarity, a property shared with many other fractals.

Beyond the Arnold family (9) **...** The decomposition of the parameter space in an open & dense set on the one hand, versus a nowhere dense, fractal set of positive measure turns out to be universal, also see [25]. To begin with, any arbitrary smooth (Poincaré) circle mapping of the more general format (7)

$$P_{\alpha,\varepsilon} : \varphi \mapsto \varphi + 2\pi\alpha + \varepsilon f(\varphi)$$

turns out to have an array of resonance tongues similar to the Arnold family (9), forming an open & dense set that corresponds to periodicity, with a fractal complement which is nowhere dense and of positive measure that corresponds to quasi-periodicity.

The only point of difference with (9) is formed by the exact 'sharpness' of the tongues, which depends on the Fourier coefficients of the function f. In particular a tongue at the tip $(\alpha, \varepsilon) = (p/q, 0)$ has transverse boundaries if and only if the qth Fourier coefficient does not vanish.

Link with Resonance

Returning to the driven oscillator or the two coupled oscillators we now link periodicity of the Poincaré mapping (7) with resonance. For simplicity we keep $|\varepsilon|$ sufficiently small to ensure this mapping to be a diffeomorphism.

As observed in section "Rotation Number" the fact that (α, ε) belongs to the p/q–tongue, i.e., that $\varrho(P_{\alpha,\varepsilon}) = p/q$, means that the motion takes place on a p:q torus knot. Generically these periodic orbits come in attracting and repelling pairs and the visible motion takes place on such a periodic attractor. In view of our general 'definition' of resonance in that case we say that the oscillators are in p:q resonance, one also speaks of *phase-locking* or *synchronisation*. In the case of 1:1 resonance sometimes the term *entrainment* is being used.

If (α, ε) is outside the tongues, by the Denjoy theory mentioned before, the torus motion takes place on a dense orbit. We also call this torus motion quasi-periodic. In this case from KAM Theory [5, 20, 45] we derive the following. For Diophantine $\varrho = \varrho(P_{\alpha,\varepsilon})$, up to a smooth transformation the Poincaré mapping reads

$$\varphi \mapsto \varphi + 2\pi\varrho.$$

and the two oscillators correspondingly have the familiar decoupled form

$$\dot{\varphi}_1 = \omega_1$$
$$\dot{\varphi}_2 = \omega_2,$$

such that $\varrho(P_{\alpha,\varepsilon}) = \omega_2/\omega_1$ for *all* ε with $|\varepsilon| \ll 1$. In the parameter space this corresponds to a piece of curve through $(\alpha, \varepsilon) = (\varrho, 0)$, parametrized by ε. We emphasize that this uncountable union of these curves has positive measure.

1.3 Conclusions and Examples

The literature on resonance phenomena is immense, apart from the references already given, for instance see [3, 20, 59, 84, 87] and their bibliographies. For even

more references see below. The present point of view models resonant systems in terms of dynamical systems depending on parameters, where resonance takes place in a persistent way.

In the parameter space the resonant set is part of the bifurcation set, which forms a catalogue for transitions to various types of dynamics. What we add to the general discussion on this subject is the overall fractal geometry that usually manifests itself in the complement of all the resonances. We now present a couple of examples.

Huygens's clocks. Returning to Huygens's synchronizing clocks we first consider the problem from the torus flow point of view. We have two almost identical oscillators that are weakly coupled. This means that in (4) for the frequencies we have $\omega_1 \approx \omega_2$ and that $|\varepsilon|$ is small. For the Poincaré mapping (7)

$$P_{\alpha,\epsilon}(\varphi) = \varphi + 2\pi\alpha + \varepsilon f(\varphi)$$

we only make the assumption that the first Fourier coefficient of $f(\varphi)$ does not vanish, which ensures that the $1/1$–tongue boundaries meet transverse at $(\alpha, \varepsilon) = (0, 0)$, where the first 0 has to be taken mod $\mathbb{Z}$. Compare with Fig. 4.

This implies that (α, ε) belongs to the $1/1$–tongue, i.e., that the pendulum clocks are in 1:1 resonance, a situation described before as entrainment which is a form of synchronization. This gives a partial explanation of the phenomena discovered by Huygens [62].

Remarks.

- Note that the 1:1 resonance of the two clocks could be obtained under quite weak assumptions. If one also wants to understand the phase and anti-phase motions, the coupling between the clocks has to be included into the dynamics, compare with [9, 77] and references therein.
- For another application of these ideas in terms of circadian rhythms and the response to stimuli see [8]. Here it turns out that next to the 1:1 'entrainment' resonance also certain other resonances have biological significance.
- The above ideas can be largely extended to the case of more than two oscillators. For examples in models for the visual neurocortex see [33, 34].

Resonances in the solar system. From ancient times on resonances have been known to occur in the solar system, which are more or less in the spirit of the present section. A well-known example is the orbital 1:2:4 resonance of Jupiter's moons Ganymede, Europa, and Io which was studied by De Sitter [52,53] using the 'méthodes nouvelles' of Poincaré [76]. The 2:5 orbital resonance between Jupiter and Saturn is described by Moser et al. [70, 71, 80]. These and other resonances by certain authors are being held responsable for gaps in the rings of Saturn and in the asteroid belt.

Another type of resonance is the spin-orbit resonance. As an example thereof, the Moon is 'captured by' the Earth in a 1:1 resonance: the lunar day with respect to the Earth is (approximately) equal to 1 month. Similarly Pluto and Charon have

caught each other in such a 1:1 resonance: as an approximately rigid body the two orbit around the Sun. Interestingly, the planet Mercury is captured in a 3:2 spin-orbit resonance around the Sun [50].

Remarks.

- The spin orbit resonances are explained by tidal forces, for instance, the rotation of the Moon has been slowed down to a standstill by tidal friction brought about largely by the reciprocal tidal forces exerted of Earth and Moon. Similarly the rotation of the Earth in the very long run will be put to a stand still by the tidal forces of mainly the Moon. But probably by that time the Sun has already turned into a red giant ...
- This brings us to the subject of adiabatically changing systems as described and summarized by Arnold [2, 3] and which may be used to model such slow changes.[2] One may perhaps expect that the 3:2 spin orbit resonance of Mercury in the very long run, and after quite a number of transitions, will evolve towards another 1:1 resonance. This part of nonlinear dynamical systems still is largely unexplored.

2 Periodically Driven Oscillators Revisited

We now return to periodically driven oscillators, showing that under certain circumstances exactly the set-up of Sect. 1.2 applies.

As a motivating example we discuss the Botafumeiro in the cathedral of Santiago de Compostela, see Fig. 6. Here a large incense container is suspended by a pully in the dome where it can swing in the longitudinal direction of the church. A few men pull up the container when it approaches the ground and let go after, thereby creating a periodic forcing and in this way creating a stable motion of exactly twice the period of the forcing.

2.1 Parametric Resonance

As another model consider the parametrically driven oscillator

$$\ddot{x} + (a + \varepsilon f(t)) \sin x = 0 \tag{11}$$

[2]Mathematical ideas on adiabatic change were used earlier by Rayleigh and Poincaré and by Landau-Lifschitz.

Fig. 6 Botafumeiro in Santiago de Compostela

with $q(t + 2\pi) \equiv q(t)$, see [22]. Here a and ε are considered as parameters.[3] For the periodic function f we have studied several examples, namely

$$\begin{aligned} f(t) &= \cos t \quad \text{and} \\ &= \cos t + \tfrac{3}{2}\cos(2t) \quad \text{and} \\ &= \text{signum}\,(\cos t), \end{aligned}$$

corresponding to the Mathieu case, the Mathieu case modified by a higher harmonic, and the square case, respectively. In this setting the issue is whether the trivial 2π–periodic solution

$$x(t) \equiv 0 \equiv \dot{x}(t)$$

is elliptic, hence stable, or not. For any of such system (11) from the points

$$(a, \varepsilon) = (\tfrac{1}{4}k^2, 0), \quad k = 0, 1, 2, \ldots$$

tongues emanate in the (a, ε)–plane, where inside the trivial 2π–periodic solution is hyperbolic, hence unstable. On the tongue boundaries this solution is parabolic. See Fig. 7 and compare with [15, 18]. We note that this gives rise to a discrete union of tongues, where again the sharpness is governed by the Fourier coefficients of the periodic function $f = f(t)$.

[3] For 'historical' reasons we use the letter a instead of α^2 as we did earlier.

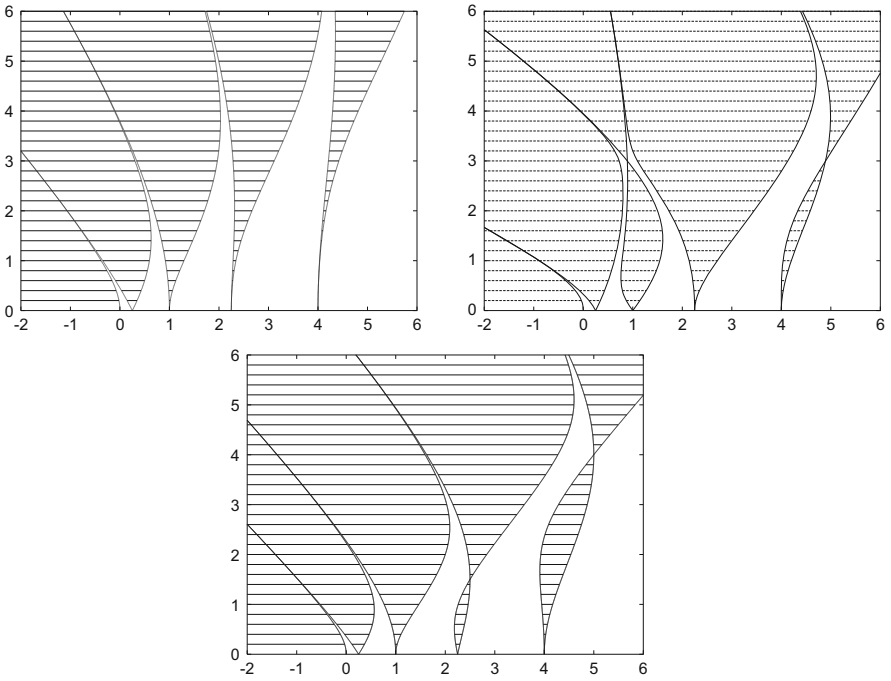

Fig. 7 Stability diagrams of Mathieu, modified Mathieu and square case [18]

Subharmonics and covering spaces. On the tongue boundaries subharmonic bifurcations occur, see [22, 23, 45] where each bifurcation can be understood in terms of a pitchfork bifurcation on a suitable covering space.

Generally, for the p:q resonance this is constructed as follows. Writing

$$z = \dot{x} + \mathrm{i}\,\frac{p}{q}x,$$

where we identify $\mathbb{C} \cong \mathbb{R}^2$, the covering map is given by the Van der Pol transformation

$$\Pi : \mathbb{C} \times \mathbb{R}/(2\pi q\mathbb{Z}) \longrightarrow \mathbb{C} \times \mathbb{R}/(2\pi\mathbb{Z})$$
$$(\zeta, t) \mapsto \left(\zeta \mathrm{e}^{\mathrm{i}tp/q}, t \ (\mathrm{mod}\ 2\pi\mathbb{Z})\right).$$

On the covering space the group $\mathscr{D}$ of decktransformations is generated by

$$(\zeta, t) \mapsto (\zeta \mathrm{e}^{2\pi p/q}, t - 2\pi),$$

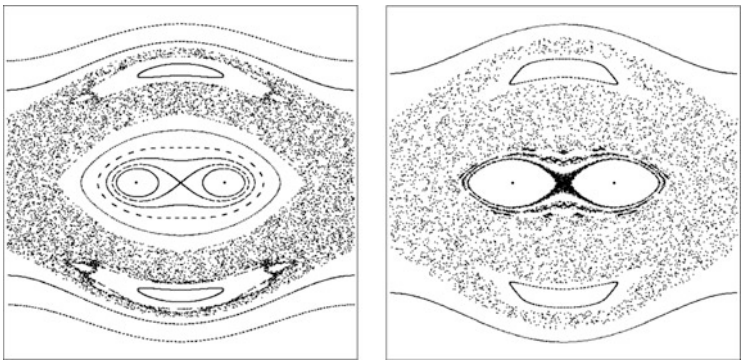

Fig. 8 Orbits of the Poincaré mapping of the swing (11)

which means that $\Pi \circ T = \Pi$ for any $T \in \mathscr{D}$.[4] Note that $\mathscr{D}$ is cyclic of order q, i.e., isomorphic to $\mathbb{Z}_q$, for details see [22, 23]. Instead of the original system in (z, t) we pull the system back along Π, so obtaining a $\mathbb{Z}_q$–equivariant system on the (ζ, t)–covering space. In fact this defines a 1:1 correspondence of systems and usually it is most convenient to work on the covering space. Generally on the covering space equivariant Singularity Theory can be practised, see [27, 57, 58] and references therein, as well as equivariant KAM Theory [24, 28, 35, 39, 45]. We refer to Sect. 5.3 for further details.

In the present case this construction is only needed for $p/q = k/2$. The strongest of these resonances occurs inside the tongue labeled by $k = 1$, where a cylinder with $\mathbb{Z}_2$–symmetry is the double cover of a Möbius strip, for a remark in this direction see [59]. This is the setting for the simplest subharmonic bifurcation, namely a period doubling bifurcation: inside the tongue the trivial 2π–periodic solution is unstable but a stable periodic orbit occurs of period 4π. At the boundary a period-doubling bifurcation takes place. The corresponding $\mathbb{Z}_2$–equivariant bifurcation on the covering space exactly is the pitchfork. The ensuing period-doubled periodic motion is exactly the one that occurs in the Botafumeiro example. See Fig. 8 for 'phase portaits' of the Poincaré mapping, left for $\varepsilon = 0.25$ and right for $\varepsilon = 0.40$

Remarks.

- The geometric complexity of the individual tongues in Fig. 7 can be described by Singularity Theory; in fact it turns out that we are dealing with type $\mathbb{A}_{2k-1}$, see [18, 22].
- The parametric 1:2 resonance sometimes also is called the *parametric roll*. By this mechanism ships have been known to capsize ...

[4] The co-ordinates (ζ, t) sometimes also are called co-rotating. Also think of the Lagrangean variation of constants.

– In Fig. 8 also invariant circles can be witnessed. KAM Theory, as discussed before, in particular an application of Moser's Twist Theorem [69], shows that the union of such invariant circles carrying quasi-periodic dynamics has positive measure.
– In both cases the cloud of points[5] is formed by just one or two orbits under the iteration of the Poincaré mapping. These clouds are associated to homoclinic orbits related to the upside down unstable periodic solution, which gives rise to horseshoes. Therefore such an orbit is chaotic since it has positive topological entropy, see [20] and references therein. A classical conjecture is that the cloud densely fills a subset of the plane of positive Lebesgue measure on which the Poincaré mapping is ergodic [4].[6]

2.2 The Hill-Schrödinger Equation

Another famous equation is a linearized version of (11) where the forcing term is quasi-periodic in t:

$$\ddot{x} + (a + \varepsilon f(t))x = 0, \tag{12}$$

where now $f(t) = F(\omega_1 t, \omega_2 t, \ldots, \omega_n t)$ for a function $F : \mathbb{T}^n \to \mathbb{R}$, see [29, 55, 72]. As in the case of Sect. 1.2 the countable union of tongues again becomes open & dense and separated by a nowhere dense set of positive measure, determined by Diophantine conditions. The geometry of the individual tongues for small $|\varepsilon|$ is exactly as in the periodic case. For larger values of $|\varepsilon|$ the situation is more complicated also involving non-reducible quasi-periodic tori, compare with [17].

The Eq. (12) happens to be the eigenvalue equation of the 1–dimensional Schrödinger operator with quasi-periodic potential. We here sketch how our geometric approach fits within the corresponding operator theory. This operator reads

$$\left(H_{\varepsilon f} x\right)(t) = -\ddot{x}(t) - \varepsilon f(t) x(t) \tag{13}$$

with *potential* εf; it acts on wave functions $x = x(t) \in L^2(\mathbb{R})$.

We like to note that in the corresponding literature usually the value of $\varepsilon = \varepsilon_0 \neq 0$ is fixed and the intersection of the horizontal line $\varepsilon = \varepsilon_0$ with a tongue is referred to as *gap*: it is a gap in the spectrum of the Schrödinger operator (13). The approach with tongues and the results of [29] regarding the $\mathbb{A}_{2k-1}$–singularity therefore leads to a generic gap closing theory.

[5] Colloquially often referred to as 'chaotic sea'.

[6] Also known as the metric entropy conjecture.

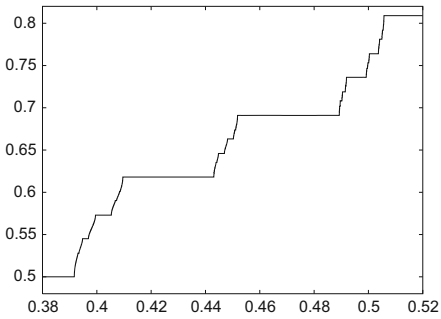

Fig. 9 Devil's staircase in the Schrödinger equation with quasi-periodic potential: $\omega_1 = 1$ and $\omega_2 = \frac{1}{2}(\sqrt{5}-1)$, see [29]

Remarks.

- In the context of Schrödinger operators the letters are chosen somewhat differently. In particular, instead of $x(t)$ one often considers $u(x)$, which gives this theory a spatial interpretation. Also instead of $\varepsilon f(t)$ one uses $V(x)$, compare with [72].
- For a fixed value $\varepsilon = \varepsilon_0$ the Diophantine Cantor set leads to Cantor spectrum. The total picture is illustrated in the devil's staircase of Fig. 9, where we took $n = 2$, $\omega_1 = 1$ and $\omega_2 = \frac{1}{2}(\sqrt{5}-1)$. The rotation number ϱ is defined almost as before [29] as a function of a.
- The nonlinear equation

$$\ddot{x} + (a + \varepsilon f(t)) \sin x = 0,$$

with q quasi-periodic is dealt with in [28]. In comparison with the case of periodic f the averaged, approximating situation, is identical. However, the infinite number of resonances and the Cantorization we saw before leads to an infinite regress of the bifurcation scenarios. For this use was made of equivariant Hamiltonian KAM Theory on a suitable covering space [24,45]. As a consequence the resonant set becomes residual and the quasi-periodic set meagre. Compare this with [7, 46–48] in the dissipative case.

2.3 Driven and Coupled Van der Pol-Like Oscillators

The examples of the driven oscillator in Sect. 1.1 were based on approximations of the damped pendulum, the free oscillation of which always tends to the lower equilibrium $x = 0, \dot{x} = 0$. Our present interest is formed by Van der Pol-like oscillators that for $|x|$ and $|\dot{x}|$ sufficiently small have negative damping, for this approach compare with [20, 45]. Such oscillators are known to occur in electronics [79, 91, 92].

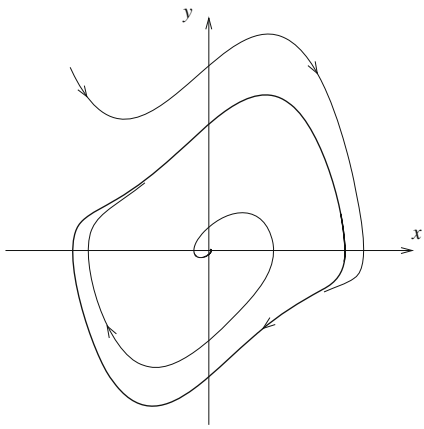

Fig. 10 Phase portrait of the free Van der Pol oscillator [20]

Therefore our starting point is the periodically driven Van der Pol oscillator in a slightly more general form

$$\ddot{x} = -\alpha^2 x - c\dot{x} - a(x, \dot{x}) + \varepsilon f(x, \dot{x}, t; \varepsilon),$$

where the function q is 2π–periodic in the time t. Van der Pol originally considered $a(x, \dot{x}) = bx^2\dot{x}$ and $f(x, \dot{x}, t; \varepsilon) = \sin t$. We here assume that a and q are sufficiently smooth, say of class C^∞ or real-analytic. The important restriction on a is that the corresponding free oscillator has a hyperbolic attractor. For a phase portrait in the $(x, \dot{x})$–plane, see Fig. 10. Passing to the system form

$$\begin{aligned} \dot{x} &= y \\ \dot{y} &= -\alpha^2 x - cy - a(x, y) + \varepsilon F(x, y, z; \varepsilon) \\ \dot{z} &= 1, \end{aligned}$$

as before, we get a 3–dimensional state space $\mathbb{R}^2 \times \mathbb{T}^1 = \{(x, y), z\}$, so with angular variable z. Let us denote the corresponding vector field by $X_{\alpha,\varepsilon}$.

This brings us back to the general setting of a 2–torus flow, with two phase angles φ_1, φ_2, e.g., with φ_1 the phase of the free oscillator, i.e., its time parametrization scaled to period 2π, and $\varphi_2 = z$. For $\varepsilon = 0$ we so obtain

$$\begin{aligned} \dot{\varphi}_1 &= \omega_1 \\ \dot{\varphi}_2 &= \omega_2, \end{aligned}$$

which is of the familiar format (4). From here the theory of Sect. 1.2 applies in al its complexity, with in the parameter space an open & dense, countable union of resonances and a fractal set of positive measure regarding quasi-periodicity.

Similar results hold for n coupled Van der Pol type oscillators, now with state space $\mathbb{T}^n$, the cartesian product of n copies of $\mathbb{T}^1$. Next to periodic and quasi-periodic motion, now also chaotic motions occur, see [20] and references therein.

3 Universal Studies

Instead of studying classes of driven or coupled oscillators we now turn to a few universal cases of 'generic' bifurcations. The first of these is the Hopf-Neĭmark-Sacker bifurcation for diffeomorphisms, which has occurrence codimension 1. This means that the bifurcation occurs persistently in generic 1–parameter families. However, the open & dense occurrence of countably many resonances and the complementary fractal geometry of positive measure in the bifurcation set are only persistent in generic 2–parameter families. A second bifurcation we study is the Hopf saddle-node bifurcation for diffeomorphisms where we use three parameters for describing the persistent complexity of the bifurcation set.

3.1 The Hopf-Neĭmark-Sacker Bifurcation

We start with the Hopf-Neĭmark-Sacker bifurcation for diffeomorphisms, but also discuss certain consequences for systems of differential equations. As an example to illustrate our ideas consider the following Duffing–Van der Pol–Liénard type driven oscillator

$$\ddot{x} + (\nu_1 + \nu_3 x^2)\dot{x} + \nu_2 x + \nu_4 x^3 + x^5 = \varepsilon(1 + x^6)\sin t, \tag{14}$$

the coefficients of which can be considered as parameters. Note that for the free oscillator at $\nu_1 = 0$ the eigenvalues of the linear part at $(x, \dot{x}) = (0, 0)$ cross the imaginary axis at $\pm \mathrm{i}\sqrt{\nu_2}$. Excluding the strong resonances where $\sqrt{\nu_2} = p/q$ for p and q relatively prime with $q \leq 5$ and assuming that the constants ν_3 and ν_4 are generically chosen, the organization of the (ν_1, ν_2)–plane, for ν_1 consists of an an open & dense union of countably many resonance tongues separated by a nowhere dense set of positive measure. This situation is comparable to the Arnold family (9) and Fig. 4, at least for large values of q.

The Nondegerate Case

The general set-up just considers a mapping

$$P : \mathbb{R}^2 \longrightarrow \mathbb{R}^2 \tag{15}$$

around a fixed point, say $P(0) = 0$, where the eigenvalues of the linear part read $e^{\nu_1 \pm 2\pi i\sqrt{\nu_2}}$ with $|\nu_1|$ small. We consider a fixed resonance $(\nu_1, \nu_2) = (0, p^2/q^2)$ with p and q relatively prime, where we will need two parameters to versally unfold the linear part [3, 45]. Our main interest is with the periodic points of period q, so in solving the equation

$$P^q(x, y) = (x, y).$$

The zeroes of $P^q - \mathrm{Id}$ are studied by a Lyapunov–Schmidt reduction, cf. Sect. 5.1. This leads to a $\mathbb{Z}_q$–equivariant family of functions

$$G_\mu(z) = zB_\mu(u) + C_\mu \bar{z}^{q-1} + \mathcal{O}(|z|^q),$$

where z is an appropriate complex variable and where B_μ is a polynomial in $u = |z|^2$ of degree less than $(q-1)/2$. We study the corresponding discriminant set given by

$$G_\mu(z) = 0 \quad \text{and} \quad \det D_z G_\mu(z) = 0. \tag{16}$$

Here μ is an unfolding-multiparameter detuning the resonance at hand. The way to study this discriminant set is by $\mathbb{Z}_q$–equivariant contact equivalence [27, 36, 40, 41, 44]. In the present non-degenerate case (16) can be reduced to the polynomial normal form

$$G^{\mathrm{NF}}_\sigma(z) = z(\sigma + |z|^2) + \bar{z}^{q-1},$$

for a complex parameter σ. See also Sect. 5.2, in particular Theorem 1. In general this set turns out to be a 'tongue' ending in a cusp of sharpness $(q-2)/2$, which is part of a familiar bifurcation diagram with two periodic orbits of period q inside that annihilate one another at the tongue boundaries in a saddle-node or fold bifurcation [3].

See Fig. 11 which is embedded in the context of the Eq. (14), of which P is a Poincaré mapping. Here the dynamics of P also has been described in terms of a Poincaré–Takens interpolating normal form approximation, e.g., see [13, 22, 23, 85] and Sect. 5.3.

Globally a countable union of such cusps is separated by a nowhere dense set of positive measure, corresponding to invariant circles with Diophantine rotation number. As before, see Fig. 4, the latter set contains the fractal geometry.

Remarks.

- The above results, summarized from [27, 36, 40, 44], are mainly obtained by $\mathbb{Z}_q$–equivariant Singularity Theory.
- The strong resonances with $q = 1, 2, 3$ and 4 form a completely different story where the Singularity Theory is far more involved [3, 85]. Still, since the higher

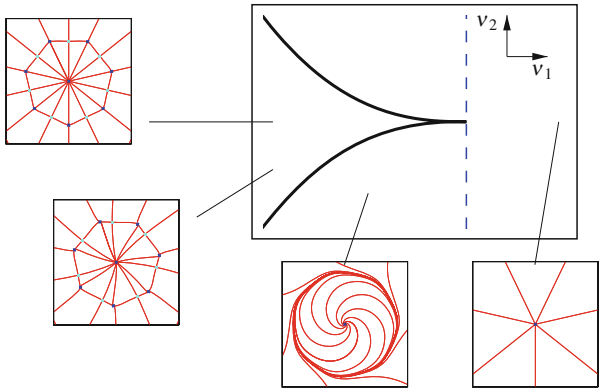

Fig. 11 Tongue in nondegenerate resonance $q = 7$ of the Hopf-Neĭmark-Sacker bifurcation [27, 36, 40, 44]

order resonances accumulate at the boundaries, there is fractal geometry around, always of positive measure.
– Regarding structural stability of unfoldings of P as in (15) under topological conjugation, all hopes had already disappeared since [66].

A Mildly Degenerate Case

In the mildly degenerate case the 'Hopf' coefficient in the previous example vanishes and is introduced as an extra parameter. This leads to another normal form

$$G^{\mathrm{NF}}_{\sigma,\tau}(z) = z(\sigma + \tau|z|^2 + |z|^4) + \overline{z}^{q-1}, \tag{17}$$

which is now parametrized over $\mathbb{C}^2 \cong \mathbb{R}^4$, hence of codimension 4. Again, cf. Sect. 5.2, in particular Theorem 1. As before [27, 41] the normal form (17) is structurally stable under $\mathbb{Z}_q$–equivariant contact equivalence. Here the Singularity Theory is more complex, involving folds, cusps, a swallowtail and a Whitney umbrella. The complete bifurcation diagram is more involved, even at the level of Poincaré–Takens normal form vector field approximations. In Fig. 12, again for the case $q = 7$, a 2–dimensional tomography is shown of the bifurcation set, in which still a tongue-like structure can be discerned, for more details see [40,44] where also 3–dimensional tomographies are presented.

To illustrate a mildly degenerate case of the Hopf–Neĭmark–Sacker bifurcation one may well consider the preceding Duffing–Van der Pol–Liénard type driven oscillator (14) where we need all four parameters.

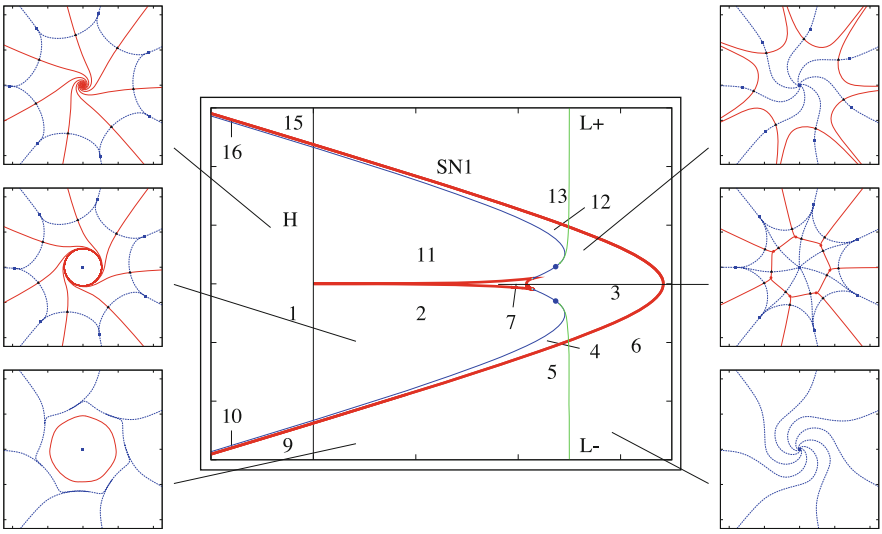

Fig. 12 Two-dimensional tomography in a mildly degenerate resonance $q = 7$ of the Hopf–Neĭmark–Sacker bifurcation [27, 36, 40, 44]

Concluding Remarks

For both cases of the Hopf–Neĭmark–Sacker bifurcation we have a good grip on the part of the bifurcation set that governs the number of periodic points. The full bifurcation set is far more involved and the corresponding dynamics is described only at the level of Poincaré–Takens normal-form vector fields [13, 40, 44]. We note that homo- and heteroclinic phenomena occur at a flat distance in terms of the bifurcation parameters [16, 19, 75].

3.2 The Hopf Saddle-Node Bifurcation for Diffeomorphisms

As a continuation of the above programme, we now consider the Hopf saddle-node (or fold Hopf) bifurcation for diffeomorphisms [37, 38, 42], in which the central singularity is a fixed point of a 3–dimensional diffeomorphism, such that the eigenvalues of the linear part at bifurcation are 1 and $e^{2\pi i\alpha}$, where

$$e^{2\pi ni\alpha} \neq 1 \quad \text{for} \quad n = 1, 2, 3 \quad \text{and} \quad 4,$$

so excluding strong resonances as in the Hopf–Neĭmark–Sacker case of Sect. 3.1. The Hopf saddle-node bifurcation for flows is well-known [21, 59], especially because of the subordinate Hopf–Neĭmark–Sacker and Šilnikov homoclinic bifurcation. Our main interest is how the Hopf–Neĭmark–Sacker bifurcation is being changed into one of the simplest quasi-periodic bifurcations near a 2:5 resonance.

From Vector Fields to Mappings

The linear part of the vector field at bifurcation has eigenvalues 0 and $\pm i\alpha$. This linear part generates an axial symmetry that in a normal form procedure can be pushed stepwise over the entire Taylor series, see [13] and references. This makes it possible to first consider axially symmetric systems, that turn out to be topologically determined by their third-order truncation given by

$$\begin{aligned}\dot{w} &= (-\beta_2 + i\alpha)w - awz - wz^2\\ \dot{z} &= -\beta_1 - sw\overline{w} - z^2\end{aligned}$$

where $w \in \mathbb{C}$ and $z \in \mathbb{R}$ and where β_1 and β_2 are unfolding parameters [59, 63]. A scaling $\beta_1 = \gamma^2, \beta_2 = \gamma^2\mu$ leads to a vector field

$$Y_{\gamma,\mu,\alpha}(z,w) = \begin{pmatrix} (-\gamma\mu + 2\pi i\alpha/\gamma)w - awz - \gamma wz^2 \\ 1 - z^2 - |w|^2 \end{pmatrix}.$$

From this an axially symmetric map

$$\begin{pmatrix} w \\ z \end{pmatrix} \mapsto \begin{pmatrix} e^{2\pi i\alpha} w[1 - \gamma(\gamma\mu + az + \gamma z^2)] \\ z - \gamma(-1 + |w|^2 + z^2) \end{pmatrix}$$

is obtained in a kind of Euler step. To study a 2:5 resonance we take $\alpha_0 = 2/5$, writing $\alpha = \alpha_0 + \gamma\delta$, and perturb to

$$G_{\mu,\delta} : \begin{pmatrix} w \\ z \end{pmatrix} \mapsto \begin{pmatrix} e^{i\alpha} w[1 - \gamma(\gamma\mu + az + \gamma z^2)] \\ z - \gamma(-1 + |w|^2 + z^2) \end{pmatrix} + \begin{pmatrix} \gamma^3(\varepsilon_1\overline{w}^4 + \varepsilon_2 z^4) \\ \gamma^4\varepsilon_3 \mathrm{Re}\, w^5 \end{pmatrix},$$

by adding axially non-symmetric order r resonant terms

$$\overline{w}^4 \frac{\partial}{\partial w} \quad \text{and} \quad \mathrm{Re}\, w^5 \frac{\partial}{\partial z}.$$

The scaling parameter γ and the other constants are fixed suitably.

In the Product of State Space and Parameter Space

In Fig. 13 a Lyapunov diagram is depicted in the parameter plane of the mapping family G. Table 1 contains the corresponding color code. In Fig. 14 we show the dynamics corresponding to two values of $(\mu, \delta/2\pi)$. Let us discuss these numerical data.

The parameter space. On the right-hand-side of the figure this method detects an attracting invariant circle of focus type (blue). In the gaps larger resonances

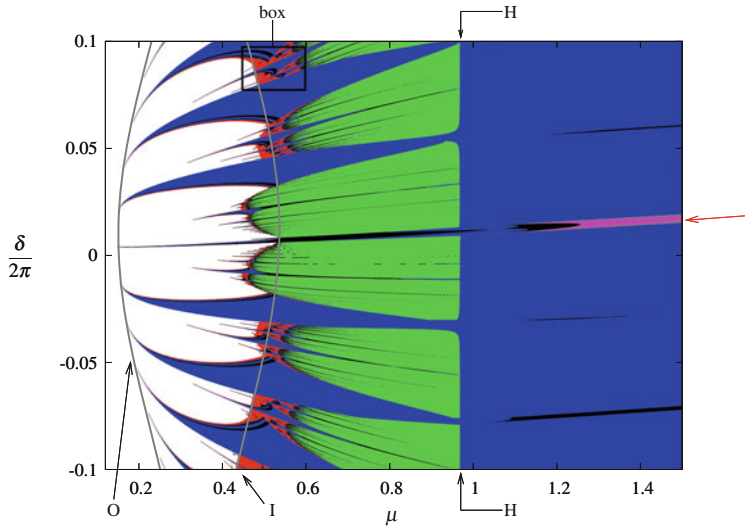

Fig. 13 Lyapunov diagram of G in the $(\mu, \delta/(2\pi))$-parameter plane. The *colors* correspond to distinct classes of attractors of G [37,42]. See Table 1 for the color coding

Table 1 Legend of the color coding for Fig. 13, see [37,42]. The attractors are classified by means of the Lyapunov exponents (ℓ_1, ℓ_2, ℓ_3)

Color	Lyapunov exponents	Attractor type
Red	$\ell_1 > 0 = \ell_2 > \ell_3$	Strange attractor
Yellow	$\ell_1 > 0 > \ell_2 > \ell_3$	Strange attractor
Blue	$\ell_1 = 0 > \ell_2 = \ell_3$	Invariant circle of focus type
Green	$\ell_1 = \ell_2 = 0 > \ell_3$	Invariant 2-torus
Black	$\ell_1 = 0 > \ell_2 > \ell_3$	Invariant circle of node type
Grey	$0 > \ell_1 > \ell_2 = \ell_3$	Fixed point of focus type
Fuchsia	$0 > \ell_1 = \ell_2 \geq \ell_3$	Fixed point of focus type
Pale blue	$0 > \ell_1 > \ell_2 > \ell_3$	Fixed point of node type
White		No attractor detected

are visible, compare with Fig. 4 for a fixed value of ε. Moving to the left, in the neighbourhood of the line indicated by H a quasi-periodic Hopf bifurcation occurs from a circle attractor to a 2–torus attractor (green). Also here the parameter space is interspersed with a resonance web of which the larger lines are visible. The remaining features, among other things, indicate invariant tori and strange attractors of various types and also more invariant circles.

The state space. The upper two figures of Fig. 14 show an invariant circle, once seen from the z–direction and once from some w–direction. The lower two figures indicate how this circle has become a strange attractor, from the same two points of view.

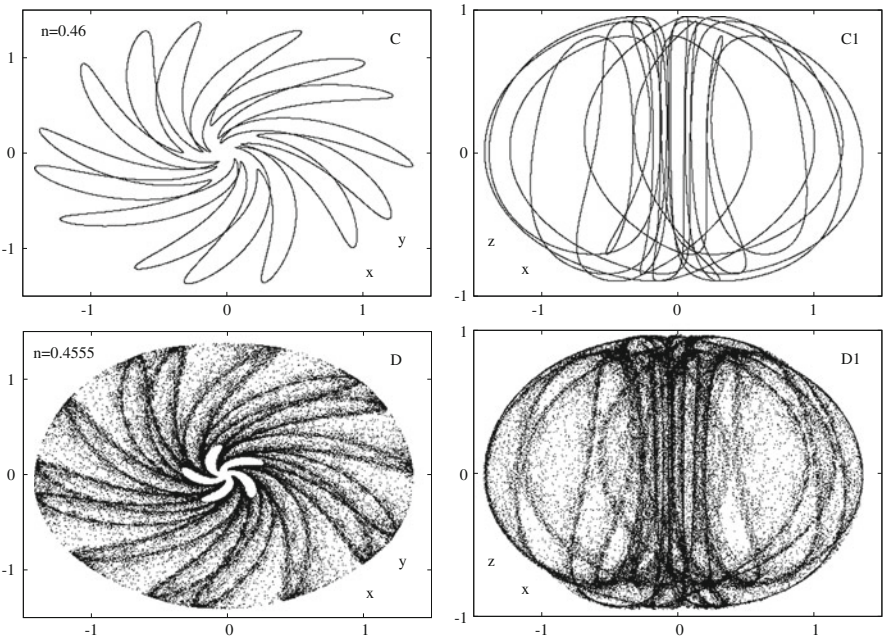

Fig. 14 Quasi-periodic (*top*) and strange attractor (*bottom*) in the Hopf saddle-node bifurcation for mappings, as seen from two different angles (*left* and *right*) [37, 42]

Part of these results can be justified mathematically, as seen from the Perturbation Theory point of view. The invariant circles all have one Lyapunov exponent equal to 0 and these are quasi-periodic, perturbations of closed integral curves of a vector field (averaging) approximation, whence their existence can be proven by KAM Theory [5,24]. A similar statement can be made about the 2–tori with two Lyapunov exponents equal to 0. In fact the transition is a quasi-periodic Hopf bifurcation as discussed by Broer et al. [10, 11, 20, 45].

By the same references, this also holds for the quasi-periodic invariant circle in the upper half of Fig. 14. The lower half of this figure is conjectured to show a *quasi-periodic Hénon-like attractor*, which is the closure of the unstable manifold of an unstable quasi-periodic invariant circle. This is the previous quasi-periodic circle that has become unstable through a quasi-periodic saddle-node bifurcation [11]. For this kind of strange attractor the mathematical background theory largely fails, so the results must remain experimental; for indications in this direction however see [42] and references therein.

For a detailed, computer-assisted bifurcation analysis of the 2:5 resonance 'bubble' we refer to [37]. Compare with earlier work of Chenciner [46–48]. We like to note that the family of mappings G forms a concrete model for the Ruelle–Takens scenario regarding the onset of turbulence. In fact it also illustrates how the earlier scenario of Hopf–Landau–Lifschitz is also included: the present multi-parameter

set-up unifies both approaches. For details and background see [20,45,60,61,64,65, 67,78].

Resonance and fractal geometry. Interestingly, the blue colors right and left correspond to quasi-periodic circle attractors. The fact that the corresponding regions of the plane look like open sets is misleading. In reality these are meagre sets, dense veined by the residual sets associated to periodicity. These details are just too fine to be detected by the computational precision used.

Particularly in the latter case, in the left half of the diagram, we are dealing with the Arnold resonance web, for a detailed analysis see [38].

4 Conclusions

We discuss a number of consequences of the present paper in terms of modelling of increasing complexity.

4.1 'Next Cases'

The Hopf saddle-node bifurcation for maps, see Sect. 3.2, can be viewed as a 'next case' in the systematic study of bifurcations as compared to, e.g., [59, 63] and many others. The nowhere dense part of parameter space, since it lacks interior points is somewhat problematic to penetrate by numerical continuation methods. Nevertheless, from the 'physical' point of view, this part surely is visible when its measure is positive or, as in the present examples, even close to full measure. Needless to say that this observation already holds for the Hopf–Neĭmark–Sacker bifurcation as described in Sect. 3.1.

Other 'next cases' are formed by the quasi-periodic bifurcations which is a joint application of Kolmogorov–Arnold–Moser Theory [5, 11, 20, 32, 45] and Singularity Theory [56–58, 86]. For overviews see [12, 49, 88]. The quasi-periodic bifurcations are inspired by the classical ones in which equilibria or periodic orbits are replaced by quasi-periodic tori. As an example, in the Hopf saddle node of Sect. 3.2 we met quasi-periodic Hopf bifurcation for mappings from circles to a 2–tori in a subordinate way. Here we witness a global geometry inspired by the classical Hopf bifurcation, which concerns the quasi-periodic dynamics associated to the fractal geometry in the parameter space, compare with Fig. 13. The gaps or tongues in between concern the resonances inside, within which we notice a further 'fractalization' or 'Cantorization'.

A similar 'next case' in complexity is given by the parametrically forced Lagrange top [31, 32], in which a quasi-periodic Hamiltonian Hopf bifurcation occurs. Indeed, we recall from [51] that in the Lagrange top a Hamiltonian Hopf bifurcation occurs, the geometry of which involves a swallowtail catastrophy. By the

periodic forcing this geometry is 'Cantorized' yielding countably many tongues with fractal geometry in between.

Remarks.

- As said before, in cases with infinite regress the fractal complement is a meagre set which has positive measure. Simon [81] describes a similar situation for 1–dimensional Schrödinger operators. Also see [6].
- It is an interesting property of the real numbers to allow for this kind of dichotomy in measure and topology, compare with Oxtoby [74]. Interestingly, although these properties in the first half of the twentieth century were investigated for theoretical reasons, they here naturally show up in the context of resonances and spectra.

4.2 Modelling

We like to note that our investigations on the Hopf saddle-node bifurcation for mappings were inspired by climate models [26, 43, 82], where in about 80–dimensional Galerkin projections of PDE models such bifurcations were detected in 3–dimensional center manifolds.

Generally speaking there exists a large-scale programme of modelling in terms of dynamical systems depending on parameters, with applications varying from climate research to mathematical physics and biological cell systems. These models often are high-dimensional and their complexity is partly explained by mechanisms of the present paper, also see [20, 78, 88]. In general such models exhibit the coexistence of periodicity (including resonance), quasi-periodicity and chaos, best observed in the product of state- and parameter space.

5 Appendix: Equivariant Singularity Theory

5.1 Lyapunov–Schmidt Reduction

Our method for finding resonance tongues—and tongue boundaries—proceeds as follows. Find the region in parameter space corresponding to points where the map P has a q-periodic orbit; that is, solve the equation $P^q(x) = x$. Using a method due to Vanderbauwhede (see [89, 90]), we can solve for such orbits by Lyapunov-Schmidt reduction. More precisely, a q-periodic orbit consists of q points $x_1, \ldots, x_q$ where

$$P(x_1) = x_2, \ldots, P(x_{q-1}) = x_q, P(x_q) = x_1.$$

Such periodic trajectories are just zeroes of the map

$$\hat{P}(x_1, \ldots, x_q) = (P(x_1) - x_2, \ldots, P(x_q) - x_1).$$

Note that $\hat{P}(0) = 0$, and that we can find all zeroes of $\hat{P}$ near the resonance point by solving the equation $\hat{P}(x) = 0$ by Lyapunov-Schmidt reduction. Note also that the map $\hat{P}$ has $\mathbb{Z}_q$ symmetry. More precisely, define

$$\sigma(x_1, \ldots, x_q) = (x_2, \ldots, x_q, x_1).$$

Then observe that

$$\hat{P}\sigma = \sigma\hat{P}.$$

At 0, the Jacobian matrix of $\hat{P}$ has the block form

$$J = \begin{pmatrix} A & -I & 0 & 0 & \cdots & 0 & 0 \\ 0 & A & -I & 0 & \cdots & 0 & 0 \\ & & & \vdots & & & \\ 0 & 0 & 0 & 0 & \cdots & A & -I \\ -I & 0 & 0 & 0 & \cdots & 0 & A \end{pmatrix}$$

where $A = (dP)_0$. The matrix J automatically commutes with the symmetry σ and hence J can be block diagonalized using the isotypic components of irreducible representations of $\mathbb{Z}_q$. (An *isotypic component* is the sum of the $\mathbb{Z}_q$ isomorphic representations. See [58] for details. In this instance all calculations can be done explicitly and in a straightforward manner.) Over the complex numbers it is possible to write these irreducible representations explicitly. Let ω be a qth root of unity. Define V_ω to be the subspace consisting of vectors

$$[x]_\omega = \begin{pmatrix} x \\ \omega x \\ \vdots \\ \omega^{q-1} x \end{pmatrix}.$$

A short calculation shows that

$$J[x]_\omega = [(A - \omega I)x]_\omega.$$

Thus J has zero eigenvalues precisely when A has qth roots of unity as eigenvalues. By assumption, A has just one such pair of complex conjugate qth roots of unity as eigenvalues.

Since the kernel of J is two-dimensional—by the simple eigenvalue assumption in the Hopf bifurcation—it follows using Lyapunov-Schmidt reduction that solving the equation $\hat{P}(x) = 0$ near a resonance point is equivalent to finding the zeros of a reduced map from $\mathbb{R}^2 \to \mathbb{R}^2$. We can, however, naturally identify $\mathbb{R}^2$ with $\mathbb{C}$, which we do. Thus we need to find the zeros of a smooth implicitly defined function

$$g : \mathbb{C} \to \mathbb{C},$$

where $g(0) = 0$ and $(dg)_0 = 0$. Moreover, assuming that the Lyapunov-Schmidt reduction is done to respect symmetry, the reduced map g commutes with the action of σ on the critical eigenspace. More precisely, let ω be the critical resonant eigenvalue of $(dP)_0$; then

$$g(\omega z) = \omega g(z). \tag{18}$$

Since p and q are coprime, ω generates the group $\mathbb{Z}_q$ consisting of all qth roots of unity. So g is $\mathbb{Z}_q$-equivariant.

We propose to use $\mathbb{Z}_q$-equivariant singularity theory to classify resonance tongues and tongue boundaries.

5.2 Equivariant Singularity Theory

In this section we develop normal forms for the simplest singularities of $\mathbb{Z}_q$-equivariant maps g of the form (18), as presented in Sect. 3.1. To do this, we need to describe the form of $\mathbb{Z}_q$-equivariant maps, contact equivalence, and finally the normal forms.

The structure of $\mathbb{Z}_q$-equivariant maps. We begin by determining a unique form for the general $\mathbb{Z}_q$-equivariant polynomial mapping. By Schwarz's theorem [58] this representation is also valid for C^∞ germs.

Lemma 1. *Every $\mathbb{Z}_q$-equivariant polynomial map $g : \mathbb{C} \to \mathbb{C}$ has the form*

$$g(z) = K(u, v)z + L(u, v)\bar{z}^{q-1},$$

where $u = z\bar{z}$, $v = z^q + \bar{z}^q$, and K, L are uniquely defined complex-valued function germs.

$\mathbb{Z}_q$ contact equivalences. Singularity theory approaches the study of zeros of a mapping near a singularity by implementing coordinate changes that transform the mapping to a 'simple' normal form and then solving the normal form equation. The kinds of transformations that preserve the zeros of a mapping are called contact equivalences. More precisely, two $\mathbb{Z}_q$-equivariant germs g and h are $\mathbb{Z}_q$-*contact equivalent* if

$$h(z) = S(z)g(Z(z)),$$

where $Z(z)$ is a $\mathbb{Z}_q$-equivariant change of coordinates and $S(z) : \mathbb{C} \to \mathbb{C}$ is a real linear map for each z that satisfies

$$S(\gamma z)\gamma = \gamma S(z)$$

for all $\gamma \in \mathbb{Z}_q$.

Normal form theorems. In this section we consider two classes of normal forms—the codimension two standard for resonant Hopf bifurcation and one more degenerate singularity that has a degeneracy at cubic order. These singularities all satisfy the nondegeneracy condition $L(0,0) \neq 0$; we explore this case first.

Theorem 1. *Suppose that*

$$h(z) = K(u,v)z + L(u,v)\overline{z}^{q-1}$$

where $K(0,0) = 0$.

1. *Let* $q \geq 5$. *If* $K_u L(0,0) \neq 0$, *then* h *is* $\mathbb{Z}_q$ *contact equivalent to*

$$g(z) = |z|^2 z + \overline{z}^{q-1}$$

with universal unfolding

$$G(z,\sigma) = (\sigma + |z|^2)z + \overline{z}^{q-1}.$$

2. *Let* $q \geq 7$. *If* $K_u(0,0) = 0$ *and* $K_{uu}(0,0)L(0,0) \neq 0$, *then* h *is* $\mathbb{Z}_q$ *contact equivalent to*

$$g(z) = |z|^4 z + \overline{z}^{q-1}$$

with universal unfolding

$$G(z,\sigma,\tau) = (\sigma + \tau|z|^2 + |z|^4)z + \overline{z}^{q-1},$$

where $\sigma, \tau \in \mathbb{C}$.

Remark 2. Normal forms for the cases $q = 3$ and $q = 4$ are slightly different. See [27] for details.

5.3 Resonances in Forced Oscillators

As indicated in Sect. 2.1 subharmonic bifurcations in periodicially forced oscillators and the can be studied by lifting the system to a suitable covering space. This section contains the details of this procedure.

Hopf-Neĭmark-Sacker bifurcations in forced oscillators. Forced oscillators depending on parameters may undergo bifurcations involving the birth or death of subharmonics. In particular, we consider 2π-periodic systems on $\mathbb{C}$ of the form

$$\dot{z} = F(z, \bar{z}, \mu) + \varepsilon G(z, \bar{z}, t, \mu), \tag{19}$$

obtained from an autonomous system by a small 2π-periodic perturbation. Here ε is a real perturbation parameter, and $\mu \in \mathbb{R}^k$ is an additional k-dimensional parameter. Subharmonics of order q may appear or disappear upon variation of the parameters if the linear part of F at $z = 0$ satisfies a $p : q$-resonance condition which is appropriately detuned upon variation of the parameter μ.

The Hopf-Neĭmark-Sacker Normal form of such systems reveals this type of bifurcation. To this end, consider a 2π-periodic forced oscillator on $\mathbb{C}$ of the form

$$\dot{z} = X(z, \bar{z}, t, \mu),$$

where

$$X(z, \bar{z}, t, \mu) = i\omega_N z + (\alpha + i\delta)z + zP(z, \bar{z}, \mu) + \varepsilon Q(z, \bar{z}, t, \mu). \tag{20}$$

Here $\mu \in \mathbb{R}^k$, and ε is a small real parameter. Furthermore we assume that P and Q contain no terms that are independent of z and $\bar{z}$ (i.e., $P(0, 0, \mu) = 0$ and $Q(0, 0, t, \mu) = 0$), and that Q does not even contain terms that are linear in z and $\bar{z}$. Any system of the form (19) with linear part $\dot{z} = i\omega_N z$ can be brought into this form after a straightforward initial transformation. See [24, Part II] for details. Applying the algorithm of, e.g., [30], this system can be brought into the following Hopf-Neĭmark-Sacker normal form:

Theorem 2 (Normal Form to order q). *The system (20) has normal form*

$$\dot{z} = i\omega_N z + (\alpha + i\delta)z + zF(|z|^2, \mu) + d\,\varepsilon\,\bar{z}^{q-1}\,e^{ipt} + O(q+1), \tag{21}$$

where $F(|z|^2, \mu)$ is a complex polynomial of degree $q-1$ with $F(0, \mu) = 0$, and d is a complex constant.

Subharmonics of order q are to be expected if the linear part satisfies a $p : q$-resonance condition, in other words, if the normal frequency ω_N is equal to $\frac{p}{q}$ (with p and q relatively prime). To explore these subharmonics further we apply the Van der Pol transformation and bring the Poincaré-map of the lifted system into its Takens Normal Form.

Existence of $2\pi q$-periodic orbits. The Van der Pol transformation. Subharmonics of order q of the 2π-periodic forced oscillator (20) correspond to q-periodic orbits of the Poincaré time 2π-map $P : \mathbb{C} \to \mathbb{C}$. These periodic orbits of the Poincaré map are brought into one-one correspondence with the zeros of a vector

field on a q-sheeted cover of the phase space $\mathbb{C} \times \mathbb{R}/(2\pi\mathbb{Z})$ via the *Van der Pol transformation*, cf. [22]. This transformation corresponds to a q-sheeted covering

$$\begin{aligned} \Pi : \mathbb{C} \times \mathbb{R}/(2\pi q\mathbb{Z}) &\to \mathbb{C} \times \mathbb{R}/(2\pi\mathbb{Z}), \\ (z, t) &\mapsto (z\mathrm{e}^{itp/q}, t \pmod{2\pi\mathbb{Z}}) \end{aligned} \tag{22}$$

with cyclic Deck group of order q generated by

$$(z, t) \mapsto (z\mathrm{e}^{2\pi i p/q}, t - 2\pi).$$

The Van der Pol transformation $\zeta = ze^{-i\omega_N t}$ lifts the forced oscillator (19) to the system

$$\dot{\zeta} = (\alpha + i\delta)\zeta + \zeta P(\zeta e^{i\omega_N t}, \overline{\zeta} e^{-i\omega_N t}, \mu) + \varepsilon Q(\zeta e^{i\omega_N t}, \overline{\zeta} e^{-i\omega_N t}, t, \mu) \tag{23}$$

on the covering space $\mathbb{C} \times \mathbb{R}/(2\pi q\mathbb{Z})$. The latter system is $\mathbb{Z}_q$-equivariant. A straightforward application of (23) to the normal form (21) yields the following normal form for the lifted forced oscillator.

Theorem 3 (Equivariant Normal Form of order q). *On the covering space, the lifted forced oscillator has the $\mathbb{Z}_q$-equivariant normal form:*

$$\dot{\zeta} = (\alpha + i\delta)\zeta + \zeta F(|\zeta|^2, \mu) + d\,\varepsilon\,\overline{\zeta}^{q-1} + O(q+1), \tag{24}$$

where the $O(q+1)$ terms are $2\pi q$-periodic.

Resonance tongues for families of forced oscillators. Bifurcations of q-periodic orbits of the Poincaré map P on the base space correspond to bifurcations of fixed points of the Poincaré map $\tilde{P}$ on the q-sheeted covering space introduced in connection with the Van der Pol transformation (22). Denoting the normal form system (21) on the base space by $\mathcal{N}$, and the normal form system (24) of the lifted forced oscillator by $\tilde{\mathcal{N}}$, we see that

$$\Pi_* \tilde{\mathcal{N}} = \mathcal{N}.$$

The Poincaré mapping $\tilde{P}$ of the normal form on the covering space now is the $2\pi q$-period mapping

$$\tilde{P} = \tilde{\mathcal{N}}^{2\pi q} + O(q+1),$$

where $\tilde{\mathcal{N}}^{2\pi q}$ denotes the $2\pi q$-map of the (planar) vector field $\tilde{\mathcal{N}}$. Following the Corollary to the Normal Form Theorem of [22, page 12], we conclude for the original Poincaré map P of the vector field X on the base space that

$$P = R_{2\pi\omega_N} \circ \tilde{\mathcal{N}}^{2\pi} + O(q+1),$$

where $R_{2\pi\omega_N}$ is the rotation over $2\pi\omega_N = 2\pi p/q$, which precisely is the Takens Normal Form of P at $(z, \mu) = (0, 0)$, see [85].

Our interest is with the q-periodic points of P_μ, which correspond to the fixed points of $\tilde{P}_\mu$. This fixed point set and the boundary thereof in the parameter space $\mathbb{R}^3 = \{a, \delta, \varepsilon\}$ is approximately described by the discriminant set of

$$(a + i\delta)\zeta + \zeta\tilde{F}(|\zeta|^2, \mu) + \varepsilon d\bar{\zeta}^{q-1},$$

which is the truncated right hand side of (24). This gives rise to the bifurcation equation that determine the boundaries of the resonance tongues. The following theorem implies that, under the conditions that $d \neq 0 \neq F_u(0, 0)$, the order of tangency at the tongue tips is generic. Here $F_u(0, 0)$ is the partial derivative of $F(u, \mu)$ with respect to u.

Theorem 4 (Bifurcation equations modulo contact equivalence). *Assume that $d \neq 0$ and $F_u(0, 0) \neq 0$. Then the polynomial (24) is $\mathbb{Z}_q$-equivariantly contact equivalent with the polynomial*

$$G(\zeta, \mu) = (a + i\delta + |\zeta|^2)\zeta + \varepsilon\bar{\zeta}^{q-1}. \tag{25}$$

The discriminant set of the polynomial $G(\zeta, \mu)$ is of the form

$$\delta = \pm\varepsilon(-a)^{(q-2)/2} + O(\varepsilon^2). \tag{26}$$

Proof. The polynomial (25) is a universal unfolding of the germ $|\zeta|^2\zeta + \varepsilon\bar{\zeta}^{q-1}$ under $\mathbb{Z}_q$ contact equivalence. See [27] for a detailed computation. The tongue boundaries of a $p : q$ resonance are given by the bifurcation equations

$$\begin{aligned} G(\zeta, \mu) &= 0, \\ \det(dG)(\zeta, \mu) &= 0. \end{aligned}$$

As in [27, Theorem 3.1] we put $u = |z|^2$, and $b(u, \mu) = a + i\delta + u$. Then $G(\zeta, \mu) = b(u, \mu)\zeta + \varepsilon\bar{\zeta}^{q-1}$. According to (the proof of) [27, Theorem 3.1], the system of bifurcation equations is equivalent to

$$\begin{aligned} |b|^2 &= \varepsilon^2 u^{q-2}, \\ b\bar{b}' + \bar{b}b' &= (q-2)\varepsilon^2 u^{q-3}, \end{aligned}$$

where $b' = \dfrac{\partial b}{\partial u}(u, \mu)$. A short computation reduces the latter system to the equivalent

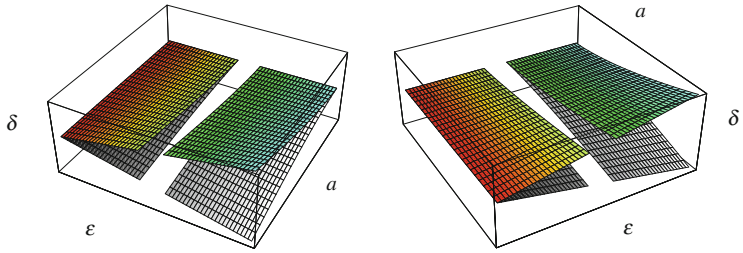

Fig. 15 Resonance zones for forced oscillator families: the Hopf-Neĭmark-Sacker phenomenon

$$(a+u)^2+\delta^2=\varepsilon^2u^{q-2},$$
$$a+u=\frac{1}{2}(q-2)\varepsilon^2u^{q-3}.$$

Eliminating u from this system of equations yields expression (26) for the tongue boundaries. □

The discriminant set of the equivariant polynomial (25) forms the boundary of the resonance tongues. See Fig. 15. At this surface we expect the Hopf-Neĭmark-Sacker bifurcation to occur; here the Floquet exponents of the linear part of the forced oscillator cross the complex unit circle. This bifurcation gives rise to an invariant 2-torus in the 3D phase space $\mathbb{C}\times\mathbb{R}/(2\pi\mathbb{Z})$. Resonances occur when the eigenvalues cross the unit circle at roots of unity $e^{2\pi ip/q}$. 'Inside' the tongue the 2-torus is phase-locked to subharmonic periodic solutions of order q.

Acknowledgements The author thanks Konstantinos Efstathiou, Aernout van Enter and Ferdinand Verhulst for their help in the preparation of this paper.

References

1. Arnol'd, V.I.: Small divisors I: on mappings of the circle onto itself. Am. Math. Soc. Transl. Ser. 2 **46**. 213–284 (1965)
2. Arnold, V.I.: Mathematical Methods of Classical Mechanics. GTM 60. Springer, New York (1978). 2nd edn. (1989)
3. Arnold, V.I.: Geometrical Methods in the Theory of Ordinary Differential Equations. Springer, New York (1983). Grundlehren der mathematischen Wissenschaften, vol. 250, 2nd edn. Springer (1988)
4. Arnold, V.I., Avez, A.: Probèmes Ergodiques de la Mécanique classique. Gauthier-Villars, Paris (1967); Ergodic Problems of Classical Mechanics. Benjamin (1968). 2nd edn. Addison-Wesley (1989)
5. Arnol'd, V.I., Kozlov, V.V., Neishtadt, A.I.: Mathematical aspects of classical and celestial mechanics. In: Arnol'd, V.I. (ed.) Dynamical Systems III. Springer, Berlin/New York (1988). 3rd edn. Springer (2006)

6. Avila, A., Damanik, D.: Generic singular spectrum for ergodic Schrödinger operators. Duke Math. J. **130**(2), 393–400 (2005)
7. Baesens, C., Guckenheimer, J., Kim, S., MacKay, R.S.: Three coupled oscillators: mode-locking, global bifurcation and toroidal chaos. Phys. D **49**(3), 387–475 (1991)
8. Beersma, D.G.M., Broer, H.W., Cargar, K.A., Efstathiou, K., Hoveijn, I.: Pacer cell response to periodic Zeitgebers. Preprint University of Groningen (2011)
9. Bennett, M., Schatz, M.F., Rockwood, H., Wiesenfeld, K.: Huygens clocks. Proc. R. Soc. Lond. A **458**, 563–579 (2002)
10. Braaksma, B.L.J., Broer, H.W.: On a quasi-periodic Hopf bifurcation. Annales Insitut Henri Poincaré, Analyse non linéaire **4**, 115–168 (1987)
11. Braaksma, B.L.J., Broer, H.W., Huitema, G.B.: Towards a quasi-periodic bifurcation theory. Mem. AMS **83**(421), 81–175 (1990)
12. Broer, H.W.: KAM theory: the legacy of Kolmogorov's 1954 paper. Bull. AMS (New Series) **41**(4), 507–521 (2004)
13. Broer, H.W.: Normal forms in perturbation theory. In: Meyers, R. (ed.) Encyclopædia of Complexity & System Science, pp. 6310–6329. Springer, New York (2009)
14. Broer, H.W.: Resonance and fractal geometry. Acta Appl. Math. **120**(1), 61–86 (2012)
15. Broer, H.W., Levi, M.: Geometrical aspects of stability theory for Hill's equations. Arch. Ration. Mech. Anal. **131**, 225–240 (1995)
16. Broer, H.W., Roussarie, R.: Exponential confinement of chaos in the bifurcations sets of real analytic diffeomorphisms. In: Broer, H.W., Krauskopf, B., Vegter, G. (eds.) Global Analysis of Dynamical Systems, pp. 167–210. IoP Publishing, Bristol (2001)
17. Broer, H.W., Simó, C.: Hill's equation with quasi-periodic forcing: resonance tongues, instability pockets and global phenomena. Bol. Soc. Bras. Mat. **29**, 253–293 (1998)
18. Broer, H.W., Simó, C.: Resonance tongues in Hill's equations: a geometric approach. J. Differ. Equ. **166**, 290–327 (2000)
19. Broer, H.W., Takens, F.: Formally symmetric normal forms and genericity. Dyn. Rep. **2**, 36–60 (1989)
20. Broer, H.W., Takens, F.: Dynamical Systems and Chaos. Applied Mathematical Sciences, vol. 172. Springer, New York (2011)
21. Broer, H.W., Vegter, G.: Subordinate Sil'nikov bifurcations near some singularities of vector fields having low codimension. Ergod. Theory Dyn. Syst. **4**, 509–525 (1984)
22. Broer, H.W., Vegter, G.: Bifurcational aspects of parametric resonance. Dyn. Rep. New Ser. **1**, 1–51 (1992)
23. Broer, H.W., Vegter, G.: Generic Hopf-Neĭmark-Sacker bifurcations in feed forward systems. Nonlinearity **21**, 1547–1578 (2008)
24. Broer, H.W., Huitema, G.B., Takens, F.: Unfoldings and bifurcations of quasi-periodic tori. Mem. Am. Math. Soc. **83**(#421), 1–82 (1990)
25. Broer, H.W., Simó, C., Tatjer, J.C.: Towards global models near homoclinic tangencies of dissipative diffeomorphisms. Nonlinearity **11**(3), 667–770 (1998)
26. Broer, H.W., Simó, C., Vitolo, R.: Bifurcations and strange attractors in the Lorenz-84 climate model with seasonal forcing. Nonlinearity **15**(4), 1205–1267 (2002)
27. Broer, H.W., Golubitsky, M., Vegter, G.: The geometry of resonance tongues: a singularity theory approach. Nonlinearity **16**, 1511–1538 (2003)
28. Broer, H.W., Hanßmann, H., Jorba, Á., Villanueva, J., Wagener, F.O.O.: Normal-internal resonances in quasi-periodically forces oscillators: a conservative approach. Nonlinearity **16**, 1751–1791 (2003)
29. Broer, H.W., Puig, J., Simó, C.: Resonance tongues and instability pockets in the quasi-periodic Hill-Schrödinger equation. Commun. Math. Phys. **241**, 467–503 (2003)
30. Broer, H.W., Golubitsky, M., Vegter, G.: Geometry of resonance tongues. In: Singularity Theory. Proceedings of the 2005 Marseille Singularity School and Conference, Marseille, pp. 327–356 (2007)
31. Broer, H.W., Hanßmann, H., Hoo, J.: The quasi-periodic Hamiltonian Hopf bifurcation. Nonlinearity **20**, 417–460 (2007)

32. Broer, H.W., Hoo, J., Naudot, V.: Normal linear stability of quasi-periodic tori. J. Differ. Equ. **232**, 355–418 (2007)
33. Broer, H.W., Efstathiou, K., Subramanian, E.: Robustness of unstable attractors in arbitrarily sized pulse-coupled systems with delay. Nonlinearity **21**, 13–49 (2008)
34. Broer, H.W., Efstathiou, K., Subramanian, E.: Heteroclinic cycles between unstable attractors. Nonlinearity **21**, 1385–1410 (2008)
35. Broer, H.W., Hanßmann, H., You, J.: On the destruction of resonant Lagrangean tori in Hamiltonian systems. In: Johann, A., Kruse, H.-P., Rupp, F., Schmitz, S. (eds.) Recent Trends in Dynamical Systems, Proceedings of a Conference in Honor of Jürgen Scheurle. Springer Proceedings in Mathematics & Statistics, vol. 35, Chapter 13 (2013 to appear). ISBN 978-3-0348-0450-9
36. Broer, H.W., Holtman, S.J., Vegter, G.: Recognition of the bifurcation type of resonance in a mildly degenerate Hopf-Neĭmark-Sacker families. Nonlinearity **21**, 2463–2482 (2008)
37. Broer, H.W., Simó, C., Vitolo, R.: The Hopf-Saddle-Node bifurcation for fixed points of 3D-diffeomorphisms, analysis of a resonance 'bubble'. Phys. D **237**, 1773–1799 (2008)
38. Broer, H.W., Simó, C., Vitolo, R.: The Hopf-Saddle-Node bifurcation for fixed points of 3D-diffeomorphisms, the Arnol'd resonance web. Bull. Belg. Math. Soc. Simon Stevin **15**, 769–787 (2008)
39. Broer, H.W., Ciocci, M.C., Hanßmann, H., Vanderbauwhede, A.: Quasi-periodic stability of normally resonant tori. Phys. D **238**, 309–318 (2009)
40. Broer, H.W., Holtman, S.J., Vegter, G., Vitolo, R.: Geometry and dynamics of mildly degenerate Hopf-Neĭmarck-Sacker families near resonance. Nonlinearity **22**, 2161–2200 (2009)
41. Broer, H.W., Holtman, S.J., Vegter, G.: Recognition of resonance type in periodically forced oscillators. Phys.-D **239**(17), 1627–1636 (2010)
42. Broer, H.W., Simó, C., Vitolo, R.: Chaos and quasi-periodicity in diffeomorphisms of the solid torus. DCDS-B **14**(3), 871–905 (2010)
43. Broer, H.W., Dijkstra, H.A., Simó, C., Sterk, A.E., Vitolo, R.: The dynamics of a low-order model for the Atlantic Multidecadal Oscillation. DCDS-B **16**(1), 73–102 (2011)
44. Broer, H.W., Holtman, S.J., Vegter, G., Vitolo, R.: Dynamics and Geometry Near Resonant Bifurcations. Regul. Chaotic Dyn. **16**(1–2), 39–50 (2011)
45. Broer, H.W., Hanßmann, H., Wagener, F.O.O.: Quasi-periodic bifurcation theory: the geometry of KAM (2012). (to appear)
46. Chenciner, A.: Bifurcations de points fixes elliptiques. I. Courbes invariantes. Publ. Math. IHÉS **61**, 67–127 (1985)
47. Chenciner, A.: Bifurcations de points fixes elliptiques. II. Orbites périodiques et ensembles de Cantor invariants. Invent. Math. **80**, 81–106 (1985)
48. Chenciner, A.: Bifurcations de points fixes elliptiques. III. Orbites périodiques de "petites" périodes et élimination résonnante des couples de courbes invariantes. Publ. Math. IHÉS **66**, 5–91 (1988)
49. Ciocci, M.C., Litvak-Hinenzon, A., Broer, H.W.: Survey on dissipative KAM theory including quasi-periodic bifurcation theory based on lectures by Henk Broer. In: Montaldi, J., Ratiu, T. (eds.) Geometric Mechanics and Symmetry: The Peyresq Lectures. LMS Lecture Notes Series, vol. 306, pp. 303–355. Cambridge University Press, Cambridge (2005)
50. Correia, A., Laskar, J.: Mercury's capture into the 3/2 spin-orbit resonance as a result of its chaotic dynamics. Nature **429**, 848–850 (2004)
51. Cushman, R.H., van der Meer, J.C.: The Hamiltonian Hopf bifurcation in the Lagrange top. In: Albert, C. (ed.) Géometrie Symplectique et Méchanique, Colloque International, La Grande Motte, 23–28 Mai 1988. Lecture Notes in Mathematics, vol. 1416, pp. 26–38 (1990)
52. de Sitter, W.: On the libration of the three inner large satellites of Jupiter. Publ. Astron. Lab. Gron. **17**, 1–119 (1907)
53. de Sitter, W.: New mathematical theory of Jupiters satellites. Ann. Sterrewacht Leiden, XII (1925)
54. Devaney, R.L.: An Introduction to Chaotic Dynamical Systems, 2nd edn. Addison-Wesley, Redwood City (1989). 2nd edn. Westview Press (2003)

55. Eliasson, L.H.: Floquet solutions for the one-dimensional quasi-periodic Schrödinger equation. Commun. Math. Phys. **146**, 447–482 (1992)
56. Golubitsky, M., Guillemin, V.: Stable Mappings and Their Singularities. Springer, New York (1973). GTM, vol. 14. Springer (1973)
57. Golubitsky, M., Schaeffer, D.G.: Singularities and Groups in Bifurcation Theory Vol. I. Springer, New York (1985)
58. Golubitsky, M., Stewart, I., Schaeffer, D.G.: Singularities and Groups in Bifurcation Theory Vol. II. Applied Mathematical Sciences, vol. 69 Springer, New York (1988)
59. Guckenheimer, J., Holmes, P.: Nonlinear Oscillations, Dynamical Systems, and Bifurcations of Vector Fields, 5th edn. Applied Mathematical Sciences, vol. 42. Springer, New York (1997)
60. Hopf, E.: A mathematical example displaying features of turbulence. Commun. (Pure) Appl. Math. **1**, 303–322 (1948)
61. Hopf, E.: Repeated branching through loss of stability, an example. In: Diaz, J.B. (ed.) Proceedings of the Conference on Differential Equations, College Park, MD 1955, pp. 49–56. University Maryland book store (1956)
62. Huygens, C.: Œvres complètes de Christiaan Huygens., vol. 5, pp. 241–263 and vol. 17, pp. 156–189. Martinus Nijhoff, La Haye (1888–1950)
63. Kuznetsov, Yu.A.: Elements of Applied Bifurcation Theory, 3rd edn. Applied Mathematical Sciences, vol. 112. Springer, New York (2004)
64. Landau, L.D.: On the problem of turbulence. Dokl. Akad. Nauk SSSR **44**, 339–342 (1944)
65. Landau, L.D., Lifshitz, E.M.: Fluid Mechanics, 2nd edn. Pergamon, Oxford/New York (1987)
66. Newhouse, S.E., Palis, J., Takens, F.: Bifurcations and stability of families of diffeomorphisms. Publ. Math. IHES **57**, 5–71 (1983)
67. Newhouse, S.E., Ruelle, D., Takens, F.: Occurrence of strange Axiom A attractors near quasi-periodic flows on $\mathbb{T}^m$, $m \leq 3$. Commun. Math. Phys. **64**, 35–40 (1978)
68. Mandelbrot, B.B.: The Fractal Geometry of Nature. Freeman, New York (1977)
69. Moser, J.K.: On invariant curves of area-preserving mappings of an annulus. Nachrichten Akademie Wissenschaften Göttingen, Mathematisch–Physikalische Klasse II. **1**, 1–20 (1962)
70. Moser, J.K.: Lectures on Hamiltonian systems. Mem. Am. Math. Soc. **81**, 1–60 (1968)
71. Moser, J.K.: Stable and Random Motions in Dynamical Systems, with Special Emphasis to Celestial Mechanics. Annals Mathematical Studies, vol. 77. Princeton University Press, Princeton (1973). Princeton Landmarks in Mathematics (2001)
72. Moser, J.K., Pöschel, J.: An extension of a result by Dinaburg and Sinai on quasi-periodic potentials. Comment. Math. Helv. **59**, 39–85 (1984)
73. Nitecki, Z.: Differentiable Dynamics. An Introduction to the Orbit Structure of Diffeomorphisms. Massachusetts Institute of Technology, Cambridge (1971)
74. Oxtoby, J.: Measure and Category. Springer, New York (1971). 2nd edn. Springer (1980)
75. Palis, J., Takens, F.: Hyperbolicity & Sensitive Chaotic Dynamics at Homoclinic Bifurcations. Cambridge University Press, Cambridge/New York (1993)
76. Poincaré, J.H.: Les Méthodes Nouvelles de la Mécanique Céleste I, II, III. Gauthier-Villars, Paris (1892, 1893, 1899). Republished by Blanchard (1987)
77. Pogromsky, A., Rijlaarsdam, D., Nijmeijer, H.: Experimental Huygens synchronization of oscillators. In: Thiel, M., Kurths, J., Romano, M.C., Moura, A., Károlyi, G. (eds.) Nonlinear Dynamics and Chaos: Advances and Perspectives. Springer Complexity, pp. 195–210. Springer, New York/Berlin/Heidelberg (2010)
78. Ruelle, D., Takens, F.: On the nature of turbulence. Commun. Math. Phys. **20**, 167–192 (1971); **23**, 343–344 (1971)
79. Sanders, J.A., Verhulst, F., Murdock, J.: Averaging Methods in Nonlinear Dynamical Systems, Rev. 2nd edn. Applied Mathematical Sciences, vol. 59. Springer, New York (2007)
80. Siegel, C.L., Moser, J.K.: Lectures on Celestial Mechanics. Springer, Berlin/New York (1971)
81. Simon, B.: Operators with singular continuous spectrum: I. General operators. Ann. Math. **141**, 131–145 (1995)
82. Sterk, A.E., Vitolo, R., Broer, H.W., Simó, C., Dijkstra, H.A.: New nonlinear mechanisms of midlatitude atmospheric low-frequency variability. Phys. D **239**(10), 702–718 (2010)

83. Stoker, J.J.: Nonlinear Vibrations in Mechanical and Electrical Systems, 2nd edn. Wiley, New York (1992)
84. Strogatz, S.H.: Nonlinear Dynamics and Chaos. Addison Wesley, Reading (1994)
85. Takens, F.: Forced oscillations and bifurcations. In: Applications of Global Analysis I. Communications of the Mathematical Institute, Rijksuniversiteit Utrecht (1974). In: Broer, H.W., Krauskopf, B., Vegter, G. (eds.) Global Analysis of Dynamical Systems. IoP Publishing, pp. 1–62 (2001)
86. Thom, R.: Stabilité Structurelle et Morphogénèse. Benjamin, Reading (1972). Addison-Wesley (1989)
87. Verhulst, F.: Nonlinear Differential Equations and Dynamical Systems. Universitext, 2nd edn. Springer, Berlin (1996). Universitext, 2nd edn. Springer (2000)
88. Vitolo, R., Broer, H.W., Simó, C.: Quasi-periodic bifurcations of invariant circles in low-dimensional dissipative dynamical systems. Regul. Chaotic Dyn. **16**(1–2), 154–184 (2011)
89. Vanderbauwhede, A.: Branching of periodic solutions in time-reversible systems. In: Broer, H.W., Takens, F. (eds.) Geometry and Analysis in Non-linear Dynamics. Volume 222 of Pitman Research Notes in Mathematics, pp. 97–113. Pitman, London (1992)
90. Vanderbauwhede, A.: Subharmonic bifurcation at multiple resonances. In: Eliady, S., Allen, F., Elkhaeder, A., Mughrabi, T., Saleh, M. (eds.) Proceedings of the Mathematics Conference, (Birzeit August 1988), pp. 254–276. World Scientific, Singapore (2000)
91. van der Pol, B.: De amplitude van vrije en gedwongen triode-trillingen. Tijdschr. Ned. Radiogenoot. **1**, 3–31 (1920)
92. van der Pol, B.: The nonlinear theory of electric oscillations. Proc. Inst. Radio Engl. **22**, 1051–1086 (1934) Reprinted in: Selected Scientific Papers. North-Holland (1960)

Inverse Jacobi Multipliers: Recent Applications in Dynamical Systems

Adriana Buică, Isaac A. García, and Susanna Maza

Abstract In this paper we show novel applications of the inverse Jacobi multiplier focusing on questions of bifurcations and existence of periodic solutions admitted by both autonomous and non-autonomous systems of ordinary differential equations. In the autonomous case we focus on dimension $n \geq 3$ whereas in the non-autonomous we study the cases with $n \geq 2$. We summarize results already published and additionally we state some recent results to appear. The principal object of this research is two fold: first to prove the existence and smoothness of inverse Jacobi multiplier V in the region of interest in the phase space and second to show that the invariant set under the flow given by the zero-set of an inverse Jacobi multiplier contains under some assumptions orbits which are relevant in its phase portrait such as periodic orbits, limit cycles, stable, unstable and center manifolds and so on. In the non-autonomous T-periodic case we show some relationships between T-periodic orbits and T-periodic inverse Jacobi multipliers.

1 Introduction

Through this paper first we will focalize our attention on autonomous systems of ordinary differential equations $\dot{x} = f(x)$ defined in an open set $U \subseteq \mathbb{R}^n$ where $x = (x_1, \ldots, x_n) \in U$ and $f : U \to \mathbb{R}^n$ is of class $C^1(U)$. We also consider its associated vector field $\mathscr{X} = \sum_{i=1}^{n} f_i(x)\partial_{x_i}$ where $f(x) = (f_1(x), \ldots, f_n(x))$.

A. Buică (✉)
Department of Applied Mathematics, Babeş-Bolyai University, Kogălniceanu 1,
400084 Cluj-Napoca, Romania
e-mail: abuica@math.ubbcluj.ro

I.A. García · S. Maza
Departament de Matemàtica, Universitat de Lleida, Avda. Jaume II, 69, 25001 Lleida, Spain
e-mail: garcia@matematica.udl.cat; smaza@matematica.udl.cat

S. Ibáñez et al. (eds.), *Progress and Challenges in Dynamical Systems*,
Springer Proceedings in Mathematics & Statistics 54,
DOI 10.1007/978-3-642-38830-9_8,

A $\mathscr{C}^1$ function $V : U \to \mathbb{R}$ non locally null in U is said to be an *inverse Jacobi multiplier* for the vector field $\mathscr{X}$ in $\mathscr{U}$ when V solves in U the linear first order partial differential equation $\mathscr{X}V = V\mathrm{div}\mathscr{X}$, where $\mathrm{div}\mathscr{X} = \sum_{i=1}^{n} \partial f_i(x)/\partial x_i$ is the divergence of the vector field $\mathscr{X}$. Clearly, for divergence-free vector fields, non-constant inverse Jacobi multipliers of $\mathscr{X}$ are just first integrals of $\mathscr{X}$. Inverse Jacobi multipliers are a natural generalization of inverse integrating factors to n-dimensional dynamical systems with $n \geq 3$. The special case $n = 2$ has been treated in many papers, see [9] and references therein. Therefore here we will only focus on the higher dimensional case $n \geq 3$.

The first appearance in the literature of the nowadays called Jacobi (last) multiplier $1/V$ was in [14]. After Jacobi, his last multiplier was mainly used to find the last additional first integral needed to get complete integrability of $\mathscr{X}$. The main idea consists in obtaining an inverse integrating factor of the final planar differential equation obtained after the elimination of $n-2$ variables thanks to the knowledge of a set $\{H_1(x), \ldots, H_{n-2}(x)\}$ of functionally independent first integrals of $\mathscr{X}$. More precisely, to fix ideas we solve (at least locally) from the equation $H_i(x) = h_i$ with arbitrary constant $h_i \in \mathbb{R}$ the variable x_i obtaining $x_i = F_i(x_{i+1}, \ldots, x_n, h_1, \ldots, h_i)$ from $i = 1, \ldots, n-2$. Then the inverse integrating factor $v(x_{n-1}, x_n)$ of the final planar differential equation between the variables x_{n-1} and x_n written in Pfaffian form

$$\omega := f_{n-1}(F_1, \ldots, F_{n-2}, x_{n-1}, x_n)\, dx_n - f_n(F_1, \ldots, F_{n-2}, x_{n-1}, x_n)\, dx_{n-1} = 0$$

will be given by $v = V \prod_{i=1}^{n-2} \frac{\partial H_i}{\partial x_i}$ where V is an inverse Jacobi multiplier of $\mathscr{X}$. The last first integral H_{n-1} of $\mathscr{X}$ is obtained by quadratures using the inverse integrating factor $v(x_{n-1}, x_n)$. More precisely the differential 1-form ω/v is exact and we get $dH_{n-1} = \omega/v$. Of course, the function H_{n-1} may be not well defined in a region which is not simply-connected.

The above mentioned procedure was the only (although useful) utility of Jacobi last multipliers until the occurrence of Sophus Lie which found a link between Jacobi last multipliers and Lie point symmetries of $\mathscr{X}$ in [15]. This connection works as follows. Assume that $\mathscr{X}$ admits in U a $(n-1)$–parameter local Lie group G of transformations with infinitesimal generators (also known as normalizers) given by $\{\mathscr{Z}_1, \ldots, \mathscr{Z}_{n-1}\}$, that is, the Lie bracket $[\mathscr{X}, \mathscr{Z}_i] = \Lambda_i \mathscr{X}$ holds for some functions $\Lambda_i : U \to \mathbb{R}$. Then an inverse Jacobi multiplier V for $\mathscr{X}$ in U is furnished by the determinant $V = \det\{\mathscr{X}, \mathscr{Z}_1, \ldots, \mathscr{Z}_{n-1}\}$ provided that this determinant is not identically zero, that is, assuming the independence condition $\mathscr{X} \wedge \mathscr{Z}_1 \wedge \ldots \wedge \mathscr{Z}_{n-1} \neq 0$ almost everywhere in U, i.e., in a full Lebesgue measure (dense) open subset of U. Notice that, under this construction, V vanishes on every integral curve of $\mathscr{X}$ in U which is invariant under the action of G in U.

We remark that although the connection between Jacobi last multipliers and Lie symmetries is quite old, recent results are still arising. As an example in [17] the authors show how to obtain a new inverse Jacobi multiplier from a given one and a normalizer. Let $\mathscr{Z}$ be a normalizer of $\mathscr{X}$ such that $[\mathscr{X}, \mathscr{Z}] = \Lambda\mathscr{X}$ and let V be a C^2 inverse Jacobi multiplier of $\mathscr{X}$. Then $\tilde{V} = (\mathrm{div}\mathscr{Z} - \Lambda)V - \mathscr{Z}(V)$ is another (maybe trivial) inverse Jacobi multiplier of $\mathscr{X}$. Of course in the trivial case ($\tilde{V} \equiv 0$ in U) no new information is giving.

It is also interesting to point out that the connections between Lie symmetries and Jacobi multipliers is recently exploited in several works analyzing systems of special relevance in physics, see for instance [20, 21] and references therein.

Now we present a brief list of some well-known properties of inverse Jacobi multipliers, see [2] for a modern proof:

- V is an inverse Jacobi multiplier of $\mathscr{X}$ in U if and only if $\mathrm{div}(\mathscr{X}/V) \equiv 0$ in the set $U \setminus V^{-1}(0)$.
- If we perform a change of coordinates $x \mapsto y$ defined by $y = \phi(x)$, then $W(y) = (V \circ \phi^{-1})(y) \det\{D\phi(\phi^{-1}(y))\}$ is an inverse Jacobi multiplier of the transformed vector field $\phi_*\mathscr{X}$. Here, since ϕ is a differentiable map, we denote its Jacobian matrix (differential) by $D\phi(x)$.
- Straightforward computations shows that if V_1 and V_2 are two linearly independent inverse Jacobi multipliers of $\mathscr{X}$ in U, then the ratio V_2/V_1 satisfies $\mathscr{X}(V_2/V_1) \equiv 0$ on $U \setminus V_1^{-1}(0)$ and therefore is a first integral of $\mathscr{X}$ in $U \setminus V_1^{-1}(0)$.
- The Jacobi multiplier can be understood as the density associated with an invariant measure. For any $x \in U$, let $\Psi_t(x)$ be the flow associated to $\mathscr{X}$ with initial condition $\Psi_0(x) = x$. Let $\Omega \subset U$ be any measurable set. Then, the integral $\int_{\Psi_t(\Omega)} 1/V(x)\,dx$ is an invariant integral (that is, it is independent of t) for $\mathscr{X}$ if and only if V is an inverse Jacobi multiplier of $\mathscr{X}$.

In this paper we show novel applications of the inverse Jacobi multiplier focusing on questions of bifurcations and existence of periodic solutions admitted by ordinary differential equations or equivalently for $\mathscr{X}$. The first work in this direction was [2]. It is a modern reference of the classical theory of Jacobi multiplier in the formal methods of integration of vector fields. Besides it gives also modern applications closely related to our point of view. The principal object of this new research is two fold: first to prove the existence and smoothness of a Jacobi multiplier V in the region of interest in the phase space and second to show that the invariant set of $\mathscr{X}$ given by the zero-set of a Jacobi multiplier $V^{-1}(0) = \{x \in U : V(x) = 0\}$ contains (under some assumptions) orbits of $\mathscr{X}$ which are relevant in its phase portrait such as periodic orbits, limit cycles, stable, unstable and center manifolds, separatrices and so on. Moreover sometimes $V^{-1}(0)$ contains also information about bifurcations occurring in perturbations of $\mathscr{X}$.

2 Autonomous Differential Systems

2.1 Invariant Manifolds Through Singularities

A point $p_0 \in U$ is a *singularity* of $\mathscr{X}$ if $\mathscr{X}(p_0) = 0$. We say that p_0 is a *nondegenerate* singular point if the Jacobian matrix $D\mathscr{X}(p_0)$ has no eigenvalues equal to zero. In addition, a singularity p_0 is called *strong* if $\operatorname{div}\mathscr{X}(p_0) \neq 0$. As usual, a hyperbolic singular point p_0 of a $\mathscr{C}^1$ vector filed $\mathscr{X}$ is named a *saddle point* when $D\mathscr{X}(p_0)$ has eigenvalues with both positive and negative real parts. Assuming that k of these real parts are positive and the remaining $n-k$ are negative, the stable manifold theorem ensures the existence of two invariant $\mathscr{C}^1$ manifolds $W^u(p_0)$ and $W^s(p_0)$ with dimensions $\dim W^u(p_0) = k$ and $\dim W^s(p_0) = n-k$, such that they intersect transversally one each other in p_0. In [2] it is proved the next result.

Theorem 1 ([2]). *Let p_0 be a nondegenerate strong singular point of the $\mathscr{C}^1$ vector field $\mathscr{X}$ having an inverse Jacobi multiplier V defined in a neighborhood of p_0. Then V vanishes on $W^u(p_0)$ (resp. $W^s(p_0)$) provided that $\operatorname{div}\mathscr{X}(p_0) < 0$ (resp. $\operatorname{div}\mathscr{X}(p_0) > 0$).*

2.2 Limit Cycles

By a *limit cycle* $\gamma = \{\gamma(t) \in U : 0 \leq t \leq T\}$ of $\mathscr{X}$ we mean a T–periodic orbit which is α or ω–limit set of another orbit of $\mathscr{X}$. We define

$$\Delta(\gamma) = \int_0^T \operatorname{div}\mathscr{X} \circ \gamma(t)\, dt\,,$$

and we recall that $\Delta(\gamma)$ is the sum of the characteristic exponents of γ. Thus if $\Delta(\gamma) > 0$ then γ is not orbitally stable. We will say that γ is a *strong* limit cycle when $\Delta(\gamma) \neq 0$ and it is a *weak* limit cycle otherwise. In [2] the next two results are proved.

Theorem 2 ([2]). *Let V be an inverse Jacobi multiplier of $\mathscr{X}$ defined in a region containing a limit cycle γ of $\mathscr{X}$. Then, $\gamma \subset V^{-1}(0)$ in the following cases:* (i) *if γ is a strong limit cycle, or* (ii) *if γ is asymptotically orbitally stable (unstable).*

Remark 1. It is important to emphasize that in the planar case $n = 2$ the corresponding Theorem 2 is stronger because always $\gamma \subset V^{-1}(0)$ independently of the nature of γ. This important property has currently several different proofs but the first was given in [13] using the machinery of de Rham cohomology.

Theorem 3 ([2]). *Let V be a Jacobi inverse multiplier defined in a neighborhood of a limit cycle γ of the vector field $\mathscr{X}$. If γ is a strong limit cycle, then*

(i) V vanishes on $W^s(\gamma)$, the stable manifold of γ, provided that $\Delta(\gamma) > 0$;
(ii) V vanishes on $W^u(\gamma)$, the unstable manifold of γ, provided that $\Delta(\gamma) < 0$.

3 Monodromic Singularities on Center Manifolds in $\mathbb{R}^3$

We consider three-dimensional systems

$$\dot{x} = -y + \mathscr{F}_1(x, y, z)\ ,\ \dot{y} = x + \mathscr{F}_2(x, y, z)\ ,\ \dot{z} = \lambda z + \mathscr{F}_3(x, y, z), \quad (1)$$

where $\lambda \in \mathbb{R} \setminus \{0\}$, $\mathscr{F} = (\mathscr{F}_1, \mathscr{F}_2, \mathscr{F}_3) : U \to \mathbb{R}^3$ is real analytic on the open neighborhood $U \subset \mathbb{R}^3$ of the origin, and $\mathscr{F}$ satisfies $\mathscr{F}(0) = 0$ and $D\mathscr{F}(0) = 0$. We let $\mathscr{X}_\lambda = (-y + \mathscr{F}_1(x, y, z))\partial_x + (x + \mathscr{F}_2(x, y, z))\partial_y + (\lambda z + \mathscr{F}_3(x, y, z))\partial_z$ denote the vector field associated to system (1).

Since the eigenvalues at the origin of system (1) are $\{\pm i, \lambda\}$ with $i^2 = -1$, it is well-known that it possesses a C^r local center manifold W^c at the origin for any $r \in \mathbb{N}$, which need not be neither unique nor analytic. It is also known that the singularity of the restricted vector field $\mathscr{X}_\lambda|W^c$ at the origin must be either a focus or a center. In the center case, [3] proves that system (1) is analytically normalizable. This means that there exists a real analytic near-identity diffeomorphism that brings system (1) into the following normal from

$$\dot{x} = -y[1 + F(x^2 + y^2)]\ ,\ \dot{y} = x[1 + F(x^2 + y^2)]\ ,\ \dot{z} = z[\lambda + G(x^2 + y^2)]\ , \quad (2)$$

where F and G are real analytic on a neighborhood of zero in $\mathbb{R}$ and moreover $F(0) = G(0) = 0$.

In the focus case, that is, when $\mathscr{X}_\lambda$ has a focus at the origin in a center manifold (hence on every center manifold), system (1) need not be analytically normalizable. But in this case (see [1]) system (1) is C^∞-conjugated to the normal form

$$\begin{aligned}
\dot{x} &= -y + \frac{1}{2}[(x + iy)A(x^2 + y^2) + (x - iy)B(x^2 + y^2)] \\
\dot{y} &= x + \frac{1}{2}[(y - ix)A(x^2 + y^2) + (y + ix)B(x^2 + y^2)] \\
\dot{z} &= z[\lambda + C(x^2 + y^2)]
\end{aligned} \quad (3)$$

where the symmetry conjugation $\overline{B(x^2 + y^2)} = A(x^2 + y^2)$ holds (so the normal form is real), $A(x^2 + y^2) + B(x^2 + y^2) \not\equiv 0$, and $\mathrm{Re}(A) \not\equiv 0$. We will denote by $\hat{\mathscr{Y}}_\lambda$ the vector field associated to system (3).

3.1 The Center Problem in $\mathbb{R}^3$

The *center problem* in $\mathbb{R}^3$ consist in determining when the origin of system (1) is a center or a focus on any local center manifold W^c. In fact, the singularity is a center of (1) if a punctured neighborhood of it is composed entirely of periodic orbits on

any W^c. Conversely, the singular point is a focus if every trajectory near the origin spirals around it on any W^c. In this last case the singular point is also called a *saddle-focus*.

The center problem in $\mathbb{R}^3$ was solved first by Liapunov in terms of a first integral, see [3]. Liapunov proved that the origin of system (1) is a center if and only if system (1) admits a real analytic local first integral of the form $H(x, y, z) = x^2 + y^2 + \cdots$ around the origin where the dots means higher order terms in the Taylor expansion at the origin. Moreover, it was also proved that when the singularity is a center, the local center manifold W^c is unique and analytic.

The inverse Jacobi multiplier has emerged as a useful tool to solve the center problem. Recently, it has been published another solution to the center problem in $\mathbb{R}^3$ given in terms of an inverse Jacobi multiplier. Moreover, new properties of the vanishing set of inverse Jacobi multipliers of system (1) has been discovered. See, [4] for a proof of the following result.

Theorem 4 ([4]). *The analytic system (1) has a center at the origin if and only if it admits a local analytic inverse Jacobi multiplier of the form $V(x, y, z) = z + \cdots$ in a neighborhood of the origin in $\mathbb{R}^3$. Moreover, in this case the local analytic center manifold $W^c \subset V^{-1}(0)$.*

The following theorem, also proved in [4], shows analogous results involving inverse Jacobi multiplier in the focus case.

Theorem 5 ([4]). *Assume that the origin is a saddle-focus for the analytic system (1). Then there exists a local C^∞ and non-flat inverse Jacobi multiplier of (1) having the expression $V(x, y, z) = z(x^2 + y^2)^k + \cdots$ for some $k \geq 2$. Moreover, there is a local C^∞ center manifold W^c such that $W^c \subset V^{-1}(0)$.*

In both the center and the focus cases, any local C^∞ and non-flat inverse Jacobi multiplier of (1) must have the form $V(x, y, z) = z(x^2 + y^2)^k + \cdots$ for some $k \geq 0$. Clearly, C^∞ inverse Jacobi multipliers are not unique neither in the center nor in the focus case. The following result proved in [7] clarifies even more the special relation between center manifolds and inverse Jacobi multipliers when the origin is a saddle-focus for system (1).

Theorem 6 ([7]). *Assume that the origin is a saddle-focus for the analytic system (1). Then the following holds:*

(i) For each locally smooth and non-flat at the origin inverse Jacobi multiplier V of (1) there is exactly one smooth center manifold W^c of (1) such that $W^c \subset V^{-1}(0)$.
(ii) Any two locally smooth and non-flat at the origin linearly independent inverse Jacobi multipliers of (1) have the same Taylor expansion at the origin.

Another property proved in [4] linking inverse Jacobi multipliers of $\mathscr{X}_\lambda$ with inverse integrating factors of the restricted planar vector field $\mathscr{X}_\lambda|W^c$ to the center manifold W^c is the following.

Theorem 7 ([4]). *Let V be a local C^∞ inverse Jacobi multiplier of system (1) and $W^c = \{z = h(x, y)\}$ be a C^∞ local center manifold at the origin. Consider the*

restricted function $V|_{W^c} : (x, y) \mapsto V(x, y, h(x, y))$. *Then, when* $W^c \subset V^{-1}(0)$, *there exists a* C^∞ *function* $W(x, y, z)$ *such that* $W(x, y, h(x, y)) \not\equiv 0$ *and the following factorization occurs* $V(x, y, z) = (z - h(x, y))\, W(x, y, z)$. *Moreover,* $v(x, y) = W|_{W^c} = W(x, y, h(x, y))$ *is an inverse integrating factor of* $\mathscr{X}_\lambda|W^c$.

A consequence of these results is the fact that, given the expression of a C^∞ and non-flat inverse Jacobi multiplier, one can find the expression of a C^∞ center manifold and, additionally, of an inverse integrating factor of the system reduced to this center manifold.

In [4] we take advantage of the above properties for solving a conjecture concerning the existence of centers on local center manifolds at equilibria of the Lü system. We recall that Lü's family is given by the following quadratic system in $\mathbb{R}^3$

$$\dot{x} = a(y - x),\ \dot{y} = cy - xz,\ \dot{z} = -bz + xy, \tag{4}$$

with parameters $(a, b, c) \in \mathbb{R}^3$. In paper [19] the authors conjecture that in the straight line $L = \{(a, b, c) \in \mathbb{R}^3 : a \neq 0, b = 2a, c = a\}$ of the parameter space, the equilibria $Q_\pm = (\pm\sqrt{bc}, \pm\sqrt{bc}, c)$ are centers of the Lü system. We gave a very simple solution to this conjecture finding the expression of an analytic inverse Jacobi multiplier $V(x, y, z) = z - \frac{x^2}{2a}$ for (4) with $(a, b, c) \in L$. Since we must have that $W^c \subset V^{-1}(0)$ we get that $W^c = \{z - \frac{x^2}{2a} = 0\}$ is a global center manifold for both singularities $Q_\pm$. Applying Theorem 7 we deduce that $v(x, y) = 1$ is an inverse integrating factor for the Lü system reduced to W^c, hence this planar system is Hamiltonian.

Another work devoted to solve the center problem in the Lü system is [18].

3.2 Multiple Hopf Bifurcation in $\mathbb{R}^3$

We consider now an analytic perturbation of system (1) of the form

$$\begin{aligned} \dot{x} &= -y + \mathscr{G}_1(x, y, z; \varepsilon)\ , \\ \dot{y} &= x + \mathscr{G}_2(x, y, z; \varepsilon)\ , \\ \dot{z} &= \lambda z + \mathscr{G}_3(x, y, z; \varepsilon)\ , \end{aligned} \tag{5}$$

where $\varepsilon \in \mathbb{R}^p$ is a finite dimensional perturbation parameter, that is, $0 < \|\varepsilon\| << 1$ and $\mathscr{G}_i(x, y, z; 0) \equiv \mathscr{F}_i(x, y, z)$ for all i. We will assume that the vector field $\mathscr{G} = (\mathscr{G}_1, \mathscr{G}_2, \mathscr{G}_3)$ is analytic for both (x, y, z) and ε in a neighborhood of the origin. Additionally we will assume that the position and monodromic nature of the singularity at the origin is not affected by such perturbation imposing that $\mathscr{G}_i(0, 0, 0; \varepsilon) = 0$ for all ε and i and that the Jacobian matrix $D\mathscr{G}(0, 0, 0; 0) = 0$. More precisely, the allowed perturbation is made so that $D\mathscr{G}(0, 0, 0; \varepsilon) = \mathrm{diag}\{\mu(\varepsilon), \mu(\varepsilon), \nu(\varepsilon)\}$ with analytic functions μ and ν near the origin such that

$\mu(0) = \nu(0) = 0$. Equivalently the eigenvalues at the origin of (5) must be $\mu(\varepsilon) \pm i$ and $\lambda + \nu(\varepsilon)$. We associate to the perturbed system (5) the vector field $\mathscr{Z}_\varepsilon$.

We focus our attention in studying the existence of periodic orbits of family (5) in a neighborhood of the origin for small values of $\|\varepsilon\|$.

Assume that we have a saddle-focus at the origin of the unperturbed system (5) for $\varepsilon = 0$. If the stability type of this point changes when ε varies near 0, then we can expect to find a small-amplitude limit cycle branching from the singular point. Such a kind of bifurcation is called *Hopf bifurcation*, also denoted by Poincaré–Andronov-Hopf bifurcation. The *cyclicity* of the saddle-focus at the origin of $\mathscr{Z}_0 = \mathscr{X}_\lambda$ under any deformation $\mathscr{Z}_\varepsilon$ is the sharp upper bound for the number of limit cycles which can bifurcate from the saddle-focus of system (1) under the perturbation (5). This sharp upper bound will be denoted by $\mathrm{Cycl}(\mathscr{Z}_\varepsilon, 0)$ throughout this paper.

The next result gives the above mentioned cyclicity from the knowledge of the Taylor expansion at the origin of an inverse Jacobi multiplier for the unperturbed analytic system (1). Its proof can be found in [6].

Theorem 8 ([6]). *Assume that the origin of* (1) *is a saddle-focus. Let* $V(x, y, z) = z(x^2 + y^2)^k + \cdots$ *with* $k \geq 2$ *be a smooth and non-flat at the origin inverse Jacobi multiplier of the unperturbed analytic system* (1). *Then* $\mathrm{Cycl}(\mathscr{Z}_\varepsilon, 0) = k - 1$.

3.3 Lie Symmetries Near Monodromic Points in $\mathbb{R}^3$

We let $[\mathscr{X}, \mathscr{Z}] = \mathscr{X}\,\mathscr{Z} - \mathscr{Z}\,\mathscr{X}$ denote the usual Lie bracket of smooth C^∞ or analytic vector fields $\mathscr{X}$ and $\mathscr{Z}$ on an open set U in $\mathbb{R}^n$. An *analytic centralizer* (resp. formal centralizer) of $\mathscr{X}$ on U is an analytic (resp. formal) vector field $\mathscr{Z}$ on U such that the commutation relation $[\mathscr{X}, \mathscr{Z}] = 0$ holds on U. The set of analytic (resp. formal) centralizers of $\mathscr{X}$ on U will be denoted by $\mathfrak{C}(\mathscr{X}, U)$ (resp. $\mathfrak{C}_{\mathrm{for}}(\mathscr{X})$). Notice that the set U is immaterial in the formal context. Clearly $\mathfrak{C}(\mathscr{X}, U) \subset \mathfrak{C}_{\mathrm{for}}(\mathscr{X})$. There is no algorithmic procedure for determining if $\mathfrak{C}(\mathscr{X}, U)$ is nontrivial, that is, to determine if $\mathfrak{C}(\mathscr{X}, U) \neq \mathbb{R}\,\mathscr{X}$.

The set $\mathfrak{C}(\mathscr{X}, U)$ is a Lie algebra which is, in general, infinite-dimensional. The work [12] investigates how whether the origin is a focus or a center of $\mathscr{X}_\lambda | W^c$, is analytically normalizable or not, and is linearizable or not is reflected in the centralizer $\mathfrak{C}(\mathscr{X}_\lambda, U)$. An important step in this study is to give a proof of the next theorem.

Theorem 9 ([12]). *Suppose the analytic system* (1) *with its associated analytic vector field* $\mathscr{X}_\lambda$ *has a focus at the origin in any center manifold. Let* $\hat{\mathscr{Y}}_\lambda$ *denote the* C^∞ *vector field associated to the formal normal form* (3) *of* (1).

(i) $\dim \mathfrak{C}_{\mathrm{for}}(\mathscr{X}_\lambda) = \dim \mathfrak{C}_{\mathrm{for}}(\hat{\mathscr{Y}}_\lambda) = 3$.
(ii) A basis of the Lie algebra $\mathfrak{C}_{\mathrm{for}}(\hat{\mathscr{Y}}_\lambda)$ *is* $\{-y\partial_x + x\partial_y + \lambda z\partial_z, z\partial_z, \hat{\mathscr{Y}}_\lambda\}$.

Clearly part (i) of Theorem (9) is trivial if the second part is proved because $\mathscr{X}_\lambda$ and $\hat{\mathscr{Y}}_\lambda$ are, in particular, formally conjugated. To prove the second part (ii) first observe that the linear vector fields $-y\partial_x + x\partial_y + \lambda z\partial_z$ and $z\partial_z$ are in $\mathfrak{C}_{\text{for}}(\hat{\mathscr{Y}}_\lambda)$ and that $\det\{-y\partial_x + x\partial_y + \lambda z\partial_z, z\partial_z, \hat{\mathscr{Y}}_\lambda\} = \frac{1}{2}z(x^2+y^2)[A(x^2+y^2)+B(x^2+y^2)]$ vanishes on a set of measure zero in a neighborhood of the origin in $\mathbb{R}^3$. Hence, it suffices to show that $\{-y\partial_x + x\partial_y + \lambda z\partial_z, z\partial_z, \hat{\mathscr{Y}}_\lambda\}$ spans $\mathfrak{C}_{\text{for}}(\hat{\mathscr{Y}}_\lambda)$. Recalling that the former determinant gives a formal inverse Jacobi multiplier of $\hat{\mathscr{Y}}_\lambda$, the key point to prove statement (ii) of Theorem 9 is the statement (ii) of Theorem 6 which in this context means that any formal inverse Jacobi multiplier of $\hat{\mathscr{Y}}_\lambda$ has the form

$$c\, z\,(x^2+y^2)[A(x^2+y^2)+B(x^2+y^2)]$$

for some constant $c \in \mathbb{R}$.

4 Non-autonomous Differential Systems and Non-autonomous Inverse Jacobi Multipliers

In the second part of this paper we shall consider non-autonomous systems of ordinary differential equations

$$\dot{x} = f(t,x)\,, \tag{6}$$

where $f : I \times \tilde{U} \to \mathbb{R}^n$ is a C^1 function where $I \subset \mathbb{R}$ is an open interval and $\tilde{U} \subset \mathbb{R}^n$ is an open set. As in the first part of the work we use the notation $x = (x_1, \ldots, x_n)$ and $f = (f_1, \ldots, f_n)$.

We associate to system (6) the vector field $\mathscr{X} = \partial_t + \sum_{i=1}^n f_i(t,x)\partial_{x_i}$ and we define a function $V : \Omega \to \mathbb{R}$ to be an inverse Jacobi multiplier of system (6) in the open set $\Omega \subset I \times \tilde{U}$, if V is of class $C^1(\Omega)$, it is not locally null and satisfies the following linear first order partial differential equation:

$$\mathscr{X} V = V \operatorname{div} \mathscr{X}\,. \tag{7}$$

The first two subsections are dedicated to the construction and some applications of inverse Jacobi multipliers of system (6) in particular classes of vector fields in the two-dimensional case $n = 2$. In the last section we turn to the arbitrary dimension $n \in \mathbb{N}$.

4.1 A Nonautonomous Extension of the Darboux Construction

We note that the problem of determining the general solution of the partial differential equation defining an inverse Jacobi multiplier should be at least as

difficult as solving the given ordinary differential equation. However, in many cases only a particular solution is needed. Therefore in practice some times the following theory is useful to obtain closed expressions of inverse Jacobi multipliers for a special class of vector fields.

Darboux in [8] studies polynomial vector fields in $\mathbb{C}^n$ where the existence of invariant algebraic surfaces is the key point to build up first integrals for the vector field. In the paper [16] the Darboux theory of integrability is extended to the class of nonautonomous vector fields defined by planar polynomials in two variables with coefficients given by C^1 functions in the independent (time) variable. More precisely, they deal with differential equations of the form

$$\dot{x} = P(t,x,y) = \sum_{0\le i+j\le m} a_{ij}(t)x^i y^j \ , \ \dot{y} = Q(t,x,y) = \sum_{0\le i+j\le m} b_{ij}(t)x^i y^j \ , \tag{8}$$

where $P, Q \in C^1(I,\mathbb{R})[x,y]$, the ring of polynomials in the real variables x and y with coefficients in $C^1(I,\mathbb{R})$, the field of C^1 functions from $I \subset \mathbb{R}$ to $\mathbb{R}$. Now we associate to system (8) the vector field $\mathscr{X} = \partial_t + P\partial_x + Q\partial_y$. The work [16] is focusing in the construction of inverse Jacobi multipliers of (8) using its invariant surfaces and exponential factors. We say that $f = 0$ is an invariant surface in $I \times \mathbb{R}^2$ of system (8) if $f \in C^1(I,\mathbb{R})[x,y]$ and satisfies the linear partial differential equation $\mathscr{X}(f) = Kf$ for some function $K \in C^1(I,\mathbb{R})[x,y]$ called cofactor. Similarly, given $g, h \in C^1(I,\mathbb{R})[x,y]$, the function $F(t,x,y) = \exp(g/h)$ is called an exponential factor of the differential system (8) if it is a solution of the linear partial differential equation $\mathscr{X}(F) = LF$ for some cofactor $L \in C^1(I,\mathbb{R})[x,y]$ of degree at most $m-1$ in x and y.

Given $f_i \in C^1(I,\mathbb{R})[x,y]$ irreducible and coprimes for $i = 1,\dots,p$, $F_j = \exp(g_j/h_j)$ with $g_j, h_j \in C^1(I,\mathbb{R})[x,y]$ for $j = 1,\dots,q$ and $G, \lambda_i, \mu_j \in C^1(I,\mathbb{R})$, any function of the form

$$\exp(G)\prod_{i=1}^{p} f_i^{\lambda_i} \prod_{j=1}^{q} F_j^{\mu_j} \tag{9}$$

will be called a generalized Darboux function.

Regarding inverse Jacobi multipliers, the main results of [8] are the following.

Theorem 10 ([8]). *Then the following statements hold.*

(i) If a nonautonomous differential system (8) has an inverse Jacobi multiplier given by a generalized Darboux function of the form (9) then the exponents $\lambda_i \in \mathbb{R}$ are all constants and the exponents $\mu_j \in \mathbb{R}$ are constants too except if $h_j \in C^1(I,\mathbb{R})$ does not depend on x and y and the degree of g_j in x and y is less or equal to $m-1$.

(ii) We assume that the differential system (8) of degree m admits the invariant surfaces $f_i = 0$ with cofactors $K_i \neq 0$ for $i = 1,\dots,p$; exponential factors

$F_j = \exp(g_j/h_j)$ with cofactors $L_j \neq 0$ for $j = 1, \ldots, q$. Let $G \in C^1(I, \mathbb{R})$ with $dG/dt = g$. We assume that all the f_i and F_j are pairwise independent and all the f_i are coprimes in the ring $C^1(I, \mathbb{R})[x, y]$. Then there exist $\lambda_i \in \mathbb{R}$ and $\mu_j \in \mathbb{R}$ not all zero such that

$$\sum_{i=1}^{p} \lambda_i K_i + \sum_{j=1}^{q} \mu_j L_j + g = \operatorname{div} \mathscr{X}$$

if and only if the function (9) is an inverse Jacobi multiplier of system (8).

4.2 Second Order Autonomous Scalar Differential Equations

In [11], the authors consider autonomous second order differential equations

$$\ddot{x} = w(x, \dot{x}) \,, \tag{10}$$

with $w \in \mathscr{C}^\infty(\mathscr{U})$ and $\mathscr{U} \subseteq \mathbb{R}^2$ an open set. They associated to (10) the first order planar system defined on $\mathscr{U}$ in the usual way

$$\dot{x} = y \,, \ \dot{y} = w(x, y) \,. \tag{11}$$

Moreover, it is associated to Eqs. (10) and (11) the vector fields $\mathscr{X} = \partial_t + \dot{x}\partial_x + w(x, \dot{x})\partial_{\dot{x}}$ and $\bar{\mathscr{X}} = y\partial_x + w(x, y)\partial_y$, respectively.

A symmetry of (10) is a diffeomorphism $\Phi : (t, x) \mapsto (\bar{t}, \bar{x})$ that maps the set of solutions of (10) into itself. Therefore, the symmetry condition for (10) is just $\bar{x}'' = w(\bar{x}, \bar{x}')$, where the prime denotes the derivative $' = d/d\bar{t}$. When the symmetry is a 1–parameter Lie group of point transformations Φ_ϵ, then $\bar{t} = t + \epsilon\xi(t, x) + O(\epsilon^2)$, $\bar{x} = x + \epsilon\eta(t, x) + O(\epsilon^2)$, for ϵ close to zero, and the vector field $\mathscr{Y} = \xi(t, x)\partial_t + \eta(t, x)\partial_x$ is called the *infinitesimal generator* of the 1–parameter Lie group of point transformations Φ_ϵ. It is well known that the *determining equations* for Lie point symmetries can be obtained from the linearized condition

$$\mathscr{Y}^{[2]}(\ddot{x} - w(x, \dot{x})) = 0 \text{ when } \ddot{x} = w(x, \dot{x}) \,, \tag{12}$$

where $\mathscr{Y}^{[2]} = \mathscr{Y} + \eta^{[1]}(t, x, \dot{x})\partial_{\dot{x}} + +\eta^{[2]}(t, x, \dot{x}, \ddot{x})\partial_{\ddot{x}}$ is the so–called *second prolongation* of the infinitesimal generator $\mathscr{Y}$ and

$$\eta^{[1]}(t, x, \dot{x}) = D_t\eta - \dot{x}D_t\xi, \qquad \eta^{[2]}(t, x, \dot{x}, \ddot{x}) = D_t\eta^{[1]} - \ddot{x}D_t\xi,$$

where $D_t = \partial_t + \dot{x}\partial_x + \ddot{x}\partial_{\dot{x}}$ is the operator total derivative with respect to t. Of course, since (10) is autonomous, it always admits the generator $\mathscr{Y} = \partial_t$ of a Lie point symmetry. Let $\mathscr{L}_r$ denotes the set of all infinitesimal generators

of 1–parameter Lie groups of point symmetries of the differential equation (10). It is known that $\mathscr{L}_r$ is a finite dimensional real Lie algebra, where we denote $r = \dim \mathscr{L}_r$. Moreover, for autonomous second order differential equation we have $r \in \{1, 2, 3, 8\}$.

For any $\mathscr{Y}_i = \xi_i(t,x)\partial_t + \eta_i(t,x)\partial_x \in \mathscr{L}_r$ we define $\mathscr{Y}_i^{[1]} = \mathscr{Y}_i + \eta_i^{[1]}(t,x,\dot{x})\partial_{\dot{x}}$ as its first prolongation of $\mathscr{Y}$. If $r \geq 2$, we define the functions

$$V_{ij}(t,x,\dot{x}) = \det\{\mathscr{X}, \mathscr{Y}_i^{[1]}, \mathscr{Y}_j^{[1]}\} = \begin{vmatrix} 1 & \dot{x} & w(x,\dot{x}) \\ \xi_i(t,x) & \eta_i(t,x) & \eta_i^{[1]}(t,x,\dot{x}) \\ \xi_j(t,x) & \eta_j(t,x) & \eta_j^{[1]}(t,x,\dot{x}) \end{vmatrix} \tag{13}$$

for $i, j \in \{1, \ldots, r\}$ with $1 \leq i < j \leq r$. It is easy to see that the functions $V_{ij}(t,x,\dot{x})$ defined in (13) satisfy the linear partial differential equation $\mathscr{X} V_{ij} = V_{ij}\ \mathrm{div}\mathscr{X}$, where $\mathscr{X} = \partial_t + \dot{x}\partial_x + w(x,\dot{x})\partial_{\dot{x}}$. Therefore $V_{ij}(t,x,y)$ are inverse Jacobi multipliers of the vector field $\mathscr{Z} = \partial_t + y\partial_x + w(x,y)\partial_y = \partial_t + \bar{\mathscr{X}}$ provided they are not identically zero.

The aim of the work [11] is to generalize the concept of inverse integrating factor $v(x,y)$ of system (11) via the non-autonomous inverse Jacobi multipliers $V_{ij}(t,x,y)$ defined in (13). In fact, in the autonomous particular case $\partial V_{ij}/\partial t \equiv 0$, we get that V_{ij} is just an inverse integrating factor of (11). On the contrary, when $\partial V_{ij}/\partial t \not\equiv 0$, in [11] it is proved that the zero–sets $v^{-1}(0)$ and $V_{ij}^{-1}(0)$ have similar properties.

Next theorem is about the invariant curves of $\bar{\mathscr{X}}$ contained in $V_{ij}^{-1}(0)$ with special emphasis on periodic orbits of (11). Recall here that a limit cycle $\gamma := \{(x(t), y(t)) \in \mathscr{U} : 0 \leq t < T\}$ is *hyperbolic* if $\Delta(\gamma) = \oint_\gamma \mathrm{div}\bar{\mathscr{X}}(x(t), y(t))dt \neq 0$. On the other hand, a $\mathscr{C}^1$ curve $f(x,y) = 0$ defined on $\mathscr{U}$ is invariant for $\bar{\mathscr{X}}$ if $\bar{\mathscr{X}} f = Kf$ for some continuous function $K : \mathscr{U} \to \mathbb{R}$ called *cofactor*.

Theorem 11 ([11]). *Let $\mathscr{U} \subset \mathbb{R}^2$ be an open set and assume that $\ddot{x} = w(x,\dot{x})$ with w smooth in $\mathscr{U}$ admits an r–dimensional Lie point symmetry algebra $\mathscr{L}_r$ with $r \geq 2$. Consider the inverse Jacobi multipliers $V_{ij}(t,x,\dot{x})$ of (11) defined in (13) for $i, j \in \{1, \ldots, r\}$ with $1 \leq i < j \leq r$. Suppose that $\gamma = (x(t), y(t)) \subset \mathscr{U}$ is a T–periodic orbit of (11). Then the next statements hold:*

(i) *If $V_{ij}(t,x,\dot{x}) = V(x,\dot{x}) \not\equiv 0$, with $V \in \mathscr{C}^1(\mathscr{U})$, then $V(x,y)$ is an inverse integrating factor of system (11) in $\mathscr{U}$. In particular, if γ is a limit cycle, then $\gamma \subset \{V(x,y) = 0\}$.*

(ii) *If $V_{ij}(t,x,\dot{x}) = F(t)G(x,\dot{x}) \not\equiv 0$ with non–constants F and $G \in \mathscr{C}^1(\mathscr{U})$, then $\dot{F} = \alpha F$ with $\alpha \in \mathbb{R}\backslash\{0\}$ and $G(x,y) = 0$ is an invariant curve of system (11). Moreover, we have:*

(ii.1) *If $\gamma \subset \{G = 0\}$ and G is analytic on $\mathscr{U}$, then G is not square–free, i.e., $G(x,y) = g^n(x,y)u(x,y)$ with a positive integer $n > 1$ and g and u are analytic functions on $\mathscr{U}$ satisfying $\gamma \subset \{g = 0\}$ and $\gamma \not\subset \{u = 0\}$.*

(ii.2) *If $\gamma \not\subset \{G = 0\}$ then γ is hyperbolic and $\alpha T = \oint_\gamma \mathrm{div}\bar{\mathscr{X}}(x(t), y(t))dt$.*

As an application of this theory to polynomial Liénard systems, in [11] it is proved among other results the next theorem.

Theorem 12 ([11]). *The polynomial Liénard differential equation* $\ddot{x} + f(x)\dot{x} + g(x) = 0$ *with* $f, g \in \mathbb{R}[x]$ *having a* r*–dimensional Lie point symmetry algebra* $\mathscr{L}_r$ *with* $r \geq 2$ *has no limit cycles in* $\mathbb{R}^2$.

Remark 2. We want to show here an elementary example. If we modify Liénard equation introducing a term $\dot{x}^2$ instead of $\dot{x}$ we get equation $\ddot{x} + f(x)\dot{x}^2 + g(x) = 0$ where we assume that f and g are C^1 functions in $\mathbb{R}$. It is straightforward to check that this equation possesses the inverse integrating factor $v(x, y) = \exp(-2F(x))$ with $F'(x) = f(x)$. Since v is $C^1(\mathbb{R}^2)$ and its zero-set is empty we get that it has no limit cycles (see Remark 1).

4.3 Inverse Jacobi Multipliers, First Integrals and Periodic Orbits

All the results of this subsection can be found in [5]. We turn to consider non-autonomous systems of ordinary differential equations (6) in arbitrary dimension $n \in \mathbb{N}$ defined in $I \times \tilde{U} \subset \mathbb{R} \times \mathbb{R}^n$.

We recall that a function $H : \Omega \subset I \times \tilde{U} \to \mathbb{R}$ is a first integral of system (6) in the open set Ω if H is of class $C^1(\Omega)$, it is not locally constant and satisfies the linear first order partial differential equation $\mathscr{X} H = 0$.

For each $(t_0, y) \in I \times \tilde{U}$ we denote by $\psi(\cdot; t_0, y)$ the solution of (6) satisfying $\psi(t_0; t_0, y) = y$ and by $I_{(t_0,y)}$ its maximal interval of existence.

For a given open subset $U \subset \tilde{U}$, we consider the open subset $\Omega^* \subset I \times \tilde{U}$ defined by $\Omega^* = \{(t, \psi(t; 0, x)),\ x \in U,\ t \in I_{(0,x)}\}$.

Theorem 13 ([5]). *Let* $F : U \to F(U)$ *be a diffeomorphism and define the function* $\tilde{H} : \Omega^* \to \mathbb{R}^n$ *as* $\tilde{H}(t, y) = F(\psi(0; t, y))$ *for any* $(t, y) \in \Omega^*$. *Then we have:*

(i) The components of $\tilde{H}$ *are first integrals in* Ω^* *of* (6).
(ii) $H : \Omega^* \to \mathbb{R}$ *is a first integral of* (6) *if and only if there exists a* C^1 *function* ϕ *which is not locally constant and such that* $H = \phi(\tilde{H})$ *on* Ω^*.
(iii) Assume in addition that f *is* C^2. *Then* $V^* : \Omega^* \to \mathbb{R}$ *defined by* $V^*(t, y) = \exp\left[\int_0^t \operatorname{div} \mathscr{X}(s, \psi(s; t, y))ds\right]$ *for any* $(t, y) \in \Omega^*$ *is an inverse Jacobi multiplier of* (6).
(iv) Assume again that f *is* C^2. *Then* $V : \Omega^* \to \mathbb{R}$ *is an inverse Jacobi multiplier of* (6) *linearly independent with* V^* *if and only if there exists a* C^1 *function* ϕ *which is not locally constant and such that* $V = \phi(\tilde{H})V^*$ *on* Ω^*.

Assume that there exists some $T > 0$ and some open subset U of $\tilde{U}$ such that $[0, T] \subset I_{(0,x)}$ for any $x \in U$. Then we introduce the Poincaré translation map at time T as $\Pi : U \to \tilde{U}$ defined by $\Pi(x) = \psi(T; 0, x)$ for any $x \in U$.

We remark that the forthcoming fundamental relation given by formula (14) was obtained for the first time in [10] in the particular case $n = 1$.

Theorem 14 ([5]). *Let $V : \Omega \to \mathbb{R}$ be an inverse Jacobi multiplier of (6) and assume that $(t, \psi(t; 0, x)) \in \Omega$ for all $t \in [0, T]$ and $x \in U$. Then for all $x \in U$ the following fundamental relation holds*

$$V(T, \Pi(x)) = V(0, x) \det D\Pi(x). \tag{14}$$

In what follows we always assume what we will call HYPOTHESIS *:

(i) System (6) is well defined for any time, that is, $I = \mathbb{R}$;
(ii) System (6) is T-periodic for some fixed minimal period $T > 0$. This means that the function $f(\cdot, x)$ is T-periodic for each $x \in \tilde{U}$;
(iii) There is an open subset $U \subset \tilde{U}$ such that $[0, T] \subset I_{(0,x)}$ for any $x \in U$.

We say that k first integrals $H_1, \ldots, H_k$ of (6) are independent in Ω if the gradient vectors $\nabla H_1(t, x), \ldots, \nabla H_k(t, x)$ are linearly independent for each $(t, x) \in \Omega$.

We say that an inverse Jacobi multiplier $V : \mathbb{R} \times U \to \mathbb{R}$ of system (6) is T-periodic if $V(\cdot, x)$ is T-periodic for any $x \in U$. Similarly we define the T-periodicity of a first integral $H : \mathbb{R} \times U \to \mathbb{R}$.

Theorem 15 ([5]). *Assume Hypothesis * and that there exists $\tilde{x} \in U$ such that $\psi(\cdot; 0, \tilde{x})$ is a T-periodic solution of (6).*

(i) If there exist n independent first integrals in $\mathbb{R} \times U$ of (6) which are T-periodic, then there exists an open neighborhood U_0 of $\tilde{x}$ such that $\psi(\cdot; 0, x)$ is T-periodic for any initial condition $x \in U_0$.
(ii) If there exist $n - 1$ independent first integrals, and an inverse Jacobi multiplier $\tilde{V}$ in $\mathbb{R} \times U$ which are T-periodic and such that $\tilde{V}(0, x) \neq 0$ for all $x \in U$, then the T-periodic solution $\psi(\cdot; 0, \tilde{x})$ is included into a 1-parameter family of T-periodic solutions $\psi(t; 0, x^*(\mu))$, where x^* is a C^1 function in some open interval of reals.

Regarding the global T-periodic behavior of solutions of (6) and the T-periodic first integrals and inverse Jacobi multipliers of (6) in $\mathbb{R} \times U_0$ with $U_0 \subset \mathbb{R}^n$ a sufficiently small open neighborhood of an equilibrium point of system (6) we have the following result.

Theorem 16 ([5]). *Assume Hypothesis * and suppose that $f(t, 0) = 0$ for all $t \in \mathbb{R}$. If $\psi(\cdot; 0, x)$ is T-periodic for all $x \in U$ then there exists an open neighborhood $U_0 \subset U$ of the origin such that $\mathbb{R} \times U_0 \subset \Omega^*$ and*

(i) Any first integral $H : \Omega^* \to \mathbb{R}$ of (6) is T-periodic in $\mathbb{R} \times U_0$.
(ii) Any inverse Jacobi multiplier $V : \Omega^* \to \mathbb{R}$ of (6) is T-periodic in $\mathbb{R} \times U_0$.

References

1. Belitskii, G.R.: Smooth equivalence of germs of vector fields with a single zero eigenvalue or a pair of purely imaginary eigenvalues. Funct. Anal. Appl. **20**, 253–259 (1986)
2. Berrone, L.R., Giacomini, H.: Inverse Jacobi multipliers. Rend. Circ. Mat. Palermo (2) **52**, 77–130 (2003)
3. Bibikov, Y.N.: Local Theory of Nonlinear Analytic Ordinary Differential Equations. Lecture Notes in Mathematics, vol. 702. Springer, New York (1979)
4. Buică, A., García, I.A., Maza, S.: Existence of inverse Jacobi multipliers around Hopf points in $\mathbb{R}^3$: emphasis on the center problem. J. Differ. Equ. **252**, 6324–6336 (2012)
5. Buică, A., García, I.A.: Inverse Jacobi multipliers for non-autonomous differential systems (2013, preprint)
6. Buică, A., García, I.A., Maza, S.: Multiple Hopf bifurcation in $\mathbb{R}^3$ and inverse Jacobi multipliers (2013, preprint)
7. Buică, A., García, I.A., Maza, S.: Some remarks on inverse Jacobi multipliers around Hopf points (2013, preprint)
8. Darboux, G.: De l'emploi des solutions particulières algébriques dans l'intégration des systèmes d'équations différentielles algébriques. Acad. Sci. Paris C. R. **86**, 1012 (1878)
9. García, I.A., Grau, M.: A survey on the inverse integrating factor. Qual. Theory Dyn. Syst. **9**, 115–166 (2010)
10. García, I.A., Giacomini, H., Grau, M.: The inverse integrating factor and the Poincaré map. Trans. Am. Math. Soc. **362**, 3591–3612 (2010)
11. García, I.A., Giné, J., Maza, S.: Periodic solutions of second–order differential equations with two–dimensional Lie point symmetry algebra. Nonlinear Anal. Real World Appl. **11**, 4128–4140 (2010)
12. García, I.A., Maza, S., Shafer, D.S.: Properties of monodromic points on center manifolds in $\mathbb{R}^3$ via Lie symmetries (2013, preprint)
13. Giacomini, H., Llibre, J., Viano, M.: On the nonexistence, existence, and uniqueness of limit cycles. Nonlinearity **9**, 501–516 (1996)
14. Jacobi, C.G.J.: Sul principio dell'ultimo moltiplicatore, e suo uso come nuovo principio generale di meccanica. Giornale Arcadico di Scienze Lettere ed Arti **99**, 129–146 (1844)
15. Lie, S.: Verallgemeinerung und neue Verwertung der Jacobischen Multiplikatortheorie. Forhandlinger Christiania **1874**, 255–274 (1875). Reprinted in Abhandlungen 3, 188–205. [November 1874.]
16. Llibre, J., Pantazi, C.: Darboux theory of integrability for a class of nonautonomous vector fields. J. Math. Phys. **50**, 102705, 19 pp (2009)
17. Llibre, J., Peralta-Salas, D.: A Note on the first integrals of vector fields with integrating factors and normalizers. SIGMA **8**, 1–9 (2012)
18. Mahdi, A., Pessoa, C., Shafer, D.S.: Centers on center manifolds in the Lü system. Phys. Lett. A **375**, 3509–3511 (2011)
19. Mello, L.F., Coelho, S.F.: Degenerate Hopf bifurcations in the Lü system. Phys. Lett. A **373**, 1116–1120 (2009)
20. Nucci, M.C., Leach, P.G.L.: Jacobi's last multiplier and symmetries for the Kepler problem plus a lineal story. J. Phys. A **37**, 7743–7753 (2004)
21. Nucci, M.C., Leach, P.G.L.: Jacobi's last multiplier and the complete symmetry group of the Ermakov-Pinney equation. J. Nonlinear Math. Phys. **12**, 305–320 (2005)

On Entropy of Non–autonomous Discrete Systems

Jose S. Cánovas

Abstract In this paper we explore the notion of entropy for non–autonomous discrete systems and solve an open question stated in Zhu et al. (J Korean Math Soc 49:165–185, 2012). Some other open questions are also proposed.

1 Introduction and Definitions

Let X be a set and let $T_{1,\infty} = (T_i)_{i=1}^{\infty}$ be a sequence of maps $T_i : X \to X$. The pair $(X, T_{1,\infty})$ is a discrete non–autonomous system. For each $x \in X$, its orbit under $T_{1,\infty}$ is given by the sequence $(x, T_1(x), T_2(T_1(x)), \ldots T_1^n(x), \ldots)$, where $T_1^n = T_n \circ \ldots \circ T_1$ for $n \geq 1$. When $T_i = T$ for all $i \geq 1$, we have a discrete dynamical system (X, T). The notion of discrete non–autonomous systems was introduced by Kolyada and Snoha in [15]. The orbits of non–autonomous discrete systems can be seen as solutions of the non–autonomous difference equation $x_{n+1} = T_n(x_n)$.

Usually, discrete systems, both dynamical and non–autonomous, are studied with additional mathematical structures. So, when $(X, \beta(X), \mu)$ is a probability space, that is, $\beta(X)$ is a σ–algebra on X and μ is a probability measure on $\beta(X)$, and consider a sequence of measure preserving transformations $T_{1,\infty} = (T_i)_{i=1}^{\infty}$, that is, measurable transformations $T_i : X \to X$ satisfying the condition $\mu(T_i^{-1}A) = \mu(A)$ for any $A \in \beta(X)$ and for any $i \in \mathbb{N}$, we analyze the ergodic properties of the system (see e.g. [19] or [10]). For instance, the convergence of the sequence

$$\frac{1}{n} S_n(f, x) = \frac{1}{n} \sum_{i=0}^{n-1} f \circ T_i \circ \ldots \circ T_1(x),$$

J.S. Cánovas (✉)
Departamento de Matemática Aplicada y Estadística, Universidad Politécnica de Cartagena, C/ Dr. Fleming sn, 30202 Cartagena, Murcia, Spain
e-mail: jose.canovas@upct.es

S. Ibáñez et al. (eds.), *Progress and Challenges in Dynamical Systems*,
Springer Proceedings in Mathematics & Statistics 54,
DOI 10.1007/978-3-642-38830-9_9,

where $f : X \to \mathbb{R}$ is a continuous map and $x \in X$ is studied in [2–6, 12]. When X is a compact topological space (usually metrizable with metric d) and $T_i : X \to X$ continuous for $i \geq 1$, we study the system in the setting of topological dynamics.

The notion of entropy has been introduced in both settings, topological (see [15]) and ergodic (see [20]). Metric entropy of autonomous systems was introduced by Kolmogorov (see e.g. [19]) and reintroduced as topological entropy by Adler, Konheim and McAndrew for open covers definition [1] and Bowen for the definition based on spanning and separated sets [7]. However, the topological version is introduced first in the setting of non–autonomous systems due to the measure preserving property is quite strong.

We introduce here the last approach originally due to Bowen for sequences of maps $T_{1,\infty}$ (see [15] and [7]). Let $\varepsilon > 0$ and $Y \subset X$. A set $E_n \subset Y$ is $(n, \varepsilon, Y, T_{1,\infty})$–separated if for any distinct points $x, y \in E_n$ there is an $i \in \{0, 1, \ldots, n-1\}$ such that

$$d(T_1^i(x), T_1^i(y)) > \varepsilon.$$

If we denote by $s_n(\varepsilon, Y, T_{1,\infty})$ the maximal cardinality of any $(n, \varepsilon, Y, T_{1,\infty})$–separated set of Y and define

$$s(\varepsilon, Y, T_{1,\infty}) := \limsup_{n\to\infty} \frac{1}{n} \log s_n(\varepsilon, Y, T_{1,\infty}).$$

A set $F_n \subset Y_1$ $(n, \varepsilon, Y, T_{1,\infty})$–spans Y if for any $x \in Y$ there is $y \in Y$ such that

$$d(T_1^i(x), T_1^i(y)) < \varepsilon$$

for all $i \in \{0, 1, 2, \ldots, n-1\}$. Denote by $r_n(\varepsilon, Y, T_{1,\infty})$ the minimal cardinality of any set $(n, \varepsilon, Y, T_{1,\infty})$–spanning Y. Let

$$r(\varepsilon, Y, T_{1,\infty}) := \limsup_{n\to\infty} \frac{1}{n} \log r_n(\varepsilon, Y, T_{1,\infty}).$$

Since the inequalities

$$r(\varepsilon, Y_1, f_{1,\infty}) \leq s(\varepsilon, Y_1, f_{1,\infty}) \leq r(\varepsilon/2, Y_1, f_{1,\infty})$$

are fulfilled, for compact metric spaces we define the *topological entropy* of $T_{1,\infty}$ as

$$h(T_{1,\infty}) := \lim_{\varepsilon\to 0} r(\varepsilon, X, T_{1,\infty}) = \lim_{\varepsilon\to 0} s(\varepsilon, X, T_{1,\infty}).$$

In the ergodic case, the definition is given in terms of finite partitions of measurable sets as follows (see [20] and [19]). A family $\mathscr{A} = \{A_1, \ldots, A_k\}$ is called a *finite partition* of X if $A_i \in \beta(X)$ for $i = 1, 2, \ldots, k$, $A_i \cap A_j = \emptyset$

if $i \neq j$, and $\bigcup_{i=1}^{k} A_i = X$. Let $\mathscr{Z}$ denote the set containing all the finite partitions of X. If $\mathscr{B} = \{B_1, \ldots, B_l\}$ is also a finite partition of X, $\mathscr{A} \vee \mathscr{B} = \left\{A_i \cap B_j : A_i \in \mathscr{A},\ B_j \in \mathscr{B}\right\}$. We write $\mathscr{A} \leq \mathscr{B}$ to mean that each element of $\mathscr{A}$ is a union of elements of $\mathscr{B}$. It is also said that $\mathscr{B}$ is *finer* than $\mathscr{A}$. Under the convention that $0 \log 0 = 0$, the *metric entropy* of the finite partition $\mathscr{A}$ is

$$H_\mu(\mathscr{A}) = -\sum_{i=1}^{k} \mu\left(A_i\right) \log \mu\left(A_i\right).$$

If $\mathscr{B}$ is also a finite partition as above, the *metric conditional entropy* of $\mathscr{A}$ relative to $\mathscr{B}$ is given by

$$H_\mu(\mathscr{A}/\mathscr{B}) = \sum_{\mu(B_j)\neq 0} \sum_{i=1}^{k} \mu(A_i \cap B_j) \log \frac{\mu(A_i \cap B_j)}{\mu(B_j)},$$

and $\rho(\mathscr{A}, \mathscr{B}) = H_\mu(\mathscr{A}/\mathscr{B}) + H_\mu(\mathscr{B}/\mathscr{A})$ defines a distance in the set of finite partitions $\mathscr{Z}$.

Let $T_{1,\infty} = (T_i)_{i=1}^{\infty}$ be a sequence of measure preserving transformations $T_i : X \to X$ with $i \in \mathbb{N}$. Let $\mathscr{A}$ be a finite partition of X. The *metric entropy of* $T_{1,\infty}$ *relative to the partition* $\mathscr{A}$ is

$$h_\mu(T_{1,\infty}, \mathscr{A}) = \limsup_{n\to\infty} \frac{1}{n} H_\mu\left(\bigvee_{i=0}^{n-1} T_1^{-n} \mathscr{A}\right).$$

and the *metric entropy* of $T_{1,\infty}$

$$h_\mu(T_{1,\infty}) = \sup_{\mathscr{A}} h_\mu(T_{1,\infty}, \mathscr{A}).$$

Let us remark that when $T_{1,\infty} = (T, T, \ldots)$ is a constant sequence of maps, then $h_\mu(T_{1,\infty}) = h_\mu(T)$ and $h(T_{1,\infty}) = h(T)$ are the metric and the topological entropies of T, respectively. Additionally, if $B = (b_i)_{i=1}^{\infty}$ is a sequence of positive integers, we consider the sequence $A = \{(a_i)_{i=1}^{\infty}$ defined by $a_i = \sum_{k=1}^{i} b_k$, which is an increasing sequence of positive integers. Then, we can construct the sequence of measure preserving transformations (resp. continuous maps) $T_{1,\infty} = (T^{b_i})_{i=1}^{\infty}$ where $T : X \to X$ is a measure preserving transformation (resp. continuous map). Then $h_\mu(T_{1,\infty}) = h_{\mu,A}(T)$ is the *metric sequence entropy* of T (see [16]) and $h_A(T) := h(T_{1,\infty})$ is the topological sequence entropy (see [11]).

2 Previous Results

In general, the basic properties satisfied by the metric entropy of sequences of measure preserving transformations are summarized below.

Theorem 1. *Let $T_{1,\infty} = (T_i)_{i=1}^{\infty}$ be a sequence of measure preserving transformations. Let $\mathscr{A}, \mathscr{B} \in \mathscr{Z}$. Then:*

(a) $h_\mu(T_{1,\infty}, \mathscr{A}) \leq H_\mu(\mathscr{A})$.
(b) $h_\mu(T_{1,\infty}, \mathscr{A} \vee \mathscr{B}) \leq h_\mu(T_{1,\infty}, \mathscr{A}) + h_\mu(T_{1,\infty}, \mathscr{B})$.
(c) If $\mathscr{A} \leq \mathscr{B}$ then $h_\mu(T_{1,\infty}, \mathscr{A}) \leq h_\mu(T_{1,\infty}, \mathscr{B})$.
(d) $h_\mu(T_{1,\infty}, \mathscr{A}) \leq h_\mu(T_{1,\infty}, \mathscr{B}) + H_\mu(\mathscr{A}/\mathscr{B})$.
(e) $h_\mu(T_{1,\infty}, \mathscr{A}) = h_\mu(T_{2,\infty}, \mathscr{A})$ *where* $T_{2,\infty} = (T_2, T_3, \ldots)$.
(f) $|h_\mu(T_{1,\infty}, \mathscr{A}) - h_\mu(T_{1,\infty}, \mathscr{B})| \leq \rho(\mathscr{A}, \mathscr{B})$. *Hence the map $h_\mu(T_{1,\infty}, \cdot) : \mathscr{Z} \to \mathbb{R}^+ \cup \{0\}$ is continuous.*

Proof. Properties (a)–(d) and (f) are proved by standard entropy theory (see e.g. [19, Chap. 4]). Now we will prove the property (e). Note that by Walters [19, Theorem 4.3] we have that

$$\begin{aligned} H_\mu\left(\bigvee_{i=0}^{n-1} T_1^{-i}\mathscr{A}\right) &\leq H_\mu(\mathscr{A}) + H_\mu\left(\bigvee_{i=1}^{n-1} T_1^{-i}\mathscr{A}\right) \\ &= H_\mu(\mathscr{A}) + H_\mu\left(T_1^{-1}\left(\bigvee_{i=1}^{n-1} T_2^{-i}\mathscr{A}\right)\right) \\ &= H_\mu(\mathscr{A}) + H_\mu\left(\bigvee_{i=1}^{n-1} T_2^{-i}\mathscr{A}\right), \end{aligned}$$

and dividing by n and taking limits at infinite we get that $h_\mu(T_{1,\infty}, \mathscr{A}) \leq h_\mu(T_{2,\infty}, \mathscr{A})$.

On the other hand, again by Walters [19, Theorem 4.3], it follows that

$$\begin{aligned} H_\mu\left(\bigvee_{i=0}^{n-1} T_2^{-i}\mathscr{A}\right) &= H_\mu\left(T_1^{-1}\left(\bigvee_{i=0}^{n-1} T_2^{-i}\mathscr{A}\right)\right) \\ &= H_\mu\left(\bigvee_{i=1}^{n} T_1^{-i}\mathscr{A}\right) \\ &\leq H_\mu\left(\bigvee_{i=0}^{n} T_1^{-i}\mathscr{A}\right). \end{aligned}$$

Again, dividing by n and taking limits when n tends to infinite, we conclude the reverse inequality $h_\mu(T_{1,\infty}, \mathscr{A}) \leq h_\mu(T_{2,\infty}, \mathscr{A})$, which concludes the proof. □

Let us remark that the equality $h(T_{1,\infty}) = h(T_{2,\infty})$ is not true in general (see [15]).

The following two technical lemmas, which will be useful in what follows, can be found in [19].

Lemma 1. *Let $r \geq 1$ be an integer. Then for all $\epsilon > 0$ there exists $\delta > 0$ such that if $\mathscr{A} = \{A_1, \ldots, A_r\}$ and $\mathscr{B} = \{B_1, \ldots, B_r\}$ are two finite partitions satisfying the inequality $\sum_{i=1}^{r} \mu(A_i \triangle B_i) < \delta$, it holds that $\rho(\mathscr{A}, \mathscr{B}) < \epsilon$.*

Lemma 2. *Let β_0 be an algebra such that the σ–algebra generated by β_0, which is denoted $\sigma(\beta_0)$, is $\beta(X)$. Let $\mathscr{A}$ be a finite partition of X containing elements from $\beta(X)$. Then, for all $\epsilon > 0$ there exists a finite partition $\mathscr{B}$ containing elements from β_0 and holding $\rho(\mathscr{A}, \mathscr{B}) < \epsilon$.*

Proposition 1. *Let $T_{1,\infty} = (T_i)_{i=1}^{\infty}$ be a sequence of measure preserving transformations. Let β_0 be an algebra such that $\sigma(\beta_0) = \beta(X)$. Let $\mathscr{Z}_0$ be the set of finite partitions of X containing elements from β_0. Then*

$$h_\mu(T_{1,\infty}) = \sup\left\{h_\mu(T_{1,\infty}, \mathscr{A}) : \mathscr{A} \in \mathscr{Z}_0\right\}.$$

Proof. By Lemma 2, given an arbitrary real number $\epsilon > 0$ and $\mathscr{B} \in \mathscr{Z}$ there exists a finite partition $\mathscr{A}_\epsilon \in \mathscr{Z}_0$ such that $H_\mu(\mathscr{B}/\mathscr{A}_\epsilon) < \epsilon$. Then by Theorem 1 (d) we have that

$$\begin{aligned} h_\mu(T_{1,\infty}, \mathscr{B}) &\leq h_\mu(T_{1,\infty}, \mathscr{A}_\epsilon) + H_\mu(\mathscr{B}/\mathscr{A}_\epsilon) \\ &\leq h_\mu(T_{1,\infty}, \mathscr{A}_\epsilon) + \epsilon. \end{aligned}$$

So

$$h_\mu(T_{1,\infty}, \mathscr{B}) \leq \epsilon + \sup\left\{h_\mu(T_{1,\infty}, \mathscr{A}) : \mathscr{A} \in \mathscr{Z}_0\right\},$$

and since ε was arbitrary it follows that

$$h_\mu(T_{1,\infty}) \leq \sup\left\{h_\mu(T_{1,\infty}, \mathscr{A}) : \mathscr{A} \in \mathscr{Z}_0\right\}.$$

The reverse inequality is obvious, and so the proof ends. □

3 Relationship Between Metric and Topological Entropies

In [20], the authors wonder on the relationship between metric and topological entropies of non–autonomous discrete systems. However, the main problem arises with the existence of invariant measures for sequences of continuous maps. While for continuous maps the set of invariant measures of t, $\mathscr{M}(X, T)$ is always

non–empty, for sequences of continuous maps $T_{1,\infty}$ the set $\mathscr{M}(X, T_{1,\infty})$ can be empty. Let us explain this fact.

Denote by $\mathscr{M}(X)$ the set of all the probability measures on $(X, \beta(X))$. A measure $\mu \in \mathscr{M}(X)$ is said invariant by a continuous map $T : X \to X$ if it is a fixed point for the map $\tilde{T} : \mathscr{M}(X) \to \mathscr{M}(X)$ defined by $\tilde{T}\mu(A) = \mu(T^{-1}A)$ for all $\mu \in \mathscr{M}(X)$ and $A \in \beta(X)$. The set of invariant measures of a continuous map is denoted by $\mathscr{M}(X, T)$. Therefore, if $\mu \in \mathscr{M}(X, T)$, then $\mu(T^{-1}A) = \mu(A)$ for all $A \in \beta(X)$.

Now we consider a sequence of continuous maps $T_{1,\infty} = (T_i)_{i=1}^{\infty}$; then the set of invariant measures for this sequence, $\mathscr{M}(X, T_{1,\infty})$, is the set of fixed points of the sequence $\tilde{T}_{1,\infty} = (\tilde{T}_i)_{i=1}^{\infty}$. That is, $\mu \in \mathscr{M}(X, T_{1,\infty})$ if and only if $\mu(T_i^{-1}A) = \mu(A)$ for all $A \in \beta(X)$ and all $i \in \mathbb{N}$. The following example shows that $\mathscr{M}(X, T_{1,\infty})$ can be empty.

Example 1. Consider the sequence $T_{1,\infty} = (f, g, g, g, \ldots.)$ where $f : [0,1] \to [0,1]$ is given by $f(x) = 1$ for all $x \in [0,1]$ and g is the standard tent map $g(x) = 1 - |2x - 1|$. The set of invariant measures for this sequence $\mathscr{M}(X, f_{1,\infty})$ is the set of fixed points of the sequence $(\tilde{f}, \tilde{g}, \tilde{g}, \tilde{g}, \ldots)$ where $\tilde{f}$ and $\tilde{g}$ are maps from $\mathscr{M}(X)$ into itself. $\tilde{f}$ has only a fixed point δ_1, the probabilistic atomic measure such that $\delta_1(\{1\}) = 1$, but this measure is not a fixed point of $\tilde{g}$ and so $\mathscr{M}(X, T_{1,\infty})$ is empty.

If we assume that the set of invariant measures $\mathscr{M}(X, T_{1,\infty})$ is not empty (for instance, when $T_{1,\infty}$ contains two commuting maps [13]), studying the above mentioned relationship makes sense. We start with the following lemma.

Lemma 3. *Let (X, d) be a metric compact space and let $T_{1,\infty}$ be a sequence of continuous maps such that $\mathscr{M}(X, T_{1,\infty}) \neq \emptyset$. Let $(\mathscr{A}_i)_{i=1}^{\infty}$ be a sequence of measurable partitions such that $\lim_{n\to\infty} \operatorname{diam}(\mathscr{A}_n) = 0$. Then for any invariant measure $\mu \in \mathscr{M}(X, T_{1,\infty})$ it holds that*

$$h_\mu(T_{1,\infty}) = \lim_{n\to\infty} h_\mu(T_{1,\infty}, \mathscr{A}_n).$$

Proof. The basic ideas to prove the statement are due to Bowen (see Theorem 8.3 from [19]). Let $\epsilon > 0$. We choose a finite partition $\mathscr{A} = \{A_1, \ldots, A_r\}$ such that:

$$h_\mu(T_{1,\infty}, \mathscr{A}) > h_\mu(T_{1,\infty}) - \epsilon \text{ if } h_\mu(T_{1,\infty}) < \infty,$$

$$h_\mu(T_{1,\infty}, \mathscr{A}) > \frac{1}{\epsilon} \text{ if } h_\mu(T_{1,\infty}) = \infty.$$

By Lemma 1, we also choose $\delta > 0$ such that if $\mathscr{B} = \{B_1, \ldots, B_r\}$ is a finite partition of X satisfying the condition $\sum_{i=1}^{r} \mu(A_i \triangle B_i) < \delta$, then it holds $H_\mu(\mathscr{A}/\mathscr{B}) + H_\mu(\mathscr{B}/\mathscr{A}) < \epsilon$.

Since any probabilistic measure on a metric space is regular (see Theorem 6.1 from [19]), we can choose compact sets $K_i \subset A_i$ with $i = 1, 2, \ldots, r$, such that

$\mu(A_i \setminus K_i) < \delta/(r+1)$. Let $\delta' = \inf_{i \neq j} d(K_i, K_j)$, and take the integer n such that $\operatorname{diam}(\mathscr{A}_n) < \delta'/2$.

For $1 \leq i \leq r-1$, let E_n^i be the set composed of all the elements of $\mathscr{A}_n$ that intersect the compact set K_i, and E_n^r the union of the sets of $\mathscr{A}_n$ that do not intersect any set K_i for $i = 1, 2, \ldots r-1$. Let $\mathscr{A}_n' = \{E_n^1, E_n^2, \ldots, E_n^r\}$ be the finite partition of X. It holds that $\mathscr{A}_n' \leq \mathscr{A}_n$. We calculate

$$\begin{aligned}\mu(E_n^i \triangle A_i) &= \mu(E_n^i \setminus A_i) + \mu(A_i \setminus E_n^i) \\ &\leq \mu\left(X \setminus \bigcup_{j=1}^{r} K_j\right) + \mu(A_i \setminus K_i) < \delta.\end{aligned}$$

Then by Lemma 1 we have that $H_\mu(\mathscr{A}/\mathscr{A}_n') \leq \epsilon$, and therefore, by Theorem 1,

$$\begin{aligned}h_\mu(T_{1,\infty}, \mathscr{A}) &\leq h_\mu(f_{1,\infty}, \mathscr{A}_n') + H_\mu(\mathscr{A}/\mathscr{A}_n') \\ &\leq h_\mu(T_{1,\infty}, \mathscr{A}_n') + \epsilon \\ &\leq h_\mu(T_{1,\infty}, \mathscr{A}_n) + \epsilon.\end{aligned}$$

Then, if $\operatorname{diam}(\mathscr{A}_n) < \delta/2$ it follows that

$$h_\mu(T_{1,\infty}, \mathscr{A}_n) \geq h_\mu(T_{1,\infty}) - 2\epsilon \text{ if } h_\mu(T_{1,\infty}) < \infty,$$

$$h_\mu(T_{1,\infty}, \mathscr{A}_n) > \frac{1}{\epsilon} - \epsilon \text{ if } h_\mu(T_{1,\infty}) = \infty,$$

and this concludes the proof. □

Proposition 2. *Let (X_i, d_i), $i = 1, 2$, be compact metric spaces and let $T_{1,\infty}$ and $S_{1,\infty}$ be two sequences of continuous maps. Consider the product sequence of compact topological spaces $(X_1 \times X_2, d_1 \times d_2)$ and the product sequence of continuous maps $T_{1,\infty} \times S_{1,\infty} = (T_i \times S_i)$. Then*

(a) $h(T_{1,\infty} \times S_{1,\infty}) \leq h(T_{1,\infty}) + h(S_{1,\infty})$.
(b) If $T_{1,\infty} = S_{1,\infty}$, *then* $h(T_{1,\infty} \times T_{1,\infty}) = 2h(T_{1,\infty})$.

Proof. First, we will prove (a). Let E_1 and E_2 be $(n, \epsilon, X_1, T_{1,\infty})$–spanning set for X_1 and $(n, \epsilon, X_2, S_{1,\infty})$–spanning set for X_2 with minimum cardinality, respectively. Then, $E_1 \times E_2$ is an $(n, \epsilon, X_1 \times X_2, T_{1,\infty} \times S_{1,\infty})$–spanning set for $X_1 \times X_2$. So

$$r_n(\epsilon, X_1 \times X_2, T_{1,\infty} \times S_{1,\infty}) \leq r_n(\epsilon, X_1, T_{1,\infty}) r_n(\epsilon, X_2, S_{1,\infty}),$$

and then we obtain that

$$\begin{aligned} h(T_{1,\infty} \times S_{1,\infty}) &= \lim_{\varepsilon \to 0} \limsup_{n \to \infty} \frac{1}{n} \log r_n(\epsilon, X_1 \times X_2, T_{1,\infty} \times S_{1,\infty}) \\ &\leq \lim_{\varepsilon \to 0} \limsup_{n \to \infty} \frac{1}{n} \log r_n(\epsilon, X_1, T_{1,\infty}) r_n(\epsilon, X_2, S_{1,\infty}) \\ &\leq \lim_{\varepsilon \to 0} \limsup_{n \to \infty} \frac{1}{n} \log r_n(\epsilon, X_1, T_{1,\infty}) \\ &\quad + \lim_{\varepsilon \to 0} \limsup_{n \to \infty} \frac{1}{n} \log r_n(\epsilon, X_2, S_{1,\infty}) \\ &= h(T_{1,\infty}) + h(S_{1,\infty}). \end{aligned}$$

Now we will prove (b). Let E_n be an $(n, \epsilon, X_1, T_{1,\infty})$–separated set with maximum cardinality. Then $E_n \times E_n$ is an $(n, \epsilon, X_1 \times X_1, T_{1,\infty} \times T_{1,\infty})$–separated set and therefore

$$s_n(\epsilon, X_1 \times X_1, T_{1,\infty} \times T_{1,\infty}) \geq s_n(\epsilon, X_1, T_{1,\infty})^2.$$

Then

$$\begin{aligned} h(T_{1,\infty} \times T_{1,\infty}) &= \lim_{\varepsilon \to 0} \limsup_{n \to \infty} \frac{1}{n} \log s_n(\epsilon, X_1 \times X_1, T_{1,\infty} \times T_{1,\infty}) \\ &\geq \lim_{\varepsilon \to 0} \limsup_{n \to \infty} \frac{1}{n} \log r_n(\epsilon, X_1, T_{1,\infty})^2 \\ &= 2h(T_{1,\infty}), \end{aligned}$$

which concludes the proof. □

Proposition 3. *Let $(X_i, \beta(X_i), \mu_i)$ be two probability spaces with $i = 1, 2$ and consider two sequences of measure preserving transformations $T_{1,\infty} = (T_i)_{i=1}^{\infty}$ and $S_{1,\infty} = (S_i)_{i=1}^{\infty}$ where $T_i : X_1 \to X_1$ and $S_i : X_2 \to X_2$ for $i \in \mathbb{N}$. Consider the product probability space $(X_1 \times X_2, \beta(X_1 \times X_2), \mu_1 \times \mu_2)$ and the sequence of measure preserving transformations $T_{1,\infty} \times S_{1,\infty} = (T_i \times S_i)_{i=1}^{\infty}$. Then*

(a) $h_{\mu_1 \times \mu_2}(T_{1,\infty} \times S_{1,\infty}) \leq h_{\mu_1}(T_{1,\infty}) + h_{\mu_2}(S_{1,\infty})$.
(b) If $S_{1,\infty} = T_{1\infty}$, it follows $h_{\mu_1 \times \mu_1}(T_{1,\infty} \times T_{1,\infty}) = 2h_{\mu}(T_{1,\infty})$.

Proof. First we will prove (a). Consider two measurable partitions, $\mathscr{A}_1$ of X_1 and $\mathscr{A}_2$ of X_2. Then $\mathscr{A}_1 \times \mathscr{A}_2$ is a measurable partition of $X_1 \times X_2$. Hence

$$H_{\mu_1 \times \mu_2}\left(\bigvee_{i=0}^{n-1} (T_1^{-i} \times S_1^{-i})(\mathscr{A}_1 \times \mathscr{A}_2)\right) = H_{\mu_1}\left(\bigvee_{i=0}^{n-1} T_1^{-i} \mathscr{A}_1\right) + H_{\mu_2}\left(\bigvee_{i=0}^{n-1} S_1^{-i} \mathscr{A}_2\right).$$

So

$$\begin{aligned} h_{\mu_1\times\mu_2}(T_{1,\infty}\times S_{1,\infty},\mathscr{A}_1\times\mathscr{A}_2) &= \limsup_{n\to\infty}\frac{1}{n}H_{\mu_1\times\mu_2}\left(\bigvee_{i=0}^{n-1}(T_1^{-i}\times S_1^{-i})(\mathscr{A}_1\times\mathscr{A}_2)\right)\\ &\le \limsup_{n\to\infty}\frac{1}{n}H_{\mu_1}\left(\bigvee_{i=0}^{n-1}T_1^{-i}\mathscr{A}_1\right)\\ &\quad+\limsup_{n\to\infty}\frac{1}{n}H_{\mu_2}\left(\bigvee_{i=0}^{n-1}S_1^{-i}\mathscr{A}_2\right)\\ &\le h_{\mu_1}(T_{1,\infty},\mathscr{A}_1)+h_{\mu_2}(S_{1,\infty},\mathscr{A}_2)\\ &\le h_{\mu_1}(T_{1,\infty})+h_{\mu_2}(S_{1,\infty}). \end{aligned}$$

Since the algebra $\beta(X_1)\times\beta(X_2)$ generates the product σ–algebra $\beta(X_1\times X_2)$, by Proposition 1, it follows that

$$\begin{aligned} h_{\mu_1\times\mu_2}(T_{1,\infty}\times S_{1,\infty}) &= \sup_{\mathscr{A}_1\times\mathscr{A}_2} h_{\mu_1\times\mu_2}(T_{1,\infty}\times S_{1,\infty},\mathscr{A}_1\times\mathscr{A}_2)\\ &\le h_{\mu_1}(T_{1,\infty})+h_{\mu_2}(S_{1,\infty}), \end{aligned}$$

and the part (a) follows.

In order to prove the part (b) consider $\mathscr{A}$ a finite partition of X and now

$$H_{\mu_1\times\mu_1}\left(\bigvee_{i=0}^{n-1}(T_1^{-i}\times T_1^{-i})(\mathscr{A}\times\mathscr{A})\right)=2H_{\mu_1}\left(\bigvee_{i=0}^{n-1}T_1^{-i}\mathscr{A}\right).$$

Therefore

$$\begin{aligned} h_{\mu\times\mu}(T_{1,\infty}\times T_{1,\infty},\mathscr{A}\times\mathscr{A}) &= \limsup_{n\to\infty}\frac{1}{n}H_{\mu_1\times\mu_1}\left(\bigvee_{i=0}^{n-1}(T_1^{-i}\times T_1^{-i})(\mathscr{A}\times\mathscr{A})\right)\\ &= \limsup_{n\to\infty}\frac{1}{n}2H_{\mu}\left(\bigvee_{i=0}^{n-1}T_1^{-i}\mathscr{A}\right)\\ &= 2h_{\mu}(T_{1,\infty},\mathscr{A}). \end{aligned}$$

Taking the supremum over all the finite partitions

$$\sup_{\mathscr{A}} h_{\mu\times\mu}(T_{1,\infty}\times T_{1,\infty},\mathscr{A}\times\mathscr{A})=2h_{\mu}(T_{1,\infty}).$$

Then

$$h_{\mu\times\mu}(T_{1,\infty}\times T_{1,\infty}) \geq 2h_{\mu}(T_{1,\infty}),$$

and using the part (a) the proof ends. □

Let us remark that for the autonomous case the inequalities (a) can be replaced by equality for metric entropy and topological entropy for maps defined in compact metric spaces. Recently, Hulse proved that the equality for product formula is even not true for Bowen's definition of entropy for non–compact spaces (see [14]).

A space X has *covering dimension* at most m if any open cover of X has an open refinement such that any non–empty intersection have at most $m+1$ elements of the subcover (see [17]). Then we write $\dim X = m$. The next result solves partially a problem stated in [20].

Theorem 2. *Let (X,d) be a metric compact space with finite covering dimension m, and let $T_{1,\infty}$ be a sequence of continuous maps such that $\mathscr{M}(X,T_{1,\infty}) \neq \emptyset$. Then*

$$\sup\{h_{\mu}(T_{1,\infty}) : \mu \in \mathscr{M}(X,T_{1,\infty})\} \leq h(T_{1,\infty}).$$

Proof. The ideas for this proof are due to Bowen and Goodman. Let $\mathscr{B}_{\epsilon} = \{B_1,\ldots,B_r\}$ be an open cover of X with $\mathrm{diam}(\mathscr{B}_{\epsilon}) < \epsilon$ and with each point of X in at most $m+1$ members of $\mathscr{B}_{\epsilon}$. Let $\mathscr{A}_{\epsilon} = \{A_1,\ldots,A_r\}$ be a measurable partition of X such that the closure $Cl(A_i) \subset B_i$ for each i. For each $x \in X$ choose an open neighborhood C_x of x intersecting at most $m+1$ A_i's (if $x \notin B_i$, then we can assume that $x \notin Cl(A_i)$). Let $\mathscr{C} = \{C_{x_1},\ldots,C_{x_s}\}$ be a finite cover of X, and let δ be a Lebesgue number for $\mathscr{C}$. Let $C(y) \in \mathscr{C}$ be the element of $\mathscr{C}$ with $Cl(B(y,\delta)) \subset C(y)$.

Let S_n be an $(n,\delta,X,T_{1,\infty})$–spanning set of X. Let

$$\mathscr{T}_n = \{(i_0,\ldots,i_{n-1}) : y \in S_n,\ A_{i_j} \cap C(f_1^j(y)) \neq \emptyset\ \forall\ 0 \leq j < n\}.$$

Now suppose that

$$x \in A(i_0,\ldots,i_{n-1}) := \bigcap_{j=0}^{n-1} T_1^{-j}(A_{i_j}).$$

Pick $y \in S_n$ so that $d(T_1^j(x),T_1^j(y)) \leq \delta$ for all $0 \leq j < n$. Then $T_1^j(x) \in A_{i_j} \cap C(T_1^j(y))$ and so $(i_0,\ldots,i_{n-1}) \in \mathscr{T}_n$. Let $U_n = \{(i_0,\ldots,i_{n-1}) : A(i_0,\ldots,i_{n-1}) \neq \emptyset\}$. Notice that $U_n \subset \mathscr{T}_n$. Since $C(T_1^j(y))$ can intersect at most $m+1$ of the A_k's, we have that

$$\mathrm{Card}(U_n) \leq \mathrm{Card}(\mathscr{T}_n) \leq (m+1)^n \mathrm{Card}(S_n) = (m+1)^n r_n(\delta,X,T_{1,\infty}). \quad (1)$$

By the properties of entropy of partitions (see page 78 from [19]), for any $\mu \in \mathscr{M}(X, T_{1,\infty})$ we have that

$$H_\mu\left(\bigvee_{i=0}^{n-1} t_1^{-i}(\mathscr{A}_\epsilon)\right) \leq \log \text{Card}(U_n). \tag{2}$$

Then, by (1) and (2)

$$\begin{aligned} h_\mu(T_{1,\infty}, \mathscr{A}_\epsilon) &= \limsup_{n\to\infty} \frac{1}{n} H_\mu\left(\bigvee_{i=0}^{n-1} T_1^{-i}(\mathscr{A}_\epsilon)\right) \\ &\leq \limsup_{n\to\infty} \frac{1}{n} \log(m+1)^n r_n(\delta, X, T_{1,\infty}) \\ &\leq \log(m+1) + h(T_{1,\infty}), \end{aligned}$$

By Lemma 3, if $\epsilon \to 0$, then

$$h_\mu(T_{1,\infty}) = \lim_{\epsilon\to 0} h_\mu(T_{1,\infty}, \mathscr{A}_\epsilon) \leq \log(m+1) + h(T_{1,\infty}).$$

By Propositions 2 and 3, and taking into account that the set $Y_n = \prod_{i=1}^n X_i$ with $X_i = X$ for each $1 \leq i \leq n$ has covering dimension nm (see [17]), we have

$$\begin{aligned} h_\mu(T_{1,\infty}) &= \frac{1}{n} h_{\mu\times\overset{n}{\ldots}\times\mu}(T_{1,\infty} \times \overset{n}{\ldots} \times T_{1,\infty}) \\ &\leq \frac{1}{n}(\log(nm+1) + h(T_{1,\infty} \times \overset{n}{\ldots} \times T_{1,\infty})) \\ &= \frac{1}{n}\log(nm+1) + h(T_{1,\infty}). \end{aligned}$$

Taking limits when n tends to infinity we have

$$h_\mu(T_{1,\infty}) \leq h(T_{1,\infty}) \ \forall \mu \in \mathscr{M}(X, T_{1,\infty}),$$

and this concludes the proof. □

4 The Power Formula

For a sequence of continuous mappings $T_{1,\infty}$ as above and a positive integer k denote by $T_{1,\infty}^{[k]}$ the sequence $(T_{ki+1}^k)_{i=1}^\infty$. In the autonomous case, the well–known power formulas $h(T^k) = kh(T)$ and $h_\mu(T^k) = kh_\mu(T)$ establish the relationship between the entropies of a map and its powers. For topological entropy the power

formula $h(T_{1,\infty}^{[k]}) = kh(T_{1,\infty})$ holds for equicontinuous sequences (see [15]). For the metric entropy, the inequality $h_\mu(T_{1,\infty}^{[k]}) \leq kh_\mu(T_{1,\infty})$ was proved in [20] and the authors wonder whether the equality is true. The next result shows that an autonomous like result is not possible in general for both topological and ergodic settings.

Theorem 3. *In general, the formulas* $h(T_{1,\infty}^{[k]}) = kh(T_{1,\infty})$ *and* $h_\mu(T_{1,\infty}^{[k]}) = kh_\mu(T_{1,\infty})$ *do not hold.*

Proof. First we make the proof for the metric entropy. By [18], there exist a family of measure preserving transformations holding that $\sup_A h_{A,\mu}(T) = \log n$, for some integer n, where the supremum is taken over all the increasing sequences of integers. Let $A = (a_i)_{i=1}^{\infty}$ be such that $h_{A,\mu}(T) = \log n - \epsilon$ for small enough $\epsilon > 0$. Since $h_{A,\mu}(T) = h_\mu(T_{1,\infty})$, where $T_{1,\infty} = (T^{a_1}, T^{a_2-a_1}, \ldots)$ and $h_\mu(T_{1,\infty}^{[k]})$ is the metric sequence entropy $h_{B,\mu}(T_{1,\infty}^{[k]})$ for a suitable sequence B, the equality cannot be true.

The same argument, using the results from [8] and [9] which establish the existence of continuous maps T such that $\sup_A h_A(T) = \log 2$, is valid to prove a similar result for the topological entropy case. □

In some particular cases the power formula can be true as the following results show.

Proposition 4. *Let* $T_{1,\infty} = (T_i)_{i=1}^{\infty}$ *be a periodic sequence of measure preserving transformations. Then the formula* $h_\mu(T_{1,\infty}^{[m]}) = mh_\mu(T_{1,\infty})$ *holds for any positive integer* m.

Proof. First of all we prove the equality for n the period of $T_{1,\infty}$. Then $T_{1,\infty}^{[n]}$ is the constant sequence $(T_i^{[n]})_{i=1}^{\infty}$ with $T_i^{[n]} = T_1^n$ for all $i \in \mathbb{N}$. For any finite partition $\mathscr{A}$ and $t = mn + r$ we have:

$$\mathscr{A}^t(T_{1,\infty}) = \left(\mathscr{A} \vee T_1^{-1}\mathscr{A} \vee \ldots \vee T_1^{-(n-1)}\mathscr{A}\right) \bigvee$$

$$\bigvee \left(T_1^{-n}\mathscr{A} \vee T_1^{-1}\mathscr{A} \vee \ldots \vee T_1^{-(2n-1)}\mathscr{A}\right) \bigvee \ldots \bigvee$$

$$\bigvee \left(T_1^{-mn}\mathscr{A} \vee T_1^{-1}\mathscr{A} \vee \ldots \vee T_1^{-(mn-1)}\mathscr{A}\right) \bigvee \left(\bigvee_{i=0}^{r-1} T_1^{-i}\mathscr{A}\right).$$

Then

$$\frac{1}{m} H_\mu\left(\mathscr{A}^{mn+r}(T_{1,\infty})\right) \leq \frac{1}{m} H_\mu\left(\mathscr{A}^m(T_{1,\infty}^{[n]})\right) + \frac{1}{m} H_\mu\left(\bigvee_{i=0}^{r-1} T_1^{-i}\mathscr{A}\right),$$

and so

$$\frac{1}{m} H_\mu \left(\mathscr{A}^m (T_{1,\infty}^{[n]}) \right) \geq \frac{1}{m} H_\mu \left(\mathscr{A}^{mn+r} (T_{1,\infty}) \right) - \frac{1}{m} H_\mu \left(\bigvee_{i=0}^{r-1} T_1^{-i} \mathscr{A} \right).$$

Since $\limsup_{m\to\infty} \frac{1}{m} H_\mu \left(\bigvee_{i=0}^{r-1} T_1^{-i} \mathscr{A} \right) = 0$, we have that

$$\begin{aligned} h_\mu \left(T_{1,\infty}^{[n]}, \bigvee_{i=0}^{n-1} T_1^{-i} \mathscr{A} \right) &= \limsup_{m\to\infty} \frac{1}{m} H_\mu \left(\mathscr{A}^m (T_{1,\infty}^{[n]}) \right) \\ &\geq \limsup_{m\to\infty} \frac{1}{m} H_\mu \left(\mathscr{A}^{mn+r} (T_{1,\infty}) \right) \\ &= n \limsup_{m\to\infty} \frac{1}{nm+r} H_\mu \left(\mathscr{A}^{mn+r} (T_{1,\infty}) \right) \\ &= n(h_\mu T_{1,\infty}, \mathscr{A}) \end{aligned}$$

and then

$$h_\mu (T_{1,\infty}^{[n]}) \geq n h_\mu (T_{1,\infty}).$$

The equality follows because the reverse inequality holds.

Now, suppose that $m = kn$ with $k \in \mathbb{N}$. Then it holds that $T_{1,\infty}^{[m]}$ is the constant sequence $(T_i^{[m]})_{i=1}^{\infty}$ where $T_i^{[m]} = (T_n \circ \ldots \circ T_1)^k$ and since it is periodic it holds that

$$\begin{aligned} h_\mu (T_{1,\infty}^{[m]}) &= h_\mu ((T_n \circ \ldots \circ T_1)^k) \\ &= k h_\mu \left(T_n \circ \ldots \circ T_1 \right) \\ &= m h_\mu (T_{1,\infty}). \end{aligned}$$

Finally, suppose that n does not divide m. Then the sequence $T_{1,\infty}^{[m]}$ is periodic with the same period as $T_{1,\infty}$. Then

$$h_\mu (T_{1,\infty}^{nm}) = n h_\mu (T_{1,\infty}^{m}),$$

and on the other hand we have that

$$h_\mu (T_{1,\infty}^{nm}) = nm h_\mu (T_{1,\infty}).$$

Combining both equalities we have that $h_\mu (T_{1,\infty}^{m}) = m h_\mu (T_{1,\infty})$ and the proof ends. □

Let $T_{1,\infty} = (T_i)_{i=1}^{\infty}$ be a sequence of measure preserving transformations. We say that $T_{1,\infty} = (T_i)_{i=1}^{\infty}$ is *eventually periodic* if there exists a positive integer k such that $T_{k,\infty}$ is periodic.

Proposition 5. *Let $T_{1,\infty} = (T_i)_{i=1}^{\infty}$ be an eventually periodic sequence of measure preserving transformations. Then for any $m \in \mathbb{N}$ we have that $h_\mu(T_{1,\infty}^{[m]}) = mh_\mu(T_{1,\infty})$.*

Proof. Let k be the first positive integer such that $T_{k,\infty}$ is periodic. Consider the sequence $T_{1,\infty}^{[m]} = (T_1^{m-1}, T_m^{2m-1} \dots T_{(i-1)m}^{im-1} \dots)$. This sequence is also eventually periodic and $(T^{[m]})_{k,\infty} = (T_{km}^{2km-1}, \dots, T_{(i-1)m}^{im-1} \dots)$ is periodic.

By Theorem 1 (e) and Proposition 4 it follows that

$$h_\mu(T_{1,\infty}^{[m]}) = h_\mu((T^{[m]})_{k,\infty}) = mh_\mu(T_{k,\infty}) = mh_\mu(T_{1,\infty}),$$

which concludes the proof. □

It is unclear whether the power formula remains true for sequences $T_{1,\infty}$ which are generated by just a finite numbers of maps $T_1,\dots,T_n$.

If $K = (k_i)_{i=1}^{\infty}$ is a sequence of integers, we may define the non–autonomous system $T_{1,\infty}^{[K]}$ as $T_{1,\infty}^{[K]} = (T_1^{k_1}, T_{k_1+1}^{k_2}, \dots)$ and, analogously to the autonomous case (see [11]), we say that $T_{1,\infty}$ is null if $sup_K h_\mu(T_{1,\infty}^{[K]}) = 0$, bounded if $sup_K h_\mu(T_{1,\infty}^{[K]})$ is bounded and unbounded if $sup_K h_\mu(T_{1,\infty}^{[K]}) = \infty$. Analogous definitions can be established for topologically null, bounded and unbounded non–autonomous systems. Let us show a property that implies that the system is null. It is unclear whether the condition can be replaced by an equivalence, as in the autonomous case (see [16]) and what happens in the bounded and unbounded cases.

Recall that given a measure preserving transformation $T : X \to X$ it can be defined a linear operator $U_T : L^2(X,\mu) \to L^2(X,\mu)$ given by $U_T(f) = f \circ T$ for all $f \in L^2(X,\mu)$. λ is said an eigenvalue of T if there exists a non zero map $f \in L^2(X,\mu)$ with $U_T(f) = \lambda f$; f is said an eigenvector of T associated to λ. We say that T has discrete spectrum if $L^2(X,\mu)$ has an orthonormal basis of eigenvectors.

Proposition 6. *Let $T_{1,\infty} = (T_i)_{i=1}^{\infty}$ be a sequence of maps preserving the same measure μ. Suppose that for all positive integer i the measure preserving transformation T_i has discrete spectrum with the same orthonormal basis. Then $T_{1,\infty}$ is null.*

Proof. Notice that $T_{1,\infty}^{[K]}$ holds the hypothesis and therefore it is enough to prove that $h_\mu(T_{1,\infty}) = 0$.

Let $f \in L^2(X,\mu)$ be a characteristic function of a set of measure $1/2$ and let M be the set of such functions contained in $L^2(X,\mu)$. Consider the map $\psi : M \to \mathscr{Z}$ such that $\psi(f) = \left\{f^{-1}(1), f^{-1}(0)\right\}$. Defining the metric ρ' in M as

$$\rho'(f,g) = \mu(f^{-1}(1) \triangle g^{-1}(1)),$$

it follows from [16] that ψ is a continuous map and if a set $K \subset M$ is compact, then $\psi(K)$ is also compact in $\psi(M)$. By Lemma 2 in [16], a closed set $L \subset \psi(M) \subset \mathscr{Z}$ is compact if and only if for any sequence $\{\xi_i\}_{i=1}^{\infty} \subset L$ it holds

$$\lim_{n\to\infty} \frac{1}{n} H_\mu \left(\bigvee_{i=1}^{n} \xi_i \right) = 0.$$

Consider the sequence of unitary operators $U_{1,\infty} = \{U_{T_1}, U_{T_2}, \ldots.\}$ where $U_{T_i}(g) = g \circ T_i$ for all $g \in L^2(X,\mu)$. If each transformation T_i has discrete spectrum with the same orthonormal basis $\{e_i\}_{i=0}^{\infty}$, then for any $f \in L^2(X,\mu)$ it follows that $\mathrm{Cl}(\{U_{T_1} \circ \ldots \circ U_{T_n}(f)\}_{n=0}^{\infty})$, the closure of the sequence $\{U_{T_1} \circ \ldots \circ U_{T_n}(f)\}_{n=0}^{\infty}$, is compact. In order to see this, we know that $U_{T_i}(e_j) = \lambda_{ij} e_j$, $|\lambda_{ij}| = 1$ for any pair $(i,j) \in \mathbb{N}^2$. For any $f \in L^2(X,\mu)$, $f = \sum_{i=0}^{\infty} a_i e_i$ with $\sum_{i=0}^{\infty} |a_i|^2 < \infty$, it follows that:

$$\mathrm{Cl}(\{U_{T_1} \circ \ldots \circ U_{T_n}(f)\}_{n=0}^{\infty}) \subset \left\{ g = \sum_{i=0}^{\infty} b_i e_i : |b_i| \leq |a_i| \right\} = B.$$

Since B is compact, our set $\mathrm{Cl}(\{U_{T_1} \circ \ldots \circ U_{T_n}(f)\}_{n=0}^{\infty})$ is compact.

Let $f \in M \subset L^2(X,\mu)$. Since $\mathrm{Cl}(\{U_{T_1} \circ \ldots \circ U_{T_n}(f)\}_{n=0}^{\infty})$ is compact and the map ψ is continuous, the set

$$\psi\left(\mathrm{Cl}(\{U_{T_1} \circ \ldots \circ U_{T_n}(f)\}_{n=0}^{\infty})\right) = \mathrm{Cl}(\{T_1^{-n}\psi(f)\}_{n=0}^{\infty})$$

is compact in $\psi(M) \subset \mathscr{Z}$ and then

$$h_\mu(T_{1,\infty}, \psi(f)) = \limsup_{n\to\infty} \frac{1}{n} H_\mu \left(\bigvee_{i=0}^{n-1} T_1^{-n} \psi(f) \right) = 0.$$

If we consider the finite partitions of X given by $\bigvee_{i=1}^{n} \xi_i$ with $\xi_i \in \psi(M)$, then by Theorem 1 we have that

$$h_\mu \left(T_{1,\infty}, \bigvee_{i=1}^{n} \xi_i \right) \leq \sum_{i=1}^{n} h_\mu(T_{1,\infty}, \xi_i) = 0.$$

Since it follows from [16] that the set of finite partitions $\bigvee_{i=1}^{n} \xi_i$ with $\xi_i \in \psi(M)$ is everywhere dense in $\mathscr{Z}$, and the map $h_\mu(T_{1,\infty}, \cdot) : \mathscr{Z} \to \mathbb{R}^+ \cup \{0\}$ is continuous, by Theorem 1, $h_\mu(T_{1,\infty}) = 0$ and the proof concludes. □

Next, we show two examples of null systems. For the first one, let $S^1 = \{z \in \mathbb{C} : |z| = 1\}$. Consider a sequence $(\alpha_i)_{i=1}^{\infty}$, $\alpha_i \in \mathbb{C}$, and construct the sequence $R_{1,\infty} = (R_i)_{i=1}^{\infty}$ where $R_i : S^1 \to S^1$ is given by $R_i(x) = \alpha_n x$, for all $x \in S^1$.

Then maps R_i are rotations on S^1. Every rotation preserves the normalized Haar measure (see page 20 from [19]). Then we can prove the following proposition.

Proposition 7. *Under the above conditions, if μ is the normalized Haar measure in S^1 we have that $h_m(R_{1,\infty}) = 0$.*

Proof. It is known that every rotation on S^1 has discrete spectrum with the same orthonormal basis (see Sect. 3.3 from [19]). Applying Proposition 6 the proof finishes. □

Now we apply Proposition 6 to the sequences of ergodic rotations on a compact group. Let G be a compact group and $a \in G$. Consider the measure preserving transformation $T_a : G \to G$ given by $T_a(g) = ag$ called rotation of "angle"a. It can be seen that each rotation preserves the Haar measure in G (see [19]). Then we can prove the following result.

Proposition 8. *Let $(a_i)_{i=1}^{\infty}$ be a sequence of elements of a compact topological group G and let $T_{1,\infty} = (T_{a_i})_{i=1}^{\infty}$ be a sequence of ergodic rotations over G. If m denotes the Haar measure, then it follows that $h_m(T_{1,\infty}) = 0$.*

Proof. Let $\hat{G}$ be the set of characters of G, that is, the set of continuous homomorphisms of G onto S^1. It is know (see Sect. 3.3 from [19]) that $\hat{G}$ is a discrete countable group, whose members are mutually orthogonal members of $L^2(G, m)$.

By Theorem 3.5 from [19], we know that every rotation T_{a_i} has discrete spectrum with basis $\hat{G}$ for all $i \in \mathbb{N}$. Now apply Proposition 6 to obtain $h_m(T_{1,\infty}) = 0$. □

There are sequences of measure preserving transformations with zero metric entropy $T_{1,\infty} = (T_i)_{i=1}^{\infty}$ satisfying that every map T_i, $i \in \mathbb{N}$, has no discrete spectrum. Let us see in the following example.

Example 2. Let $\Sigma^2 = \{0,1\}^{\mathbb{Z}}$. Denote by β the product σ–algebra of Σ^2 and by μ the product measure satisfying $\mu([i]) = 1/2$ where

$$[i] = \{\{x_i\}_{i=-\infty}^{\infty} : x_0 = i\} \text{ with } i = 0, 1.$$

Let $\sigma : \Sigma^2 \to \Sigma^2$ be the shift map. Since $h_\mu(\sigma) = h_\mu(\sigma^{-1}) = \log 2$, σ and σ^{-1} have not discrete spectrum (see [16]). Consider the periodic sequence $\sigma_{1,\infty} = \left(\sigma, \sigma^{-1}, \sigma, \sigma^{-1}, \ldots\right)$. By Theorem 4 we have that $h_\mu(\sigma_{1,\infty}^2) = 2h_\mu(\sigma_{1,\infty})$. Since $\sigma_{1,\infty}^2 = (Id, Id, \ldots)$ with Id the identity map on Σ^2 we have that $h_\mu(\sigma_{1,\infty}^2) = 0$ and then $h_\mu(\sigma_{1,\infty}) = 0$. Moreover, it is straightforward to check that the non–autonomous system is null.

Acknowledgements This paper has been partially supported by the grants MTM2011-23221 from Ministerio de Economía y Competitividad (Spain) and 08667/PI/08 from Fundación Séneca, Agencia de Ciencia y Tecnología de la Comunidad Autónoma de la Región de Murcia (II PCTRM 2007–10).

References

1. Adler, R.L., Konheim, A.G., McAndrew, M.H.: Topological entropy. Trans. Am. Math. Soc. **114**, 309–319 (1965)
2. Below, A., Losert, V.: On sequences of density zero in ergodic theory. Contemp. Math. **26**, 49–60 (1984)
3. Blum, J.R., Hanson, D.L.: On the mean ergodic theorem for subsequences. Bull. Am. Math. Soc. **66**, 308–311 (1960)
4. Bourgain, J.: On the maximal ergodic theorem for certain subsets of the integers. Irsael J. Math. **61**, 39–72 (1988)
5. Bourgain, J.: On the maximal ergodic theorem on L^p for arithmetic sets. Irsael J. Math. **61**, 73–84 (1988)
6. Bourgain, J.: Almost sure convergence and bounded entropy. Irsael J. Math. **63**, 79–97 (1988)
7. Bowen, R.: Entropy for group endomorphism and homogeneous spaces. Trans. Am. Math. Soc. **153**, 401–414 (1971)
8. Cánovas, J.S.: Topological sequence entropy of interval maps. Nonlinearity **17**, 49–56 (2004)
9. Cánovas, J.S.: Topological sequence entropy of circle maps. Appl. Gen. Topol. **2**, 1–7 (2001)
10. Denker, M., Grillenberger, C., Sigmund, K.: Ergodic Theory on Compact Spaces. Lecture Notes in Mathematics. Springer, Berlin (1976)
11. Goodman, T.N.T.: Topological sequence entropy. Proc. Lond. Math. Soc. **29**, 331–350 (1974)
12. Halmos, P.R.: Lectures on Ergodic Theory. The Mathematical Society of Japan, Tokyo (1956)
13. Hu, H.: Some ergodic properties of commuting diffeomorphisms. Ergod. Theory Dyn. Syst. **13**, 73–100 (1993)
14. Hulse, P.: Counterexamples to the product rule for entropy. Dyn. Syst. **24**, 81–95 (2009)
15. Kolyada, S., Snoha, L.: Topological entropy of nonautonomous dynamical systems. Random Comput. Dyn. **4**, 205–233 (1996)
16. Kushnirenko, A.G.: On metric invariants of entropy type. Russ. Math. Surv. **22**, 53–61 (1967)
17. Nagata, J.: Modern Dimension Theory. Wiley, New York (1965)
18. Pickel, B.S.: Some properties of A–entropy. Mat. Zametki **5**, 327–334 (1969). (Russian)
19. Walters, P,: An Introduction to Ergodic Theory. Springer, New York (1982)
20. Zhu, Y., Liu, Z., Xu, X., Zhang, W.: Entropy of nonautonomous dynamical systems. J. Korean Math. Soc. **49**, 165–185 (2012)

Interlacing and Separation of Solutions of Linear Meromorphic ODEs

Félix Álvaro Carnicero and Fernando Sanz

Abstract Solutions of two-dimensional linear systems of ODEs with real meromorphic coefficients may have two very distinct kinds of relative behaviour when they approach to a singular point: either any two of them are linked or either any two of them can be separated by a linear projection. In this paper, we are interesting in the question of the decidability of the dichotomy linked/separated for the whole family of systems. First, we rewrite the known result which asserts that the dichotomy is determined in terms of a semialgebraic set (is decidable) on a truncation of the Taylor expansion of the coefficients of the system. After that, we study the question of the decidability of that dichotomy in terms of the coefficients of the system themselves as elements of the ordered Hardy field of real meromorphic functions.

1 Introduction and Statements

This paper deals with real meromorphic linear systems of two ordinary differential equations; that is, systems of the form

$$Y' = AY + B, \quad Y = \begin{pmatrix} y_1 \\ y_2 \end{pmatrix} \tag{1}$$

where A is a 2×2 matrix and B is a 2-dimensional column vector, both with entries in the field $K = \mathbb{R}(\{x\})$ of real meromorphic series. The *Poincaré rank* of the system is the minimum $q \in \mathbb{Z}_{\geq -1}$ such that $x^{q+1}A$ has no pole at $x = 0$.

F.Á. Carnicero (✉) · F. Sanz
University of Valladolid, Departamento de Álgebra, Análisis Matemático, Geometría y Topología, Facultad de Ciencias, Campus Miguel Delibes, Paseo Belén, 7, E-47011, Valladolid, Spain
e-mail: carnicero_fac@hotmail.com; fsanz@agt.uva.es

S. Ibáñez et al. (eds.), *Progress and Challenges in Dynamical Systems*,
Springer Proceedings in Mathematics & Statistics 54,
DOI 10.1007/978-3-642-38830-9_10,

Classical studies of meromorphic linear systems of ODEs (in any dimension) usually deals with the complex case; i.e., the entries are meromorphic series with complex coefficients. They cover the search of fundamental systems of solutions in terms of exponential of polynomial functions and formal power series, summation processes of the formal part of the solutions in sectors at $0 \in \mathbb{C}$, Stokes phenomena and other related topics (see [1,7]).

Here, we concentrate in the real situation and we do not treat or use those type of results from the complex case. In what follows, a *solution* of the system (1) will be a map $x \mapsto Y(x) \in \mathbb{R}^2$ defined and of class C^1 on a right neighborhood $(0, \varepsilon)$ of 0 that satisfies the equation; that is, so that $\frac{dY}{dx}(x) = A(x)Y(x) + B(x)$ for any $x \in (0, \varepsilon)$. (An analogous study can be made for solutions defined in a left neighborhood of 0.) Assuming that $x = 0$ is a singular point of the system (i.e. some of the entries of A or B has a pole at $x = 0$), we are interested in the asymptotic behavior of solutions when x goes to 0.

More precisely, we are interested in the relative asymptotic behavior of two such solutions and, particularly, in the concepts of linking and separation of solutions which come from the concepts of "spiralement" and "enlacement" introduced in [2,3] for trajectories of three-dimensional vector fields.

Roughly speaking (see Definition 1 below), two different solutions $Y(x)$ and $Z(x)$ are said to be *asymptotically interlaced* (resp. *separated*) if the vector $Y(x) - Z(x)$ of $\mathbb{R}^2$ spirals around the origin (resp. it has a well defined limit direction) when x goes to 0. It is not hard to see (we recall below a proof) that, given a system (1), either any pair of solutions is asymptotically interlaced or any pair of solutions is separated, thus allowing to say, correspondingly, that the system is *interlaced* or *separated*. Another remark is that a system as in (1) is interlaced or separated iff it is so for its homogenized system (the system consisting on the same coefficient matrix A but with $B = 0$).

The question now is to determine criteria that permit to know if a given system is interlaced or separated. In the paper [5], this problem is treated in the more general setting where the entries of the coefficient matrix A and those of the vector B belong to a *Hardy field* H. By definition, a Hardy field is a subfield of the ring of germs at $x = 0$ of differentiable real functions on a right interval $(0, \varepsilon)$ which is closed by taking the derivative with respect to x. This concept captures some of the good finiteness properties that we have for real analytic functions: non-zero elements in H have finitely many zeros, they have a limit in $\mathbb{R} \cup \{+\infty, -\infty\}$ when $x \to 0$, L'Hôpital's rule holds for elements of H, H is a totally ordered field by $f \leq g$ iff $f(x) \leq g(x)$ for any x in a right neighborhood of 0, etc. (see [4] for an extensive exposition of the theory of Hardy fields, or [6] for a recent summary). The main result in [5] is that a system as in (1) with matrix coefficient $A = \begin{pmatrix} a & b \\ c & d \end{pmatrix}$ in a Hardy field H is separated if and only if the associated *Riccati equation*

$$y' = cy^2 + (a - d)y - b \tag{2}$$

has a solution $x \mapsto y(x) \in \mathbb{R}$ defined for every x in a right neighborhood of $x = 0$. Moreover, in that case, the extension of the field H of coefficients by the family of all solutions of the system (their germs at $x = 0$) is again a Hardy field.

The result thus provides a criterium for a system to be interlaced or separated in terms of the Riccati equation of the system. However, this criterium, being completely general for any Hardy field, is far from being constructive. Restricting to our special case where the field of coefficients is $H = K = \mathbb{R}(\{x\})$, the general question now is:

> Can we expect a constructive criterium for deciding the dichotomy interlaced/separated for linear ODEs with real meromorphic coefficients?

This paper is an introductory work to the program that we have started regarding this question. We present just the first results obtained so far devoted to the task of finding what kind of "constructiveness" can we hope for such a criterium.

Before stating the results, let us fix some useful notation. First, as we have mentioned, for distinguishing between interlaced or separated systems we can restrict ourselves to homogenized ones. The whole family of such systems will be identified with K^4 by the natural identification

$$Y' = AY \longleftrightarrow A = \begin{pmatrix} a & b \\ c & d \end{pmatrix} \in K^4.$$

Denote by $\mathscr{S}$ (resp. $\mathscr{I}$) the family of separated (resp. interlaced) systems, so that we have the partition $K^4 = \mathscr{S} \cup \mathscr{I}$. For any $q \geq 0$, let

$$\mathscr{F}^q = \{A \in K^4 \ : \ x^{q+1}A \text{ has no pole at } x = 0\}$$

be the family of systems with Poincaré rank not greater than q and denote by $\mathscr{F}^q = \mathscr{S}^q \cup \mathscr{I}^q$ the corresponding partition into separated and interlaced systems. An element $A \in \mathscr{F}^q$ will be written as a Laurent power series

$$A = \sum_{j=-(q+1)}^{\infty} x^j A_j$$

where each A_j is a matrix with real entries denoted by $A_j = \begin{pmatrix} a_j & b_j \\ c_j & d_j \end{pmatrix}$. Given two integers l, m with $m \geq l \geq -(q+1)$, we will speak of the (l, m)-*truncation* of the system A to refer to the vector

$$\Pi_{[l,m]}(A) = (A_l, A_{l+1}, \ldots, A_m) \equiv (a_l, b_l, \ldots, c_m, d_m) \in \mathbb{R}^{4(m-l+1)}. \qquad (3)$$

The first result about constructiveness of the criterium for the dichotomy interlacing/separation is the following.

Theorem 1. *For any $q \geq 0$, there exists a semi-algebraic set $\Sigma_q \subset \mathbb{R}^{4(2q+2)}$ such that a system $A \in \mathscr{F}^q$ belongs to $\mathscr{S}^q$ if and only if $\Pi_{[-(q+1),q]}(A) \in \Sigma_q$.*

We recall that, by definition, a semi-algebraic set of $\mathbb{R}^n$ is a finite union of sets of the form

$$\{\mathbf{x} \in \mathbb{R}^n : P(\mathbf{x}) = 0, Q_1(\mathbf{x}) > 0, \ldots, Q_r(\mathbf{x}) > 0\}$$

where $P, Q_j \in \mathbb{R}[X_1, \ldots, X_n]$ are real polynomials in n variables.

This result appears already in the cited Ref. [5]. We present below a sketch of the proof in the way it will be useful for what follows. It establishes constructiveness for deciding interlacing/separation for systems with bounded Poincaré rank in terms of semi-algebricity of a finite jet of the Taylor expansion of the entries of the coefficient matrix of the system. In other words, we can state: for any q there exists a finite algorithm, which uses only the operations of $\mathbb{R}$ as an ordered field, whose input is a vector of real numbers corresponding to a finite Taylor expansion of a system A in $\mathscr{F}^q$ and whose output is the answer to the question of whether the system is interlaced or separated.

Our objective is to look for such a constructive criterium or finite algorithm in terms of the entries of the matrix as elements of the Hardy field $K = \mathbb{R}(\{x\})$, instead of their Taylor expansions. In order to formulate more precisely this objective, let us say that a subset of K^n is *K-semialgebraic in K^n* if it is a finite union of sets of the form

$$\{\mathbf{x} \in K^n : P(\mathbf{x}) = 0, Q_1(\mathbf{x}) > 0, \ldots, Q_r(\mathbf{x}) > 0\}$$

where $P, Q_j \in K[X_1, \ldots, X_n]$ (recall that we have defined the order in K as $a > 0$ iff $a(x) > 0$ for any x in a right neighborhood of 0).

Our next results are in the negation of existence of such constructive criterium.

Theorem 2. *For any $q \geq 1$, neither $\mathscr{S}^q \subset K^4$ nor $\mathscr{I}^q \subset K^4$ is K-semialgebraic in K^4.*

Using the fact that $\mathscr{F}^q \subset K^4$ is K-semialgebraic (see Example 2 (ii) below), we obtain

Corollary 1. *Neither the set $\mathscr{S}$ of separated systems nor the set $\mathscr{I}$ of interlaced ones is K-semialgebraic in K^4.*

The above negative results motivate the search of constructive criteria by using other operations of the Hardy field K besides the ones corresponding to an ordered field. The first natural such operation is the derivative. Accordingly to this, we will say that a subset $\Omega \subset K^n$ is *K-differentially-semialgebraic* (or *(K, d)-semialgebraic* for short) if it is a finite union of subsets of the form

$$\{\mathbf{x} \in K^n : P(\mathbf{x}, \mathbf{x}', \mathbf{x}'', \ldots) = 0, Q_1(\mathbf{x}, \mathbf{x}', \mathbf{x}'', \ldots) > 0, \ldots, Q_r(\mathbf{x}, \mathbf{x}', \mathbf{x}'', \ldots) > 0\}$$

where $P, Q_j \in K < X >= K[X, X^{(1)}, X^{(2)}, \ldots]$ are differential polynomials in n variables (i.e., any $X^{(i)}$ denotes a vector of n indeterminates) and $\mathbf{x}', \mathbf{x}''$, etc. denotes the vector of successive derivatives of the components of $\mathbf{x}$.

Our next result complements the result in Theorem 2. It states that if we allow to take derivatives, a constructive criterium for deciding the dichotomy interlacing/separation exists for systems with bounded Poincaré rank.

Theorem 3. *For any $q \geq 0$, both $\mathscr{S}^q$ and $\mathscr{I}^q$ are (K, d)-semialgebraic subsets of K^4.*

Finally, the next natural question is to know wether the use of the operation of taking derivatives suffices in order to obtain a constructive criterium for the whole family of systems, i.e. with no bound on the Poincaré rank. We claim that the answer to this question is negative, although at the time of submission of this work we had not a fully detailed proof of it. In more precise terms, we can announce

Claim (Yet unproved). Neither the set $\mathscr{S}$ nor $\mathscr{I}$ is a (K, d)-semialgebraic subset of K^4.

2 Interlaced Versus Separated

Consider a system (1) of linear meromorphic ODEs as in the introduction. If $\varepsilon > 0$ is small enough, we can assume that any entry of the matrices A and B is a well defined and analytic real function in the interval $(0, \varepsilon) \subset \mathbb{R}$. Since the map $(x, Y) \mapsto A(x)Y + B(x)$ is Lipschitz with respect to the variables $Y = (Y_1, Y_2)$, given any initial condition $(x_0, Y_0) \in (0, \varepsilon) \times \mathbb{R}^2$, there exists a unique solution of the system $x \mapsto Y(x) \in \mathbb{R}^2$ defined for any $x \in (0, \varepsilon)$ and such that $Y(x_0) = Y_0$.

Given two such different solutions Y, Z, we have $Y(x) \neq Z(x)$ for any $x \in (0, \varepsilon)$. Identifying $\mathbb{R}^2$ with the complex plane by $(y_1, y_2) \equiv y_1 + iy_2$ as usual, we can write

$$Y(x) - Z(x) = \rho(x)e^{i\theta(x)}$$

where $\rho(x) =|| Y(x) - Z(x) ||$ and $\theta_{Y,Z} : (0, \varepsilon) \to \mathbb{R}$ is a continuous (in fact analytic) function. The function $\theta_{Y,Z}$ is only well defined up to translation by $2\pi\mathbb{Z}$ (and up to translation by $\pi\mathbb{Z}$ if we interchange Y, Z); any such choice will be called in the sequel an *angle function* between Y and Z.

Definition 1. The solutions Y, Z are called *interlaced* if their angle function $\theta_{Y,Z}(x)$ diverges either to $+\infty$ or to $-\infty$ when x goes to 0. They are called *separated* if $\theta_{Y,Z}(x)$ has a finite real limit when x goes to 0.

The name "separated" makes reference to the following fact: if Y, Z are separated and $\lim_{x\to 0} \theta_{Y,Z}(x) = \theta_0$, for any plane L in coordinates (z, y_1, y_2) which contains the x-axis and is transversal to the direction where $y_2/y_1 = \tan\theta_0$, the orthogonal

linear projections of the graphs of Y, Z onto L do not intersect for x sufficiently small. On the contrary, if Y, Z are interlaced, for any such plane L, their projections intersect infinitely many times when x goes to 0.

Two different solutions can only have one of the two opposite relative behavior interlacing/separation. Moreover, we have the following result.

Theorem 4 (Dichotomy for systems). *Consider a system $Y' = AY + B$ of linear ODEs with meromorphic coefficients. Then either any two distinct solutions are interlaced or any two distinct solutions are separated. The system is called correspondingly interlaced or separated.*

Proof. A proof of this result (even in a more general setting) can be found in [5]. Let us sketch here the principal arguments for an alternative proof in our particular case.

Let $Y(x), Z(x)$ be two different solutions and let $\theta(x) = \theta_{Y,Z}(x)$ be an angle function. Let q be the Poincaré rank of the system and write $A = x^{-(q+1)}\begin{pmatrix} a_{11} & a_{12} \\ a_{21} & a_{22} \end{pmatrix}$ where the a_{ij} are real analytic functions at $x = 0$. Then $\theta(x)$ satisfies the differential equation

$$x^{q+1}\theta' = -a_{12}\, sen^2\theta + (a_{22} - a_{11})\, sen\theta cos\theta + a_{21}\, cos^2\theta. \tag{4}$$

Notice that this equation is independent of the chosen pair of solutions Y, Z of the system. Thus, it is enough to prove that either any solution $\theta(x)$ of (4), defined for x in a right neighborhood of 0, has a finite limit when x goes to 0 or any solution $\theta(x)$ diverges to $+\infty$ or $-\infty$ when x goes to 0. On the other hand, notice that, since two different solutions of (4) take different values for any positive x where they are defined, it is enough to prove that a single solution $\theta(x)$ has one of those two types of asymptotic behaviors.

The second member of Eq. (4) is an analytic function on the strip $(x, \theta) \in (0, \varepsilon) \times \mathbb{R}$, periodic in the second variable θ. Let k be the minimum of the orders of the functions a_{ij} at $x = 0$. If $k \geq q + 1$ then we can divide both sides of Eq. (4) by x^{q+1} so that the function $\theta(x)$ satisfies $\theta'(x) = R(x, \theta(x))$ where R is analytic on $(-\varepsilon, \varepsilon) \times \mathbb{R}$. In this case, by integration, there exists a limit of $\theta(x)$ when x goes to 0. Assume that $k < q + 1$ and write Eq. (4) as

$$x^{q-k+1}\theta' = R(x, \theta) \tag{5}$$

where R is analytic in $(-\varepsilon, \varepsilon) \times \mathbb{R}$, periodic in θ and such that $R(0, \theta) \not\equiv 0$. It will be sufficient to prove that if $\Lambda \subset \mathbb{R}$ is the set of accumulation values of a solution $\theta(x)$ of (5) when x goes to 0 then Λ is contained in the set of zeros of the function $\theta \mapsto R(0, \theta)$. Now, let $\theta_0 \in \mathbb{R}$ be such that $R(0, \theta_0) \neq 0$ and assume for instance that $R(0, \theta_0) > 0$. Using the fact that $q - k + 1 > 0$, we can see that there exists a box $C = (0, \delta) \times [\theta_0 - \delta, \theta_0 + \delta]$ such that if φ is a solution of equation (5) with initial condition on C, then the intersection of the graph of φ with C is the

graph of a restriction of φ to a closed subinterval $[a, b] \subset (0, \delta)$ and such that $\varphi(a) \in (0, \delta) \times \{\theta_0 - \delta\}$ and $\varphi(b) \in (0, \delta) \times \{\theta_0 + \delta\}$. This property prevents the value θ_0 to be an accumulation value of the solution $\theta(x)$ (a continuous function on a right neighborhood of $x = 0$). □

Remark 1. Since the difference of two solutions of the system $Y' = AY + B$ is a solution of its homogenized system $Y' = AY$, both systems are separated or both are interlaced. Thus, from now on, we will only consider homogeneous systems $Y' = AY$, each of them identified with the coefficient matrix $A \in K^4$ where $K = \mathbb{R}(\{x\})$ is the field of real meromorphic series in one variable.

Looking more carefully the proof sketched above, we have the following proposition which describes a good family of systems for which it is easy to decide whether it is separated or interlaced. Such a family will be used several times later on and thus it merits a definition first.

Definition 2. Consider a system $A \in K^4$ with Poincaré rank not greater than $q \geq 0$ and write $A = \sum_{j=-(q+1)}^{\infty} x^j A_j$, where each A_j is a matrix with real entries. Let $k = k(A)$ be the first integer (or infinity) such that A_k is not a multiple of the identity matrix. We will say that the system is in *final form* if either $k \geq 0$ or $k < 0$ and $\Delta(A_k) \neq 0$, where Δ is the discriminant.

Proposition 1. *With the same notations as above, assume that the system $A \in K^4$ is in final form. Then the system is interlaced if and only if $k < 0$ and $\Delta(A_k) < 0$.*

Proof. Use the same notations of the proof of Theorem 4. If $k \geq 0$, we have seen that the angle function $\theta(x)$ between two solutions of the system has a limit when x goes to 0, showing that the system is separated. If $k < 0$ and $\Delta(A_k) < 0$ then in the Eq. (5) we have that $\theta \mapsto R(0, \theta)$ never vanishes. From the proof of Theorem 4, we obtain then that $\theta(x)$ can not have any finite accumulation value and therefore it diverges to $+\infty$ or to $-\infty$, showing that the system is interlaced. Finally, if $k < 0$ and $\Delta(A_k) > 0$ then $\theta \mapsto R(0, \theta)$ change sign and their zeros can be accumulation values of the angle function $\theta(x)$. The proof of Theorem 4 also shows that solutions of (5) near a point θ_0 where $R(0, \theta_0) \neq 0$ are monotonous on x, increasing if $R(0, \theta_0) > 0$ and decreasing if $R(0, \theta_0) < 0$. This property prevents the angle function $\theta(x)$ to diverge and thus it has a limit when x goes to 0, showing that the system is separated. □

3 Proof of Theorem 1

In this paragraph we sketch a proof of Theorem 1 following the Ref. [5] where it first appears.

A first remark is that Theorem 1 is true for the family of systems in final form (cf. Definition 2). More precisely, and in the same terms and notation of

the statement of Theorem 1, we can state the following result which is an easy consequence of the respective definitions and of Proposition 1.

Lemma 1. *For any $q \geq 0$, there exists a semi-algebraic set Σ'_q in $\mathbb{R}^{4(q+1)}$ such that, given $A \in \mathscr{F}^q$, the system A is in final form and separated if and only if $\Pi_{[-(q+1),-1]}(A) \in \Sigma'_q$.*

(Recall the notation of the truncation $\Pi_{[l,m]}$ in Eq. (3)). The proof of Theorem 1 in the general case will be a consequence of the existence of a process that converts a given system in a system in final form and that involves only a finite truncation of the system, the number of terms in this truncation depending on the Poincaré rank of the initial system. This process is an avatar of the classical Turritin's algorithm for the search of a formal fundamental matrix of solutions of a linear meromorphic system of ODEs (in any dimension). It can be seen with details in the Refs. [7] or [1]. In our case, the process is simpler. For the sake of completeness, we sketch here the principal arguments (see also [3] for a proof in this special case).

We consider the following types of coordinate transformations in $\mathbb{R}^3$:

$$
\begin{aligned}
&T_L : x = \tilde{x}, (y_1, y_2) = (\tilde{y}_1, \tilde{y}_2)L^t, \text{ where } L \in \mathscr{M}_{2\times 2}(\mathbb{R}) \text{ with } \det L \neq 0\\
&B : x = \tilde{x}, y_1 = \tilde{y}_1, y_2 = x\tilde{y}_2\\
&R : x = \tilde{x}^2
\end{aligned}
$$

The first one is a linear transformation with constant coefficients (and leaving the independent variable x fixed); the notation B for the second one stands for *blowing-up* (with center the y_1-axis ($x = y_2 = 0$)) and the notation R for the third one stands for *ramification* (over the x-plane and of order 2). Any of such types of transformations will be called in the sequel a *permissible transformation*.

The first interesting property about permissible transformation is that they preserve the character interlaced/separated of the system: given a system $Y' = AY$ with $A \in K^4$, a permissible transformation $\psi : (x, y_1, y_2) \mapsto (\tilde{x}, \tilde{y}_1, \tilde{y}_2)$ produces a new system $\tilde{Y}' = \tilde{A}\tilde{Y}$ (where $\tilde{Y} = (\tilde{y}_1, \tilde{y}_2)$ and the derivative $\tilde{Y}'$ is with respect to $\tilde{x}$) such that the systems $A, \tilde{A}$ are both interlaced or both separated. We will use the notation $\tilde{A} = \psi_* A$.

From a computational point of view, the transformed system $\tilde{A}$ can be obtained from the system A according to the following rules: if we write

$$
\begin{aligned}
A &= x^{-(q+1)}A_{-(q+1)} + x^{-q}A_{-q} + \cdots, \ A_j = \begin{pmatrix} a_j & b_j \\ c_j & d_j \end{pmatrix}\\
\tilde{A} &= x^{-(\tilde{q}+1)}\tilde{A}_{-(\tilde{q}+1)} + x^{-\tilde{q}}A_{-\tilde{q}} + \cdots, \ \tilde{A}_j = \begin{pmatrix} \tilde{a}_j & \tilde{b}_j \\ \tilde{c}_j & \tilde{d}_j \end{pmatrix},
\end{aligned}
$$

then

– In the case of the linear transformation T_L, we have

$$\tilde{q} = q \text{ and } \tilde{A}_j = L^{-1}A_j L, \ \forall j. \tag{6}$$

– In the case of the blowing-up transformation B, and if $c_{-(q+1)} = 0$, we have

$$\tilde{q} = q, \quad \tilde{a}_j = a_j, \tilde{b}_j = b_{j-1}, \tilde{c}_j = c_{j+1} \,\forall\, j$$
$$\tilde{d}_j = d_j \text{ for } j \neq -1 \text{ and } \tilde{d}_{-1} = d_{-1} - 1. \tag{7}$$

– In the ramification transformation R, we have

$$\tilde{q} = 2q \text{ and } \tilde{A}_{-(\tilde{q}+1)+2j} = 2A_{-(q+1)+j}, \ \tilde{A}_{-(\tilde{q}+1)+2j+1} = 0, \ \forall\, j \geq 0. \tag{8}$$

Permissible transformations permit to transform any system into a system in final form. More precisely, we have the following result that states that the process of transforming a system into one in final form only depends on a finite truncation of the original system.

Proposition 2. *Let $A \in \mathscr{F}^q$ be a system with Poincaré rank not greater than q. Then there exists a composition $\phi_A = \psi^n \circ \psi^{n-1} \circ \cdots \circ \psi^1$ of finitely many permissible transformations such that*

$$(\phi_A)_* A = \psi^n_*(\psi^{n-1}_*(\cdots(\psi^1_* A)\cdots))$$

is in final form. Moreover, the collection of ϕ_A for $A \in \mathscr{F}^q$ can be constructed so that the following properties hold:

(i) If $A, A' \in \mathscr{F}^q$ are such that $\Pi_{[-(q+1),q]}(A) = \Pi_{[-(q+1),q]}(A')$ then $\phi_A = \phi_{A'}$.
(ii) There is a semialgebraic set $\Omega = \Omega(q) \subset \mathbb{R}^{4(2q+2)}$ such that, if we denote $\Omega_1 = \Omega$, $\Omega_2 = \mathbb{R}^{4(2q+2)} \setminus \Omega$ and $q_1 = q$, $q_2 = 2q$ then, for $i = 1, 2$, we have

(ii1) $\Pi_{[-(q+1),q]}(A) \in \Omega_i \Rightarrow (\phi_A)_* A \in \mathscr{F}^{q_i}$.
(ii2) The truncation $\Pi_{[-(q_i+1),-1]}((\phi_A)_* A)$ only depends on $\Pi_{[-(q+1),q]}(A)$.
(ii3) The map $h_i : \Omega_i \to \mathbb{R}^{4(q_i+1)}$ defined by

$$h_i : \Pi_{[-(q+1),q]}(A) \mapsto \Pi_{[-(q_i+1),-1]}((\phi_A)_* A)$$

is semialgebraic (its graph is a semialgebraic set of $\mathbb{R}^{4(2q+2+q_i+1)}$).

Proposition 2, together with Lemma 1 and the basic properties of semialgebraic geometry (notably that the direct image as well as the inverse image of a semialgebraic set by a semialgebraic map is semialgebraic) provides a proof of Theorem 1.

Sketch of the proof of Proposition 2. The set $\Omega = \Omega(q)$ will be constructed in the following way. We describe two families $\{E^i\}_{i=1}^r$, $\{\Omega^i\}_{i=1}^r$ of semialgebraic subsets of $\mathbb{R}^{4(2q+2)}$ with

$$\mathbb{R}^{4(2q+2)} = E^1 \cup E^2 \cup \cdots E^r, \ E^i \cap E^j = \emptyset \text{ for } i \neq j \text{ and } \Omega^i \subset E^i \tag{9}$$

such that, for $i = 1, 2, \ldots, r$, we have

(i′) Statement (i) holds with $\pi^{-1}_{[-(q+1),q]}(E^i)$ in the place of $\mathscr{F}^q$.

(ii′) Statement (ii) holds with E^i and Ω^i in the place of $\mathbb{R}^{4(2q+2)}$ and Ω, respectively.

After that, the required set $\Omega = \Omega(q)$ in (ii) will be then the union of the Ω^i and the proof of Proposition 2 will be achieved.

Denote by Σ_Δ the semialgebraic set of $\mathbb{R}^4$ consisting of those matrices $L \in \mathscr{M}_{2\times 2}(\mathbb{R})$ with $\Delta(L) = 0$, where we identify $\mathbb{R}^4 \equiv \mathscr{M}_{2\times 2}(\mathbb{R})$.

We proceed by induction on q.

Consider the case $q = 0$. For any $A \in \mathscr{F}^0$ we write $A = x^{-1}A_{-1} + A_0 + \cdots$ and $(A_{-1}, A_0) \equiv \Pi_{[-1,0]}(A)$. If $\Delta(A_{-1}) \neq 0$ then A is already in final form and we will take $\phi_A = id$ (i.e., no permissible transformation at all) for such a system. Thus, our first set in the partition (9) is $E^1 = (\mathbb{R}^4 \setminus \Sigma_\Delta) \times \mathbb{R}^4$ for which we put $\Omega^1 = E^1$ (so that (i′) and (ii′) hold for E^1, Ω^1). We look for other members of the partition inside $\Sigma_\Delta \times \mathbb{R}^4$. For any system A such that $\Delta(A_{-1}) = 0$, there exists a non singular matrix $L = L(A_{-1})$, whose entries are polynomials in the entries of A_{-1}, and such that $L^{-1}A_{-1}L$ is upper triangular. For any such A, we consider the permissible transformation $\psi^1 = T_{L(A_{-1})}$ (which only depends on $\Pi_{[-1,0]}(A)$, in fact only on $\Pi_{[-1,-1]}(A) = A_{-1}$), put $A^{(1)} = \psi^1_* A$ and use the notation

$$\Pi_{[-1,0]}(A^{(1)}) = (A^{(1)}_{-1}, A^{(1)}_0) \text{ with } A^{(1)}_j = \begin{pmatrix} a^{(1)}_j & b^{(1)}_j \\ c^{(1)}_j & d^{(1)}_j \end{pmatrix}.$$

Notice that each entry of $A^{(1)}_j$ for $j = -1, 0$ is a semialgebraic function on the entries of A_{-1} and A_0 (using the rule (6) for ψ^1). The equation $\{c^{(1)}_0 = 0\}$ thus defines a semialgebraic subset $E^2 \subset \Sigma_\Delta \times \mathbb{R}^4$. Put also $E^3 = \Sigma_\Delta \times \mathbb{R}^4 \setminus E^2$ and $\Omega^i = E^i$ for $i = 2, 3$. We claim that (i′) and (ii′) hold for the two pairs of semialgebraic sets E^2, Ω^2 and E^3, Ω^3, giving the desired partition (9) for $q = 0$. To prove this claim, if $A \in \mathscr{F}^0$ is such that $\Pi_{[-1,0]}(A) \in E^2$ then we consider $\phi_A = \psi^2 \circ \psi^1$ where ψ^2 is the blowing-up transformation and $\psi^1 = T_{L(A_{-1})}$. Put $A^{(2)} = (\phi_A)_* A = \psi^2_* A^{(1)}$ where $A^{(1)} = \psi^1_* A$ and write $\Pi_{[-1,0]}(A^{(2)}) = (A^{(2)}_{-1}, A^{(2)}_0)$. The rule (7) for ψ^2 shows that $\Delta(A^{(2)}_{-1}) \neq 0$ and thus $A^{(2)}$ is in final form. This shows (i′) and (ii′) for E^2 and Ω^2. On the other hand, if $A \in E^3$ then we put $\phi_A = \psi^3 \circ \psi^2 \circ \psi^1$ where $\psi^1 = T_{L(A_{-1})}$, ψ^2 is the ramification R and ψ^3 is the blowing-up B. Applying the rules (8) and (7) we see that in this case $\tilde{A} = (\phi_A)_* A \in \mathscr{F}^0$ (that is, $q_2 = 2q = 0$ as required in (ii1)) and, if we write $\tilde{A} = x^{-1}\tilde{A}_{-1} + \tilde{A}_0 + \cdots$, then $\tilde{A}_{-1} = a^{(1)}_{-1} I_2$ where I_2 is the identity matrix. This proves that $\tilde{A}$ is in final form and we can conclude the properties (i′) and (ii′) for E^3, Ω^3.

Suppose now that $q \geq 1$. Given $A \in \mathscr{F}^q$ we write $A = x^{-(q+1)}A_{-(q+1)} + x^{-q}A_{-q} + \cdots$. Analogous to the previous case, we put $E^1 = (\mathbb{R}^4 \setminus \Sigma_\Delta) \times \mathbb{R}^{4(2q+1)}$ and $\Omega^1 = E^1$ as the first element in the partition (9). Now, for a system A with $\Delta(A_{-(q+1)}) = 0$, there exists a non singular matrix $L = L(A_{-(q+1)})$, whose entries

are polynomials in the entries of $A_{-(q+1)}$, and such that $L^{-1}A_{-(q+1)}L$ is upper triangular. For such an A, consider $\psi^1 = T_{L(A_{-(q+1)})}$ and $A^{(1)} = \psi^1_* A$, written as $A^{(1)} = x^{-(q+1)}A^{(1)}_{(q+1)} + x^{-q}A^{(1)}_{-q} + \cdots$. The truncations $\Pi_{[-(q+1),q]}(A)$ of those systems A for which $A^{(1)}_{-(q+1)}$ is diagonal (and thus a multiple of the identity) form a semialgebraic set $\mathscr{D} \times \mathbb{R}^{4(2q+1)}$ in $\mathbb{R}^{4(2q+2)}$. Using the induction hypothesis, there exists a semialgebraic set $\Omega(q-1) \subset \mathbb{R}^{4(2(q-1)+2)}$ satisfying property (ii) for $q-1$. Therefore, if we put

$$E^2 = \mathscr{D} \times \mathbb{R}^{4(2q+1)},\ \Omega^2 = \mathscr{D} \times \Omega(q-1) \times \mathbb{R}^4 \subset E^2,$$

we have a second element of the partition (9) such that (i′) and (ii′) hold for E^2, Ω^2. It remains to describe the other members of the partition inside $(\mathbb{R}^4 \setminus \mathscr{D}) \times \mathbb{R}^{4(2q+1)}$. With the notations as above, assume that $A^{(1)}_{-(q+1)}$ is upper triangular but not diagonal and write $A^{(1)}_j = \begin{pmatrix} a^{(1)}_j & b^{(1)}_j \\ c^{(1)}_j & d^{(1)}_j \end{pmatrix}$. The equation $\{c^{(1)}_{-q} = 0\}$ defines a semialgebraic set E^3 in $(\mathbb{R}^4 \setminus \mathscr{D}) \times \mathbb{R}^{4(2q+1)}$. For a system A with truncation in E^3 we put ψ^2 equal to the blowing-up transformation B and $A^{(2)} = (\psi^2 \circ \psi^1)_* A \in \mathscr{F}^q$. Its first coefficient $A^{(2)}_{-(q+1)}$ is a multiple of the diagonal. Moreover, by the rule (7), for any $l \geq -(q+1)$, the truncation $\Pi_{[-(q+1),l]}(A^{(2)})$ is the image of $\Pi_{[-(q+1),l+1]}(A^{(1)})$ (and thus of $\Pi_{[-(q+1),l+1]}(A)$) by a semialgebraic map. Therefore, if we put

$$\Omega^3 = E^3 \cap \mathbb{R}^4 \times \Omega(q-1) \times \mathbb{R}^4 \subset \mathbb{R}^{4(2q+2)},$$

we obtain a third member of the required partition (9) so that (i′) and (ii′) hold for E^3, Ω^3. Finally, put $E^4 = (\mathbb{R}^4 \setminus \mathscr{D}) \times \mathbb{R}^{4(2q+1)} \setminus E^3$ and $\Omega^4 = \emptyset$. To finish, let us show properties (i′) and (ii′) for the pair $E^4, \Omega^4 = \emptyset$. If a system A is such that $\Pi_{[-(q+1),q]}(A) \in E^4$ then $c^{(1)}_{-q} \neq 0$ with the notations as above. We consider the permissible transformations $\psi^2 = R$, $\psi^3 = B$ and the composition $\phi_A = \psi^3 \circ \psi^2 \circ \psi^1$ which does not depend on A chosen so that $\Pi_{[-(q+1),q]}(A) \in E^4$. Put $\tilde{A} = (\phi_A)_* A$. Using the rules (8) and (7) we can see that $\tilde{A} \in \mathscr{F}^{2q}$ and, if we write $\tilde{A} = x^{-(2q+1)}\tilde{A}_{-(2q+1)} + x^{-2q}\tilde{A}_{-2q} + \cdots$, then $\tilde{A}_{-(2q+1)}$ is a multiple of the identity matrix and

$$\tilde{A}_{-2q} = \begin{pmatrix} 0 & b^{(1)}_{-(q+1)} \\ c^{(1)}_{-q} & 0 \end{pmatrix}.$$

This proves that $\tilde{A}$ is in final form. On the other hand, $\Pi_{[-(2q+1),2q-1]}(\psi^2_* A^{(1)})$ is the image of $\Pi_{[-(q+1),q]}(A^{(1)})$ by a semialgebraic map and $\Pi_{[-(2q+1),2q-2]}(\tilde{A})$ is the image of $\Pi_{[-(2q+1),2q-1]}(\psi^2_* A^{(1)})$ by a semialgebraic map. This shows the properties (i′) and (ii′) for the pair $E^4, \Omega^4 = \emptyset$ and we are done. □

Remark 2. If we look more carefully the proof of Proposition 2, we can realize that in the statement of Theorem 1 we can in fact put $\Sigma_q \subset \mathbb{R}^{4(2q+1)}$ and $A \in \mathscr{F}^q$ separated if and only if $\Pi_{[-(q+1),q-1]}(A) \in \Sigma_q$.

Examples 1. We may point out also that there is an algorithmic way to obtain the semialgebraic set Σ_q in Theorem 1 (that is, a finite collection of polynomial identities or inequalities describing it). This algorithm is not explicit in the proof we have provided. However, as an illustration, and for a further use in the next paragraph, we want to give here a partial description of the set Σ_q (contained in $\mathbb{R}^{4(2q+1)}$ according to the remark above) in the cases $q = 0$ and $q = 1$.

Use in both cases the notation, for $A \in \mathscr{F}^q$,

$$A = x^{-(q+1)} A_{-(q+1)} + x^{-q} A_{-q} + \cdots, \; A_j = \begin{pmatrix} a_j & b_j \\ c_j & d_j \end{pmatrix}.$$

Denote also by $\Delta(L)$ the discriminant of a (square, two-dimensional) matrix L.

(i) For $q = 0$ we have

$$A \text{ separated } \Leftrightarrow \Delta(A_{-1}) = (a_{-1} - d_{-1})^2 + 4b_{-1}c_{-1} \geq 0,$$

which gives a complete description of $\Sigma_0 \subset \mathbb{R}^4$ (depending only on $A_{-1} \in \mathbb{R}^4$).

(ii) For $q = 1$, the complete description of $\Sigma_1 \subset \mathbb{R}^{12}$ is longer and requires several steps. We have that Σ_1 is contained in the set $\{\Delta(A_{-2}) \geq 0\} \times \mathbb{R}^8$ and contains its interior $\{\Delta(A_{-2}) > 0\} \times \mathbb{R}^8$, but not the whole frontier $\{\Delta(A_{-2}) = 0\} \times \mathbb{R}^8$. One explicit semialgebraic subset of Σ_1 in which we are interested is the following. Given a matrix A_{-2} with $c_{-2} \neq 0$, we consider the linear real polynomial in four variables

$$H_{A_{-2}}(Z) = -\frac{(d_{-2} - a_{-2})}{2} Z_1 + c_{-2} Z_2 - \frac{(d_{-2} - a_{-2})^2}{4c_{-2}} Z_3 + \frac{(d_{-2} - a_{-2})}{2} Z_4. \quad (10)$$

Then we have

$$\begin{aligned} &\{(A_{-2}, A_{-1}) \in \mathbb{R}^8 : \Delta(A_{-2}) = 0, c_{-2} \neq 0, H_{A_{-2}}(A_{-1}) > 0\} \times \mathbb{R}^4 \subset \Sigma_1 \\ &\{(A_{-2}, A_{-1}) \in \mathbb{R}^8 : \Delta(A_{-2}) = 0, c_{-2} \neq 0, H_{A_{-2}}(A_{-1}) < 0\} \times \mathbb{R}^4 \subset \mathbb{R}^8 \setminus \Sigma_1 \end{aligned} \quad (11)$$

(Where we use the obvious notation $H_{A_{-2}}(A_{-1}) = H_{A_{-2}}(a_{-1}, b_{-1}, c_{-1}, d_{-1})$). The proof of (11) follows from the proof of Proposition 2: if $\Delta(A_{-2}) = 0$ and $c_{-2} \neq 0$, the matrix $Q = \begin{pmatrix} 0 & 2 \\ 2c_{-2} & d_{-2} - a_{-2} \end{pmatrix}$ is inversible and $QA_{-2}Q^{-1}$ is upper triangular with equal elements in the diagonal and entry equal to 1 above the diagonal. The linear transformation $T_{Q^{-1}}$ gives rise to a new system where the new coefficient, $QA_{-1}Q^{-1}$, of degree -1 has an entry precisely equal to $H_{A_{-2}}(A_{-1})$ below the diagonal. After a ramification followed by a blowing-up

transformation, we will have a new system in $\mathscr{F}^2$ with first term a multiple of the identity matrix and a second term equal to $\begin{pmatrix} 0 & 1 \\ H_{A_{-2}}(A_{-1}) & 0 \end{pmatrix}$. The sign of $H_{A_{-2}}(A_{-1})$ then gives the sign of the discriminant of this second term and then we have (11), using Proposition 1.

4 Proof of Theorem 2

In this paragraph we prove Theorem 2. Recall the standard (total) order in the field $K = \mathbb{R}(\{x\})$ of real meromorphic functions (germs at $x = 0$):

$$a \in K,\, a > 0 \Leftrightarrow \exists \varepsilon > 0, a(x) > 0 \forall x \in (0, \varepsilon).$$

We recall also the standard terminology: a subset Ω of K^n is called a *basic K-semialgebraic set* if it is of the form

$$\Omega = \{\mathbf{x} \in K^n : P(\mathbf{x}) = 0, Q_1(\mathbf{x}) > 0, \ldots, Q_r(\mathbf{x}) > 0\} \subset K^n \tag{12}$$

where $P, Q_j \in K[X_1, \ldots, X_n]$. Such a set Ω will be said to be an *open (basic K-semialgebraic set)* if there is no equation $P(\mathbf{x}) = 0$ in its description (or that P is the zero polynomial). A subset of K^n will be called *K-semialgebraic* if it is a union of finitely many basic K-semialgebraic sets of K^n. The finite unions and intersections of K-semialgebraic sets of K^n are again K-semialgebraic, as well as their complements in K^n. Notice that the intersection of two basic K-semialgebraic sets (resp. open basic K-semialgebraic sets) is again a basic K-semialgebraic set (resp. open basic K-semialgebraic set), but not necessarily its union.

Examples 2. The following examples of K-semialgebraic sets will be useful in what follows.

(i) For any $r \in \mathbb{Z}$, the set $\mathscr{L}^r = \{a \in K : -a^2 + x^{2r-1} > 0\}$ is K-semialgebraic in K and consists exactly on the set of meromorphic series with order greater or equal to r. Also, the set of series with order exactly r, which equals $\mathscr{L}^r \setminus \mathscr{L}^{r+1}$, is K-semialgebraic in K.

(ii) As a consequence of the precedent example, for any $q \geq 0$, the subset $\mathscr{F}^q = (\mathscr{L}^{-(q+1)})^4$ of systems with Poincaré rank not greater than q is K-semialgebraic in K^4.

(iii) The subset $\mathscr{S}^0 \subset K^4$ of separated systems with Poincaré rank not greater than 0 is K-semialgebric: using the notations of Example 1 (i), a system $A \in \mathscr{F}^0$ is separated if and only $(a_{-1} - d_{-1})^2 + 4b_{-1}c_{-1} \geq 0$ which is equivalent to say that $A = \begin{pmatrix} a & b \\ c & d \end{pmatrix}$ is in $\mathscr{F}^0$ and, either $(a-d)^2 + 4bc$ has order greater or equal to -1 or $(a-d)^2 + 4bc$ has order exactly -2 and $(a-d)^2 + 4bc > 0$.

Recall the notation $\mathscr{S}$ (resp. $\mathscr{S}^q$) for the subset of separated systems (resp. separated systems in $\mathscr{F}^q$). Example 2 (iii) shows that Theorem 2 can not be extended to the case $q = 0$. On the other hand, using Example 2 (ii) and taking into account that $\mathscr{S}^1 = \mathscr{F}^1 \cap \mathscr{S}^q$, for any $q \geq 1$, and also that $\mathscr{S}^1 = \mathscr{F}^1 \cap \mathscr{S}$ and that $\mathscr{I} = K^4 \setminus \mathscr{S}$, in order to prove Theorem 2 and Corollary 1, it suffices to prove the particular case $q = 1$:

Theorem 5. *The set $\mathscr{S}^1$ is not K-semialgebraic in K^4.*

The rest of this paragraph is devoted to the proof of Theorem 5.

We start by introducing some notations. If $A = x^{-2}A_{-2} + x^{-1}A_1 + \cdots \in \mathscr{F}^1$, we will put for $j \geq -2$

$$\Pi_j : \mathscr{F}^1 \to \mathbb{R}^4,\ \Pi_j(A) := \Pi_{[j,j]}(A) = A_j \equiv (a_j, b_j, c_j, d_j).$$

On the other hand, given $P \in K[\underline{X}]$ with $\underline{X} = (X_1, X_2, X_3, X_4)$, we write

$$P = \sum_{I \in \mathbb{N}^4} P_I \underline{X}^I \text{ with } P_I(x) = \sum_{k=\nu_I}^{\infty} P_{I,k} x^k \in K\ ,\ P_{I,k} \in \mathbb{R} \text{ and } \nu_I \in \mathbb{Z}.$$

We use the usual notation $\underline{X}^I = X_1^{i_1} X_2^{i_2} X_3^{i_3} X_4^{i_4}$ and $|I| = i_1 + i_2 + i_3 + i_4$ if $I = (i_1, i_2, i_3, i_4)$. We consider the *weight map*

$$\rho : \mathbb{N}^4 \times \mathbb{Z},\ \rho(I, k) = k - 2|I|$$

and define

$$\beta = \beta(P) = \min\{\rho(I, k) / P_{I,k} \neq 0\}$$

which is a well defined integer number associated to the polynomial P if $P \not\equiv 0$, called the *ρ-order* of P. Then we write the polynomial as a series

$$P(\underline{X}) = P^{(\beta)}(\underline{X}) + P^{(\beta+1)}(\underline{X}) + \cdots \tag{13}$$

where

$$P^{(j)}(\underline{X}) = \sum_{(I,k) \in \mathbb{N}^4 \times \mathbb{Z} : \rho(I,k) = j} P_{I,k} x^k \underline{X}^I \in K[\underline{X}] \text{ for } j \geq \beta$$

is called the *homogeneous ρ-component* of P of degree j. On the other hand, for any system $A \in \mathscr{F}^1$, we will use the following notation for the Laurent expansion of the series $P(A) \in \mathbb{R}(\{x\})$:

$$P(A) = C_\beta(P, A)x^\beta + C_{\beta+1}(P, A)x^{\beta+1} + \cdots\ ,\ C_j(P, A) \in \mathbb{R}.$$

Despite of the notation, each coefficient $C_j(P, A)$ depends only on a finite truncation of the system A. It is possible to give explicit formulas for the value of $C_j(P, A)$ in terms of the homogeneous ρ-components of P. However, we will only describe those formulas for the family of systems that we are going to use in what follows.

Consider the subset T of systems in $\mathscr{F}^1$ given by

$$T = \{A = x^{-2}A_{-2} + x^{-1}A_{-1} : \Delta(A_{-2}) = 0\}. \tag{14}$$

Recall that Δ denotes the discriminant. Denote by $\Sigma_\Delta = (\Delta = 0)$ the semialgebraic subset of $\mathbb{R}^4$ of those matrices with zero discriminant and, for any $L \in \mathbb{R}^4$, denote by $D_L\Delta$ the differential of the discriminant at L (considered as a differentiable function $\Delta : \mathbb{R}^4 \to \mathbb{R}$).

Lemma 2. *Let $P \in K[\underline{X}]$ be a non-zero polynomial and denote by $\beta \in \mathbb{Z}$ its ρ-order. Then there exists a natural number $t = t(P) \geq 0$ and finitely many real polynomials*

$$R_1, R_2, \ldots, R_n \in \mathbb{R}[\underline{X}],$$

none of which is divisible by Δ, such that, we have for any $A \in T$

$$\begin{array}{l} C_\beta(P, A) = 0,\ C_{\beta+1}(P, A) = 0,\ \ldots,\ C_{\beta+t-1}(P, A) = 0, \\ C_{\beta+t}(P, A) = \sum_{i=0}^{n} R_i(A_{-2})(D_{A_{-2}}\Delta(A_{-1}))^i \end{array} \tag{15}$$

where $A_j = \Pi_j(A)$, $j = -2, -1$.

Proof. Consider the decomposition (13) of P in homogeneous ρ-components and put for any $j \geq \beta$,

$$\overline{P}^{(j)} = \sum_{(I,k)\in\mathbb{N}^4\times\mathbb{Z}:\rho(I,k)=j} P_{I,k}\underline{X}^I \in \mathbb{R}[\underline{X}].$$

Then we have, for any natural number $s \geq 0$ and $A \in T$,

$$P^{(\beta+s)}(A) = x^{\beta+s}\overline{P}^{(\beta+s)}(A_{-2} + xA_{-1}).$$

Using the Taylor formula for functions in several variables, we obtain, for $s \geq 0$,

$$C_{\beta+s}(P, A) = \sum_{i=0}^{s} \frac{1}{i!} D^i_{A_{-2}}\overline{P}^{(\beta+s-i)}(A_{-1}, \overset{(i)}{\ldots}, A_{-1}), \tag{16}$$

where, if f is a function of class C^∞ in a domain $U \subset \mathbb{R}^n$ and $a \in \mathbb{R}^n$ then $D^i_a f$ denotes the i-th iterated differential of f at a, a multilinear form on $\mathbb{R}^n$ of degree i (see [4]).

Now, for $s \geq 0$, let k_s be equal to ∞ if $\overline{P}^{(\beta+s)} = 0$ or the maximum non-negative integer k such that Δ^k divides the polynomial $\overline{P}^{(\beta+s)}$, otherwise. If $k_s \neq \infty$ we write

$$\overline{P}^{(\beta+s)} = \Delta^{k_s} R^{(s)},$$

where $R^{(s)} \in \mathbb{R}[\underline{X}]$ is not divisible by Δ. In this case, an iteration of Leibnitz's formula for the derivative of a product gives, for any $A = x^{-2}A_{-2} + x^{-1}A_{-1} \in T$,

$$\begin{array}{l} D^i_{A_{-2}} \overline{P}^{(\beta+s)}(A_{-1}, \overset{(i)}{\ldots}, A_{-1}) = 0 \text{ if } i < k_s \text{ and} \\ D^{k_s}_{A_{-2}} \overline{P}^{(\beta+s)}(A_{-1}, \overset{(k_s)}{\ldots}, A_{-1}) = k_s!(D_{A_{-2}}\Delta(A_{-1}))^{k_s} R^{(s)}(A_{-2}) \end{array} \tag{17}$$

Let us see that the natural number

$$t = t(P) = \min\{k_i + i \ : \ i \geq 0\}$$

has the required properties. In one hand, if $0 \leq s < t$ then $k_{s-i} > i$ for $i = 0, 1, \ldots, s$. We will have in this case, from (16) and (17), that $C_{\beta+s}(P, A) = 0$ for any $A \in T$. On the other hand, notice $k_{t-i} \geq i$ for $i = 0, 1, \ldots, t$ and then, for any such i, again using (16) and (17), we have

$$D^i_{A_{-2}} \overline{P}^{(\beta+t-i)}(A_{-1}, \overset{(i)}{\ldots}, A_{-1}) = \begin{cases} 0, & \text{if } k_{t-i} > i; \\ i!(D_{A_{-2}}\Delta(A_{-1}))^i R^{(\beta+t-i)}(A_{-2}), & \text{if } k_{t-i} = i. \end{cases}$$

Take finally $n = \#\{i \in \{0, \ldots, t\} \ : \ k_{t-i} = i\}$ and rename the polynomials $R^{(\beta+t-i)}$ in the above equation for which $k_{t-i} = i$ in order to have (15). □

The next lemma establishes that a non-zero polynomial can only vanish inside T in a "small" subset (where T is given in (14)). For a topological space X and a subset $Y \subset X$ we use the notation $Int^X(Y)$ for the interior of Y in X.

Lemma 3. *Let $P \in K[\underline{X}]$ with $P \neq 0$ and let $E = T \cap \{P = 0\}$ be the subset of systems A in T for which $P(A) = 0$. Then the set*

$$\mathscr{D}_P = \{A_{-2} \in \Sigma_\Delta \ : \ Int^{\mathbb{R}^4}\left(\Pi_{-1}((\Pi_{-2})^{-1}(A_{-2}) \cap E)\right) \neq \emptyset\} \tag{18}$$

has empty interior inside Σ_Δ.

Proof. Let t, n and $R_1, \ldots, R_n$ be as in Lemma 2 satisfying (15) and let

$$\Gamma = \Sigma_\Delta \cap \{L \in \mathbb{R}^4 \ : \ R_0(L) = 0\}.$$

It is a semialgebraic subset having empty interior inside Σ_Δ (since Δ does not divide R_0). Consider for any $A_{-2} \in \Sigma_\Delta$ the polynomial

$$F_{A_{-2}}(\underline{Z}) = \sum_{l=0}^{n} (D_{A_{-2}}\Delta(\underline{Z}))^l R_l(A_{-2}) \in \mathbb{R}[\underline{Z}].$$

By construction, $F_{A_{-2}}$ is a polynomial with non-zero constant term if $A_{-2} \notin \Gamma$ (notice that $D_L\Delta(\underline{Z})$ is a homogeneous polynomial of degree 1 for any L). In particular, for $A_{-2} \notin \Gamma$, $F_{A_{-2}}$ is not divisible by Δ and $\{F_{A_{-2}} = 0\} \cap \Sigma_\Delta$ has empty interior inside Σ_Δ.

On the other hand, if $A \in E$ then $C_j(P, A) = 0$ for any $j \geq \beta = \beta(P)$ with the notations introduced before Lemma 2. In particular, and using (15), $C_{\beta+t}(P, A) = F_{A_{-2}}(A_{-1}) = 0$ for any $A \in E$. That is,

$$\Pi_{-1}((\Pi_{-2})^{-1}(A_{-2}) \cap E) \subset \{F_{A_{-2}} = 0\}.$$

We conclude that if $A_{-2} \notin \Gamma$ then $A_{-2} \notin \mathscr{D}_P$ and we are done. □

We need a third lemma before the proof of Theorem 5. For that, we will use the notations of Example 1 (ii). In particular, we make use of the homogeneous polynomial $H_{A_{-2}} \in \mathbb{R}[\underline{Z}]$ of degree 1 defined in (10). Recall that $H_{A_{-2}}$ is defined for every $A_{-2} \in \Sigma_\Delta$ except for a semialgebraic subset $\Gamma_1 \subset \Sigma_\Delta$ which satisfies $Int^{\Sigma_\Delta}(\Gamma_1) = \emptyset$ (Γ_1 defined by $\{c_{-2} = 0\}$ with the notations of the mentioned example). Furthermore, it is easy to see that there exists a semialgebraic set $\Gamma \subset \Sigma_\Delta$ with $\Gamma_1 \subset \Gamma$ and $Int^{\Sigma_\Delta}(\Gamma) = \emptyset$ such that $H_{A_{-2}}$ and $D_{A_{-2}}\Delta$ are linearly independent over $\mathbb{R}$ if $A_{-2} \in \Sigma_\Delta \setminus \Gamma$. For $A_{-2} \in \Sigma_\Delta \setminus \Gamma$ and $\varepsilon > 0$ we consider the *ε-positive quadrant relative to A_{-2}* as the set $\mathscr{Q}^\varepsilon_{A_{-2}}$ of systems A in T defined by the equations

$$\Pi_{-2}(A) = A_{-2},\ D_{A_{-2}}\Delta(\Pi_{-1}(A)) > \varepsilon\, ||\Pi_{-1}(A)||,\ H_{A_{-2}}(\Pi_{-1}(A)) > 0.$$

By (11), systems in the ε-positive quadrant are separated, that is:

$$A_{-2} \in \Sigma_\Delta \setminus \Gamma \Rightarrow \mathscr{Q}^\varepsilon_{A_{-2}} \subset T \cap \mathscr{S}^1 \tag{19}$$

Lemma 4. *Suppose that we can write $\mathscr{S}^1 = \Omega_1 \cup \Omega_2 \cup \cdots \Omega_r$ where each Ω_i is a basic K-semialgebraic set in K^4. Then there exists $i_0 \in \{1, 2, \ldots, r\}$ such that Ω_{i_0} satisfies:*

(i) Ω_{i_0} is an open basic K-semialgebraic set.
(ii) $Int^{\Sigma_\Delta}(\Pi_{-2}(T \cap \Omega_{i_0})) \neq \emptyset$.
(iii) For any $i = 1, \ldots, r$, consider the set $B(\Omega_i) \subset \Sigma_\Delta$ of those matrices $A_{-2} \notin \Gamma$ for which there exists some $\varepsilon > 0$ such that $\Pi_{-1}(\mathscr{Q}^\varepsilon_{A_{-2}} \cap \Omega_i)$ is non empty and unbounded. Then

$$Int^{\Sigma_\Delta}(\Pi_{-2}(T \cap \Omega_{i_0}) \cap B(\Omega_{i_0})) \neq \emptyset. \tag{20}$$

Proof. Define the partition $\{1, 2, \ldots, r\} = J_1 \cup J_2 \cup J_3$ where

$$\begin{aligned} J_1 &= \{i \ : \ \Omega_i \text{ is not open basic }\}, \\ J_2 &= \{i \ : \ \Omega_i \text{ is open basic and } Int^{\Sigma_\Delta}(\Pi_{-2}(T \cap \Omega_j)) = \emptyset\}, \\ J_3 &= \{i \ : \ \Omega_i \text{ is open basic and } Int^{\Sigma_\Delta}(\Pi_{-2}(T \cap \Omega_j)) \neq \emptyset. \end{aligned}$$

For $i \in J_1$, by definition of open basic set, there exists a polynomial equation $\{P_i = 0\}$ in the description of Ω_i, where $P_i \in K[\underline{X}]$ is non zero. Consider for such P_i the set $\mathscr{D}_{P_i}$ given in Lemma 3, a subset with empty interior in Σ_Δ. If Lemma 4 is not true then the following set has empty interior in Σ_Δ:

$$M = \bigcup_{i \in J_1} \mathscr{D}_{P_i} \cup \bigcup_{i \in J_2} \Pi_{-2}(T \cap \Omega_i) \cup \bigcup_{i \in J_3} \Pi_{-2}(T \cap \Omega_i) \cap B(\Omega_i).$$

Fix a matrix $A_{-2} \in \Sigma_\Delta \setminus \Gamma$ which is not in M. Fix $\varepsilon > 0$. By (19), we have

$$\mathscr{Q}^\varepsilon_{A_{-2}} = \mathscr{Q}^\varepsilon_{A_{-2}} \cap \mathscr{S}^1 = \mathscr{Q}^\varepsilon_{A_{-2}} \cap \bigcup_{i=1}^{r} \Omega_i$$

and hence

$$\Pi_{-1}(\mathscr{Q}^\varepsilon_{A_{-2}}) = \bigcup_{i=1}^{r} \Pi_{-1}(\mathscr{Q}^\varepsilon_{A_{-2}} \cap \Omega_i).$$

If $i \in J_2$ then $\mathscr{Q}^\varepsilon_{A_{-2}} \cap \Omega_i = \emptyset$ since $A_{-2} \notin \Pi_{-2}(T \cap \Omega_i)$; if $i \in J_1$ then $\Pi_{-1}(\mathscr{Q}^\varepsilon_{A_{-2}} \cap \Omega_i)$ has empty interior in $\mathbb{R}^4$ since $A_{-2} \notin \mathscr{D}_{P_i}$; if $i \in J_3$ then $\Pi_{-1}(\mathscr{Q}^\varepsilon_{A_{-2}} \cap \Omega_i)$ is bounded since $A_{-2} \notin B(\Omega_i)$. We find therefore the desired contradiction with the fact that $\Pi_{-1}(\mathscr{Q}^\varepsilon_{A_{-2}})$ is open and unbounded in $\mathbb{R}^4$. □

Proof of Theorem 5. Assume that $\mathscr{S}^1$ is a K-semialgebraic set and let us look for a contradiction. By definition, $\mathscr{S}^1$ is a finite union of basic K-semialgebraic sets $\mathscr{S}^1 = \Omega_1 \cup \Omega_2 \cup \cdots \Omega_r$.

By Lemma 4, one of those basic sets has the properties (i)–(iii) of that lemma, which we denote here simply by Ω. Write

$$\Omega = \{A \in K^4 \ : \ Q_1(A) > 0, \ldots, Q_l(A) > 0\}$$

where each $Q_j \in K[\underline{X}]$ is a non zero polynomial. Apply Lemma 2 to Q_j so that we have $t_j = t(Q_j) \in \mathbb{N}_{\geq 0}$ and real polynomials $R_{j,1}, \ldots, R_{j,n_j} \in \mathbb{R}[\underline{X}]$, none of them divisible by Δ, such that, for any $A \in T$,

$$C_{\beta(Q_j)+s}(Q_j, A) = \begin{cases} 0, & \text{if } 0 \leq s < t_j; \\ \sum_{i=1}^{n_j} R_{j,i}(\Pi_{-2}(A)) \left(D_{\Pi_{-2}(A)} \Delta(\Pi_{-1}(A))\right)^i, & \text{if } s = t_j. \end{cases} \tag{21}$$

Using (20) in Lemma 4 (iii), there exists a matrix $A_{-2} \in \Sigma_\Delta$ which is in $B(\Omega)$ and such that $R_{j,n_j}(A_{-2}) \neq 0$ for any $j = 1, \ldots, l$. By definition of $B(\Omega)$, this means that $\Pi_{-1}(\mathscr{Q}^\varepsilon_{A_{-2}} \cap \Omega)$ is unbounded. By definition of the ε-positive quadrant, $D_{\Pi_{-2}(A)}\Delta(\Pi_{-1}(A)) > \varepsilon \mid\mid \Pi_{-1}(A) \mid\mid$ for any $A \in \mathscr{Q}^\varepsilon_{A_{-2}}$. Therefore, taking $A \in \mathscr{Q}^\varepsilon_{A_{-2}} \cap \Omega$ with $\mid\mid \Pi_{-1}(A) \mid\mid$ sufficiently big, $C_{\beta(Q_j)+n_j}(Q_j, A)$ in (21) will be non zero and its sign will be that of $R_{j,n_j}(A_{-2})$, for any j. Since $A \in \Omega$ and $C_{\beta(Q_j)+n_j}(Q_j, A)$ is the first non zero coefficient of the series $Q_j(A)$, we must have

$$R_{j,n_j}(A_{-2}) > 0 \quad \forall j = 1, 2, \ldots, l. \tag{22}$$

Now recall that $A_{-2} \in B(\Omega)$ means in particular that $A_{-2} \notin \Gamma$ and then the two linear polynomials $D_{A_{-2}}\Delta, H_{A_{-2}} \in \mathbb{R}[\underline{Z}]$ are not proportional. Thus, the set $N = \{A_{-1} \in \mathbb{R}^4 : D_{A_{-2}}\Delta(A_{-1}) > 0, H_{A_{-2}} < 0\}$ is non empty and unbounded. If $A_{-1} \in N$ has a norm sufficiently big and $A \in T$ satisfies $\Pi_{-2}(A) = A_{-2}$ and $\Pi_{-1}(A) = A_{-1}$ then (21) and (22) imply that $Q_j(A) > 0$ for any $j = 1, 2, \ldots, l$ and thus $A \in \Omega$. But this is a contradiction with the fact that such a system A is interlaced by (11), since $H_{A_{-2}} < 0$.

This finishes the proof of Theorem 5. □

5 Proof of Theorem 3

In this paragraph we prove Theorem 3. We must show that, for any $q \geq 0$, the set $\mathscr{S}^q \subset K^4$ of separated systems in $\mathscr{F}^q$ is a finite union of sets of the form

$$\{A \in K^4 : P(A) = 0, Q_1(A) > 0, \ldots, Q_r(A) > 0\}$$

where P and the Q_j are K-differential polynomials in four variables.

Recall that a K-differential polynomial in n variables is an element

$$P(\underline{Z}, \underline{Z}^{(1)}, \ldots, \underline{Z}^{(m)}) \in K<\underline{Z}>= K[\underline{Z}, \underline{Z}^{(1)}, \ldots, \underline{Z}^{(m)}, \ldots]$$

where $\underline{Z}^{(j)} = (Z_1^{(j)}, Z_2^{(j)}, \ldots, Z_n^{(j)})$ (with $\underline{Z}^{(0)} = \underline{Z}$) and all involved $Z_i^{(j)}$ are independent variables. Also, for $n = 4$, if $A \in K^4$ is written as a matrix $A = \begin{pmatrix} a & b \\ c & d \end{pmatrix}$, then by definition we put

$$P(A) := P((a, b, c, d), (a', b', c', d'), (a'', b'', c'', d''), \ldots, (a^{(m)}, b^{(m)}, c^{(m)}, d^{(m)})),$$

where $a', a'', .., a^{(m)}$, etc. denote the successive derivates of the series $a \in \mathbb{R}(\{x\})$ with respect to x.

Theorem 3 will be easily obtained from Theorem 1 once we notice several facts concerning K-differential polynomials in one variable ($n = 1$), collected in the following lemma.

Lemma 5. *Let $Z = Z_1$ be a single variable. Fix $r \in \mathbb{Z}$. Define recursively for any natural number $s \geq 0$ the K-differential polynomials*

$$\begin{aligned} R_{r,0} &= xZ^{(1)} - rZ \in K[Z, Z^{(1)}] \subset K<Z> \\ R_{r,s} &= R_{r+s,0}(R_{r+s-1,s-1}) \in K[Z, Z^{(1)}, \dots Z^{(s)}] \subset K<Z> \text{ if } s \geq 1, \\ \tilde{R}_{r,s} &= \frac{R_{r,s}}{s! x^{r+s}} \in K<Z> . \end{aligned}$$

Then, if $a = \sum_{i \geq r} a_i x^i$ is a series with order not smaller than r ($a \in \mathscr{L}^r$ in the notation of Example 2 (i)), then we have for any $s \geq 0$ that $\tilde{R}_{r,s}(a)$ is a series of order at least 0 and $\tilde{R}_{r,s}(a)(0) = a_{r+s}$.

The proof is a simple computation in differential algebra. Perhaps we must recall that composition of two differential polynomials in one variable is defined in the standard way by extending by linearity the composition rule on monomials

$$\begin{aligned} &Z^{(1)}(bZ^{l_0}(Z^{(1)})^{l_1} \cdots (Z^{(m)})^{l_m}) = b' Z^{l_0}(Z^{(1)})^{l_1} \cdots (Z^{(m)})^{l_m} \\ &+ \textstyle\sum_{i=0}^{m} l_i Z^{l_0}(Z^{(1)})^{l_1} \cdots (Z^{(l_i+1)})^{l_i - 1} \cdots (Z^{(l_m)})^{l_m}, \quad b \in K. \end{aligned}$$

This lemma permits to prove Theorem 3 from Theorem 1 in the following way. Let $Q_1, Q_2, \dots, Q_l \in \mathbb{R}[\underline{X}]$ be all the real polynomials (in $4(2q+2)$ variables) that appears in a description of the semialgebraic set $\Sigma_q \subset \mathbb{R}^{4(2q+2)}$ given by Theorem 1. Using the notation

$$A = \begin{pmatrix} a & b \\ c & d \end{pmatrix}, \; a = a_{-(q+1)} x^{-(q+1)} + a_{-q} x^{-q} + \cdots, etc.,$$

Lemma 5 permits to show, for any $j = 1, \dots, l$,

(i) $Q_j(a_{-(q+1)}, \dots, d_{-(q+1)}, \dots, a_q, \dots, d_q) > 0$ if and only if the series

$$Q_j(\tilde{R}_{-(q+1),0}(a), \dots, \tilde{R}_{-(q+1),0}(d), \dots, \tilde{R}_{-(q+1),2q+1}(a), \dots, \tilde{R}_{-(q+1),2q+1}(d))$$

is positive and has order 0.

(ii) $Q_j(a_{-(q+1)}, \dots, d_{-(q+1)}, \dots, a_q, \dots, d_q) = 0$ if and only if the series

$$Q_j(\tilde{R}_{-(q+1),0}(a), \dots, \tilde{R}_{-(q+1),0}(d), \dots, \tilde{R}_{-(q+1),2q+1}(a), \dots, \tilde{R}_{-(q+1),2q+1}(d))$$

belongs to $\mathscr{L}^1$.

We substitute any of the inequalities $Q_j > 0$ or equations $Q_j = 0$ in the description of Σ_q by its corresponding condition on K-differential polynomials according to (i) and (ii) above. We conclude from Theorem 1 that $\mathscr{S}^q$ is (K, d)-semialgebraic (taking into account Example 2 (i)), thus proving Theorem 3.

References

1. Balser, W.: Formal Power Series and Linear Systems of Meromorphic Ordinary Differential Equations. Universitext. Springer, New York (2000)
2. Cano, F., Moussu, R., Sanz, F.: Oscillation, spiralement, tourbillonnement. Comment. Math. Helv. **75**, 284–318 (2000)
3. Cano, F., Moussu, R., Sanz, F.: Pinceaux de courbes intégrales d'un champ de vecteurs analytique. Astérisque **297**, 1–34 (2004)
4. Dieudonné, J.: Éléments d'analyse. Tome I: Fondements de l'analyse moderne. Gauthier-Villars, Éditeur, Paris (1968)
5. LeGal, O., Sanz, F., Speissegger, P.: Non-interlaced solutions of 2-dimensional systems of linear ordinary differential equations. Proc. Am. Math. Soc. **141**, 2429–2438 (2013)
6. Miller, C.: Basics of O-minimality and Hardy Fields. In: Lecture Notes on O-minimal Structures and Real Analytic Geometry. Fields Institute Communications, vol. 62. Springer, New York (2012)
7. Wasow, W.: Asymptotic Expansions for Ordinary Differential Equations. Intersciencie, New York (1965) (Re-edited Dover, 1987)

A Walk Through the New Methods of Celestial Mechanics

Alain Chenciner

Abstract

En ce qui concerne le problème des trois corps, je ne suis pas sorti du cas suivant : Je considère trois masses, la première très grande, la seconde petite mais finie, la troisième infiniment petite ; je suppose que les deux premières décrivent un cercle autour de leur centre de gravité commun et que la troisième se meut dans le plan de ces cercles. Tel serait le cas d'une petite planète troublée par Jupiter, si l'on négligeait l'excentricité de Jupiter et l'inclinaison des orbites. (Concerning the Three-Body Problem, I did not venture away from the following case: I consider three masses, the first one very big, the second one small but finite, the third one infinitesimal; I suppose that the first two describe a circle around their common center of mass and that the third moves in the plane of these circles. Such would be the case of a small planet perturbed (*maybe "troubled" better conveys the charm of the eighteen century flavoured "troublé"*) by Jupiter if one was neglecting Jupiter's eccentricity and the inclination of the orbits.)

This is how, at the beginning of his memoir *On the three-body problem and the equations of dynamics* which, in 1889, wins the prize given by the king Oscar of Sweden, Poincaré describes the setting which will be developped in *The New Methods of Celestial Mechanics*. This work was indeed built in order to correct the sentence which, in the first version of the memoir, followed the one above:

Dans ce cas particulier, j'ai démontré rigoureusement la stabilité. (In this particular case, I have rigorously proved stability.)

Originally published as "Une promenade dans les Méthodes Nouvelles de la Mécanique Céleste" in "SMF, Gazette des mathématiciens" 134, octobre 2012, p. 37–47 (French).
English translation by the author
DOI 10.1007/978-3-642-38830-9

A. Chenciner (✉)
Observatoire de Paris, IMCCE (UMR 8028), ASD, 77, avenue Denfert-Rochereau,
75014 Paris, France

Département de mathématique, Université Paris VII, Paris, France
e-mail: chenciner@imcce.fr

S. Ibáñez et al. (eds.), *Progress and Challenges in Dynamical Systems*,
Springer Proceedings in Mathematics & Statistics 54,
DOI 10.1007/978-3-642-38830-9_11,

Respectively published by Gauthier-Villars in 1892, 1893 et 1899 these three volumes (1,268 pages + 10 pages for the tables of contents) will cause Paul Appell to say in 1925: *"It is likely that, during the next half-century, this book will be the mine from which more modest researchers will extract their material"*. The prediction came true: more than a century later, we contemplate some of these nuggets, whose brightness has not weakened. (This text is essentially a translation by the author of A. Chenciner [7] (*Une promenade dans les Méthodes nouvelles de la mécanique céleste*, Gazette des Mathématiciens, $n^0$134, October 2012, 37–47, and Quadrature, special issue dedicated to Henri Poincaré, November 2012). A much more technical text on the same subject is A. Chenciner (*Poincaré and the Three-Body Problem*, "Poincaré seminar" (also called "Bourbaphy"), XVI, November 2012, 45–133, www.bourbaphy.fr/novembre2012.html). As in this last text, I have chosen to leave in French Poincaré's quotations, the translation being given in footnotes. The hope is that some readers be given the chance to appreciate Poincaré's superb style.)

1 The General Problem of Dynamics

In Chap. I, Sect. 13, titled *"The general problem of dynamics"*, Poincaré gives the scope of his work:

> Nous sommes donc conduit à nous proposer le problème suivant:
> Etudier les équations canoniques
>
> $$\frac{dx_i}{dt} = \frac{dF}{dy_i}, \quad \frac{dy_i}{dt} = -\frac{dF}{dx_i}, \tag{1}$$
>
> en supposant que la fonction $F(x, y, \mu)$ peut se développer suivant les puissances d'un paramètre très petit μ de la manière suivante ;
>
> $$F = F_0 + \mu F_1 + \mu^2 F_2 + \cdots,$$
>
> en supposant de plus que F_0 ne dépend que des x et est indépendant des y et que $F_1, F_2, \cdots$ sont des fonctions périodiques de période 2π par rapport aux y.[1]

In other words, the system is a small perturbation of the "completely integrable" system associated to $F_0(x)$, for which (x, y) are "action-angle" coordinates and whose solutions are:

---

[1] Hence we are led to propose the following problem: study the canonical equations

$$\frac{dx_i}{dt} = \frac{dF}{dy_i}, \quad \frac{dy_i}{dt} = -\frac{dF}{dx_i},$$

while supposing that the function $F(x, y, \mu)$ may be expanded in powers of a very small parameter μ in the following way;

$$F = F_0 + \mu F_1 + \mu^2 F_2 + \cdots,$$

where moreover we suppose that F_0 depends only on the x variables and is independant of the y's and that $F_1, F_2, \cdots$ are 2π-periodic functions of the y's.

$$x_i = x_i^0, \quad y_i = n_i t + y_i^0, \text{ where } n_i = -\frac{dF_0}{dx_i}(x^0). \tag{2}$$

The phase space, which is the product by a torus $\mathbb{T}^N$ (coordinates y) of a bounded domain in $\mathbb{R}^N$ (coordinates x), is then foliated by N-dimensional "invariant tori" $x = x^0 = (x_1^0, \cdots, x_N^0)$ which bear quasi-periodic solutions whose frequencies n_i depend only on x^0. In particular, if this dependance is effective, there is a dense family of these tori filled with periodic solutions. For a small planet whose Keplerian motion around the Sun is "troubled" by Jupiter, the small parameter is the ratio of the mass of Jupiter to the one of the Sun, that is approximately $1/1{,}000$. But similar equations rule the motions of the Earth-Moon couple troubled by the Sun, the small parameter taking also into account the ratio of the distances Earth-Moon and Earth-Sun, that is about $1/400$. The works of G.W. Hill on this last problem had a great influence on Poincaré's study of what we call to-day the "Circular planar three-body problem" (or circular planar RTBP). In a rotating frame, the equations take the same form as above, F being now the "Jacobi constant". Together with the "geodesic flow" on an almost spherical surface, which Poincaré studied at the end of his life, these are examples of generic – and in particular "non-integrable" – Hamiltonian systems with $N = 2$ degrees of freedom. More generally, this form of the equations holds for the $(1+n)$-body problem in the planetary case with a Sun of mass 1 and n planets whose masses are $O(\mu)$ and whose motions around the center of mass of the system are almost circular and coplanar. But a new difficulty appears: as for a given negative energy, all solutions of the Kepler problem are periodic with the same period, the function F_0, which describes n uncoupled Kepler problems, depends only on some of the action variables x.

2 Periodic Solutions

The periodic solutions appear in Sect. 36 of Chap. III.

> Le problème que nous allons traiter ici est le suivant : Supposons que, dans les équations (1),[2] les fonctions X_i dépendent d'un certain paramètre μ ; supposons que dans le cas de $\mu = 0$ on ait pu intégrer les équations, et qu'on ait reconnu ainsi l'existence d'un certain nombre de solutions périodiques. Dans quelles conditions aura-t-on le droit d'en conclure que les équations comportent encore des solutions périodiques pour les petites valeurs de μ ?"[3]

These solutions are found throughout the three volumes, and their study by perturbation methods anticipates some aspects of the theory of singularities; "characteristic exponents" are introduced in Chap. IV, "asymptotic solutions" (to-day the stable

[2] that is in equations $dx_i/dt = X_i(x_1, \cdots, x_n),\ i = 1, \cdots, n$.

[3] The problem we are going to address is the following: suppose that, in Eq. (1), the functions X_i depend on some parameter μ; suppose that, when $\mu = 0$ one has integrated the equations and recognized the existence of some periodic solutions. Under what conditions shall we be able to conclude that for small values of μ the equations still possess periodic solutions?

and unstable manifolds) in Chap. VII, finally, periodic solutions are the main responsible for the non-integrability. Announcing the existence of an infinity of periodic solutions of the planetary three-body problem when the planetary masses are sufficiently small, Poincaré justifies his efforts in the following way:

> Il semble d'abord que ce fait ne puisse être d'aucun intérêt pour la pratique. En effet, il y a une probabilité nulle pour que les conditions initiales du mouvement soient précisément celles qui correspondent à une solution périodique. Mais il peut arriver qu'elles en diffèrent très peu, et cela a lieu justement dans les cas où les méthodes anciennes ne sont plus applicables. On peut alors avec avantage prendre la solution périodique comme première approximation, comme *orbite intermédiaire*, pour employer le langage de M. Gylden.
>
> Il y a même plus : voici un fait que je n'ai pu démontrer rigoureusement, mais qui me paraît pourtant très vraisemblable.
>
> Étant données des équations de la forme définie dans le numéro 13 et une solution particulière quelconque de ces équations, on peut toujours trouver une solution périodique (dont la période peut, il est vrai, être très longue), telle que la différence entre les deux solutions soit aussi petite qu'on le veut, pendant un temps aussi long qu'on le veut. D'ailleurs, ce qui nous rend ces solutions périodiques si précieuses, c'est qu'elles sont, pour ainsi dire, la seule brèche par où nous puissions essayer de pénétrer dans une place jusqu'ici réputée inabordable.[4]

A little further, in Sect. 39, Poincaré recalls his classification of periodic solutions in three sorts:

> ... j'ai été conduit à distinguer trois sortes de solutions périodiques: pour celles de la première sorte, les inclinaisons sont nulles et les excentricités très petites ; pour celles de la deuxième sorte, les inclinaisons sont nulles et les excentricités finies ; enfin, pour celles de la troisème sorte, les inclinaisons ne sont plus nulles.[5]

Then, describing Hill's research on the Moon, he further explains the importance of the construction of approximate periodic solutions:

> Supposons que, dans le mouvement d'un astre quelconque, il se présente une inégalité[6] très considérable. Il pourra se faire que le mouvement véritable de cet astre diffère fort peu de celui d'un astre idéal dont l'orbite correspondrait à une solution périodique.

---

[4]It seems at first that this fact cannot be of any interest in practice. Indeed, there is zero probability that the initial conditions of motion be precisely those which correspond to a periodic solution. But it may happen that they differ very little, and this occurs precisely where the old methods no longer apply. We can then use the periodic solution as a first approximation, as an *intermediate orbit*, to use the language of Mr. Gyldén. There is even more: here is a fact that I could not prove rigorously, but which nevertheless seems very likely to me. Given equations of the form defined in n^o 13 and an arbitrary solution of these equations, one can always find a periodic solution (with a period which, admitedly, may be very long), such that the difference between the two solutions be arbitrarily small. In fact, what makes these solutions so precious to us, is that they are, so to say, the only opening through which we can try to enter a place which, up to now, was deemed inaccessible.

[5]I was led to distinguish three kinds of periodic solutions: for those of the first sort, the inclinations are equal to zero and the eccentricities are very small, for those of the second sort, the inclinations are equal to zero and the eccentricities are finite; finally for those of the third sort, the inclinations are no more equal to zero.

[6]C'est-à-dire une déviation du mouvement elliptique due à l'action du Soleil.

> Il arrivera alors assez souvent que l'inégalité considérable dont nous venons de parler aura sensiblement le même coefficient pour l'astre réel et pour cet astre idéal ; mais ce coefficient pourra se calculer beaucoup plus facilement pour l'astre idéal dont le mouvement est plus simple et l'orbite périodique.
>
> C'est à M. Hill que nous devons la première application de ce principe. Dans sa théorie de la Lune, il remplace ce satellite dans une première approximation par une Lune idéale, dont l'orbite est périodique. Le mouvement de cette Lune idéale est alors celui qui a été décrit au $n^o 41$, où nous avons parlé de ce cas particulier des solutions périodiques de la première sorte, dont nous devons la connaissance à M. Hill.
>
> Il arrive alors que le mouvement de cette Lune idéale, comme celui de la Lune réelle, est affecté d'une inégalité considérable bien connue sous le nom de *variation* ; le coefficient est à peu près le même pour les deux Lunes. M. Hill calcule sa valeur pour sa Lune idéale avec un grand nombre de décimales. Il faudrait, pour passer au cas de la nature, corriger le coefficient ainsi obtenu en tenant compte des excentricités, de l'inclinaison et de la parallaxe. C'est ce que M. Hill eût sans doute fait s'il avait achevé la publication de son admirable Mémoire.[7]

3 Non-existence of Uniform First Integrals

Bruns had shown that the only first integrals of the Newtonian n-body problem which are algebraic in the velocities, are the ones which come from the symmetries of the problem, namely the energy and the angular momentum. Using a completely different method, intimately related to the behavior of periodic solutions, Poincaré shows in Chaps. V and VI the non-existence of new first integrals which are analytic in x, y and μ, that is which depend analytically of the (small enough) masses of the planets:

> Le théorème qui précède est plus général en un sens que celui de M. Bruns, ... Mais, en un autre sens, le théorème de M. Bruns est plus général que le mien ; j'établis seulement, en effet, qu'il ne peut pas exister d'intégrale algébrique pour toutes les valeurs suffisamment

[7] Suppose that, in the motion of some star, there is a very strong inequality. It may happen that the true motion of this star will differ very little from the motion of an ideal star whose orbit would correspond to a periodic solution. It will often happen that the large inequality which we just mentioned will have approximately the same coefficient for the real star and for this ideal star; but this coefficient will be much more easily computed for the ideal star whose motio, is simpler and the orbit is periodic. It is to Mr Hill that we owe the first application of this principle. In his Lunar theory, he replaces this satellite in first approximation by an ideal Moon, whose orbit is periodic. The motion of this ideal Moon is then the one describe in section $n^0 41$, where we discussed of this special case of periodic solutions of the first sort, which we know thanks to Mr Hill. It then arrives that the motion of this ideal Moon is affected of a very large inequality, well known under the name of variation; the coefficient is approximately the dame for the two Moons. Then Mr Hill computes its value for his ideal Moon with a large number of decimals? In order to treat the case of nature, one would need correct the coefficient obtaient in this way by taking into account the eccentricities, the inclination and the parallax. This is most probably what Mr Hill would have done if he had completed the publication of his admirable Memoir.

> petites des masses ; et M. Bruns démontre qu'il n'en existe pour aucun système de valeurs des masses.[8]

The proof consists in a difficult reasoning on the presence of sufficiently many non-zero coefficients in the Fourier expansion in the angle y of the "perturbing function", which amounts to the "genericity" of the periodic solutions and in particular to the fact that they do not constitute continua which fill invariant tori as it is the case when $\mu = 0$: an invariant torus which contains dense orbits is the closure of any one of them and thus has dynamical significance; on the contrary, an invariant torus which is the mere union of periodic solutions has no dynamical reason to exist and hence is very likely to be destroyed under the effect of a small perturbation by giving birth to a finite number of "generic" periodic solutions. These reasonings constitute the very technical Chap. VI in which Poincaré generalises to functions of two complex variables a method used by Darboux relating the behaviour of their Fourier coefficients of high orders to their analytical properties, more precisely to the behaviour of their singularities and to the obstructions to the deformation of integration countours caused by the pinching of these singularities:

> M. Flamme applique à chacun des facteurs la méthode de M. Darboux. Cet artifice ne saurait nous suffire pour notre objet ; il nous faut, au contraire, appliquer directement à la fonction perturbatrice la méthode de M. Darboux et pour cela étendre cette méthode au cas des fonctions de deux variables.[9]

4 Quasi-periodic Solutions

The second volume of the "New methods" is devoted to the study of the perturbation series, which are the main tool used by astronomers to "solve" the equations of motion. Poincaré starts by showing in Chap. IX that which is the essence of the "new methods": namely, the existence of formal quasi-periodic solutions of Eqs. (1), analogous to what the solutions (2) would become after a formal change of coordinates depending on μ. These are the *Lindstedt series*, a name given by Poincaré who nevertheless was the first who proved their existence:

> Mais il y a une autre difficulté plus grave ; on constate aisément que la méthode est applicable dans les premières approximations, mais on peut se demander si l'on ne sera pas arrêté dans les approximations suivantes; M. Lindstedt n'avait pu l'établir rigoureusement et conservait même à ce sujet quelques doutes. Ces doutes n'étaient pas fondés et sa belle méthode est toujours légitime; je l'ai démontré d'abord par l'emploi des invariants intégraux

[8] The theorem above is in some sense more general than the one of M. Bruns, ... But, in another sense, the theorem of M. Bruns is more general than mine; indeed I prove only that there does not exist algebraic integrals valid for all sufficiently small values of the masses; and M. Bruns proves that such integral exists for no system of values of the masses.

[9] Mr. Flamme applies M. Darboux's method to each of the factors. This is not sufficient for our purpose, and we must, on the contrary, apply directly M. Darboux's method to the perturbing function and for that extend this method to the case of functions of two variables.

dans le *Bulletin astronomique, t. III, p. 57*, puis, sans me servir de ces invariants, dans les *Comptes rendus, t. CVIII, p. 21.*[10]

These series – where the time is present only "under sines and cosines", and not in polynomial terms as in the formidable "secular terms", which then appear to be only artefacts originating from Taylor expansions of these sines and cosines[11] (the "old methods") – are of the following form (I do not follow here Poincaré's notations):

$$\begin{cases} x = x^0 + \mu\Phi_1(w) + \mu^2\Phi_2(w) + \cdots, \\ y = w + \mu\Psi_1(w) + \mu^2\Psi_2(w) + \cdots, \end{cases} \tag{3}$$

where the Φ_j and the Ψ_j are mappings from $\mathbb{T}^N$ to $\mathbb{R}^N$ and where

$$w = (w_1, w_2, \cdots, w_N), \quad w_i(t) = \overline{w}_i(\mu) + n_i(\mu)t,$$

the $\overline{w}_i(\mu)$ et $n_i(\mu)$ being formal series in μ.

It is in the famous Sect. 149 of Chap. XIII that Poincaré approaches the convergence question; he distinguishes the series with "variable frequencies", whose divergence is related to the "genericity" of the periodic solutions (in fact independantly of the non-integrability), from those with "fixed frequencies" about which he writes:

Il nous reste à traiter la deuxième question ; on peut encore, en effet, se demander si ces séries ne pourraient pas converger pour les petites valeurs de μ, quand on attribue aux x_i^0 certaines valeurs convenablement choisies. . . .

⋯ Supposons, pour simplifier, qu'il y ait deux degrés de liberté ; les séries ne pourraient-elles pas, par exemple, converger quand x_1^0 et x_2^0 ont été choisis de telle sorte que le rapport $\frac{n_1}{n_2}$ soit incommensurable, et que son carré soit au contraire commensurable (ou quand le rapport $\frac{n_1}{n_2}$ est assujetti à une autre condition analogue à celle que je viens d'énoncer un peu au hasard)?

Les raisonnements de ce Chapitre ne me permettent pas d'affirmer que ce fait ne se présentera pas. Tout ce qu'il m'est permis de dire, c'est qu'il est fort invraisemblable.[12]

---

[10] But there is another, more serious, difficulty; one checks easily that the method can be applied in the first approximations, but one can ask if one will not be stopped in the next approximations; M. Lindstedt had not been able to prove it and he was even somewhat doubting it. These doubts were not founded and his beautiful method is always legitimate; I first proved it in the *Bulletin astronomique*, t. III, p. 57, by using the integral invariants, then without using them in the *Comptes rendus*, t. CVIII, p. 21.

[11] The idea of eliminating such powers of t by making the frequencies vary is already present in d'Alembert's lunar theory of 1748.

[12] It remains to deal with the second question; we can still, in fact, ask whether the series can not converge for small values of μ, when the x_i^0 are given certain suitably chosen values . . . Suppose, for simplicity, that there are two degrees of freedom; could, for example, the series converge when x_1^0 and x_2^0 have been chosen so that the ratio $\frac{n_1}{n_2}$ is non commensurable, and its square is on the contrary commensurable (or when the ratio $\frac{n_1}{n_2}$ is subject to a condition similar to the one I have just stated somewhat at random)? The arguments of this chapter do not allow me to affirm that such a case will not arise. All I can say is that it is highly unlikely.

The existence of quasi-periodic solutions of equations (1) whose frequencies satisfy some diophantine hypotheses will be proved for the first time by A. N. Kolmogorov in 1954 [10]; the convergence of Lindstedt series with fixed frequencies satisfying such diophantine hypotheses – which follows as soon as one knows the analyticity of these solutions with respect to the parameter μ – will be proved by Moser in [11]. Second victory on the "small denominators" after the one of C. L. Siegel in 1942, it implies a very strong stability in the restricted problem. Kolmogorov's proof will be extended by V. I. Arnold [1] to the degenerate case of the three-body problem and adapted to the differentiable (i.e. non analytic) case by J. Moser [11], which explains the present acronym of "KAM theory" (see [2]).

5 Integral Invariants

> Pour bien faire comprendre l'origine et la portée de la notion des invariants intégraux, je crois utile de commencer par l'étude d'un exemple particulier emprunté à une application physique. ... Examinons en particulier le cas des liquides ; c'est celui où le fluide est incompressible, c'est-à-dire où le volume d'une masse fluide est invariable. Supposons alors que la figure F_0 soit un volume, au bout du temps t la masse fluide qui remplissait ce volume occupera un volume différent qui ne sera autre chose que la figure F. Le volume de la masse fluide n'a pas dû changer ; donc F_0 et F ont même volume : ...[13]

It is by this example of the *motion of a stationary permanent fluid* that Sect. 233 of Chap. XXII opens the third volume: having proved the non-existence of first integrals independent of the known ones, Poincaré considers the integral invariants as an ersatz consisting in the replacement of the equations of motion by the "variational equations" which indeed admit first integrals. Let us see how, in Sect. 242, he explains this relation which is somewhat forgotten in the modern presentations:

> Reprenons le système
>
> $$\frac{dx_1}{X_1} = \frac{dx_2}{X_2} = \cdots = \frac{dx_n}{X_n} = dt. \tag{1}$$
>
> Nous pouvons former les équations aux variations correspondantes telles qu'elles ont été définies au début du Chapitre IV. Pour former ces équations, on change dans les

[13] In order that the origin and the scope of the notion of integral invariant be clearly understood, I think it useful to start with the study of an example taken from a physical application. ... Let us look in particular to the case of liquids; it is the case when the fluid is incompressible, i.e. when the volume of a mass of fluid is invariable. Suppose then that the figure F_0 be a volume, after a time t the fluid filling this volume will fill a different volume which will be nothing but figure F. The volume of the fluid massha to remain constant; hence F_0 and F have the same volume: ...

équations (1) x_i en $x_i + \xi_i$ et l'on néglige les carrés des ξ_i ; on trouve ainsi le système d'équations linéaires

$$\frac{d\xi_k}{dt} = \frac{dX_k}{dx_1}\xi_1 + \frac{dX_k}{dx_2}\xi_2 + \cdots + \frac{dX_k}{dx_n}\xi_n. \tag{2}$$

Il y a, entre les intégrales des équations (2) et les invariants intégraux des équations (1), un lien intime qu'il est aisé d'apercevoir.

Soit $F(\xi_1, \xi_2, \cdots, \xi_n) =$ const., une intégrale quelconque des équations (2). Ce sera une fonction homogène par rapport aux ξ, et dépendant d'ailleurs des x d'une manière quelconque. Je pourrai toujours supposer que cette fonction F est homogène de degré 1 par rapport aux ξ ; car s'il n'en était pas ainsi, je n'aurais qu'à élever F à une puissance convenable pour trouver une fonction homogène de degré 1. Considérons maintenant l'expression

$$\int F(dx_1, \cdots, dx_n),$$

je dis que c'est un invariant intégral du système (1).[14]

Let us recall that the theoretical structure of classical mechanics is in great part founded on the existence of the "Poincaré-Cartan integral invariant" or "energy-momentum tensor"

$$\sum_i p_i dq_i - H(p, q, t)dt.$$

6 "à la Poisson" Stability

Le mot stabilité a été entendu sous les sens les plus différents, et la différence de ces divers sens deviendra manifeste si l'on se rappelle l'histoire de la Science. Lagrange a démontré qu'en négligeant les carrés des masses, les grands axes des orbites deviennent invariables. Il voulait dire par là qu'avec ce degré d'approximation les grands axes peuvent se développer en séries dont les termes sont de la forme $A\sin(\alpha t + \beta)$, A, α et β étant des constantes.[15]

[14]Let us take back the system (1) $\frac{dx_1}{X_1} = \frac{dx_2}{X_2} = \cdots = \frac{dx_n}{X_n} = dt$. We can form the corresponding variational equations as they were defined at the beginning of Chap. IV. In order to form these equations one changes x_i into $x_i + \xi_i$ in Eq. (1) and one neglects the squares of the ξ_i; one finds in this way the system of linear equations (2) $\frac{d\xi_k}{dt} = \frac{dX_k}{dx_1}\xi_1 + \frac{dX_k}{dx_2}\xi_2 + \cdots + \frac{dX_k}{dx_n}\xi_n$. There is, between the integrals of Eqs. (2) and the integral invariants of Eqs. (1), an intimate relation which is easy to see. Let $F(\xi_1, \xi_2, \cdots, \xi_n) =$ const., be any integral of Eqs. (2). It is a function, homogeneous of degree 1 in the ξ_i and depending in an arbitrary way on the x; indeed, if this was not the case, it would be enough to raise F to a conveniently chosen power in order to obtain a function homogeneous of degree 1. Now, let us consider the expression $\int F(dx_1, \cdots, dx_n)$, I say it is an integral invariant of system (1).

[15]The word stability has been taken in very different meanings, and the difference between these meanings will become obvious if one remembers history of Science. Lagrange has proved that if one neglects the squares of the mases, the major axes of the orbits become invariable. He wanted to say that with this degree of approximation the major axes can be expanded in series whose terms are of the form $A\sin(\alpha t + \beta)$, where A, α and β are constants.

The title of Chap. XXVI is not innocent. Having wrongly announced in the memoir of 1889 a very strong stability result in the restricted problem of three bodies, Poincaré wants to crown his treatise with a stability result which, even if weaker than the previous one, has still a great importance. Indeed, based on the "recurrence theorem", it is the forerunner of "ergodic theory". The word "à la Poisson stability" alludes to the absence of purely secular terms (i.e. of terms which grow indefinitely when time goes on) in the planetary semi-major axes at the second order of the classical theory of perturbations (i.e. if the cubes of the planetary masses are neglected) which, at this order of approximation, implies a recurrent behaviour of these semi-major axes. (S. Haretu will show that this property does not subsist at higher orders.) Using an argument of volume conservation in a domain of finite volume, Poincaré shows that, in the case he is considering, the preservation of the integral invariant implies that a "generic" solution of the restricted problem will return infinitely often in an arbitrarily small neighborhood of a given point in the phase space. The following quotation (Chap. XXVI Sect. 296) justifies the consideration of the generic case in a way which announces Borel's zero measure sets:

> En résumé, les molécules qui ne traversent U_0 qu'un nombre fini de fois sont exceptionnelles au même titre que les nombres commensurables qui ne sont qu'une exception dans la série des nombres, pendant que les nombres incommensurables sont la règle. Si donc Poisson a cru pouvoir répondre affirmativement à la question de la stabilité telle qu'il l'avait posée, bien qu'il eût exclu les cas où le rapport des moyens mouvements est commensurable, nous aurons de même le droit de regarder comme démontrée la stabilité telle que nous la définissons, bien que nous soyons forcés d'exclure les molécules exceptionnelles dont nous venons de parler.[16]

Titled *Probabilities*, this Sect. 296 is particularly visionary: ignoring the fears of J. Bertrand about the "paradoxes" of continuous probabilities, Poincaré understands perfectly that any choice of a regular density will lead to the same notion of sets whose probability is negligible:

> Mais il faut d'abord que j'explique le sens que j'attache au mot *probabilité*. Soit $\varphi(x, y, z)$ une fonction quelconque positive des trois coordonnées x, y, z ; je conviendrai de dire que la probabilité pour qu'à l'instant $t = 0$ une molécule se trouve à l'intérieur d'un certain volume est proportionnelle à l'intégrale
>
> $$J = \int \varphi(x, y, z) dx dy dz$$

[16] Summarizing, the molecules which pass through U_0 only a finite number of times are exceptional in the same way as the rational numbers which are but an exception in the series of numbers, while the irrational numbers are the rule. Hence, if Poisson considered that he could reply affirmatively to the question of the stability as he had set it, although he had excluded the case when the mean motions are commensurable, we shall have in the same way the right of considering the stability as proved, although we are forced to exclude the exceptional molecules that we have just mentioned.

étendue à ce volume. . . . Nous pouvons choisir arbitrairement la fonction φ et la probabilité se trouve ainsi complètement définie. ⋯ Nous retombons donc sur les mêmes résultats *qui sont ainsi indépendants du choix de la fonction* φ.[17]

A nice analysis of this part of the text is found in the thesis of Anne Robadey [13].

7 Theory of "Consequents"

As, once written in rotating axes, the circular planar restricted three-body problem becomes a two degrees of freedom Hamiltonian system, a constant energy hypersurface is a three-dimensional manifold. In the Sect. 305 of Chap. XXVII, Poincaré exhibits a halph-plane (indeed a disc from which one point of its boundary is sent "to infinity") embedded in such a manifold, which is cut transversely by every integral curve except its boundary, and hence acts as a stroboscope:

Le point M_1 sera dit le *conséquent* de M_0. Ce qui justifie cette dénomination, c'est que, si l'on considère le faisceau des courbes qui satisfont aux équations différentielles (1) ; si, par le point M_0, on fait passer une courbe et qu'on la prolonge jusqu'à ce qu'elle rencontre de nouveau le demi-plan ($y = 0, x > 0$), cette nouvelle rencontre aura lieu en M_1.[18]

The existence of an integral invariant implies that the "first return map" on this "surface of section", preserves a measure with a smooth density with respect to Lebesgue measure (which, of course, Poincaré could not know) and finite total mass:

Ainsi, *l'intégrale (5) a même valeur pour une aire quelconque et sa conséquente.*[19]

From this property, Poincaré deduces an important result of intersection with its "consequent" of a closed curve made of segments asymptotic manifolds of periodic solutions.

Later on, Birkhoff will build an annulus playing the same role as Poincaré's halfplane (disc). This annulus (see [6, 8]), whose second component of the boundary is obtained by blowing up the fixed point in Poincaré's disc, is at the origin of the

[17]But I must first explain the meaning I give to the word *probability*. Let $\varphi(x, y, z)$ any positive function of the three coordinates x, y, z; I shall agree to say that the probability for a molecule to be at time 0 inside a certain volume is proportional to the integral

$$J = \int \varphi(x, y, z)dxdydz$$

extended to this volume. . . . We may choose arbitrarily the function φ and the probability is then completely defined. ⋯ So doing, we get again the same results *which hence are independant of the choice of the function* φ.

[18]What justifies this denomination is that, considering the set of curves which satisfy the differential equations (1), if by the point M_0 passes one such curve and if one continues this curve until it cuts again the halph-plane ($y = 0, x > 0$), this new intersection will take place in M_1.

[19]Hence, the integral (5) takes the same value for any area and its consequent.

study of "conservative monotone distortions of the annulus" which, in the second half of twentieth century, played an important role in the development of qualitative conservative dynamics and in the birth of symplectic topology (Poincaré-Birkhoff's fixed point theorem and Arnold's conjecture). It is Birkhoff's annulus rather than Poincaré's half-plane that I have chosen to represent in the figure of Sect. 9. The return map may be loosely interpreted as describing the successive positions of the perihelion (or the aphelion) of the zero mass body.

8 Doubly Asymptotic Solutions

Recall the wrong assertion of the memoir of 1889:

> Donc *les surfaces asymptotiques sont des surfaces fermées.* Mais au début de ce travail, nous avons montré que pour établir la stabilité, il suffit de démontrer l'existence de surfaces trajectoires fermées.[20]

In fact, even if they coincide at all orders of the theory of perturbations (see the exponentially small estimation of the intersection angle given in the case of a perturbed pendulum in Chap. XXI), the stable and instable asymptotic surfaces of a periodic solution of the restricted problem have no reason to coincide and hence they do not define closed surfaces which would confine the solutions in a fixed energy surface [3, 14]. This non coincidence is a manifestation of the divergence of the "Bohlin series" in $\sqrt{\mu}$, which Poincaré had thought to be convergent in the first version of the memoir.[21]

Understanding the extreme complexity of the intersections of these two asymptotic surfaces, Poincaré writes (one should say "exclaims") :

> Que l'on cherche à se représenter la figure formée par ces deux courbes et leurs intersections en nombre infini dont chacune correspond à une solution doublement asymptotique, ces intersections forment une sorte de treillis, de tissu, de réseau à mailles infiniment serrées ; chacune des deux courbes ne doit jamais se recouper elle-même, mais elle doit se replier sur elle-même d'une manière très complexe pour venir recouper une infinité de fois toutes les mailles du réseau.
>
> On sera frappé de la complexité de cette figure, que je ne cherche même pas à tracer. Rien n'est plus propre à nous donner un idée de la complication du problème des trois corps et en général de tous les problèmes de Dynamique où il n'y a pas d'intégrale uniforme et où les série de Bohlin sont divergentes.[22] (Chap. XXXIII, Sect. 397.)

[20] Hence the asymptotic surfaces are closed surfaces. But at the beginning of this work, we have shown that in order to establish the stability, it is enough to prove the existence of closed surface trajectories.

[21] See [12] for an in depth study of the way Poincaré deals with divergent series.

[22] Let us try to represent the figure formed by these two curves and their intersections in infinite number, each corresponding to a doubly asymptotic solution, these intersections form a kind of mesh, of fabric, of infinitely tight network; each of the two curves must never intersect itself, but it

At the origin of what some people have (mis)named "chaos theory", this complexity of the mesh of homoclinic or heteroclinic intersections (i.e. the intersections of stable and unstable manifolds) can be analyzed to-day by methods of symbolic dynamics but, although a partial vision can be gained through the use of computers, it is still hard to imagine the whole picture.

9 A Summary in the Form of a Picture*

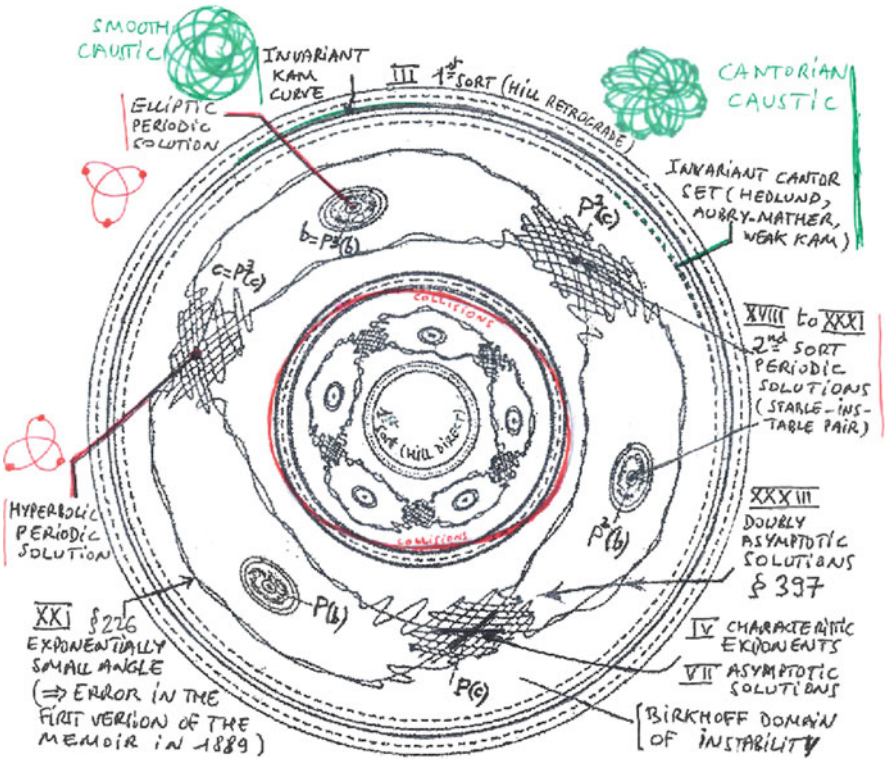

must fold back on itself in a very complex way in order to cross an infinite number of times all the meshes of the network.

On will be struck by the complexity of this figure, which I do not even try to draw. Nothing is more likely to give us an idea of the complexity of the three-body problem and in general of all the problems of dynamics where there is no uniform integral and where the Bohlin series are divergent.

*The figure in this section is a revised version of Figure 39 in [15], published with kind permission of © Encyclopædia Universalis France S.A. 2005. All Rights Reserved.

10 A Letter to Gauthier-Villars

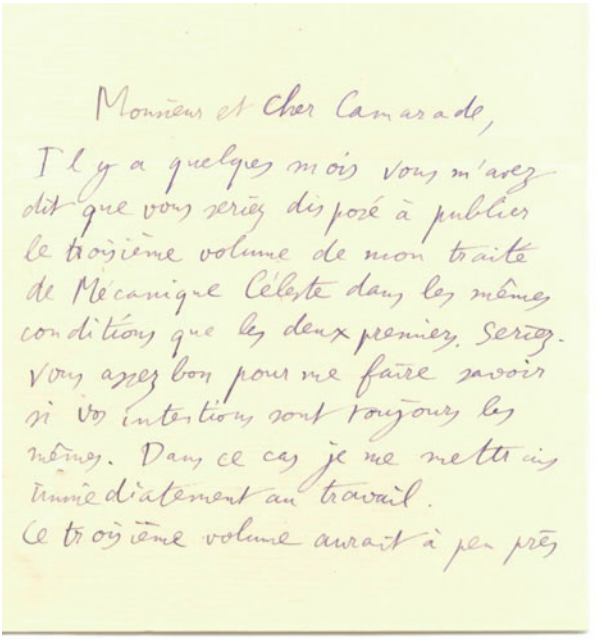

Monsieur et Cher Camarade,

Il y a quelques mois vous m'avez dit que vous seriez disposé à publier le troisième volume de mon traité de Mécanique Céleste dans les mêmes conditions que les deux premiers. Seriez-vous assez bon pour me faire savoir si vos intentions sont toujours les mêmes. Dans ce cas je me mettrai immédiatement au travail.
Ce troisième volume aurait à peu près

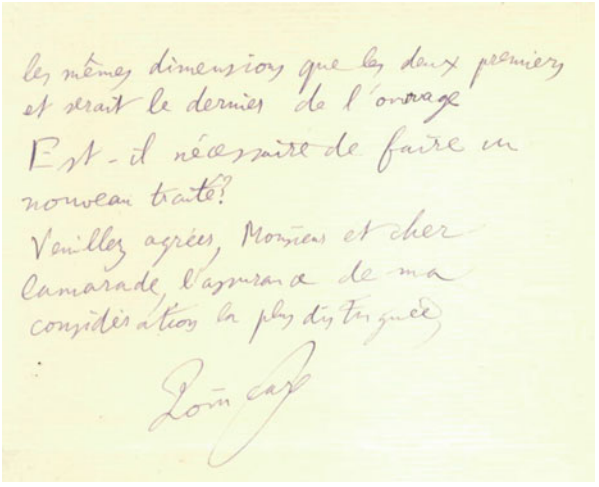

les mêmes dimensions que les deux premiers et serait le dernier de l'ouvrage
Est-il nécessaire de faire un nouveau traité?
Veuillez agréer, Monsieur et cher Camarade, l'assurance de ma considération la plus distinguée
:

Poincaré

11 A Seminar

From 1988 to 1990, Jacques Laskar and I had organized at the Bureau des Longitudes a seminar dedicated to the reading of the "New methods of celestial mechanics". Bringing together mathematicians and astronomers, this seminar is at the origin of the creation of the ASD (Astronomy and Dynamical Systems) group in which we try to continue the collaboration between astronomers and mathematicians. We knew that the Poincaré research on differential equations, and in particular on the three-body problem were the source of entire sections of to-day mathematics: dynamical systems, differential forms, ergodic theory, topology, ... But we have discovered the visionary precision with which these three volumes exposed ideas that we had thought to be recent. The three papers [4, 5, 9] were published on this occasion.

Warm thanks to the friends of the Dynamical Systems group of the University of Oviedo for having organized such a nice celebration of Poincaré.

References

1. Arnold, V.I.: Petits dénominateurs et problème de la stabilité du mouvement en mécanique classique et céleste. Usp. Mat. Nauk **18**, 91–192 (1963)
2. Arnold, V.I., Kozlov, V.V., Neishtadt, A.I.: Mathematical aspects of classical and celestial mechanics. In: Dynamical Systems III, 3rd edn. Encyclopædia of Mathematical Sciences, vol. 3. Springer, Berlin (2006)
3. Barrow-Green, J.: Poincaré and the Three Body Problem. History of Mathematics, vol. 11. AMS, Providence (1997)
4. Chenciner, A.: Intégration du problème de Kepler par la méthode de Hamilton-Jacobi : coordonnées "action-angles" de Delaunay; Laskar, J.: Les variables de Poincaré et le développement de la fonction perturbatrice. Notes scientifiques et techniques du Bureau des Longitudes 5026 (mars 1989)
5. Chenciner, A.: Séries de Lindstedt. Notes scientifiques et techniques du Bureau des Longitudes 5028 (février 1990)
6. Chenciner, A.: Three-body problem. Scholarpedia **2**(10), 2111 (2007)
7. Chenciner, A.: Une promenade dans les Méthodes nouvelles de la mécanique céleste. Gazette des Mathématiciens, $n^0$134, pp. 37–47, SMF Paris, Oct 2012. Quadrature, special issue dedicated to Henri Poincaré, Nov 2012
8. Chenciner, A.: Poincaré and the Three-Body Problem. "Poincaré seminar" (also called "Bourbaphy"), XVI, pp. 45–133, Nov 2012. www.bourbaphy.fr/novembre2012.html
9. Ferraz-Mello, S.: The Method of Delaunay; Jupp, A.: Chapter XIX Bohlin method. Notes scientifiques et techniques du Bureau des Longitudes 5036 (avril 1992)
10. Kolmogorov, A.N.: On the conservation of conditionnally periodic motions under small perturbations of the Hamiltonian. Dokl. Akad. Nauk SSSR **98**, 527–530 (1954)
11. Moser, J.: On invariant curves of area preserving mappings of an annulus. Nachr. Akad. Wiss. Gött., Math. Phys. Kl. **II**, 1–20 (1962)
12. Ramis, J.P.: Poincaré et les développements asymptotiques (Première partie). Gazette des mathématiciens 133, pp. 33–72, SMF Paris, juillet 2012
13. Robadey, A.: Différentes modalités de travail sur le général dans les recherches de Poincaré sur les sytèmes dynamiques. Thèse Paris (2006)
14. Yoccoz, J.C.: Une erreur féconde du mathématicien Henri Poincaré. Gazette des mathématiciens **107**, 19–26 (2006)
15. Systèmes Dynamiques Différentiables, © Encyclopædia Universalis France S.A. (2005)

Porcupine-Like Horseshoes: Topological and Ergodic Aspects

L.J. Díaz and K. Gelfert

Abstract We introduce a class of topologically transitive and partially hyperbolic sets called porcupine-like horseshoes. The dynamics of these sets is a step skew product over a horseshoe. The fiber dynamics is given by a one-dimensional genuinely noncontracting iterated function system. We study this dynamics and explain how the properties of the iterated function system can be translated to topological and ergodic properties of the porcupines.

1 Introduction

1.1 General Setting

In this paper we summarize and explain the main ingredients in the series of papers [10–13, 26] about topological and ergodic properties of the so-called *porcupine-like horseshoes*. The naive image of these sets, that justifies their name, is the following: in $\mathbb{R}^3$ consider a horseshoe in $\mathbb{R}^2 \times \{0\}$ and for a dense subset of the horseshoe glue spines (segments) parallel to the direction $\{0^2\} \times \mathbb{R}$. This is done in such a way that the resulting set is partially hyperbolic (one-dimensional center parallel to the spines) and topologically transitive. These systems are step skew products

L.J. Díaz (✉)
Departamento de Matemática, PUC-Rio, Marquês de São Vicente 225, Gávea, Rio de Janeiro 225453-900, Brazil
e-mail: lodiaz@mat.puc-rio.br

K. Gelfert
Instituto de Matemática, Universidade Federal do Rio de Janeiro, Av. Athos da Silveira Ramos 149, Cidade Universitária – Ilha do Fundão, Rio de Janeiro 21945-909, Brazil
e-mail: gelfert@im.ufrj.br

S. Ibáñez et al. (eds.), *Progress and Challenges in Dynamical Systems*, Springer Proceedings in Mathematics & Statistics 54,
DOI 10.1007/978-3-642-38830-9_12,

over a horseshoe (hyperbolic part) whose central dynamics is defined in terms of a one-dimensional (noncontracting) iterated function system (IFS) of fiber maps.

The fiber IFS has finitely many generators, one of them reversing the orientation of the fibers. These systems exhibit topologically interesting features that contrast what has been studied in other contexts. For instance, iterated function systems with monotonically increasing fiber maps possess invariant sets being a finite union of graphs. As some examples we can name the famous Weierstrass function [19], pinched skew products over a minimal base dynamics with strange nonchaotic attractors [22], and skew-products over a shift space with a finite number of attractor-repeller pairs [24].

Let us outline some motivations of this line of research. The starting point are the results in [11] about bifurcations of hyperbolic homoclinic classes and their topological properties, followed by investigations of their ergodic properties and, in particular, their Lyapunov exponents in [26]. Second, the topological examples of recurrent sets of fibered systems over a shift space, so-called *bony attractors*, by Ilyashenko in [20]. These attractors have the following significant property: the map has an invariant manifold, and the intersection of the attractor with that manifold, called a *bone*, is much larger than the attractor of the restriction of the map to the invariant manifold. Bony attractors with one-dimensional bones were discovered in [25] and [21] provides further examples with higher-dimensional bones. Another motivation comes from the results about iterated function systems and skew product dynamics in [17, 18].

Let us now say a few words about our examples of porcupines. For notational simplicity, in what follows we assume that the ambient space is three-dimensional. The porcupine horseshoe in [11, 26] is essentially hyperbolic with a two-dimensional contracting direction and has *attached* one hyperbolic saddle with one-dimensional stable direction, we say that this point is *exposed*. All the saddles in the transitive set different from the exposed one are hyperbolic with *unstable index* one (dimension of the unstable direction) and, in fact, such saddles are all *homoclinically related* (their invariant manifolds meet cyclically and transversely). Moreover, the porcupine is their *homoclinic class* (closure of the transverse intersections of the invariant manifolds of the saddle). This configuration has immediate implications for the ergodic properties: all ergodic measures are hyperbolic, the only measure with positive central exponent is the Dirac measure supported on the exposed saddle, the central spectrum (Lyapunov exponents corresponding to the central direction) forms an interval of the form $[a, 0] \cup \{b\}$, where $b > 0$ is the exponent of the exposed saddle. This is an example of a nonhyperbolic set which is hyperbolic in the sense that all its ergodic measures are hyperbolic (have nonvanishing Lyapunov exponents). Other examples of different nature can be found in [2,7], but the novelty in [11, 26] is that measures have different type of hyperbolicity.

The examples in [10, 12–14] can be considered as extensions of [11] to genuinely nonhyperbolic settings. These extensions rely on a detailed study of the topological and ergodic properties of the underlying fibered iterated function system. The complexity of the dynamics is also related to the complexity of the exposed part of the porcupine (see Definition 2). In [10] we consider porcupines whose central

spectrum contains a gap and an interval of positive and negative values. Here the exposed piece is also just a saddle. The examples in [12] are an extension of [10] exhibiting porcupines whose exposed pieces are horseshoes and deriving ergodic consequences of this fact (equilibrium states and special phase transitions for some geometric potentials). Finally, in [14] we consider more complicated exposed pieces that give raise to multiple gaps in the Lyapunov spectrum. A complete analysis of the Lyapunov spectrum and related properties is presented in [13].

Let us observe that porcupines are simple examples of nonhyperbolic transitive sets with rich dynamics. Many features of nonhyperbolic dynamics can be easily checked and explained. In general, when trying to understand the dynamics, the simplest examples to start with are iterated function systems and step skew products. The complexity increases for general skew products (where the fiber maps depend on the base point). In this context, the most complex case corresponds to partially hyperbolic dynamics with one-dimensional center. Note that under quite general and natural assumptions one can translate properties of general skew products to partially hyperbolic dynamical systems, see [16, 23].

Another motivation comes from the study of elementary pieces of dynamics that generalize the concept of basic sets in uniformly hyperbolic systems. In some cases homoclinic classes provide the right generalizing concept, see [4, Chap. 10]. Porcupines are significant examples of nonhyperbolic homoclinic classes.

Finally, the gaps in the spectrum explained in [12, 14, 26] provide examples of a new type of phase transitions for geometric potentials (in our case the potential $\varphi_c = -\log |dF|_{E^c}|$ associated to the derivative of the diffeomorphism in the central direction), that is, nondifferentiability of the topological pressure. Pressure is a central object in ergodic theory as it joins various dynamical quantifiers such as Lyapunov exponents, dimension, entropy, decay of correlations, equilibrium states among others (see [29, 32]) and its regularity is of great interest. Such phase transitions come along with the co-existence of equilibriums states with positive entropy and with different exponents. Let us point out that an essential point in our examples is transitivity. Clearly when a system has several transitive components (though they could be intermingled) then this will be reflected dynamically (see [15] for an example of renormalizable unimodal maps). If, however, a dynamical system is transitive but there exist pieces that are "exposed" in a sense that dynamically and topologically they form extreme points then we still can observe the phenomenon of phase transitions and coexistence of equilibrium states.

1.2 Porcupine-Like Horseshoes

In this section we give some definitions and discuss more precisely some features of porcupines. We consider invariant sets having a dominated splitting with three nontrivial directions $E^s \oplus E^c \oplus E^u$, where E^s is uniformly contracting, E^u is uniformly expanding, and E^c is one-dimensional and nonhyperbolic. In this case we say that the splitting is *strongly partially hyperbolic*.

Definition 1 (Porcupines). We call a compact F-invariant compact set Λ of a (local) diffeomorphism F a *porcupine-like horseshoe* or *porcupine* if

- Λ is the maximal invariant set in a compact set $\mathbf{C}$, *transitive* (existence of a dense orbit), and strongly partially hyperbolic,
- There is a subshift of finite type $\sigma\colon \Sigma \to \Sigma$ and a semiconjugation $\pi\colon \Lambda \to \Sigma$ such that $\sigma \circ \pi = \pi \circ F$, $\pi^{-1}(\xi)$ contains a continuum for uncountably many $\xi \in \Sigma$ and a single point for uncountably many $\xi \in \Sigma$.

We call $\pi^{-1}(\xi)$ a *spine* and say that it is *nontrivial* if it contains a continuum. The *spine of a point* $X \in \Lambda$ is the set $\pi^{-1}(\pi(X))$.

Given a saddle P of F, its *homoclinic class* $H(P, F)$ is the closure of the transverse intersections of the stable and unstable manifolds of the orbit of P. Two saddle points P and Q are *homoclinically related* if the invariant manifolds of their orbits meet cyclically and transversally. Note that there are points whose homoclinic classes are equal but are not homoclinically related. A homoclinic class is *nontrivial* if it contains at least two different orbits. Given a neighborhood U of P, we call the closure of the set of points R that are in the transverse intersections of the stable and unstable manifolds of P and whose orbit is entirely contained in U the *homoclinic class of P relative to U* and denote this set by $H_U(P, F)$. The homoclinic class of a saddle P is always a transitive set and the hyperbolic periodic points of the same unstable index as P are dense in the class. However, a homoclinic class may fail to be hyperbolic and may contain points of different unstable indices. Indeed, the porcupines illustrates this situation. We can define the (relative) homoclinic class of a transitive hyperbolic set similarly.

Definition 2 (Exposed piece). We call a compact F-invariant subset E of a porcupine Λ an *exposed piece* if E is transitive and satisfies $H_{\mathbf{C}}(E) = E$, where $\mathbf{C}$ is a cube such that $\Lambda = \cap_{i\in\mathbb{Z}} F^i(\mathbf{C})$.

In some sense the exposed pieces cannot be "reached" by the remaining dynamics of the porcupine. This unattainability has two aspects. First, the orbits of the porcupine outside the exposed piece only accumulate on "one side" of it. Second, the existence of the spectral gap immediately implies that the dynamics does not satisfy the specification property [30]. Though such pieces do not break topological transitivity – which perhaps can be considered a concept to weak to capture the phenomena observed. Let us observe that in a slightly different context [6] provides examples of a chain recurrent class that properly contains a homoclinic class besides "exposed orbits" that correspond to heteroclinic intersections between saddles of different unstable indices.

So far we have studied three types of exposed pieces of porcupines:

- The exposed piece is a fixed point [10, 11]. This leads to a central spectrum of the form $[a, b] \cup \{c\}$, where $a < 0 \le b < c$. This spectrum provides a phase transition of the geometric potential φ_c at some critical parameter.

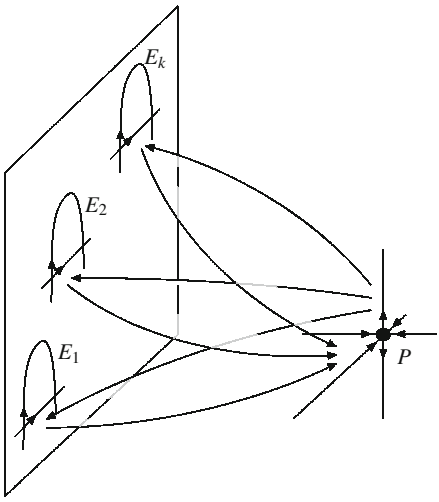

Fig. 1 Exposed pieces and connections to a saddle P

- The exposed piece is a horseshoe [12]. This leads to a central spectrum of the form $[a, b] \cup [c, d]$, where $a < 0 < b < c < d$. This spectrum provides a rich phase transition for the geometrical potential φ_c at some critical parameter.
- The exposed piece is composed by a finite number of disjoint horseshoes [14]. These horseshoes have disjoint central Lyapunov spectrum and appropriate entropies. This leads to a central spectrum of the form $[c_0, d_0] \cup [c_1, d_1] \cup \ldots \cup [c_k, d_k]$, where $c_0 < 0 < d_0 < c_1 < d_1 < \ldots < c_k < d_k$. This gives k rich phase transitions of the potential φ_c.

The exposed pieces mentioned above are connected by a heterodimensional cycles to one saddle in the porcupine (see Fig. 1). This sort of configuration is nongeneric. It was shown in [1] that C^1 generically the Lyapunov spectrum of a homoclinic class is convex. This implies immediately that spectra with gap(s) similar to our examples only can occur in nongeneric situations.

Further, we would like to mention that in terms of an iterated function system the above mentioned heterodimensional cycle corresponds to a cycle condition for the fiber maps. This seems to play a role similar to the Misiurewicz property in one-dimensional dynamics as, for example, in the case of the quadratic map $f(x) = 1 - 2x^2$ or of Chebyshev polynomials [27, 28] where there is a periodic point that is "dynamically exposed" in the sense that it is immediately post-critical.

Above we focused mainly on topological aspects of porcupines. Let us observe that these topological properties have implications in the ergodic level. First, the fact that the central direction of the porcupine is one-dimensional implies that its topological entropy coincides with the one of its base [8]. Dynamics on the fibers does not generate additional entropy. Furthermore, this implies upper semicontinuity of the entropy function [9] which in turn is essential to guarantee existence of equi-

librium states (measure of maximal entropy etc.) [32]. Observe also that porcupines are transitive sets of saddle-type containing intermingled hyperbolic sets of different unstable indices. Thus the one-dimensional central direction of the porcupine is contracting for some of these sets and expanding for others. Hence, a first question is to determine the dominating behavior. Indeed, intuitively it can be seen that it topologically behaves essentially contracting, this is illustrated by the fact that the maps of the underlying IFS map the interval $[0, 1]$ into itself. We will support this observation by studying the ergodic properties of relevant measures on the porcupine.

The content of this paper is the following. In Sect. 2 we introduce the porcupines and explain the main properties of their fiber maps. In Sect. 3 we derive some properties for the underlying IFS of the porcupine. These properties can be summarized as follows: every point has forward and backward iterates which are uniformly expanding. An important consequence of this fact is the minimality of the IFS. Another consequence of this fact and the cycle property of the IFS is the existence of a spectral gap. The topological properties of the porcupines (transitivity, structure of the fibers, distribution of periodic poins) are studied in Sect. 4. In Sect. 5.1 we translate the spectral properties of the IFS in Sect. 3.6 to properties of the central spectrum of the porcupine. Finally, in Sect. 5.2 we study thermodynamical properties and see how the gaps in the spectrum lead to phase transitions of the geometrical potential φ_c.

2 The Dynamics of the Porcupine

We now introduce the class of step skew-product maps that we will consider. Given the square $\hat{\mathbf{C}} = [0, 1]^2$ of $\mathbb{R}^2$ and a planar diffeomorphism Φ having an affine horseshoe Γ in $\hat{\mathbf{C}}$ that is conjugate to the full shift $\sigma\colon \Sigma_i \to \Sigma_i$ ($\Sigma_i := \{0, \dots, i-1\}^{\mathbb{Z}}$ for $i = 2$ or 3 is the symbolic space) we consider the sub-cubes $\hat{\mathbf{C}}_i$, of $\hat{\mathbf{C}}$ given by the "first level" rectangles defined as the connected components of $\Phi^{-1}([0, 1]^2) \cap [0, 1]^2$. Let $\mathbf{C} = [0, 1]^3$ and $\mathbf{C}_i = \hat{\mathbf{C}}_i \times [0, 1]$ and consider the map $F\colon \mathbf{C} \to \mathbb{R}^3$ defined by

$$F(X) := (\Phi(\hat{x}), f_i(x)) \quad \text{if } X = (\hat{x}, x) \in \mathbf{C}_i. \tag{1}$$

Here the maps $f_i\colon [0, 1] \to [0, 1]$ are C^1 injective maps satisfying the following two basic properties:

(F0) The map f_0 is increasing and has exactly two hyperbolic fixed points in $[0, 1]$, the point $q_0 = 0$ (repelling) and the point $p_0 = 1$ (attracting). Let $\beta_0 = f_0'(0) > 1 > \lambda_0 = f_0'(1) > 0$.

(F1) The map f_1 is an affine contraction $f_1(x) := \gamma\,(1 - x)$ where $\gamma \in (\lambda_0, 1)$. We denote by p_1 the attracting fixed point of f_1. Note that f_1 satisfies the *cycle condition* $f_1(1) = 0$.

Further properties of these maps (and also of f_2 when $i = 3$) are specified in Sect. 3.1, compare Fig. 2.

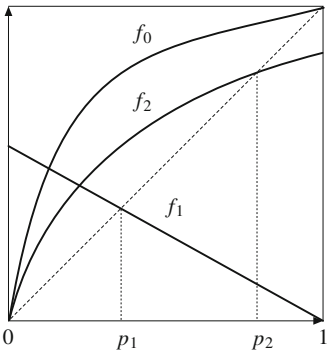

Fig. 2 Fiber maps of the IFS

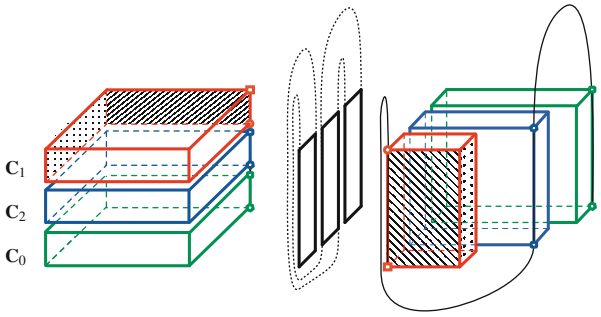

Fig. 3 Level 1 rectangles and the dynamics of F

To complete the definition of F in $\mathbf{C}$ we will consider some appropriate C^1-continuation of F such that $F(\text{int}\,(\mathbf{C} \setminus \bigcup_i \mathbf{C}_i)) \cap \mathbf{C} = \emptyset$.

We now briefly discuss some basic dynamical properties of the local diffeomorphism F, compare Fig. 3. We focus on the dynamics of F on its maximal invariant set Λ in $\mathbf{C}$ defined by

$$\Lambda := \bigcap_{i \in \mathbb{Z}} F^i(\mathbf{C}). \tag{2}$$

By an appropriate choice of the horseshoe Γ, the set Λ is partially hyperbolic for F with central direction $E^c = \{(0^s, 0^u)\} \times \mathbb{R}$. Associated to the fixed points $\theta_0 \in \hat{\mathbf{C}}_0$ and $\theta_1 \in \hat{\mathbf{C}}_1$ of the horseshoe there are the following fixed points of Λ, $P_0 = (\theta_0, 1)$ and $P_1 = (\theta_1, p_1)$, with contracting central direction, and $Q_0 = (\theta_0, 0)$ with expanding central direction.

Conditions (F0) (implying that $f_0^i(x) \to 1$ and $f_0^{-i}(x) \to 0$ as $i \to \infty$ if $x \in (0, 1)$) and (F1) (stating $f_1(1) = 0$) imply that F has a heterodimensional cycle

associated to the saddles P_0 and Q_0: the stable manifold of P_0 meets the unstable one of Q_0 and the unstable manifold of P_0 meets the stable one of Q_0, see Fig. 3.

Under the additional condition (F01) the set Λ is transitive (actually it is a relative homoclinic class) where intermingled hyperbolic sets with different indices coexist. Indeed these hyperbolic sets are cyclically related. This fact generates a rich dynamics mixing hyperbolicity of different types.

This system also exhibits an interesting fiber structure. Recall that the horseshoe Γ in the base is conjugate to the shift $\sigma\colon \Sigma \to \Sigma$ (where $\Sigma = \Sigma_2$ or Σ_3, according to the case). Then there is a semiconjugation $\varpi\colon \Lambda \to \Sigma$ such that $\sigma \circ \varpi = \varpi \circ F$. We call a set $\varpi^{-1}(\xi) \subset \Lambda$ a *spine* and say that it is *nontrivial* if it contains a continuum. The spines are connected sets tangent to the central direction. We will see that the spines $\varpi^{-1}(\xi)$ are nontrivial for a uncountable dense subset of Σ and a single point for a residual subset of Σ.

Finally note that any point $X \in \Lambda$ is of the form $X = (X_\xi, x)$, $X_\xi \in \Gamma$ and $x \in [0, 1]$, where $\xi = \varpi(X)$.

3 The Underlying Iterated Function System

In this section we present a simplest case of our model and deduce some key properties of the IFS.

3.1 The Fiber Maps

We now complete the description of the fiber maps $f_i\colon [0, 1] \to [0, 1]$, see Fig. 2. For most topological conditions (as backward minimality and existence of forward expanding itineraries) it is enough to consider just the maps f_0 and f_1 and the properties (F0) and (F1) above and (F01) below. These properties provide the covering and expanding key properties for forward orbits in Lemma 2. These properties will imply the transitivity of Λ and that it is the relative homoclinic class of a saddle of unstable index two in **C**.

Forward Expanding-Like Condition

Recall the definitions of γ, λ_0, and β_0 above. We assume that f_0 and f_1 satisfy the following:

(F01) The derivative f_0' is decreasing in $[0, 1]$ and satisfies

$$\gamma\, \lambda_0^3\, (1 - \lambda_0)(1 - \beta_0^{-1})^{-1} > 1.$$

Given $\gamma, \lambda_0 \in (0, 1)$, condition (F01) holds if $\beta_0 > 1$ is sufficiently close to 1.

This condition provides a fundamental domain $J = [f_0^{-1}(b), b] \in (0,1)$ of f_0 (b close to 0) and a large N such that $f_1 \circ f_0^N(J) \subset (0,b)$, and the restriction of $f_1 \circ f_0^N$ to J is uniformly expanding. This is the key for defining expanding itineraries (see Sect. 3.3).

Backward Expanding-Like Condition

In some cases we consider an extra hypotheses to get a more accurate description of the dynamics or a dynamics with a richer structure. We introduce two types of conditions. A blender-like condition implying some expansion for backward iterates is the following:

(F_B) $f_0'(x) \in (0,1)$ for all $x \in [\gamma, 1] = [f_1(0), 1]$.

Lateral Horseshoe Condition

To get an exposed set containing a horseshoe we need to consider the following condition:

(F2) The map f_2 is increasing and has two hyperbolic fixed points in $[0,1]$, the point $q_2 = 0$ (repelling) and the point $p_2 \in (0,1)$ (attracting). Let $\beta_2 = f_2'(0) > 1$. This map is close to f_0.

This condition implies that the set Λ contains a horseshoe Λ_{02} in $(\hat{C}_0 \cup \hat{C}_1) \times \{0\}$ conjugate to the full shift of two symbols. The set of central Lyapunov exponent of this horseshoe is the closed interval of extremes $\log \beta_2$ and $\log \beta_0$. This condition will imply the rich phase transitions in Sect. 5.2.

3.2 Admissible Sequences: Notation

In what follows, for the IFS associated to $\{f_0, f_1, f_2\}$ we use the standard cylinder notation, given *finite* sequences $(\xi_0 \dots \xi_n)$ and $(\xi_{-m} \dots \xi_{-1})$, $\xi_i \in \{0,1,2\}$, we let

$$f_{[\xi_0 \dots \xi_n]} := f_{\xi_n} \circ \dots \circ f_{\xi_1} \circ f_{\xi_0} : [0,1] \to [0,1]$$

and

$$f_{[\xi_{-m} \dots \xi_{-1}.]} := (f_{\xi_{-1}} \circ \dots \circ f_{\xi_{-m}})^{-1} = (f_{[\xi_{-m} \dots \xi_{-1}]})^{-1}.$$

Note that the maps $f_{[\xi_{-m} \dots \xi_{-1}.]}$ are in general only defined on a closed subinterval of $[0,1]$. The finite sequence $(\xi_{-m} \dots \xi_{-1})$ is *admissible* for $x \in [0,1]$ if the map $f_{[\xi_{-m} \dots \xi_{-1}.]}$ is well-defined at x (i.e., $f_{[\xi_{-j} \dots \xi_{-1}.]}(x) \in [0,1]$ for all $j = 1, \dots, m-1$).

Every sequence $\xi = (\ldots \xi_{-1}.\xi_0\xi_1 \ldots) \in \Sigma$ is of the form $\xi = \xi^-.\xi^+$, where $\xi^+ \in \Sigma^+$ and $\xi^- \in \Sigma^-$ ($\Sigma^\pm$ are defined in the obvious way). A one-sided infinite sequence $\xi^- = (\ldots \xi_{-2}\xi_{-1}.) \in \Sigma^-$ is *admissible* for x if $(\xi_{-m} \ldots \xi_{-1})$ is admissible for x for all $m \geq 1$. Note that admissibility of a sequence ξ does not depend on ξ^+. By writing (ξ, x) we always suppose that ξ^- is admissible for x.

3.3 Expanding Itineraries and Covering Property

We begin by stating a simple (but important) expansion property of the IFS generated by f_0 and f_1.

Lemma 1 (Expansion property). *Assume that conditions (F0), (F1), and (F01) hold. Then there are $\kappa > 1$ and $b > 0$ close to 0 such that for any interval $J \subset [f_0^{-2}(b), b]$ there is a number $n(J)$ (uniformly bounded) such that for every $x \in J$*

$$\left(f_1 \circ f_0^{n(J)}\right)(x) \in (0, b] \quad \text{and} \quad |(f_1 \circ f_0^{n(J)})'(x)| \geq \kappa$$

Proof. For simplicity assume linearity of f_0 close to 0 and 1. Note that there are small $b > 0$ and large n such that (recall the definitions of β_0 and λ_0)

$$f_0^n([\beta_0^{-1} b, b]) = [1 - b, 1 - \lambda_0 b],$$

From the monotonicity of f_0' and $J \subset [\beta_0^{-2} t, t]$ we get that, for all $x \in J$,

$$(f_0^n)'(x) \geq \frac{\lambda_0^2 (1 - \lambda_0)}{1 - \beta_0^{-1}}.$$

Let $n(J) = n$ if $f_0^n(J) \subset [1 - b, 1]$ and $n(J) = n + 1$ otherwise. This implies that for all $x \in J$ we have

$$(f_0^{n(J)})'(x) \geq \frac{\lambda_0^3 (1 - \lambda_0)}{1 - \beta_0^{-1}}.$$

Thus, by (F01),

$$|(f_1 \circ f_0^{n(J)})'(x)| \geq \gamma \left(\frac{\lambda_0^3 (1 - \lambda_0)}{1 - \beta_0^{-1}}\right) > \kappa > 1.$$

Noting that $f_0^{n(J)}(J) \subset [1 - b, 1 - \lambda_0^2 b]$ we get $f_1 \circ f_0^{n(J)}(J) \subset (0, \gamma b] \subset (0, b]$, proving the lemma. □

We now deduce some consequences from the above lemma. To each interval $J \subset [f_0^{-2}(b), b]$ we associate the sequence $\xi(J) = (0^{n(J)}\,1\,0^{m(J)})$, where $m(J)$ is the first positive integer such that $(f_0^k \circ f_1 \circ f_0^{n(J)})(J)$ intersects $[f_0^{-1}(b), b)]$. Note that $m(J) \geq 0$ and that the restriction of $f_0^{m(J)} \circ f_1 \circ f_0^{n(J)}$ to J is uniformly expanding. Moreover, there is κ independent of J such that

$$|f_{[\xi(J)]}(J)| = |f_{[0^{n(J)}10^{m(J)}]}(J)| \geq \kappa |J|.$$

We say that $\xi(J)$ is the *expanding return* of J to $[f_0^{-2}(b), b]$ and that $f_{[\xi(J)]}(J)$ is the *expanded successor* of J.

Lemma 2 (Covering and expanding properties). *Assume that conditions (F0), (F1), and (F01) hold. Then for every interval $J \subset [f_0^{-2}(b), b]$ there is a finite sequence $\eta(J) = (0^{n_0}\,1\,0^{m_0} \ldots 0^{n_\ell}\,1\,0^{m_\ell})$ such that*

1. *$f_{[\eta(J)]}$ is uniformly expanding in J,*
2. *$f_{[\eta(J)]}(J)$ contains $[f_0^{-2}(b), f_0^{-1}(b)]$.*

This above lemma follows from considering recursively the expanding returns and the expanded successors of J. Let $J = J_0$ and inductively define J_{j+1} to be the expanded successor of $J_j \subset [f_0^{-2}(b), b]$. Since

$$|J_{j+1}| \geq \kappa\, |J_j| \geq \kappa^{j+1}\, |J_0|,$$

and $\kappa > 1$ there is smallest number $\ell = \ell(J)$ such that $J_{\ell+1}$ is not contained in $[f_0^{-2}(b), b]$ and thus contains $[f_0^{-2}(b), f_0^{-1}(b)]$. Now it is enough to consider the concatenation $\eta(J)$ of the expanding returns $\xi(J_0), \xi(J_1), \ldots, \xi(J_\ell)$.

An immediate consequence of the previous lemma is the following.

Corollary 1. *Assume that conditions (F0), (F1), and (F01) hold. Consider any closed interval $J \subset [f_0^{-2}(b)\, f_0^{-1}(b)]$ and its sequence $\eta(J)$. Then the map $f_{[\eta(J)]}$ has an expanding fixed point $q_J^* \in J$ whose unstable manifold $W^u(q_J^*, f_{[\eta(J)]})$ contains $[f_0^{-2}(b), f_0^{-1}(b)]$.*

An important property of the previous construction is that it *only* involves iterations in an interval that does not contain the point 0.

Remark 1 (Backward covering property). Condition (F_B) guarantees that for every point $x \in [0, 1]$

$$\max \left\{ |(f_0^{-1})'(x)|, |(f_1^{-1})'(x)| \right\} \geq \varrho > 1.$$

This implies that every point $x \in [0, 1]$ has an admissible negative sequence $\eta^- = (\ldots, \eta_{-n} \ldots \eta_{-1})$ satisfying for every n

$$|f'_{[\eta_{-n} \ldots \eta_{-1}.]}(x)| > \varrho^n.$$

This property is used to define backward expanding successors in the same spirit as before. Arguing as in [3], we get that the pre-orbit of any open interval $J \subset [0,1]$ contains the point $(1-\gamma)$ and therefore the points $0 = f_1^{-1}(1-\gamma)$ and $1 = f_1^{-1}(0)$. In particular, since $W^u(1, f_1) \supset (0,1]$, the backward orbit of J covers the whole interval $(0,1]$. This covering property for backward iterations is similar to the one in Lemma 2 (for forward iterations).

3.4 Minimality

We now study the minimality of the IFS generated by the fiber maps. Recall that a map $f: X \to X$ defined on a metric space X is *minimal* if any closed proper subset Y of X with $f(Y) \subset Y$ is empty. Consider now the IFS by $\{f_0, f_1\}$, this IFS is *forward minimal* if each closed proper subset $Y \subset [0,1]$ such that $f_{[\xi_0 \dots \xi_k]}(Y) \subset Y$ for all finite sequence $(\xi_0 \dots \xi_k)$ is empty.

Given a point $x \in [0,1]$ consider the set of all forward images of x,

$$\mathcal{O}^+(x) := \{f_{[\eta_0 \dots \eta_n]}(x) : \eta_i \in \{0,1\},\ n \geq 0\}$$

The forward minimality of the IFS is equivalent to the density of $\mathcal{O}^+(x)$ in $[0,1]$ for every x.

We can also study backward minimality of this IFS considering the inverse maps f_0^{-1}, f_1^{-1} and a characterization using dense backward orbits. Observe that not all backward concatenations are possible and that we need to focus on the admissible ones. Consider the set of all pre-images of x under the IFS.

$$\mathcal{O}^-(x) := \{f_{[\eta_{-n} \dots \eta_{-1}.]}(x) : \eta^- \text{ is admissible for } x \text{ and } n \geq 1\}.$$

Note that in our case $\mathcal{O}^-(1) = \{1\}$ and $\mathcal{O}^-(0) = \{0,1\}$ and thus the IFS is not backward minimal. However, next proposition claims that these two points are the only points of exception.

Proposition 1 (Minimality). *Assume that (F0), (F1), (F01), and (F_B) are satisfied. Then the set $\mathcal{O}^+(x)$ is dense in $[0,1]$ for every $x \in [0,1]$ and the set $\mathcal{O}^-(x)$ is dense in $[0,1]$ for every $x \in (0,1)$.*

The density of $\mathcal{O}^+(x)$ follows from Remark 1 that implies that for every point $x \in (0,1]$ and every open set $U \subset [0,1]$ there are a open set $V \subset U$ and a finite sequence $(\eta_{-n} \dots \eta_{-1})$ such that $x \in f_{[\eta_{-n} \dots \eta_{-1}.]}(V)$. Thus $f_{[\eta_{-1} \dots \eta_{-n}]}(x) \in V$. This implies the density of $\mathcal{O}^+(x)$ for all $x \in (0,1]$. For $x = 0$ just note that $f_1(0) \in (0,1)$ and thus the forward orbit of 0 is also dense in $[0,1]$.

To get the density of the pre-orbits $\mathcal{O}^-(x)$ it is enough to see that for every open interval $J \subset [0,1]$ and every point $p \in (0,1)$ there is a sequence $(\eta_0 \dots \eta_m)$ with $p \in f_{[\eta_0 \dots \eta_m]}(J)$. This is guaranteed by the next lemma.

Lemma 3. *Assume that (F0), (F1), and (F01) hold. Then for every* $p \in (0,1)$ *and every interval* $J \subset (0,1)$ *there is a finite sequence* $(\eta_0 \dots \eta_m)$ *such that*

$$f_{[\eta_0 \dots \eta_m]}(J) \supset [p - \delta/2, p + \delta/2].$$

An important fact in this lemma (in order to control derivatives) is that the covering property holds in some sense uniformly: if $p \in (\Delta, 1-\Delta)$, $J \subset (\Delta, 1-\Delta)$, and $|J| \geq \tau$ then the length of the finite sequence $(\eta_0 \dots \eta_m)$ can be bounded uniformly by some number depending only on Δ and τ.

Lemma 3 immediately follows from Lemma 2 when p and J are contained in $[f_0^{-2}(b), f_0^{-1}(b)]$. In the general case, note that for ℓ sufficiently large $f_0^{\ell}(J)$ is close to 1 and thus $f_1 \circ f_0^{\ell}(J) \subset (0, f^{-2}(b))$. Considering further iterations by f_0 we get $m > 0$ such that (after shrinking J if necessary)

$$J_0 = f_0^m \circ f_1 \circ f_0^{\ell}(J) \subset [f^{-2}(b), f_0^{-1}(b)].$$

We can now consider forward expanding returns of the interval J_0 to eventually cover $[f^{-2}(b), f_0^{-1}(b)]$. This provides a finite sequence $(\xi_0 \dots \xi_k)$ such that

$$[f_0^{-2}(b), f_0^{-1}(b)] \subset f_{[\xi_0 \dots \xi_k]}(J).$$

As $[f_0^{-2}(b), f_0^{-1}(b)]$ is a fundamental domain of f_0 and the forward orbit of b by f_0 accumulates to 1 this implies that

$$[f_0^{-2}(b), 1) \subset \bigcup_{i \geq 0} f_{[\xi_0 \dots \xi_k 0^i]}(J).$$

The cycle property $f_1(1) = 0$ and the fact that b is close to 0 imply that

$$(0,1) \subset \Big(\bigcup_{i \geq 0} f_{[\xi_0 \dots \xi_k 0^i]}(J) \Big) \cup \Big(\bigcup_{i \geq 0} f_{[\xi_0 \dots \xi_k 0^i 1]}(J) \Big),$$

which implies the lemma.

3.5 *Creation of Periodic Points*

An uniform version of Lemma 3 implies that given any interval $[p - \delta, p + \delta] \subset (0,1)$, small $\delta > 0$, there is a sequence $(\eta_0 \dots \eta_m)$ with $f_{[\eta_0 \dots \eta_m]}([p - \delta, p + \delta]) \supset [p - \delta, p + \delta]$. This provides a fixed point q of $f_{[\eta_0 \dots \eta_m]}$ close to p. If the sequence $(\eta_0 \dots \eta_m)$ mainly consists of segments corresponding to expanding returns one gets an expanding point. Much more interesting is that it is possible to choose (with some constrains, see Sect. 3.6) the value of $f'_{[\eta_0 \dots \eta_m]}(q)$. For this one considers

combinations of expanding returns (providing expansion) and consecutive iterates of f_0 (providing contraction). Of course, bounded variation of the derivatives and control of the distortion are involved in these calculations.

3.6 Spectral Gap

We now discuss the existence of an spectral gap. First, given a point $x \in [0,1]$ and a sequence $\xi \in \Sigma$, the *upper (forward) Lyapunov exponent* of x with respect to ξ is defined by

$$\overline{\chi}^+(\xi, x) := \limsup_{n\to\infty} \frac{1}{n} \log |(f_{[\xi_0 \dots \xi_{n-1}]})'(x)|.$$

The lower exponent $\underline{\chi}^+$ is defined analogously taking lim inf instead of lim sup. We can also define backward exponents $\overline{\chi}^-$ and $\underline{\chi}^-$ in a similar way. In this case we can only consider admissible pairs (ξ, x) When the lim inf and the lim sup are equal we speak simply of forward and backward Lyapunov exponents $\chi^\pm$.

Assume, for instance, that $\Sigma = \Sigma_3$ and consider the set $\mathcal{E}$ of *exceptional points* defined by

$$\begin{aligned}\mathcal{E} := \big\{(\xi, 0) &: \xi \in \{0,2\}^{\mathbb{Z}}\big\} \cup \\ &\big\{\big((0^{-\mathbb{N}}.0^k\, 1\, \xi^+), 1\big), \big((0^{-\mathbb{N}}\, 1\, \xi_k.\xi^+), 0\big) : k \geq 0, \xi_k \in \{0,2\}^k, \xi^+\big\} \quad (3)\end{aligned}$$

where $\xi^+ \in \{0,2\}^{\mathbb{N}}$. That is, the set $\mathcal{E}$ codes all points in the "full lateral horseshoe" Λ_{02} (recall "Lateral Horseshoe Condition" in Sect. 3.1) together with its stable manifold.

Let us assume that $\log \beta_2$ is close to but smaller than $\log \beta_0$. For points in the exceptional set $\mathcal{E}$ the exponents are in $[\log \beta_2, \log \beta_0]$. We claim that the points in $\Lambda \setminus \Lambda_{02}$ have exponent less than some number $\log \tilde{\beta} < \log \beta_2$. The heuristic argument is the following. Due to monotonicity of the maps f_0, f_2 and their derivatives, the only way that a point $x \in \Lambda \setminus \Lambda_{02}$ could have a central Lyapunov exponent close to $[\log \beta_2, \log \beta_0]$ is when its orbit would stay close to Λ_{02} for a long time. By the cycle configuration, such an orbit previously visited a small neighborhood of 1 for a long time (a comparable amount of time). The latter introduces a contraction that compensates the expansion corresponding to the iterates close to Λ_{02}. Consequently the central Lyapunov exponent of these points is smaller than some number $\log \tilde{\beta} < \log \beta_2$.

Proposition 2 (Spectral gap). *Under hypotheses (F0), (F1), (F2), and (F01),*

$$\exp\Big(\sup\big\{\overline{\chi}^+(\xi, x) : (\xi, x) \notin \mathcal{E}\big\}\Big) := \tilde{\beta} < \beta_2.$$

This result holds also for the case of two generators (in such a case (F2) is superfluous). Indeed, in [13] it is proved that under quite natural conditions the central spectrum has exactly one gap. More precisely we have the following.

Theorem 1. *Under assumptions (F0), (F1), (F01), and (F_{B}) the IFS satisfies the following: There is $0 < \tilde{\beta} < \beta_0$ such that*
Forward spectrum:

(i) For every $\chi \in [0, \log \tilde{\beta}\,]$ the set of points y such that there exists $\xi^+ \in \Sigma^+$ with $\chi_+(y, \xi^+) = \chi$ is dense in $[0, 1]$.
(ii) For every $\chi \in [\log \lambda, 0]$ there exists $\xi^+ \in \Sigma^+$ with $\chi_+(y, \xi^+) = \chi$ for every $y \in [0, 1]$.

Backward spectrum:

(iii) For every $\chi \in [0, \log \tilde{\beta}\,]$ and for every $y \in (0, 1)$ there exists $\xi^- \in \Sigma^-$ with $\chi_-(y, \xi^-) = \chi$.
(iv) For every $\chi \in [\log \lambda, 0]$ the set of points y for which there exists $\xi^- \in \Sigma^-$ with $\chi_-(y, \xi^-) = \chi$ is dense in $[0, 1]$.

In view of these constructions, the problem of the existence of examples whose spectrum has several gaps raises in a natural way. In [14] there are given examples where the lateral horseshoe splits into finitely many disjoint horseshoes Λ_j coded by a subshift H_j, $j = 1, \ldots, \ell$, such that

$$\{\underline{\chi}(\xi, 0), \overline{\chi}(\xi, 0) \colon \xi \in H_\ell\} = [\alpha_j^-, \alpha_j^+],$$

where $\alpha_j^+ < \alpha_{j+1}^-$. This construction leads to a Lyapunov spectrum with gaps $(\alpha_\ell^+, \alpha_{\ell-1}^-), \ldots, (\alpha_2^-, \alpha_1^+)$.

4 Topological Dynamics

We next discuss aspects of the topological dynamics of the porcupine horseshoes. These properties are consequence of the properties of the IFS in the previous section. In the next result we assume that the porcupine is fibered over a horseshoe conjugate to Σ_2 (i.e., we just consider the maps f_0 and f_1). A similar result can be stated for porcupines fibered over Σ_3.

Theorem 2. *Assume that conditions (F0), (F1), and (F01) hold and let F be the associated skew-product diffeomorphism. Then the maximal invariant set Λ of F in* **C***, see (2), satisfies the following properties:*

- *The set Λ is the relative homoclinic class in* **C** *of a saddle of unstable index two. In particular, Λ is transitive and the set of periodic points of unstable index two is dense in Λ.*
- *The set of periodic points of unstable index one is dense in Λ.*

- *There is an uncountable and dense subset of sequences $\xi \in \Sigma$ such that $\varpi^{-1}(\xi)$ is nontrivial. The set of nontrivial spines is dense in Λ.*
- *There is a residual subset of sequences $\xi \in \Sigma$ such that $\varpi^{-1}(\xi)$ is trivial. The set of trivial spines is dense in Λ.*

4.1 Transitivity

We now sketch the proof of the transitivity of Λ. Let $q^* = q^*_J$ be the expanding point of $f_{[\eta(J)]}$ in Corollary 1. Consider the periodic sequence $(\eta(J))^{\mathbb{Z}}$ and the periodic point Q^* of F associated to it whose central coordinate is q^*. This point has unstable index two. We see that Λ is the homoclinic class of Q^* relative to $\mathbf{C}$.

Condition $[f_0^{-2}(b), f_0^{-1}(b)] \subset W^u(q^*, f_{[\eta(J)]})$ implies that the unstable manifold of the orbit of Q^* transversely intersects every stable segment of the form $[0,1] \times \{(x^u, x)\}$ with $x \in (0,1)$. Similarly, the stable manifold $W^s(Q^*, F)$ of the orbit of Q^* transversely intersects any center-unstable disk $\{x^s\} \times [0,1] \times J$ such that $J \subset (0,1)$ is a fundamental domain of f_0.

An *inner point* of Λ is a point $X = (x^s, x^u, x) \in \Lambda$ such that for all $i \in \mathbb{Z}$ the central central coordinate x_i of $F^i(X) = (x_i^s, x_i^u, x_i)$ belongs to $(0,1)$. Let us just explain why inner points are in in the (relative) homoclinic class of Q^*. This is the main step of the proof of the transitivity of Λ.

Given any small $\delta > 0$ consider the stable segment centered at X,

$$\Delta^s_\delta(X) := [x^s - \delta, x^s + \delta] \times \{(x^u, x)\}.$$

Using that F^{-1} uniformly expands the x^s-direction, we get some n such that

$$F^{-n}(\Delta^s_\delta(X)) \supset [0,1] \times \{(x^u_n, x_n)\}.$$

By the previous comments, $\Delta^s_\delta(X)$ transversely intersects the unstable manifold $W^u(Q^*, F)$ of the orbit of Q^*. Let

$$X_\delta := (x^s_\delta, x^u, x) \in \Delta^s_\delta(X) \pitchfork W^u(Q^*, F)$$

and for small $\varepsilon > 0$ consider the center-unstable rectangle

$$\Delta^{cu}_\varepsilon(X_\delta) := \{x^s_\delta\} \times [x^u - \varepsilon, x^u + \varepsilon] \times [x - \varepsilon, x + \varepsilon] \subset W^u(Q^*, F).$$

We claim that $\Delta^{cu}_\varepsilon(X_\delta)$ intersects $W^s(Q^*, F)$ transversely. This immediately implies $\Delta^{cu}_\varepsilon(X(\delta))$ contains a transverse homoclinic Y point of Q^*. As δ and ε can be chosen arbitrarily small, the point Y can be taken arbitrarily close to X. Moreover, since we just consider iterations in $\mathbf{C}$, the whole orbit of Y is contained in $\mathbf{C}$. Thus Y is a transverse homoclinic point relative to $\mathbf{C}$ and hence X is in the relative homoclinic class of Q^*.

To prove our claim, $\Delta^{cu}_{\varepsilon}(X_\delta) \pitchfork W^s(Q^*, F)$, note first that (due to uniform expansion in the x^u-direction) after positive iterations by F of $\Delta^{cu}_{\varepsilon}(X(\delta))$ one gets a "large disk" of the form $\{y^s\} \times [0,1] \times I$, where I is an interval in $(0,1)$. Using the heterodimensional cycle associated to P_0 and Q_0, after further forward iterates, one gets a disk $\{z^s\} \times [0,1] \times J$, where $J \subset (f_0^{-2}(b), b)$. We can now apply Lemma 2 to the interval J to get a finite sequence $(\xi_0 \dots \xi_m)$ such that $f_{[\xi_0 \dots \xi_m]}(J)$ covers a fundamental domain D of f_0 in $(0,1)$. Putting together these comments we get large N such that $F^N(\Delta^{cu}_{\varepsilon}(X(\delta)))$ contains a center-unstable rectangle of the form $\{x^s\} \times [0,1] \times D$. As D is a fundamental domain of f_0 the comments above imply that $W^s(Q^*, F)$ transversely meets $\Delta^{cu}_{\varepsilon}(X(\delta))$.

This type of arguments can be used to prove that every pair of interior saddles of unstable index two are homoclinically related. Note that the interior assumption is essential: the exposed saddle Q_0 of unstable index two is not related to other saddles.

Finally, let us observe that if condition (F_B) is satisfied the same kind or arguments implies that Λ is the relative homoclinic class of P_0 (indeed of any saddle of unstable index one in Λ).

4.2 Structure of the Spines

First observe that any spine containing a saddle of unstable index two (thus expanding in the central direction) is nontrivial. This immediately follows from $f_i([0,1]) \subset [0,1]$, that implies that the extremes of a periodic spine are either attracting or neutral in the central direction. As the periodic points of unstable index two are dense in Λ, the set of nontrivial spines is also dense in Λ.

To describe the spines, given a sequence $\xi = \xi^- \xi^+$, $\xi^- = (\dots \xi_{-m} \dots \xi_{-1})$ we define the pre-spine of m-th generation by $I_{[\xi_{-m} \dots \xi_{-1}.]}$ as the domain of definition of $f_{[\xi_{-m} \dots \xi_{-1}.]}$. These sets are nontrivial sub-intervals of $[0,1]$ forming a decreasing nested sequence. Note that if $-m-1=0$ then $I_{[\xi_{-m-1}\xi_{-m} \dots \xi_{-1}.]} = I_{[\xi_{-m} \dots \xi_{-1}.]}$. We define

$$I_{[\xi]} := \bigcap_{m \geq 1} = I_{[\xi_{-m} \dots \xi_{-1}.]}.$$

Note that the positive of a tail of ξ plays no role in the definition of $I_{[\xi]}$. By construction, we obtain the spine $\varpi^{-1}(\xi) = \{X_\xi\} \times I_{[\xi]}$.

Note that for each m the map $\xi \mapsto |I_{[\xi_{-m} \dots \xi_{-1}.]}|$ is continuous. This implies that the map $\xi \mapsto |I_{[\xi]}|$ is upper semi-continuous. Also it is not difficult to see that the set of ξ whose spines have length less than $1/n$ is open and dense in Σ. These two facts immediately implies that the set of sequences with trivial spines is a residual subset of Σ.

Roughly speaking, to get a trivial spine it is enough to consider sequences whose negative tail contains long sequences of consecutive 1s, that corresponds to

backward expansions. This implies that after some negative iterations a significant part of the m-th spine will be mapped outside $[0,1]$ and thus be removed. Conversely, to get nontrivial spines one considers sequences whose negative part contains a huge amount of 0s.

5 Ergodic Properties

5.1 Central Spectrum: Lyapunov Exponents

Note that the porcupine Λ is partially hyperbolic with a dominated splitting $E^s \oplus E^c \oplus E^u$, where E^c is parallel to $\{0^2\} \times \mathbb{R}$. In particular, for every Lyapunov regular point $R \in \Lambda$ this splitting coincides with the Oseledec one provided by the multiplicative ergodic theorem. Thus the *Lyapunov exponent associated to the central direction* E^c at such regular point R is well-defined and equal to the Birkhoff average of the continuous map $R \mapsto \log \|dF|_{E^c_R}\|$,

$$\chi_c(R) := \lim_{n\to\infty} \frac{1}{n} \log \|dF^n|_{E^c_R}\| = \lim_{n\to\infty} \frac{1}{n} \sum_{k=0}^{n-1} \log \|dF|_{E^c_{F^k(R)}}\|.$$

Write $R = (r^s, r^u, r) \in \Lambda$ and consider the sequence $\xi = (\ldots \xi_{-1}.\xi_0\xi_1 \ldots) = \pi(R)$. Since the central dynamics is determined by the fiber IFS we have that

$$\chi_c(R) = \lim_{n\to\infty} \frac{1}{n} \log |(f_{[\xi_0 \ldots \xi_{n-1}]})'(r)|.$$

This formula estates the relation between the Lyapunov exponents of the IFS studied in Sect. 3.6 and the central Lyapunov exponents of the porcupine.

Finally, observe that the remaining exponents of the porcupine are associated to the stable and the unstable hyperbolic directions, thus they are uniformly bounded away from zero.

Let us observe that as a consequence of our results and the methods for constructing nonhyperbolic ergodic measures with large support introduced in [18] and further developed in [5] one can construct ergodic measures with full support in the porcupine having a central exponent in $[\log \lambda_0, \log \tilde{\beta})$.

5.2 Thermodynamic Formalism

Let us finally explain the thermodynamic consequences of the spectral gaps. Given a continuous function $\varphi\colon \Lambda \to \mathbb{R}$, the topological pressure $P(\varphi)$ of φ is defined in

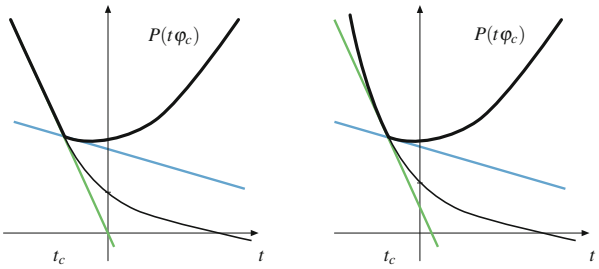

Fig. 4 First order and rich first order phase transitions

purely topological terms, but can be expressed in measure-theoretic terms via the variational principle [32]

$$P(\varphi) = \sup_{\mu \in \mathcal{M}(\Lambda)} \left(h(\mu) + \int \varphi \, d\mu \right), \tag{4}$$

where $h(\mu)$ denotes the entropy of the measure μ and the supremum is considered in the set $\mathcal{M}(\Lambda)$ of ergodic F-invariant measures supported on Λ. A measure μ is called *equilibrium state* if it attains the supremum in (4). By [9,32] such states exist.

Non-differentiability of P is closely related to the coexistence of equilibrium states. The question of existence and uniqueness of equilibrium states has been studied in several contexts already. In [31] in the context of uniformly expanding C^2 circle maps uniqueness was derived for any φ satisfying $P(\varphi) > \sup \varphi$. This condition is essential.

It is an immediate consequence of (4) that for every $t \in \mathbb{R}$ we have $P(t\varphi_c) \geq \sup(t\varphi_c)$. Observe that to each measure μ the graph of the map $t \mapsto h(\mu) - t \int \varphi_c \, d\mu$ gives a line below the graph of the function $P(t) := P(t\varphi_c)$. Hence, by (4) the function $P(t)$ is convex. Recall that $P(t)$ is real analytic if Λ is a basic set [29]. The pressure function $P(t)$ exhibits a *phase transition* at a characteristic parameter t_* if it fails to be real analytic at t_*.

In the case that $\sup(-\varphi_c)$ is attained in a single point $R \in \Lambda$ (which is the case in one of our models, where R is the exposed saddle) then exactly one of the following two cases is true: either $P(t)$ converges to the line $t \mapsto t\varphi_c(R)$ as $t \to -\infty$ (in which case there would be ergodic measures with central exponent converging to $-\varphi_c(R)$) or we have $P(t) = t\varphi_c(R)$ for every $t \leq t_*$ for some $t_* < 0$ (in which case $P(t)$ is not analytic at t_*). As we showed that there is a gap in the central Lyapunov spectrum, we are in the second case. In fact, it implies that there is a *first order phase transition* at t_*, that is, $P(t)$ fails to be differentiable at t_* and there exist (at least two) ergodic equilibrium states with exponents equal to the negative of the left/right derivatives at t_*. We call this transition *rich* if there exist (at least two) equilibrium states with positive entropy. This is exactly what happens in the case when the exposed piece is a horseshoe.

Two different types of phase transitions we obtain are depicted in Fig. 4 (compare also the examples of different types of exposed pieces discussed in Sect. 1.2).

Studying in [12] extensions of Bernoulli measures in the lateral horseshoe, it can be concluded that the transitive set containing intermingled hyperbolic sets of different indices is in a sense essentially contracting: the part with nonpositive central exponent carries larger entropy. The right derivative of the pressure function at $t = 0$ is nonnegative (there is a measure of maximal entropy with nonpositive central Lyapunov exponent). This has as a consequence that the maximal entropy that can be obtained from an embedded hyperbolic horseshoe with unstable index 2 is smaller than the one obtained from horseshoes with unstable index 1.

Acknowledgements This paper was partially supported by CNPq (research grants and Projeto Universal), CNE Faperj, and Pronex (Brazil) and Balzan Research Project of J. Palis.

References

1. Abdenur, A., Bonatti, Ch., Crovisier, S., Díaz, L.J., Wen, L.: Periodic points and homoclinic classes. Ergod. Theory Dyn. Syst. **27**, 1–22 (2007)
2. Baladi, V., Bonatti, Ch., Schmitt, B.: Abnormal escape rates from nonuniformly hyperbolic sets. Ergod. Theory Dyn. Syst. **19**, 1111–1125 (1999)
3. Bonatti, Ch., Díaz, L.J., Viana, M.: Discountinuity of Hausdorff dimension of hyperbolic sets. Comptes Rendus de Academie de Sciencies de Paris **320-I**, 713–718 (1995)
4. Bonatti, Ch., Díaz, L.J., Viana, M.: Dynamics Beyond Uniform Hyperbolicity: A Global Geometric and Probabilistic Perspective. Mathematical Physics, III (Encyclopaedia of Mathematical Sciences, vol. 102). Springer, Berlin (2005)
5. Bonatti, Ch., Díaz, L.J., Gorodetski, A.: Non-hyperbolic ergodic measures with large support. Nonlinearity **23**, 687–705 (2010)
6. Bonatti, Ch., Crovisier, S., Gourmelon, N., Potrie, R.: Tame dynamics and robust transitivity (2011, Preprint). arXiv:1112.1002
7. Cao, Y., Luzzatto, S., Rios, I.: Some non-hyperbolic systems with strictly non-zero Lyapunov exponents for all invariant measures: horseshoes with internal tangencies. Discret. Contin. Dyn. Syst. **15**, 61–71 (2006)
8. Cowieson W., Young, L.-S.: SRB measures as zero-noise limits. Ergod. Theory Dyn. Syst. **25**, 1115–1138 (2005)
9. Díaz, L.J., Fisher, T.: Symbolic extensions and partially hyperbolic diffeomorphisms. Discret. Contin. Dyn. Syst. **29**, 1419–1441 (2011)
10. Díaz, L. J., Gelfert, K.: Procupine-like horseshoes: transitivity, Lyapunov spectrum, and phase transitions. Fundam. Math. **216**, 55–100 (2012)
11. Díaz, L.J., Horita, V., Rios, I., Sambarino, M.: Destroying horseshoes via heterodimensional cycles: generating bifurcations inside homoclinic classes. Ergod. Theory Dyn. Syst. **29**, 433–473 (2009)
12. Díaz, L.J., Gelfert, K., Rams, M.: Rich phase transitions in step skew products. Nonlinearity **24**, 3391–3412 (2011)
13. Díaz, L.J., Gelfert, K., Rams, M.: Almost complete Lyapunov spectrum in step skew-products. Dyn. Syst. **28**, 76–110 (2013)
14. Díaz, L.J., Gelfert, K., Rams, M.: Abundant rich phase transitions in step skew products (2013, Preprint). arXiv:1303.0581
15. Dobbs, N.: Renormalisation induced phase transitions for unimodal maps. Commun. Math. Phys. **286**, 377–387 (2009)
16. Gorodetski, A.: Minimal attractors and partially hyperbolic invariant sets of dynamical systems. PhD thesis, Moscow State University (2001)

17. Gorodetski, A., Ilyashenko, Yu.: Certain new robust properties of invariant sets and attractors of dynamical systems. Funct. Anal. Appl. **33**, 95–105 (1999)
18. Gorodetski, A., Ilyashenko, Yu., Kleptsyn, V., Nalskij, M.: Non-removable zero Lyapunov exponent. Funct. Anal. Appl. **39**, 27–38 (2005)
19. Hardy, G.H.: Weierstrass's non-differentiable function. Trans. Am. Math. Soc. **17**, 301–325 (1916)
20. Ilyashenko, Yu.: Thick and bony attractors. Conference talk at the topology, geometry, and dynamics, Rokhlin Memorial, St. Petersburg, 11–16 Jan (2010)
21. Ilyashenko, Yu.: Multidimensional bony attractors. Funct. Anal. Appl. **46**, 239–248 (2012)
22. Keller, G.: A note on strange nonchaotic attractors. Fundam. Math. **151**, 139–148 (1996)
23. Kleptsyn, V., Nalsky, M.: Persitence of nonhyperbolic measures for C^1-diffeomorphisms. Funct. Anal. Appl. **41**, 271–283 (2007)
24. Kleptsyn, V., Volk, D.: Skew products and random walks on the unit interval (2011, Preprint). arXiv:1110.2117
25. Kudryashov, Yu.G.: Bony attractors. Funct. Anal. Appl. **44**, 219–222 (2010)
26. Leplaideur, R., Oliveira, K., Rios, I.: Equilibrium states for partially hyperbolic horseshoes. Ergod. Theory Dyn. Syst. **31**, 179–195 (2011)
27. Makarov N., Smirnov, S.: Phase transition in subhyperbolic Julia sets. Ergod. Theory Dyn. Syst. **16**, 125–157 (1996)
28. Makarov, N., Smirnov, S.: On 'thermodynamics' of rational maps: I. Negative spectrum. Commun. Math. Phys. **211**, 705–743 (2000)
29. Ruelle, D.: Thermodynamic Formalism. The Mathematical Structures of Classical Equilibrium Statistical Mechanics. Encyclopedia of Mathematics and Its Applications. Addison-Wesley, Reading (1978)
30. Sigmund, K.: On dynamical systems with the specification property. Trans. Am. Math. Soc. **190**, 285–299 (1974)
31. Urbaśki, M.: Invariant subsets of expanding mappings of the circle. Ergod. Theory Dyn. Syst. **7**, 627–645 (1987)
32. Walters, P.: An Introduction to Ergodic Theory. Graduate Texts in Mathematics, vol. 79. Springer, New York (1981)

Planar Filippov Systems with Maximal Crossing Set and Piecewise Linear Focus Dynamics

Emilio Freire, Enrique Ponce, and Francisco Torres

Abstract This paper includes some new results and a survey of known bifurcations for a family of Filippov systems. Such a family is constituted by planar piecewise linear systems with a discontinuity line where the crossing set is maximal and it has two dynamics of focus type. From the natural 12 parameters needed we obtain, under some generic conditions, a Liénard canonical form topologically equivalent to the original system with only four parameters. We describe, taking into account the number of equilibria inside each zone of linearity: zero, one or two, the qualitatively different phase portraits that can occur and the bifurcations connecting them.

1 Introduction

Piecewise linear systems (PWL) are the natural extension of linear systems in order to capture nonlinear behavior. They are extensively used to model biological process as well as electronics and mechanical devices, see for instance [2] and [11]. The simplest family of PWL systems is the planar case constituted by two linear systems continuously matched along a straight line. Such a family was carefully studied in [3], where some canonical forms with only four parameters were introduced. In particular, the existence of at most one limit cycle was established.

Enforced by new applications in nonlinear engineering and mathematical biology, planar PWL systems with a straight line as the discontinuity manifold have deserved the attention by researchers. To fix ideas, let us assume without loss of generality that the phase plane is divided in the two linearity regions

$$S^- = \{(x, y) : x < 0\}, \quad S^+ = \{(x, y) : x > 0\},$$

E. Freire (✉) · E. Ponce · F. Torres
Departamento Matemática Aplicada II, E.T.S. Ingeniería, 41092-Sevilla, Spain
e-mail: efrem@us.es; eponcem@us.es; ftorres@us.es

S. Ibáñez et al. (eds.), *Progress and Challenges in Dynamical Systems*,
Springer Proceedings in Mathematics & Statistics 54,
DOI 10.1007/978-3-642-38830-9_13,

so that our systems are constituted by two linear systems discontinuously gluing along the line $\Sigma = \{(x, y) : x = 0\}$. That is, the systems to be studied are,

$$\dot{\mathbf{x}} = \mathbf{F}(\mathbf{x}) = \begin{cases} \mathbf{F}^-(\mathbf{x}) = \left(F_1^-(\mathbf{x}), F_2^-(\mathbf{x})\right)^T = A^-\mathbf{x} + \mathbf{b}^-, & x \in S^-, \\ \mathbf{F}^+(\mathbf{x}) = \left(F_1^+(\mathbf{x}), F_2^+(\mathbf{x})\right)^T = A^+\mathbf{x} + \mathbf{b}^+, & x \in S^+. \end{cases} \tag{1}$$

where $\mathbf{x} = (x, y)^T$, A^+ and A^- are 2×2 matrices and $\mathbf{b}^+ = (b_1^+, b_2^+)^T$ and $\mathbf{b}^- = (b_1^-, b_2^-)^T$ are constant vectors.

Obviously, the orbits living in only one zone are well defined. When a orbit arrives to the discontinuity line Σ we should adopt some rules, so that the solutions are uniquely defined in forward time. Different things can happen.

If $F_1^-(0, y)F_1^+(0, y) = (a_{12}^- y + b_1^-)(a_{12}^+ y + b_1^+) > 0$, then both vector fields are transversal to the discontinuity line having their normal components the same sign. In this case, the orbits are concatenated in the natural way, so that an orbit coming from a linearity zone crosses towards the other linearity zone with a discontinuity in the vector tangent. We say that this point is a *crossing point* and the set of the crossing points is termed the *crossing set* Σ^c.

If $F_1^-(0, y)F_1^+(0, y) \leq 0$, then either the normal components of vector fields to the discontinuity line have opposite sign or at least one of them vanishes. Here, we speak of a *sliding point* and the set of the sliding points, which is the complementary of the crossing set, is named the *sliding set* Σ^s. In this case, according to the convex method of Filippov, we should assume that the orbit slides along the sliding set with a particular dynamics, see [9].

As the taxonomy is large, here we mainly pay attention to the case of systems having maximal crossing set and no proper sliding set.

Since our goal is to study nonlinear phenomena, we look for possible periodic orbits Γ not totally contained in S^- or S^+. If the orbit Γ has sliding points will be called a *sliding periodic orbit*. Otherwise we speak of *crossing periodic orbits* whose study constitute the main goal of this contribution.

If $a_{12}^+ a_{12}^- \leq 0$, it is easy to see that the crossing set, if it exists, is an open interval of the $y-$axis, bounded for $a_{12}^+ a_{12}^- < 0$ and unbounded for $a_{12}^+ a_{12}^- = 0$. In both cases, the $x-$component of both vector fields has constant sign at the crossing set and elementary qualitative arguments preclude the existence of crossing periodic orbits. Thus, crossing periodic orbits only can exist when $a_{12}^- a_{12}^+ > 0$. Note also that for $a_{12}^- a_{12}^+ > 0$ the crossing set is unbounded while the sliding set is bounded. If furthermore, we want there to be a maximal crossing set and accordingly the sliding set should shrink to a point, we must impose the existence of a point $(0, \bar{y})$ such that $F^-(0, \bar{y}) = F^+(0, \bar{y}) = 0$, that is when the conditions

$$a_{12}^- a_{12}^+ > 0, \quad a_{12}^+ b_1^- = a_{12}^- b_1^+ \tag{2}$$

are true. In this case, the sliding set is the point $(0, \bar{y}) = \left(0, -b_1^-/a_{12}^-\right)$.

In what follows we assume that the conditions (2) hold. For such systems, we propose a canonical form with six parameters which is able to cover all the cases where self-sustained oscillations are possible. Furthermore, in this paper we restrict our attention to the interesting case where the two linear systems involved are of focus type, a situation where the number of parameters can be reduced to four.

The rest of the paper is outlined as follows. In Sect. 2, the promised Liénard canonical form is introduced as well as a reduced canonical form for the focus-focus case. Next, some results about limit cycles are given for the cases of having only virtual or boundary equilibria (Sect. 3), only one real equilibrium (Sect. 4) and two real equilibria (Sect. 5). With these results, all the phase portraits are completely characterized excepting some cases with two real equilibria, where certain conjectures are stated.

2 Canonical Forms

As mentioned in the recent work by Huang and Yang, see [7], the study of discontinuous PWL is a formidable task if you do not have a canonical form that can cope with a sufficient broad class of systems, in contrast to what can be done for the continuous case, see [3]. This emphasizes the importance of the canonical form introduced in [4], which is reviewed in the sequel.

The quoted canonical form can be obtained by making a piecewise linear change of variables such that the resulting transformation will be a homeomorphism, keeping invariant the half-planes S^-, S^+ and the discontinuity line Σ. We want to stress that generically, such a homeomorphism does not produce a topological equivalent dynamical in the sliding set. In our case, as such set is a singleton, the topological equivalence is preserved.

Denoting by T^- and T^+ and by D^- and D^+ the traces and determinant of matrices A^- and A^+, respectively, we state the following result.

Proposition 1 (The Liénard canonical form). *Assume that* $a_{12}^- a_{12}^+ > 0$ *and* $a_{12}^+ b_1^- = a_{12}^- b_1^+$ *in system* (1). *Then the homeomorphism* $\tilde{\mathbf{x}} = h(\mathbf{x})$ *given by*

$$\tilde{\mathbf{x}} = \begin{pmatrix} 1 & 0 \\ a_{22}^- & -a_{12}^- \end{pmatrix} \mathbf{x} - \begin{pmatrix} 0 \\ b_1^- \end{pmatrix}, \quad \mathbf{x} \in S^- \cup \Sigma$$

and

$$\tilde{\mathbf{x}} = \frac{1}{a_{12}^+} \begin{pmatrix} a_{12}^- & 0 \\ a_{12}^- a_{22}^+ & -a_{12}^- a_{12}^+ \end{pmatrix} \mathbf{x} - \begin{pmatrix} 0 \\ b_1^- \end{pmatrix}, \quad \mathbf{x} \in S^+ \cup \Sigma,$$

after dropping tildes, transforms system (1) *into the canonical form*

$$\begin{aligned}\dot{\mathbf{x}} &= \mathbf{G}^-(\mathbf{x}) = \begin{pmatrix} T^- & -1 \\ D^- & 0 \end{pmatrix}\mathbf{x} - \begin{pmatrix} 0 \\ a^- \end{pmatrix}, \quad \mathbf{x} \in S^-, \\ \dot{\mathbf{x}} &= \mathbf{G}^+(\mathbf{x}) = \begin{pmatrix} T^+ & -1 \\ D^+ & 0 \end{pmatrix}\mathbf{x} - \begin{pmatrix} 0 \\ a^+ \end{pmatrix}, \quad \mathbf{x} \in S^+, \end{aligned} \tag{3}$$

where

$$a^- = a_{12}^- b_2^- - a_{22}^- b_1^-, \quad a^+ = \frac{a_{12}^-}{a_{12}^+}(a_{12}^+ b_2^+ - a_{22}^+ b_1^+).$$

Furthermore, the crossing set and the sliding point of the original system (1) *are transformed by the homeomorphism h into the crossing set* $\Sigma^c = \{(0, y) : y \neq 0\}$ *and the origin respectively and systems* (1) *and* (3) *are topologically equivalent.*

Proof. To obtain the vector field (3) is a direct computation. From the equalities

$$\mathbf{G}_1^-(h(0, y)) \cdot \mathbf{G}_1^+(h(0, y)) = \left(a_{12}^- y + b_1^-\right)^2 = \frac{a_{12}^-}{a_{12}^+}\mathbf{F}_1^-(0, y) \cdot \mathbf{F}_1^+(0, y)$$

we see that the only sliding point $(0, \bar{y})$ and the crossing set of system (1) are transformed into the only sliding point of (3) (the origin) and the crossing set of system (3), respectively.

Since orbits totally contained in one of the two half-planes are transformed in a homeomorphic way and the orbits arriving at the crossing set are continued by a natural concatenation that preserves the orbits, the topological equivalence between systems (1) and (3) follows. □

Note that for $a^- = a^+$ system (3) turns out to be continuous. Thus Proposition 1 assures that certain discontinuous systems 1 can be transformed into continuous systems by means of a continuous but non-smooth piecewise linear change of variables. In particular, we see that systems (1) with $a_{12}^- a_{12}^+ > 0$ and $\mathbf{b}^- = \mathbf{b}^+ = \mathbf{0}$ can always be transformed in a continuous system. Thus, for instance, the class of bimodal systems considered in [8] and the analysis done in [12] can be completely recast into the continuous cases studied in [3].

2.1 Reduced Liénard Canonical Form in the Focus-Focus Case

In the remainder of this work, we only pay attention to one of the most important cases in practice, in which both dynamics are of focus type; that is, $T^2 - 4D < 0$ in both zones. In this case, the eigenvalues of matrices $A^\pm$ are $\lambda^\pm = \alpha^\pm \pm i\omega^\pm$ and we can give a simpler canonical form only depending on four parameters. The proof comes from a direct computation.

Proposition 2. *Assume that* $T^{\pm} = 2\alpha^{\pm}, D^{\pm} = (\alpha^{\pm})^2 + (\omega^{\pm})^2$ *with* $\omega^{\pm} > 0$ *in the canonical form* (3) *and we introduce the parameters*

$$\gamma_L = \frac{\alpha^-}{\omega^-}, \quad \gamma_R = \frac{\alpha^+}{\omega^+}, \quad a_L = \frac{a^-}{\omega^-}, \quad a_R = \frac{a^+}{\omega^+}.$$

Then the change of variables (different for each half-plane)

$$(x, y, t) \to \left(\frac{x}{\omega(x)}, y, \frac{t}{\omega(x)}\right), \quad \omega(x) = \begin{cases} \omega^-, & x < 0, \\ \omega^+, & x > 0, \end{cases}$$

transforms the canonical form (3) *into the form*

$$\begin{aligned} \dot{\mathbf{x}} &= \begin{pmatrix} 2\gamma_L & -1 \\ 1+\gamma_L^2 & 0 \end{pmatrix} \mathbf{x} - \begin{pmatrix} 0 \\ a_L \end{pmatrix}, \quad \mathbf{x} \in S^-, \\ \dot{\mathbf{x}} &= \begin{pmatrix} 2\gamma_R & -1 \\ 1+\gamma_R^2 & 0 \end{pmatrix} \mathbf{x} - \begin{pmatrix} 0 \\ a_R \end{pmatrix}, \quad \mathbf{x} \in S^+. \end{aligned} \tag{4}$$

A necessary condition for the existence of crossing periodic orbits will be given in the next proposition. Its proof is deduced from Green's formula, see Proposition 3.7 and Remark 3.8 in [4].

Proposition 3. *If system* (4) *has a crossing periodic orbit then either* $\gamma_L \gamma_R < 0$ *or* $\gamma_L = \gamma_R = 0$.

The above result is also useful to exclude the existence of crossing periodic orbits in certain cases, see the next remark.

Remark 1. We remark that for $\gamma_L \gamma_R \geq 0$ with $|\gamma_L| + |\gamma_R| \neq 0$, the necessary condition for existence of crossing periodic orbits cannot be fulfilled, and so system (4) cannot have crossing periodic orbits.

Regarding the possible equilibria, tangency points and pseudoequilibria of system (4), we give the next proposition, whose proof is elementary and will not shown. For precise definitions of visible and invisible tangency points, as well as boundary equilibrium points, see for instance [6] and [9].

Proposition 4. *For system* (4) *the following statements hold.*

1. *There is one equilibrium point in the left zone when* $a_L < 0$, *and no equilibria in that zone when* $a_L > 0$. *Analogously, there is one equilibrium point in the right zone when* $a_R > 0$, *and no equilibria in that zone when* $a_R < 0$.
2. *If* $a_L \neq 0$, *then the origin is a left tangency point, visible for* $a_L < 0$ *and invisible for* $a_L > 0$. *If* $a_L = 0$, *then the origin is a boundary equilibrium point.*
3. *If* $a_R \neq 0$, *then the origin is a right tangency point, visible for* $a_R > 0$ *and invisible for* $a_R < 0$. *If* $a_R = 0$, *then the origin is a boundary equilibrium point.*

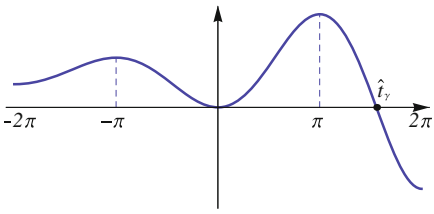

Fig. 1 The graph of function φ_γ for $\gamma > 0$. We note that $\varphi_\gamma(\hat{t}_\gamma) = 0$ where $\pi < \hat{t}_\gamma < 2\pi$

4. *If $a_R a_L \neq 0$, then the origin is a double tangency point. It behaves as a regular point for $a_R a_L > 0$, being a pseudoequilibrium point for $a_R a_L < 0$; in fact, the origin is a pseudofocus for $a_R < 0 < a_L$ and a pseudosaddle for $a_L < 0 < a_R$.*

When $a_L > 0$ or $a_R < 0$ we will speak of virtual equilibria which still govern the dynamics of the corresponding zone, not being real equilibria since they are located in the "wrong" zone.

2.2 The Parametric Definition of the Poincaré Map

For system (4), the direction of the flow at the line $x = 0$ assures that orbits starting at points $(0, y_0)$ with y_0 big enough go into the zone S^- until they reach Σ at a point $(0, y_1)$ with $y_1 \leq 0$ after a time t. Thus, we can define a left Poincaré map as $y_1 = P_L(y_0)$ in a certain subset of $\mathbf{R}^+$. To determine the map P_L we consider different cases, see Proposition 7.1 in [4].

If $a_L \gamma_L = 0$, then $P_L(y_0) = -e^{\gamma_L \pi} y_0, \quad y_0 \geq 0$.

If $a_L \gamma_L \neq 0$, then we resort to the auxiliary function $\varphi_\gamma(t) = 1 - e^{\gamma t}(\cos t - \gamma \sin t)$. This function φ_γ was introduced in [1] and for $\gamma > 0$ has a first positive zero at a value $\hat{t}_\gamma \in (\pi, 2\pi)$, see Fig. 1. Then we get the parametric representation of the left Poincaré map,

$$y_0 = \frac{a_L}{1+\gamma_L^2} \frac{e^{-\gamma_L t}\varphi_{\gamma_L}(t)}{\sin t}, \quad P_L(y_0) = -\frac{a_L}{1+\gamma_L^2} \frac{e^{\gamma_L t}\varphi_{-\gamma_L}(t)}{\sin t}. \tag{5}$$

where $\pi < t \leq \hat{t}_{\gamma_L}$ for $a_L < 0$ and $\gamma_L < 0$, being $\hat{t}_{\gamma_L}$ the first positive zero of the function $\varphi_{-\gamma_L}(t)$, and $0 < t < \pi$ otherwise.

Integrating the system in the zone S^+ from the point $(0, z_0)$ with $z_0 < 0$ and big enough, after a time t, we arrive at the point $(0, z_1)$, with $z_1 \geq 0$. So we define the right Poincaré map P_R as $z_1 = P_R(z_0)$. Different cases appear in the determination of map P_R, see Proposition 7.2 in [4].

If $a_R \gamma_R = 0$, then $P_R(z_0) = -e^{\gamma_R \pi} z_0, \quad z_0 \leq 0$.

If $a_R \gamma_R \neq 0$, we get the parametric representation of the right Poincaré map,

$$z_0 = \frac{a_R}{1+\gamma_R^2} \frac{e^{-\gamma_R t}\varphi_{\gamma_R}(t)}{\sin t}, \quad P_R(z_0) = -\frac{a_R}{1+\gamma_R^2} \frac{e^{\gamma_R t}\varphi_{-\gamma_R}(t)}{\sin t}, \tag{6}$$

where $\pi < t \leq \hat{t}_{\gamma_R}$ for $a_R > 0$ and $\gamma_R < 0$, being $\hat{t}_{\gamma_R}$ the first positive zero of the function $\varphi_{-\gamma_R}(t)$ and $0 < t < \pi$ otherwise.

Finally, as the main tool in looking for crossing periodic orbits we define the Poincaré map as the composition $P = P_R \circ P_L$, when possible.

3 The System has Only Virtual or Boundary Equilibria

In this section we only pay attention to the case where the system (4) has only either virtual or boundary equilibria. Then, according to Proposition 4, the condition $a_R \leq 0 \leq a_L$ holds.

Clearly, the origin is a topological focus. In the next proposition, which is basically Proposition 4.2 in [4], we characterize its stability.

Proposition 5. *Assuming $a_R \leq 0 \leq a_L$ in system (4), the following statements hold.*

1. *The origin is asymptotically stable for $a_L\gamma_R < a_R\gamma_L$ and unstable for $a_L\gamma_R > a_R\gamma_L$.*
2. *If $a_L\gamma_R = a_R\gamma_L$, then the origin is unstable for $\gamma_L + \gamma_R > 0$, asymptotically stable for $\gamma_L + \gamma_R < 0$ and a global center for $\gamma_L + \gamma_R = 0$.*

In the next results, the existence of periodic orbits is established as well as the global asymptotic stability of the origin, see Theorem 4.3 and Corollary 4.4 in [4].

Theorem 1. *Assuming $a_R \leq 0 \leq a_L$ in system (4), the following statements hold.*

1. *If $\gamma_L + \gamma_R = 0$, then there is a global nonlinear center around the origin for $a_L\gamma_R = a_R\gamma_L$ and no crossing periodic orbits when $a_L\gamma_R \neq a_R\gamma_L$.*
2. *If $\gamma_L + \gamma_R \neq 0$ and $\gamma_L\gamma_R \geq 0$, then there are no crossing periodic orbits.*
3. *If $\gamma_L + \gamma_R \neq 0$ and $\gamma_L\gamma_R < 0$, then for $(\gamma_L + \gamma_R)(a_L\gamma_R - a_R\gamma_L) < 0$ there is only one crossing periodic orbit, which is stable for $\gamma_L + \gamma_R < 0$ and unstable for $\gamma_L + \gamma_R > 0$.*

   When $(\gamma_L + \gamma_R)(a_L\gamma_R - a_R\gamma_L) \geq 0$ there are no crossing periodic orbits.

Corollary 1. *Under the condition $a_R \leq 0 \leq a_L$, the origin is globally asymptotically stable in the two cases: (i) when $a_L\gamma_R < a_R\gamma_L$ and $\gamma_L + \gamma_R \leq 0$, and (ii) when $a_L\gamma_R = a_R\gamma_L$ and $\gamma_L + \gamma_R < 0$.*

In Fig. 2, we sketch a global (γ_L, γ_R) bifurcation set for the generic case $a_R \leq 0 < -a_R < a_L$, according to Proposition 5 and Theorem 1. Under these conditions, there are no real equilibrium and only one a pseudofocus at the origin. Two bifurcation lines appear in the quoted figure,

$$H_\infty = \{(\gamma_L, \gamma_R) : \gamma_L + \gamma_R = 0\}, \quad H_0 = \{(\gamma_L, \gamma_R) : a_L\gamma_R + a_R\gamma_L = 0\}$$

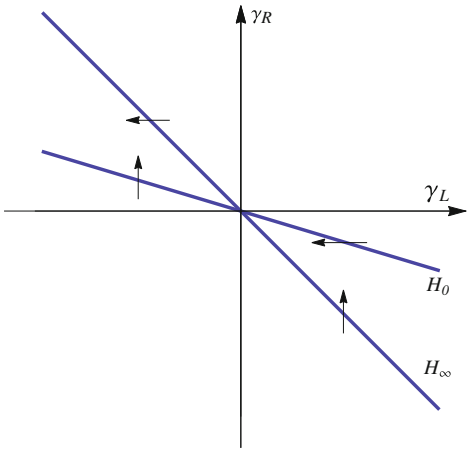

Fig. 2 Bifurcation set of system (4) for $a_R \leq 0 < a_L$ and $|a_R/a_L| < 1$. The pseudofocus is unstable above (stable below) the line H_0. The point at infinity is attractive above (repulsive below) the line H_∞. At the line H_∞ a Hopf bifurcation at infinity occurs and at the line H_0 we have a Hopf bifurcation at the origin. There is one periodic orbit in the sectors of second and fourth quadrants limited by the straight lines H_0 and H_∞. The periodic orbit is stable for $\gamma_L < 0$ and unstable for $\gamma_L > 0$

At the line H_∞ the point at infinity changes its stability and a Hopf bifurcation at infinity appears. At the line H_0 the pseudofocus changes its stability and a Hopf bifurcation of the origin occurs. Both bifurcations are supercritical for $\gamma_L < 0$ and subcritical for $\gamma_L < 0$.

An analogous case could be stated for $a_R < 0 \leq a_L$ with $|a_L/a_R| < 1$.

4 The System has One Real and One Virtual Equilibrium Point

In this section we consider the case where there is only one equilibrium point in the interior of the two half-planes. Then, according to Proposition 4, we have either $a_L < 0$ and $a_R < 0$ or $a_L > 0$ and $a_R > 0$.

Firstly, note that system (3) is invariant under the transformation

$$(x, y, t, \gamma_L, \gamma_R, a_L, a_R) \to (-x, -y, t, \gamma_R, \gamma_L, -a_R, -a_L) \tag{7}$$

where t stands for the independent variable. Thus, without loss of generality, we can assume $a_R < 0$ and $a_L < 0$, that is, the only equilibrium is located in the left zone, otherwise it suffices to apply the transformation (7).

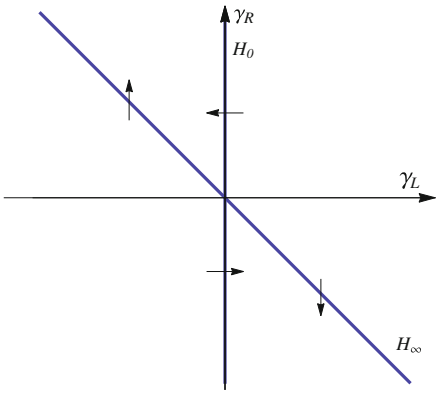

Fig. 3 Bifurcation set of system (4) for $a_L < 0$ and $a_R < 0$. The only equilibrium point is stable for $\gamma_L < 0$ and unstable for $\gamma_L > 0$. The point at infinity is attractive above (repulsive below) the line H_∞. At the line H_∞ a Hopf bifurcation at infinity occurs and at the line H_0 we have a focus-center limit cycle bifurcation. There is one periodic orbit in the sectors in the second and third quadrants limited by the straight lines H_0 and H_∞. The periodic orbit is unstable for $\gamma_L < 0$ and stable for $\gamma_L > 0$

Since the equilibrium point is in the interior of the left zone, its stability is clearly determined by the sign of the parameter γ_L. The next result deals with the existence of crossing periodic orbits, see Theorem 1 in [5].

Theorem 2. *Assuming $a_L < 0$ and $a_R < 0$ in system (4), the following statements hold.*

1. *If $\gamma_L\gamma_R \geq 0$ and $\gamma_L + \gamma_R \neq 0$, then there are no crossing periodic orbits.*
2. *If $\gamma_L = \gamma_R = 0$, then every orbit is a periodic orbit and the configuration is a global center.*
3. *If $\gamma_L\gamma_R < 0$ and $\gamma_L(\gamma_L + \gamma_R) \geq 0$, then there are no periodic orbits.*
4. *If $\gamma_L\gamma_R < 0$ and $\gamma_L(\gamma_L + \gamma_R) < 0$, then there is only one periodic orbit which is stable for $\gamma_L > 0$ and unstable for $\gamma_L < 0$.*

In Fig. 3, we sketch a global (γ_L, γ_R) bifurcation set for the case $a_L < 0$ and $a_R < 0$, according to Theorem 2. Under these conditions, there are only one real equilibrium which is located in the left zone. Two bifurcation lines appear in the quoted figure,

$$H_\infty = \{(\gamma_L, \gamma_R) : \gamma_L + \gamma_R = 0\}, \quad H_0 = \{(\gamma_L, \gamma_R) : \gamma_L = 0\}$$

At the line H_∞ the point at infinity changes its stability and a Hopf bifurcation at infinity appears. At the line H_0 the equilibrium point changes its stability, and one limit cycle with finite amplitude is born; this bifurcation is called focus-center limit cycle bifurcation and is thoroughly studied in [10]. Both bifurcations are subcritical for $\gamma_L > 0$ and supercritical for $\gamma_L < 0$.

5 The System has Two Real Equilibria

In this section we consider the system when there are two real equilibrium points. Then, according to Proposition 4, we have $a_L < 0$ and $a_R > 0$.

Since the equilibrium points are in the interior of each zone, their stability is clearly determined by the sign of the parameters γ_L and γ_R.

Before proceeding, we will introduce some significative values needed to establish the next results. From (5) we realize that for $\gamma_L < 0$ and taking $t = \hat{t}_{\gamma_L}$ we see that $P_L(y_0) = 0$. We define $\hat{y} = y_0(\hat{t}_{\gamma_L}) > 0$ that satisfies $P_L(\hat{y}) = 0$. Similarly, for $\gamma_L > 0$, we have $y_0(\hat{t}_{\gamma_L}) = 0$ and $y^* = P_L(0) < 0$, see Fig. 4. After some direct computations we obtain

$$\hat{y} = a_L \sin(\hat{t}_{\gamma_L}) e^{-\gamma_L \hat{t}_{\gamma_L}}, \quad y^* = -a_L \sin(\hat{t}_{\gamma_L}) e^{\gamma_L \hat{t}_{\gamma_L}} \tag{8}$$

Analogously, from (6), for $\gamma_R < 0$ we define $\hat{z} = z_0(\hat{t}_{\gamma_R}) < 0$ so that $P_R(\hat{z}) = 0$, while for $\gamma_R > 0$ we have $z_0(\hat{t}_{\gamma_R}) = 0$ and define $z^* = P_R(0) > 0$, see again Fig. 4. We get,

$$\hat{z} = a_R \sin(\hat{t}_{\gamma_R}) e^{-\gamma_R \hat{t}_{\gamma_R}}, \quad z^* = -a_R \sin(\hat{t}_{\gamma_R}) e^{\gamma_R \hat{t}_{\gamma_R}} \tag{9}$$

Our last result is the following theorem.

Theorem 3. *Assuming $a_L < 0 < a_R$ in system (4), the following statements hold.*

1. *If $\gamma_L \gamma_R \geq 0$ and $\gamma_L + \gamma_R \neq 0$, then there are no periodic orbits.*
2. *If $\gamma_L = \gamma_R = 0$, then there exists a double homoclinic connection at the origin and all the other orbits are periodic orbits foliating the plane.*
3. *$\gamma_L \gamma_R < 0$, the following cases arise.*
   - *(a) If $a_L + a_R = \gamma_L + \gamma_R = 0$ then there exist one homoclinic connection to the origin, a bounded continuum of heteroclinic connections, and one unbounded continuum of periodic orbits surrounding the above structure.*
   - *(b) If $\gamma_L < 0$ and $(\gamma_L + \gamma_R)(\hat{y} - z^*) > 0$, then there is at least one crossing periodic orbit, which is unstable for $\gamma_L + \gamma_R > 0$ and stable for $\gamma_L + \gamma_R < 0$.*
   - *(c) If $\gamma_L > 0$ and $(\gamma_L + \gamma_R)(\hat{z} - y^*) < 0$, then there is at least one crossing periodic orbit, which is unstable for $\gamma_L + \gamma_R > 0$ and stable for $\gamma_L + \gamma_R < 0$.*

Proof. For the sake of brevity, we only outline the proof. Statement (1) follows directly from Proposition 3 and Remark 1.

If $\gamma_L = \gamma_R = 0$, then both equilibria are linear centers and the orbits living in only one zone are periodic excepting the two orbits corresponding to the tangencies at the origin, which determine a double pseudosaddle connection. From the parametric representation of the left and right Poincaré maps we know that $P_L(y) = -y$ for $y > 0$ and $P_R(z) = -z$ for $z < 0$, so that the full Poincaré

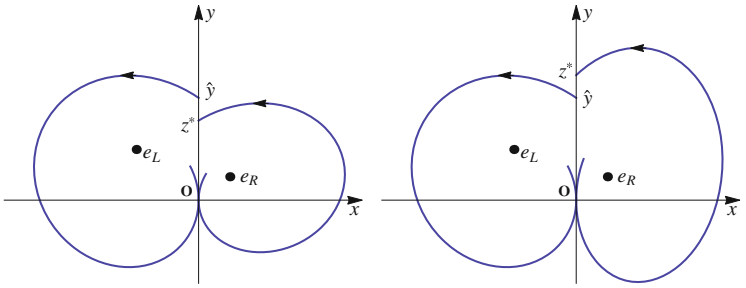

Fig. 4 Two different cases in system (4) for $\gamma_L < 0$ and $\gamma_R > 0$. *Left panel*: In this case $z^* < \hat{y}$ and the system is contractive in a neighborhood of the origin. *Right panel*: In this case $z^* > \hat{y}$ and the system is expansive in a neighborhood of the origin. In both cases the system has a periodic orbit when $(\gamma_L + \gamma_R)(\hat{y} - z^*) > 0$. When $\hat{y} = z^*$ there exists a homoclinic connection to the origin

map is given by $P(y) = P_R(P_L(y)) = y$. That is every orbit living in the two zones is a crossing periodic orbit and statement (2) is shown.

Assuming now $\gamma_L \gamma_R < 0$, we consider the following cases.

If $\gamma_L + \gamma_R = a_L + a_R = 0$, then it is not restrictive to assume that $\gamma_L < 0$, otherwise it suffices to apply the symmetry

$$(x, y, t, \gamma_L, \gamma_R, a_L, a_R) \to (x, -y, -t, -\gamma_L, -\gamma_L, a_L, a_R)$$

that leaves invariant system (4). From (8) and (9), we see that $\hat{y} = z^*$ and so there exists one homoclinic connection to the origin, see Fig 4. The orbits through the points in the interval $(0, \hat{y})$ asymptotically tend to the right equilibrium e_R for $t \to -\infty$ and to the left equilibrium e_L for $t \to \infty$, making up one bounded continuum of heteroclinic connections. Finally, from the parametric representation of the left and right Poincaré maps we obtain $P_L(y) = P_R^{-1}(y)$ for all $y > \hat{y}$, consequently, we obtain $P(y) = y$, and so every orbit touching the y-axis at a point $y > \hat{y}$ is a crossing periodic orbit and statement 3.*a* is proved.

In order to prove statement 3.*b* we consider the zeroes of the residual function $d(y) = P(y) - y$. Firstly assume that $\gamma_L + \gamma_R > 0$, then from the hypotheses we have $\hat{y} > z^*$. From the properties of Poincaré map we obtain that the derivative of the Poincaré map satisfies

$$\lim_{y \to \infty} P'(y) = e^{(\gamma_L + \gamma_R)\pi} > 1,$$

which implies that $P(y) > y$ in a neighborhood of the point at infinity. Since we can write $P(\hat{y}) = P_R(P_L(\hat{y}) = P_R(0) = z^*$, from the inequality $z^* < \hat{y}$, we obtain $P(\hat{y}) < \hat{y}$, and so $P(y) < y$ for small $y - \hat{y} > 0$. Hence at least a point $\bar{y}$ must exist where the function $d(y) = P(y) - y$ vanishes, which corresponds to an unstable crossing limit cycle.

The proofs of the case $\gamma_L + \gamma_R < 0, z^* > \hat{y}$, and the ones of statement 3.*c* are very similar and they will not be shown. □

Note that the above theorem does not consider all the possible cases. In particular the two cases $z^* = \hat{y}$ and $y^* = \hat{z}$ deserve additional attention, to be paid elsewhere. However, based on extensive numerical simulation we state the following conjectures.

Conjecture 1. Assuming $a_L < 0 < a_R$ and $\gamma_L \gamma_R < 0$ in system (4), then the system has at most one crossing periodic orbit.

Conjecture 2. Assuming $a_L < 0 < a_R$ and $\gamma_L \gamma_R < 0$ in system (4), then the following statements hold.

1. If $\gamma_L < 0$ and $(\gamma_L + \gamma_R)(\hat{y} - z^*) < 0$, the system has no crossing periodic orbits.
2. If $\gamma_L > 0$ and $(\gamma_L + \gamma_R)(\hat{z} - y^*) > 0$, the system has no crossing periodic orbits.

Acknowledgements Authors are partially supported by the *Ministerio de Ciencia y Tecnología, Plan Nacional* $I + D + I$, in the frame of projects MTM2009-07849, MTM2012-31821 and by the *Consejería de Educación y Ciencia de la Junta de Andalucía* under the gants TIC-0130 and P08-FQM-03770.

References

1. Andronov, A.A., Vitt, A.A., Khaikin, S.E.: Theory of Oscillators. Pergamon, Oxford (1966)
2. di Bernardo, M., Budd, C.J., Champneys, A.R., Kowalczyk, P.: Piecewise-smooth dynamical systems. In: Theory and Applications. Springer, London (2008)
3. Freire, E., Ponce, E., Rodrigo, F., Torres, F.: Bifurcation sets of continuous piecewise linear systems with two zones. Int. J. Bifurc. Chaos **8**, 2073 (1998)
4. Freire, E., Ponce, E., Torres, F.: Canonical discontinuous planar piecewise linear systems. SIAM J. Appl. Dyn. Syst. **11**, 181 (2012)
5. Freire, E., Ponce, E., Torres, F.: The discontinuous matching of two planar foci can have three nested limit cycles. Publications Matemàtiques, Volume EXTRA, (2013, to appear). Proceedings of the Conference "New Trends in Dynamical Systems" held in Salou (Tarragona), Spain, 1–5 Oct 2012
6. Guardia, M., Seara, T.M., Teixeira, M.A.: Generic bifurcations of low codimension of planar Filippov systems. J. Differ. Equ. **250**, 1967 (2001)
7. Huan, S., Yang, W.: On the number of limit cycles in general planar piecewise linear systems. Discret. Contin. Dyn. Syst. **32**, 2147 (2012)
8. Iwatani, Y., Hara, S.: In: Stability Analysis and Stabilization for Bimodal Piecewise Linear Systems Based on Eigenvalue Loci. Mathematical Engineering Technical Reports (2004). Available on line at http://www.keisu.t.u-tokyo.ac.jp/research/techrep/data/2004/METR04-34.pdf
9. Kuznetsov, Y., Rinaldi, S., Gragnani, A.: One-parameter bifurcations in planar piecewise Filippov systems. Int. J. Bifurc. Chaos **13**, 2157 (2003)
10. Ponce, E., Ros, J., Vela, E.: The focus-center limit cycle bifurcation in planar discontinuous piecewise linear systems without sliding. In: Ibáñez, S. et al. (eds) Progress and Challenges in Dynamical Systems, Springer Proceedings in Mathematics & Statistics, vol. 54 (this volume)
11. Stoker, J.J.: Nonlinear Vibrations in Mechanical and Electrical Systems. John Wiley, New York (1950)
12. Zou, Y., Kupper, T., Bein, W.J.: Generalized Hopf bifurcations for planar Filippov systems continuous at the origin. J. Nonlinear Sci. **16**, 159 (2006)

Some Applications of the Extended Bendixson-Dulac Theorem

Armengol Gasull and Hector Giacomini

Abstract During the last years the authors have studied the number of limit cycles of several families of planar vector fields. The common tool has been the use of an extended version of the celebrated Bendixson-Dulac Theorem. The aim of this work is to present an unified approach of some of these results, together with their corresponding proofs. We also provide several applications.

1 The Bendixson-Dulac Theorem

Ivar Bendixson and Henri Dulac are the fathers of the today known as Bendixson-Dulac Theorem. The classical version of this theorem appears in most textbooks on differential equations; see [14, 31, 37, 38] with many applications. Let us recall it. Consider a $\mathscr{C}^1$-planar differential system

$$\dot{x} = P(x, y), \quad \dot{y} = Q(x, y), \tag{1}$$

defined in some open simply connected subset $\mathscr{U} \subset \mathbb{R}^2$, and set $X = (P, Q)$. Assume that there exists a $\mathscr{C}^1$ function $D : \mathscr{U} \to \mathbb{R}$, such that

$$\operatorname{div}(DX)|_{\mathscr{U}} = \frac{\partial(D(x, y)P(x, y))}{\partial x} + \frac{\partial(D(x, y)Q(x, y))}{\partial y}\bigg|_{\mathscr{U}} \geq 0 \quad (\text{or} \quad \leq 0),$$

A. Gasull (✉)
Departament de Matemàtiques, Universitat Autònoma de Barcelona, Edifici C 08193 Bellaterra, Barcelona, Spain
e-mail: gasull@mat.uab.cat

H. Giacomini
Laboratoire de Mathématiques et Physique Théorique, Faculté des Sciences et Techniques, Université de Tours, C.N.R.S. UMR 7350. 37200 Tours, France
e-mail: Hector.Giacomini@lmpt.univ-tours.fr

S. Ibáñez et al. (eds.), *Progress and Challenges in Dynamical Systems*,
Springer Proceedings in Mathematics & Statistics 54,
DOI 10.1007/978-3-642-38830-9_14,

vanishing only on a set of zero Lebesgue measure. Then system (1) has no periodic orbits contained in $\mathscr{U}$. This function D is usually called a *Dulac function* of the system.

This theorem has been extended to multiple connected regions, see for instance [5, 17, 27, 36] obtaining then a method for determining upper bounds of the number of limit cycles in $\mathscr{U}$. In the next section we recall this extension and present the proof given in [17].

As we will see this extension can be used if it is possible to find a suitable function V, a real number s, and a domain $\mathscr{U} \subset \mathbb{R}^2$ such that

$$M = \frac{\partial V}{\partial x} P + \frac{\partial V}{\partial y} Q + s\Big(\frac{\partial P}{\partial x} + \frac{\partial Q}{\partial y}\Big) V \Big|_{\mathscr{U}}$$

does not change sign and vanishes on a set of zero Lesbesgue measure. Moreover, the upper bound given by the method for the number of limit cycles depends on the number and distribution of the ovals of $\{V(x, y) = 0\}$ in $\mathscr{U}$.

When all the involved functions P, Q and V are polynomials this approach relates both parts of Hilbert's Sixteenth Problem. Recall that the first part deals with the number and distribution of ovals of a real algebraic curve in terms of its degree while the second part asks to find an uniform bound of the number of limit cycles of systems of the form (1) when both polynomials have a given degree; see [24, 35].

Notice that the importance of the use of the Bedixson-Dulac results is that in many cases they translate the problem of knowing the number of periodic solutions of a planar polynomial differential equation to a problem of semi-algebraic nature: the control of the sign of a polynomial in a suitable domain.

Analogously to Lyapunov functions, the first difficulty to apply these results is to find a suitable Dulac function. The problem of its existence, in the basin of attraction of critical points, is treated in [3]. A second difficulty of the method is to find a suitable region $\mathscr{U}$.

The aim of this paper is to present an unified point of view of some of the results obtained by the authors in [17–19, 21], together with some proofs. These results give methods to find Dulac functions D, or equivalently functions V and values s, for which the corresponding expression M is simple and so its sign can be easily studied. We also apply the method to give an upper bound of the number of limit cycles for several families of planar systems.

The Bendixson-Dulac approach has been extended in several directions: to prove non-existence of periodic orbits in higher dimensions, see [15, 26]; to control the number of isolated periodic solutions of some non-autonomous Abel differential equations, see for instance [1, 9]; to prove non-existence of periodic orbits for some difference equations, see [29].

We can not end this introduction without talking about the contributions on the use of Dulac functions of our friend and colleague Leonid Cherkas, sadly recently deceased. His important work in this subject started many years ago and arrives until the actuality, continued by his collaborators, see for instance [4–10] and the reference therein. In fact, one of the main motivations for the fist author to work in

this direction were the pleasant conversations with him walking around the beautiful gardens of the Beijing University in the summer of 1990.

1.1 The Bendixson-Dulac Theorem for Multiple Connected Regions

An open subset $\mathscr{U}$ of $\mathbb{R}^2$ with smooth boundary, is said to be ℓ-*connected* if its fundamental group, $\pi_1(\mathscr{U})$ is $\mathbb{Z} * \overset{(\ell)}{\cdots} * \mathbb{Z}$, or in other words if $\mathscr{U}$ has ℓ holes. We will say that $\ell(\mathscr{U}) = \ell$. We state and prove, following [17], the extension of the Bendixson-Dulac Theorem to more general domains; see other proofs in [5, 27, 36]. As usual, $\langle \cdot, \cdot \rangle$ denotes the scalar product in $\mathbb{R}^2$.

Extended Bendixson-Dulac Theorem. *Let $\mathscr{U}$ be an ℓ-connected open subset of $\mathbb{R}^2$ with smooth boundary. Let $D \colon \mathscr{U} \to \mathbb{R}$ be a $\mathscr{C}^1$ function such that*

$$M := \operatorname{div}(DX) = \frac{\partial D}{\partial x} P + \frac{\partial D}{\partial y} Q + D \left(\frac{\partial P}{\partial x} + \frac{\partial Q}{\partial y} \right) = \langle \nabla D, X \rangle + D \operatorname{div}(X) \tag{2}$$

does not change sign in $\mathscr{U}$ and vanishes only on a null measure Lebesgue set, such that $\{M = 0\} \cap \{D = 0\}$ does not contain periodic orbits of (1). Then the maximum number of periodic orbits of (1) contained in $\mathscr{U}$ is ℓ. Furthermore each one of them is a hyperbolic limit cycle that does not cut $\{D = 0\}$ and its stability is given by the sign of DM over it.

Proof. Observe that $M|_{\{D=0\}} = \langle \nabla D, X \rangle|_{\{D=0\}} \geq 0$ does not change sign in $\mathscr{U}$. Since, by hypothesis, there are no periodic orbits of (1) contained in $\{M = 0\} \cap \{D = 0\}$, we have that the periodic orbits of (1) do not cut $\{D = 0\}$.

If $\mathscr{U}$ is simply connected ($\ell = 0$) then by the Bendixson-Dulac Theorem we have that (1) has no periodic orbits in $\mathscr{U}$. We give now a proof for an arbitrary ℓ. Assume that system (1) has $\ell + 1$ different periodic orbits γ_i, included in $\mathscr{U}$. These orbits induce $\ell + 1$ elements $\overline{\gamma}_i$ in the first homology group of $\mathscr{U}$, $H_1(\mathscr{U}) = \mathbb{Z} \oplus \overset{(\ell)}{\cdots} \oplus \mathbb{Z}$. Since this group has at most ℓ linearly independent elements it follows that there is a non trivial linear combination of them giving $0 \in H_1(\mathscr{U})$. Then $\sum_{i=1}^{\ell+1} m_i \overline{\gamma}_i = 0$, with $(m_1, \ldots, m_{\ell+1}) \neq 0$.

This last fact means that the curve $\sum_{i=1}^{\ell+1} m_i \gamma_i$ is the boundary of a two cell C for which Stokes Theorem can be applied. Then

$$\iint_C \operatorname{div}(DX) = \int_{\sum_{i=1}^{\ell+1} m_i \gamma_i} \langle D\, X, \mathbf{n} \rangle.$$

Note that the right hand term in this equality is zero because DX is tangent to the curves γ_i and that the left one is non-zero by our hypothesis. This fact leads to a contradiction. So ℓ is the maximum number of periodic orbits of (1) in $\mathscr{U}$.

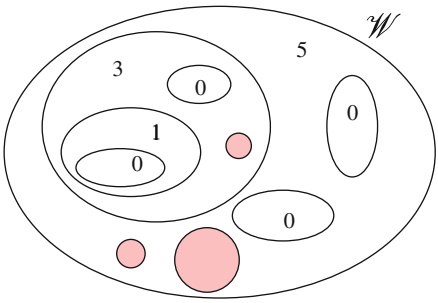

Fig. 1 Open set $\mathscr{W}$ with $\ell(\mathscr{W}) = 3$. The *filled circles* are *holes* in $\mathscr{W}$ and the *thick lines* correspond to $\{V = 0\}$. The numbers displayed are the values $\ell(\mathscr{U})$ for each connected component $\mathscr{U}$ of $\mathscr{W} \setminus \{V = 0\}$. For this example $c(\mathscr{W}, V) = 6$ and $\ell(\mathscr{W}, V) = 9$

Let us prove their hyperbolicity. Fix one periodic orbit $\gamma = \{(x(t), y(t)), t \in [0, T]\} \subset \mathscr{U}$, where T is its period. Remember that $\gamma \cap \{D = 0\} = \emptyset$. In order to study its hyperbolicity and stability we have to compute $\int_0^T \operatorname{div} X(x(t), y(t))dt$, and to prove that it is not zero. This fact follows by integrating the equality

$$\operatorname{div} X = \frac{\partial P}{\partial x} + \frac{\partial Q}{\partial y} = \frac{\operatorname{div}(DX)}{D} - \frac{\frac{\partial D}{\partial x} P + \frac{\partial D}{\partial y} Q}{D},$$

because the last term of the right hand side of the above equality coincides with $\frac{d}{dt} \ln |D(x(t), y(t))|$. □

To apply the above theorem, we consider a function $D(x, y)$ of the form $|V(x, y)|^m$ where V is a smooth function in two variables in $\mathbb{R}^2$ and m is a real number.

Before giving the result for this particular choice of V we introduce some more notation. Given an open subset $\mathscr{W}$ with smooth boundary and a smooth function $V : \mathscr{W} \to \mathbb{R}$ we denote by $\ell(\mathscr{W}, V)$ the sum of $\ell(\mathscr{U})$ where $\mathscr{U}$ ranges over all the connected components of $\mathscr{W} \setminus \{V = 0\}$. Finally, we denote by $c(\mathscr{W}, V)$ the number of closed ovals of $\{V = 0\}$ contained in $\mathscr{W}$. See Fig. 1 for an illustration of these definitions.

Corollary 1. *Assume that there exist a real number s and an analytic function V in $\mathbb{R}^2$ such that*

$$M_s := \frac{\partial V}{\partial x} P + \frac{\partial V}{\partial y} Q + s\Big(\frac{\partial P}{\partial x} + \frac{\partial Q}{\partial y}\Big) V = \langle \nabla V, X \rangle + sV \operatorname{div}(X)$$

does not change sign in an open region $\mathscr{W} \subset \mathbb{R}^2$ with regular boundary and vanishes only in a null measure Lebesgue set. Then the limit cycles of system (1) are either totally contained in $\mathscr{V}_0 := \{V = 0\}$, or do not intersect $\mathscr{V}_0$.

Moreover the number of limit cycles contained in $\mathscr{V}_0$ is at most $c(\mathscr{W}, V)$ and the number N of limit cycles that do not intersect $\mathscr{V}_0$ satisfies

$$N \leq \begin{cases} \ell(\mathscr{W}) & \text{if} \quad s > 0, \\ 0 & \text{if} \quad s = 0, \\ \ell(\mathscr{W}, V) & \text{if} \quad s < 0, \end{cases}$$

Furthermore for any $s \neq 0$ the limit cycles of this second type are hyperbolic.

Proof. First observe that since M_s does not change sign we have that on the analytic curves $\mathscr{V}_0$, $\langle \nabla V, X \rangle$ does not change sign. Therefore these curves are either solutions of (1) or curves crossed by the flow generated by (1) in just one direction. Hence all limit cycles in $\mathscr{W}$ are either contained in the connected components of $\mathscr{W} \setminus \mathscr{V}_0$ or in $\mathscr{V}_0$. This fact implies the first assertions of the Theorem. In order to bound the number of limit cycles of (1) we apply the extended Bendixson-Dulac Theorem to each one of the connected components $\mathscr{U}$ of $\mathscr{W} \setminus \mathscr{V}_0$. The fact that when $D = |V|^m$,

$$\operatorname{div}(DX) = \langle \nabla D, X \rangle + D\operatorname{div}(X) = \operatorname{sign}(V) m |V|^{m-1} \left[\langle \nabla V, X \rangle + \frac{1}{m} V \operatorname{div}(X) \right],$$

gives the theorem by taking $m = 1/s$. Observe that the difference between the cases $s > 0$ and $s < 0$ comes from the fact that in the first case the function D is well defined in the whole plane. For the case $s = 0$ the proof is easier because $M_0 = dV/dt = \langle \nabla V, X \rangle$. □

The above corollary shows that the study of the functions

$$M_s = \frac{\partial V}{\partial x} P + \frac{\partial V}{\partial y} Q + s \Big(\frac{\partial P}{\partial x} + \frac{\partial Q}{\partial y} \Big) V \tag{3}$$

gives a tool for controlling the number of limit cycles of system (1). As we will see this approach turns out to be useful for many families of planar vector fields. This function is also often used in the quoted works of Cherkas and his coauthors.

1.2 Some Simple Examples

As paradigmatic examples we will give short and easy proofs of the non-existence of limit cycles for a generalization of the Lotka-Volterra system and of the uniqueness of the limit cycle of the van der Pol system. The first one is a folklore prove and the second one is given by Cherkas, see [11, p. 105]. We will prove also a more general non-existence result for Kolmogorov systems.

Non-existence of Limit Cycles for Some Predator-Prey Systems

Consider the following extension of the celebrated Lotka-Volterra system

$$\dot{x} = x(ax + by + c), \quad \dot{y} = y(dx + ey + f), \tag{4}$$

where all the parameters are real numbers. It appears in most texts books of mathematical ecology. By uniqueness of solutions it is clear that if it has periodic orbits then they do not intersect the coordinate axes. By making the change of variables $x \to \pm x$, $y \to \pm y$, if necessary, we can restrict our attention to the first quadrant $\mathscr{U}$ and prove that the system has no periodic orbit in it. To do this consider the Dulac function $D(x, y) = x^A y^B$, where the real numbers A and B have to be determined. Then the function M appearing in (2) is

$$\begin{aligned} M(x, y) &= \langle \nabla D(x, y), X(x, y) \rangle + D(x, y) \operatorname{div} X(x, y) \\ &= x^A y^B \left((aA + dB + 2a + d)x + (bA + eB + 2e + b)y + (cA + fB + c + f) \right). \end{aligned}$$

When $ae - bd \neq 0$ we can solve the linear system obtained vanishing the coefficients of x and y with unknowns A and B. Call the solution $A = \alpha$ and $B = \beta$. Then

$$M(x, y) = \frac{abf + ced - aef - ace}{ae - bd} x^\alpha y^\beta := R x^\alpha y^\beta.$$

When $R \neq 0$ we can apply the Bendixson-Dulac Theorem and since $\mathscr{U}$ is simply connected ($\ell(\mathscr{U}) = 0$) the system has no limit cycles. When $R = 0$ then it $x^\alpha y^\beta$ is an integrating factor. Hence the system is integrable and its first integral is smooth in $\mathscr{U}$. Thus it can not have isolated periodic orbits, i.e. it has no limit cycles. This case includes the famous Lotka-Volterra system. Recall that it has a center in $\mathscr{U}$, surrounded by periodic orbits.

When $ae - bd = 0$ then either the linear system $ax + by + c = 0$, $dx + ey + f = 0$, with unknowns x and y has no solutions or its solutions are either the full plane or a whole line. In the first case the only critical points of system (4) are on the axes, so the system can not have periodic orbits. Otherwise it is either the trivial system $\dot{x} = 0$, $\dot{y} = 0$ or is a reparameterization of the simple system $\dot{x} = gx$, $\dot{y} = hy$, for some real numbers g, h, which clearly can not have periodic orbits either.

Non-existence of Limit Cycles for a Class of Kolmogorov Systems

Following [2] we give a non-existence criterion for a family of Kolmogorov systems. This result can be applied to the Gause-type systems considered in [30] or to the systems studied in [23].

Proposition 1. *Consider the $\mathscr{C}^1$-system*

$$\dot{x} = x\left(g_0(x) + g_1(x)y\right), \quad \dot{y} = y\left(h_0(x) + h_1(x)y + h_2(x)y^2\right), \tag{5}$$

for $x \geq 0$, $y \geq 0$. For any $\lambda \in \mathbb{R}$ define the functions:

$$S_\lambda(x) = x[g_0'(x)g_1(x) - g_0(x)g_1'(x)] + \lambda h_0(x)g_1(x) - (1+\lambda)g_0(x)h_1(x),$$
$$T_\lambda(x) = (2+\lambda)h_2(x)g_1(x).$$

Let $\mathscr{I} \subset \mathbb{R}^+$ be an open interval. Assume that there exists a value of λ such that $S_\lambda(x)T_\lambda(x) \geq 0$, for all $x \in \mathscr{I}$, and all its zeroes are isolated. Then system (5) does not have periodic orbits in the strip $\mathscr{U} = \mathscr{I} \times (0, +\infty)$.

Proof. First, let us prove that if the system has a limit cycle then it can not intersect the set $\{(x, y) \,|\, x > 0, g_1(x) = 0\}$. This holds because if $\bar{x} > 0$ is such that $g_1(\bar{x}) = 0$ then either $x = \bar{x}$ is an invariant line (i.e. also $g_0(\bar{x}) = 0$) or it is a line without contact, i.e. $\dot{x}\,|_{x=\bar{x}} = \bar{x}g_0(\bar{x}) \neq 0$. Hence, in the region where (5) can have periodic orbits we can always assume that g_1 does not vanish.

Consider now the family of Dulac functions $D(x, y) = y^{\lambda-1}Z(x)$, where λ is given in the statement and Z is an unknown function. Computing the function (2),

$$\begin{aligned} M(x,y) &= \operatorname{div}\left(D(x,y)X(x,y)\right) \\ &= \left[\left(xg_0(x)Z(x)\right)' + \lambda h_0(x)Z(x) + \left(\left(xg_1(x)Z(x)\right)' + (\lambda+1)h_1(x)Z(x)\right)y \right. \\ &\quad \left. + \left((\lambda+2)h_2(x)Z(x)\right)y^2\right]y^{\lambda-1}. \end{aligned}$$

The solutions of the differential equation

$$\left(xg_1(x)Z(x)\right)' + (\lambda+1)h_1(x)Z(x) = 0 \tag{6}$$

are

$$Z_{x_0}(x) = \frac{\exp\left[-(\lambda+1)\displaystyle\int_{x_0}^{x} \frac{h_1(s)}{sg_1(s)}\,ds\right]}{xg_1(x)},$$

where $x_0 > 0$ is an arbitrary contant. By taking the Dulac function $\tilde{D}(x, y) = y^{\lambda-1}Z_{x_0}(x)$, for a given $x_0 > 0$, and taking into account that $Z_{x_0}(x)$ satisfies (6), we obtain after some computations that

$$M(x, y) = \frac{Z_{x_0}(x)}{g_1(x)}\left(S_\lambda(x) + T_\lambda(x)y^2\right)y^{\lambda-1}.$$

Since on $\mathscr{I}$, $S_\lambda(x)T_\lambda(x) \geq 0$ we have proved that M does not change sign in $\mathscr{U} = I \times (0, +\infty)$, which is simply connected, and vanishes on a set of zero Lebesgue measure given by some vertical straight lines. Hence, by the Bendixson-Dulac Theorem, the result is proved. □

Observe that the function $S_\lambda(x)$ of Proposition 1 can also be written as

$$S_\lambda(x) = g_1^2(x)\left[x\left(\frac{g_0(x)}{g_1(x)}\right)' + \lambda\frac{h_0(x)}{g_1(x)} - (1+\lambda)\frac{g_0(x)h_1(x)}{g_1^2(x)}\right].$$

When $h_1(x) \equiv 0$, it essentially coincides with the one given in the non-existence criterion presented in [25, Theorem 4.1].

Uniqueness of the Limit Cycle for the van der Pol Equation

The second order van der Pol equation $\ddot{x} + \varepsilon(x^2 - 1)\dot{x} + x = 0$, can be written as the planar system

$$\dot{x} = y, \qquad \dot{y} = -\varepsilon(x^2 - 1)y - x.$$

Taking $V(x, y) = x^2 + y^2 - 1$ we obtain that the associated function M_s given in (3) is

$$M_s(x, y) = -\varepsilon(x^2 - 1)(sx^2 + (2 + s)y^2 - s).$$

Choosing $s = -2$ we get that $M_{-2}(x, y) = 2\varepsilon(x^2-1)^2$. So, for $\varepsilon \neq 0$, this function does not change sign and vanishes on two straight lines. Hence since, $\ell(\mathbb{R}^2, V) = 1$ and $s < 0$, by Corollary 1, we obtain the van der Pol system has at most one limit cycle, which when exists is hyperbolic, and lies outside the unit circle. This approach does not provide the existence of the limit cycle. The existence, for $\varepsilon \neq 0$, can be obtained studying the behavior of the flow at infinity.

2 Control of the Function M_s

To apply the Dulac method to concrete examples the main difficulty is to find a suitable couple $s \in \mathbb{R}$ and V and then control the sign of the function M_s given in (3). Many times a good trick consists in trying to reduce the question to a one variable problem. This approach is developed in Sect. 2.1 following [17, 18].

Another point of view is to work in polar coordinates. Then the control of the corresponding function M_s takes advantage of writing the functions as polynomials of the radial component with coefficients depending periodically on the angle. This approach has been followed in [19] and some results are presented in Sect. 2.2.

2.1 The Function M_s Is Reduced to a One Variable Function

A First Method

Proposition 2. *Consider a $\mathscr{C}^1$ system of the form*

$$\dot{x} = p_0(x) + p_1(x)y = P(x,y), \quad \dot{y} = q_0(x) + q_1(x)y + q_2(x)y^2 = Q(x,y), \tag{7}$$

with $p_1(x) \not\equiv 0$. For each $s \in \mathbb{R}$ and for each $n \in \mathbb{N}$ it is possible to associate to it a $(n+1)$-parameter family of functions $V_n(x, y; c_0, c_1, \ldots, c_n) := V_n(x, y)$ of the form

$$V_n(x,y) = v_0(x) + v_1(x)y + v_2(x)y^2 + \cdots + v_n(x)y^n,$$

such that for each one of them the function (3),

$$M_{s,n}(x) = \langle \nabla V_n, (P,Q)\rangle + sV_n \operatorname{div}(P,Q)$$

is a function only of the x-variable.

Proof. Direct computations give

$$\begin{aligned}
&\langle \nabla V_n, (P,Q)\rangle + sV_n \operatorname{div}(P,Q) = \\
&\quad = \left[\left\{\left(sp_1' + 2sq_2 + nq_2\right)v_n + p_1 v_n'\right\} y^{n+1} + \mathscr{F}_n(v_n, v_{n-1})y^n + \right. \\
&\quad + \left\{\mathscr{F}_{n-1}(v_{n-1}, v_{n-2}) + nq_0(x)v_n(x)\right\} y^{n-1} + \cdots + \\
&\quad + \left.\left\{\mathscr{F}_1(v_1, v_0) + 2q_0(x)v_2(x)\right\} y + \left\{(sp_0' + sq_1)v_0 + p_0 v_0' + q_0 v_1\right\}\right],
\end{aligned}$$

where for each $j = 1, 2 \ldots, n$,

$$\begin{aligned}
\mathscr{F}_j(v_j, v_{j-1}) =& (sp_0' + sq_1 + jq_1)v_j(x) + \\
& p_0 v_j'(x) + (sp_1' + 2sq_2 + (j-1)q_2)v_{j-1}(x) + p_1 v_{j-1}'(x).
\end{aligned}$$

From the above expressions we can obtain a 1-parameter family of functions $v_n^*(x; c_n) := v_n^*(x)$ such that the coefficient of y^{n+1} vanishes, by solving a linear first order ordinary differential equation. Once we have v_n^*, from $\mathscr{F}_n(v_n^*, v_{n-1}) = 0$ we get $v_{n-1}^*(x; c_n, c_{n-1}) := v_{n-1}^*(x)$ and so on until we have found $v_n^*, v_{n-1}^*, \ldots, v_0^*$. Finally, we obtain

$$\langle \nabla V_n, (P,Q)\rangle + sV_n \operatorname{div}(P,Q) = \left[(sp_0' + sq_1)v_0^* + p_0(v_0^*)' + q_0 v_1^*\right] = M_{s,n}(x),$$

as we wanted to prove. □

Corollary 2. *Consider the generalized Liénard system*

$$\dot{x} = y - F(x) := P(x, y), \quad \dot{y} = -g(x) := Q(x, y).$$

If we take

$$V_2(x, y) = \left(\frac{s(s+1)}{2}(F(x))^2 + c_1 s F(x) + 2G(x) + c_0\right) + (sF(x) + c_1)y + y^2,$$

where $G(x) = \int_0^x g(z)\,dz$, *then*

$$\begin{aligned} M_{s,2}(x) &= \langle \nabla V_2, (P, Q)\rangle + sV_2 \operatorname{div}(P, Q) \\ &= -\frac{s(s+1)(s+2)}{2}(F(x))^2 F'(x) - s(s+1)c_1 F(x)F'(x) \\ &\quad - (s+2)g(x)F(x) - 2sF'(x)G(x) - sc_0 F'(x) - c_1 g(x). \end{aligned}$$

In particular, for $s = -1$ *we have*

$$V_2(x, y) = (-c_1 F(x) + 2G(x) + c_0) + (-F(x) + c_1)y + y^2,$$

and

$$M_{-1,2}(x) = 2F'(x)G(x) + c_0 F'(x) - g(x)F(x) - c_1 g(x).$$

As an application of the above results we prove here the uniqueness and hyperbolicity of the limit cycle of a Liénard system with a rational F. The uniqueness (without proving the hyperbolicity) for this system was already proved in [13, 33]; see also [20]. Other applications are given in [17].

Proposition 3. *The Liénard system*

$$\dot{x} = y - F(x), \quad \dot{y} = -x, \quad \text{with} \quad F(x) = \frac{x(1 - cx^2)}{(1 + cx^2)} \tag{8}$$

and c *a real positive constant, has at most one limit cycle. Furthermore, when it exists it is hyperbolic and unstable.*

Proof. We apply Proposition 2 and Corollary 2 with $s = -1$, $n = 2$ and $V(x, y)$ given by the rational function:

$$V(x, y) = y^2 - F(x)y + x^2\,.$$

Then

$$M_{-1,2}(x) = \frac{-4cx^4}{(1 + cx^2)^2} < 0 \quad \text{for all} \quad x \neq 0\,.$$

The function $V(x, y) = 0$ is a second degree polynomial in the variable y, with discriminant

$$\Delta = x^2\left(\left(\frac{1-cx^2}{1+cx^2}\right)^2 - 4\right) = -\frac{x^2(cx^2+3)(3cx^2+1)}{(1+cx^2)^2} < 0 \qquad \text{for} \quad \text{all } x \neq 0\,.$$

Hence the set $\{V = 0\}$ reduces to the origin. Therefore $c(\mathbb{R}^2, V) = 0$ and $\ell(\mathbb{R}^2, V) = 1$. From Corollary B we conclude that system (8) has at most one limit cycle. The origin is the only critical point of this system and it is stable. Then, when the limit cycle exists it is hyperbolic and unstable. □

A Second Method

Proposition 4. *Consider a $\mathscr{C}^1$ system of the form*

$$\dot{x} = y = P(x, y), \quad \dot{y} = h_0(x) + h_1(x)y + h_2(x)y^2 + y^3 = Q(x, y),$$

and fix a positive integer number n. There is a constructive procedure to obtain an $(n+1)$-th order linear differential equation

$$y^{(n+1)}(x) + r_{n,n}(x)\, y^{(n)}(x) + \cdots + r_{n,1}(x)\, y'(x) + r_{n,0}(x)\, y(x) = 0, \qquad (9)$$

such that if $y(x) = v_n(x)$ is any of its solutions, we can define a function

$$V_n(x, y) := v_{n,0}(x) + v_{n,1}(x)y + v_{n,2}(x)y^2 + \cdots + v_{n,n}(x)y^n,$$

where $v_{n,n}(x) = v_n(x)$ and $v_{n,i}(x), i = 0 \ldots n-1$, are obtained from given expressions involving $h_i(x), i = 0, 1, 2, v_n(x)$ and their derivatives, such that the corresponding function M_s given in (3) with $s = -n/3$,

$$M^{[n]} := M_{-n/3} = \langle \nabla V_n, (P, Q)\rangle - \frac{n}{3} V_n \operatorname{div}(P, Q),$$

is a function only of the x-variable.

Proof. For sake of simplicity we present the details of the proof only for the case $n = 2$. Also, for sake of brevity and during this proof, when it appears a function of the x variable that we do not want to specify we simply will write $*$.

Take $V_2(x, y) = v_{2,0}(x) + v_{2,1}(x)y + v_{2,2}(x)y^2 := v_0(x) + v_1(x)y + v_2(x)y^2$. Then

$$M^{[2]} = \langle \nabla V_n, (P, Q)\rangle - \frac{2}{3}\operatorname{div}(P, Q)V_2 =$$
$$\left(v_2'(x) + \frac{2}{3}\, v_2(x)\, h_2(x) - v_1(x)\right) y^3 +$$

$$\left(v_1'(x)+\frac{4}{3}v_2(x)h_1(x)-\frac{1}{3}v_1(x)h_2(x)-2v_0(x)\right)y^2+$$
$$\left(v_0'(x)+\frac{1}{3}v_1(x)h_1(x)-\frac{4}{3}h_2(x)v_0(x)+2v_2(x)h_0(x)\right)y+$$
$$\left(v_1(x)h_0(x)-\frac{2}{3}h_1(x)v_0(x)\right).$$

By choosing the following expressions for v_0 and v_1

$$v_0(x)=\frac{1}{2}\left(v_1'(x)+\frac{4}{3}v_2(x)h_I(x)-\frac{1}{3}v_I(x)h_2(x)\right),$$
$$v_1(x)=v_2'(x)+\frac{2}{3}v_2(x)h_2(x),$$

we get that the coefficients of y^2 and y^3 in $M^{[2]}$ vanish. Observe that $v_1(x) = v_2'(x) + *v_2(x)$ and that $v_0(x) = v_2''(x)/2 + *v_2'(x) + *v_2(x)$. Hence if we substitute these equalities in the coefficient of y in the expression of $M^{[2]}$ we get that it writes as $v_2'''(x)/2 + *v_2''(x) + *v_2'(x) + *v_2(x)$. By imposing that this last expression be identically zero we get the linear ordinary differential equation (9) given in the statement of the lemma. Hence for these values of the functions $v_i, i = 0, 1, 2$ the expression of $M^{[2]}$ is the function of one variable

$$M^{[2]}(x)=v_1(x)h_0(x)-\frac{2}{3}h_1(x)v_0(x),$$

as we wanted to prove. □

The advantage of the above result is that for each it n gives the freedom to choose any solution of a linear ordinary differential equation of order $n + 1$. Then using it we have to prove that the corresponding $M^{[n]}$ does not change sign. This approach is used in [19] to study the particular case $a = e = 0$ of the challenging question proposed in [12]:

Question. Consider the planar semi-homogeneous system

$$\dot{x}=ax+by,\quad \dot{y}=cx^3+dx^2y+exy^2+fy^3.$$

Is two its maximum number of limit cycles?

2.2 Computations in Polar Coordinates

To work in polar coordinates we will need the expression of M_s in terms of the expression of the vector field (1) in polar coordinates,

$$\begin{aligned}\dot{r} &= R(r,\theta) := P(r\cos\theta, r\sin\theta)\cos\theta + Q(r\cos\theta, r\sin\theta)\sin\theta, \qquad (10)\\ \dot{\theta} &= \Theta(r,\theta) := \frac{1}{r}\Big(Q(r\cos\theta, r\sin\theta)\cos\theta - P(r\cos\theta, r\sin\theta)\sin\theta\Big).\end{aligned}$$

Lemma 1. *Let $\dot{r} = R(r,\theta)$, $\dot{\theta} = \Theta(r,\theta)$ be the expression (10) of system (1) in polar coordinates. Then the function M_s given in (3) writes as*

$$\begin{aligned}M_s &= \frac{\partial V}{\partial x}P + \frac{\partial V}{\partial y}Q + s\left(\frac{\partial P}{\partial x} + \frac{\partial Q}{\partial y}\right)V\\ &= \frac{\partial V}{\partial r}R + \frac{\partial V}{\partial \theta}\Theta + s\left(\frac{\partial R}{\partial r} + \frac{\partial \Theta}{\partial \theta} + \frac{R}{r}\right)V.\end{aligned}$$

Theorem 1. *Consider the planar differential system (1),*

$$\dot{x} = P(x,y), \qquad \dot{y} = Q(x,y),$$

where P and Q are real polynomials of degree n and $P(0,0) = Q(0,0) = 0$. Define the polynomial

$$p(r^2) := \frac{1}{2\pi r}\int_0^{2\pi} R(r,\theta)\, d\theta,$$

where R is given in (10) and set $w(r) = r^2 p'(r^2)$. Denote by d the degree of w and by N^+ its number of non-negative roots. For each fixed $s \in \mathbb{R}$ consider the function

$$\begin{aligned}M_s(r,\theta) :&= R(r,\theta)w'(r) + s\left(\frac{\partial R(r,\theta)}{\partial r} + \frac{\partial \Theta(r,\theta)}{\partial \theta} + \frac{R(r,\theta)}{r}\right)w(r)\\ &=: \sum_{i=1}^{n+d-1} m_i(s,\theta)r^i,\end{aligned}$$

and, for any $i \geq 1$, let $\mu_i(s)$ be such that $\max_{\theta\in[0,2\pi]} m_i(s,\theta) \leq \mu_i(s)$.

Then, if the polynomial

$$\Phi_s(r) := \sum_{i=1}^{n+d-1} \mu_i(s)r^i$$

is negative for all $r \in (0,\infty)$*, system* (1) *has at most* N^+ *limit cycles and all of them are hyperbolic.*

Proof. We want to apply Corollary 1 to system (1) with $V(x,y) = w(r)$ and the value s given in the statement of the Theorem. By hypothesis, we have

$$M_s = M_s(r,\theta) = \sum_{i=1}^{n+d-1} m_i(s,\theta) r^i \le \sum_{i=1}^{n+d-1} \mu_i(s) r^i = \Phi_s(r) < 0$$

for all $r \in (0,\infty)$. Notice that by the proof of Corollary 1 and because M_s does no vanish there are no limit cycles in $\{w(r) = 0\}$. Hence the maximum number of limit cycles is $\ell(\mathbb{R}^2) = 0$ when $s \ge 0$ and $\ell(\mathbb{R}^2, w)$ if $s < 0$. In fact notice that $\{w(r) = 0\}$ is formed by the origin and $N^+ - 1$ disjoint concentric cercles. Therefore $\ell(\mathbb{R}^2, w) = N^+$ and again by Corollary 1 the theorem follows. □

Remark 1. (i) The choice of the function $V(x,y) = w(r)$ in Theorem 1 is motivated by the following fact: for the simple system that in polar coordinates writes as $\dot r = r p(r^2)$, $\dot\theta = q(r^2)$, where q is any arbitrary polynomial, it holds that the corresponding M_{-1}, given in (3), is always negative.

(ii) Following the proof of Corollary 1 it is not difficult to see that under the hypotheses of the Theorem 1, if the system has only the origin as a critical point then it has at least $N^+ - 2$ limit cycles, with alternating stability. The reason is that two consecutive circles of $\{w(r) = 0\}$ always are the boundaries of positive or negative invariant regions.

We end this subsection with a concrete application of Theorem 1 to a 3-parameter family of planar vector fields. Consider the system

$$\begin{aligned} \dot x &= x(1-(x^2+y^2))(2-(x^2+y^2)) - y + ax^2 y + bx^2 y^2, \\ \dot y &= x + y(1-(x^2+y^2))(2-(x^2+y^2)) + cx^2. \end{aligned} \tag{11}$$

We will prove that if a, b and c are such that

$$\Psi_{a,b,c}(r) := -10 + \frac{9}{4}(|a|+|c|) + \frac{9}{4}|b| r + (12 + |a| + |c|)\, r^2 + |b| r^3 - 4r^4 < 0$$

for all $r > 0$, then system (11) has at most two (hyperbolic) limit cycles. Moreover, when they exist, one is included in the disc $\mathscr{D} := \{x^2 + y^2 \le 3/2\}$ and is stable and the other one is outside the disc and it is unstable.

To apply Theorem 2 we compute $p(s) = 2 - 3s + s^2$. Then taking $w(r) = r^2 p'(r^2) = r^2(-3 + 2r^2)$ and $s = -1$, we obtain

$$M_{-1}(r,\theta) = \frac{1}{4}\left(-40 + a\left(6\sin(2\theta) - 3\sin(4\theta)\right) + c\left(6\sin(2\theta) + 3\sin(4\theta)\right)\right) r^4$$
$$+ \frac{3}{8} b\left(2\cos(\theta) - 3\cos(3\theta) + \cos(5\theta)\right) r^5$$
$$+ \left(12 + a\sin(4\theta) - c\sin(4\theta)\right) r^6 - \frac{b}{2}\left(-\cos(3\theta) + \cos(5\theta)\right) r^7 - 4r^8.$$

Hence, for the values of the parameters considered, we can prove that

$$M_{-1}(r,\theta) \leq r^4 \Psi_{a,b,c}(r) < 0$$

for all $r > 0$. Thus we can apply Theorem 2. Since $N^+ = 2$ we have proved that system (11) has at most two (hyperbolic) limit cycles.

For instance the condition on $\Psi_{a,b,c}$ holds for $a = 1/8$, $b = 1/15$ and $c = 1/20$. Moreover for these parameters it is not difficult to prove, by using resultants and the Sturm's theorem, that the origin is the unique critical point, which is unstable. Finally, by studying the flow on $\{x^2 + y^2 = R^2\}$, for R big enough, and on $\{x^2 + y^2 = 3/2\}$, we prove the existence of both limit cycles.

3 More Applications

This section contains an extension of a Massera's result extracted from [21] and a study of an extension of the van der Pol system introduced in [34].

3.1 A Generalization of a Result of Massera

Consider the generalized smooth second order Liénard equation.

$$\ddot{x} + f(x)\dot{x} + g(x) = 0,$$

with f and g smooth functions. It can be written as the planar system

$$\dot{x} = y, \qquad \dot{y} = -f(x)y - g(x). \tag{12}$$

We define $G(x) = \int_0^x g(z)\,dz$.

Using once more the extended Bendixson-Dulac Theorem and its Corollary 1 we can prove the following result.

Proposition 5. *Let $\mathscr{W} = \mathscr{I} \times \mathbb{R}$ be a vertical strip of $\mathbb{R}^2$, where $\mathscr{I}$ is an open interval containing the origin. Assume that the functions f and g are of class $\mathscr{C}^1$,*

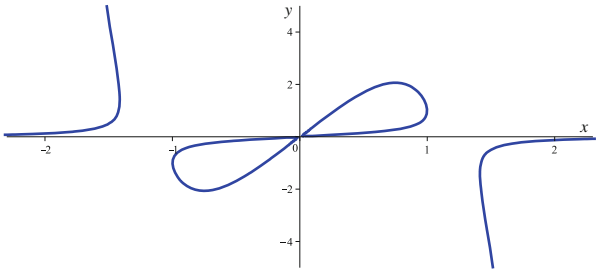

Fig. 2 Example of set $\{V = 0\}$, under the hypotheses of Proposition 5

that g only vanishes at the origin and that $f + 2(f/g)'G$ does not change sign on $\mathscr{I}$, vanishing only at $x = 0$. Then system (12) has at most one periodic orbit which entirely lies in $\mathscr{W}$, and when it exists it is a hyperbolic limit cycle.

Proof. By taking $V(x, y) = y^2 + (2Gf)y/g + 2G$ and $s = -1$ we can compute M_s given in (3), obtaining that

$$M_{-1} = \left(f + 2G(f/g)'\right) y^2.$$

Notice that G/g and $(f/g)'G$ are well–defined at the origin. By the hypotheses, M_-1 does not change sign on $\mathscr{W}$ and $\{M_{-1} = 0\} = \{xy = 0\}$. Moreover this set does not contain periodic orbits. Hence we can apply Corollary 1. Since $s < 0$ we have to compute $\ell(\mathscr{W}, V)$. The function V has degree 2 in y and when $x = 0$ the only point in $\mathscr{V}_0 := \{V = 0\}$ is $(0, 0)$. Therefore the set $\mathscr{V}_0$ has no oval surrounding the origin. Moreover, since the origin is the only critical point of the system and $\mathscr{V}_0$ is without contact by the flow of the system, then $\mathscr{V}_0$ does not contain ovals at all. In Fig. 2 we illustrate a possible set $\mathscr{V}_0$, taking $f(x) = -4 + x^2 + x^4$ and $g(x) = x$. Then $V(x, y) = y^2 + (-4 + x^2 + x^4)xy + x^2$ and $M_{-1}(x, y) = 2(1 + 2x^2)x^2y^2$. Hence, in general, all the connected regions of $\mathscr{W} \setminus \mathscr{V}_0$ are simply connected but one and $\ell(\mathscr{W}, V) = 1$. Thus we have proved the uniqueness of the limit cycle. □

We remark that Proposition 5 when $g(x) = x$, contains the following classical result, which was proved by Massera [28] and Sansone [32].

Massera's Theorem. *Consider the Liénard differential system (12) with $g(x) = x$, $f(0) < 0$ and $f'(x)x > 0$ if $x \neq 0$. Then system (12) has at most one limit cycle.*

3.2 A Generalization of van der Pol Equation

The system

$$\dot{x} = y, \quad \dot{y} = -x + (b^2 - x^2)(y + y^3), \tag{13}$$

is introduced and studied in [34] as a generalization of the van der Pol equation. In the papers [22, 34] it is proved that it has at most one (hyperbolic) limit cycle and that it exists if and only if $b \in (0, b^*)$ for some $0 < b^* < \sqrt[6]{9\pi^2/16} \approx 1.33$. This bifurcation value is refined in [16], proving that $b^* \in (0.79, 0.817)$. In fact, numerically it can be seen that $b^* \approx 0.80629$. In this section we will prove the uniqueness of the limit cycle when $b \in (0, 0.6]$ using a suitable Bendixson-Dulac function. This idea is developed in [16] where the authors prove, with the same method, the uniqueness and hyperbolicity of the limit cycle holds when $b \in (0, 0.817)$ and its non-existence when $b \in [0.817, \infty)$.

To give an idea of how we have found the function V and the value s to find the function M_s that we will use in our proof we first study again the van der Pol system. As we will see the main difficulty of this example is that the function M_s is a function of two variables.

The van der Pol Equation (A Second Approach)

The van der Pol equation studied in Sect. 1.2 (see "Uniqueness of the Limit Cycle for the van der Pol Equation"), after a rescaling of variables, is equivalent to the system

$$\dot{x} = y, \quad \dot{y} = -x + (b^2 - x^2)y. \tag{14}$$

Arguing like in Sect. 2.1 (see "A First Method") it is natural to start considering functions of the form

$$V(x, y) = v_2 y^2 + v_1(x)y + v_0(x),$$

with $s = -1$. Then the corresponding M_{-1} given in (3) is a polynomial of degree 2 in y, with coefficients being functions of x. In particular the coefficient of y^2 is

$$v_1'(x) + v_2(b^2 - x^2).$$

Taking $v_1(x) = (x^2 - 3b^2)v_2 x/3$ we get that this coefficient vanishes. Next, fixing $v_2 = 6$, and imposing to the coefficient of y to be zero we obtain that $v_0(x) = 6x^2 + c$, for any constant c. Finally, taking $c = b^2(3b^2 - 4)$, we arrive to

$$V(x, y) = 6y^2 + 2(x^2 - 3b^2)xy + 6x^2 + b^2(3b^2 - 4). \tag{15}$$

Then

$$M_{-1}(x, y) = 4x^4 + b^2(3b^2 - 4)(x^2 - b^2).$$

It is easy to see that for $b \in (0, 2/\sqrt{3}) \approx (0, 1.15)$, $M_{-1}(x, y) > 0$. Hence we can apply Corollary 1. As $V(x, y)$ is quadratic in y, $V(x, y) = 0$ has at most one oval, see Fig. 3 for $b = 1$. Hence $\ell(\mathbb{R}^2, V) = 1$ and we have proved the uniqueness

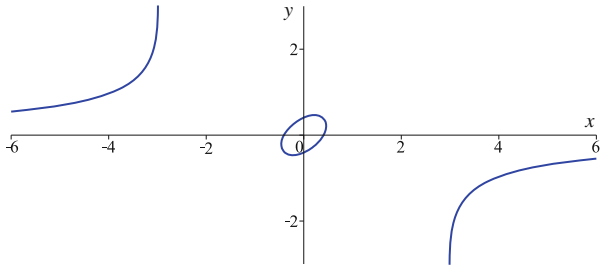

Fig. 3 The algebraic curve $V(x, y) = 0$ with $b = 1$

and hyperbolicity of the limit cycle when $b < 2/\sqrt{3}$. Recall that the proof given in Sect. 1.2 (see "Uniqueness of the Limit Cycle for the van der Pol Equation") is simpler and valid for all values of the parameter. We have included this one as a motivation for the construction of the function $V(x, y)$ used to study system (13).

3.3 *System* (13) *with* $b \leq 0.6$

By making some modifications to the function V given by (15), we propose the following function V,

$$\begin{aligned} V(x, y) =& \big(2x^3 + 6b^2(1 - b^2)x\big)y^3 + 6(1 - b^2)y^2 + 2(x^2 - 3b^2)xy \\ &+ 6(1 - b^2)x^2 + b^2(3b^2 - 4) \end{aligned} \tag{16}$$

and again $s = -1$. Some computations give that

$$\begin{aligned} M_{-1}(x, y) = 6\big((2 - 3b^2)x^4y^2 - 2b^2(2 - b^2)x^3y^3 + (2 - b^2)x^2y^4\big) + 2(2 - 3b^2)x^4 \\ -3b^2(14 - 15b^2)x^2y^2 + 12b^4(2 - b^2)xy^3 - b^2(4 - 9b^2)x^2 \\ +3b^4(2 - 3b^2)y^2 + b^4(4 - 3b^2). \end{aligned}$$

Then we need to study the shape of the connected components of set $\mathbb{R}^2\backslash\{V = 0\}$ and the sign of $M_{-1}(x, y)$. It can be seen that the algebraic curve $V(x, y) = 0$, with $V(x, y)$ given by (16), has no singular points and at most one closed oval for $b \in (0.0.85]$. Moreover $M_{-1}(x, y)$ does not vanish for $b \in (0, 0.651)$. Hence we can apply again Corollary 1. Since $\ell(\mathbb{R}^2, V) = 1$ we have proved the uniqueness and hyperbolicity of the limit cycle for $b \leq 0.6$ (in fact for $b \leq 0.651$).

The tools used to prove the above assertions are given in [16]. Among other methods the authors use discriminants, double discriminants, Sturm sequences and the study of the points at infinity of the algebraic curves.

Acknowledgements First author is supported by the MICIIN/FEDER grant number MTM2008-03437 and the Generalitat de Catalunya grant number 2009SGR410.

References

1. Álvarez, M.J., Gasull, A., Giacomini, H.: A new uniqueness criterion for the number of periodic orbits of Abel equations. J. Differ. Equ. **234**, 161–176 (2007)
2. Álvarez, M.J., Gasull, A., Prohens, R.: Limit cycles for two families of cubic systems. Nonlinear Anal. **75**, 6402–6417 (2012)
3. Chamberland, M., Cima, A., Gasull, A., Mañosas, F.: Characterizing asymptotic stability with Dulac functions. Discret. Contin. Dyn. Syst. **17**, 59–76 (2007)
4. Cherkas, L.A.: Estimation of the number of limit cycles of autonomous systems. Differ. Equ. **13**, 529–547 (1977)
5. Cherkas, L.A.: Dulac function for polynomial autonomous systems on a plane. Differ. Equ. **33**, 692–701 (1997)
6. Cherkas, L.A., Grin', A.A.: A second-degree polynomial Dulac function for a cubic system on the plane. Differ. Equ. **33**, 1443–1445 (1997)
7. Cherkas, L.A., Grin', A.A.: A Dulac function in a half-plane in the form of a polynomial of the second degree for a quadratic system. Differ. Equ. **34**, 1346–1348 (1998)
8. Cherkas, L.A., Grin', A.A.: On the Dulac function for the Kukles system. Differ. Equ. **46**, 818–826 (2010)
9. Cherkas, L.A., Grin', A.A.: A function of limit cycles of the second kind for autonomous functions on a cylinder. Differ. Equ. **47**, 462–470 (2011)
10. Cherkas, L.A., Grin', A.A., Schneider, K.R.: Dulac-Cherkas functions for generalized Liénard systems. Electron. J. Qual. Theory Differ. Equ. **35**, 23 (2011)
11. Chicone, C.: Ordinary differential equations with applications. In: Texts in Applied Mathematics, vol. 34, 2nd edn. Springer, New York (2006)
12. Cima, A., Gasull, A., Mañosas, F.: Limit cycles for vector fields with homogeneous components. Appl. Math. (Warsaw) **24**, 281–287 (1997)
13. Conti, R.: Soluzioni periodiche dell'equazione di Liénard generalizatta. Esistenza ed unicità, Bolletino della Unione Matematica Italiana **3**, 111–118 (1952)
14. Dumortier, F., Llibre, J., Artés, J.C.: Qualitative theory of planar differential systems. UniversiText, Springer, New York (2006)
15. Fečkan, M.: A generalization of Bendixson's criterion. Proc. Am. Math. Soc. **129**, 3395–3399 (2001)
16. García-Saldaña, J.D., Gasull, A., Giacomini, H.: Bifurcation values for a family of planar vector fields of degree five (2012, preprint). arXiv:1202.1919
17. Gasull, A., Giacomini, H.: A new criterion for controlling the number of limit cycles of some generalized Liénard equations. J. Differ. Equ. **185**, 54–73 (2002)
18. Gasull, A., Giacomini, H.: Upper bounds for the number of limit cycles through linear differential equations. Pac. J. Math. **226**, 277–296 (2006)
19. Gasull, A., Giacomini, H.: Upper bounds for the number of limit cycles of some planar polynomial differential systems. Discret. Contin. Dyn. Syst. **27**, 217–229 (2010)
20. Gasull, A., Guillamon, A.: Non-existence, uniqueness of limit cycles and center problem in a system that includes predator-prey systems and generalized Liénard equations. Differ. Equ. Dyn. Syst. **3**, 345–366 (1995)
21. Gasull, A., Giacomini, H., Llibre, J.: New criteria for the existence and non-existence of limit cycles in Liénard differential systems. Dyn. Syst. **24**, 171–185 (2009)
22. Han, M., Qian, T.: Uniqueness of periodic solutions for certain second-order equations. Acta Math. Sci. (Engl. Ser.) **20**, 247–254 (2004)
23. Hsu, S.B., Huang, T.W.: Global stability for a class of predator-prey systems. SIAM J. Appl. Math. **55**, 763–783 (1995)
24. Ilyashenko, Yu.: Centennial history of Hilbert's 16th problem. Bull. Am. Math. Soc. (N.S.) **39**, 301–354 (2002)
25. Kuang, Y.: Global stability of Gause-type predator-prey systems. J. Math. Biol. **28**, 463–474 (1990)

26. Li, Y., Muldowney, J.S.: On Bendixson's criterion. J. Differ. Equ. **106**, 27–39 (1993)
27. Lloyd, N.G.: A note on the number of limit cycles in certain two-dimensional systems. J. Lond. Math. Soc. **20**(2), 277–286 (1979)
28. Massera, J.L., Sur un théorème de, G.: Sansone sur l'équation di Liénard (French). Boll. Un. Mat. Ital. **9**(3), 367–369 (1954)
29. McCluskey, C.C., Muldowney, J.S., James, S.: Bendixson-Dulac criteria for difference equations. J. Dynam. Differ. Equ. **10**, 567–575 (1998)
30. Moreira, H.N.: On Liénard's equation and the uniqueness of limit cycles in predator-prey systems. J. Math. Biol. **28**, 341–354 (1990)
31. Perko, L.M.: Differential equations and dynamical systems. In: Texts in Applied Mathematics, vol. 7, 3rd edn. Springer, New York (2001)
32. Sansone, G.: Soluzioni periodiche dell'equazione di Liénard. Calcolo del periodo (Italian). Univ. e Politecnico Torino. Rend. Sem. Mat. **10**, 155–171 (1951)
33. Sansone, G., Conti, R.: Equazioni differenziali non lineari (Italian). Edizioni Cremonese, Roma (1956)
34. Wang, X., Jiang, J., Yan, P.: Analysis of global bifurcation for a class of systems of degree five. J. Math. Anal. Appl. **222**, 305–318 (1998)
35. Wilson, G.: Hilbert's sixteenth problem. Topology **17**, 53–73 (1978)
36. Yamato, K.: An effective method of counting the number of limit cycles. Nagoya Math. J. **76**, 35–114 (1979)
37. Yan Qian Ye, et al.: Theory of limit cycles. In: Translations of Mathematical Monographs, vol. 66. American Mathematical Society, Providence (1986)
38. Zhi Fen Zhang, et al.: Qualitative theory of differential equations. In: Translations of Mathematical Monographs, vol. 101. American Mathematical Society, Providence (1992)

On Solutions of Zero Exponential Type for Some Inhomogeneous Differential-Difference Equations in a Banach Space

Sergey Gefter and Tetyana Stulova

Abstract Let A be a closed linear operator on a Banach space having a bounded inverse operator and f be an entire function of zero exponential type. The problem on well-possedeness of the differential-difference equation $w'(z) = Aw(z-h) + f(z)$ in the space of entire functions of zero exponential type is considered. Moreover, an explicit formula for the zero exponential type entire solution is found.

The present paper deals with special holomorphic solutions of the following simple inhomogeneous linear differential-difference equation

$$w'(z) = Aw(z-h) + f(z). \tag{1}$$

in a Banach space. Here $h \in C$ and A is a closed linear operator on a complex Banach space E with the domain $D(A)$ which is not necessarily dense in E. Note for $h = 0$, we obtain the classical linear differential equation. Here we suppose that A has a bounded inverse. These operators appear in studying some boundary-value problems for parabolic type equations (see [4, 8, 17–19]). For example, this case appears in the problem on the heat conduction equation on the finite segment $[0, l]$ with zero boundary conditions. In this situation we can consider $E = C[0, l]$, and operator $A = \frac{d^2}{dx^2}$ with the domain of definition $D(A) = \{u \in C^2[0, l] : u(0) = u(l) = 0\}$. In studying Eq. (1) we suppose that $f(z)$ is an E-valued entire function and by a solution of the equation we imply an entire E-valued function $w(z)$, such that $w(z) \in D(A)$ and Eq. (1) is fulfilled. The properties of holomorphic and entire solutions of the differential equation $w'(z) = Aw(z) + f(z)$

S. Gefter (✉) · T. Stulova
Department of Mechanics and Mathematics, Kharkiv National University,
4 sq. Svoboda, Kharkiv, 61022 Ukraine
e-mail: gefter@univer.kharkov.ua; stutestella@rambler.ru

S. Ibáñez et al. (eds.), *Progress and Challenges in Dynamical Systems*,
Springer Proceedings in Mathematics & Statistics 54,
DOI 10.1007/978-3-642-38830-9_15, © Springer-Verlag Berlin Heidelberg 2013

were examined in numerous works (see, for example, [1, 5, 10–14, 16]). The reader can find the results concerning the continuously differentiable solutions of linear difference-differential equations in a Banach space in *semi-axes* in [2, 3, 7] (in the case of finite dimensional space) and [6, 8, 9, 15, 20] (in the case of abstract delay differential equation).

The main result of the paper is the well-possedeness proof of Eq. (1) in the space of entire functions of zero exponential type (see Theorems 2 and 3). Let us recall that entire E-valued function $f(z)$ is of zero exponential type if for $f(z)$ the following condition

$$\forall \varepsilon > 0 \; \exists C_\varepsilon > 0 \; \forall z \in C : \|f(z)\| \leq C_\varepsilon e^{\varepsilon |z|}$$

is fulfilled. In the present paper we consider such entire functions as the simplest generalizations of polynomials (see in this connection results Corollaries 6 and 4). Note that we obtain the solution of zero exponential type of Eq. (1) under a single assumption of invertibility of the operator A, and we do not impose another conditions on its resolvent. The proofs of the main theorems are based on the analysis of the implicit differential-difference equation $Tw'(z+h) + g(z) = w(z)$ (see Theorem 1). In the paper some examples of ordinary differential-difference equations and partial differential-difference equations are considered (see Examples 1–6).

1 Main Results

Let E be a complex Banach space and $g : C \longrightarrow E$ be an entire function.

Lemma 1. *The function $g(z)$ is of zero exponential type if and only if $g'(z)$ is of zero exponential type. Moreover, the following condition is fulfilled*
$\forall \varepsilon > 0 \; \exists \, M > 0 \; \forall n \in N \cup \{0\} : \; \left\| g^{(n)}(z) \right\| \leq M \; \varepsilon^n e^{\varepsilon |z|}, \; z \in C.$

Proof. Let $g(z) = \sum\limits_{m=0}^{\infty} \alpha_m z^m$ be of zero exponential type and $\varepsilon > 0$.
As $\sqrt[m]{m! \, \|\alpha_m\|} \to 0$ then $m! \, \|\alpha_m\| \leq M \cdot \varepsilon^m$, i.e. $\|\alpha_m\| \leq M \frac{\varepsilon^m}{m!}$ for some $M > 0$ and all $m \in N$. Hence $\left\| g^{(n)}(z) \right\| =$

$$= \left\| \sum_{m=n}^{\infty} \alpha_m m(m-1) \ldots (m-(n-1)) z^{m-n} \right\| = \left\| \sum_{m=0}^{\infty} \frac{(m+n)!}{m!} \alpha_{m+n} z^m \right\| \leq$$

$$\leq \sum_{m=0}^{\infty} \frac{(m+n)!}{m!} \|\alpha_{m+n}\| \cdot |z^m| \leq \sum_{m=0}^{\infty} \frac{M}{m!} \cdot \varepsilon^{m+n} \cdot |z|^m = M \cdot \varepsilon^n \sum_{m=0}^{\infty} \frac{(\varepsilon |z|)^m}{m!} = M \varepsilon^n e^{\varepsilon |z|}.$$

Conversely, let $g'(z) = \sum\limits_{k=0}^{\infty} \beta_k z^k$ be of zero exponential type. Then $g(z) = g(0) + \int\limits_0^z g'(\xi)\, d\xi = g(0) + z \sum\limits_{k=0}^{\infty} \frac{\beta_k}{k+1} z^k$ and $\sqrt[k]{k! \left\| \frac{\beta_k}{k+1} \right\|} = \frac{\sqrt[k]{k! \|\beta_k\|}}{\sqrt[k]{k+1}} \to 0$, that is the function $g(z)$ is of zero exponential type as well. □

Let $T : E \to E$ be an arbitrary bounded linear operator and $h \in \mathbb{C}$. We first consider the inhomogeneous implicit differential-difference equation of the form

$$Tw'(z+h) + g(z) = w(z), \tag{2}$$

Theorem 1. *Let g be of zero exponential type. Then Eq. (2) has a unique entire solution of zero exponential type*

$$w(z) = \sum_{n=0}^{\infty} T^n g^{(n)}(z + nh). \tag{3}$$

Proof. Let $g(z) = \sum\limits_{m=0}^{\infty} \alpha_m z^m$, $\varepsilon > 0$ and $\varepsilon e^h < \frac{1}{\|T\|}$. Then by Lemma 1 we obtain: $\exists M > 0\ \forall n \in N : \left\| g^{(n)}(z + nh) \right\| \le M \varepsilon^n e^{\varepsilon |z+nh|} \le M \varepsilon^n e^{\varepsilon |z|} e^{nh}$, $z \in C$. We show that the series $\sum\limits_{n=0}^{\infty} T^n g^{(n)}(z + nh)$ converges uniformly in any disk and the sum is an entire function of zero exponential type. Let $|z| \le R$. Then $\left\| T^n g^{(n)}(z + nh) \right\| \le$ $\le M \|T\|^n \varepsilon^n e^{\varepsilon R} e^{nh} = M e^{\varepsilon R} (\varepsilon \cdot \|T\| e^h)^n$ and $\sum\limits_{n=0}^{\infty} \left(\varepsilon \|T\| e^h \right)^n < +\infty$. Therefore, the series $\sum\limits_{n=0}^{\infty} T^n g^{(n)}(z + nh)$ converges uniformly in the disk $|z| \le R$. So, the function $w(z) = \sum\limits_{n=0}^{\infty} T^n g^{(n)}(z + nh)$ is entire. It is easy to check that $w(z)$ is a solution of Equation (2). Apart from that $\|w(z)\| \le \sum\limits_{n=0}^{\infty} \left\| T^n g^{(n)}(z + nh) \right\| \le$ $\le M e^{\varepsilon |z|} \sum\limits_{n=0}^{\infty} \left(\varepsilon \|T\| e^h \right)^n = \frac{M}{1 - \varepsilon \|T\| e^h} \cdot e^{\varepsilon |z|}$, $z \in C$. Hence, $w(z)$ is of zero exponential type.

Let us prove the uniqueness of the entire solution of zero exponential type. Let $w(z)$ be a solution of the homogeneous equation $Tw'(z + h) = w(z)$. Then $T^n w^{(n)}(nh) = w(0)$ and $\|w(0)\| \le \|T^n\| \|w^{(n)}(nh)\| \le \|T^n\| M \varepsilon^n e^{\varepsilon R} e^{nh} \le$ $\le M e^{\varepsilon R} (\varepsilon \cdot \|T\| e^h)^n$. So $\lim\limits_{n \to \infty} \left(\sqrt[n]{\|w(0)\|} \right) \le \varepsilon \|T\| e^h < 1$, that is $w(0) = 0$. Note that the function $w^{(k)}(z)$ satisfies the homogeneous equation $Tw'(z + h) = w(z)$. Moreover, it is an entire function of zero exponential type (see Lemma 1). Therefore, $w_k = 0$, $k \in N$, that is $w = 0$. Theorem is proved. □

Corollary 1. *Let g be of zero exponential type. Then Equation*

$$Tw^{(m)}(z+h)+g(z)=w(z), \tag{4}$$

has the unique entire solution of zero exponential type

$$w(z)=\sum_{n=0}^{\infty}T^n g^{(nm)}(z+nh).$$

If $h=0$, then we obtain the following corollary.

Corollary 2. *Let g be of zero exponential type. Then the following differential equation*

$$Tw^{(m)}(z)+g(z)=w(z), \tag{5}$$

has a unique entire solution of zero exponential type

$$w(z)=\sum_{n=0}^{\infty}T^n g^{(nm)}(z). \tag{6}$$

Let us make some remarks relating to Theorem 1.

Remark 1. If instead of entire functions of zero exponential type we shall consider entire functions of positive exponential type, then the conclusion of Theorem 1 is even incorrect in one-dimensional case. In fact, the homogeneous equation $w'(z+e)=w(z)$ has the nonzero solution $w(z)=e^{z/e}$. Moreover, if we consider inhomogeneous equation $w'(z+h)+g(z)=w(z)$, where $h=e$ and $g(z)=e^{z/e}$, then the series $\sum_{n=0}^{\infty}g^{(n)}(z+nh)$ diverges for all $z\in C$.

Remark 2. We claim that if $g(z)$ is an entire function of positive exponential type, then Eq. (2) cannot even have a continuously differentiable solution in the real axes. In order to show that we consider the following shift operator on a Hilbert space E with an orthonormalized basis $\{e_n\}_{n=0}^{\infty}$: $Te_n=e_{n+1}$. Let $g(z)=e^z e_0$. If $w(t)=\sum_{n=0}^{\infty}w_n(t)\,e_n$ is a solution of Equation $Tw'(t+1)+g(t)=w(t)$ in the real axes, then

$$\begin{cases} e^t=w_0(t) \\ w_n'(t+1)=w_{n+1}(t), \quad n\geq 0. \end{cases}$$

Hence, $w_n(t)={w_0}^{(n)}(t+n)$. Therefore, $w_n(t)=e^{t+n}$ and $w_n(0)=e^n$. Hence, $\sum_{n=0}^{\infty}|w_n(0)|^2=+\infty$, contradicting that w is an E-valued function.

Remark 3. Considering of an arbitrary bounded operator in the series (3) essentially leads to the use of entire functions of a zero exponential type. Namely, let $g(z)$ be a vector-function which is holomorphic in a neighborhood of zero and the series $\sum\limits_{n=0}^{\infty} T^n g^{(n)}(0)$ converges for any bounded linear operator T. If $g(z) = \sum\limits_{m=0}^{\infty} \alpha_m z^m$, then $g^{(n)}(0) = n!\alpha_n$ and we find that the sequence $\{n!T^n\alpha_n\}$ is bounded. Therefore, $\overline{\lim\limits_{n\to\infty}} \sqrt[n]{n!\,\|T^n\alpha_n\|} \le 1$. Taking as T the operator $\frac{1}{\varepsilon}\cdot I$, where $\varepsilon > 0$ and I is the identity operator, we find that $\overline{\lim\limits_{n\to\infty}} \sqrt[n]{n!\,\|\alpha_n\|} \le \varepsilon$, that is $\lim\limits_{n\to\infty} \sqrt[n]{n!\,\|\alpha_n\|} = 0$. Thus, g is an entire function of zero exponential type.

Now let us consider the following generalizations of Theorem 1 and Corollary 1. We examine the following differential-difference equation of the m-th order

$$T_m w^{(m)}(z+mh) + T_{m-1} w^{(m-1)}(z+(m-1)h) + \ldots + T_1 w'(z+h) + g(z) = w(z), \tag{7}$$

where $T_1, T_2, \ldots, T_m$ are bounded linear operators on E and $g(z)$ is an entire E-valued function of zero exponential type.

We set

$$\tilde{w}(z) = \begin{pmatrix} w(z) \\ w'(z+h) \\ \vdots \\ w^{(m-1)}(z+(m-1)h) \end{pmatrix}, \quad \tilde{T} = \begin{pmatrix} 0 & 1 & 0 & \cdots & 0 \\ 0 & 0 & 1 & \cdots & 0 \\ \cdots & \cdots & \cdots & \cdots & \cdots \\ 0 & 0 & 0 & \cdots & 1 \\ T_1 & T_2 & T_3 & \cdots & T_m \end{pmatrix},$$

$$\tilde{g}(z) = \begin{pmatrix} g(z) \\ 0 \\ 0 \\ \vdots \\ 0 \end{pmatrix}.$$

Consider the space $V = \underbrace{E \oplus E \oplus \ldots \oplus E}_{n}$, with $\|v\| = \max\limits_{1\le k\le n} \|v_k\|$, if $v = \begin{pmatrix} v_1 \\ v_2 \\ \vdots \\ v_n \end{pmatrix}$.

Then V is a Banach space, $\tilde{T}$ is a bounded operator on V, $\tilde{g}$ is a V-valued entire function of zero exponential type, and Eq. (7) has the following form

$$\tilde{T}\tilde{w}'(z+h) + \tilde{g}(z) = \tilde{w}(z).$$

According to Theorem 1, Eq. (7) has a unique entire solution of zero exponential type. In particular, if $h = 0$, then we have the following statement.

Corollary 3. *Let $T_1, T_2, \ldots, T_m$ be bounded linear operators on E and $g(z)$ be an entire E-valued function of zero exponential type. Then the differential equation*

$$T_m w^{(m)} + T_{m-1} w^{(m-1)} + \ldots + T_1 w' + g(z) = w(z) \tag{8}$$

has a unique entire solution of zero exponential type.

Let us return to the entire solutions of the Equation (1).

Theorem 2. *Let A be a closed linear operator on a Banach space, where the domain of definition $D(A)$ of A is not necessarily dense. If A has a bounded inverse operator and $f(z)$ is an entire function of zero exponential type, then Eq. (1) has a unique entire solution of zero exponential type*

$$w(z) = -\sum_{n=0}^{\infty} A^{-(n+1)} f^{(n)}(z + (n+1)h). \tag{9}$$

Moreover, the Cauchy problem

$$\begin{cases} w'(z) = Aw(z-h) + f(z) \\ w(0) = w_0 \end{cases} \tag{10}$$

has an entire solution of zero exponential type if and only if
$w_0 + \sum_{n=0}^{\infty} A^{-(n+1)} f^{(n)}((n+1)h) = 0.$

Proof. Let $T = A^{-1}$ and $g(z) = -A^{-1} f(z+h)$. Then T is bounded, $g(z)$ is an entire function of zero exponential type and Eq. (1) is equivalent to Eq. (2). According to Theorem 1, Eq. (1) has the unique entire solution of zero exponential type
$w(z) = \sum_{n=0}^{\infty} T^n g^{(n)}(z+nh) = -\sum_{n=0}^{\infty} A^{-(n+1)} f^{(n)}(z+(n+1)h)$ and
$w(0) = -\sum_{n=0}^{\infty} A^{-(n+1)} f^{(n)}((n+1)h)$. The theorem is proved. □

Corollary 4. *Let A be a closed linear operator on a Banach space where the domain of definition $D(A)$ of A is not necessarily dense. Consider the following differential equation*

$$w^{(m)}(z) = Aw(z-h) + f(z). \tag{11}$$

If A has a bounded inverse operator and $f(z)$ is an entire function of zero exponential type, then Eq. (11) has the unique entire solution of zero exponential type $w(z) = -\sum_{n=0}^{\infty} A^{-(n+1)} f^{(mn)}(z+nh)$. Moreover, the Cauchy problem

$$w'(z) = Aw(z-h) + f(z), \quad w^{(j)}(0) = 0, \quad j = 0, \ldots, m-1.$$

has the entire solution of zero exponential type if and only if
$w_0 + \sum_{n=0}^{\infty} A^{-(n+1)} f^{(mn)}((n+1)h) = 0.$

Proof. Let $T = A^{-1}$ and $g(z) = -A^{-1} f(z+h)$. Then $D(T) = E$, T is bounded, $g(z)$ is an entire function of zero exponential type and Eq. (1) is equivalent to Eq. (5). According to Theorem 1, Eq. (5) has the unique entire solution of zero exponential type
$w(z) = \sum_{n=0}^{\infty} T^n g^{(mn)}(z+nh) = -\sum_{n=0}^{\infty} A^{-(n+1)} f^{(mn)}(z+(n+1)h)$ and
$w(0) = -\sum_{n=0}^{\infty} A^{-(n+1)} f^{(mn)}((n+1)h)$. The corollary is proved. □

Corollary 5. *Let E_1 and E_2 be Banach spaces, $Q : E_1 \to E_2$ be an arbitrary bounded linear operator, and A be a closed linear operator from E_1 to E_2 with the domain $D(A)$, that is not necessarily dense in E_1. Consider the following implicit differential-difference equation*

$$Qw'(z) = Aw(z-h) + g(z), \tag{12}$$

where $g(z)$ is an E_2-valued entire function. If A has a bounded inverse operator and g is of zero exponential type, then Eq. (12) has the unique entire solution of zero exponential type $w(z) = -\sum_{n=0}^{\infty} \left(A^{-1}Q\right)^n A^{-1} g^{(n)}(z+(n+1)h)$.

From Theorem 2 we obtain the following interesting algebraic and arithmetical corollaries:

Corollary 6. *Let E be a finite-dimensional space and $f(z)$ be an E-valued polynomial of degree m. Consider the system of differential-difference equations $w'(z) = Aw(z-h) + f(z)$, where A is an invertible matrix. Then this system has the unique polynomial solution of degree m,*
$w(z) = -\sum_{n=0}^{m} A^{-(n+1)} f^{(n)}(z+(n+1)h)$.

Corollary 7. *Consider the system of differential-difference equations $w'(z) = Aw(z-h) + f(z)$, where A is a matrix with integer coefficients, $f(z)$ is a polynomial with integer coefficients and $h \in Z$. If* $\det A = \pm 1$, *then this system has a unique polynomial solution and this solution is a polynomial with integer coefficients.*

Proof. It follows from Cramer's rule that A^{-1} has integer coefficients. □

Remark 4. Let matrix A have integer coefficients and $\det A \neq \pm 1$ (in particular, $det A = 0$). It is easy to show that there is polynomial $f(z)$ with integer coefficients such that System (10) either does not have polynomial solutions with integer coefficients at all or can have polynomial solutions with nonintegral coefficients ($\det A = 0$).

Now let us consider the space $\widetilde{E_0}$ of all E-valued entire functions of zero exponential type. Then $\widetilde{E_0} = \bigcap_{\varepsilon>0} E_\varepsilon$, where E_ε is a Banach space that consists of all entire functions such that $\|f\|_\varepsilon := \sup_{z\in C} \|f(z)\| e^{-\varepsilon|z|} < +\infty$. The space $\widetilde{E_0}$ is a Frechet space with the natural topology of projective limit of Banach spaces.

Theorem 3. *Let the operator A have bounded inverse and $g(z)$ be an E-valued entire function of zero exponential type. The unique solution (9) of Eq. (2) is continuously dependent upon the function g in the topology of the space $\widetilde{E_0}$.*

Proof. Consider the differentiation operator on the space $\widetilde{E_0}$: $(Dg)(z) = g'(z)$ (see Lemma 2). Show that this operator is continuous on $\widetilde{E_0}$. As $\widetilde{E_0}$ is a Frechet space, it is sufficient to check that D is closed. Let $\{g_n\} \in \widetilde{E_0}$, $g_n \to 0$ and $Dg_n \to h$ in $\widetilde{E_0}$. Let $\varepsilon_0 > 0$. Therefore, $g_n \to 0$ in the space $\widetilde{E_{\varepsilon_0}}$. Thus, $g_n(z) \to 0$ uniformly in every disk. Hence, $g_n'(z) \to 0$ uniformly in every disk as well. But as $Dg_n \to h$ in $\widetilde{E_{\varepsilon_0}}$, then $(Dg_n)(z) \to h(z)$ uniformly in every disk. Thus, $h(z) = 0$, $z \in C$.

Now consider the operator $\tilde{S}$ on the space $\widetilde{E_0}$: $(\tilde{S}g)(z) = Tw'(z+h)$, where $T = A^{-1}$. Then $\tilde{S} = \tilde{T}DU_h$, where $(\tilde{T}f)(z) = Tf(z)$, $(U_h f)(z) = f(z+h)$. It is not difficult to check that operators $\tilde{S}$ and U_h are bounded on any space $\widetilde{E_\varepsilon}$, $\varepsilon > 0$. Therefore, they are continuous on the space $\widetilde{E_0}$. Hence, $\tilde{S}$ is continuous on $\widetilde{E_0}$. Rewrite Eq. (1) in the following form $(I - \tilde{S})w = g$, where $g = -A^{-1}f(z+h)$. According to Theorem 1, the operator $I - \tilde{S}$ is invertible, and $((I-\tilde{S})^{-1}g)(z) =$

$= \sum_{n=0}^{\infty} T^n g^{(n)}(z+nh)$, $g \in \widetilde{E_0}$. From the Banach theorem on inverse operator, we find that the operator $(I - \tilde{S})^{-1}$ is continuous. The theorem is proved. □

Remark 5. We suppose that all conditions of the Theorem 1 are fulfilled, and T and g are fixed. Using the inequality from the proof of Theorem 1 it can be shown that the solutions of Equation (2) as $h \to 0$ converges uniformly in every disk to the solution of the corresponding differential equation
$Tw'(z) + g(z) = w(z)$.

Consider some examples.

Example 1. Let $E = C$ and $A = I$. Consider the differential-difference equation $w'(z) = w(z-h) + f(z)$. If $f(z)$ is an entire function of zero exponential type, then this equation has a unique entire solution of zero exponential type
$w(z) = -\sum_{n=0}^{\infty} f^{(n)}(z + (n+1)h)$ and this solution is continuously dependent upon f in the topology of the space $\widetilde{E_0}$.

Example 2. Let $E = C$ and $A = I$. Consider the differential-difference equation $w^{(m)}(z) = w(z-h) + f(z)$. If $f(z)$ is an entire function of zero exponential type, then this equation has a unique entire solution of zero exponential type
$w(z) = -\sum_{n=0}^{\infty} f^{(mn)}(z + (n+1)h)$.

Example 3. Consider the following differential-difference equation $\ddot{x}(t)+\omega^2 x(t-h)=f(t)$, where $h,\omega>0$ and $f(t)$ is the trace on the real axes of an entire function of zero exponential type. With $h=0$, this equation becomes the equation of forced oscillations. Using Corollary 1, we find that this equation has a unique solution, which can be extended to an entire function of zero exponential type,

$$x(t)=\sum_{k=0}^{\infty}\frac{(-1)^{k+1}}{\omega^{2k+2}}f^{(2k)}(t+(n+1)h).$$

Example 4. Let $dimE=2$ and $detT=0$. We have the singular system of two differential-difference equations

$$Tw'(z+h)+g(z)=w(z),$$

where $T=\begin{pmatrix} a & b\\ c & d\end{pmatrix}$ and $g(z)=\begin{pmatrix} g_1(z)\\ g_2(z)\end{pmatrix}$ is an entire function of zero exponential type. As $detT=0$, then $T^2=\lambda T$ where $\lambda=a+d$ is an eigenvalue of T. Hence, $T^n=\lambda^{n-1}T, n\geq 1$. Therefore, the unique zero exponential type entire solution for this equation becomes $w(z)=g(z)+T\sum\limits_{n=1}^{\infty}\lambda^{n-1}g^{(n)}(z+nh)$.

Example 5. Let $E=C[0,1]$, $A=\frac{d}{dx}$ and $D(A)=\{u\in C^1[0,1]:u(0)=0\}$.

Then $\left(A^{-1}v\right)(x)=\int\limits_0^x v(y)\,dy$ and $\left(A^{-(n+1)}v\right)(x)=\frac{1}{n!}\int\limits_0^x(x-y)^n v(y)\,dy$.

In the transition to the real axis, Eq. (12) has the following form

$$\begin{cases}\frac{\partial w}{\partial t}(x,t)=\frac{\partial w}{\partial x}(x,t-h)+f(t,x), & t\in R,\ x\in(0,1)\\ w(t,0)=0.\end{cases}\tag{13}$$

If $f(t,x)=\sum\limits_{n=0}^{\infty}c_n(x)\,t^n$, where $c_n\in C[0,1]$ and $\lim\limits_{n\to\infty}\sqrt[n]{n!\,\|c_n\|}=0$, then in the class of such functions Problem (13) has the unique solution

$$w(t,x)=-\sum_{n=0}^{\infty}\frac{1}{n!}\int_0^x(x-y)^n\frac{\partial^n f}{\partial t^n}(t+(n+1)h,y)\,dy.$$

In particular, if $h=0$ using Taylor's formula, we have

$$w(t,x)=-\sum_{n=0}^{\infty}\frac{1}{n!}\int_0^x(x-y)^n\frac{\partial^n f}{\partial t^n}(t,y)\,dy=-\int_0^x f(t+x-y,y)\,dy.$$

It is important to note that for $h = 0$ Problem (13) has only the zero solution for the homogeneous equation even in the class of continuously differentiable functions.

Example 6. Let $E = C[0,\ 1]$, $A = \frac{d^2}{dx^2}$, $D(A) = \left\{u \in C^2[0,\ 1] : u(0) = u(1) = 0\right\}$. Then the operator A is invertible, $\left(A^{-1}h\right)(x) = \int\limits_0^1 G(x,\ y)\ h(y)dy$, where G is the Green function of the corresponding boundary problem. In this case $\left(A^{-(n+1)}h\right)(x) = \int\limits_0^1 G_{n+1}(x,\ y)\ h(y)\,dy$, where $G_1(x,\ y) = G(x, y)$, $G_{n+1}(x,\ y) = \int\limits_0^1 G_n(x,\ s)\ G(s,\ y)\,ds$. In the transition to the real axis, Eq. (1) has the form of the heat equation on $(0,\ 1)$ with zero boundary conditions

$$\begin{cases} \frac{\partial w}{\partial t}(t, x) = \frac{\partial^2 w}{\partial x^2}(t - h, x) + f(t, x), \quad t \in R,\ x \in (0,\ 1) \\ w(t,\ 0) = w(t,\ 1) = 0 \end{cases} \tag{14}$$

If $f(t, x) = \sum\limits_{n=0}^{\infty} c_n(x)\ t^n$, where $c_n \in C[0, 1]$ and $\lim\limits_{n\to\infty} \sqrt[n]{n!\,\|c_n\|} = 0$, then the problem (14) has the solution $w(t, x) = -\sum\limits_{n=0}^{\infty} \int\limits_0^1 G_{n+1}(x, y)\, \frac{\partial^n f}{\partial t^n}(t + (n + 1)h, y)\,dy$.

Example 7. Let $T, Q : E \to E, TQ = QT, \sigma(Q) = \{0\}, v \in E$, and $g(z) = e^{zQ}v$. Consider the equation $Tw'(z+h)+e^{zQ}v = w(z)$. As the operator Q is quasinilpotent, then $g(z)$ is of zero exponential type. According to Theorem 1,

$$w(z) = \sum_{n=0}^{\infty} T^n g^{(n)}(z + nh) = \sum_{n=0}^{\infty} T^n Q^n e^{(z+nh)Q} v = \sum_{n=0}^{\infty} (TQ)^n \left(e^{hQ}\right)^n e^{zQ} v =$$

$$= \sum_{n=0}^{\infty} \left(TQe^{hQ}\right)^n e^{zQ} v = \left(1 - TQe^{hQ}\right)^{-1} e^{zQ} v.$$

In particular, if $h = 0$, then we obtain the differential equation $Tw' + e^{zQ}v = w(z)$, which has the unique solution of zero exponential type $w(z) = (1 - TQ)^{-1} e^{zQ} v$. Note that the function $w(z)$ is a solution of this equation for a weaker assumption. Instead of the condition $\sigma(Q) = \{0\}$ we can consider that Q is such a bounded linear operator for which $1 \notin \sigma(TQ)$.

References

1. Balser, W., Duval, A., Malek, S.: Summability of formal solutions for abstract Cauchy problems and related convolution equations. Ulmer Seminare über Funktionalanalysis und Differetialgleichungen. **11**, 29–44 (2007)

2. Bellman, R., Cooke, K.L.: Differential-Difference Equations. Mathematics in Science and Engineering. The RAND Corporation, Santa Monica/New York Academic Press, London (1963)
3. Campbell, S.L.: Singular linear systems of differential equations with delays. Appl. Anal. **11**, 129–136 (1980)
4. Da Prato, G., Sinestrati, E.: Differential operators with non dense domain. Annali della scuola normale superiore. Di Pisa. **14**, 285–344 (1987)
5. Dalec'kii, Ju., Kreĭn, M.: Stability of differential equations in Banach space. American Mathematical Society, Providence (1974)
6. Datko, R.: Linear autonomous neutral differential equations in a banach space. J. Differ. Equ. **25**, 258–274 (1977)
7. Diekmann, O., van Gils, S.A., Verduyn Lunel, S.M., Walther, H.O.: Delay equations. Springer, New York (1995)
8. Engel, K.I., Nagel, R.: One-Parameter Semigroups for Linear Evolution Equations. Springer, New York (2000)
9. Favini, A., Vlasenko L.: Degenerate non-stationary differential equations with delay in Banach spaces. J. Differ. Equ. **192**(1), 93–110 (2003)
10. Gefter, S., Stulova, T.: On Holomorphic Solutions of Some Implicit Linear Differential Equation in a Banach Space. Operator Theory: Advances and Applications, vol. 191, pp. 323–332. Birkhauser Verlag, Basel (2009)
11. Gefter, S., Stulova, T.: On entire solutions of some inhomogeneous linear differential equations in a banach space. In: Proceedings of the 3rd Nordic EWM Summer School for PhD Students in Mathematics. TUCS General Publication, vol. 53, pp. 211–214. Turku Centre for Computer Science, Turku (2009). www.doria.fi/bitstream/handle/10024/66221/TUCSGeneral53.pdf
12. Gorbachuk, M.: An operator approach to the Cauchy-Kovalevskay theorem. J. Math. Sci. **5**, 1527–1532 (2000)
13. Gorbachuk, M.: On analytic solutions of operator-differential equations. Ukr. Math. J. **52**(5), 680–693 (2000)
14. Gorbachuk, M., Gorbachuk, V.: On the well-posed solvability in some classes of entire functions of the Cauchy problem for differential equations in a Banach space. Methods Funct. Anal. Topol. **11**(2), 113–125 (2005)
15. Hale, J.K.: Theory of Functional Differential Equations. Springer, New York (1977)
16. Hille, E.: Ordinary Differential Equations in the Complex Domain. Wiley-InterScience, New York/London (1976)
17. Kreĭn, S.: Linear Differential Equations in Banach Space. Translations of Mathematical Monographs, vol. 29. American Mathematical Society, Providence (1971)
18. Sil'chenko, Yu.T.: Differential equations with non-densely defined operator coefficients, generating semigroups with singularities. Nonlinear Anal. A Theory Methods **36**(3), 345–352 (1999)
19. Sil'chenko, Yu.T., Sobolevskii, P.E.: Solvability of the Cauchy problem for an evolution equation in a Banach space with a non-densely given operator coefficient which generates a semigroup with a singularity (Russian). Sib. Math. J. **27**(4), 544–553 (1986)
20. Vlasenko, L.A.: On a class of neutral functional differential equations. Funct. Differ. Equ. **13**(2), 305–321(2006)

Homoclinic Solutions to Infinity and Oscillatory Motions in the Restricted Planar Circular Three Body Problem

Marcel Guardia, Pau Martín, and Tere M. Seara

Abstract The circular restricted three body problem models the motion of a massless body under the influence of the Newtonian gravitational force caused by two other bodies, the primaries, which describe circular planar Keplerian orbits. The system has a first integral, the Jacobi constant. The existence of oscillatory motions for the restricted planar circular three body problem, that is, of orbits which leave every bounded region but which return infinitely often to some fixed bounded region, was proved by Llibre and Simó [18] in 1980. However, their proof only provides such orbits for values of the ratio between the masses of the two primaries exponentially small with respect to the Jacobi constant. In the present work, we extend their result proving the existence of oscillatory motions for any value of the mass ratio. The existence of these motions is a consequence of the transversal intersection between the stable and unstable manifolds of infinity, which guarantee the existence of a symbolic dynamics that creates the oscillatory orbits. We show that this intersection does happen for any value of the mass ratio and for big values of the Jacobi constant. We remark that, since in our setting the mass ratio is no longer small, this transversality cannot be checked by means of classical perturbation theory respect to the mass ratio. Furthermore, since our method is

M. Guardia (✉)
Department of Mathematics, Mathematics Building, University of Maryland, College Park, MD 20742-4015, USA
e-mail: marcel.guardia@upc.edu; mguardia@umd.edu

P. Martín
Departament de Matemàtica Aplicada IV, Universitat Politècnica de Catalunya, Campus Nord, Edifici C3, C. Jordi Girona, 1-3. 08034 Barcelona, Spain
e-mail: martin@ma4.upc.edu

T.M. Seara
Departament de Matemàtica Aplicada I, Universitat Politècnica de Catalunya, Diagonal 647, 08028 Barcelona, Spain
e-mail: tere.m-seara@upc.edu

S. Ibáñez et al. (eds.), *Progress and Challenges in Dynamical Systems*,
Springer Proceedings in Mathematics & Statistics 54,
DOI 10.1007/978-3-642-38830-9_16,

valid for all values of mass ratio, we are able to detect a curve in the parameter space, formed by the mass ratio and the Jacobi constant, where cubic homoclinic tangencies between the invariant manifolds of infinity appear.

1 Introduction

The restricted three body problem is a simplified model of the three body problem, where one of the bodies is assumed to be massless and, consequently, its movement does not affect the other two, *the primaries*. Thus, the orbits of the primaries are governed by the classical Kepler's laws. Let us assume that the primaries, whose motion lies on a plane, perform circular orbits and that the movement of the massless body takes place in the same plane. This particular case of the three body problem is known as the restricted planar circular three body problem (RPC3BP from now on). Normalizing the total mass of the system to be one, the RPC3BP depends on one parameter μ, which measures the quotient between the masses of the two primaries and therefore satisfies $\mu \in [0, 1/2]$. Using the appropriate units, the RPC3BP is Hamiltonian with respect to

$$H(q, p, t; \mu) = \frac{\|p\|^2}{2} - \frac{1-\mu}{\|q + \mu q_0(t)\|} - \frac{\mu}{\|q - (1-\mu)q_0(t)\|} \tag{1}$$

where $q, p \in \mathbb{R}^2$ and $-\mu q_0(t)$ and $(1-\mu)q_0(t)$, $q_0(t) = (\cos t, \sin t)$, are the positions of the primaries. Although the Hamiltonian (1) has two and a half degrees of freedom, it has a conserved quantity, the *Jacobi constant*, defined as

$$\mathscr{J}(q, p, t; \mu) = H(q, p, t; \mu) - (q_1 p_2 - q_2 p_1). \tag{2}$$

The purpose of this work is to prove the existence of oscillatory orbits for the RPC3BP, that is, orbits such that

$$\limsup_{t \to \pm\infty} \|q\| = +\infty \quad \text{and} \quad \liminf_{t \to \pm\infty} \|q\| < +\infty.$$

When $\mu = 0$, there is only one primary. In this case, the motion of the massless body satisfies Kepler's laws. In particular, oscillatory motions cannot exist. In this work we show that oscillatory orbits do exist for any value of the mass ratio $\mu \in (0, 1/2]$.

Chazy proposed the existence of oscillatory motions (see, for instance, Arnold et al. [1]). In 1922, he gave a complete classification of all possible states that a three body problem can approach as time tends to infinity. For the restricted three body problem, in all its instances, there are only four possible final states, namely

- $H^{\pm}$ (hyperbolic): $\|q(t)\| \to \infty$ and $\|\dot{q}(t)\| \to c > 0$ as $t \to \pm\infty$.
- $P^{\pm}$ (parabolic): $\|q(t)\| \to \infty$ and $\|\dot{q}(t)\| \to 0$ as $t \to \pm\infty$.

- $B^{\pm}$ (bounded): $\limsup_{t\to\pm\infty} \|q\| < +\infty$.
- $OS^{\pm}$ (oscillatory): $\limsup_{t\to\pm\infty} \|q\| = +\infty$ and $\liminf_{t\to\pm\infty} \|q\| < +\infty$.

Chazy himself gave examples of all these types of motion, except the oscillatory ones. Sitnikov, in [27], was the first to prove the existence of oscillatory motions. He considered a particular configuration of the restricted spatial three body problem with mass ratio $\mu = 1/2$, called now *the Sitnikov example*. A new proof was given later by Moser [22]. In his approach, he studied the invariant manifolds of infinity and proved that they intersect transversally. This fact allowed him to establish the existence of symbolic dynamics close to these invariant manifolds which lead to the existence of oscillatory motions.

In the case of the RPC3BP, the first ones to obtain oscillatory motions were Simó and Llibre [18]. Nevertheless, they had to assume μ small enough. As in [22], they checked that the invariant manifolds of infinity intersect transverally for those values of the mass ratio. In fact, for $\mu = 0$, the system is integrable, and these manifolds coincide. To check that the intersection is transversal for $\mu \neq 0$ they used the classical Poincaré–Melnikov Theory [21, 25]. However, in order to compute the Melnikov integral, they had to assume the Jacobi constant large enough, which, in turn, made the Melnikov integral exponentially small. For this reason, they had to assume the mass ratio to be exponentially small with respect to the Jacobi constant. It is worth to remark that the orbits they obtained have large Jacobi constant, which implies that they are far from the primaries and, hence, far from collisions. Using the real-analyticity of the invariant manifolds of infinity, this result was extended by Xia [29] to any mass ratio $\mu \in (0, 1/2]$ except for a finite number of values. See also [22] for a similar argument for the Sitnikov problem.

Using Simó and Llibre's approach, in [23] the restricted planar *elliptic* three body problem was considered. There some formal computations were performed to show that the invariant manifolds of infinity intersect transversally for arbitrarily small mass ratio. A rigorous computation of the Melnikov function is done in [6], assuming the eccentricity small enough.

Another related problem were oscillatory motions have also been found is the (non necessarily restricted) collinear three body problem [19].

All these works follow Moser's approach, that is, oscillatory motions appear linked to transversal homoclinic points to infinity and symbolic dynamics. A different approach using Aubry-Mather theory and semi-infinite regions of instability has been recently developed in [9–11]. Using this new approach the authors have proven the existence of orbits which initially are in the range of our Solar System and become oscillatory as time tends to infinity for the RPC3BP with a realistic mass ratio for the Sun-Jupiter pair.

With respect to the abundance of oscillatory motions in Celestial Mechanics, the recent paper [12] deals with the Hausdorff dimension of the set of oscillatory motions for the Sitnikov example and the RPC3BP. Using [22] and [18], they prove that for both problems and a Baire generic subset of an open set of parameters (the eccentricity of the primaries in the Sitnikov example and the mass ratio and the Jacobi constant in the RPC3BP) the Hausdorff dimension is maximal. As pointed

out to us by V. Kaloshin and A. Gorodetski, the present work and the techniques developed by them in [12] lead to the proof of the existence of a set of maximal Hausdorff dimension of oscillatory motions for any value of the mass ratio and a Baire generic subset of an open set of Jacobi constants.

The purpose of this work is to improve the results of [18] and [29]. We prove that, provided $\mathscr{J}$ is large enough, the invariant manifolds of infinity intersect transversally *for any value of* $\mu \in (0, 1/2]$, from which we can deduce the existence of oscillatory motions for those values of the parameters. Furthermore, our approach allows us to detect a curve in the parameter plane $(\mu, \mathscr{J})$ where the stable and unstable invariant manifolds of infinity undergo a cubic homoclinic tangency. Note that for these values of the parameters the classical Poincaré–Melnikov Theory does not apply due to the exponentially smallness with respect to the Jacobi constant $\mathscr{J}$ of the difference between the invariant manifolds. This phenomenon was already known by Poincaré [25], and he called it the *Fundamental problem of mechanics*. It has been under research in the past decades but, due to its difficulty, it has essentially only been considered in toy models [4,8,14,16,28] or in general systems under hypothesis that typically do not apply when one wants to study problems from Celestial Mechanics [2,3,5,7,13].

We would like to remark the novelty of the present work in two different aspects. On the one hand, it is the first one in Celestial Mechanics where, without assuming artificial smallness conditions on the parameters of the problem, exponentially small splitting of separatrices is shown. On the other, it is the first one dealing with an irrational Hamiltonian.

The main result of the present work is the following.

Theorem 1 (Main Theorem). *Fix any* $\mu \in (0, 1/2]$. *Then, there exists* $J_0 > 0$ *big enough, such that for any* $J > J_0$ *there exists an orbit* $(q_J(t), p_J(t))$ *of* (1) *in the hypersurface* $\mathscr{J}(q, p, t; \mu) = J$ *which is oscillatory. Namely, it satisfies*

$$\limsup_{t\to\pm\infty} \|q_J\| = +\infty \quad \textit{and} \quad \liminf_{t\to\pm\infty} \|q_J\| < +\infty.$$

Moreover, if we take $\mu^* \in (0, 1/2)$, *there exists* $J^* > 0$ *big enough such that, for any* $J > J^*$ *and* $\mu \in (0, \mu^*]$, *the previous claims hold.*

As we have already mentioned, the main difficulty of the proof lies in proving the tranversal intersection of the invariant manifolds of infinity, which we need to define. First, writing the system in rotating coordinates, it becomes a two degrees of freedom Hamiltonian system. At each energy level, infinity corresponds to a periodic orbit with two dimensional stable and unstable manifolds. Their intersection is studied in Sect. 2. Theorem 2 gives an asymptotic formula for their difference and Theorem 3 claims that they intersect transversally for any $\mu \in (0, 1/2]$ and $\mathscr{J}$ large enough and gives a formula for the area of the lobes between two consecutive homoclinic points in an associated Poincaré map. Theorem 1 follows from Theorem 3 using the reasoning in [18]. Finally, Theorem 4 describes the cubic homoclinic tangency between the manifolds appearing in a bifurcation curve in the parameter space (μ, J).

In Sect. 3, we give some ideas of the proof of the theorems. Following [17, 26], we look for parameterizations of the invariant manifolds as graphs of generating functions in a suitable domain using the Hamilton-Jacobi equation and we state Theorem 5, which gives the difference of these generating functions. Then, Theorems 2 and 3 follow easily from Theorem 5. The proof of Theorems 4 and 5 can be found in [15].

2 The Invariant Manifolds of Infinity

To study the invariant manifolds of infinity, it is more convenient to express the Hamiltonian (1) in polar coordinates. It is given by

$$\begin{aligned} H(r,\alpha,y,G,t;\mu) =& \frac{y^2}{2}+\frac{G^2}{2r^2}-\tilde{U}(r,\alpha-t;\mu) \\ =& \frac{y^2}{2}+\frac{G^2}{2r^2}-\frac{1}{r}-U(r,\alpha-t;\mu), \end{aligned} \tag{3}$$

where (r,α) are the polar coordinates of the configuration space and (y,G) are the symplectic conjugate variables. That is, y is the radial velocity (or momentum) and G is the angular momentum. The function $\tilde{U}$ is the Newtonian potential

$$\tilde{U}(r,\phi;\mu)=\frac{1-\mu}{(r^2-2\mu r\cos\phi+\mu^2)^{1/2}}+\frac{\mu}{(r^2+2(1-\mu)r\cos\phi+(1-\mu)^2)^{1/2}}$$

and satisfies $\tilde{U}(r,\phi;\mu)=\frac{1}{r}+U(r,\phi;\mu)$, with $U=\mathcal{O}(\mu)$ (although, in our case, μ is not necessarily small).

The associated equations are

$$\begin{aligned} &\dot{r}=y, \qquad \dot{y}=\frac{G^2}{r^3}-\frac{1}{r^2}+\partial_r U(r,\alpha-t;\mu), \\ &\dot{\alpha}=\frac{G}{r^2}, \quad \dot{G}=\partial_\alpha U(r,\alpha-t;\mu). \end{aligned} \tag{4}$$

Call $\Phi_{t,t_0}=(\Phi^r_{t,t_0},\Phi^y_{t,t_0},\Phi^\alpha_{t,t_0},\Phi^G_{t,t_0})$ to the flow associated to this equation. Then, the stable and unstable manifolds of infinity are defined as

$$\begin{aligned} \mathcal{W}^s_\infty &= \left\{ z\in\mathbb{R}^2\times\mathbb{T}\times\mathbb{R} : \lim_{t\to+\infty}\Phi^r_{t,t_0}(z;\mu)=\infty, \lim_{t\to+\infty}\Phi^y_{t,t_0}(z;\mu)=0 \right\} \\ \mathcal{W}^u_\infty &= \left\{ z\in\mathbb{R}^2\times\mathbb{T}\times\mathbb{R} : \lim_{t\to-\infty}\Phi^r_{t,t_0}(z;\mu)=\infty, \lim_{t\to-\infty}\Phi^y_{t,t_0}(z;\mu)=0 \right\}, \end{aligned} \tag{5}$$

where $\mathbb{T}=\mathbb{R}/(2\pi\mathbb{Z})$. These invariant manifolds are analytic (see [20]).

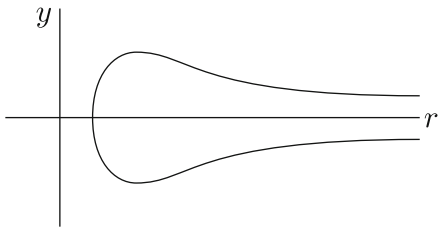

Fig. 1 Projection on the (r, y) plane of the separatrix (6) of system (4) with $\mu = 0$. It also correspond to the separatrix of the Poincaré map $\mathbb{P}_{G_0,\phi_0}$ in (16)

When $\mu = 0$, the RPC3BP is reduced to a central force equation. Hence, the energy H and the angular momentum G are conserved and the system is integrable. The invariant manifolds of infinity coincide along a *homoclinic manifold*, $\mathscr{W}^s_\infty = \mathscr{W}^u_\infty$, formed by a family of homoclinic orbits to infinity which perform Keplerian parabolic orbits. By "infinity" we mean $(r, y) = (+\infty, 0)$. Then, "infinity" is foliated by the periodic orbits parameterized by the angular momentum G_0

$$\Lambda_{G_0} = \{(r, \alpha, y, G) : r = \infty, y = 0, \alpha \in \mathbb{T}, G = G_0\}.$$

Their homoclinic orbits belong to the energy level $H = 0$ and can be parameterized by G_0 and their initial condition in the angular variable. We denote them by

$$z_{\mathrm{h}}(u; G_0, \alpha_0) = (r_{\mathrm{h}}(u; G_0), \alpha_0 + \alpha_{\mathrm{h}}(u; G_0), y_{\mathrm{h}}(u; G_0), G_0), \tag{6}$$

and we fix the origin of time such that $y_{\mathrm{h}}(0; G_0) = 0$ and $\alpha_{\mathrm{h}}(0; G_0) = 0$ (see Fig. 1), which makes the homoclinic orbit with $\alpha_0 = 0$ symmetric,

2.1 The RPC3BP as a Nearly Integrable Hamiltonian System with Two Time Scales

Exponentially small phenomena often arise in systems with two different time scales. More concretely, the exponentially small splitting of separatrices often appears when the system has combined elliptic and hyperbolic (or parabolic) behavior in such a way that the elliptic one is much faster than the hyperbolic (or parabolic) one. This is also the case in our problem.

It is easy to explain why this system has two time scales. If the Jacobi constant is large, the massless body is very far from the primaries. Moreover, the oscillatory motions lie close to the invariant manifolds of the "parabolic" infinity, that is, orbits whose speed tends to zero as their position tends to infinity. Hence, the massless body moves slowly in comparison with the primaries. Therefore, rescaling time in such a way that the massless body has a speed of order one, the primaries perform rapid rotations.

For system (4) neither H nor G are preserved, but there is still a conserved quantity, the Jacobi constant. In polar coordinates, it is given by

$$\mathscr{J}(r,\alpha,y,G,t;\mu) = H(r,\alpha,y,G,t;\mu) - G. \tag{7}$$

We fix $\mathscr{J} = G_0$ and, in this invariant hypersurface, we consider the new variables

$$r = G_0^2\tilde{r}, \quad y = G_0^{-1}\tilde{y}, \quad \alpha = \tilde{\alpha} \quad \text{and} \quad G = G_0\tilde{G} \tag{8}$$

and we rescale time as

$$t = G_0^3 s. \tag{9}$$

Calling

$$V(\tilde{r},\phi;\mu,G_0) = G_0^2 U(G_0^2\tilde{r},\phi;\mu),$$

we have that

$$\begin{aligned} V(\tilde{r},\phi;\mu,G_0) = & \frac{1-\mu}{\left(\tilde{r}^2 - 2(\frac{\mu}{G_0^2})\tilde{r}\cos\phi + (\frac{\mu}{G_0^2})^2\right)^{1/2}} \\ & + \frac{\mu}{\left(\tilde{r}^2 + 2(\frac{1-\mu}{G_0^2})\tilde{r}\cos\phi + (\frac{1-\mu}{G_0^2})^2\right)^{1/2}} - \frac{1}{\tilde{r}}, \end{aligned} \tag{10}$$

and we obtain that system (4) becomes

$$\begin{aligned} &\frac{d}{ds}\tilde{r} = \tilde{y}, \quad \frac{d}{ds}\tilde{y} = \frac{\tilde{G}^2}{\tilde{r}^3} - \frac{1}{\tilde{r}^2} + \partial_{\tilde{r}} V(\tilde{r},\tilde{\alpha} - G_0^3 s;\mu,G_0), \\ &\frac{d}{ds}\tilde{\alpha} = \frac{\tilde{G}}{\tilde{r}^2}, \quad \frac{d}{ds}\tilde{G} = \partial_{\alpha} V(\tilde{r},\tilde{\alpha} - G_0^3 s;\mu,G_0). \end{aligned} \tag{11}$$

Now the two time scales become clear. Indeed, in these variables we have that $d\tilde{y}/ds \sim d\tilde{r}/ds \sim 1$, which are the variables that will define the separatrix, whereas the perturbation dependence on time is fast. Note that $V \sim \mu G_0^{-2}$ and thus, since we are taking $G_0 \gg 1$, we are dealing with a *fast oscillating small* perturbation. When one studies the splitting of separatrices phenomena in the resonances of nearly integrable Hamiltonian systems typically the perturbation has the same size as the integrable unperturbed system (see [3, 13, 28]). This is not the case in the present problem. In this sense, its study is simpler and does not need the use of *inner equations*, *complex matching techniques* or *continuous averaging* as in those papers.

The new system (11) is Hamiltonian with respect to

$$\tilde{H}(\tilde{r},\tilde{\alpha},\tilde{y},\tilde{G},s;\mu,G_0)=\frac{\tilde{y}^2}{2}+\frac{\tilde{G}^2}{2\tilde{r}^2}-\frac{1}{\tilde{r}}-V(\tilde{r},\tilde{\alpha}-G_0^3 s;\mu,G_0). \tag{12}$$

The Jacobi constant is now $\mathscr{J}=G_0^{-2}\tilde{H}-G_0\tilde{G}$ and the periodic orbit at infinity is given by $(\tilde{r},\tilde{\alpha},\tilde{y},\tilde{G})=(\infty,\tilde{\alpha},0,1)$, which belongs to the surface of Jacobi constant

$$\mathscr{J}\left(G_0^2\tilde{r},\tilde{\alpha},G_0^{-1}\tilde{y},\tilde{G}_0 G,G_0^3 s;\mu\right)=-G_0.$$

One of the main advantages of this new set of coordinates is that the parameterization of the separatrix of the unperturbed system (6) in the rescaled variables,

$$(\tilde{r},\tilde{\alpha},\tilde{y},\tilde{G})=(\tilde{r}_{\rm h}(s),\tilde{\alpha}_{\rm h}(s),\tilde{y}_{\rm h}(s),\tilde{G}_{\rm h}(s)), \tag{13}$$

is independent of G_0 (and also of μ). In particular, $\tilde{G}_{\rm h}(s)\equiv 1$. Moreover, note that after the rescaling we still have

$$\tilde{y}_{\rm h}(0)=0 \quad \text{and} \quad \tilde{\alpha}_{\rm h}(0)=0. \tag{14}$$

2.2 Main Result: Intersection of the Invariant Manifolds

Let $\tilde{\mathscr{W}}^s_\infty$ and $\tilde{\mathscr{W}}^u_\infty$ be the rescaling of the invariant manifolds $\mathscr{W}^s_\infty$ and $\mathscr{W}^u_\infty$ in (5).

Note that the dependence on s in (12) is only through $\tilde{\alpha}-G_0^{-3}s$. Thus, defining the new angle $\phi=\tilde{\alpha}-G_0^{-3}s$, we obtain the Hamiltonian

$$\mathscr{H}(\tilde{r},\phi,\tilde{y},\tilde{G};\mu,G_0)=\frac{\tilde{y}^2}{2}-G_0^3\tilde{G}+\frac{\tilde{G}^2}{2\tilde{r}^2}-\frac{1}{\tilde{r}}-V(\tilde{r},\phi;\mu,G_0), \tag{15}$$

which is autonomous with conserved energy $\mathscr{H}$, which is a rescaling of the Jacobi constant: $\mathscr{H}(\tilde{r},\tilde{\alpha}-G_0^3 s,\tilde{y},\tilde{G};\mu,G_0)=G_0^2\mathscr{J}(G_0^2\tilde{r},\tilde{\alpha},G_0^{-1}\tilde{y},G_0\tilde{G},G_0^3 s;\mu)$. This new set of coordinates is usually called (rescaled) rotating polar coordinates since they are set in a rotating frame with respect to the primaries.

The invariant manifolds $\tilde{\mathscr{W}}^s_\infty$ and $\tilde{\mathscr{W}}^u_\infty$ are three dimensional. In the energy level $\mathscr{H}(\tilde{r},\phi,\tilde{y},\tilde{G};\mu,G_0)=-G_0^3$, the corresponding invariant manifolds

$$\mathscr{W}^{u,s}_{\infty,G_0}=\tilde{\mathscr{W}}^{u,s}_\infty\cap\left\{\mathscr{H}(\tilde{r},\phi,\tilde{y},\tilde{G};\mu,G_0)=-G_0^3\right\}$$

are two dimensional. Moreover, if G_0 is large enough, in a neighborhood of these invariant manifolds $\dot{\phi}\neq 0$. Consequently, the flow associated to (15) restricted to $\mathscr{H}=-G_0^3$ induces a Poincaré map

$$\begin{aligned}\mathbb{P}_{G_0,\phi_0}:&\{\phi=\phi_0\}\longrightarrow\{\phi=\phi_0+2\pi\}\\&(r,y)\qquad\mapsto\quad\mathbb{P}_{G_0,\phi_0}(r,y).\end{aligned} \tag{16}$$

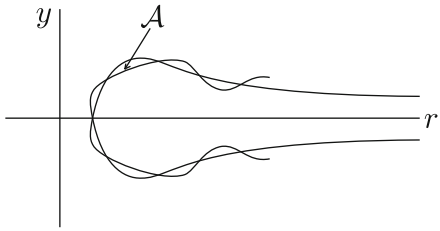

Fig. 2 Stable and unstable invariant manifolds of infinity for the Poincaré map $\mathbb{P}_{G_0,\phi_0}$ in (16)

This Poincaré map is a two dimensional area preserving map (it preserves the symplectic form $\Omega = dr \wedge dy$). The invariant manifolds become invariant curves $\gamma^{u,s}$ (see Fig. 2). We consider a parameterization of $\gamma^{u,s}$ of the form

$$\tilde{r} = \tilde{r}_{\mathrm{h}}(v), \quad \tilde{y} = Y_{\phi_0}^{u,s}(v;\mu,G_0), \tag{17}$$

where $\tilde{r}_{\mathrm{h}}(v)$ is the $\tilde{r}$ component of the separatrix parameterization (13). Then, following [26], to measure the distance between the invariant manifolds along a section $\tilde{r} = \text{const}$, it suffices to measure the difference between the functions $Y_{\phi_0}^{u,s}$.

Theorem 2. *Consider the invariant manifolds of infinity $\mathscr{W}^s_{\infty,G_0}$ and $\mathscr{W}^u_{\infty,G_0}$ of the system associated to Hamiltonian (15) in the level of energy $\mathscr{H} = -G_0^3$ and the corresponding invariant curves $\gamma^{u,s}$ of the Poincaré map $\mathbb{P}_{G_0,\phi_0}$. Then, there exists $G_0^* > 0$ such that for any $G_0 > G_0^*$ and $\mu \in (0, 1/2]$,*

- *The curves $\gamma^{u,s}$ have a parameterization of the form (17) and*
- *If we fix a section $\tilde{r} = \tilde{r}^*$, the distance d between these curves along this section is given by*

$$\begin{aligned} d = {} & \tilde{y}_{\mathrm{h}}(v^*)^{-1}\mu(1-\mu)\sqrt{\pi}\left[\frac{1-2\mu}{2\sqrt{2}}G_0^{3/2}e^{-\frac{G_0^3}{3}}\sin\left(\phi_0-\tilde{\alpha}_{\mathrm{h}}(v^*)+G_0^3v^*\right)\right. \\ & + 8G_0^{7/2}e^{-\frac{2G_0^3}{3}}\sin 2\left(\phi_0-\tilde{\alpha}_{\mathrm{h}}(v^*)+G_0^3v^*\right) \\ & \left. + \mathscr{O}\left((1-2\mu)G_0e^{-\frac{G_0^3}{3}}+G_0^3e^{-\frac{2G_0^3}{3}}\right)\right], \end{aligned}$$

where v^* is the only $v > 0$ such that $\tilde{r}(v^*) = \tilde{r}^*$ and $\tilde{y}_{\mathrm{h}}(v)$ and $\tilde{\alpha}_{\mathrm{h}}(v)$ are the $\tilde{y}$ and $\tilde{\alpha}$ components of the unperturbed homoclinic (13).

This theorem follows from Theorem 5 in Sect. 3, whose proof can be found in [15]. Observe that the distance is exponentially small with respect to G_0, which is taken as a large parameter. Moreover, note that the size of the first order in the formula of Theorem 2 is significantly different depending whether $\mu \neq 1/2$ or $\mu = 1/2$. The reason is that Hamiltonian (15) is periodic with respect to ϕ with period 2π, in the first case, and π, in the second one. Figure 3 illustrates why the

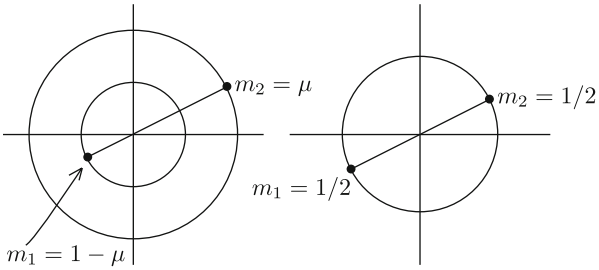

Fig. 3 The motion of the primary bodies in the cases $\mu \neq 1/2$ and $\mu = 1/2$ respectively

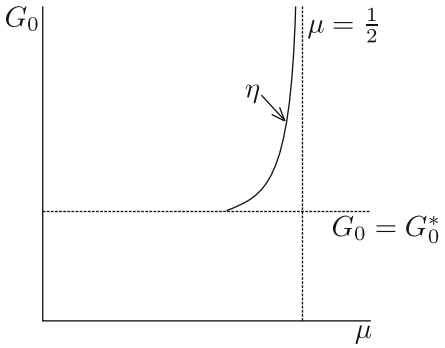

Fig. 4 Bifurcation curve η in the parameter space where the homoclinic tangency is undergone

periodicity of the system changes for $\mu = 1/2$. As usual in these problems, the smaller the period of the fast perturbation, the smaller the distance between the manifolds (see for instance [24]).

Looking at the formula given in Theorem 2, the zeros of the distance are given, up to first order, by the zeros of the function

$$f(x) = (1-2\mu)\sin x + 16\sqrt{2}G_0^2 e^{-\frac{G_0^3}{3}}\sin 2x \quad \text{where } x = \phi_0 - \tilde{\alpha}_{\mathrm{h}}(v) + G_0^3 v.$$

The number of zeros for $x \in [0, 2\pi)$ and their nondegeneracy depend on the parameters μ and G_0. For $\mu \neq 1/2$ and $G_0 > 0$ big enough, $f(x) \sim (1-2\mu)\sin x$ and has two nondegenerate zeros, which give rise to two transversal homoclinic points. On the contrary, for $\mu = 1/2$ and G_0 big enough, $f(x) \sim 16\sqrt{2}G_0^2 e^{-G_0^3/3}\sin 2x$, which has four nondegenerate zeros. Theorem 3 collects these facts. Between these two regimes the system undergoes a global bifurcation: one of the two transversal intersections becomes a cubic tangency where two new homoclinic points are born. This occurs in a curve η in the parameter plane (see Fig. 4) as is stated in Theorem 4.

Theorem 3. *Fix $\mu \in (0, 1/2]$. Then there exists $G^* > 0$ such that for any $G_0 > G^*$,*

- *The invariant curves $\gamma^{u,s}$ of the Poincaré map $\mathbb{P}_{G_0,\phi_0}$ intersect transversally and*
- *The area of the lobes between the invariant curves $\gamma^{u,s}$ between two transversal consecutive homoclinic points is given by*

$$\mathscr{A} = \mu(1-\mu)\sqrt{\pi}\left[\frac{1-2\mu}{\sqrt{2}} G_0^{-3/2} e^{-\frac{G_0^3}{3}} + 8 G_0^{1/2} e^{-\frac{2G_0^3}{3}}\right]\left(1 + \mathscr{O}\left(G_0^{-1/2}\right)\right).$$

Theorem 4. *Let $G_0^* > 0$ be the constant introduced in Theorem 2. Then, there exists a curve η in the parameter region*

$$(\mu, G_0) \in \left(0, \frac{1}{2}\right] \times (G_0^*, +\infty),$$

of the form

$$\mu = \mu^*(G_0) = \frac{1}{2} - 16\sqrt{2} G_0^2 e^{-\frac{G_0^3}{3}} \left(1 + \mathscr{O}\left(G_0^{-1/2}\right)\right),$$

such that, for $(\mu, G_0) \in \eta$,

- *The invariant curves $\gamma^{u,s}$ of the Poincaré map $\mathbb{P}_{G_0,\phi_0}$ have a cubic homoclinic tangency and a transversal homoclinic point and*
- *The area of the lobes between the invariant curves $\gamma^{u,s}$ between the homoclinic tangency and a consecutive transversal homoclinic point is given by*

$$\mathscr{A} = 10\sqrt{\pi} G_0^{1/2} e^{-2\frac{G_0^3}{3}} \left(1 + \mathscr{O}\left(G_0^{-1/2}\right)\right).$$

Theorem 3 is proven in Sect. 3. The proof of Theorem 4 can be found in [15].

2.3 From Transversal Homoclinic Points to Oscillatory Motions

The arguments used by Llibre and Simó in [18] to obtain oscillatory motions in the RPC3BP follow the ones developed by Moser in [22]. As a first step, it is necessary to control the local behavior near infinity by using McGehee coordinates [20], in which infinity becomes a parabolic point at the origin, and then the so-called Shilnikov coordinates to study the local map near zero.

The local behavior at infinity is independent of the values of the parameters, provided that G_0 is big enough. Indeed, in McGehee coordinates (see [18]) the system becomes

$$\frac{dx}{d\theta} = \frac{x^3 y}{4} + K\frac{x^7 y}{32} + \mathscr{O}_{10}(x, y)$$
$$\frac{dy}{d\theta} = \frac{x^4}{4} - K^2\frac{x^6}{32} + 3K\frac{x^6 y^2}{16} - \lambda(\theta;\mu)x^8 + \mathscr{O}_{10}(x, y)$$

where $K = \mathscr{J} - \mu(1-\mu)$ and $\lambda(\theta;\mu) = \frac{3}{32}\mu(1-\mu)(1-3\cos^2\theta)$. Since the dependence on μ only appears in the higher order terms, the local behavior is the same regardless the value of the parameter $\mu \in [0, 1/2]$. Therefore, the techniques in [22] and [18] are also valid in our setting.

The second step of the proof is to show that the invariant stable and unstable manifolds of infinity intersect transversally, which follows from Theorem 3.

Hence combining this fact with the local results of [18] we obtain Theorem 6.1 of [18] for any value of $\mu \in (0, 1/2]$, which shows that there exists a Cantor set in the phase space where certain return map associated to system (4) is conjugated with a shift of infinitely many symbols. From this result, Theorem 1 follows directly.

3 Parameterizations of the Invariant Manifolds as Generating Functions

To study the difference between the invariant manifolds of infinity, we follow the approach proposed in [17,26]. We consider the Hamilton-Jacobi equation associated to Hamiltonian (15) and we look for functions $S(\tilde{r}, \phi; \mu, G_0)$ such that

$$(\tilde{y}, \tilde{G}) = \left(\partial_{\tilde{r}} S(\tilde{r}, \phi; \mu, G_0), \partial_\phi S(\tilde{r}, \phi; \mu, G_0)\right)$$

parameterize the invariant manifolds. The Hamilton-Jacobi equation reads

$$\mathscr{H}(\tilde{r}, \phi, \partial_{\tilde{r}} S, \partial_\phi S; \mu, G_0) = -G_0^3. \tag{18}$$

For the unperturbed Hamiltonian this equation simply reads

$$\frac{1}{2}\left(\partial_{\tilde{r}} S\right)^2 - G_0^3 \partial_\phi S + \frac{1}{2\tilde{r}^2}\left(\partial_\phi S\right)^2 - \frac{1}{\tilde{r}} = -G_0^3.$$

It has a solution of the form

$$S_0(\tilde{r}, \phi) = \phi + f(\tilde{r}), \tag{19}$$

where f is any solution of

$$\frac{1}{2}\left(\partial_{\tilde{r}} f\right)^2 + \frac{1}{2\tilde{r}^2} - \frac{1}{\tilde{r}} = 0.$$

We look for solutions of (18) close to (19). To this end, we write $S = S_0 + S_1$ and then the equation for S_1 becomes

$$\partial_{\tilde{r}} f\, \partial_{\tilde{r}} S_1 + \frac{1}{2}\left(\partial_{\tilde{r}} S_1\right)^2 - G_0^3 \partial_\phi S_1 + \frac{1}{\tilde{r}^2}\partial_\phi S_1 + \frac{1}{2\tilde{r}^2}\left(\partial_\phi S_1\right)^2 - V(\tilde{r}, \phi; \mu, G_0) = 0.$$

To look for solutions of this equation we proceed as in [17, 26] and we reparameterize the variables $(\tilde{r}, \phi)$ through the unperturbed separatrix (13). Namely, we consider the change

$$(\tilde{r}, \phi) = (\tilde{r}_{\rm h}(v), \xi + \tilde{\alpha}_{\rm h}(v)). \tag{20}$$

We define the new generating function

$$T(v, \xi; \mu, G_0) = S(\tilde{r}_{\rm h}(v), \xi + \tilde{\alpha}_{\rm h}(v); \mu, G_0), \tag{21}$$

which can be correspondingly written as $T = T_0 + T_1$ where

$$T_0(v, \xi) = S_0(\tilde{r}_{\rm h}(v), \xi + \tilde{\alpha}_{\rm h}(v))$$

and

$$T_1(v, \xi; \mu, G_0) = S_1(\tilde{r}_{\rm h}(v), \xi + \tilde{\alpha}_{\rm h}(v); \mu, G_0),$$

whose associated Hamilton-Jacobi equation is

$$\partial_v T_1 - G_0^3 \partial_\xi T_1 + \frac{1}{2\tilde{y}_{\rm h}^2}\left(\partial_v T_1 - \frac{1}{\tilde{r}_{\rm h}^2}\partial_\xi T_1\right)^2 + \frac{1}{2\tilde{r}_{\rm h}^2}\left(\partial_\xi T_1\right)^2 - V\left(\tilde{r}_{\rm h}, \xi + \tilde{\alpha}_{\rm h}; \mu, G_0\right) = 0. \tag{22}$$

We look for two solutions $T_1^{u,s}$ of this equation such that

$$\lim_{v \to -\infty} \tilde{y}_{\rm h}^{-1}(v) \partial_v T_1^u(v, \xi; \mu, G_0) = 0, \qquad \lim_{v \to -\infty} \partial_\xi T_1^u(v, \xi; \mu, G_0) = 0,$$

and analogous ones for T_1^s, the stable manifold, taking $v \to +\infty$.

Theorems 2 and 3 follow from the study of the difference of the generating functions T_1^u and T_1^s and from the difference between their derivatives given in Theorem 5 below. Theorem 4 needs the use of additional symmetries.

We define

$$L(v, \xi; \mu, G_0) = \int_{-\infty}^{+\infty} V(\tilde{r}_{\rm h}(v + s), \xi - G_0^3 s + \tilde{\alpha}_{\rm h}(v + s); \mu, G_0) ds, \tag{23}$$

where V is the rescaled perturbed Newtonian potential defined in (10). Note that the classical Poincaré function is the first order in μ of this function, that is

$$\int_{-\infty}^{+\infty} \partial_\mu V(\tilde{r}_{\rm h}(v+s), \xi - G_0^3 s + \tilde{\alpha}_{\rm h}(v+s); \mu, G_0)\big|_{\mu=0}\, ds.$$

It is possible to compute, for large values of G_0, an expression for (23).

Proposition 1. *The function $L(v, \xi; \mu, G_0)$ satisfies*

$$L(v, \xi; \mu, G_0) = L^{[0]}(\mu, G_0) + 2\sum_{\ell=1}^{+\infty} L^{[\ell]}(\mu, G_0)\cos\ell\left(\xi + G_0^3 v\right),$$

where

$$\begin{aligned}
L^{[1]}(\mu, G_0) &= -\mu(1-\mu)\sqrt{\pi}\frac{1-2\mu}{4\sqrt{2}} G_0^{-3/2} e^{-\frac{G_0^3}{3}}\left(1 + \mathscr{O}\left(G_0^{-2}\right)\right)\\
L^{[2]}(\mu, G_0) &= -2\mu(1-\mu)\sqrt{\pi} G_0^{1/2} e^{-\frac{2G_0^3}{3}}\left(1 + \mathscr{O}\left(G_0^{-1/2}\right)\right)\\
L^{[\ell]}(\mu, G_0) &= \left(G_0^{\ell-3/2} e^{-\frac{\ell G_0^3}{3}}\right), \quad \text{for } \ell \geq 3.
\end{aligned}$$

Finally, next theorem ensures that L is indeed the main term of the difference $T_1^u - T_1^s$.

Theorem 5. *There exist $0 < v_- < v_+$, $G_0^* > 0$ and $K > 0$ such that, for any $G_0 > G_0^*$ and $\mu \in (0, 1/2]$, the generating functions $T_1^{u,s}$ are defined for $(v, \xi) \in (v_-, v_+) \times \mathbb{T}$. They satisfy*

$$\left|T_1^u(v,\xi) - T_1^s(v,\xi) - L(v,\xi) - E\right| \leq K\mu^2(1-2\mu) G_0^{-2} e^{\frac{G_0^{-3}}{3}} + K G_0^{-1/2}\mu^2 e^{\frac{2G_0^{-3}}{3}},$$

for a constant $E \in \mathbb{R}$, which might depend on μ and G_0, and

$$\begin{aligned}
&\left|\partial_v^m \partial_\xi^n T_1^u(v,\xi) - \partial_v^m \partial_\xi^n T_1^s(v,\xi) - \partial_v^m \partial_\xi^n L(v,\xi)\right| \leq\\
&\qquad K\mu^2(1-2\mu) G_0^{-2+3m} e^{\frac{G_0^{-3}}{3}} + K G_0^{-1/2+3m}\mu^2 e^{\frac{2G_0^{-3}}{3}}
\end{aligned}$$

for $0 < m + n \leq 2$, $0 \leq m, n$, where we have omitted the dependence on μ and G_0 of $T_1^{u,s}$, L and E to simplify the notation.

The proof of this theorem can be found in [15].

Acknowledgements The authors have been partially supported by the Spanish MINECO-FEDER Grants MTM2009-06973, MTM2012-31714 and the Catalan Grant 2009SGR859. M. G. and P. M warmly thank the Institute for Advanced Study for their hospitality, stimulating atmosphere and support. During his stay in the Institute for Advanced Study, M. G. was also partially supported by the NSF grant DMS-0635607.

References

1. Arnold, V.I., Kozlov, V.V., Neishtadt, A.I.: Dynamical Systems III. Volume 3 of Encyclopaedia of Mathematical Sciences. Springer, Berlin (1988)
2. Baldomá, I., Fontich, E.: Exponentially small splitting of invariant manifolds of parabolic points. Mem. Am. Math. Soc. **167**(792), x–83 (2004)
3. Baldomá, I., Fontich, E., Guàrdia, M., Seara, T.M.: Exponentially small splitting of separatrices beyond Melnikov analysis: rigorous results. J. Differ. Equ. **253**(12), 3304–3439 (2012)
4. Delshams, A., Seara, T.M.: An asymptotic expression for the splitting of separatrices of the rapidly forced pendulum. Commun. Math. Phys. **150**(3), 433–463 (1992)
5. Delshams, A., Seara, T.M.: Splitting of separatrices in Hamiltonian systems with one and a half degrees of freedom. Math. Phys. Electron. J. **3**, Paper 4, 40 pp. (electronic) (1997)
6. Delshams, A., Kaloshin, V., de la Rosa, A., Seara, T.: Parabolic orbits in the restricted three body problem (2012, preprint)
7. Gelfreich, V.G.: Melnikov method and exponentially small splitting of separatrices. Phys. D **101**(3–4), 227–248 (1997)
8. Gelfreich, V.G.: Separatrix splitting for a high-frequency perturbation of the pendulum. Russ. J. Math. Phys. **7**(1), 48–71 (2000)
9. Galante, J., Kaloshin, V.: Destruction of invariant curves using the ordering condition. Preprint, available at http://www.terpconnect.umd.edu/~vkaloshi (2010)
10. Galante, J., Kaloshin, V.: The method of spreading cumulative twist and its application to the restricted circular planar three body problem. Preprint, available at http://www.terpconnect.umd.edu/~vkaloshi (2010)
11. Galante, J., Kaloshin, V.: Destruction of invariant curves in the restricted circular planar three-body problem by using comparison of action. Duke Math. J. **159**(2), 275–327 (2011)
12. Gorodetski, A., Kaloshin, V.: Hausdorff dimension of oscillatory motions for restricted three body problems. Preprint, available at http://www.terpconnect.umd.edu/~vkaloshi (2012)
13. Guardia, M.: Splitting of separatrices in the resonances of nearly integrable Hamiltonian systems of one and a half degrees of freedom. Discret. Contin. Dyn. Syst. **33**(7), 2829–2859 (2013)
14. Guardia, M., Olivé, C., Seara, T.M.: Exponentially small splitting for the pendulum: a classical problem revisited. J. Nonlinear Sci. **20**(5), 595–685 (2010)
15. Guardia, M., Martín, P., Seara, T.M.: Oscillatory motions for the restricted planar circular three body problem. Preprint available at http://http://arxiv.org/abs/1207.6531 (2012)
16. Holmes, P., Marsden, J., Scheurle, J.: Exponentially small splittings of separatrices with applications to KAM theory and degenerate bifurcations. In: Meyer, K.R., Saari, D.G. (eds.) Hamiltonian Dynamical Systems. Volume 81 of Contemporary Mathematics. American Mathematical Society, Providence (1988)
17. Lochak, P., Marco, J.-P., Sauzin, D.: On the splitting of invariant manifolds in multidimensional near-integrable Hamiltonian systems. Mem. Am. Math. Soc. **163**(775), viii + 145 (2003)
18. Llibre, J., Simó, C.: Oscillatory solutions in the planar restricted three-body problem. Math. Ann. **248**(2), 153–184 (1980)
19. Llibre, J., Simó, C.: Some homoclinic phenomena in the three-body problem. J. Differ. Equ. **37**(3), 444–465 (1980)

20. McGehee, R.: A stable manifold theorem for degenerate fixed points with applications to celestial mechanics. J. Differ. Equ. **14**, 70–88 (1973)
21. Melnikov, V.K.: On the stability of the center for time periodic perturbations. Trans. Moscow Math. Soc. **12**, 1–57 (1963)
22. Moser, J.: Stable and Random Motions in Dynamical Systems. Princeton University Press, Princeton (1973). With special emphasis on celestial mechanics, Hermann Weyl Lectures, the Institute for Advanced Study, Princeton, Annals of Mathematics Studies, No. 77
23. Martínez, R., Pinyol, C.: Parabolic orbits in the elliptic restricted three body problem. J. Differ. Equ. **111**(2), 299–339 (1994)
24. Neĭshtadt, A.I.: The separation of motions in systems with rapidly rotating phase. Prikl. Mat. Mekh. **48**(2), 197–204 (1984)
25. Poincaré, H.: Sur le problème des trois corps et les équations de la dynamique. Acta Math. **13**, 1–270 (1890)
26. Sauzin, D.: A new method for measuring the splitting of invariant manifolds. Ann. Sci. École Norm. Sup. **34**(4), 159–221 (2001)
27. Sitnikov, K.: The existence of oscillatory motions in the three-body problems. Sov. Phys. Dokl. **5**, 647–650 (1960)
28. Treschev, D.: Separatrix splitting for a pendulum with rapidly oscillating suspension point. Russ. J. Math. Phys. **5**(1), 63–98 (1997)
29. Xia, Z.: Mel′nikov method and transversal homoclinic points in the restricted three-body problem. J. Differ. Equ. **96**(1), 170–184 (1992)

Partial Symmetry Breaking and Heteroclinic Tangencies

Isabel S. Labouriau and Alexandre A.P. Rodrigues

Abstract We study some global aspects of the bifurcation of an equivariant family of volume-contracting vector fields on the three-dimensional sphere. When part of the symmetry is broken, the vector fields exhibit Bykov cycles. Close to the symmetry, we investigate the mechanism of the emergence of heteroclinic tangencies coexisting with transverse connections. We find persistent suspended horseshoes accompanied by attracting periodic trajectories with long periods.

1 Introduction

Heteroclinic cycles and networks associated to equilibria, periodic solutions and chaotic sets may be responsible for intermittent dynamics in nonlinear systems. Heteroclinic cycles may also be seen as the skeleton for the understanding of complicated switching between physical states – see Field [10], Golubitsky and Stewart [11] and Melbourne et al. [19].

The homoclinic cycle associated to a saddle-focus [14] provides one of the main examples for the occurrence of chaos involving suspended hyperbolic horseshoes and strange attractors; the complexity of the dynamics near these cycles was discovered by the pioneer L. P. Shilnikov [27, 28, 30]. The simplest heteroclinic cycles between two saddle-foci of different Morse indices where one heteroclinic connection is structurally stable and the other is not were first studied by Bykov [8] and are thus called *Bykov cycles*. Recently there has been a renewal of interest on this type of heteroclinic bifurcation in different contexts – see [14, 17, 24] and references therein. We also refer to Lamb et al. [18] who have studied Bykov cycles in the context of reversible systems.

I.S. Labouriau (✉) · A.A.P. Rodrigues
Centro de Matemática da Universidade do Porto and Faculdade de Ciências da Universidade do Porto, Rua do Campo Alegre 687, 4169–007 Porto, Portugal
e-mail: islabour@fc.up.pt; alexandre.rodrigues@fc.up.pt

S. Ibáñez et al. (eds.), *Progress and Challenges in Dynamical Systems*,
Springer Proceedings in Mathematics & Statistics 54,
DOI 10.1007/978-3-642-38830-9_17,

Explicit examples of vector fields for which such cycles may be found are reported in Aguiar et al. [3] and Rodrigues and Labouriau [25]. These examples start with a differential equation with symmetry, $\dot{x} = f_0(x)$ whose flow has a globally attracting three-dimensional sphere, containing an asymptotically stable heteroclinic network with two saddle-foci. When part of the symmetry is destroyed by a small non-equivariant perturbation, it may be shown by the Melnikov method that the two-dimensional invariant manifolds intersect transversely. When some symmetry remains, the connection of the one-dimensional manifolds is preserved, giving rise to Bykov cycles forming a network.

The main goal of this article is to describe and characterize the transition from the dynamics of the flow of the fully symmetric system $\dot{x} = f_0(x)$ and the perturbed system $\dot{x} = f_\lambda(x)$, for small $\lambda \neq 0$. For $\dot{x} = f_0(x)$, there is a heteroclinic network Σ^0 whose basin of attraction has positive Lebesgue measure. When $\lambda \neq 0$, the intersection of the invariant manifolds is transverse giving rise to a network $\Sigma^\star$ that cannot be removed by any small smooth perturbation. The transverse intersection implies that the set of all trajectories that lie for all time in a small neighbourhood of $\Sigma^\star$ has a locally-maximal hyperbolic set, admiting a complete description in terms of symbolic dynamics [29]. Labouriau and Rodrigues [17] proved that for the perturbed system $\dot{x} = f_\lambda(x)$, the flow contains a Bykov network $\Sigma^\star$ and uniformly hyperbolic horseshoes accumulating on it.

Suppose the fully symmetric network Σ^0 is asymptotically stable and let V^0 be a neighbourhood of Σ^0 whose closure is compact and positively flow-invariant; hence it contains the ω–limit sets of all its trajectories. The union of these limit sets is a maximal invariant set in V^0. For $\dot{x} = f_0(x)$, this union is simply the network Σ_0. For symmetry-breaking perturbations of f_0 it contains, but does not coincide with, a nonwandering set $\Omega_\lambda(\Sigma^\star)$ of trajectories that remain close to $\Sigma^\star$, the suspension of horseshoes accumulating on $\Sigma^\star$. The goal of this article is to investigate a larger limit set that contains nontrivial hyperbolic subsets and attracting limit cycles with long periods in V^0. This is what Gonchenko et al. [12] call a *strange attractor*: an attracting limit set containing nontrivial hyperbolic subsets as well as attracting periodic solutions of extremely long periods.

When $\lambda \to 0$, the horseshoes in $\Omega_\lambda(\Sigma^\star)$ lose hyperbolicity giving rise to *heteroclinic tangencies* with infinitely many sinks nearby. A classical problem in this context is the study of heteroclinic bifurcations that lead to the birth of stable periodic sinks – see Afraimovich and Shilnikov [1] and Newhouse [21, 22]. When we deal with a heteroclinic tangency of the invariant manifolds, the description of all solutions that lie near the cycle for all time becomes more difficult. The problem of a *complete description* is unsolvable: the source of the difficulty is that arbitrarily small perturbations of any differential equation with a quadratic homo/heteroclinic tangency (the simplest situation) may lead to the creation of new tangencies of higher order, and to the birth of degenerate periodic orbits – Gonchenko [13].

Large-scale invariant sets of planar Poincaré maps vary discontinuously in size under small perturbations. Global bifurcations of observable sets, such as the emergence of attractors or metamorphoses of their basin boundaries, are easily detected numerically and regularly described. However, in the example described in

[25], the global bifurcation from a neighbourhood of $\Sigma^\star$ to V^0 is still a mystery. The present paper contributes to a better understanding of the transition between uniform hyperbolicity (Smale horseshoes with infinitely many slabs) and the emergence of heteroclinic tangencies in a dissipative system close the symmetry.

1.1 Framework of the Paper

This paper is organised as follows. In Sect. 3 we state our main result and review some of our recent results related to the object of study, after some basic definitions given in Sect. 2. Coordinates and notation used in the rest of the article are presented in Sect. 4, where we also obtain a geometrical description of the image by the flow of a curve of initial conditions lying across the stable manifold of an equilibrium. In Sect. 5, we investigate the limit set that contains nontrivial hyperbolic subsets and we explain how the horseshoes in $\Omega_\lambda(\Sigma^\star)$ lose hyperbolicity, as $\lambda \to 0$. The first obstacle towards hyperbolicity is the emergence of tangencies and the existence of thick suspended Cantor sets near the network. In Sect. 6, we prove that there is a sequence of parameter values λ_i accumulating on 0 such that the flow of f_{λ_i} has heteroclinic tangencies and thus infinitely many attracting periodic trajectories. We include in Sect. 7 a short conclusion about the results.

2 Preliminaries

Let f be a C^1 vector field on $\mathbf{R}^n$ with flow given by the unique solution $x(t) = \varphi(t, x_0) \in \mathbf{R}^n$ of $\dot{x} = f(x)$ and $x(0) = x_0$. Given two equilibria p and q, an m-dimensional *heteroclinic connection* from p to q, denoted $[p \to q]$, is an m-dimensional connected flow-invariant manifold contained in $W^u(p) \cap W^s(q)$. There may be more than one trajectory connecting p and q.

Let $\mathscr{S} = \{p_j : j \in \{1, \ldots, k\}\}$ be a finite ordered set of mutually disjoint invariant saddles (sometimes called *nodes*). Following Field [10], we say that there is a *heteroclinic cycle* associated to $\mathscr{S}$ if

$$\forall\, j \in \{1, \ldots, k\}, W^u(p_j) \cap W^s(p_{j+1}) \neq \emptyset \pmod{k}.$$

A *heteroclinic network* is a finite connected union of heteroclinic cycles. Throughout this article, all nodes will be hyperbolic; the dimension of the local unstable manifold of an equilibrium p will be called the *Morse index* of p.

In a three-dimensional manifold, a *Bykov cycle* is a heteroclinic cycle associated to two hyperbolic saddle-foci with different Morse indices, in which the one-dimensional manifolds coincide and the two-dimensional invariant manifolds have a transverse intersection. It arises as a bifurcation of codimension 2, also called a *T–point*.

Let μ denote a measure on a smooth manifold M locally equivalent to the Lebesgue measure on charts. Given $x \in M$, let

$$\omega(x) = \bigcap_{T>0} \overline{\{\varphi(t,x) : t \geq T\}}$$

denote the ω-limit set of the solution through x. If $X \subset M$ is a compact and flow-invariant subset, we let $\mathscr{B}(X) = \{x \in M : \omega(x) \subset X\}$ denote the *basin of attraction* of X. A compact invariant subset X of M is a *Milnor attractor* if $\mu(\mathscr{B}(X)) > 0$ and for any proper compact invariant subset Y of X, $\mu(\mathscr{B}(X) \backslash \mathscr{B}(Y)) > 0$.

3 The Object of Study

3.1 The Organising Centre

The starting point of the analysis is a differential equation $\dot{x} = f_0(x)$ on the unit sphere $\mathbf{S}^3 = \{X = (x_1, x_2, x_3, x_4) \in \mathbf{R}^4 : ||X|| = 1\}$ where $f_0 : \mathbf{S}^3 \to \mathbf{TS}^3$ is a C^1 vector field with the following properties:

(P1) The vector field f_0 is equivariant under the action of $\mathbf{Z}_2 \oplus \mathbf{Z}_2$ on $\mathbf{S}^3$ induced by the two linear maps on $\mathbf{R}^4$:

$$\gamma_1(x_1, x_2, x_3, x_4) = (-x_1, -x_2, x_3, x_4)$$

and

$$\gamma_2(x_1, x_2, x_3, x_4) = (x_1, x_2, -x_3, x_4)$$

(P2) The set $Fix(\mathbf{Z}_2 \oplus \mathbf{Z}_2) = \{x \in \mathbf{S}^3 : \gamma_1 x = \gamma_2 x = x\}$ consists of two equilibria $\mathbf{v} = (0,0,0,1)$ and $\mathbf{w} = (0,0,0,-1)$ that are hyperbolic saddle-foci, where:

- The eigenvalues of $df_0(\mathbf{v})$ are $-C_\mathbf{v} \pm \alpha_\mathbf{v} i$ and $E_\mathbf{v}$ with $\alpha_\mathbf{v} \neq 0, C_\mathbf{v} > E_\mathbf{v} > 0$
- The eigenvalues of $df_0(\mathbf{w})$ are $E_\mathbf{w} \pm \alpha_\mathbf{w} i$ and $-C_\mathbf{w}$ with $\alpha_\mathbf{w} \neq 0$, $C_\mathbf{w} > E_\mathbf{w} > 0$.

(P3) The flow-invariant circle $Fix(\langle\gamma_1\rangle) = \{x \in \mathbf{S}^3 : \gamma_1 x = x\}$ consists of the two equilibria $\mathbf{v}$ and $\mathbf{w}$, a source and a sink, respectively, and two heteroclinic trajectories from $\mathbf{v}$ to $\mathbf{w}$ that we denote by $[\mathbf{v} \to \mathbf{w}]$.

(P4) The f_0-invariant sphere $Fix(\langle\gamma_2\rangle) = \{x \in \mathbf{S}^3 : \gamma_2 x = x\}$ consists of the two equilibria $\mathbf{v}$ and $\mathbf{w}$, and a two-dimensional heteroclinic connection from $\mathbf{w}$ to $\mathbf{v}$. Together with the connections in (P3) this forms a heteroclinic network that we denote by Σ^0.

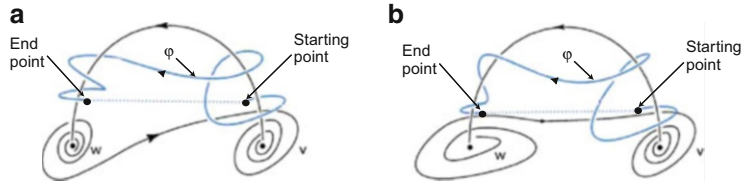

Fig. 1 There are two different possibilities for the geometry of the flow around a Bykov cycle depending on the orientation of trajectories around the heteroclinic connection [$\mathbf{v} \to \mathbf{w}$]. We assume here that all trajectories turn in the same direction near $\mathbf{v}$ and near $\mathbf{w}$ as drawn on the *left* (**a**). When the endpoints of the trajectory are joined, the closed curve is linked to the cycle. The case where trajectories turn in opposite directions around the connection is shown in (**b**). In this case, when the endpoints of the trajectory are joined, the closed curve may not be linked to the cycle

(P5) For sufficiently small open neighbourhoods V and W of $\mathbf{v}$ and $\mathbf{w}$, respectively, given any trajectory φ going once from V to W, if one joins the starting point of φ in ∂V to the end point in ∂W by a line segment, one obtains a closed curve that is linked to Σ^0 (Fig. 1), where ∂V and ∂W denote the boundary of V and W, respectively.

Condition (P5) means that the curve φ and the cycle Σ^0 cannot be separated by an isotopy. This property is persistent under perturbations: if it holds for the organising centre f_0, then it is still valid for vector fields near it, as long as the heteroclinic connection remains. An explicit example of a family of differential equations where this assumption is valid is constructed in Rodrigues and Labouriau [25].

3.2 The Heteroclinic Network of the Organising Centre

The heteroclinic connections in the network Σ^0 are contained in fixed point subspaces satisfying the hypothesis (H1) of Krupa and Melbourne [16]. Since the inequality $C_{\mathbf{v}}C_{\mathbf{w}} > E_{\mathbf{v}}E_{\mathbf{w}}$ holds, the Krupa and Melbourne stability criterion [16] may be applied to Σ^0 and we have:

Proposition 1. *Under conditions (P1)–(P4) the heteroclinic network Σ^0 is asymptotically stable.*

In particular, we obtain:

Corollary 1. *The basin of attraction of the heteroclinic network Σ^0 whose vector field satisfies (P1)–(P4) has positive Lebesgue measure.*

Proposition 1 implies that there exists an open neighbourhood V^0 of the network Σ^0 such that every trajectory starting in V^0 remains in it for all positive time and is forward asymptotic to the network. The neighbourhood may be taken to have its boundary transverse to the vector field f_0.

The fixed point hyperplane defined by $Fix(\langle\gamma_2\rangle) = \{(x_1, x_2, x_3, x_4) \in \mathbf{S}^3 : x_3 = 0\}$ divides $\mathbf{S}^3$ in two flow-invariant connected components, preventing jumps between the two cycles in Σ^0. Due to the $\langle\gamma_2\rangle$–symmetry, trajectories whose initial condition lies outside the invariant subspaces will approach one of the cycles in positive time. Successive visits to both cycles require breaking this symmetry.

3.3 Bykov Cycles

Since $\mathbf{v}$ and $\mathbf{w}$ are hyperbolic equilibria, then any vector field close to f_0 in the C^1 topology still has two equilibria $\mathbf{v}$ and $\mathbf{w}$ with eigenvalues satisfying (P2). The dimensions of the local stable and unstable manifolds of $\mathbf{v}$ and $\mathbf{w}$ do not change. If we retain the symmetry γ_1, then the one-dimensional connection of (P3) remains, as it takes place in the flow-invariant circle $Fix(\langle\gamma_1\rangle)$, but generically when the symmetry γ_2 is broken, the two dimensional heteroclinic connection is destroyed, since the fixed point subset $Fix(\mathbf{Z}_2(\langle\gamma_2\rangle))$ is no longer flow-invariant. Generically, the invariant two-dimensional manifolds meet transversely at two trajectories, for small $\langle\gamma_1\rangle$-equivariant perturbations of the vector field. We denote these heteroclinic connections by $[\mathbf{w} \to \mathbf{v}]$. This gives rise to a network Σ^* consisting of four copies of the simplest heteroclinic cycle between two saddle-foci of different Morse indices, where one heteroclinic connection is structurally stable and the other is not. This cycle is a *Bykov cycle*. Note that the networks Σ^0 and Σ^* are not of the same nature (*i. e.* they are qualitatively different).

Transversality ensures that the neighbourhood V^0 is still positively invariant for vector fields C^1 close to f_0 and contains the network Σ^*. Since the closure of V^0 is compact and positively invariant it contains the ω-limit sets of all its trajectories. The union of these limit sets is a maximal invariant set in V^0. For f_0, this is the cycle Σ^0, by Proposition 1, whereas for symmetry-breaking perturbations of f_0 it contains Σ^* but does not coincide with it. From now on, our aim is to obtain information on this invariant set.

A systematic study of the dynamics in a neighbourhood of the Bykov cycles in Σ^* was carried out in Aguiar et al. [2], Labouriau and Rodrigues [17] and Rodrigues [24]; we proceed to review these local results. In the next section we will discuss some global aspects of the dynamics.

Given a Bykov cycle Γ involving $\mathbf{v}$ and $\mathbf{w}$, let V and W $\subset V^0$ be disjoint neighbourhoods of these points. Let S_p and S_q be local cross-sections of f_λ at two points p and q in the connections $[\mathbf{v} \to \mathbf{w}]$ and $[\mathbf{w} \to \mathbf{v}]$, respectively, with $p, q \notin V \cup W$. Saturating the cross-sections by the flow, one obtains two flow-invariant tubes joining V and W containing the connections in their interior. We call the union of these tubes, V and W a *tubular neighbourhood* V^Γ of the Bykov cycle.

With these conventions we have:

Theorem 1 (Labouriau and Rodrigues [17]). *If a vector field f_0 satisfies (P1)–(P5), then the following properties are satisfied generically by vector fields in an*

open neighbourhood of f_0 in the space of $\langle\gamma_1\rangle$–equivariant vector fields of class C^1 on $\mathbf{S}^3$:

1. *There is a heteroclinic network Σ^* consisting of four Bykov cycles involving two equilibria $\mathbf{v}$ and $\mathbf{w}$, two heteroclinic connections $[\mathbf{v} \to \mathbf{w}]$ and two heteroclinic connections $[\mathbf{w} \to \mathbf{v}]$;*
2. *The only heteroclinic connections from $\mathbf{v}$ to $\mathbf{w}$ are those in the Bykov cycles and there are no homoclinic connections;*
3. *Any tubular neighbourhood V^Γ of a Bykov cycle Γ in Σ^* contains points not lying on Γ whose trajectories remain in V^Γ for all time;*
4. *Any tubular neighbourhood V^Γ of a Bykov cycle Γ in Σ^* contains at least one n-pulse heteroclinic connection $[\mathbf{w} \to \mathbf{v}]$;*
5. *Given a cross-section $S_q \subset V^\Gamma$ at a point q in $[\mathbf{w} \to \mathbf{v}]$, there exist sets of points such that the dynamics of the first return to S_q is uniformly hyperbolic and conjugate to a full shift over a finite number of symbols. These sets accumulate on the cycle.*

Notice that assertion 4 of Theorem 1 implies the existence of a bigger network: beyond the original transverse connections $[\mathbf{w} \to \mathbf{v}]$, there exist infinitely many subsidiary heteroclinic connections turning around the original Bykov cycle. We will restrict our study to one cycle.

It is a folklore result that a non-trivial hyperbolic invariant set of a C^2–diffeomorphism has zero Lebesgue measure – see Bowen [7]. However, since the authors of [17] worked in the C^1 category, this chain of horseshoes might have positive Lebesgue measure as the "fat Bowen horseshoe" described in [6]. Rodrigues [24] proved that this is not the case:

Theorem 2 (Rodrigues [24]). *Let V^Γ be a tubular neighbourhood of one of the Bykov cycles Γ of Theorem 1. Then in any cross-section $S_q \subset V^\Gamma$ at a point q in $[\mathbf{w} \to \mathbf{v}]$ the set of initial conditions in $S_q \cap V^\Gamma$ that do not leave V^Γ for all time has zero Lebesgue measure.*

It follows from Theorem 2 that the shift dynamics does not trap most trajectories in the neighbourhood of the cycle. In particular, the cycle cannot be Lyapunov stable (and therefore cannot be asymptotically stable).

One astonishing property of the heteroclinic network Σ^* is the possibility of shadowing it by the property called *switching*: any infinite sequence of pseudo-orbits defined by admissible heteroclinic connections can be shadowed, as we proceed to define.

A *path* on Σ^* is an infinite sequence $s^k = (c_j)_{j\in\mathbf{N}}$ of heteroclinic connections $c_j = [A_j \to B_j]$ in Σ^* such that $A_j, B_j \in \{\mathbf{v}, \mathbf{w}\}$ and $B_j = A_{j+1}$. Let $V, W \subset V^0$ be neighbourhoods of $\mathbf{v}$ and $\mathbf{w}$. For each heteroclinic connection in Σ^*, consider a point p on it and a small neighbourhood $U_p \subset V^0$ of p. We assume that all these neighbourhoods are pairwise disjoint.

The trajectory $\varphi(t, q)$ of $\dot{x} = f_\lambda(x)$, *follows* the path $s^k = (c_j)_{j\in\mathbf{N}}$ within a given set of neighbourhoods as above, if there exist two monotonically increasing

sequences of times $(t_i)_{i\in\mathbf{N}}$ and $(z_i)_{i\in\mathbf{N}}$ such that for all $i \in \mathbf{N}$, we have $t_i < z_i < t_{i+1}$ and:

- $\varphi(t,q) \subset V^0$ for all $t \geq 0$;
- $\varphi(t_i,q) \in V \cap W$ and $\varphi(z_i,q) \in U_p$, $p \in c_i$ and
- For all $t \in (z_i, z_{i+1})$, $\varphi(t,q)$ does not visit the neighbourhood of any other node except A_{i+1}.

There is *switching* near Σ^* if for each path there is a trajectory that follows it within every set of neighbourhoods as above.

Theorem 3 (Aguiar et al. [2]). *There is switching on the network Σ^*.*

The solutions that realise switching lie for all positive time in the union of tubular neighbourhoods V^Γ of all cycles $\Gamma \subset \Sigma^*$. Hence we may adapt the proof of Theorem 2 to obtain:

Corollary 2. *The switching of Theorem 3 is realised by a set of initial conditions with zero Lebesgue measure.*

3.4 Non-hyperbolic Dynamics

When the symmetry γ_2 is broken, the dynamics changes dramatically, as can be seen in the next result:

Theorem 4. *If a vector field f_0 satisfies (P1)–(P5), then in any open neighbourhood of f_0 in the space of $\langle\gamma_1\rangle$-equivariant vector fields of class C^1 on $\mathbf{S}^3$, there are vector fields f_* whose flow has a heteroclinic tangency between $W^u(\mathbf{w})$ and $W^s(\mathbf{v})$ in V^0.*

Theorem 4 is proved in Sect. 6. The vector fields f_* will be obtained in a generic one-parameter unfolding f_λ of f_0, for which we will find a sequence of λ_i converging to zero such that the flow of f_{λ_i} has the required property. When $\lambda_i \to 0$, these tangencies accumulate on the transverse connections. Persistent tangencies in a dissipative diffeomorphism are related to the coexistence of infinitely many sinks and sources [21, 22]. Moreover, any parametrised family of diffeomorphisms going through a heteroclinic tangency associated to a dissipative cycle must contain a sequence of Hénon-like families [9, 20]. Hence, for $\lambda \approx 0$, return maps to appropriate domains close to the tangency are conjugate to Hénon-like maps and thus:

Corollary 3. *Suppose a vector field f_0 satisfies (P1)–(P5). Then in the space of $\langle\gamma_1\rangle$-equivariant vector fields of class C^3 on $\mathbf{S}^3$, there is a set $\mathscr{C}$ of vector fields accumulating on f_0 such that all $f_\lambda \in \mathscr{C}$ possess infinitely many strange (coexisting) attractors in V^0.*

Proof. In Ovsyannikov and Shilnikov [23], it is shown that there are small perturbations of f_0 with a periodic solution as close as desired to the cycle whose

stable and unstable manifolds are tangent. By Colli [9], the result follows. Note that although the statement in [9] asks for C^∞ perturbations, in [5] the coexistence of strange attractors only requires C^3. □

4 Local Dynamics Near the Network

In order to obtain results on $\langle\gamma_1\rangle$–equivariant vector fields C^1 close to f_0 we study the bifurcation of a generic one-parameter family of differential equations $\dot{x} = f_\lambda(x)$ on the unit sphere $\mathbf{S}^3 = \{X = (x_1, x_2, x_3, x_4) \in \mathbf{R}^4 : ||X|| = 1\}$. The unfolding $f_\lambda : \mathbf{S}^3 \to \mathbf{TS}^3$ of f_0 is a family of C^1 vector fields with the following properties:

(P6) For each λ the vector field f_λ is $\langle\gamma_1\rangle$–equivariant.

(P7) There are two equilibria $\mathbf{v}$ and $\mathbf{w}$ satisfying (P2) and (P3).

(P8) For $\lambda \neq 0$, the local two-dimensional manifolds $W^u(\mathbf{w})$ and $W^s(\mathbf{v})$ intersect transversely at two trajectories. Together with the connections in (P3) this forms a Bykov heteroclinic network that we denote by $\Sigma^\star$. For $\lambda = 0$ we denote it by Σ^0.

In order to describe the dynamics around the Bykov cycles, we start by introducing local coordinates near the saddle-foci $\mathbf{v}$ and $\mathbf{w}$ and we define some terminology that will be used in the rest of the paper. Since by assumption (P2) we have $C_\mathbf{v} \neq E_\mathbf{v}$ and $C_\mathbf{w} \neq E_\mathbf{w}$, then by Samovol's Theorem [26], the vector field f_λ is C^1–conjugate to its linear part around each saddle-focus – see also Homburg and Sandstede [15] (Sect. 3.1). Assuming that $\alpha_\mathbf{v} = \alpha_\mathbf{w} = 1$, in cylindrical coordinates (ρ, θ, z) the linearization at $\mathbf{v}$ takes the form

$$\dot{\rho} = -C_\mathbf{v}\rho \qquad \dot{\theta} = 1 \qquad \dot{z} = E_\mathbf{v} z$$

and around $\mathbf{w}$ it is given by:

$$\dot{\rho} = E_\mathbf{w}\rho \qquad \dot{\theta} = 1 \qquad \dot{z} = -C_\mathbf{w} z.$$

We consider cylindrical neighbourhoods V and W in $\mathbf{S}^3$ of $\mathbf{v}$ and $\mathbf{w}$, respectively, of radius $\varepsilon > 0$ and height 2ε – see Fig. 2. After a linear rescaling of the local variables, we may take $\varepsilon = 1$. Their boundaries consist of three components: the cylinder wall parametrized by $x \in \mathbf{R} \pmod{2\pi}$ and $|y| \leq 1$ with the usual cover $(x, y) \mapsto (1, x, y) = (\rho, \theta, z)$ and two discs (top and bottom of the cylinder). We take polar coverings of these discs $(r, \varphi) \mapsto (r, \varphi, \pm 1) = (\rho, \theta, z)$ whith $0 \leq r \leq 1$ and $\varphi \in \mathbf{R} \pmod{2\pi}$ and use the following terminology, as in Fig. 2:

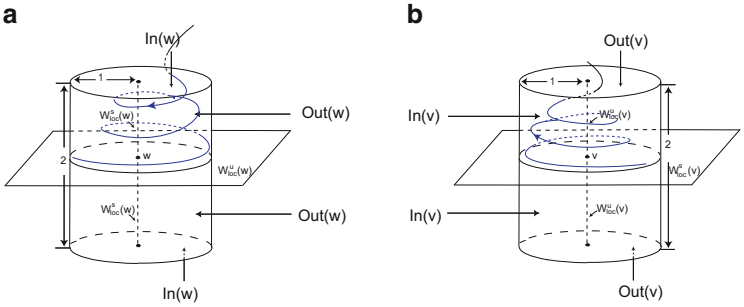

Fig. 2 Cylindrical neighbourhoods of the saddle-foci **w** (**a**) and **v** (**b**)

- $In(\mathbf{v})$, the cylinder wall of V, consists of points that go inside V in positive time;
- $Out(\mathbf{v})$, the top and bottom of V, consists of points that go inside V in negative time;
- $In(\mathbf{w})$, the top and bottom of W, consists of points that go inside W in positive time;
- $Out(\mathbf{w})$, the cylinder wall of W, consists of points that go inside W in negative time.

The flow is transverse to these sets and moreover the boundaries of V and of W may be written as the closures of the disjoint unions $In(\mathbf{v}) \cup Out(\mathbf{v})$ and $In(\mathbf{w}) \cup Out(\mathbf{w})$, respectively. The trajectories of all points (x, y) in $In(\mathbf{v})\backslash W^s(\mathbf{v})$, leave V at $Out(\mathbf{v})$ at

$$\Phi_{\mathbf{v}}(x, y) = \left(|y|^{\delta_{\mathbf{v}}}, -\frac{\ln|y|}{E_{\mathbf{v}}} + x \right) = (r, \varphi) \qquad \text{where} \qquad \delta_{\mathbf{v}} = \frac{C_{\mathbf{v}}}{E_{\mathbf{v}}} > 1\,. \quad (1)$$

Similarly, points (r, ϕ) in $In(\mathbf{w})\backslash W^s(\mathbf{w})$, leave W at $Out(\mathbf{w})$ at

$$\Phi_{\mathbf{w}}(r, \varphi) = \left(-\frac{\ln r}{E_{\mathbf{w}}} + \varphi, \pm r^{\delta_{\mathbf{w}}} \right) = (x, y) \qquad \text{where} \qquad \delta_{\mathbf{w}} = \frac{C_{\mathbf{w}}}{E_{\mathbf{w}}} > 1\,. \quad (2)$$

We will denote by $W^u_{loc}(\mathbf{v})$ the portion of $W^u(\mathbf{v})$ that goes from $\mathbf{v}$ up to $In(\mathbf{w})$ not intersecting the interior of W. Similarly, $W^s_{loc}(\mathbf{v})$ is the portion of $W^s(\mathbf{v})$ outside W that goes directly from $Out(\mathbf{w})$ into $\mathbf{v}$, and $W^u_{loc}(\mathbf{w})$ and $W^s_{loc}(\mathbf{w})$ connect $\mathbf{w}$ to ∂V, not intersecting the interior of V.

The flow sends points in $Out(\mathbf{v})$ near $W^u_{loc}(\mathbf{v})$ into $In(\mathbf{w})$ along the connection $[\mathbf{v} \to \mathbf{w}]$. We will assume that this map $\Psi_{\mathbf{v}\to\mathbf{w}}$ is the identity, this is compatible with hypothesis (P5); nevertheless all the results follow if $\Psi_{\mathbf{v}\to\mathbf{w}}$ is either a uniform contraction or a uniform expansion. We make the convention that one of the connections $[\mathbf{v} \to \mathbf{w}]$ links points with $y > 0$ in V to points with $y > 0$ in W. There is also a well defined transition map $\Psi_{\mathbf{w}\to\mathbf{v}} : Out(\mathbf{w}) \longrightarrow In(\mathbf{v})$ that will be discussed later.

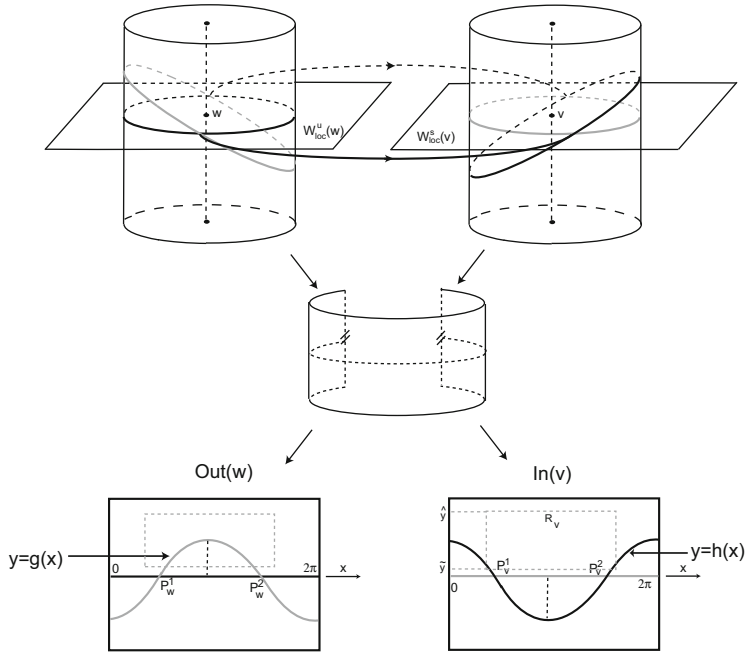

Fig. 3 For λ close to zero, we are assuming that $W^s(\mathbf{v})$ intersects the wall $Out(\mathbf{w})$ of the cylinder W on a closed curve – this is the expected unfolding from the coincidence of the invariant manifolds of the equilibria

By (P8), the manifolds $W^u(\mathbf{w})$ and $W^s(\mathbf{v})$ intersect transversely for $\lambda \neq 0$. For λ close to zero, we are assuming that $W^s(\mathbf{v})$ intersects the wall $Out(\mathbf{w})$ of the cylinder W on a closed curve represented in Fig. 3 by an ellipse – this is the expected unfolding from the coincidence of the invariant manifolds of the equilibria.

From the geometrical behaviour of the local transition maps (1) and (2), we need some definitions: a *segment* β on $In(\mathbf{v})$ is a smooth regular parametrized curve $\beta : [0, 1] \to In(\mathbf{v})$ that meets $W^s_{loc}(\mathbf{v})$ transversely at the point $\beta(1)$ only and such that, writing $\beta(s) = (x(s), y(s))$, both x and y are monotonic functions of s.

A *spiral* on a disc D around a point $p \in D$ is a curve $\alpha : [0, 1) \to D$ satisfying $\lim_{s\to 1^-} \alpha(s) = p$ and such that if $\alpha(s) = (r(s), \theta(s))$ is its expression in polar coordinates around p then the maps r and θ are monotonic, and $\lim_{s\to 1^-} |\theta(s)| = +\infty$.

Consider a cylinder C parametrized by a covering $(\theta, h) \in \mathbf{R} \times [a, b]$, with $a < b \in \mathbf{R}$ where θ is periodic. A *helix* on the cylinder C *accumulating on the circle* $h = h_0$ is a curve $\gamma : [0, 1) \to C$ such that its coordinates $(\theta(s), h(s))$ satisfy $\lim_{s\to 1^-} h(s) = h_0$, $\lim_{s\to 1^-} |\theta(s)| = +\infty$ and the maps θ and h are monotonic.

Using these definitions and the expressions (1) and (2) for $\Phi_{\mathbf{v}}$ and $\Phi_{\mathbf{w}}$, respectively, we get:

Proposition 2 (Aguiar et al. [4]). *When (P5) holds, then a segment on $In(\mathbf{v})$ is mapped by $\Phi_{\mathbf{v}}$ into a spiral on $Out(\mathbf{v})$ around $W^u_{loc}(\mathbf{v}) \cap Out(\mathbf{v})$. This spiral is mapped by $\Psi_{\mathbf{v}\to\mathbf{w}}$ into another spiral around $W^s_{loc}(\mathbf{w}) \cap In(\mathbf{v})$, which is mapped by $\Phi_{\mathbf{w}}$ into a helix on $Out(\mathbf{w})$ accumulating on the circle $Out(\mathbf{w}) \cap W^u(\mathbf{w})$.*

5 Hyperbolicity

In this section we show that the hyperbolicity of Theorem 1 only holds when we restrict our attention to trajectories that remain near the cycles in the network. The construction also indicates how the geometrical content of Theorems 1–3 is obtained.

Let $(P^1_{\mathbf{w}}, 0)$ and $(P^2_{\mathbf{w}}, 0)$ with $0 < P^1_{\mathbf{w}} < P^2_{\mathbf{w}} < 2\pi$ be the coordinates of the two points in $W^u_{loc}(\mathbf{w}) \cap W^s_{loc}(\mathbf{v}) \cap Out(\mathbf{w})$ where the connections $[\mathbf{w} \to \mathbf{v}]$ meet $Out(\mathbf{w})$, as in Fig. 3. Analogously, let $(P^1_{\mathbf{v}}, 0)$ and $(P^2_{\mathbf{v}}, 0)$ be the coordinates of the two corresponding points in $W^u_{loc}(\mathbf{w}) \cap W^s_{loc}(\mathbf{v}) \cap In(\mathbf{v})$ where $[\mathbf{w} \to \mathbf{v}]$ meets $In(\mathbf{v})$, with the convention that $(P^j_{\mathbf{w}}, 0)$ and $(P^j_{\mathbf{v}}, 0)$ are on the same trajectory for $j = 1, 2$.

For small $\lambda > 0$ we may write $W^s(\mathbf{v}) \cap Out(\mathbf{w})$ as the graph of a smooth function $y = g(x)$, with $g(P^j_{\mathbf{w}}) = 0$, $j = 1, 2$. Similarly, $W^u(\mathbf{w}) \cap In(\mathbf{v})$ is the graph of a smooth function $y = h(x)$, with $g(P^j_{\mathbf{v}}) = 0$, $j = 1, 2$. We number the points in the connections so that $g'(P^1_{\mathbf{w}}) > 0$. Hence $g'(P^2_{\mathbf{w}}) < 0$, and $h'(P^1_{\mathbf{v}}) < 0$, $h'(P^2_{\mathbf{v}}) > 0$.

Proposition 3. *For the first hit map $\eta = \Phi_{\mathbf{w}} \circ \Psi_{\mathbf{v}\to\mathbf{w}} \circ \Phi_{\mathbf{v}} : In(\mathbf{v}) \longrightarrow Out(\mathbf{w})$, we have:*

(i) Any horizontal line segment $[a, b] \times \{y_0\} \subset In(\mathbf{v})$ is mapped by η into a horizontal line segment $[c, d] \times \{y_0^\delta\} \subset Out(\mathbf{w})$, with $\delta > 1$;

(ii) Any vertical line segment $\{x_0\} \times [0, y_0] \subset In(\mathbf{v})$ is mapped by η into a helix accumulating on the circle $Out(\mathbf{w}) \cap W^u_{loc}(\mathbf{w})$;

(iii) Given x_0, there are positive constants $a < b \in \mathbf{R}$ and a sequence of intervals $\mathscr{I}_n = \{x_0\} \times [e^{-2n\pi/K} e^a, e^{-2n\pi/K} e^b]$ such that $\eta(\mathscr{I}_n)$ crosses $W^s_{loc}(\mathbf{v}) \cap Out(\mathbf{w})$ twice transversely;

(iv) If $K > 1$ then the intervals $\mathscr{I}_n$ are disjoint.

Proof. Assertion (i) is immediate from the expression of $\eta = \Phi_{\mathbf{w}} \circ \Psi_{\mathbf{v}\to\mathbf{w}} \circ \Phi_{\mathbf{v}}$ in coordinates:

$$\eta(x, y) = \left(x - K \ln y, y^\delta\right) \quad \text{where} \quad K = \frac{C_{\mathbf{v}} + E_{\mathbf{w}}}{E_{\mathbf{v}} E_{\mathbf{w}}} > 0 \quad \text{and} \quad \delta = \delta_{\mathbf{v}} \delta_{\mathbf{w}} > 1$$

and assertion (ii) follows from Proposition 2.

For (iii) let y_* be the maximum value of $g(x)$ and let $m \in \mathbf{Z}$ such that $x_0 - P^1_{\mathbf{w}} \leq \frac{K}{\delta} \ln y_* + 2m\pi$. We take $a = (x_0 - P^2_{\mathbf{w}} - 2m\pi)/K$ and $b = (x_0 - P^1_{\mathbf{w}} - 2m\pi)/K$. Then $a < b$, the second coordinate of $\eta(x_0, e^b)$ is less than y_*, its first coordinate is $P^1_{\mathbf{w}} + 2m\pi$, and that of $\eta(x_0, e^a)$ is $P^2_{\mathbf{w}} + 2m\pi$. Hence the curve $\eta(\mathscr{I}_0)$ goes across

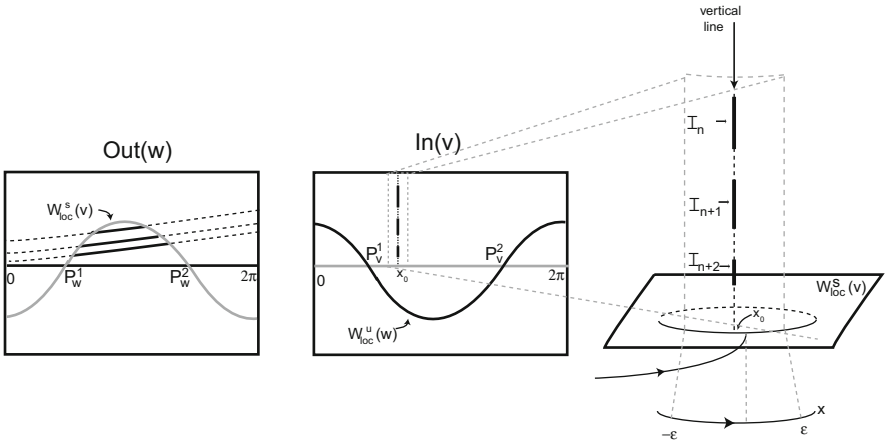

Fig. 4 Proof of (iii) in Proposition 3: the transition map η sends the intervals $\mathscr{I}_n$ into curves that cross $W^s_{loc}(\mathbf{v})$ transversely

the graph of $g(x)$ that corresponds to $W^s(\mathbf{v})$ as in Fig. 4. The first coordinates of the end points of $\eta(\mathscr{I}_n)$ for the other intervals are $P^2_{\mathbf{w}}+2(m+n)\pi$ and $P^1_{\mathbf{w}}+2(m+n)\pi$ and their second coordinates are also less than y_*, so each curve $\eta(\mathscr{I}_n)$ also crosses the graph of $g(x)$ transversely.

If $K > 1$, and since $P^2_{\mathbf{w}} - P^1_{\mathbf{w}} < 2\pi < 2K\pi$, then

$$x_0 - P^2_{\mathbf{w}} - 2m\pi - 2K\pi < x_0 - P^1_{\mathbf{w}} - 2m\pi$$

and hence $b - 2(n+1)\pi/K < a - 2n\pi/K$, implying that $\mathscr{I}_n \cap \mathscr{I}_{n+1} = \emptyset$. □

We are interested in the images of rectangles in $In(\mathbf{v})$ under iteration by the first return map to $In(\mathbf{v})\backslash W^s_{loc}(\mathbf{v})$ given by $\zeta = \Psi_{\mathbf{w}\to\mathbf{v}} \circ \eta$.

Consider a rectangle $R_{\mathbf{v}} = [P^1_{\mathbf{v}} - \tau, P^1_{\mathbf{v}} + \tau] \times [\tilde{y}, \hat{y}] \subset In(\mathbf{v})$ with $\tau > 0$ small and $0 < \tilde{y} < \hat{y} < 1$. This is mapped by η into a strip whose boundary consists of two horizontal line segments and two pieces of helices. A calculation similar to that in Proposition 3 shows that there are many choices of $\tilde{y}$ and $\hat{y}$ for which the strip crosses $W^s_{loc}(\mathbf{v})$ transversely near $P^1_{\mathbf{w}}$. This strip is then mapped by $\Psi_{\mathbf{w}\to\mathbf{v}}$ into $In(\mathbf{v})$ crossing $W^s_{loc}(\mathbf{v})$ transversely. The final strip $\zeta(R_{\mathbf{v}}) = \Psi_{\mathbf{w}\to\mathbf{v}} \circ \eta(R_{\mathbf{v}})$ remains close to $W^u_{loc}(\mathbf{w})$. Hence the effect of ζ is to stretch $R_{\mathbf{v}}$ in the vertical direction and map it with the stretched direction approximately parallel to $W^u_{loc}(\mathbf{w})$. Since $R_{\mathbf{v}}$ has been chosen to contain a piece of $W^u_{loc}(\mathbf{w})$, then $\zeta(R_{\mathbf{v}})$ will cross $R_{\mathbf{v}}$. Repeating the process for successive disjoint intervals $[\tilde{y}, \hat{y}]$ give rise to horseshoes.

This is the idea of the proof of the local results of Theorem 1: in a neighbourhood of the connection point $(P^1_{\mathbf{v}}, 0)$, one finds infinitely many disjoint rectangles, each one containing a Cantor set of points whose orbits under ζ remain in the Cantor set, and hence return to a neighbourhood of $(P^1_{\mathbf{v}}, 0)$ for all future iterations. In the

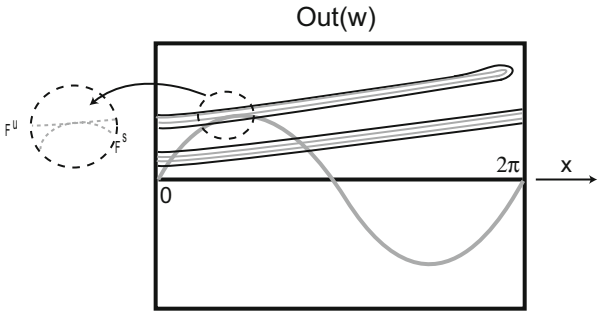

Fig. 5 Near the point of maximum height of $W^s_{loc}(\mathbf{v}) \cap Out(\mathbf{w})$ the unstable manifold of some point is tangent to $W^s(\mathbf{v})$. By varying λ this point may be taken to be in the Cantor set of points that remain near the cycle

gaps between these rectangles one finds another set of disjoint rectangles that are first mapped by ζ into a neighbourhood of the other connection point $(P^2_{\mathbf{v}}, 0)$. Repeating the construction near the second connection one obtains the switching of Theorem 3.

It can also be shown that the first return map ζ is uniformly hyperbolic at the points in the rectangle $R_{\mathbf{v}}$, with the choices of $\tilde{y}, \hat{y}$ above. This means that at each of these points there is a well defined contraction direction and this is the main tool in the proof of Theorem 2.

Since this takes place inside a positively invariant neighbourhood V^0, it would be natural to try to extend this reasoning to larger rectangles in $In(\mathbf{v})$. We finish this section explaining why this fails.

Consider a rectangle $R_{\mathbf{v}}$ as above, containing points of the Cantor set. Since η expands vertical lines, the local unstable manifolds of these points forms a lamination on $R_{\mathbf{v}}$ whose sheets are approximately vertical. Now, take a larger rectangle $\hat{R}_{\mathbf{v}}$ with $y \in [\tilde{y}, \bar{y}]$, $\bar{y} > \hat{y}$, so as to have the maximum of the curve $y = g(x)$ lying in $\eta(\hat{R}_{\mathbf{v}})$, and increasing τ if necessary. The sheets of the lamination still follow the vertical direction in the enlarged rectangle, and their image by η is approximately a helix on $Out(\mathbf{w})$. Changing the value of the bifurcation parameter λ moves the graph $y = g(x)$ (the stable manifold of $\mathbf{v}$) but does not affect the map η. Hence, by varying λ we can get a sheet of the lamination tangent to $y = g(x)$, say, $W^u(x_0, y_0)$ for some point (x_0, y_0) in the Cantor set as in Fig. 5. This breaks the hyperbolicity, since it means that $W^u(x_0, y_0)$ is tangent to $W^s(\mathbf{v})$. This phenomenon has been studied by Gonchenko et al. [12] – it corresponds to a decrease in topological entropy as in Fig. 6. As the images of the rectangles move down, each time one of them crosses a rectangle a sequence of saddle-node bifurcations starts, together with a period-doubling cascade, as on the right hand side of Fig. 6.

A more rigorous construction will be made in the next section.

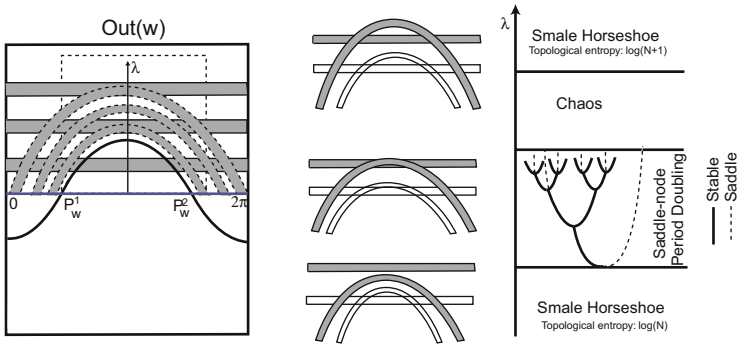

Fig. 6 When λ decreases, the Cantor set of points of the horseshoes that remain near the cycle is losing topological entropy, as the set loses hyperbolicity. This happens when the unstable manifold of some point in the Cantor set is tangent to $W^s(\mathbf{v})$

6 Heteroclinic Tangency

In this section we show how to find values of the bifurcation parameter λ for which $W^u(\mathbf{w})$ is tangent to $W^s(\mathbf{v})$.

Proof (of Theorem 4). With the notation of Sect. 5, the two points $(P^1_{\mathbf{w}}, 0)$ and $(P^2_{\mathbf{w}}, 0)$ divide the closed curve $y = g(x)$ where $W^s_{loc}(\mathbf{v})$ intersects $Out(\mathbf{w})$ in two components, corresponding to different signs of the second coordinate. With the conventions of Sect. 5, we get $g(x) > 0$ for $x \in \left(P^1_{\mathbf{w}}, P^2_{\mathbf{w}}\right)$. Then the region in $Out(\mathbf{w})$ delimited by $W^s_{loc}(\mathbf{v})$ and $W^u_{loc}(\mathbf{w})$ between $P^1_{\mathbf{w}}$ and $P^2_{\mathbf{w}}$ gets mapped by $\Psi_{\mathbf{w}\to\mathbf{v}}$ into the $y < 0$ component of $In(\mathbf{v})$, while all other points in $Out(\mathbf{w})$ with positive second coordinates, are mapped ito the $y > 0$ component of $In(\mathbf{v})$ as in Fig. 7. The maximum value of the coordinate y for the curve $W^s_{loc}(\mathbf{v}) \cap Out(\mathbf{w})$ is of the order of λ, attained at some point $(x, y) \approx (x_m, \lambda)$ with $P^1_{\mathbf{w}} < x_m < P^2_{\mathbf{w}} \pmod{2\pi}$.

Consider now the closed curve where $W^u_{loc}(\mathbf{w})$ intersects $In(\mathbf{v})$. For small values of λ this is approximately an ellipse, crossing $W^s_{loc}(\mathbf{v})$ at the two points $(P^1_{\mathbf{v}}, 0)$ and $(P^2_{\mathbf{v}}, 0)$, see Fig. 3. With the conventions of Sect. 5, this is the graph $y = h(x)$ with $h(x) > 0$ for $x \in \left(P^2_{\mathbf{v}}, P^1_{\mathbf{v}}\right)$. In particular, the portion of this curve that lies in the upper half of $In(\mathbf{v})$, parametrised by (x, y), $y > 0$, may be written as the union of two segments σ_1 and σ_2 that meet at the point where the coordinate y attains its maximum value on the curve. Without loss of generality, let (x_*, λ) be the coordinates in $In(\mathbf{v})$ of this point, whith $P^2_{\mathbf{v}} < x_* < P^1_{\mathbf{v}} \pmod{2\pi}$.

By Proposition 2, the image of each segment σ_j by η is a helix on $Out(\mathbf{w})$ accumulating on $W^u_{loc}(\mathbf{w})$. Hence, the curve $\eta(\sigma_1 \cup \sigma_2)$ is a double helix. The projection of this curve into $W^u_{loc}(\mathbf{w})$ is regular at all points, except for a fold at $\eta(x_*, \lambda) = (x_* - K \ln \lambda, \lambda^\delta) = (x(\lambda), y(\lambda))$, as in Fig. 8. As λ decreases to zero, the first coordinate $x(\lambda)$ of $\eta(x_*, \lambda)$ tends to infinity, hence the point $\eta(x_*, \lambda)$ makes infinitely many turns around the cylinder $Out(\mathbf{w})$.

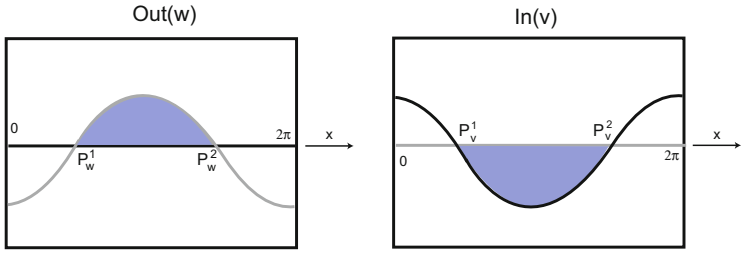

Fig. 7 The transition map $\Psi_{\mathbf{w}\to\mathbf{v}}$ sends the shaded area in $Out(\mathbf{w})$, between $W^s_{loc}(\mathbf{v})$ and $W^u_{loc}(\mathbf{w})$ and with positive second coordinate, into the *shaded area* in $In(\mathbf{v})$ with negative second coordinate. Conventions: *black line* stands for $W^u_{loc}(\mathbf{w})$, *grey line* is $W^s_{loc}(\mathbf{v})$. The rest of the *upper part* of $Out(\mathbf{w})$ is mapped into the *upper part* of $In(\mathbf{v})$

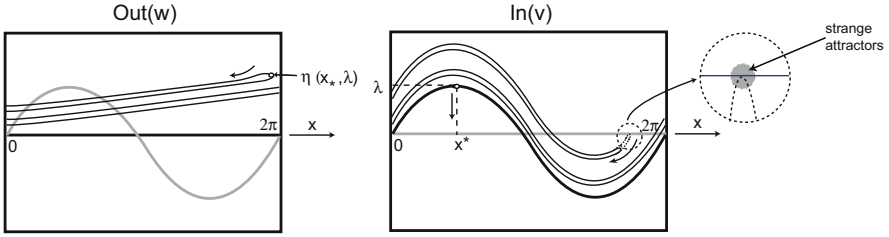

Fig. 8 In any open neighbourhood of f_0 in the space of $\langle\gamma_1\rangle$–equivariant vector fields of class C^1 on $\mathbf{S}^3$, there is a sequence of vector fields f_{λ_i} accumulating of f_0 whose flow has a heteroclinic tangency between $W^u(\mathbf{w})$ and $W^s(\mathbf{v})$

On the other hand, $y(\lambda) = \lambda^\delta$ with $\delta > 1$, so $y(\lambda)$ decreases to zero faster than λ, the maximum height of the curve $W^s_{loc}(\mathbf{v}) \cap Out(\mathbf{w})$. Therefore, given any small $\lambda_0 > 0$, there exists a positive $\lambda_1 < \lambda_0$ such that $x(\lambda_1) = x_m$ and moreover $\eta(x_*, \lambda_1) = (x(\lambda_1), y(\lambda_1))$ lies in the region in $Out(\mathbf{w})$ between $W^s_{loc}(\mathbf{v})$ and $W^u_{loc}(\mathbf{w})$ that gets mapped into the lower part of $In(\mathbf{v})$. For $\lambda = \lambda_1$, the points on the curve $W^u_{loc}(\mathbf{w}) \cap In(\mathbf{v})$ close to (x_*, λ_1) are also mapped by η into the lower half of $Out(\mathbf{w})$.

Furthermore, there exists a positive $\lambda_2 < \lambda_1$ such that $P^2_{\mathbf{w}} < x(\lambda_2) < P^1_{\mathbf{w}}$ (mod 2π) and hence $\eta(x_*, \lambda_2) = (x(\lambda_2), y(\lambda_2))$ is mapped by $\Psi_{\mathbf{w}\to\mathbf{v}}$ into the upper part of $In(\mathbf{v})$. Again, for $\lambda = \lambda_2$, points on the curve $W^u_{loc}(\mathbf{w}) \cap In(\mathbf{v})$ close to (x_*, λ) return to the upper part of $Out(\mathbf{w})$.

Therefore, for some λ_*, with $\lambda_2 < \lambda_* < \lambda_1$, the image of the curve $W^u_{loc}(\mathbf{w}) \cap In(\mathbf{v})$ by the first return map to $In(\mathbf{v})$ is tangent to $W^s_{loc}(\mathbf{v}) \cap In(\mathbf{v})$, given in local coordinates by $y = 0$. This completes the proof of Theorem 4 – given any $\lambda_0 > 0$ we have found a positive $\lambda_* < \lambda_0$ such that $W^u(\mathbf{w})$ is tangent to $W^w(\mathbf{v})$ for f_{λ_*}. □

7 Conclusion

For the present study, we have used the symmetry γ_1 and its flow invariant fixed point subspace to ensure the persistence of the connections $[\mathbf{v} \to \mathbf{w}]$ of one-dimensional manifolds. The symmetry is not essential for our exposition but its existence makes it more natural. In particular, the networks we describe are persistent within the class of differential equations with the prescribed symmetry.

As a global structure, the transition of the dynamics from $\dot{x} = f_0(x)$ to $\dot{x} = f_\lambda(x)$, $\lambda \approx 0$ is intriguing and has not always attracted appropriate attention. There is a neighbourhood V^0 with positive Lebesgue measure that is positively invariant for the flow of $\dot{x} = f_\lambda(x)$. For $\lambda = 0$ all trajectories approach the network Σ^0. For $\lambda > 0$ and for a sufficiently small tubular neighbourhood $V^\Gamma \subset V^0$ of any of the Bykov cycles in $\Sigma^\star$, almost all trajectories might return to V^Γ but they do not necessarily remain there for all future time. Trajectories that remain in V^Γ for all future time form an infinite set of suspended horseshoes with zero Lebesgue measure.

For a fixed $\lambda > 0$, when we take a larger tubular neighbourhood V^Γ of a Bykov cycle Γ, the suspended horseshoes lose hyperbolicity. While small symmetry-breaking terms generically destroy the attracting cycle Σ^0, there will still be an attractor lying close to the original cycle. This is the main point of Sect. 5: when local invariant manifolds are extended, they develop tangencies, which explain the attractivity. The existence of primary heteroclinic tangencies is proved in Sect. 6.

Heteroclinic tangencies give rise to attracting periodic trajectories of large periods and small basins of attraction, appearing in large (possibly infinite) numbers. Heteroclinic tangencies also create new tangencies near them in phase space and for nearby parameter values. We know very little about the geometry of these strange attractors, we also do not know the size and the shape of their basins of attraction.

When $\lambda \to 0$, the infinite number of periodic sinks lying close to the network of Bykov cycles will approach the ghost of Σ^0. For the parameter values where we observe heteroclinic tangencies, each Bykov cycle possesses infinitely many sinks whose basins of attractions have positive three-dimensional Lesbesgue measure. The attractors must lie near $\overline{W^s(\mathbf{v})} \cup \overline{W^u(\mathbf{w})}$ and they collapse into Σ^0 as $\lambda \to 0$. A lot more needs to be done before the subject is well understood.

Acknowledgements The authors would like to thank Maria Carvalho for helpful discussions.

CMUP is supported by the European Regional Development Fund through the programme COMPETE and by the Portuguese Government through the Fundação para a Ciência e a Tecnologia (FCT) under the project PEst-C/MAT/UI0144/2011. A.A.P. Rodrigues was supported by the grant SFRH/BPD/84709/2012 of FCT.

References

1. Afraimovich, V.S., Shilnikov, L.P.: Strange attractors and quasiattractors. In: Barenblatt, G.I., Iooss, G., Joseph, D.D. (eds.) Nonlinear Dynamics and Turbulence, pp. 1–51. Pitman, Boston (1983)
2. Aguiar, M., Castro, S.B., Labouriau, I.S.: Dynamics near a heteroclinic network. Nonlinearity **18**, 391–414 (2005)
3. Aguiar, M., Castro, S.B., Labouriau, I.S.: Simple vector fields with complex behaviour. Int. J. Bifurc. Chaos **16**(2), 369–381 (2006)
4. Aguiar, M., Labouriau, I.S., Rodrigues, A.A.P.: Swicthing near a heteroclinic network of rotating nodes. Dyn. Syst. Int. J. **25**(1), 75–95 (2010)
5. Bonatti, C., Díaz, L., Viana, M.: Dynamics beyond uniform hyperbolicity. Springer, Berlin/Heidelberg (2005)
6. Bowen, R.: A horseshoe with positive measure. Invent. Math. **29**, 203–204 (1975)
7. Bowen, R.: Equilibrium States and the Ergodic Theory of Anosov Diffeomorphisms. Lecture Notes in Mathematics. Springer, Berlin/New York (1975)
8. Bykov, V.V.: Orbit structure in a neighbourhood of a separatrix cycle containing two Saddle-Foci. Am. Math. Soc. Transl. **200**, 87–97 (2000)
9. Colli, E.: Infinitely many coexisting strange attractors. Ann. Inst. Henri Poincaré Anal. Non Linéaire **15**, 539–579 (1998)
10. Field, M.: Lectures on Bifurcations, Dynamics and Symmetry. Pitman Research Notes in Mathematics Series, vol. 356. Longman, Harlow (1996)
11. Golubitsky, M., Stewart, I.: The Symmetry Perspective, Birkhauser, Basel/Boston (2000)
12. Gonchenko, S.V., Shilnikov, L.P., Turaev, D.V.: Quasiattractors and homoclinic tangencies. Comput. Math. Appl. **34**(2–4), 195–227 (1997)
13. Gonchenko, S.V., Ovsyannikov, I.I., Turaev, D.V.: On the effect of invisibility of stable periodic orbits at homoclinic bifurcations. Phys. D **241**, 1115–1122 (2012)
14. Homburg, A.J.: Periodic attractors, strange attractors and hyperbolic dynamics near homoclinic orbit to a saddle-focus equilibria. Nonlinearity **15**, 411–428 (2002)
15. Homburg, A.J., Sandstede, B.: Homoclinic and Heteroclinic Bifurcations in Vector Fields. Handbook of Dynamical Systems, vol. 3, pp. 379–524. North Holland, Amsterdam (2010)
16. Krupa, M., Melbourne, I.: Asymptotic stability of heteroclinic cycles in systems with symmetry. Ergod. Theory Dyn. Syst. **15**, 121–147 (1995)
17. Labouriau, I.S., Rodrigues, A.A.P.: Global generic dynamics close to symmetry. J. Differ. Equ. **253**(8), 2527–2557 (2012)
18. Lamb, J.S.W., Teixeira, M.A., Webster, K.N.: Heteroclinic bifurcations near Hopf-zero bifurcation in reversible vector fields in $\mathbf{R}^3$. J. Differ. Equ. **219**, 78–115 (2005)
19. Melbourne, I., Proctor, M.R.E., Rucklidge, A.M.: A heteroclinic model of geodynamo reversals and excursions. In: Chossat, P., Armbruster, D., Oprea, I. (eds.) Dynamo and Dynamics, a Mathematical Challenge, pp. 363–370. Kluwer, Dordrecht (2001)
20. Mora, L., Viana, M.: Abundance of strange attractors. Acta Math. **171**, 1–71 (1993)
21. Newhouse, S.E.: Diffeomorphisms with infinitely many sinks. Topology **13**, 9–18 (1974)
22. Newhouse, S.E.: The abundance of wild hyperbolic sets and non-smooth stable sets for diffeomorphisms. Publ. Math. Inst. Hautes Etudes Sci. **50**, 101–151 (1979)
23. Ovsyannikov, I.M., Shilnikov, L.P.: On systems with saddle-focus homoclinic curve. Math. USSR Sb. **58**, 557–574 (1987)
24. Rodrigues, A.A.P.: Repelling dynamics near a Bykov cycle. J. Dyn. Differ. Equ. (2013, to appear). doi:10.1007/s10884-013-9289-2
25. Rodrigues, A.A.P., Labouriau, I.S.: Spiraling sets near a heteroclinic network. Preprint – CMUP n. 2011–22 available at arXiv:1304.5283v1
26. Samovol, V.S.: Linearization of a system of differential equations in the neighbourhood of a singular point. Sov. Math. Dokl. **13**, 1255–1959 (1972)

27. Shilnikov, L.P.: Some cases of generation of periodic motion from singular trajectories. Math. USSR Sb. **61**(103), 443–466 (1963)
28. Shilnikov, L.P.: A case of the existence of a denumerable set of periodic motions. Sov. Math. Dokl. **6**, 163–166 (1965)
29. Shilnikov, L.P.: On a Poincaré–Birkhoff problem. Math. USSR Sb. **3**, 353–371 (1967)
30. Shilnikov, L.P.: The existence of a denumerable set of periodic motions in four dimensional space in an extended neighbourhood of a saddle-focus. Sov. Math. Dokl. **8**(1), 54–58 (1967)

Finding Periodic Orbits in the Hindmarsh-Rose Neuron Model

M. Angeles Martínez, Roberto Barrio, and Sergio Serrano

Abstract In this work we apply a modified search method based on the stability transformation method, combined with the Newton method, to the classical neuronal model proposed by Hindmarsh and Rose in 1984. We have selected two values of parameter b corresponding to chaotic-bursting behavior ($b = 2.69$ and $b = 3.05$). For these values we have studied the changes of the chaotic attractors by obtaining the complete set of unstable periodic orbits up to multiplicity four. For $b = 2.69$ we have found 1, 1, 2 and 3 POs of multiplicity one to four, respectively, and for $b = 3.05$ we have found 1, 1, 0, 1 POs of multiplicity one to four, and thus giving a different chaotic attractor.

1 Introduction

The study of brain behaviour is one of the challenges of this century. But the brain itself is too much complicated to understand how it works; we need first to know how its components (the neurons) work. Knowing the behaviour of a neuron helps to improve the interneuronal models and therefore the brain behaviour knowledge. Neurons are characterized by oscillations in the potential membrane. The accumulation of these oscillations can be seen, for example, in the electroencephalograms. These oscillations play an important role in some neurological deceases such as Parkinson or epilepsy [10] and make their study so important.

From a mathematical point of view, a neuron is a dynamical system [7] which can be characterized by a set of differential equations and parameters that describe how the neuron activity evolves in time. Several neuron models have been

M.A. Martínez (✉) · R. Barrio · S. Serrano
Departamento de Matemática Aplicada and IUMA, Universidad de Zaragoza, E-50009 Zaragoza, Spain
e-mail: gelimc@unizar.es; rbarrio@unizar.es; sserrano@unizar.es

S. Ibáñez et al. (eds.), *Progress and Challenges in Dynamical Systems*,
Springer Proceedings in Mathematics & Statistics 54,
DOI 10.1007/978-3-642-38830-9_18,

provided during the last decades. One of the most famous and complete is the one formulated by Hodgkin-Huxley [7]. Ought to the complexity of their system, several simplifications have been developed as the Hindmarsh and Rose (HR) model [6] that reproduce very fairly the two main characteristics of neurons: spiking and bursting oscillations.

Modeling a neuron as a dynamical system, allows us to carry out a bifurcation study to see when the qualitative changes of the system are produced or which parameters have to be varied to change the system. Sometimes this bifurcation study shows us some chaotic regions in which chaotic attractors can be found (Sect. 2). Chaotic attractors are composed by Unstable Periodic Orbits (UPOs). The more unstable the orbits are, the more difficult is to found them. That is why we have developed and applied a periodic orbit search method based on the stability transformation combined with the Newton method (Sect. 3). Finally we present a summary and some conclusions of this work (Sect. 4).

2 Hindmarsh and Rose Model

Hindmarsh and Rose [6] proposed in 1984 a model of neuronal activity described by three nonlinear Ordinary Differential Equations (ODEs):

$$\begin{cases} \dot{x} = y - ax^3 + bx^2 - z + I \\ \dot{y} = c - dx^2 - y \\ \dot{z} = \epsilon[s(x - x_0) - z] \end{cases} \tag{1}$$

where x is the membrane potential, y the fast and z the slow gating variables for ionic current. The parameters are typically set as follow: $a = 1$, $c = 1$, $d = 5$, $s = 4$, $x_0 = -1.6$, $\epsilon = 0.01$ and we consider with detail two particular cases $b = 2.69$, $I = 4.155571635$ and $b = 3.05$, $I = 2.774963821$. The bifurcation parameter b determines the bursting or spiking behavior and we will study the system by changing the values of this parameter.

This HR model fulfills the two basic conditions of being computationally simple but at the same time it is able to reproduce the main behavior (the rich firing patterns) exhibited by the real biological neuron.

In Fig. 1 we present the brute-force bifurcation diagram obtained by means of multiple numerical integrations of the systems using the spike-counting method [4]. First we define a grid of 1,000 by 1,000 points in the (b, I) plane. For each pair of the grid parameter values we integrate using the recently developed software TIDES [2] (Taylor Integrator for Differential EquationS). After rejecting points during the transient time we look for periodicity by considering the maximum of the z value. The color-coded bar gives the spike-number range [4]. In this work we have selected several values of parameter b in the chaotic-bursting region corresponding to a positive first Lyapunov exponent. We have observed that the structure of the chaotic

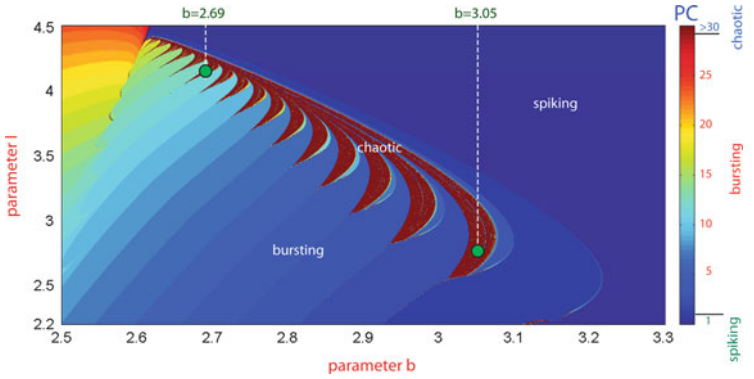

Fig. 1 Spike counting diagram giving regular spiking and bursting regions with chaotic bursting zones, and selected b values in the chaotic region

attractor changes with the b parameter (other b and I values have been studied in the chaotic region but the main differences can be seen in these two extreme cases).

In Fig. 2 we show, for two different values of the b parameter, the chaotic attractor together with the stable manifold of the equilibrium point. In all cases the equilibrium point lies far from the chaotic invariant set but its stable manifold go through it. However the structure of the attractors is clearly different.

3 Periodic Orbit Search Method

Our periodic orbit search method is based on the stability transformation (ST) method [9] combined with the Newton method. The ST method was developed in [9] to detect unstable periodic orbits in chaotic dynamical systems by modifying the system in order to increase or create a basin of attraction to any UPO. Although it was created for discrete dynamical systems it can be extended to time-continuous systems by the reduction of the continuous flow to a Poincaré map which is then searched for fixed points [8].

Let us consider a continuous chaotic system given by a set of ordinary differential equations

$$U : \dot{\mathbf{x}} = \mathbf{F}(\mathbf{x}).$$

To find fixed points of U we carry on a set of transformations which change U into new dynamical systems (S_k) where each unstable fixed point in U became stable. For each S_k a different set of fixed points of U is stabilized.

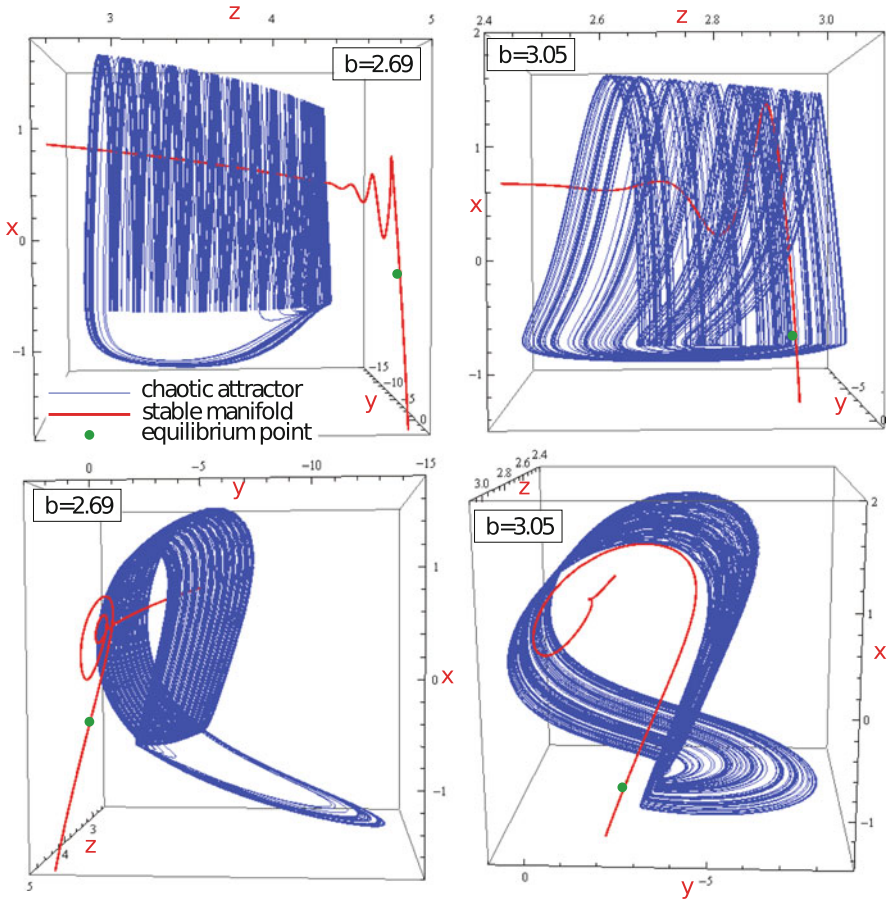

Fig. 2 Chaotic attractors together with their equilibrium point (in *green*) and the stable manifold (in *red*). We can appreciate that the structure is clearly different

The new stabilized systems S_k are defined as follows:

$$S_k : \mathbf{x}_{i+1} = \mathbf{x}_i + \Lambda_k(\mathbf{F}(\mathbf{x}_i) - \mathbf{x}_i),$$

where Λ_k is an invertible constant $n \times n$ matrix. In [9] it was proposed to use $\Lambda_k = \lambda C_k$ with $0 < \lambda \ll 1$. Matrices C_k are defined to have only one non vanishing entry $+1$ or -1 in each row and column, and thus they are orthogonal. These matrices configure the so-called *minimal set* [9].

As it can be seen in [9] one advantage of this method is the increment of the convergent region since the extension of the basins of attraction is larger than the corresponding in the Newton method. Another advantage is that we do not need any previous knowledge about the dynamical system under consideration.

Therefore, the three key components in the ST method when applied to time-continuous systems are: a good positioning of the Poincaré Surfaces of Section (PSS), a suitable distribution of the initial points and an appropriate value for the parameter λ. The extended explanation of the proper choice of these components can be seen in [3].

As explained in [5, 8] the numerical efficiency of the ST method can be significantly improved by combining with the Newton method. After a certain number of iterations of the ST method, this is replaced by the Newton one. A proper choice of this step-size is essential for the overall performance of the POs search [3]. In the case of the Newton method we use the development made by Abad et al. [1] considering only the double-precision implementation.

As a whole, our search method works as follows. First we obtain a well distributed set of points to use as initial conditions (obtained saving the intersection points of a chaotic orbit with the PSS). Second, we calculate the critical value ($\lambda_c = 1/\max_i \|\lambda_i\|$) using the inverse of the largest modulus of the eigenvalues of the stability matrix. Then we propagate each initial point until it intersects again the PSS, and we obtain the difference between the initial point and its propagation. If the difference is lower than the desired accuracy we have found one periodic orbit. If it is greater than the desired accuracy but lower than a chosen step-size we use Newton method to look for the periodic orbit. If the difference is greater than the chosen step-size we continue with the ST method which implies multiplying that difference by λ and one matrix of the minimal set, and adding this quantity to the initial point. We consider this new point as the initial point and we repeat the process for each matrix of the minimal set until we reach a periodic orbit or we get the maximum number of iterations. It has to be noted that one initial point can reach different periodic orbits by using different matrices of the minimal set.

In some cases of high multiplicity we use only the ST method because even for an initial point very close to the solution ($\sim 10^{-8}$), Newton method does not converge. In these cases we have to relax the accuracy and play with other components as λ, number of iterations or number of points. As the multiplicity increases, we should decrease the λ value and therefore, increase the number of iterations.

To be sure that all periodic orbits have been detected we use the information provided by a suitable First Return Map (FRM). In Fig. 3 we plot the FRM for the two selected values of parameter b considering a PSS at $x = 0$ for the y coordinate. In the first map (top-left picture) we plot in the abscissa axis the y_i coordinate and in the ordinates the y_{i+1}, which means that when $y_i = y_{i+1}$, i.e. in the diagonal, we have a periodic orbit of multiplicity one. In the second map (FRM^2) we plot y_i versus y_{i+2}, and now when $y_i = y_{i+2}$ we have a periodic orbit of multiplicity two and so on. Looking for the intersection with the diagonal (marked with a colour point in the two first maps) we can know how many periodic orbit have to be found for a selected multiplicity. Multiplicity one orbits have one intersection point, multiplicity two have two intersection points and so on. We can see that in the third map (FRM^3) for $b = 2.69$ there exist seven intersection points distributed as follows, one corresponds to the multiplicity one orbit, three to a multiplicity three orbit and other three to another multiplicity three orbit. However, for $b = 3.05$ there

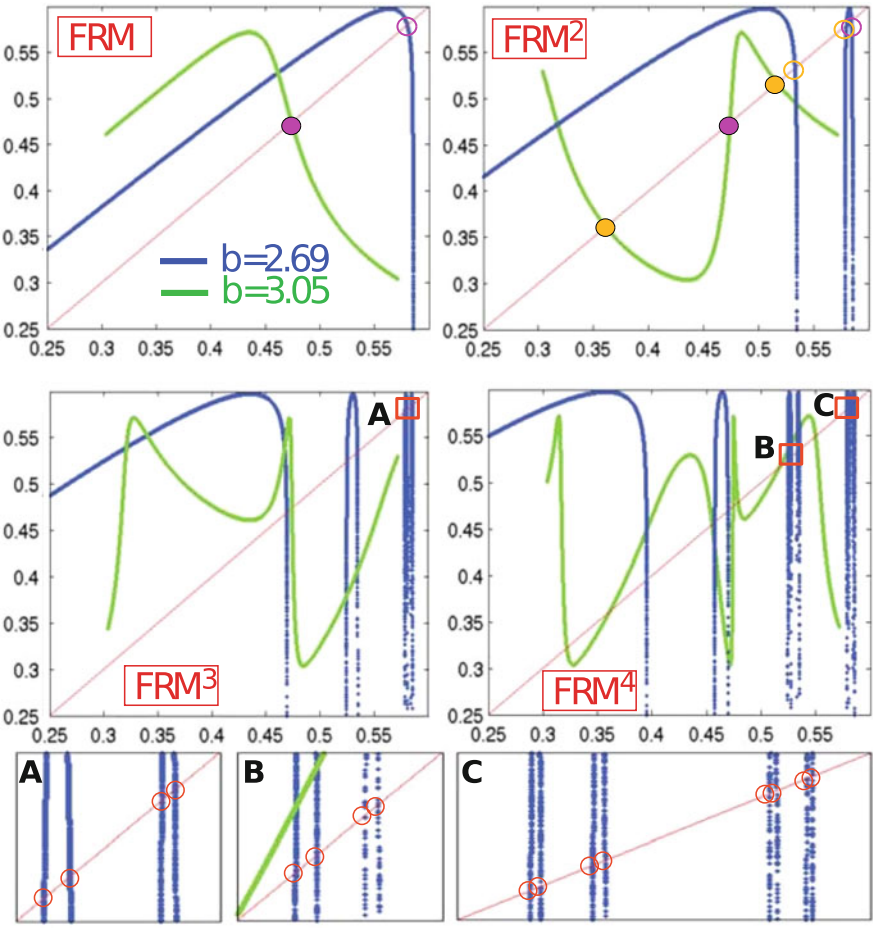

Fig. 3 First Return map (FRM) to fourth return map (FRM^4) of the two selected chaotic attractors. On the *bottom* we zoom several areas to see exactly how many intersection points with the diagonal there exist

Table 1 Number of unstable periodic orbits up to multiplicity four for the two selected b values

b	$m = 1$	$m = 2$	$m = 3$	$m = 4$
2.69	1	1	2	3
3.05	1	1	0	1

exist only one intersection point with the diagonal corresponding to the multiplicity one orbit (see the first map). The number of periodic orbits to be found for each case is summarized in Table 1 where we present for each selected value b (column 1) the number of periodic orbits for each multiplicity (columns 2–5).

Table 2 Initial conditions for the unstable periodic orbits

m	x	y	z	T
$b = 2.69$				
1	0	−2.231322821	4.417443232	24.82412578
2	0	−2.209228569	4.424424035	47.76420192
3	0	−2.499189513	4.328419675	72.21468385
3	0	−2.455015665	4.343676744	68.34909310
4	0	−2.453720291	4.344120618	86.86090563
4	0	0.524652133	4.218528182	92.36872603[a]
4	0	0.580751898	4.309261197	97.07999229[a]
$b = 3.05$				
1	0	−4.659567370	2.917404632	57.82253022
2	0	0.517041996	2.842272431	81.54102149
4	0	0.549814747	2.895139780	184.9712929

[a]Only with ST method

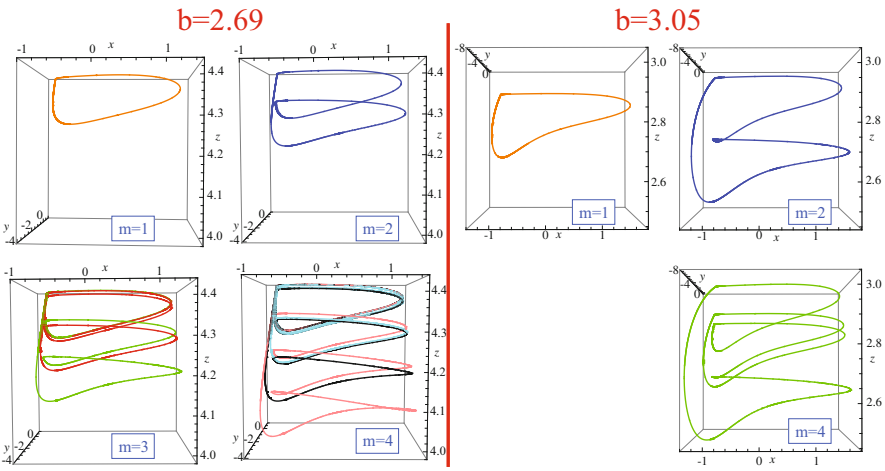

Fig. 4 Unstable periodic orbits foliated to the two chaotic attractors

In Table 2 we present all the UPOs of the system, for the two selected cases, up to multiplicity 4. First column of the table corresponds to the multiplicity of the orbit. Since in some multiplicities more than one orbit is found, we see the multiplicity repeated. At columns 2–4 we find the initial conditions which together with the period in column 5 define the orbit.

In Fig. 4 we plot the periodic orbits for the two cases. We note that for $b = 3.05$ we have not found any orbit of multiplicity 3 (which has been confirmed with the FRM) and only one of multiplicity 4. On the other hand, in $b = 2.69$ we have found two orbits of multiplicity 3 and three orbits of multiplicity 4. We can see that both chaotic attractors (see Fig. 2) are completely different in appearance, and moreover in the UPOs foliated to it, which means that topologically both attractors

are different. In the $b = 2.69$ case all orbits go through the first loop and as the multiplicity increases, the orbits cover more attractor surface. We have to remark that when the POs are very close each other it is much more difficult to find them numerically, as it occurs in this case. Actually blue and black cases in $m = 4$ had been found using only ST method since the Newton method do not converge even for points very near to the solution.

4 Summary and Conclusions

In this paper we have studied, for the first time, all the unstable periodic orbits up to multiplicity four, for the Hindmarsh-Rose neuron model using two different values of the parameter b corresponding to the chaotic region. We have shown that these two cases present a different chaotic attractor, as the number of unstable periodic orbits foliated to them is different, and thus giving a different topological template. A more detailed analytical and numerical study is in progress.

Acknowledgements This work is supported by Spanish Research project AYA2008-05572 (to M.A.M.) and by the Spanish Research project MTM2012-31883 (to R.B. and S.S.). We acknowledge Prof. Andrey Shilnikov for valuable comments and fruitful discussions about neuron models.

References

1. Abad, A., Barrio, R., Dena, A.: Computing periodic orbits with arbitrary precision. Phys. Rev. E **84**, 6 (2011)
2. Abad, A., Barrio, R., Blesa, F., Rodríguez, M.: Algorithm 924: TIDES, a Taylor series integrator for differential equations. ACM Trans. Math. Softw. **39**, 5:1–5:28 (2012). http://gme.unizar.es/software/tides
3. Abad, A., Barrio, R., Martínez, M.A., Serrano, S.: Finding Periodic Orbits in Time Continuous Dynamical Systems (in preparation)
4. Barrio, R., Shilnikov, A.: Parameter-sweeping techniques for temporal dynamics of neuronal systems: case study of Hindmarsh-Rose model. J. Math. Neurosci. **1**, 6 (2011)
5. Davidchack, R.L., Lai, Y.C.: Efficient algorithm for detecting unstable periodic orbits in chaotic systems. Phys. Rev. E **60**, 6172 (1999)
6. Hindmarsh, J.L., Rose, R.M.: A model of the nerve impulse using three coupled first-order differential equations. Proc. R. Soc. Lond. **B221**, 87–102 (1984)
7. Hodgkin, A.L., Huxley, A.F.: A quantitative description of membrane current and its application to conduction and excitation in nerve. J. Physiol. **117**, 500–544 (1952)
8. Pingel, D., Schemelcher, P., Diakonos, F.K.: Detecting unstable periodic orbits in chaotic continuous-time dynamical systems. Phys. Rev. E **64**, 026214 (2001)
9. Schemelcher, P., Diakonos, F.K.: Detecting unstable periodic orbits of chaotic dynamical systems. Phys. Rev. Lett. **78**, 4733 (1997)
10. Uhlhaas, P.J., Singer, W.: Neural synchrony in brain disorders: relevance for cognitive dysfunctions and pathophysiology. Neuron **52**, 155–168 (2006)

Realization Problems in the Theory of Foliations

Daniel Peralta-Salas

Abstract Can any embedded 3-sphere be realized as a leaf of a codimension two foliation of $\mathbb{R}^5$? Does there exist a submersion $\Phi : \mathbb{R}^3 \to \mathbb{R}^2$ with a knotted fibre $\Phi^{-1}(0)$? For any link L, does there exist a non vanishing Morse-Smale flow in $\mathbb{R}^3$ whose whole set of periodic trajectories is given by L? These apparently unrelated problems can be addressed using the theory of integrable embeddings recently introduced by Gilbert Hector and the author. In this paper I will provide a leisurely introduction to this theory, focused on the applications to the aforementioned problems. The theory of integrable embeddings is a very rich framework where many classical tools from differential and algebraic topology play a prominent role: Gromov h-principle, Hirsch-Smale theory of immersions, complete intersections and obstruction theory.

1 Introduction

The problem of deciding whether a manifold L of dimension k is diffeomorphic to a leaf of a foliation of another manifold M of dimension $n > k$ (the realization problem) is a classical question in the theory of foliations that can be traced back to [20]. Since every manifold is a leaf of a product foliation $L \times \mathbb{R}$ or $L \times \mathbb{S}^1$, the main difficulty consists in fixing some properties of the ambient manifold M or the qualitative structure of the realizing foliation. For example, when L is open and M is compact, many realization (and non realization) theorems have been obtained for the last 30 years, e.g. [2,7,11,18]. When M is the Euclidean space $\mathbb{R}^n$, in 1993 E. Vogt raised the problem [21] of characterizing which closed (orientable) 3-manifolds can

D. Peralta-Salas (✉)
Instituto de Ciencias Matemáticas (ICMAT), Consejo Superior de Investigaciones Científicas, Madrid, Spain
e-mail: dperalta@icmat.es

S. Ibáñez et al. (eds.), *Progress and Challenges in Dynamical Systems*,
Springer Proceedings in Mathematics & Statistics 54,
DOI 10.1007/978-3-642-38830-9_19, © Springer-Verlag Berlin Heidelberg 2013

be realized as leaves of foliations of a Euclidean space with all leaves compact, in particular:

Question 1. Can $\mathbb{S}^3$ be a leaf of a codimension two foliation of $\mathbb{R}^5$ or a codimension three foliation of $\mathbb{R}^6$?

This question has an affirmative answer in $\mathbb{R}^n$ for $n \geq 7$. Indeed, a foliation realizing $\mathbb{S}^3$ in $\mathbb{R}^7$ can be easily constructed using the Hopf fibration $\mathbb{S}^3 \to \mathbb{S}^7 \to \mathbb{S}^4$ and identifying $\mathbb{R}^7$ with $\mathbb{S}^7 \backslash \{N\}$, N being the north pole of $\mathbb{S}^7$. Obviously, all the leaves of this foliation are diffeomorphic to $\mathbb{S}^3$ except for one leaf which is diffeomorphic to $\mathbb{R}^3$. This construction extends to $\mathbb{R}^n$, $n \geq 7$, just by taking the product foliation $\mathbb{R}^7 \times \mathbb{R}^{n-7}$. Let me remark that, as a consequence of Wu's theorem [1], all the embeddings of $\mathbb{S}^3$ in $\mathbb{R}^n$, $n \geq 7$, are isotopic, and hence the realization problem does not depend on the way $\mathbb{S}^3$ is embedded in these dimensions. This is not the case in $\mathbb{R}^5$ and $\mathbb{R}^6$, where there are infinitely many non isotopic "knotted" embeddings.

The realization problem for foliations of open manifolds admitting a maximal number of independent first integrals has also attracted considerable attention. These foliations, usually called *simple foliations*, are given by the intersection of the level sets of m functions $\Phi_i : M \to \mathbb{R}$, m being the codimension of the foliation, so that $rank(d\Phi_1, \cdots, d\Phi_m) = m$ at each point of M. In other words, a simple foliation is defined by the union of the connected components of the fibres $\Phi^{-1}(c)$ of a submersion $\Phi : M \to \mathbb{R}^m$. These types of foliations appear very naturally in several contexts, as e.g. completely integrable vector fields, where $m = n - 1$, and Liouville integrable Hamiltonian systems, where M is a symplectic manifold and $m = n/2$. In general, a submersion does not define a fibre bundle and simple foliations can exhibit interesting behaviors, as the coexistence of open and compact leaves separated by fractal boundaries. In 1988, motivated by the study of the Szebehely equation in classical mechanics, the authors of [8] raised the question:

Question 2. Let L be a knot in $\mathbb{R}^3$. Does there exist a submersion $\Phi : \mathbb{R}^3 \to \mathbb{R}^2$ such that its zero fibre is given by L, i.e. $\Phi^{-1}(0) = L$?

It is obvious that this question has a negative answer in $\mathbb{R}^2$. Indeed, any function $\Phi : \mathbb{R}^2 \to \mathbb{R}$ whose zero fibre is a closed curve $L \subset \mathbb{R}^2$ has a critical point in the region bounded by L. Moreover, a submersion $\Phi : \mathbb{R}^3 \to \mathbb{R}^2$ all of whose fibres are compact is a fibration by Ehresmann's theorem, and since $\mathbb{R}^3$ cannot be fibred by circles [6], it follows that any submersion Φ with a compact fibre must have open fibres as well. Question 2 was answered affirmatively in a paper by S. Miyoshi [14], but his proof is seriously flawed, as we showed in [13].

Part of the literature on realization problems concerns the existence of knotted and linked trajectories of non vanishing vector fields (hence 1-dimensional foliations) satisfying some assumptions. A remarkable result in this direction is Wada's theorem [22], which classifies the link types that can be realized as sets of periodic orbits of non vanishing Morse-Smale flows in $\mathbb{S}^3$. These structures are called zero-entropy links, and the method of proof exploits the round handle decomposition of $\mathbb{S}^3$ that can be defined using a Morse-Smale flow, which imposes strong constraints

on the admissible types of knots and links. This approach does not work in $\mathbb{R}^3$ (the infinity plays an important role), so it is natural to ask the following question:

Question 3. Let L be a link in $\mathbb{R}^3$. Can L be realized as the whole set of periodic trajectories of a non vanishing Morse-Smale flow in $\mathbb{R}^3$?

In this paper I will assume that the link L has a locally finite number of connected components, although this is not necessarily the general case [4]. This question was affirmatively answered by N. Watanabe [23] using a quite sophisticated geometric construction of a codimension two simple foliation of $\mathbb{R}^3$ realizing the link L as a set of leaves. In this paper I will provide a simpler proof of this result using an explicit analytic construction.

The paper is organized as follows. In Sects. 2 and 3 I will introduce the theory of weakly and strongly integrable embeddings [13], which allows us to tackle all these problems under a unified framework. Sections 4–6 are dedicated to solve Questions 1–3 using the methods explained in the previous sections. To conclude, in Sect. 7 I pose some open questions related to the realization problem. The aim of this paper is not to provide detailed proofs of the results that will be stated but to introduce the main ideas and methods that we have developed to address these types of problems. Further technical details can be consulted in [13].

2 The Theory of Weakly Integrable Embeddings

Let L be a properly embedded k-dimensional submanifold of $\mathbb{R}^n$, and denote by $m := n - k \geq 1$ its codimension. In this paper I will assume that all manifolds are smooth, oriented and without boundary, but not necessarily connected nor compact, and that all maps are smooth. It is well known that, if the normal bundle of L is trivial, there is a map $\Phi : \mathbb{R}^n \to \mathbb{R}^m$ such that L is contained in the zero set $\Phi^{-1}(0)$ and the Jacobian matrix $d\Phi(x)$ is onto (or equivalently, it has maximum rank) at each point $x \in L$. If the $m \times n$ matrix $d\Phi(x)$ is onto at each point of $\mathbb{R}^n$, the map Φ is a submersion.

Definition 1. We say that L is weakly integrable (WI) if there exists a submersion $\Phi : \mathbb{R}^n \to \mathbb{R}^m$ such that $L \subset \Phi^{-1}(0)$, that is L is a union of connected components of the zero fibre $\Phi^{-1}(0)$. The map Φ is called a WI equation of L.

The main goal of the theory of integrable embeddings [13] is to characterize weakly integrable submanifolds. In particular, does the weak integrability of L depend only on its topological properties or also on the way it is embedded in $\mathbb{R}^n$? Recall that all the embeddings of L in $\mathbb{R}^n$ are isotopic if $n \geq 2k + 2$, but this is not the general case if $n \leq 2k + 1$ (e.g. knots and links in $\mathbb{R}^3$). The theory that I have developed, in collaboration with Gilbert Hector, works for any non compact ambient manifold M, but I will restrict myself to $M = \mathbb{R}^n$ in this paper. Let me summarize two basic properties of WI submanifolds.

Property 1. Any WI submanifold has trivial normal bundle. Indeed, writing the map Φ in components, $\Phi = (\Phi_1, \cdots, \Phi_m)$, the gradient vector fields $\nabla\Phi_i(x)$ with respect to the Euclidean metric yield m independent vectors at each point $x \in L$ lying on a plane orthogonal to L (of dimension m). The existence of this global normal framing implies the desired property.

Property 2. Any WI submanifold is parallelizable. It is obvious that the submanifold L is a union of leaves of the codimension m foliation $\mathscr{F}_\Phi$ of $\mathbb{R}^n$ defined by the connected components of the level sets $\Phi^{-1}(c)$. We also have that the tangent bundle $T(L)$ of L extends as a subbundle of $T(\mathbb{R}^n)$ using the tangent bundle of the foliation $\mathscr{F}_\Phi$. Since any bundle over $\mathbb{R}^n$ is trivial, the claim then follows.

As noticed in Property 2, any WI submanifold is a union of leaves of a codimension m foliation $\mathscr{F}_\Phi$ of $\mathbb{R}^n$. By construction, this foliation admits m independent first integrals, is without holonomy, and its leaf space is a (possibly non Hausdorff) manifold of dimension m. These types of foliations are usually called simple in the literature. In the following examples I illustrate that simple foliations are not so "simple". The common denominator of all these examples is that the submersions Φ, whose level sets define the foliations, are not fibre bundles because they have critical points at infinity (more precisely, asymptotic critical values in the sense of Rabier [17]).

Example 1. The leaves of a simple foliation do not need to be diffeomorphic to each other. Consider the submersion $\Phi : \mathbb{R}^3 \to \mathbb{R}$ defined in cartesian coordinates as $\Phi(x, y, z) = x^2 + y^2 + \arctan z$. It is easy to check that the fibre $\Phi^{-1}(c)$ is diffeomorphic to $\mathbb{S}^1 \times \mathbb{R}$ if $c \geq \pi/2$ and diffeomorphic to $\mathbb{R}^2$ if $c \in (-\pi/2, \pi/2)$. Moreover, the codimension one foliation $\mathscr{F}_\Phi$ admits a global section and its leaf space is diffeomorphic to $\mathbb{R}$.

Example 2. All the leaves of a simple foliation of $\mathbb{R}^3$ can be diffeomorphic to $\mathbb{S}^1 \times \mathbb{R}$ (Palmeira's example [15]). To construct the corresponding submersion $\Phi : \mathbb{R}^3 \to \mathbb{R}$, we define the set $\Sigma := \{(x, y, z) \in \mathbb{R}^3 : x = 0, y \geq 0, \bigcup_{n\in\mathbb{Z}}(z = n\pi + 2 \arctan y)\}$. The main observation is that the open manifold $\mathbb{R}^3 \backslash \Sigma$ is diffeomorphic to $\mathbb{R}^3$, that is there exists a smooth diffeomorphism $H : \mathbb{R}^3 \backslash \Sigma \to \mathbb{R}^3$. It then follows that the map $\Phi = z \circ H^{-1}$ is a submersion whose fibres are all diffeomorphic to cylinders. The corresponding codimension one foliation $\mathscr{F}_\Phi$ also admits a global section and its leaf space is diffeomorphic to $\mathbb{R}$.

Example 3. Simple foliations of codimension bigger than one can have compact leaves. Consider the submersion $\Phi_1 : \mathbb{R}^3 \to \mathbb{S}^2$ obtained from the Hopf fibration $\mathbb{S}^1 \to \mathbb{S}^3 \to \mathbb{S}^2$ by removing the north pole of $\mathbb{S}^3$. Obviously the product $\mathbb{S}^2 \times \mathbb{R}$ can be immersed in $\mathbb{R}^3$ using an embedding $H : \mathbb{S}^2 \times \mathbb{R} \to \mathbb{R}^3$. It then follows that the map $\Phi : \mathbb{R}^4 \to \mathbb{R}^3$ defined as $\Phi := H \circ \Phi_1$ is a submersion whose fibers are connected and most of them diffeomorphic to $\mathbb{S}^1$. The associated simple foliation of codimension three does not admit a global section (Hopf fibration is not trivial) and its leaf space is diffeomorphic to $\mathbb{S}^2 \times \mathbb{R}$.

To study WI submanifolds we need to introduce two tools from differential and algebraic topology, respectively: Gromov h-principle and obstruction theory. Let me explain their main ideas.

Gromov h-principle is an important and quite general tool to prove the existence of solutions of partial differential relations satisfying some appropriate hypotheses. In this paper we shall only need the particular case which concerns submersions, a nice and comprehensive survey on this topic is Haefliger's paper [12].

Let M be a matrix-valued function of $\mathbb{R}^n$ which assigns an $m \times n$ matrix $M(x)$ to each point $x \in \mathbb{R}^n$. Assume that $M(x)$ is onto (i.e. it has maximum rank m) for each point x. In this case, Gromov h-principle then asserts the following:

Theorem 1 (Gromov). *There exists a continuous deformation $M_t(x)$, $t \in [0,1]$, such that for all $x \in \mathbb{R}^n$ the following properties hold:*

1. $M_0(x) = M(x)$.
2. *$M_t(x)$ is an $m \times n$ matrix which is onto for all $t \in [0,1]$.*
3. *$M_1(x) = d\Phi(x)$ for some submersion $\Phi : \mathbb{R}^n \to \mathbb{R}^m$, where $d\Phi(x)$ is the Jacobian matrix of Φ at the point x.*

Moreover, a relative version also holds. Indeed, if the matrix-valued function $M(x)$ coincides with the Jacobian matrix of a submersion Φ_0 in the closure of some open set $U \subset \mathbb{R}^n$, then $M_t(x) = M(x) = d\Phi_0(x)$ for all $x \in U$ and $t \in [0,1]$, provided that $\mathbb{R}^n \backslash U$ has no compact components. Accordingly, $\Phi(x) = \Phi_0(x)$ for $x \in U$.

Theorem 1 allows us to reduce the problem of weak integrability to a question on the extension of maps in homotopy theory. Indeed, if a submanifold $L \subset \mathbb{R}^n$ has trivial normal bundle, which is a necessary condition to be WI (cf. Property 1), we can associate an orthonormal basis of m vectors $\{v_1(x), \cdots, v_m(x)\}$ lying on the normal plane of L at each point $x \in L$. We call this set of vectors a *normal framing* $\mathcal{N}_L$ of L. Observe that, in general, there exist infinitely many non equivalent normal framings, which correspond to different trivializations of the normal bundle. Gromov h-principle then shows that the study of weakly integrable submanifolds is equivalent to the following question:

Question 4. Is it possible to extend the normal framing $\mathcal{N}_L = \{v_1, \cdots, v_m\}$ to a set of m independent vector fields $\{u_1, \cdots, u_m\}$ on all $\mathbb{R}^n$ so that $u_i|_L = v_i$ for each i?

To see that any WI submanifold admits a normal framing which extends over all $\mathbb{R}^n$ it is enough to consider an extension of the normal bundle of L as a subbundle of $T\mathbb{R}^n$ (using the foliation $\mathscr{F}_\Phi$) and then take a global trivialization of this subbundle. To prove the converse implication, i.e. that a submanifold L is WI if there is a normal framing of L which extends over all $\mathbb{R}^n$, we make use of Gromov h-principle. Indeed, we can define an $m \times n$ matrix valued function $M(x)$ on $\mathbb{R}^n$ using the vector fields $u_i(x)$ as rows. Applying Theorem 1 (the relative version) we can homotop this matrix to a Jacobian matrix of a submersion $\Phi : \mathbb{R}^n \to \mathbb{R}^m$ which coincides in a neighborhood N_L of L with the trivialization $\Phi_0 : N_L \to D$ defined by the normal framing $\mathcal{N}_L$, here $D \subset \mathbb{R}^m$ is the unit m-disk. Since the zero fibre of Φ_0 is the submanifold L we conclude that $L \subset \Phi^{-1}(0)$ as desired. Observe that Gromo v

h-principle does not provide enough control on the map Φ to guarantee that the zero fibre of Φ is exactly given by L. Summarizing, we have proved the following result:

Theorem 2. *A submanifold $L \subset \mathbb{R}^n$ such that $\mathbb{R}^n \setminus L$ has no bounded components is WI if and only if there is a normal framing $\mathcal{N}_L$ that can be extended to m independent vector fields over all $\mathbb{R}^n$.*

This theorem does not claim that any normal framing of a WI submanifold extends, but there is at least one. In fact, it can be proved [13] that the key point in this regard is how large is the dimension n compared with k: if $n \leq 2k$ any normal framing of a WI submanifold extends, but if $n \geq 2k+1$ this extension property depends on the normal framing. Also note that the assumption on the complement $\mathbb{R}^n \setminus L$ in the statement of Theorem 2 is equivalent to require either that the codimension $m \geq 2$ or that the codimension is $m = 1$ and all the components of L are non compact.

On account of Theorem 2 we can focus on Question 4 to approach the study of WI submanifolds. Using the canonical parallelism of $\mathbb{R}^n$ it is immediate to define a *normal map* $\sigma : L \to \mathbb{V}_{nm}$ from a normal framing $\mathcal{N}_L$. Here $\mathbb{V}_{nm}$ stands for the Stiefel manifold of orthonormal m-frames in $\mathbb{R}^n$. Question 4 is then equivalent to see if the map σ is homotopic to a constant, i.e. $[\sigma] = 0$, in which case there is a global map $\tilde{\sigma} : \mathbb{R}^n \to \mathbb{V}_{nm}$ which extends σ so that $\tilde{\sigma}|_L = \sigma$. This observation is key in the study of WI submanifolds, as it reduces the problem to study the homotopy class of the normal map σ, for which the main tool is *obstruction theory* in algebraic topology. If all the connected components of the submanifold L are assumed to be non compact, it is very easy to compute the homotopy class of the normal map associated to any normal framing, which allows us to prove the following theorem.

Theorem 3. *Let L be a k-dimensional submanifold of $\mathbb{R}^n$ with trivial normal bundle and whose connected components are all non compact. Then L is WI.*

Proof. The normal bundle of L being trivial, let us take a normal framing $\mathcal{N}_L$ and define its associated normal map $\sigma : L \to \mathbb{V}_{nm}$. Since $\mathbb{V}_{nm}$ is $(k-1)$-connected, we derive from obstruction theory that the set of homotopy classes of maps from L to $\mathbb{V}_{nm}$ is given by the k-cohomology group of L with coefficients in the homotopy group $\pi_k(\mathbb{V}_{nm})$, that is

$$[L, \mathbb{V}_{nm}] = H^k(L; \pi_k(\mathbb{V}_{nm}))\,.$$

The fact that no connected component of L is compact implies that $H^k(L; G) = 0$ for any field of coefficients G, and therefore we get that $[\sigma] = 0$ for any choice of the normal framing $\mathcal{N}_L$. This is equivalent to saying that any normal framing extends over all $\mathbb{R}^n$, which combined with Theorem 2, proves the desired result. Observe that $\mathbb{R}^n \setminus L$ has no bounded pieces because all the components of L are non compact. □

A straightforward consequence of this theorem is that any connected, non compact submanifold L of $\mathbb{R}^n$ with trivial normal bundle can be realized as a proper

leaf of a codimension m foliation of $\mathbb{R}^n$. In particular, any non compact hypersurface is WI, and hence a leaf of a codimension one foliation of $\mathbb{R}^n$, because its normal bundle is trivial (due to the fact that L is oriented). Additionally, Property 2 and Theorem 3 imply that any non compact submanifold L with trivial normal bundle is parallelizable, a property that is not at all obvious a priori.

In contrast with Theorem 3, the computation of the homotopy class of the normal map in the case that the submanifold L has compact components is much more complicated. For example, if L is compact and connected, it can be proved that the set of homotopy classes of maps from L to $\mathbb{V}_{nm}$ is given by:

- $[L, \mathbb{V}_{nm}] = \mathbb{Z}$ if k is even or if k is odd and $n = k + 1$.
- $[L, \mathbb{V}_{nm}] = \mathbb{Z}_2$ if k is odd and $n > k + 1$.

Accordingly, the study of the existence of a normal framing whose corresponding normal map is in the zero class of $[L, \mathbb{V}_{nm}]$ is a very subtle problem in the compact case, and requires the introduction of the whole machinery of the theory of immersions and embeddings. In this paper, motivated by Question 1, we shall only deal with the particular case that $L = \mathbb{S}^3$, see Sect. 4.

I finish this section with a theorem that establishes the equivalence between being a proper leaf of a foliation of $\mathbb{R}^n$ and being WI. One direction of the equivalence is obvious and has already been mentioned: any WI submanifold is a union of leaves of the simple foliation $\mathscr{F}_\Phi$ defined by the level sets of the submersion Φ; the converse implication is more surprising, as a foliation realizing L as a union of proper leaves does not need to be simple, e.g. it can have non trivial holonomy. The magic appears thanks to the powerful Gromov h-principle. Theorem 4 below lays bare the interest of the theory of weakly integrable embeddings for the realization problem in the theory of foliations.

Theorem 4. *A submanifold L such that $\mathbb{R}^n \backslash L$ has no bounded components is a union of proper leaves of a foliation of $\mathbb{R}^n$ if and only if it is WI.*

Proof. L being a union of proper leaves of a foliation, its normal bundle can be extended as a subbundle of $T\mathbb{R}^n$ using the normal bundle of the foliation. Since $\mathbb{R}^n$ is contractible, the extended subbundle is trivial, and hence, taking a global trivialization, we infer the existence of a normal framing $\mathscr{N}_L$ of L which extends over all $\mathbb{R}^n$. The result now follows from Theorem 2. □

3 The Theory of Strongly Integrable Embeddings

The theory of weakly integrable embeddings leaves open the problem of realizing a submanifold L as the whole fibre $\Phi^{-1}(0)$ of a submersion Φ. Indeed, Gromov h-principle does not allow us to control the appearance of extra components in the zero set of Φ when the matrix-valued function $M(x)$ is homotoped to the Jacobian matrix $d\Phi(x)$, see the discussion before Theorem 2. To address this problem we introduce the following definition.

Definition 2. We say that L is strongly integrable (SI) if there exists a submersion $\Phi : \mathbb{R}^n \to \mathbb{R}^m$ such that $L = \Phi^{-1}(0)$, that is L is a fibre of Φ. The map Φ is called a SI equation of L.

It is clear that any SI submanifold is also WI, but the converse implication does not need to hold. In fact, the study of SI submanifolds is much more subtle than that of WI submanifolds and requires the introduction of another tool: *complete intersections*.

Definition 3. We say that a submanifold $L \subset \mathbb{R}^n$ is a complete intersection (CI) if there exists a map $\Psi : \mathbb{R}^n \to \mathbb{R}^m$ such that 0 is a regular value and $L = \Psi^{-1}(0)$. The map Ψ is called a complete intersection equation of L. It is obviously not unique.

It follows from the definition that any complete intersection has trivial normal bundle, but it is not SI in general because the map Ψ can possess critical points in the complement of L (i.e. points where the Jacobian matrix $d\Psi(x)$ has rank smaller than m). An easy example is the unit sphere in $\mathbb{R}^3$, which is CI with an equation given by the polynomial $\Psi(x) = |x|^2 - 1$, but it cannot be SI because any function vanishing on the unit sphere must have critical points in the region that it bounds. Moreover, a complete intersection does not need to be parallelizable, although it is stably parallelizable because it is embedded with trivial normal bundle. On the other hand, it is obvious that any SI submanifold is CI.

A theorem by Bochnak and Kucharz [5] shows that the property of CI is equivalent to the existence of a *Seifert manifold*, that is a $(k+1)$-dimensional submanifold $S \subset \mathbb{R}^n$, not necessarily compact, with trivial normal bundle and whose boundary is $\partial S = L$. From this property it follows that any stably parallelizable k-manifold can be embedded as a complete intersection in $\mathbb{R}^{2k+1}$. In contrast, there are examples of stably parallelizable manifolds (even-dimensional exotic spheres) that cannot be embedded as complete intersections in $\mathbb{S}^n$ for any n, thus implying that any Seifert manifold of such a submanifold L is non compact.

A necessary condition in order that a submanifold L be SI is that it has to be WI and CI. We shall see in Sect. 5 that this condition is not sufficient in general. The key additional property that must be satisfied is certain compatibility relation between the CI equation Ψ and the condition of weak integrability. More precisely, assume that there exists a CI equation Ψ whose associated normal framing $\mathcal{N}_L$ extends over all $\mathbb{R}^n$ to a set of m independent vectors fields. Then, combining Theorem 2 with the fact that the extended framing corresponds to a CI equation we can prove the following result.

Theorem 5. *A submanifold $L \subset \mathbb{R}^n$ such that $\mathbb{R}^n \setminus L$ has no bounded components is SI if and only if there is a normal framing $\mathcal{N}_L$ associated to a CI equation of L that can be extended to m independent vector fields over all $\mathbb{R}^n$.*

It is apparent that the condition for being SI is much stronger than that for being WI: the existence of a normal framing that can be extended is not enough, it has to be a normal framing associated to a CI equation. In the setting of algebraic topology, the SI property is equivalent to the map $\sigma : L \to \mathbb{V}_{nm}$ being homotopically trivial,

i.e. $[\sigma] = 0$, where σ is the normal map obtained from the normal framing defined by a CI equation. If σ and $\hat{\sigma}$ are normal maps associated to normal framings $\mathscr{N}_L$ and $\hat{\mathscr{N}_L}$ respectively, their homotopy classes are different in general, $[\sigma] \neq [\hat{\sigma}]$, so it may happen that a submanifold is WI and CI with the normal class corresponding to a WI equation $[\sigma] = 0$ and the normal class corresponding to a CI equation $[\hat{\sigma}] \neq 0$. Of course, if the homotopy class of σ does not depend on the normal framing, it is obvious that WI + CI = SI, as in the following theorem.

Theorem 6. *Let L be a k-dimensional submanifold of $\mathbb{R}^n$ which is a complete intersection and whose connected components are all non compact. Then L is SI.*

Proof. Let $\sigma : L \to \mathbb{V}_{nm}$ be a normal map associated to a normal framing that corresponds to a CI equation Ψ of L. Since all the components of L are non compact, we obtained in the proof of Theorem 3 that the set of homotopy classes $[L, \mathbb{V}_{nm}] = 0$, and hence any normal map is homotopic to a constant (its homotopy class does not depend on the normal framing), thus implying that $[\sigma] = 0$ and the desired result after applying Theorem 5. □

As in the case of WI submanifolds, the most problematic situation is when L has compact components. In this paper, motivated by Question 2, I will only consider the particular case that L is a knot in $\mathbb{R}^3$, see Sect. 5. To finish this section, let me observe that the theory of strong integrability is related to the study of *critical submanifolds*. We say that L is critical if there exists a function $F : \mathbb{R}^n \to \mathbb{R}$ such that $L = \{x \in \mathbb{R}^n : \nabla F(x) = 0\}$. The fundamental result in this direction is the following.

Theorem 7. *A submanifold $L \subset \mathbb{R}^n$ that is SI is also critical.*

Proof. The submanifold L is the zero fibre of a map $\Phi : \mathbb{R}^n \to \mathbb{R}^m$. Calling Φ_i, with $i = 1, \cdots, m$, the coordinate functions of Φ, we can define the function $F := \sum_{i=1}^{m} \Phi_i^2$. It is then easy to check that $L = \{x \in \mathbb{R}^n : \nabla F(x) = 0\}$. □

4 Question 1: Vogt's Problem

As an application of the theory of weakly integrable embeddings introduced in Sect. 2, I am going to solve Vogt's problem stated in Question 1. Let me first observe that, according to Property 2 and Theorem 4, $\mathbb{S}^k$ cannot be a leaf of a foliation in any $\mathbb{R}^n$ provided that $k \notin \{1, 3, 7\}$, as the only parallelizable spheres are $\mathbb{S}^1, \mathbb{S}^3$ and $\mathbb{S}^7$. The case $k = 1$ will be addressed in the following section.

Concerning the realization problem for the embeddings of $\mathbb{S}^3$ in $\mathbb{R}^n$, the only non trivial cases correspond to $n \in \{5, 6\}$. Indeed, $\mathbb{S}^3$ cannot be a leaf in $\mathbb{R}^4$ because the Euler characteristic of the domain that it bounds (a 4-ball) is one. On the other hand, any embedding of $\mathbb{S}^3$ in $\mathbb{R}^n$ can be realized as a leaf if $n \geq 7$, as explained in Sect. 1. The remaining cases correspond to Vogt's question, and are particularly

delicate because there exist infinitely many non isotopic ways of embedding $\mathbb{S}^3$ in $\mathbb{R}^5$ and $\mathbb{R}^6$. The following theorem gives a (somehow surprising) answer to this question.

Theorem 8. *No embedded $\mathbb{S}^3$ can be realized as a leaf of a codimension two foliation of $\mathbb{R}^5$ and a codimension three foliation of $\mathbb{R}^6$.*

Proof. Any embedded $\mathbb{S}^3$ in $\mathbb{R}^5$ and $\mathbb{R}^6$ has trivial normal bundle, so let us take a normal framing $\mathscr{N}_L$ associated to a trivialization of the normal bundle. It can be proved that the normal map defined by $\mathscr{N}_L$ is not homotopic to a constant, i.e. $[\sigma] \neq 0$, for any choice of the normal framing, proving the desired result after applying Theorems 2 and 4. The proof that $[\sigma] \neq 0$ for any normal framing is technically demanding and makes use of rather subtle results in the theory of immersions and embeddings. It follows from the following facts:

1. The homotopy class of σ does not depend on the normal framing.
2. The WI property does not depend on the embedding, so very surprisingly, either all the embeddings are WI or none is.

On account of the previous points, we can restrict ourselves to the study of the unit 3-sphere in $\mathbb{R}^4$, which defines a natural embedding in the products $\mathbb{R}^4 \times \mathbb{R} = \mathbb{R}^5$ and $\mathbb{R}^4 \times \mathbb{R}^2 = \mathbb{R}^6$. A normal framing of the unit 3-sphere in $\mathbb{R}^4$ is given by a radial vector field, and adding one or two additional vector fields in the transverse directions to $\mathbb{R}^4$ we obtain a natural normal framing of these embeddings in $\mathbb{R}^5$ and $\mathbb{R}^6$ respectively. It is an easy exercise in homotopy theory to show that $[\sigma] \neq 0$ for this natural normal framing. □

Similarly, it can be proved that no embedded $\mathbb{S}^7$ can be realized as a leaf of a foliation of $\mathbb{R}^n$ for $n \leq 14$. I would like to observe that it is known that any embedding of $\mathbb{S}^7$ in $\mathbb{R}^n$ has trivial normal bundle, except for $n = 11$. The method of proof of Theorem 8 can be generalized to deal with any compact 3-manifold, thus yielding the following remarkable result, which classifies all the 3-manifolds that can be realized as leaves of codimension two foliations of $\mathbb{R}^5$. Recall that any (oriented) 3-manifold is parallelizable and any of its embeddings in $\mathbb{R}^5$ has trivial normal bundle. A complete solution to the realization problem in $\mathbb{R}^n$ for any dimension and codimension is established in [13].

Theorem 9. *A compact, connected 3-manifold $L \subset \mathbb{R}^5$ is a leaf of a codimension two foliation of $\mathbb{R}^5$ if and only if its first Betti number is odd.*

5 Question 2: Knotted Fibres

In this section I will explain how to solve the problem posed in Question 2 using the theory of strongly integrable embeddings introduced in Sect. 3. Let me first recall that any knot in $\mathbb{R}^3$ admits a Seifert surface and hence it is a complete

intersection (both in $\mathbb{R}^3$ and $\mathbb{S}^3$). Additionally, it is easy to show that any knot is WI, as established in the following proposition.

Proposition 1. *Any locally finite link in $\mathbb{R}^3$ is WI. Moreover, there exists a WI equation such that the compact components of the zero fibre $\Phi^{-1}(0)$ are exactly L.*

Proof. It is standard that there exists a 1-dimensional foliation of $\mathbb{R}^3$ containing L as a union of leaves. Applying Theorem 4 we conclude that L is WI. Accordingly, there is a WI equation $\Phi : \mathbb{R}^3 \to \mathbb{R}^2$, so that L is a union of compact components of $\Phi^{-1}(0)$. Now assume that each $C_i \subset \mathbb{R}^3$ is a compact component of the zero fibre $\Phi^{-1}(0)$ that is not contained in L, and take a point $p_i \in C_i$ in each component to define properly embedded half-lines $\gamma_i \subset \mathbb{R}^3$, non intersecting with L, whose end-points are given by p_i. Since there is a diffeomorphism $\Theta : \mathbb{R}^3 \to \mathbb{R}^3 \backslash (\cup_i \gamma_i)$ (which can be taken to be the identity in a neighborhood of L), we get a WI equation of L by defining $\Phi' := \Phi \circ \Theta$. Observe that the zero set of Φ' contains L and its compact components coincide with L because all the curves $C_i \backslash \{p_i\}$ are open, thus finishing the proof of the proposition. □

To study the strong integrability of a knot one has to check the compatibility between normal framings associated to CI and WI equations. This problem was addressed in [14], where Miyoshi claimed an affirmative answer to the knotted fibres question. In 2010 we found a counterexample to Miyoshi's theorem:

Example 4. The unknot in $\mathbb{R}^3$ is not SI. Consider the unknot given by the zero set of the CI equation $\Psi_0 = (x^2 + y^2 - 1, z) : \mathbb{R}^3 \to \mathbb{R}^2$, whose associated normal framing is $\mathcal{N}_L = \{\partial_r, \partial_z\}$ in cylindrical coordinates. An easy computation using homotopy theory shows that the normal map σ_0 defined by the normal framing $\mathcal{N}_L$ is not homotopically trivial, i.e. $[\sigma_0] \neq 0$, therefore the framing $\mathcal{N}_L$ does not extend to all $\mathbb{R}^n$. A key property proved in [13] is that any normal framing defined by a CI equation of the unknot is homotopic to the normal framing $\mathcal{N}_L$ above. The desired result then follows from Theorem 5.

Using the machinery of knot theory (mainly Seifert surfaces and appropriate knot invariants), the following theorem, which is a negative answer to Question 2, can be proved. Applying the same tools it is possible to classify all the links in $\mathbb{R}^3$ that are SI in terms of the linking number (e.g. the Hopf link is SI while the Borromean rings are not).

Theorem 10. *No knot in $\mathbb{R}^3$ is SI, and hence no knot is a fibre of a submersion $\Phi : \mathbb{R}^3 \to \mathbb{R}^2$.*

It is very striking that this theorem had already been observed in theoretical physics [3, 9]. Indeed, Berry and Dennis noticed that any knotted wave dislocation is linked by a line of critical points. A knotted wave dislocation L is a knot in $\mathbb{R}^3$ that is the zero set of a complex valued map $\Psi : \mathbb{R}^3 \to \mathbb{C}$ for which zero is a regular value, so identifying $\mathbb{C} = \mathbb{R}^2$, we get that L is a complete intersection with equation Ψ. As this map Ψ cannot be a global submersion on account of Theorem 10, we conclude that Ψ has a non empty critical set, and that this critical

set contains (generically) a line L', not necessarily compact, linking L. Roughly speaking, the reason L' must be linked with L is that otherwise all the critical points of Ψ (including L') are contained in the complement of a 3-ball $B \supset L$, and hence Ψ would be a CI equation of L in $B \approx \mathbb{R}^3$ without critical points, which is impossible by Theorem 10.

6 Question 3: Morse-Smale Flows

In this section I will show the existence of a non vanishing vector field in $\mathbb{R}^3$ that is Morse-Smale and whose set of limit cycles is given by any fixed link L, thus answering Question 3. These kinds of inverse problems for limit cycles of vector fields have a long tradition in the theory of dynamical systems. For example, in [16] I proved a realization theorem for limit cycles of polynomial vector fields, while in [10] we solved a long standing conjecture on the existence of periodic trajectories of any knot and link type for vector fields satisfying the steady Euler equation of fluid mechanics.

Using the theory of weakly integrable embeddings (concretely Proposition 1) and a construction that I introduced in [16], let me prove the main result of this section. This theorem was first established by Watanabe in [23], but his method of proof is much more complicated.

Theorem 11. *Let L be a locally finite link in $\mathbb{R}^3$. Then it can be realized as the whole set of limit cycles of a non vanishing Morse-Smale vector field in $\mathbb{R}^3$. Moreover, the limit cycles are asymptotically stable.*

Proof. On account of Proposition 1, there is a submersion $\Phi = (\Phi_1, \Phi_2) : \mathbb{R}^3 \to \mathbb{R}^2$ such that the link L is given by the union of compact components of the zero set $\Phi^{-1}(0)$. Following [16], let me define the vector field:

$$X := \nabla\Phi_1 \wedge \nabla\Phi_2 - \nabla(\Phi_1^2 + \Phi_2^2)\,,$$

where $\wedge$ is the standard vector product in $\mathbb{R}^3$. I claim that this vector field satisfies the statement of the theorem. To prove this, let me observe the following properties:

1. X is non vanishing because Φ is a submersion and hence the set of vectors $\{\nabla\Phi_1(x), \nabla\Phi_2(x), \nabla\Phi_1(x) \wedge \nabla\Phi_2(x)\}$ forms a basis at each point $x \in \mathbb{R}^3$.
2. L is a set of periodic trajectories of X. This follows from the fact that X is tangent to the zero set $\Phi^{-1}(0) \supset L$.
3. The function $F := \Phi_1^2 + \Phi_2^2$ is a Lyapunov function of X because

$$X \cdot \nabla F = -(\nabla F)^2\,.$$

Since $\nabla F = 2\Phi_1\nabla\Phi_1 + 2\Phi_2\nabla\Phi_2$, we deduce that $\{\nabla F = 0\}$ coincides with the zero fibre of Φ. Accordingly, the Lyapunov function implies that all the periodic trajectories contained in L are asymptotically stable.

4. Each periodic trajectory of X contained in L is hyperbolic. This is easily proved using the equations:

$$\dot{\Phi}_1 = X \cdot \nabla\Phi_1 = -2\Phi_1(\nabla\Phi_1)^2 - 2\Phi_2(\nabla\Phi_1 \cdot \nabla\Phi_2)$$

$$\dot{\Phi}_2 = X \cdot \nabla\Phi_2 = -2\Phi_2(\nabla\Phi_2)^2 - 2\Phi_1(\nabla\Phi_1 \cdot \nabla\Phi_2)$$

(roughly speaking, these equations show that the functions Φ_1 and Φ_2 are linearly contracted over L by the flow of X, which implies the hyperbolicity. The details are left to the interested reader.)

5. Since the only compact components of $\Phi^{-1}(0)$ are given by L, the existence of the Lyapunov function F easily implies that the set of non wandering points of X is exactly L.

Summarizing, these properties imply that X is non-vanishing and its non wandering set is given by the link L. Since L consists of hyperbolic periodic trajectories that are asymptotically stable, the transversality condition in the definition of Morse-Smale flows is trivially satisfied, thus proving the theorem. □

Let me remark that there is no contradiction with the fact that X is non vanishing and all its limit cycles are asymptotically stable, i.e. local attractors, due to the presence of unstable singularities at infinity. Of course, the link L cannot be a global attractor because $\mathbb{R}^3$ cannot be deform retracted over a link, and therefore there must exist a non compact invariant set at the boundary of the attracting basins of the limit cycles.

7 Open Problems

In this paper I have worked in the C^∞ class, but the extension of the theory of weakly and strongly integrable embeddings to the real-analytic setting (C^ω) can be easily done using a deep theorem by Shiota [19]. This theorem ensures that for any smooth submersion $\Phi : \mathbb{R}^n \to \mathbb{R}^m$ there exists a global smooth chart $\Theta : \mathbb{R}^n \to \mathbb{R}^n$ where the submersion is real-analytic, that is $\Phi \circ \Theta$ is C^ω. Much more delicate is the algebraic context, where two fundamental problems arise: first, it is not known if polynomial submersions $Sub_{pol}(\mathbb{R}^n, \mathbb{R}^m)$ are dense in smooth submersions $Sub(\mathbb{R}^n, \mathbb{R}^m)$ in some C^k-weak topology; second, it is difficult to classify which complete intersections are also *algebraic* complete intersections. In particular, the following problem seems to be completely open:

Problem 1. Does there exist, up to isotopy, a polynomial weak equation $\Phi : \mathbb{R}^3 \to \mathbb{R}^2$ for any finite link $L \subset \mathbb{R}^3$?

All the realization theorems that we have seen in this paper are existential, and a constructive approach is very difficult because our proofs rely on Gromov h-principle. In particular, we have no idea of the geometric structure of the foliations realizing prescribed compact leaves as e.g. in Theorem 9. Moreover, taking into account applications as in [3, 9], it would be very interesting to obtain explicit WI and SI equations, as in the following problem:

Problem 2. Is it possible to construct an explicit weak equation $\Phi : \mathbb{R}^3 \to \mathbb{R}^2$ (using elementary functions) for any knot in $\mathbb{R}^3$?

In Sect. 5 I showed that any knot in $\mathbb{R}^3$ is WI and CI but not SI. It remains open to obtain examples of WI submanifolds that are not SI because they are not CI. This is a difficult question because, in fact, the only known examples of submanifolds with trivial normal bundle that are not CI are certain even-dimensional exotic spheres, which are not WI because they are not parallelizable. We finish this paper with the following related question:

Problem 3. Does there exist a parallelizable submanifold of $\mathbb{R}^n$ with trivial normal bundle that is not a complete intersection?

Acknowledgements The author is grateful to Mark Dennis for pointing out Refs. [3, 9] and for valuables comments concerning Theorem 10. This work is supported in part by the Spanish MINECO under grant no. MTM2010-21186-C02-01 and the ICMAT Severo Ochoa project SEV-2011-0087. The author acknowledges the Spanish Ministry of Science for financial support through the Ramón y Cajal program.

References

1. Adachi, M.: Embeddings and Immersions. AMS, Providence (1993)
2. Attie, O., Hurder, S.: Manifolds which cannot be leaves of foliations. Topology **35**, 335–353 (1996)
3. Berry, M., Dennis, M.: Topological events on wave dislocation lines: birth and death of loops, and reconnection. J. Phys. A **40**, 65–74 (2007)
4. Birman, J., Williams, R.: Knotted periodic orbits in dynamical systems. Topology **22**, 47–82 (1983)
5. Bochnak, J., Kucharz, W: Complete intersections in differential topology and analytic geometry. Boll. Un. Mat. Ital. B **10**, 1019–1041 (1996)
6. Borel, A., Serre, J.-P.: Impossibilité de fibrer un espace euclidien par des fibres compactes. C. R. Acad. Sci. Paris **230**, 2258–2260 (1950)
7. Cantwell, J., Conlon, L.: Every surface is a leaf. Topology **26**, 265–285 (1987)
8. Costa, A.F., Gascón, F.G., González-López, A.: On codimension one submersions of Euclidean spaces. Invent. Math. **93**, 545–555 (1988)
9. Dennis, M.: Local phase structure of wave dislocation lines: twist and twirl. J. Opt. A **6**, 202–208 (2004)
10. Enciso, A., Peralta-Salas, D.: Knots and links in steady solutions of the Euler equation. Ann. Math. **175**, 345–367 (2012)
11. Ghys, E.: Une variete qui n'est pas une feuille. Topology **24**, 67–73 (1985)
12. Haefliger, A.: Lectures on the theorem of Gromov. Lect. Notes Math. **209** 128–141 (1971)

13. Hector, G., Peralta-Salas, D.: Integrable embeddings and foliations. Am. J. Math. **134**, 773–825 (2012)
14. Miyoshi, S.: Links and globally completely integrable vector fields on an open 3-manifold. Topology **34**, 383–387 (1995)
15. Palmeira, C.F.B.: Feuilletages par cylindres fermés de $\mathbb{R}^3$. C. R. Acad. Sci. Paris **290**, 419–421 (1980)
16. Peralta-Salas, D.: Note on a paper of J. Llibre and G. Rodríguez concerning algebraic limit cycles. J. Differ. Equ. **217**, 249–256 (2005)
17. Rabier, P.J.: Ehresman fibrations and Palais-Smale conditions for morphisms of Finsler manifolds. Ann. Math. **146**, 647–691 (1997)
18. Schweitzer, P.: Riemannian manifolds not quasi-isometric to leaves in codimension one foliations. Ann. Inst. Fourier **61**, 1599–1631 (2011)
19. Shiota, M.: Equivalence of differentiable mappings and analytic mappings. IHES Publ. Math. **54**, 237–322 (1981)
20. Sondow, J.D.: When is a manifold a leaf of some foliation? Bull. Am. Math. Soc. **81**, 622–624 (1975)
21. Vogt, E.: Existence of foliations of Euclidean spaces with all leaves compact. Math. Ann. **296**, 159–178 (1993)
22. Wada, M.: Closed orbits of nonsingular Morse-Smale flows on $\mathbb{S}^3$. J. Math. Soc. Jpn. **41**, 405–413 (1989)
23. Watanabe, N.: On knotted preimages of submersions. Topology **32**, 251–257 (1993)

A Hopf-Zero Degenerated Case in Symmetric Piecewise Linear Systems

Enrique Ponce, Javier Ros, and Elísabet Vela

Abstract A possible degeneration of the Hopf-zero bifurcation for symmetric three-dimensional piecewise linear differential systems with three zones is studied in a two-parameter plane. We show that around the critical point in such parameter plane the unfolding is very similar to the one appearing in the generalized Hopf bifurcation of differentiable dynamics.

1 Introduction and Preliminary Results

In models of physical devices giving rise to symmetric vector fields (invariant under the change of the sign in the state variables), the origin is always an equilibrium point. The simplest local bifurcations that this equilibrium point can undergo are the pitchfork (involving only equilibria), and the Hopf (leading to periodic behavior).

The simultaneous occurrence of both linear degeneracies results in a bifurcation called Hopf-pitchfork interaction also called Hopf-zero bifurcation. In this situation, one must expect the presence of complex tridimensional dynamical behaviors: quasiperiodic, aperiodic, homoclinic and heteroclinic, ... (see [4, 6], and [1] for the analysis of a concrete smooth system).

When dealing with non-smooth systems, as is the case of continuous piecewise linear systems, the analogous bifurcation appears associated to the presence of a zero eigenvalue and a imaginary pair of eigenvalues in the relevant linear part of the system. The lack of differentiable dynamics makes the analysis much farther from being complete than in the case of the Hopf-zero bifurcation for smooth systems, and it has been recently started in [7], by using specific tools for symmetric piecewise linear systems with three zones. In the quoted paper, the appearance of

E. Ponce (✉) · J. Ros · E. Vela
Departamento Matemática Aplicada II, E.T.S. Ingeniería, 41092-Sevilla, Spain
e-mail: eponcem@us.es; javieros@us.es; elivela@us.es

S. Ibáñez et al. (eds.), *Progress and Challenges in Dynamical Systems*,
Springer Proceedings in Mathematics & Statistics 54,
DOI 10.1007/978-3-642-38830-9_20,

the Hopf-zero bifurcation is proved, assuring the possible generation of at least three limit cycles. One of these bifurcating periodic orbits lives in the three zones of linearity and it is symmetrical respect the origin while the other two limit cycles only use two zones forming a symmetric pair.

In this paper we consider a degenerate case for such Hopf-zero bifurcation, detecting a parameter region where two different three-zones periodic orbits coexist and a bifurcation curve corresponding to a saddle-node bifurcation appears, where these two orbits collide to disappear.

We consider the same family of piecewise linear differential systems studied in [7] written in the Luré form,

$$\dot{\mathbf{x}} = \mathbf{F}(\mathbf{x}) = A_R\mathbf{x} + \mathbf{b}\,\mathrm{sat}(x), \tag{1}$$

where $\mathbf{x} = (x, y, z)^T \in \mathbb{R}^3$ and the dot represents the derivative with respect to the time τ. The matrices A_R and $\mathbf{b}$ has the following expressions

$$A_R = \begin{pmatrix} t & -1 & 0 \\ m & 0 & -1 \\ d & 0 & 0 \end{pmatrix} \quad \text{and} \quad \mathbf{b} = \begin{pmatrix} T - t \\ M - m \\ D - d \end{pmatrix}, \tag{2}$$

where t, m, d, T, M and D are certain parameters. As it is well known, the saturation function is given by

$$\mathrm{sat}(u) = \begin{cases} 1 \text{ if } u > 1, \\ u \text{ if } |u| \leqslant 1, \\ -1 \text{ if } u < -1. \end{cases}$$

System (1) and (2) has the following properties:

(a) It is symmetric with respect to the origin, i.e. $\mathbf{F}(\mathbf{x}) = -\mathbf{F}(-\mathbf{x})$.
(b) In the region with $|x| \leqslant 1$ it becomes the homogeneous system

$$\dot{\mathbf{x}}(\tau) = A_C\mathbf{x}(\tau) = \begin{pmatrix} T & -1 & 0 \\ M & 0 & -1 \\ D & 0 & 0 \end{pmatrix} \mathbf{x}(\tau). \tag{3}$$

(c) The coefficients t, m, d and T, M, D are the linear invariants (trace, sum of principal minors and determinant) of the matrices A_R and A_C, respectively.

Note that $A_C = A_R + \mathbf{b}\mathbf{e}_1^T$, where $\mathbf{e}_1 = (1, 0, 0)^T$, and that the considered family of systems is in the so-called generalized Liénard form, see [2], which is in fact equivalent to the observable canonical form in control theory [3]. Thus, under generic conditions for every system of the form (1), after some change of variables, we can get the matrices in the form given in (2) and (3).

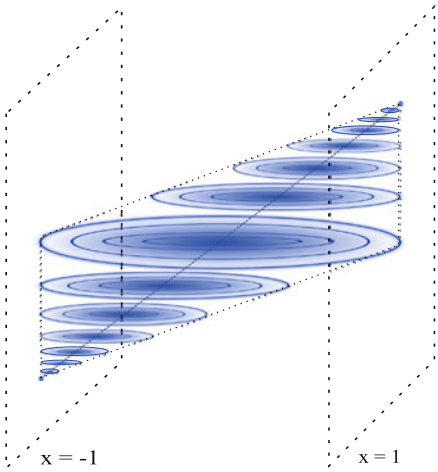

Fig. 1 Structure of the periodic orbits for $\varepsilon = 0$ in the central zone. The two solid cones are completely foliated by periodic orbits surrounding the segment of equilibrium points $\{(x, 0, x\omega^2)^T : |x| \leqslant 1\}$

As done in [7], we introduce ε as a first bifurcation parameter such that the three eigenvalues of the matrix A_C are $-\varepsilon$ and $\rho\varepsilon \pm \omega i$, where $\rho \in \mathbb{R}$ and $\omega \in \mathbb{R}^+$ are auxiliary fixed parameters. Thus for $\varepsilon = 0$ the three eigenvalues are 0 and $\pm\omega i$, which are located on the imaginary axis of the complex plane. Accordingly we choose

$$T(\varepsilon) = (2\rho - 1)\varepsilon,\ M(\varepsilon) = \omega^2 + \rho\varepsilon^2(\rho - 2),\ D(\varepsilon) = -\varepsilon(\rho^2\varepsilon^2 + \omega^2), \tag{4}$$

to be assumed hereinafter.

Note that for $\varepsilon = 0$, the solutions of system (3) give rise to orbits that, if they are completely contained in the central zone, define planar ellipses forming a bounded set foliated by periodic orbits, which has the shape of two solid cones sharing the elliptic disc $\omega^2 x^2 + y^2 \leqslant \omega^2$ in the plane $z = 0$ as their common basis, see Fig. 1.

Regarding the non-smooth Hopf-zero bifurcation of this type of dynamical systems, the following results have been obtained in [7], where much more qualitative and quantitative information can be found.

Theorem 1. *Let us consider system* (1) *and* (2) *under conditions* (4) *where it is assumed* $\rho \neq 0$ *and* $\delta = d - t\omega^2 \neq 0$ *and fixed. For* $\varepsilon = 0$ *the system* (1) *and* (2) *undergoes a tri-zonal limit cycle bifurcation, that is, from the configuration of periodic orbits that exists in the central zone for* $\varepsilon = 0$*, one limit cycle appears for* $\rho\delta\varepsilon > 0$ *and* $|\varepsilon|$ *sufficiently small. It is symmetric with respect to the origin and bifurcates from the ellipse* $\Gamma = \{(x, y, z)^T \in \mathbb{R}^3 : \omega^2 x^2 + y^2 = \omega^2, z = 0\}$*. Furthermore, the bifurcating limit cycle is stable if and only if* $t < 0$*,* $\delta > 0$ *and* $d < 0$*.*

In the case $\delta = 0$, that is when $d = t\omega^2$ with $d \neq 0$, it can be shown a similar result but requiring a special consideration, see [7].

Theorem 2. *Assume for system* (1) *and* (2) *under conditions* (4) *that* $\rho \neq 0$, $m \neq \omega^2$ *and* $d = t\omega^2 \neq 0$, *and fixed. For* $\varepsilon = 0$ *the system* (1) *and* (2) *undergoes a tri-zonal limit cycle bifurcation. For* $|\varepsilon|$ *sufficiently small and* $\rho\varepsilon t(\omega^2 - m) > 0$ *one limit cycle bifurcates from the ellipse* $\Gamma = \{(x, y, z)^T \in \mathbb{R}^3 : \omega^2 x^2 + y^2 = \omega^2, z = 0\}$. *This limit cycle is symmetric with respect to the origin and it is stable if and only if* $t < 0$ *and* $\rho\varepsilon > 0$.

The specific treatment needed in [7] to show this last result, suggested the existence of a degeneration of the bifurcation for $\delta = 0$, which is precisely the issue to be clarified in this paper.

2 The Hopf-Zero Degenerated Case

In this section we tackle the degenerated case of the Hopf-zero bifurcation, analyzing what happens near $\delta = 0$, which requires $t\, d > 0$. We use the parameters of the central zone to characterize this bifurcation, and since $\delta = d - t\omega^2$ we choose ω as the second bifurcation parameter, working in the parameter plane (ε, ω). In this plane, as we already know, the Hopf-zero bifurcation takes place at the straight line $\varepsilon = 0$. On this line, δ vanishes at the point

$$(\varepsilon_*, \omega_*) = \left(0, \sqrt{d/t}\right). \tag{5}$$

We introduce the critical parameter deviations $\tilde{\varepsilon} = \varepsilon - \varepsilon_* = \varepsilon$ and $\tilde{\omega} = \omega - \omega_*$, to place the critical point $(\varepsilon_*, \omega_*)$ at the origin of the new parameter plane $(\tilde{\varepsilon}, \tilde{\omega})$. From the proof of Theorem 1, we know (see Sect. 4 of [7]) that there exists a symmetric periodic orbit using the three zones of linearity and with a flight time τ_R in the external zones, for the values of $\tilde{\varepsilon}$ satisfying

$$\begin{aligned}\tilde{\varepsilon} = {} & \frac{(\omega_* + \tilde{\omega})\left[d - t(\omega_* + \tilde{\omega})^2\right]}{12\pi\rho}\tau_R^3 + \\ & + \frac{(\omega_* + \tilde{\omega})\left[d(t^2 - 6m) + (\omega_* + \tilde{\omega})^2(9d + 12mt - t^3 - 15t(\omega_* + \tilde{\omega})^2)\right]}{720}\tau_R^5 + \\ & + O(\tau_R^6),\end{aligned}$$

which can be seen as the local definition of a surface in the space $(\tilde{\varepsilon}, \tilde{\omega}, \tau_R)$. In each point of the above surface we can assure the existence of a periodic orbit near the critical ellipse Γ that exists for $(\tilde{\varepsilon}, \tilde{\omega}) = (0,0)$. To analyze the above expression near the critical point $(\tilde{\varepsilon}, \tilde{\omega}) = (0, 0)$ we substitute $d = t\omega_*^2$ and write

$$\tilde{\varepsilon} = \left(-\frac{t\omega_*^2}{6\pi\rho}\tilde{\omega} + O(\tilde{\omega}^2)\right)\tau_R^3 + \left(\frac{(\omega_*^2 - m)t\omega_*^3}{120\pi\rho} + O(\tilde{\omega})\right)\tau_R^5 + O(\tau_R^6). \tag{6}$$

Disregarding higher order terms, we obtain the equality

$$\tilde{\varepsilon} + \frac{t\omega_*^2}{6\pi\rho}\tilde{\omega}\tau_R^3 + \frac{(m-\omega_*^2)t\omega_*^3}{120\pi\rho}\tau_R^5 = 0. \tag{7}$$

To determine the number of positive solutions in τ_R of (7), we enunciate the following auxiliary result.

Proposition 1. *Consider the function* $h(x) = b_0 + b_3x^3 + b_5x^5$, *and assume* $b_5 \neq 0$. *Then, the number of non-negative solutions of equation*

$$h(x) = 0, \tag{8}$$

behaves as follows.

(a) For $b_0 = 0$, *the equation always has the zero solution, it has no positive solution if* $b_3b_5 > 0$ *and it has the solution* $x = \sqrt{-b_3/b_5} > 0$ *when* $b_3b_5 < 0$.
(b) For $b_3 = 0$, *the equation has no positive solution if* $b_0b_5 > 0$, *having one positive solution for* $b_0b_5 < 0$.
(c) If $b_0b_5 > 0$ *and* $b_0b_3 > 0$, *there are no positive solutions.*
(d) If $b_0b_5 < 0$, *there is only one positive solution.*
(e) When $b_0b_3 < 0$ *and* $b_0b_5 > 0$, *the following cases arise after defining in the parameter plane* (b_0, b_3) *the expression*

$$h_*(b_0, b_3) = b_0 + \frac{2}{5}b_3\left(\frac{-3b_3}{5b_5}\right)^{3/2}. \tag{9}$$

(i) If $b_0h_*(b_0, b_3) < 0$ *then Eq. (8) has two positive solutions.*
(ii) If $h_*(b_0, b_3) = 0$, *then Eq. (8) has only one positive solution, namely* $x = \sqrt{-3b_3/5b_5}$.
(iii) If $b_0h_*(b_0, b_3) > 0$, *then Eq. (8) has no positive solutions.*

Proof. Statements (a), (b), and (c) are trivial.

Under hypotheses of statement (d), as there is one sign variation in the coefficients of $h(x)$, there exists only one positive solution from Descartes Rule of signs.

We now assume the hypotheses of statement (d) and also, without loss of generality, $b_5 > 0$. Thus, we have $b_0 > 0$ and $b_3 < 0$. Computing the discriminant of the polynomial $h(x)$, we have

$$b_0^2b_5(108b_3^5 + 3{,}125b_0^2b_5^3),$$

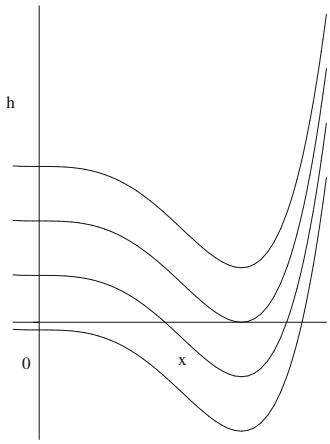

Fig. 2 The graph of function h for statements (d) and (e) of Proposition 1 with different values of b_0

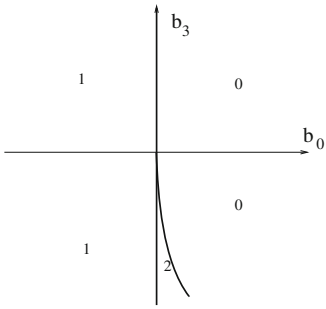

Fig. 3 Number of positive solutions of (8) in the parameter plane (b_0, b_3) for $b_5 > 0$

and so the number of positive roots changes by two where the above expression vanishes. Equivalently, the discriminant is zero for

$$b_0^2 = -\frac{108b_3^5}{3{,}125b_5^3} = \frac{2^2}{5^2}b_3^2\left(\frac{-3b_3}{5b_5}\right)^3$$

and, taking into account $b_0 b_3 < 0$, we arrive at the vanishing of expression (9). The three different cases, depending on the sign of the discriminant, follow easily and the proof is complete. □

Of course, the above result agrees with the fact that the set $\{1, x^3, x^5\}$ is an extended Chebyshev system in $\mathbb{R}^+$ and, since there is at most two positive zeros taking into account their multiplicity, any configuration of zeros can appear, see [5].

In Fig. 2 we show the graph of function $h(x)$ according to different situations of statements (d) and (e) of the above proposition by moving the parameter b_0. In Fig. 3, the number of positive solutions of (8) for different regions of the parameter plane (b_0, b_3) is represented for the case $b_5 > 0$, where the change from two positive roots to none happens at the curve

$$b_0 = -\frac{2}{5} b_3 \left(\frac{-3b_3}{5b_5} \right)^{3/2}. \tag{10}$$

with $b_3 < 0$.

The following theorem is the main result of this work.

Theorem 3. *Suppose $\rho \neq 0$, $t\,d > 0$ and $m \neq \omega_*^2$ for system (1) and (2) under conditions (4). Consider in the plane $(\tilde{\varepsilon}, \tilde{\omega})$ a sufficiently small neighborhood of the origin. This neighborhood is crossed by the straight line $\tilde{\varepsilon} = 0$, where the Hopf-zero bifurcation takes place. For parameter values in such neighborhood, the number of periodic orbits within a tubular neighborhood of the ellipse Γ is as follows.*

(a) In the region of the $(\tilde{\varepsilon}, \tilde{\omega})$ plane where condition $\rho t (m - \omega_*^2)\tilde{\varepsilon} < 0$ holds, there exists only one limit cycle born from the Hopf-zero bifurcation.

(b) In the region of the $(\tilde{\varepsilon}, \tilde{\omega})$ plane where condition $\rho t (m - \omega_*^2)\tilde{\varepsilon} > 0$ and within the zone where $\rho t \tilde{\varepsilon}\tilde{\omega} > 0$, there are no periodic solutions.

(c) In the region of the $(\tilde{\varepsilon}, \tilde{\omega})$ plane where condition $\rho t (m - \omega_*^2)\tilde{\varepsilon} > 0$ and within the zone where $\rho t \tilde{\varepsilon}\tilde{\omega} < 0$, there is a curve in the plane $(\tilde{\varepsilon}, \tilde{\omega})$ with local expression

$$\tilde{\varepsilon}_{SN} = \frac{-1}{15\pi} \frac{t\omega_*^2 \tilde{\omega}}{\rho} \left(\frac{12\tilde{\omega}}{\omega_*(\omega_*^2 - m)} \right)^{3/2} + O(\tilde{\omega}^3), \tag{11}$$

so that there are two periodic orbits when $\tilde{\varepsilon}$ is between $\tilde{\varepsilon}_{SN}$ and zero, only one if $\tilde{\varepsilon} = \tilde{\varepsilon}_{SN}$, and no periodic orbits otherwise.

Proof. To prove this theorem, we consider Eq. (7). We study this equation in a neighborhood of $(\tilde{\varepsilon}, \tilde{\omega}, \tau_R) = (0, 0, 0)$ small enough. We can assure that the number of solutions of Eq. (7) with $\tau_R > 0$ is equal, when $m \neq \omega_*^2$, to the number of periodic orbits of system (1) that bifurcate from the critical ellipse Γ in a neighborhood of $(\tilde{\varepsilon}, \tilde{\omega}) = (0, 0)$, see [7].

If we denote the coefficients of Eq. (7)

$$b_0 = \tilde{\varepsilon},\ b_3 = \frac{t\omega_*^2 \tilde{\omega}}{6\pi\rho} \text{ and } b_5 = \frac{(m - \omega_*^2) t \omega_*^3}{120\pi\rho},$$

given that $\omega_* > 0$, by its definition, we can observe that

$$\begin{aligned} \operatorname{sgn}(b_0) &= \operatorname{sgn}(\tilde{\varepsilon}), \\ \operatorname{sgn}(b_3) &= \operatorname{sgn}(t\rho\tilde{\omega}), \\ \operatorname{sgn}(b_5) &= \operatorname{sgn}(t\rho(m - \omega_*^2)). \end{aligned} \tag{12}$$

Since from our hypotheses we have $b_5 \neq 0$, we can neglect higher order terms in determining the local number of solutions of (7) and apply Proposition 1 using the above expressions for b_0, b_3 and b_5. The statement (d) of this proposition implies that Eq. (7) has only one positive solution when $b_5\tilde{\varepsilon} < 0$. Taking into account the

equalities (12), this condition is equivalent to $\rho t(m-\omega_*^2)\tilde{\varepsilon} < 0$, so that under this hypothesis and for points of the plane $(\tilde{\varepsilon}, \tilde{\omega})$ sufficiently near the origin, Eq. (6) also has a unique positive solution. Then the statement (a) of Theorem 3 is proved.

Using equalities (12), the conditions $b_5\tilde{\varepsilon} > 0$ and $b_3\tilde{\varepsilon} > 0$ are equivalent to $\rho t(m-\omega_*^2)\tilde{\varepsilon}$ and $\rho t\tilde{\varepsilon}\tilde{\omega} > 0$, so that from statement (c) of Proposition 1, Eq. (7) has no positive solutions and statement (b) of Theorem 3 is proved.

If $b_5\tilde{\varepsilon} > 0$ and $b_3\tilde{\varepsilon} < 0$, statement (e) of Proposition 1 assures the existence of a curve $h^*(b_0, b_3) = 0$, where the number of solutions changes by two. From (9), a first order approximation of such curve, in a neighborhood of $(b_0, b_3) = (0, 0)$, is given in (10). Thus, using (12) and assuming $\rho t(m-\omega_*^2)\tilde{\varepsilon} > 0$ and $\rho t\tilde{\varepsilon}\tilde{\omega} < 0$, we can deduce the existence of a curve in the plane $(\tilde{\varepsilon}, \tilde{\omega})$ where the number of positive solutions of (6) is equal to one, establishing the transition from two solutions to none. Substituting the values of b_0, b_3 and b_5 in (10), such curve is given locally by the expression

$$\tilde{\varepsilon}_{\mathrm{SN}} = \frac{-1}{15\pi}\frac{t\omega_*^2\tilde{\omega}}{\rho}\left(\frac{-12\tilde{\omega}}{\omega_*(m-\omega_*^2)}\right)^{3/2} + O(\tilde{\omega}^3). \tag{13}$$

The condition $b_0h^*(b_0, b_3) < 0$ of Proposition 1 $(e.i)$ written in the variables $\tilde{\varepsilon}$ and $\tilde{\omega}$ near the origin translates to

$$\tilde{\varepsilon}\,(\tilde{\varepsilon} - \tilde{\varepsilon}_{\mathrm{SN}}) < 0.$$

Then, for $\tilde{\varepsilon}$ between zero and the value $\tilde{\varepsilon}_{\mathrm{SN}}$ given in (13), in a neighborhood of $(\tilde{\varepsilon}, \tilde{\omega}) = (0, 0)$, Eq. (6) has two positive solutions corresponding to periodic orbits. The remaining cases of statement (c) follow in an analogous way. Theorem 3 is proved. □

We emphasize that around the origin, in the parameter plane $(\tilde{\varepsilon}, \tilde{\omega})$, the unfolding is very similar to the one appearing in the generalized Hopf bifurcation of differentiable dynamics.

The above theorem constitutes a second step in the analysis started in [7]. Future work should be directed to complete this analysis by considering the excluded case $m = \omega_*^2$, which corresponds to a higher degeneracy.

Acknowledgements Authors are partially supported by the *Ministerio de Ciencia y Tecnología, Plan Nacional I+D+I*, in the frame of projects MTM2009-07849, MTM2010-20907, MTM2012-31821, and by the *Consejería de Educación y Ciencia de la Junta de Andalucía* under grants TIC-0130 and P08-FQM-03770.

References

1. Algaba, A., Freire, E., Gamero, E., Merino, M., Rodríguez-Luis, A.J.: On the hopf pitchfork bifurcation in the Chua's equation. Int. J. Bifurc. Chaos **10**, 291–305 (2000)
2. Carmona, V., Freire, E., Ponce, E., Torres, F.: On simplifying and classifying piecewise-linear systems. IEEE Trans. Circuits Syst. **49**, 609–620 (2002)

3. Chen, C.-T.: Linear System Theory and Design, 3rd edn. Oxford University Press, New York (1998)
4. Guckenheimer, J., Holmes, P.: Nonlinear Oscillations, Dynamical Systems and Bifurcations of Vector Fields. Applied Mathematical Sciences, vol. 42. Springer, New York (1983)
5. Karlin, S., Studden, W.J.: Tchebycheff Systems: With Applications in Analysis and Statistics. Pure and Applied Mathematics. Interscience, New York (1966)
6. Kuznetsov, Yu.A.: Elements of Applied Bifurcation Theory, 3rd edn. Applied Mathematical Sciences, vol. 112. Springer, New York (2004)
7. Ponce, E., Ros, J., Vela, E.: Unfolding the fold-Hopf bifurcation in piecewise linear continuous differential systems with symmetry. Phys. D: Nonlinear Phenom. **250**, 34–46 (2013)

The Focus-Center-Limit Cycle Bifurcation in Discontinuous Planar Piecewise Linear Systems Without Sliding

Enrique Ponce, Javier Ros, and Elísabet Vela

Abstract Planar discontinuous piecewise linear systems with two linearity zones, one of them being of focus type, are considered. By using an adequate canonical form under certain hypotheses, the bifurcation of a limit cycle, when the focus changes its stability after becoming a linear center, is completely characterized. Analytic expressions for the amplitude, period and characteristic multiplier of the bifurcating limit cycle are provided. The studied bifurcation appears in real world applications, as shown with the analysis of an electronic Wien bridge oscillator without symmetry.

1 Introduction and Main Results

Nowadays, the analysis of discontinuous piecewise-linear systems is an active field of research since certain modern devices are well modeled by this class of systems, see [5]. For the simplest situation however, as is the case of the aggregation of two planar linear systems, there are bifurcations that still require a thorough analysis.

Recently, in [7] it has been proposed a canonical form for the case of planar discontinuous systems with two zones of linearity, to be denoted D2PWLS$_2$ for short. In the quoted paper, there are shown some bifurcation results for the case when both linear dynamics are of focus type without visible tangencies, that is, there are no real equilibrium points in the interior of each half-plane. Here, by resorting to the canonical form given in [7], we consider a different situation when we have an equilibrium point of focus type in the interior of a half plane without specifying the linear dynamics type in the other half plane. Our goal is to describe qualitatively and quantitatively the possible bifurcation of limit cycles through the change of

E. Ponce (✉) · J. Ros · E. Vela
Departamento Matemática Aplicada II, E.T.S. Ingeniería, 41092-Sevilla, Spain
e-mail: eponcem@us.es; javieros@us.es; elivela@us.es

S. Ibáñez et al. (eds.), *Progress and Challenges in Dynamical Systems*,
Springer Proceedings in Mathematics & Statistics 54,
DOI 10.1007/978-3-642-38830-9_21, © Springer-Verlag Berlin Heidelberg 2013

stability of such an equilibrium point. Thus, this work is a relevant generalization to discontinuous vector fields of the bifurcation studied in [6] for the continuous case.

To begin with, we assume without loss of generality that the linearity regions in the phase plane are the left and right half-planes,

$$S^- = \{(x, y) : x < 0\}, \quad S^+ = \{(x, y) : x > 0\},$$

separated by the straight line $\Sigma = \{(x, y) : x = 0\}$. The systems to be studied become

$$\dot{\mathbf{x}} = \begin{cases} \left(F_1^+(\mathbf{x}), F_2^+(\mathbf{x})\right)^T = A^+\mathbf{x} + \mathbf{b}^+, & \text{if } x \in S^+, \\ \left(F_1^-(\mathbf{x}), F_2^-(\mathbf{x})\right)^T = A^-\mathbf{x} + \mathbf{b}^-, & \text{if } x \in S^-, \end{cases} \tag{1}$$

where $\mathbf{x} = (x, y)^T \in \mathbb{R}^2$, $A^+ = (a_{ij}^+)$ and $A^- = (a_{ij}^-)$ are 2×2 constant matrices, $\mathbf{b}^+ = (b_1^+, b_2^+)^T$, $\mathbf{b}^- = (b_1^-, b_2^-)^T$ are constant vectors of $\mathbb{R}^2$, and the definition of the vector field in Σ is not relevant for our purposes.

We assume the generic condition $a_{12}^+ a_{12}^- > 0$, which means that orbits can cross the discontinuity line in opposite directions, allowing the existence of period orbits that use the two half planes. By applying Proposition 3.1 of [7], system (1) can be written in the canonical form

$$\begin{aligned} \dot{\mathbf{x}} &= \begin{pmatrix} T_- & -1 \\ D_- & 0 \end{pmatrix} \mathbf{x} - \begin{pmatrix} 0 \\ a_- \end{pmatrix} \text{ if } \mathbf{x} \in S^-, \\ \dot{\mathbf{x}} &= \begin{pmatrix} T_+ & -1 \\ D_+ & 0 \end{pmatrix} \mathbf{x} - \begin{pmatrix} -b \\ a_+ \end{pmatrix} \text{ if } \mathbf{x} \in S^+, \end{aligned} \tag{2}$$

where

$$a_- = a_{12}^- b_2^- - a_{22}^- b_1^-, \quad b = \frac{a_{12}^-}{a_{12}^+} b_1^+ - b_1^-, \quad a_+ = \frac{a_{12}^-}{a_{12}^+}(a_{12}^+ b_2^+ - a_{22}^+ b_1^+),$$

and $T_\pm = \mathrm{tr}(A^\pm)$, $D_\pm = \det(A^\pm)$ are the linear invariants of each zone.

The canonical form (2) has seven parameters; apart from the mentioned linear invariants, we find the two parameters a_+ and a_- related to the position of equilibria, and a parameter b which is responsible for the existence of a sliding set, where both vector fields cannot be concatenated in a natural way. In fact, there exists a sliding set which is a segment joining the origin and the point $(0, b)$, see [7] for more details. These two endpoints are tangency points, the origin for the left region and the point $(0, b)$ for the right one. Furthermore, the sliding set becomes attractive for $b < 0$ and repulsive for $b > 0$, shrinking to the origin when $b = 0$.

By computing the sign of $\ddot{x}$ at the tangency points, we obtain $\ddot{x}|_{(x,y)=(0,0)} = a_-$, $\ddot{x}|_{(x,y)=(0,b)} = a_+$, so that the left (right) tangency is called visible for $a_- < 0$ ($a_+ > 0$), being invisible for $a_- > 0$ ($a_+ < 0$), see [7]. Thus the $a_\pm$ parameters are

related to the visibility of the tangencies, and when they vanish we have boundary equilibrium points, see [10] and also [11].

The possible equilibria (real or virtual) are located at $(a_-/D_-, a_-T_-/D_-)$ and $(a_+/D_+, b + a_+T_+/D_+)$ where it is assumed $D_+D_- \neq 0$. Without loss of generality, we assume that there exists an equilibrium of focus type in the left zone, that is, $T_-^2 - 4D_- < 0$ (what implies $D_- > 0$), and $a_- < 0$.

Our interest is to study what happens when the trace T_- passes through the critical value zero, that is when the focus passes from stable to unstable or vice versa. Note that for $T_- = 0$ in the left half plane we have a center configuration which terminates in a visible tangency at the origin. To avoid other non-local phenomena it is then natural to impose that in the right zone we have also a tangency at the origin of invisible character, what amounts to require $b = 0$. In fact, if we allow to move this parameter b in a neighborhood of zero, then we should have the possibility of new bifurcations, namely the collision of tangencies, which has been reported in [10]. Thus, our study can be seen as a first step in the analysis of the codimension-two bifurcation that appears when the parameter b is allowed to be moved. Such codimension-two bifurcation will be the aim of a future work, since it turns out to be a non-generic case, not included in the extensive analysis done in [8].

Thus, there are no proper sliding set nor jumps in the right dynamics with respect to the critical center. Under these assumptions our first result is the following.

Proposition 1. *Under the hypotheses $T_-^2 - 4D_- < 0$, $a_- < 0$ (left focus dynamics with visible tangency at the origin) and assuming that in the right zone we have an invisible tangency at the origin, that is, $b = 0$ and $a_+ < 0$, system (2) is topologically equivalent to the system*

$$\begin{cases} \dot{x} = Tx - y, \\ \dot{y} = Dx + a, \end{cases} \quad \text{if } x > 0, \qquad \begin{cases} \dot{x} = 2\gamma x - y, \\ \dot{y} = (1+\gamma^2)(x+1), \end{cases} \quad \text{if } x < 0, \tag{3}$$

where $T = T_+$, $D = D_+$, $\gamma = \alpha/\omega$, with $2\alpha = T_-$, $\omega > 0$ is such that $4D_- - T_-^2 = 4\omega^2$, and $a = D_-a_+/(\omega a_-) > 0$.

The proof of Proposition 1 appears in Sect. 3. With this result, we manage to describe the left dynamics with only one parameter, needing other three parameters to deal with the right region. The following remark should be taken into account.

Remark 1. System (3) represents in general a discontinuous vector field since for $x = 0$ we will have generically $a \neq 1 + \gamma^2$. The original system (2) is continuous only in the case $a_+ = a_-$ and $b = 0$, but even in such non-generic case, the new system provided by Proposition 1 will be discontinuous. Thus, the analysis of system (3) is relevant for some continuous cases that could be also studied by alternative methods within a continuous vector field context. This fact will be illustrated later in Sect. 2.

Regarding equilibrium points, in the zone $x < 0$, there exists a focus at $(\overline{x}, \overline{y}) = (-1, -2\gamma)$, to be stable for $\gamma < 0$ and unstable for $\gamma > 0$. When $\gamma = 0$, we have a linear center. In the zone $x > 0$, since $a > 0$, there will be

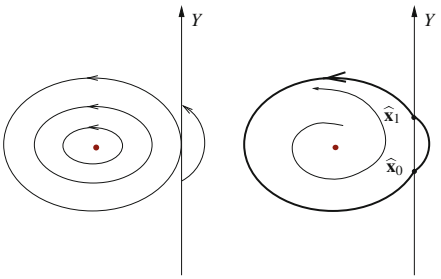

Fig. 1 (*Left*) The critical situation for $\gamma = 0$. (*Right*) The bifurcating limit cycle for $\gamma T < 0$ and $|\gamma|$ small

no equilibrium points if $D = 0$; otherwise, the possible equilibrium point will be located at $(-a/D, -aT/D)$.

We will take γ in (3) as the bifurcation parameter, having its critical value at $\gamma = 0$, where the center configuration takes place, see Fig. 1. Our first main result is the following.

Theorem 1. *Consider system* (3) *with* $a > 0$ *and under the assumption* $T \neq 0$. *The linear center configuration restricted to the zone* $x \leq 0$, *that exists for* $\gamma = 0$ *gives place to a unique periodic oscillation for* $\gamma T < 0$ *and* $|\gamma|$ *sufficiently small.*

More precisely, for $T < 0$ *the limit cycle bifurcates for* $\gamma > 0$ *and it is stable, while for* $T > 0$ *the limit cycle bifurcates for* $\gamma < 0$ *and it is unstable. If we denote with* $\hat{\mathbf{x}}_0 = (0, \hat{y}_0)^T$ *the lower crossing point of the bifurcating limit cycle, then the peak-to-peak amplitude* A_{pp} *in* x, *the period* P *of the periodic oscillation, the characteristic multiplier* ϱ *of the periodic orbit and the coordinate* $\hat{y}_0$ *are analytic functions at* 0 *in the variable* $\gamma^{1/3}$. *Namely, for* $\gamma T < 0$ *and* $|\gamma|$ *sufficiently small we have*

$$
\begin{aligned}
A_{pp} &= 2 + \frac{(3\pi)^{2/3}}{2}\frac{1+a}{(T^2 a)^{1/3}}\gamma^{2/3} + O(\gamma^{4/3}),\\
P &= 2\pi + 2(3\pi)^{1/3}\frac{a-1}{(a^2 T)^{1/3}}\gamma^{1/3}\\
&\quad - \frac{2\pi}{15}\frac{(15a^2 - 12D + T^2 - a(3D+T^2))}{a^2 T}\gamma + O(\gamma^{4/3}),\\
\varrho &= 1 - 2(3\pi)^{1/3}\left(\frac{T}{a}\right)^{2/3}\gamma^{1/3} + 2(3\pi)^{2/3}\left(\frac{T}{a}\right)^{4/3}\gamma^{2/3}\\
&\quad + \frac{2\pi}{15}\frac{15a^2 + 12D - 31T^2}{a^2}\gamma + O(\gamma^{4/3}),
\end{aligned}
$$

and

$$
\hat{y}_0 = \left(\frac{3\pi a}{T}\right)^{1/3}\gamma^{1/3} + \left(\frac{\pi^2 T}{3a}\right)^{1/3}\gamma^{2/3} + \frac{\pi\left(15a^2 + 3D + T^2\right)}{15aT}\gamma + O(\gamma^{4/3}).
$$

It should be noted that the sign of the parameter D is not relevant for the bifurcation and thus our result covers the cases the focus-antisaddle case ($D > 0$),

the case of $D = 0$ (parabolic case) and the saddle case ($D < 0$). Of course, the uniqueness of the bifurcating limit cycle is referred to a neighborhood of the most external periodic orbit of the linear center existing for $\gamma = 0$, and so it is a local uniqueness. The case $T = 0$ is explicitly excluded from our result because then we should have a global center for the critical value $\gamma = 0$; the possible bifurcation of limit cycles for such non-generic case requires different techniques, as considered in [3].

Undoing the changes of variables introduced in the proof of Proposition 1, it is easy now to get a similar result for system (2) with $b = 0$ and adequate hypotheses.

Theorem 2. *Consider system (2) under the hypotheses $T_-^2 - 4D_- < 0$, $a_- < 0$, $a_+ < 0$, $T_+ \neq 0$ and assume that in the zone $x > 0$ we have an invisible tangency at the origin, that is $b = 0$. The linear center configuration restricted to the zone $x \leq 0$, that exists for $T_- = 0$ gives place to a unique periodic oscillation for $T_- T_+ < 0$ and $|T_-|$ sufficiently small.*

More precisely, for $T_+ < 0$ the limit cycle bifurcates for $T_- > 0$ and it is stable, while for $T_+ > 0$ the limit cycle bifurcates for $T_- < 0$ and it is unstable. If we denote by $\hat{\mathbf{x}}_0 = (0, \hat{y}_0)^T$ the lower crossing point of the bifurcating limit cycle, the peak-to-peak amplitude A_{pp} in x, the period P, the characteristic multiplier ϱ and $\hat{y}_0$ are analytic functions at 0 in the variable $T_-^{1/3}$. Namely, for $T_- T_+ < 0$ and $|T_-|$ sufficiently small we have

$$A_{pp} = -2\frac{a_-}{D_-} - \frac{1}{2}\left(\frac{3\pi}{2}\right)^{2/3} \frac{a_+ + a_-}{D_-} \left(\frac{a_-}{a_+}\right)^{1/3} \left(\frac{T_-}{T_+}\right)^{2/3} + O(T_-)^{4/3}, \tag{4}$$

$$\begin{aligned} P = {} & \frac{2\pi}{\sqrt{D_-}} - (12\pi)^{1/3} \frac{a_- - a_+}{a_-^{1/3} a_+^{2/3} \sqrt{D_-}} \left(\frac{T_-}{T_+}\right)^{1/3} \\ & + \frac{\pi}{15} \frac{\left[15a_+^2 D_- - 3D_+(4a_-^2 + a_- a_+) + T_+^2 a_-(a_- - a_+)\right]}{a_+^2 D_-^{3/2}} \frac{T_-}{T_+} + O(T_-)^{4/3}, \end{aligned} \tag{5}$$

$$\begin{aligned} \varrho = {} & 1 + \frac{(12\pi)^{1/3}}{\sqrt{D_-}} T_+ \left(\frac{a_-}{a_+}\right)^{2/3} \left(-\frac{T_-}{T_+}\right)^{1/3} \\ & + (18\pi^2)^{1/3} \frac{T_+^2}{D_-} \left(\frac{a_-}{a_+}\right)^{4/3} \left(\frac{T_-}{T_+}\right)^{2/3} \\ & + \frac{\pi}{15} \frac{45a_+^2 + a_-^2(12D_+ - 31T_+^2)}{a_+^2 D_-^{3/2}} T_- + O(T_-)^{4/3}, \end{aligned}$$

and

$$\begin{aligned} \hat{y}_0 = {} & \left(\frac{3\pi}{2}\right)^{1/3} \frac{a_+^{1/3} a_-^{2/3}}{\sqrt{D_-}} \left(-\frac{T_-}{T_+}\right)^{1/3} - \left(\frac{\pi^2}{12}\right)^{1/3} \frac{a_-^{4/3} T_+}{a_+^{1/3} D_-} \left(\frac{T_-}{T_+}\right)^{2/3} \\ & - \frac{\pi}{30} \frac{15a_+^2 D_- + a_-^2(3D_+ + T_+^2)}{a_+ D_-^{3/2}} \frac{T_-}{T_+} + O(T_-)^{4/3}. \end{aligned} \tag{6}$$

This theorem is an extension of the results obtained in [6], where only the continuous case was analyzed. Consequently, if we put in the above expressions $a^+ = a^-$ the continuous case is recovered. The expressions (4)–(6) have been computed with the help of symbolic computation systems (both Mathematica [12] and Maple [2]) and only the first coefficients of the series are explicitly shown. More terms can be computed with the same techniques, if required.

The rest of the paper is organized as follows. An application of Theorem 2 to the study of the dynamics of an electronic circuit is given in Sect. 2. The proofs of main results along with other technical lemmas appear finally in Sect. 3.

2 Application to the Dynamics of a Wien Bridge Oscillator

In [9] a realistic model for an operational amplifier is proposed to illustrate the jump transition to oscillation in the Wien bridge oscillator (Fig. 2). The problem leads to a idealized symmetric model that can be settled down in a continuous vector field context, see [6]. Here, we will assume a more general situation in the sense that the nonlinear characteristic of the electronic device is allowed to have some lack of symmetry. This assumption implies that in the birth of oscillations only two linear zones are involved, and we can discard one of the most external regions. Thus we assume that the circuit model is given by

$$\begin{cases} \ddot{v} + 2\Gamma\dot{v} + v = 0, & v > 1, \\ \ddot{v} - 2\Gamma\varepsilon\dot{v} + v = 0, & v \leq 1, \end{cases}$$

where v is the dimensionless input voltage in the operational amplifier, Γ is a positive constant parameter which depends on the passive elements of the circuit, and ε is taken as the bifurcation parameter, see [9] for more details.

The above equations, after the translation $v = x + 1$, can be written in the form

$$\dot{x} = y, \quad \dot{y} = \begin{cases} -x - 2\Gamma y - 1, & \text{if } x > 0, \\ -x + 2\varepsilon\Gamma y - 1, & \text{if } x \leq 0. \end{cases} \tag{7}$$

System (7) is in the formulation (1.1) given in [7] and we can apply the Proposition 3.1 of that paper in order to put system (7) in Liénard form. The homeomorphism

$$\tilde{\mathbf{x}} = \begin{pmatrix} 1 & 0 \\ -2\Gamma & -1 \end{pmatrix} \mathbf{x} \quad \text{if } x > 0, \qquad \tilde{\mathbf{x}} = \begin{pmatrix} 1 & 0 \\ 2\varepsilon\Gamma & -1 \end{pmatrix} \mathbf{x} \quad \text{if } x \leq 0,$$

transforms system (7) in

$$\dot{x} = \begin{cases} -2\Gamma x - y, & \text{if } x > 0, \\ 2\varepsilon\Gamma x - y, & \text{if } x < 0, \end{cases} \qquad \dot{y} = x + 1, \tag{8}$$

where the tildes have been dropped for the sake of simplicity.

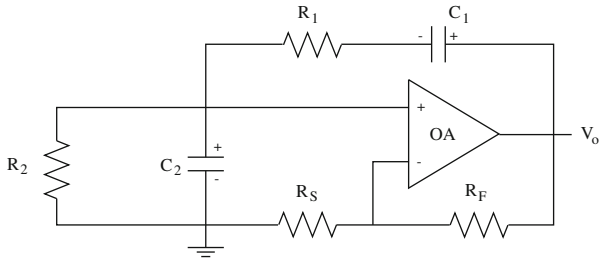

Fig. 2 Scheme of the Wien bridge oscillator. The power supply needed to bias the operational amplifier is not shown

Now, we can apply Theorem 2 to system (8) by taking $T_+ = -2\Gamma$, $T_- = 2\varepsilon\Gamma$, $D_+ = D_- = 1$, $a_+ = a_- = -1$ and $b = 0$, obtaining that the bifurcation takes place for $\varepsilon = 0$, the limit cycle exists for sufficiently small $\varepsilon > 0$ and it is stable.

The peak-to-peak amplitude, the period and the characteristic multiplier of the limit cycle are

$$A_{pp} = 2 + \left(\frac{3\pi}{2}\right)^{2/3} \varepsilon^{2/3} - \frac{\pi^{4/3}(99 + 52\Gamma^2)}{40 \cdot 18^{1/3}} \varepsilon^{4/3} + O(\varepsilon^{5/3}),$$

$$P = 2\pi + \frac{4(18\pi^5)^{1/3}}{5} \varepsilon^{5/3} + O(\varepsilon^2),$$

$$\varrho = 1 - 2(12\pi)^{1/3}\Gamma\varepsilon^{1/3} + 4(18\pi^2)^{1/3}\Gamma^2\varepsilon^{2/3} + \frac{2\pi}{15}\Gamma(27 - 124\Gamma^2)\varepsilon + \frac{4}{5}\left(\frac{4\pi}{9}\right)^{1/3} \Gamma(34\pi\Gamma^3 - 27\pi\Gamma - 5)\varepsilon^{4/3} + O(\varepsilon^{5/3}).$$

We note that the order $\varepsilon^{5/3}$ term in the last expression of the period P is not explicitly shown in Theorem 1. It has been computed with the same procedure of the proof of Theorem 1, increasing the number of terms in (17).

We emphasize that the above series are very useful to describe accurately all the features of the nonlinear oscillation for parameters near the critical value corresponding to the bifurcation. Of course, we could have obtained the same results applying Proposition 1 and Theorem 1.

3 Proofs of Main Results

We give first the proof of Proposition 1.

Proof (Proof of Proposition 1). Clearly, the assumption on right tangency at the origin, that is $\dot{x}\,|_{(x,y)=(0,0)} = 0$, reduces to $b = 0$, and this tangency will be invisible for $a_+ < 0$.

Under the hypotheses, if we define $\omega > 0$ such that $\omega^2 = D_- - T_-^2/4$ and $\alpha = T_-/2$, the eigenvalues of the linear part at S^- in (2) are $\alpha \pm \mathbf{1}\omega$. We make first the change $X = \omega x$, $Y = y$, $\tau = \omega t$ for the variables in the half plane S^-, without altering variables and time in S^+. Note that we do not change the coordinate y, so that periodic orbits using both half planes are preserved. Then, we get

$$\frac{\mathrm{d}X}{\mathrm{d}\tau} = \frac{1}{\omega}\frac{\mathrm{d}X}{\mathrm{d}t} = \frac{\mathrm{d}x}{\mathrm{d}t} = \frac{X}{\omega}T_- - Y,$$
$$\frac{\mathrm{d}Y}{\mathrm{d}\tau} = \frac{1}{\omega}\frac{\mathrm{d}Y}{\mathrm{d}t} = \frac{1}{\omega}\frac{\mathrm{d}y}{\mathrm{d}t} = \frac{1}{\omega}\left(D_-\frac{X}{\omega} - a_-\right) = \frac{D_-}{\omega^2}X - \frac{a_-}{\omega}.$$

Introducing the parameter $\gamma = \alpha/\omega$, we see that $T_- = 2\gamma\omega$ and $D_- = (\gamma^2 + 1)\omega^2$. Making in the whole plane a homothety of factor k to be defined below and removing the factor k in the equations, we have for $x < 0$,

$$\frac{\mathrm{d}x}{\mathrm{d}\tau} = k\frac{\mathrm{d}X}{\mathrm{d}\tau} = k\left(2\gamma\frac{x}{k} - \frac{y}{k}\right) = 2\gamma x - y,$$
$$\frac{\mathrm{d}y}{\mathrm{d}\tau} = k\frac{\mathrm{d}Y}{\mathrm{d}\tau} = k\left[(\gamma^2+1)\frac{x}{k} - \frac{a_-}{\omega}\right] = (\gamma^2+1)x - k\frac{a_-}{\omega},$$

while for $x > 0$ we have $\dot{x} = Tx - y$, and $\dot{y} = Dx - ka_+$. By imposing now that $k = -(\gamma^2+1)\omega/a_- > 0$, we get the expressions given in the statement. □

Before giving the proof of Theorem 1, we need first some technical results.

Let us consider system (1). We assume that the orbit of vector field F^+ starting at a point $\hat{\mathbf{x}}_0 = (0, \hat{y}_0)$ with $F_1^+(\hat{\mathbf{x}}_0) > 0$, lies in S^+ and eventually comes back to the discontinuity line arriving transversally at the point $\hat{\mathbf{x}}_1 = (0, \hat{y}_1)$, where $F_1^+(\hat{\mathbf{x}}_1) < 0$.

Lemma 1. *If we denote as $\hat{\delta}^+(t) = (x(t, \hat{\mathbf{x}}_0), y(t, \hat{\mathbf{x}}_0))$ the solution of $\dot{\mathbf{x}} = F^+(x)$ satisfying $\hat{\delta}^+(0) = \hat{\mathbf{x}}_0$, then a value $\tau^+ > 0$ exists such that $x(t, \hat{\mathbf{x}}_0) > 0$ for $0 < t < \tau^+$ and $x(\tau^+, \hat{\mathbf{x}}_0) = 0$, $y(\tau^+, \hat{\mathbf{x}}_0) = \hat{y}_1$. Then we can define a right Poincaré map P_R in a neighborhood of the point $\hat{\mathbf{x}}_0$ such that $P_R(\hat{y}_0) = \hat{y}_1$ and the first derivative of map P_R at $\hat{y}_0$ is given by*

$$P_R'(\hat{y}_0) = \frac{F_1^+(\hat{\mathbf{x}}_0)}{F_1^+(\hat{\mathbf{x}}_1)} \exp\left(\int_0^{\tau^+} \operatorname{div}\left(F^+\right)\right).$$

Proof. Let us consider the differential system $\dot{\mathbf{x}} = F^+(\mathbf{x})$ defined in $\mathbb{R}^2$, and let us denote as $\delta^+(t) = (x(t, \mathbf{x}_0), y(t, \mathbf{x}_0))$, the solution satisfying $\delta^+(0) = \mathbf{x}_0$ where $\mathbf{x}_0 = (x_0, y_0)$. Let us introduce the equation $\mathbf{Z}(t, \mathbf{x}_0, y_1) = \mathbf{0}$, where

$$\mathbf{Z}(t, \mathbf{x}_0, y_1) = \begin{pmatrix} x(t, \mathbf{x}_0) \\ y(t, \mathbf{x}_0) - y_1 \end{pmatrix},$$

and from our hypotheses we have $\mathbf{Z}(\tau^+, \hat{\mathbf{x}}_0, \hat{y}_1) = \mathbf{0}$ and $F_1^+(0, \hat{y}_1) \neq 0$. Then the Jacobian matrix

$$\frac{\partial(Z_1, Z_2)}{\partial(t, y_1)}(\tau^+, \hat{\mathbf{x}}_0, \hat{y}_1) = \left.\begin{pmatrix} \dfrac{\partial x}{\partial t} & \dfrac{\partial x}{\partial y_1} \\ \dfrac{\partial y}{\partial t} & \dfrac{\partial y}{\partial y_1} \end{pmatrix}\right|_{(\tau^+, \hat{\mathbf{x}}_0, \hat{y}_1)} = \begin{pmatrix} F_1^+(0, \hat{y}_1) & 0 \\ F_2^+(0, \hat{y}_1) & -1 \end{pmatrix}$$

is nonsingular.

Then, we conclude from the implicit function theorem the existence of two functions $\varphi(\mathbf{x}_0)$, $\psi(\mathbf{x}_0)$ defined in a neighborhood of $\mathbf{x}_0$, such that

$$x(\varphi(\mathbf{x}_0), \mathbf{x}_0) = 0, \quad y(\varphi(\mathbf{x}_0), \mathbf{x}_0) - \psi(\mathbf{x}_0) = 0, \tag{9}$$

with $\varphi(\hat{\mathbf{x}}_0) = \tau^+$, $\psi(\hat{\mathbf{x}}_0) = \hat{y}_1$.

Thus, we can define the right Poincaré map P_R in a neighborhood of the point $\mathbf{x}_0$ as $y_1 = P_R(y_0) = \psi(0, y_0)$, which satisfies $\hat{y}_1 = P_R(\hat{y}_0) = \psi(\hat{\mathbf{x}}_0)$.

To compute the first derivative of Poincaré map, we take derivatives with respect to (x_0, y_0) in Eqs. (9) to get

$$\frac{\partial \mathbf{Z}}{\partial t}(\varphi(\mathbf{x}_0), \mathbf{x}_0, \psi(\mathbf{x}_0)) \cdot D_{\mathbf{x}}\varphi(\mathbf{x}_0) + B(\mathbf{x}_0) - \begin{pmatrix} \mathbf{0} \\ D_{\mathbf{x}}\psi(\mathbf{x}_0) \end{pmatrix} = \mathbf{0}, \tag{10}$$

where

$$\frac{\partial \mathbf{Z}}{\partial t}(\varphi(\mathbf{x}_0), \mathbf{x}_0, \psi(\mathbf{x}_0)) = \begin{pmatrix} \dfrac{\partial x}{\partial t}(\varphi(\mathbf{x}_0), \mathbf{x}_0) \\ \dfrac{\partial y}{\partial t}(\varphi(\mathbf{x}_0), \mathbf{x}_0) \end{pmatrix} = F^+(\mathbf{x}_1)$$

and

$$B(\mathbf{x}_0) = D_{\mathbf{x}}\mathbf{Z}(\varphi(\mathbf{x}_0), \mathbf{x}_0, \psi(\mathbf{x}_0)) = \begin{pmatrix} \dfrac{\partial x}{\partial x_0}(\varphi(\mathbf{x}_0), \mathbf{x}_0) & \dfrac{\partial x}{\partial y_0}(\varphi(\mathbf{x}_0), \mathbf{x}_0) \\ \dfrac{\partial y}{\partial x_0}(\varphi(\mathbf{x}_0), \mathbf{x}_0) & \dfrac{\partial y}{\partial y_0}(\varphi(\mathbf{x}_0), \mathbf{x}_0) \end{pmatrix}$$

satisfies the equality

$$B(\mathbf{x}_0)F^+(\mathbf{x}_0) = F^+(\mathbf{x}_1), \tag{11}$$

due to the elementary properties of variational equations.

By right-multiplying (10) by the vector $(0,1)^T$, we get

$$\varphi_y(\mathbf{x}_0)F^+(\mathbf{x}_1) + B(\mathbf{x}_0)\begin{pmatrix}0\\1\end{pmatrix} - \begin{pmatrix}0\\ \psi_y(\mathbf{x}_0)\end{pmatrix} = \mathbf{0},$$

and so

$$B(\mathbf{x}_0)\begin{pmatrix}0\\-1\end{pmatrix} = \begin{pmatrix}F_1^+(\mathbf{x}_1)\varphi_y(\mathbf{x}_0)\\ F_2^+(\mathbf{x}_1)\varphi_y(\mathbf{x}_0) - \psi_y(\mathbf{x}_0)\end{pmatrix}. \tag{12}$$

Taking into account (11) and (12) we can write

$$\begin{pmatrix}F_1^+(\mathbf{x}_1) & 0\\ F_2^+(\mathbf{x}_1) & -1\end{pmatrix}\begin{pmatrix}1 & \varphi_y(\mathbf{x}_0)\\ 0 & \psi_y(\mathbf{x}_0)\end{pmatrix} = B(\mathbf{x}_0)\begin{pmatrix}F_1^+(\mathbf{x}_0) & 0\\ F_2^+(\mathbf{x}_0) & -1\end{pmatrix}$$

and taking determinants we arrive at the relation

$$F_1^+(\mathbf{x}_1)\psi_y(\mathbf{x}_0) = F_1^+(\mathbf{x}_0)\exp\left(\int_0^{\varphi(\mathbf{x}_0)} \operatorname{div}(F^+)dt\right), \tag{13}$$

where we have used Liouville's formula in computing $\det B(\mathbf{x}_0)$. If we take $\mathbf{x}_0 = \hat{\mathbf{x}}_0$ in (13), then $\mathbf{x}_1 = \hat{\mathbf{x}}_1 = (0, P_R(\hat{y}_0))$. Since $P_R'(\hat{y}_0) = \psi_y(\mathbf{x}_0)$, the proof is finished. □

The following result is given without proof since it appeared in [6].

Lemma 2. *Let $\eta = \xi^n\varrho(\xi)$ with n odd, where ϱ is a real analytic function in a neighborhood of the origin and such that $\varrho(0) \neq 0$. Then there exists a real analytic function χ in a neighborhood of the origin with $\chi(0) \neq 0$ such that $\xi = \eta^{1/n}\chi(\eta^{1/n})$.*

We are now ready to show Theorem 1.

Proof (Proof of Theorem 1). If $\gamma = 0$, then it is easy to see that system (3) has a linear center for $x \leq 0$, because the eigenvalues of the linearization matrix are $\pm\mathbf{1}$.

For $\gamma \neq 0$ in the zone with $x \leq 0$, the linearization matrix has complex eigenvalues $\gamma \pm \mathbf{1}$, that is, the equilibrium point at $(-1, -2\gamma)^T$ is a focus.

We want to analyze the possible bifurcation of a limit cycle from the linear center existing in the zone $x \leq 0$ for $\gamma = 0$. It should be born from the most external periodic orbit of the center, which is tangent to the frontier $x = 0$ at the origin.

Let us assume the existence of a limit cycle living in the two zones of linearity with intersections $\hat{\mathbf{x}}_0 = (0, \hat{y}_0)^T$ and $\hat{\mathbf{x}}_1 = (0, \hat{y}_1)^T$ with $x = 0$, as it is shown in Fig. 1.

Let consider the orbit of system (3) that starts from the point $\hat{\mathbf{x}}_0 = (0, \hat{y}_0)^T$ and enters the zone $x > 0$. The points of that orbit are given by the expression

$$(x_R(\tau), y_R(\tau))^T = \mathrm{e}^{A_R\tau}\left(\hat{\mathbf{x}}_0 - \mathbf{x}_{eq_R}\right) + \mathbf{x}_{eq_R},$$

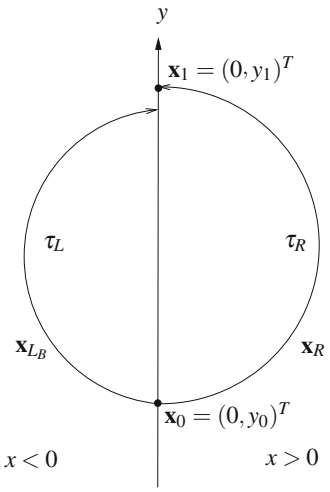

Fig. 3 A typical orbit with the notation used in the proof of Theorem 1

where the subindices R stand for the right zone, and so A_R is the linearization matrix for the right zone of (3) and $\mathbf{x}_{eq_R} = (-a/D, -aT/D)^T$ (Fig. 3).

If starting again from point $\hat{\mathbf{x}}_0$ we integrate backwards in time, we use the zone $x < 0$ and we obtain the orbit given by

$$(x_{L_B}(\tau), y_{L_B}(\tau))^T = \mathrm{e}^{-A_L \tau} \left(\hat{\mathbf{x}}_0 - \mathbf{x}_{eq_L}\right) + \mathbf{x}_{eq_L},$$

where the subindices L stand for the left zone, being A_L the linearization matrix of the left zone, and $\mathbf{x}_{eq_L} = (-1, -2\gamma)^T$.

The assumed existence of limit cycle implies that there exist two positive values τ_R and τ_L such that

$$\begin{pmatrix} x_R(\tau) \\ y_R(\tau) \end{pmatrix} = \hat{\mathbf{x}}_1 = \begin{pmatrix} 0 \\ \hat{y}_1 \end{pmatrix} = \begin{pmatrix} x_{L_B}(\tau) \\ y_{L_B}(\tau) \end{pmatrix}.$$

This expression is equivalent to the following equalities

$$\begin{cases} x_{L_B}(\tau_L) = 0, \\ x_R(\tau_R) = 0, \\ y_R(\tau_R) - y_{L_B}(\tau_L) = 0, \end{cases} \tag{14}$$

where $\hat{y}_1$ has been removed from the computations. Apart from the bifurcation parameter γ, Eqs. (14) have three unknowns: τ_L, τ_R, $\hat{y}_0$, and it will be referred as to the closing equations. The use of these equations goes back to Andronov and coworkers [1]. The closing equations (14) for $\mathbf{z} = (\tau_L, \tau_R, \hat{y}_0, \gamma)$ will be denoted by

$$\mathbf{H}(\mathbf{z}) = \mathbf{0}. \tag{15}$$

The outermost periodic orbit of the existing linear center in zone $x < 0$ for $\gamma = 0$ satisfies (15) for the values $\tau_L = 2\pi$, $\tau_R = 0$, $\hat{y}_0 = 0$, $\gamma = 0$, and it is associated to the solution $\bar{\mathbf{z}} = (2\pi, 0, 0, 0)$.

Obviously, we are interested in a branch of solutions of (15) passing through $\bar{\mathbf{z}}$, and leading to positive values of τ_L and τ_R. It turns out that system (15) has a trivial branch of solutions that passes through $\bar{\mathbf{z}}$ and can be parameterized as $\mathbf{z}(\mu) = (2\pi, 0, \mu, 0)$ for every real μ. This trivial branch is a spurious branch because, for $\mu \neq 0$, these solutions do not correspond to periodic orbits of the system (15). The Jacobian matrix of $\mathbf{H}$ at $\bar{\mathbf{z}}$ has not full rank, namely

$$\left.\frac{\partial \mathbf{H}}{\partial \mathbf{z}}\right|_{\mathbf{z}=\bar{\mathbf{z}}} = \begin{pmatrix} 0 & 0 & 0 & -2\pi \\ 0 & 0 & 0 & 0 \\ 1 & a & 0 & 0 \end{pmatrix}.$$

In order to apply the Implicit Function Theorem we must remove the spurious branch. The second equation of (15), namely $H_2(\mathbf{z}) = 0$ is satisfied for every $\mathbf{z}$ with $\tau_R = 0$. The function $\tilde{H}_2(\mathbf{z})$ such that $H_2(\mathbf{z}) = \tau_R \tilde{H}_2(\mathbf{z})$ is an analytic function in a neighborhood of $\bar{\mathbf{z}}$. If we define the modified closing equations

$$\mathbf{G}(\mathbf{z}) = \mathbf{0}, \tag{16}$$

where $G_2 = \tilde{H}_2$ and $G_i = H_i$ for $i \neq 2$, then the solution set of (16) in a neighborhood of $\bar{\mathbf{z}}$ is the solution set of (15) excepting the spurious branch solution. In other words, we have desingularized the closing equations.

The Jacobian matrix of system (16) is the following

$$J = \begin{pmatrix} 0 & 0 & 0 & -2\pi \\ 0 & -a/2 & -1 & 0 \\ 1 & a & 0 & 0 \end{pmatrix}.$$

If we neglect the second column (corresponding to τ_R), the determinant of the resulting matrix is $-2\pi \neq 0$ and hence the matrix has full rank. From the Implicit Function Theorem for analytic functions (see [4]) we obtain that in a neighborhood of $\bar{\mathbf{z}}$ there exist three unique analytic functions $\tau_L = \varphi_1(\tau_R)$, $\hat{y}_0 = \varphi_2(\tau_R)$ and $\gamma = \varphi_3(\tau_R)$, such that $\mathbf{H}(\varphi_1(\tau_R), \varphi_2(\tau_R), \varphi_3(\tau_R), \tau_R) = \mathbf{0}$. Thus, we can assume the existence of series expansions in τ_R, for the three functions. These series, computed for safety with two symbolic manipulators (Mathematica [12] and Maple [2]), are

$$\begin{aligned} \tau_L(\tau_R) &= 2\pi - a\tau_R + \frac{a(a^2 - D)}{12}\tau_R^3 + O(\tau_R^5), \\ \hat{y}_0(\tau_R) &= -\frac{a}{2}\tau_R + \frac{aT}{12}\tau_R^2 - \frac{aD}{24}\tau_R^3 + \frac{aT(7D - T^2)}{720}\tau_R^4 + O(\tau_R^5), \\ \gamma(\tau_R) &= -\frac{a^2 T}{24\pi}\tau_R^3 + \frac{a^2 T(15a^2 - 12D + T^2)}{1{,}440\pi}\tau_R^5 - \frac{a^5 T}{288\pi^2}\tau_R^6 + O(\tau_R^7). \end{aligned} \tag{17}$$

Since $a > 0$, we can invert the series for $\gamma(\tau_R)$ applying Lemma 2, after taking $n = 3$, $\xi = \tau_R$ and $\eta = \gamma$, so that we obtain

$$\tau_R(\gamma) = -2\left(\frac{3\pi}{a^2 T}\right)^{1/3}\gamma^{1/3} - \frac{2\pi(15a^2 - 12D + T^2)}{15a^2 T}\gamma - \frac{4a\pi^{1/3}}{(9a^2T^4)^{1/3}}\gamma^{4/3} + O(\gamma^{5/3}). \tag{18}$$

Since τ_R provides the time spent by the orbit in the zone $x > 0$, τ_R must be positive for $|\gamma|$ sufficiently small, and then γT must be negative. Replacing $\tau_R(\gamma)$ in (17) we obtain the expressions of $P = \tau_L(\gamma) + \tau_R(\gamma)$ and $y_0(\gamma)$ that appear in the statement of Theorem 1.

The peak-to-peak amplitude in x is measured as the difference between the maximum value in x reached in the periodic orbit and its minimum. Let us denote by $\tau_{R_{max}}$ the time for which $x(\tau)$ reaches its maximum value $x(\tau_{R_{max}})$ in the zone with $x > 0$. In the same way, let us denote by $\tau_{L_{min}}$ the time for which $x(\tau)$ reaches its minimum value $x(\tau_{L_{min}})$ in the zone $x < 0$.

In a similar way to what happens for the solution values of τ_L, $\hat{y}_0$ and γ, the time $\tau_{R_{max}}$ has a series expansion in terms of τ_R. As we assume that the coordinate x of the periodic orbit reaches its maximum value for $\tau = \tau_{R_{max}}$, the following equality must hold

$$\dot{x} = T x_R(\tau_{R_{max}}) - y_R(\tau_{R_{max}}) = 0, \tag{19}$$

where

$$\begin{pmatrix} x_R(\tau_{R_{max}}) \\ y_R(\tau_{R_{max}}) \end{pmatrix} = \mathbf{x}_{eq_R} + \mathrm{e}^{A_R \tau_{R_{max}}(\tau_R)}\left[\begin{pmatrix} 0 \\ \hat{y}_0(\tau_R) \end{pmatrix} - \mathbf{x}_{eq_R}\right]. \tag{20}$$

From equalities (17), (19) and (20) it is easy to compute the series expansion for $\tau_{R_{max}}$, namely

$$\tau_{R_{max}} = \frac{\tau_R}{2} + \frac{T}{24}\tau_R^2 + \frac{2DT - T^3}{2{,}880}\tau_R^4 + O(\tau_R^6). \tag{21}$$

Using (17) and (21) in (20) we obtain the following expansion

$$x_R(\tau_{R_{max}}) = \frac{a}{8}\tau_R^2 + \frac{a(15D - 2T^2)}{1{,}152}\tau_R^4 + O(\tau_R^6). \tag{22}$$

We compute now for the time $\tau_{L_{min}}$ its series expansion with respect to τ_R. The following equality must hold

$$\dot{x} = 2\gamma x_{L_B}(\tau_{L_{min}}) - y_{L_B}(\tau_{L_{min}}) = 0, \tag{23}$$

where

$$\begin{pmatrix} x_{L_B}(\tau_{L_{min}}) \\ y_{L_B}(\tau_{L_{min}}) \end{pmatrix} = \mathbf{x}_{eq_L} + \mathrm{e}^{-A_L \tau_{L_{min}}(\tau_R)} \left[\begin{pmatrix} 0 \\ \hat{y}_0(\tau_R) \end{pmatrix} - \mathbf{x}_{eq_L} \right]. \tag{24}$$

From equalities (17), (23) and (24) it is easy to compute the series expansion for $\tau_{L_{min}}$, namely

$$\tau_{L_{min}} = \pi - \frac{a}{2}\tau_R + \frac{aT}{12}\tau_R^2 + \frac{a(a^2 - D)}{24}\tau_R^3 + \frac{aT(7D - T^2 - 15a^2)}{720}\tau_R^4 + O(\tau_R^5). \tag{25}$$

Using (17) and (25) in (24) we obtain

$$x_{L_B}(\tau_{L_{min}}) = -2 - \frac{a^2}{8}\tau_R^2 + \frac{a^2(9a^2 - 24D - 4T^2)}{1{,}152}\tau_R^4 + O(\tau_R^5). \tag{26}$$

Finally, from $A_{pp} = x_R(\tau_{R_{max}}) - x_{L_B}(\tau_{L_{min}})$ we get the expression of Theorem 1.

In order to determine the stability of the limit cycle, first we apply Lemma 1 to system (3), obtaining

$$P_R'(\hat{y}_0) = \frac{-\hat{y}_0}{-\hat{y}_1} \exp\left(\int_0^{\tau_R} T\, d\tau \right) = \frac{\hat{y}_0}{\hat{y}_1} \exp(T\tau_R).$$

For the part of the limit cycle with $x \leq 0$, an analogous result to Lemma 1 provides the derivative of the left Poincaré map

$$P_L'(\hat{y}_1) = \frac{F_1^-(\hat{\mathbf{x}}_1)}{F_1^-(\hat{\mathbf{x}}_0)} \exp\left(\int_0^{\tau^-} \mathrm{div}(F^-) \right) = \frac{\hat{y}_1}{\hat{y}_0} \exp(2\gamma\tau_L).$$

For the full Poincaré map we get $P'(\hat{y}_0) = P_L'\left(P_R(\hat{y}_0)\right) P_R'(\hat{y}_0) = P_L'(\hat{y}_1) P_R'(\hat{y}_0)$; hence, the characteristic multiplier of the periodic orbit is $\varrho = P'(\hat{y}_0) = \exp(T\tau_R + 2\gamma\tau_L)$. Substituting the series $\tau_L(\tau_R)$ from (17) in the above expression of ϱ, using the series $\tau_R(\gamma)$ from (18) and finally computing the series expansion of ϱ with respect to γ, we obtain the expression given for ϱ in Theorem 1. □

Finally, we will show the proof of Theorem 2.

Proof (Proof of Theorem 2). To prove Theorem 2 it suffices to consider the statements in Theorem 1 for the system (3), to substitute the parameters T, a and γ by their expressions provided in Proposition 1, and undo the changes that convert the system (2) in (3).

In particular, to get the new expression in the period P, we start from (18) and the first expression in (17). This last expression is rescaled by $1/\omega$ and added to (18), which after written in terms of the original parameters in (2) leads to the expression given in (5).

Similarly, to get the expression in (4) we must start from (22) and (26). This last expression should be affect by a factor $1/(\omega k)$ while (22) must be multiplied by $1/k$. After substituting in such expressions the value of τ_R given in (18), and resorting to the original parameters we arrive at (4).

To get the new expression for the characteristic multiplier, it suffices to use the original parameters, while to get the expression (6) we only must divide by k the expression for $\hat{y}_0$ in Theorem 1. □

Acknowledgements Authors acknowledge the fruitful suggestions of Prof. F. Torres on a preliminary version of the manuscript. They are partially supported by the *Ministerio de Ciencia y Tecnología, Plan Nacional I+D+I*, in the frame of projects MTM2009-07849, MTM2010-20907, MTM2012-31821, and by the *Consejería de Educación y Ciencia de la Junta de Andalucía* under grants TIC-0130 and P08-FQM-03770.

References

1. Andronov, A.A., Vitt, A.A., Khaikin, S.E.: Theory of Oscillators. Pergamon Press, Oxford (1966)
2. Bernardin, L., Chin, P., DeMarco, P., Geddes, K.O., Hare, D.E.G.: Maple 16 Maple Programming Guide. Maplesoft, Waterloo (2012)
3. Carmona, V., Fernández-García, S., Freire, E., Torres, F.: Melnikov theory for a class of planar hybrid systems. Physica D: Nonlinear Phenom. **248**, 44–54 (2013). ISSN: 0167-2789. doi:10.1016/j.physd.2013.01.002
4. Chow, S.N., Hale, J.K.: Methods of Bifurcation Theory. Grundlehren der Mathematischen Wissenschaften. Springer, New York (1982)
5. Di Bernardo, M., Budd, C., Champneys, A.R., Kowalczyk, P.: Piecewise-Smooth Dynamical Systems: Theory and Applications. Volume 163 of Applied Mathematical Sciences. Springer, New York/London (2007)
6. Freire, E., Ponce, E., Ros, J.: Limit cycle bifurcation from center in symmetric piecewise-linear systems. Int. J. Bifurc. Chaos **9**, 895–907 (1999)
7. Freire, E., Ponce, E., Torres, F.: Canonical discontinuous planar piecewise linear systems. SIAM J. Appl. Dyn. Syst. **11**, 181–211 (2012)
8. Guardia, M., Seara, T.M., Teixeira, M.A.: Generic bifurcations of low codimension of planar Filippov systems. J. Differ. Equ. **250**, 1967–2023 (2011)
9. Kriegsmann, G.A.: The rapid bifurcation of the Wien bridge oscillator. IEEE Trans. Circuits Syst. **34**, 1093–1096 (1987)
10. Kuznetsov, Y.A., Rinaldi, S., Gragnani, A.: One-parameter bifurcations in planar filippov systems. Int. J. Bifurc. Chaos **13**(8), 2157–2188 (2003)
11. Pagano, D., Ponce, E., Torres, F.: On double boundary equilibrium bifurcations in piecewise smooth planar systems. Qual. Theory Dyn. Syst. **10**, 277–301 (2011)
12. Wolfram Research, Inc.: Mathematica Edition: Version 8.0. Wolfram Research, Inc (2010)

Piecewise Linear Bidimensional Maps as Models of Return Maps for 3D Diffeomorphisms

A. Pumariño, J.A. Rodríguez, J.C. Tatjer, and E. Vigil

Abstract The goal of this paper is to study the dynamics of a simple family of piecewise linear maps in dimension two, that we call Expanding Baker Maps (EBM), which is a simplified model of a quadratic limit return map which appears in the study of certain homoclinic bifurcations of two-parameter families of three-dimensional dissipative diffeomorphisms. In spite of its simplicity the EBM capture some of the more relevant dynamics of the quadratic family, specially that related to the evolution of 2D strange attractors.

1 Introduction

The main objects of study of dissipative families of dynamical systems are the attracting invariant sets. In general, it is important to find which types of attractors can be detected and the mechanisms of creation and destruction of such sets. The simplest attractors are periodic, but there are other attracting sets as invariant tori or strange attractors. One of the most important mechanisms of creation of strange attractors is the unfolding of a homoclinic bifurcation. For one-parameter families of two-dimensional dissipative diffeomorphisms, we can find strange attractors near homoclinic tangencies of a saddle fix or periodic point. The main tool in order to prove their existence is to build a return map near one of such homoclinic tangency. This return map is close to a one-dimensional logistic map, for which it is possible to prove the existence of strange attractors (see Mora and Viana [2]).

A. Pumariño (✉) · J.A. Rodríguez · E. Vigil
Departamento de Matemáticas, Universidad de Oviedo, Calvo Sotelo s/n, 33007 Oviedo, Spain
e-mail: apv@uniovi.es; jarodriguez@uniovi.es; vigilkike@gmail.com

J.C. Tatjer
Departamento de Matemàtica Aplicada i Anàlisi, Universitat de Barcelona, Gran Via 585, 08007 Barcelona, Spain
e-mail: jcarles@maia.ub.es

S. Ibáñez et al. (eds.), *Progress and Challenges in Dynamical Systems*,
Springer Proceedings in Mathematics & Statistics 54,
DOI 10.1007/978-3-642-38830-9_22,

Suppose that $f_{a,b} : \mathbb{R}^3 \to \mathbb{R}^3$ is a two-parametric family of three dimensional diffeomorphisms, having a dissipative saddle fixed point $p = p(a, b)$ for all $a, b \in \mathbb{R}$. If the eigenvalues of p are real and the unstable invariant manifold of p is two-dimensional, the return map $f_{a,b}^n$ associated to a homoclinic bifurcation of codimension two (called generalized homoclinic tangency) can be approximated for n large, after an n-dependent change of variables and parameters, by a two-dimensional non-invertible quadratic two-dimensional family $T_{a,b}$, independent of n. A study of this family shows that it has a very rich dynamics including the existence of several types of attractors: periodic orbits, invariant curves and strange attractors with one or two positive Lyapunov exponents. For $a = -4$ and $b = -2$ it is possible to prove that $T_{a,b}$ has a two-dimensional attractor with an absolutely continuous and ergodic invariant measure, and that it is conjugate to a non-invertible piecewise linear map (bidimensional tent map). In order to have a qualitative description of the dynamics of the family $T_{a,b}$, we define a one-parameter family of piecewise linear and continuous maps, that we call Expanding Baker Maps. The goal of this paper is to study the dynamics of the EBM and compare it with the quadratic map. We have that there are only two types of attractors: periodic orbits or attracting sets with two positive Lyapunov exponents that seem to be strange attractors. For values of the parameter in some interval $[c, d]$ there are only strange attractors. The evolution of these attractors is as follows: If we call t the parameter of the family, for $t = d$ we have a simply connected attractor. When the value of the parameter decreases, first one hole inside the attractor appears and after that, the attractor is divided in eight pieces. This phenomenon seems to repeat again an again, in the sense that each piece is divided in several pieces. We have also identify some of this behaviours in the original quadratic map $T_{a,b}$.

The paper is organized as follows: in Sect. 2 we recall the concept of limit return map and explain how this map is in the case of a type of codimension-two homoclinic tangency called generalized homoclinic tangency. Moreover we give some of the principal properties of the limit return map. In Sect. 3 we construct the piecewise linear model of the limit return map and study the different kinds of attractors that can appear. Finally, we identify in the quadratic limit return map some attractors which the same behaviour as that of the piecewise linear map. We finish the paper with a section of conclusions and open questions.

2 Generalized Homoclinic Tangencies and Return Maps

In this section we will recall the definition of limit return map, generalized homoclinic tangency and its associated limit return map. Let us recover the definition of limit return map following Tatjer [7].

2.1 Limit Return Map

This concept is related to a homoclinic bifurcation of a dissipative fixed point of a diffeomorphism, that is a fixed point such that the product of its associated eigenvalues is less than one in absolute value.

Definition 1. Let $\{f_a\}_{a\in V}$ be a smooth family of diffeomorphisms in some m-dimensional manifold M, depending on a parameter $a \in V \subset \mathbb{R}^k$, V being an open subset. Suppose that for $a = a_0$ there exists a homoclinic orbit O_0 of some dissipative fixed point p_0 of f_{a_0}. We say that the family $\{f_a\}_{a\in V}$ has a family of **limit return maps** associated to the homoclinic orbit O_0, in the C^l topology, if there exists a point q of the homoclinic orbit and a natural number N, such that for any positive integer $n \geq N$ there exist reparametrizations $a = M_n(\tilde{a})$ of the a variable and $\tilde{a}$-dependent coordinate transformations $x = \Psi_{n,\tilde{a}}(\tilde{x})$ satisfying the following properties:

1. For each compact set K in the $(\tilde{a}, \tilde{x})$ space the images of K under the maps

$$(\tilde{a}, \tilde{x}) \to \left(M_n(\tilde{a}), \Psi_{n,\tilde{a}}(\tilde{x})\right)$$

   converge, for $n \to \infty$, in the $(\tilde{a}, \tilde{x})$ space, to (a_0, q).
2. The domains of the maps

$$(\tilde{a}, \tilde{x}) \to \left(\tilde{a}, \left(\Psi_{n,\tilde{a}}^{-1} \circ f_{M_n(\tilde{a})}^n \circ \Psi_{n,\tilde{a}}\right)(\tilde{x})\right)$$

   converge, for $n \to \infty$, to $\mathbb{R}^{m+k}$, and the maps converge, in the C^l topology, to some map of the form

$$(\tilde{a}, \tilde{x}) \to \left(\tilde{a}, \tilde{f}_{\tilde{a}}(\tilde{x})\right).$$

In this case, we say that $\left\{\tilde{f}_{\tilde{a}}\right\}_{\tilde{a}\in\mathbb{R}^k}$ is a family of limit return maps associated to the homoclinic orbit O_0.

The existence of a family $\left\{\tilde{f}_{\tilde{a}}\right\}_{\tilde{a}\in\mathbb{R}^k}$ of limit return maps means that, up to a change of coordinates, the dynamics (in a neighbourhood of some homoclinic point) of a sufficiently large power of f_a looks like the dynamics of some $\tilde{f}_{\tilde{a}}$. The main advantage to work with a family of limit return maps is that it is valid for generic situations: the same family of limit return maps "represents" a generic set of families of diffeomorphisms $\{f_a\}_{a\in V}$ having homoclinic tangencies unfolding generically.

For generic one-parameter families of diffeomorphisms on surfaces unfolding a homoclinic tangency, i.e., when $k = 1$ and $m = 2$, it can be shown that the family of "bidimensional" limit return maps $\left\{\tilde{f}_{\tilde{a}}\right\}_{\tilde{a}\in\mathbb{R}}$ is given by

$$\tilde{f}_{\tilde{a}}(\tilde{x}_1, \tilde{x}_2) = \left(1 - \tilde{a}\tilde{x}_1^2, 0\right) \tag{1}$$

(see [2] and [3]). Therefore, these limit return maps essentially behave as the one-dimensional logistic family $Q_a(x) = 1 - ax^2$. Hence, a new advantage arises when a family of limit return maps is obtained: while the original family of diffeomorphisms is defined on a bidimensional space, the family of limit return maps is essentially defined in a one-dimensional domain. The family given at (1) has played a very important role for understanding the dynamics associated to the unfolding of homoclinic tangencies in dimension two, see for instance [2] and [8].

The same family of limit return maps (1) works for generic one-parameter families of diffeomorphisms on an m-dimensional manifold when $\dim(W^u(p_0)) = 1$ and p_0 is sectionally dissipative: the eigenvalues $\lambda_1, \ldots, \lambda_m$ of $Df_{a_0}(p_0)$ satisfy $|\lambda_1| \leq \ldots \leq |\lambda_{m-1}| < 1 < |\lambda_m|$ and $|\lambda_{m-1}\lambda_m| < 1$. In the sectionally dissipative case, these limit return maps were already used to prove the coexistence of infinitely many sinks, see [4], and the existence of persistent strange attractors, see [10].

2.2 Generalized Homoclinic Tangencies

We have seen in the previous cases that the limit return map was always a one dimensional map. The explanation of this behaviour is that the fixed point is sectionally dissipative. However there are cases (for dimension greater than or equal to three) for which the limit return map is essentially a two-dimensional non-invertible map. Let us introduce an important case.

Let us consider a two-parameter family $\{f_{a,b}\}_{a,b}$ of three-dimensional diffeomorphisms having a hyperbolic saddle fixed point p_0 for $(a,b) = (0,0)$ with real eigenvalues λ_1, λ_2 and λ_3 satisfying the following properties (we refer the reader to [7] for the definition of generalized homoclinic tangency and the statement of the linearization assumption):

1. The eigenvalues satisfy $0 < |\lambda_1| < 1 < |\lambda_2| < |\lambda_3|$. We remark that from this assumption the corresponding fixed point is never sectionally dissipative.
2. The invariant manifolds of p_0 have a generalized homoclinic tangency which unfolds generically (we only remark here that in the set of two-parameter families of three-dimensional diffeomorphisms unfolding homoclinic tangencies those ones unfolding a **generalized** homoclinic tangency are generic).
3. The family $\{f_{a,b}\}_{a,b}$ satisfies the linearization assumption (generic condition for families of diffeomorphisms having saddle fixed points).

In [7] (see Theorem 1) it is proved that the corresponding family of limit return maps is given by

$$\tilde{f}_{\tilde{a},\tilde{b}}(\tilde{x},\tilde{y},\tilde{z}) = \left(\tilde{z}, \tilde{a} + \tilde{b}\tilde{y} + \tilde{z}^2, \tilde{y}\right). \tag{2}$$

Let us point out that, for each $\left(\tilde{a}, \tilde{b}\right) \in \mathbb{R}^2$, every point in $\mathbb{R}^3$ "falls" by one iteration of the map $\tilde{f}_{\tilde{a},\tilde{b}}$ into the surface

$$C_{\tilde{a},\tilde{b}} = \left\{(\tilde{x}, \tilde{y}, \tilde{z}) : \tilde{y} = \tilde{a} + \tilde{b}\tilde{z} + \tilde{x}^2\right\}.$$

Hence, $C_{\tilde{a},\tilde{b}}$ is invariant by $\tilde{f}_{\tilde{a},\tilde{b}}$ and it is enough to study the dynamics of $\tilde{f}_{\tilde{a},\tilde{b}}$ on $C_{\tilde{a},\tilde{b}}$. It is not difficult to see that the map restricted to $C_{\tilde{a},\tilde{b}}$ is conjugate to the family of bidimensional endomorphisms defined on $\mathbb{R}^2$ by

$$T_{a,b}(x, y) = \left(a + y^2, x + by\right), \tag{3}$$

where we have written, in order to avoid excessive notation, $a = \tilde{a}$ and $b = \tilde{b}$.

Remark. There is another case of generalized homoclinic tangency when the unstable invariant manifold of the fixed point is one-dimensional but the fixed point is not sectionally dissipative (see [1, 7]).

2.3 An Overview of the Family $T_{a,b}$

In spite of its simplicity, the family $T_{a,b}$ has a very interesting dynamical behaviour. We can find several kinds of attractors: periodic points, invariant circles and strange attractors with one or two positive Lyapunov exponents. This map has been extensively studied in [5, 6]. We can see such complexity in Fig. 1. In this figure, we show a region $B \subset \mathbb{R}^2$ of the parameter plane for which the map $T_{a,b}$ has an invariant domain. Moreover, we also distinguish between four subdomains according to the following criterion: parameters for which the attractor reduces to a periodic point (the region in pale grey or blue in the electronic version of the paper); parameters for which one attractor presents a zero Lyapunov exponent and therefore we expect that the attractor becomes a finite union of closed curves (the region in intermediate grey or green in the electronic version). Let us observe that these two regions are clearly separated by a segment which matches with a Hopf bifurcation line. Moreover, the two endpoints of this Hopf bifurcation line correspond to codimension-two bifurcations: Bogdanov-Takens bifurcation for $(a, b) = (\frac{1}{4}, 2)$ and a 1:2 resonance for $(a, b) = (-\frac{7}{4}, -2)$. The region in dark grey (or red in the electronic version of the paper) corresponds to values of the parameter for which the sum and the product of the two Lyapunov exponents of an attractor is negative (one-dimensional strange attractors) and finally, the region in black represents those parameters for which the sum of the Lyapunov exponents of an attractor is positive (two-dimensional strange attractors).

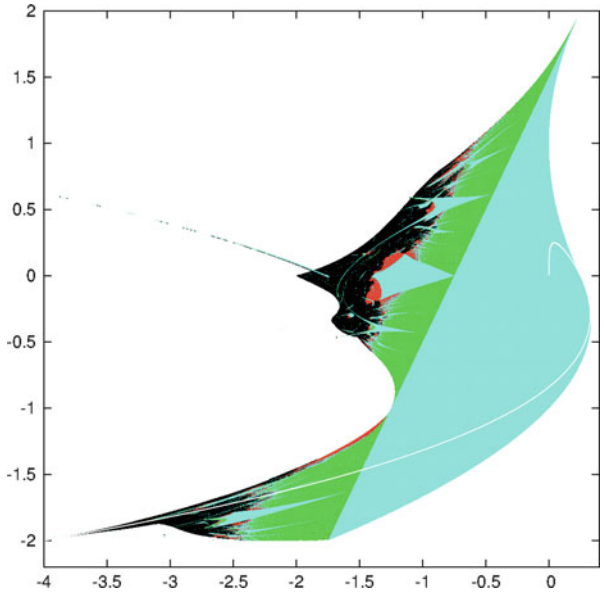

Fig. 1 Region of parameters a, b for which there are attractors

We observe, moreover, that there exists a curve $G \subset \mathbb{R}^2$ such that for $(a, b) \in G$, the map $T^2_{a,b}$ has an invariant line. This curve ends at $(-4, -2)$ and it is drawn in white. We can parametrize this curve as

$$G = \{(a(t), b(t)) \ : \ t \in [0, 2]\},$$

where

$$(a(t), b(t)) = \left(-\frac{1}{4}t^3(t^3 - 2t^2 + 2t - 2), -t^2 + t\right).$$

The invariant line is

$$L^1 = L^1(t) = \left\{(x, y) \in \mathbb{R}^2 : \ x = A + By; \ A = \frac{1}{2}\left(t - t^2\right)t^2; \ B = t^2\right\} \quad . \tag{4}$$

2.4 The Curve of Parameters $(a(t), b(t))$

Now we have a new family of maps depending on the parameter t. Let us suppose that $(a, b) = (a(t), b(t)) \in G$. The two fixed points of $T_{a,b}$ are

$$P_{a,b} = ((1 - b)y_+, y_+), \qquad \tilde{P}_{a,b} = ((1 - b)y_-, y_-), \tag{5}$$

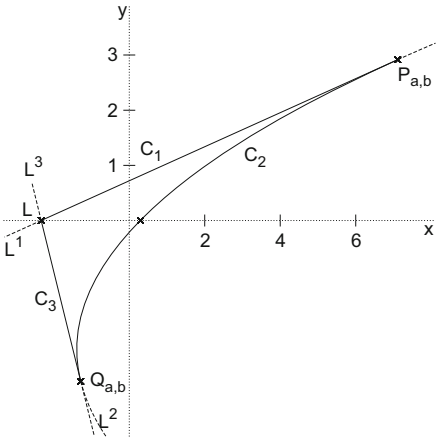

Fig. 2 The shape of R_t, for $t = 1.8$

where

$$y_{\pm} = \frac{1 - b \pm \sqrt{(b-1)^2 - 4a}}{2}.$$

The invariant line L^1, see (4), contains the fixed point $P_{a,b}$.

For every t, let us denote by $C_1 = C_1(t)$ the segment of L^1 joining $P_{a,b}$ with the point $L = (A, 0)$, see (4) for the definition of $A = A(t)$. One can show that, taking the parabola

$$L^2 = L^2(t) = \left\{ (x, y) \in \mathbb{R}^2 : x = \left(\frac{y - A}{b + B} \right)^2 + a \right\},$$

then L^2 contains $P_{a,b}$ and $T_{a,b}(C_1) \subset L^2$. On the other hand, if $Q_{a,b} = Q_{a,b}(t)$ is the unique point different from $P_{a,b}$ satisfying $T_{a,b}(Q_{a,b}) = P_{a,b}$, then $Q_{a,b}$ belongs to L^2 and, denoting by $C_2 = C_2(t)$ the arcs on L^2 joining $Q_{a,b}$ with $P_{a,b}$ then $T_{a,b}(C_2) \subset L^1$.

Finally, denoting by $C_3 = C_3(t)$ the segment on

$$L^3 = L^3(t) = \left\{ (x, y) \in \mathbb{R}^2 : x = A - (2b + B)\, y \right\}$$

joining L with $Q_{a,b}$, then $T_{a,b}(C_3) \subset L^2$.

For every $(a(t), b(t)) \in G$, let us denote by R_t the bounded set limited by the arcs C_1, C_2 and C_3. Then, one may check that $T_{a,b}(R_t) \subset R_t$, for every $t \in (0, 2]$. In fact, for $t = 2$, or $(a, b) = (-4, -2)$, one has $T_{-4,-2}(R_2) = R_2$. After this limit situation there always exist critical points inside R_t whose orbits leave the domain R_t, which is no longer invariant. This is also the behaviour of the critical point of the quadratic one-dimensional family $Q_a(x) = 1 - ax^2$ for values of the parameter greater than 2. In Fig. 2, we show the region R_t for $t = 1.8$ and we also remark that,

at least for $t \in (0, 2]$, the fixed point, $\tilde{P}_{a,b}$, given in (5) belongs to the interior of R_t, while the other fixed point, $P_{a,b}$, stays at the boundary of R_t.

The case $t = 2$ ($a = -4$, $b = -2$) is specially interesting. Indeed, it can be proved that (see [5]):

1. $T_{-4,-2}$ restricted to R_2 is topologically conjugate to the what we call *bidimensional tent map*:

$$F(u, v) = \begin{cases} (u + v, u - v), & \text{if } u + v \leq 1 \\ (2 - (u + v), u - v) & \text{if } u + v \geq 1. \end{cases}$$

   on the triangle $T_0 = \{(u, v) : 0 \leq u \leq 1, 0 \leq v \leq u\}$.
2. $T_{-4,-2}$ restricted to R_2 is topologically conjugate to the restriction of the shift to a suitable subset of the space of sequences with two symbols.
3. $T_{-4,-2}$ has an absolutely continuous and ergodic measure with support on R_2.
4. For almost all $x \in R_2$, the Lyapunov exponent is positive (and equal to $\frac{1}{2} \log 2$), in the direction of all non-zero vector.

3 A Simplified Model of the 2D Quadratic Limit Map

The goal of this section is to simplify the map (3) in order to obtain some information about its behaviour. As in the logistic map, one interesting problem is to know the nature and the abundance of strange attractors. Unlike the case of the logistic family, we can have strange attractors with two positive Lyapunov exponents, as we have seen. However, except for the case of $(a, b) = (-4, -2)$ and other trivial cases when $b = 0$, it is not known if there are more values of the parameters for which such attractors exist and which is the measure of the corresponding subset of parameters. However, numerical explorations suggest that the set of values of parameters for which strange attractors with two positive Lyapunov exponents seems to have positive (and not very small) measure. As it can be done for the logistic map, we can replace our family of maps by a suitable family of piecewise linear maps, which will preserve some of the characteristics of the original family. To begin with the simplest case, we have consider the one-parameter family $T_{a(t),b(t)}$. In the first place, we have the following proposition, in which we obtain a family of maps conjugate to the family $T_{a(t),b(t)}$, that in certain sense is closer to be piecewise linear:

Proposition 1. *For all $t \in [1, 2]$ there exists a homeomorphism $\Gamma_t : R_t \to T_0$ such that $\tilde{F}_t = \Gamma_t \circ T_{a(t),b(t)} \circ \Gamma_t^{-1}$, defined on T_0 satisfies:*

1. $\tilde{F}_2 = F$,
2. $\tilde{F}_t(T_0) \subset T_0$,
3. *The critical set of $\tilde{F}_t$ is* $\mathbf{c} = T_0 \cap \{(u, v) \in \mathbb{R}^2 : u + v = 1\}$.

4. $\tilde{F}_t(\mathbf{c}) = \overline{UT}$, *where* $\overline{UT}$, *is a segment with endpoints*

$$T = \frac{1}{\pi}(\arccos(1-t), \arccos(1-t)), \qquad U = \frac{1}{\pi}(\arccos(1-t), 0).$$

5. *Let* $P = (0,0)$, $Q = (1,1)$, $R = (1,0)$ *be the vertices of the triangle* $T_0 = \widehat{PQR}$ *and* $S = (1/2, 1/2)$. *Then* $\tilde{F}_t(\widehat{PRS}) = \tilde{F}_t(\widehat{QRS}) = \widehat{PTU}$, *and* $\tilde{F}_t$ *restricted to* $\widehat{PRS}$ *and* $\widehat{QRS}$ *is a homeomorphism.*

Proof. First, we define the homeomorphism Γ_t: When $t = 2$, $\Gamma_2 : R_2 \to \mathbb{R}^2$ is defined by

$$\Gamma_2(x,y) = \frac{1}{\pi}\left(\arccos\left(\frac{y - \sqrt{y^2+8y-4x}}{4}\right), \arccos\left(\frac{y + \sqrt{y^2+8y-4x}}{4}\right)\right).$$

In general, for $t \in [1,2]$:

$$\Gamma_t = \Gamma_2 \circ \Gamma_{1,t},$$

where $\Gamma_{1,t} : \mathbb{R}^2 \to \mathbb{R}^2$, is defined by

$$\Gamma_{1,t}(x,y) = \left(\frac{16}{t^4}x + \frac{16(2-t)}{t^3}y + 4 - \frac{8}{t}, \frac{8}{t^3}y\right).$$

Now we have:

1. It is a result proved in [5].
2. It is true since $T_{a(t),b(t)}(R_t) \subset R_t$, $\Gamma_{1,t}(R_t) = R_2$ and $\Gamma_2(R_2) = T_0$, (see again [5]).
3. As $\{(x,y) \mid y = 0\} \cap R_t$ is the critical line of $\Gamma_{1,t} \circ T_{a(t),b(t)} \circ \Gamma_{1,t}^{-1}$ and

$$\Gamma_2^{-1}(\{(x,y) \mid y = 0\} = \{(u,v) \mid u + v = 1\},$$

   then the result is true.
4. A straightforward calculation yields

$$\tilde{F}_t(u, 1-u) = \left(\frac{1}{\pi}\arccos(1-t), \frac{1}{\pi}\arccos(1 - t\cos^2(\pi u))\right),$$

   which implies the result.
5. It is an easy consequence of the previous results. □

In Fig. 3 we have drawn the triangle T_0, some points and their images and the critical line and its image for some $1 < t < 2$. Here c is the critical line and $\tilde{F}_t(c_1) \subset c_2$, $\tilde{F}_t(c_2) \subset c_1$, $\tilde{F}_t(c_3) \subset c_2$, $\tilde{F}_t(c) = d$, $\tilde{F}_t(P) = P$, $\tilde{F}_t(S) = U$, $\tilde{F}_t(Q) = P$, $\tilde{F}_t(R) = T$.

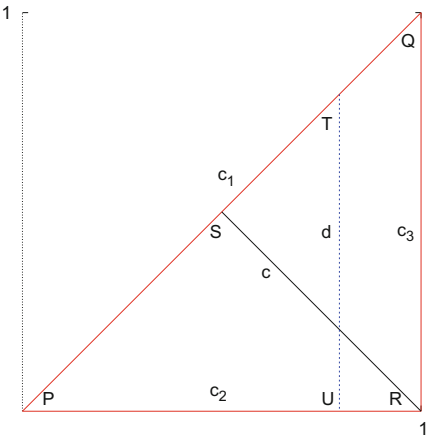

Fig. 3 The *triangle* T_0 and some points and lines and their images by $\tilde{F}_t$. See explanation in the text

To find a simplified model $\{G_t\}$ of the previous family, we impose the following conditions:

1. G_t is piecewise linear.
2. The discontinuities of the differential of G_t are in the straight line $u + v = 1$.
3. $\tilde{G}_t(P) = P$, $\tilde{G}_t(S) = U$, $\tilde{G}_t(Q) = P$, $\tilde{G}_t(R) = T$, where $P = (0, 0)$, $Q = (1, 1)$, $R = (1, 0)$, $S = (1/2, 1/2)$, $T = (t, t)$, $U = (t, 0)$.

Then it is easy to prove the following proposition:

Proposition 2. *For any t, there is one and only one map G_t satisfying the previous conditions. This map is defined by*

$$G_t(u, v) = (t(1 - |1 - u - v|), t(u - v)).$$

Moreover, $\tilde{G}_t(T_0) \subset T_0$, and for $t = 1$ we recover the bidimensional tent map.

We call the map G_t a Expanding Baker Map *(EBM).*

By simplicity reasons, we will use another (conjugate) form of the EBM: if we perform the change of coordinates $\tilde{u} = u + v$, $\tilde{v} = u - v$, and call again u, v the new coordinates, we have a map $H_t = A_t \circ \mathscr{S}$, where

$$\mathscr{S}(u, v) = \begin{cases} (u, v) & \text{if } (x, y) \in T_1 \\ (2 - u, v) & \text{if } (x, y) \in T_2 \end{cases},$$

$$A_t = \begin{pmatrix} t & t \\ t & -t \end{pmatrix}.$$

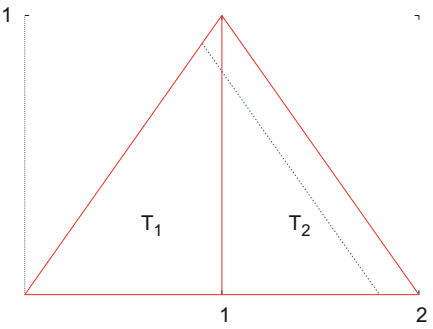

Fig. 4 The expanding baker map H_t in the new coordinates

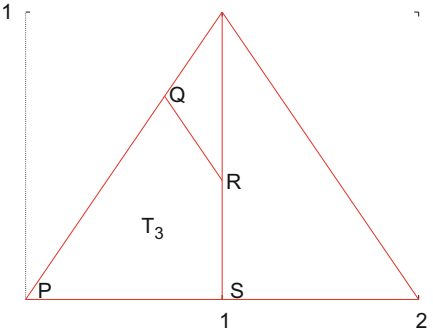

Fig. 5 The case $t = 1/\sqrt{2}$. We have $H_t(P) = P$, $H_t(Q) = S$, $H_t(R) = R$, and $H_t(S) = Q$

Then we have that $H_t|T_1$ and $H_t|T_2$ are invertible maps, the critical line is contained in $u = 1$ and the image of the critical line is a segment in a line contained in a straight line parallel to $u + v = 2$ and contained in the triangle $T = T_1 \cup T_2$. See Fig. 4.

Now we can give some preliminary properties of the EBM:

Proposition 3. *Suppose that* $0 \leq t \leq 1$. *Then, the map* H_t *has the following properties:*

1. *The triangle* $T_1 \cup T_2$ *is invariant.*
2. *If* $0 \leq t < 1/\sqrt{2}$, $(0, 0)$ *is an attracting (node) fixed point. It is a global attractor in* $T_1 \cup T_2$
3. *If* $t > 1/\sqrt{2}$, $(0, 0)$ *is a repelling node and* $\mathscr{P} = \left(\frac{2t(2t+1)}{2t^2+2t+1}, \frac{2t}{2t^2+2t+1}\right)$ *is a repelling focus.*
4. *The Lyapunov exponent of any point in* T *which is not a preimage of the straight line* $u = 1$ *in any non-zero direction is* $\log(\sqrt{2}t)$.
5. *All the periodic orbits with no critical points are repelling if* $t > 1/\sqrt{2}$.
6. *If* $t = 1/\sqrt{2}$ *then there is a region* T_3 *such that* $H_t^2|T_3$ *is the identity. Moreover,* $H_t^2(T) = T_3$, *where* T_3 *is the bounded set and its boundary is made of the union of the segments* $\overline{PQ}$, $\overline{QR}$, $\overline{RS}$ *and* $\overline{SP}$ *(see Fig. 5).*

The proof of the proposition is elementary.

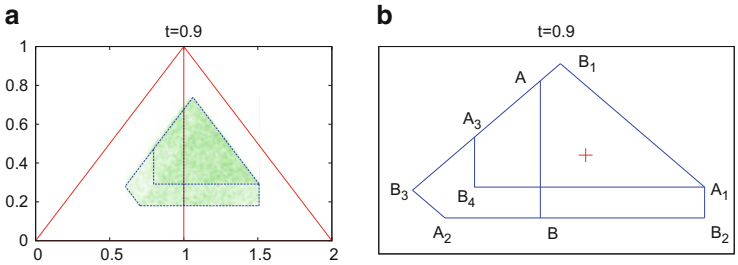

Fig. 6 (**a**) A 1-piece strange attractor for $t = 0.9$ (case 1). We have also drawn the invariant *triangle* T and the critical line. The lines enclosing the attractor are images of the critical line. (**b**) A magnification of the previous figure. See explanations in the text

3.1 Numerical Results

We have performed some computations in order to find attractors of the EBM, and compare them with the attractors displayed by the original quadratic map. We recall that there are no attracting periodic orbits if $t > 1/\sqrt{2} \approx 0.7071068$, and all the attractors have two positive Lyapunov exponents. We will assume that these attractors are strange, in the sense that they have a dense orbit, although we have not a proof of this fact yet. The results are the following:

1. When $1/2^{1/3} < t \leq 1$ there is a 1-piece simply connected strange attractor. In Fig. 6, we have and example of this attractor for $t = 0.9$: In (a) we have drawn the attractor inside the invariant triangle. In (b) we have drawn some images of the segment $\overline{AB}$ in the critical line. There, $A_i = H_t^i(A)$ and $B_i = H_t^i(B)$. If R is the strange attractor, R_1 is the region with boundary the union of the segments $\overline{AB}$, $\overline{BA_2}$, $\overline{A_2B_3}$ and $\overline{B_3A}$, R_2 is the region with boundary the union of the segments $\overline{AB}$, $\overline{BB_2}$, $\overline{B_2A_1}$, $\overline{A_1B_1}$ and $\overline{B_1A}$, then $R = R_1 \cup R_2$, $H_t(R_1) = S$ and $H_t(R_2) = R$, where S is the region with boundary the union of the segments $\overline{A_1B_4}$, $\overline{B_4A_3}$, $\overline{A_3B_1}$ and $\overline{B_1A_1}$. Moreover, H_t restricted to R_1 and R_2 is invertible. We note that the repelling focus (represented by a cross) belongs to the interior of S. Finally, the point A is $(1, 1-4t^2+4t^3)$, intersection of the critical line and its third image, and B is the point $(1, 2t - 2t^2)$, intersection of the critical line and its second image.
2. When $1/4^{1/5} < t < 1/2^{1/3}$ there is 1-piece strange attractor with a hole and this hole disappears when $t = 1/2^{1/3}$ because the repelling focus belongs to the fourth image of the critical line. In Fig. 7 we see the hole surrounding the repelling focus. We observe that in this case the fixed point does not belong to the region S. This implies that we have a smaller invariant set than before, because we can remove a small neighbourhood of the repelling focus.

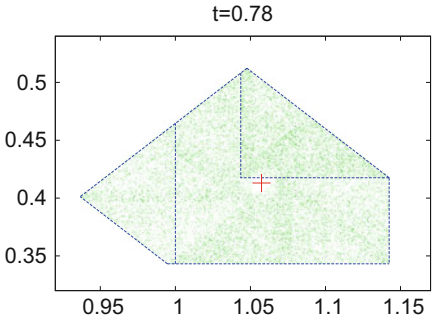

Fig. 7 A one-piece strange attractor with a hole for $t = 0.78$ (case 2)

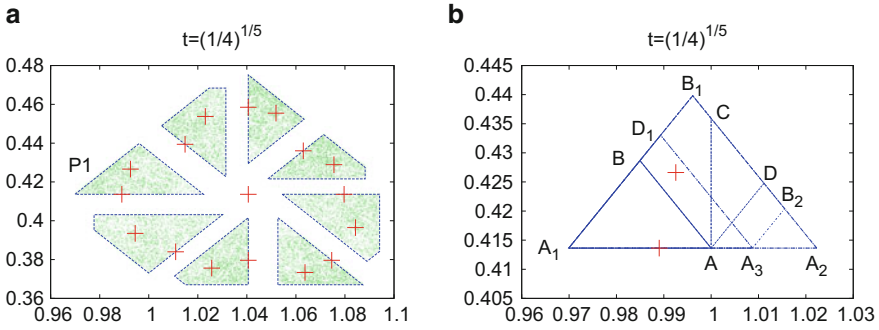

Fig. 8 (**a**) A 8-pieces strange attractor for $t = 1/4^{1/5}$. (**b**) Magnification of the piece P1. See explanations in the text

3. When $0.723 \approx t_0 < t < 1/4^{1/5}$ we have a 8-pieces strange attractor that merges to a one piece for $t = 1/4^{1/5}$ due to the existence of a point c_0 in the critical line such that $H_t^6(c_0)$ is a 8-periodic point and it belongs to the border of one of the pieces of the attractor. In Fig. 8a we have drawn for $t = 1/4^{1/5}$ the attractor and images of points of the critical line. Some of these images form the boundary of the attractor. Moreover, in each piece of the attractor there are two periodic points of period 8 and in the center a fixed point (represented by crosses). In Fig. 8b we have a magnification of the figure (a), where the boundary of the one of the 8 pieces of the attractor (P1) is drawn. We can split the region P1 in four regions: R_1 with boundary the triangle with vertices A_1, A and B, R_2 a quadrilateral with vertices A, B, B_1 and C, R_3 a triangle with vertices A, C and D, and R_4 a triangle with vertices A, D and A_2. In this four regions the map H_t^8 is invertible and $H_t^8(R_1) = R_1 \cup R_2 \cup R_3 \cup R_4$, $H_t^8(R_2)$ is the quadrilateral determined by the vertices A_1, A_3 B_2 and B_1, $H_t^8(R_3)$ is the triangle determined by the vertices A_1, D_1 and A_3, and $H_t^8(R_4) = H_t^8(R_3)$. Moreover, $H_t^8(A) = A_1$, $H_t^8(A_i) = A_{i+1}$, $i = 1, 2$, $H_t^8(B) = B_1$, $H_t^8(B_1) = B_2$ $H_t^8(C) = A_3$ and $H_t^8(D) = D_1$, and the

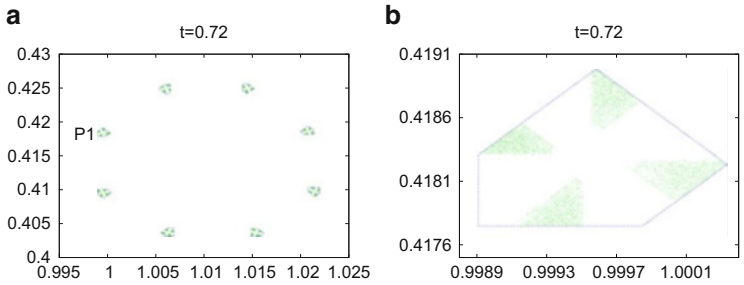

Fig. 9 (**a**) A 32-pieces (4×8) strange attractor for $t = 0.72$. The four pieces in the set P1 have been magnified in (**b**). We have also drawn the images of segments of the critical line which form the boundary of the previous 8-pieces strange attractor

crosses inside the region R_2 and in the segment $\overline{AA_1}$ are repelling 8-periodic points. For values of t larger than $1/4^{1/5}$, the periodic point enters inside the region, and this produces that all the pieces of the attractor merge into one piece with a hole.

4. When $0.711 \approx t_1 < t < t_0$ there is a 4×8-pieces strange attractor. This means that each piece of the previous attractor is divided in four pieces. See Fig. 9.
5. For values below t_1 it seems that this process of division of the attractor continues more and more. It begins with a $4 \times 4 \times 8$ pieces, and each piece is divided again and again. We recall that this behaviour has to finish for $t = 1/\sqrt{2} \approx 0.7071$.

3.2 The Quadratic Map Revisited

The behaviour of the quadratic non-invertible map is more involved than the previous map because there are more kinds of attractors, and they can coexist for the same value of the parameter. However, we can find easily examples of two-dimensional strange attractors (with two positive Lyapunov exponents) with the same behaviour for the piecewise linear and the quadratic map. For example, if we consider the map $T_{a(t),b(t)}$ we have for $t = 2$ a one-piece strange attractor, for $t = 1.9$ one-piece strange attractor with a hole, for $t = 1.8896$ a 8-pieces strange attractor and for $t = 1.88817$ a 8-pieces strange attractor with a hole. For small values of t the strange attractor does not exist and after some transformations, it becomes a 8-periodic attracting invariant circle. Finally, due to a Hopf bifurcation, this periodic invariant circle transformed into an attracting fixed point. In Fig. 10, we have some of these attractors.

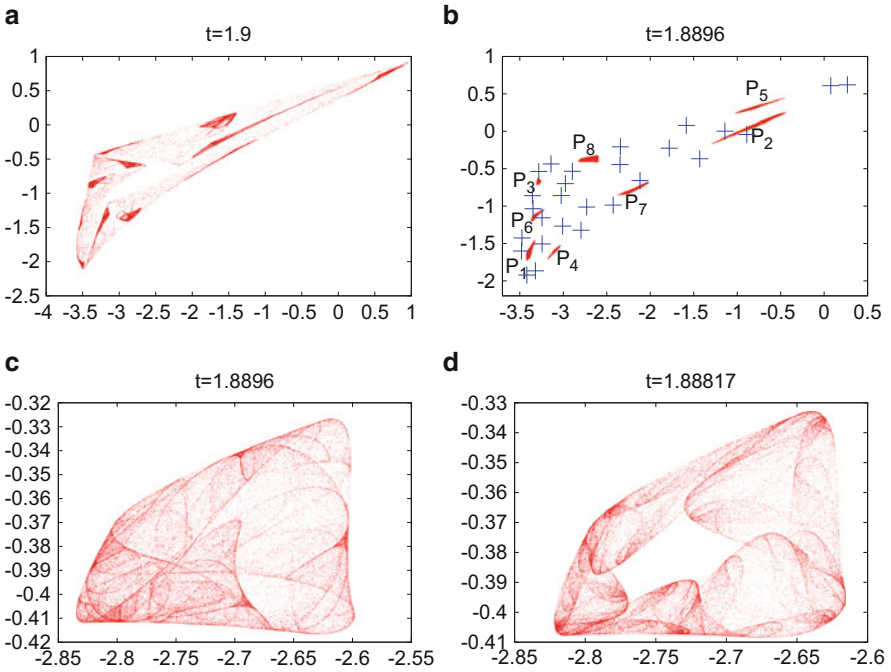

Fig. 10 Several attractors for the map $T_{a(t),b(t)}$: (**a**) A 1-piece attractor with a hole. (**b**) A 8-pieces strange attractor. Here, $T_{a,b}(P_i) = P_{i+1}$. There is also another attractor: a 27-periodic orbit. (**c**) Magnification of the piece P_8 of the previous attractor. (**d**) The same piece of the 8-pieces attractor of picture (**c**), but now with a hole

4 Conclusions and Open Questions

We have studied some properties of a piecewise linear one-parametric family of two-dimensional maps (that we call Expanding Baker Maps – EBM), which is a simplified model of limit return maps associated to some class of homoclinic bifurcations of two-parametric families of three-dimensional dissipative diffeomorphisms. We have observed that, if t is the parameter of the family of EBM, for $t = 1$ we have a one-piece strange attractor with two positive Lyapunov exponents. When t decreases first a hole appears inside the attractor and later the attractor is divided in several pieces, these pieces are divided again and so on. We think that some type of renormalization procedure could be used to explain this type of behaviour. The principal problem to implement this renormalization is that unlike the one-dimensional piecewise linear case, the iterates of EBM are not EBM. But it seems that we can include this family in a larger family more suitable for the renormalization. Other questions to clarify are if (as the numerical results seem to indicate) the basin of attraction of any attractor contains points of the critical line and if there is only one attractor for every EBM. On the other hand, as the maps

we consider are expanding, there exist finitely many invariant absolutely continuous ergodic invariant measures with an open basin (see [9]). We do not know, however, if there is a ergodic measure with support on the attractor in the cases we have studied except for the case $t = 1$.

Finally, it is important to stress that the type of attractors we have found for the EBM appear for the original limit return map, which gives more sense to the expression 'simplified model' for the EBM.

Acknowledgements This work has been supported by the MEC grants MTM2009-09723 and MTM2011-22956 and the CIRIT grant 2009 SGR 67.

References

1. Gonchenko, S.V., Gonchenko, V.S., Tatjer, J.C.: Bifurcations of three-dimensional diffeomorphisms with non-simple quadratic homoclinic tangencies and generalized Hénon maps. Regul. Chaotic Dyn. **12**, 233–266 (2007)
2. Mora, L., Viana, M.: Abundance of strange attractors. Acta Math. **171**, 1–71 (1993)
3. Palis, J., Takens, F.: Hyperbolicity and Sensitive Chaotic Dynamics at Homoclinic Bifurcations. Cambridge University Press, Cambridge (1993)
4. Palis, J., Viana M.: High dimension diffeomorphisms displaying infinitely many sinks. Ann. Math. **140**, 91–136 (1994)
5. Pumariño, A., Tatjer, J.C.: Dynamics near homoclinic bifurcations of three-dimensional dissipative diffeomorphisms. Nonlinearity **19**, 2833–2852 (2006)
6. Pumariño, A., Tatjer, J.C.: Attractors for return maps near homoclinic tangencies of three-dimensional dissipative diffeomorphisms. Discret. Contin. Dyn. Syst. Ser. B **8**, 971–1006 (2007)
7. Tatjer, J.C.: Three-dimensional dissipative diffeomorphisms with homoclinic tangencies. Ergod. Theory Dyn. Syst. **21**, 249–302 (2001)
8. Tatjer, J.C., Simó, C.: Basins of attraction near homoclinic tangencies. Ergod. Theory Dyn. Syst. **14**, 351–390 (1994)
9. Tsujii, M.: Absolutely continuous invariant measures for expanding piecewise linear maps. Invent. Math. **143**, 349–373 (2001)
10. Viana, M.: Strange attractors in higher dimensions. Bol. Soc. Bras. Mat. **24**, 13–62 (1993)

Practical Stability Domains Near $L_{4,5}$ in the Restricted Three-Body Problem: Some Preliminary Facts

C. Simó, P. Sousa-Silva, and M. Terra

Abstract We consider the problem of stability around the triangular libration points in the Restricted Three-Body Problem. The "local stability" is decided thanks to KAM theory and Nekhorosev-like estimates, as it is well known. The question addressed in this note is which is the extend of the domains of "practical stability".

1 Introduction: The Problem and Some Previous Results

We consider the Restricted Three-Body Problem (RTBP), see e.g. [19]. This is a good simple model for the motion of small bodies in the solar system under the action of Sun and Jupiter and also for the design of several space missions. It has fixed points in a rotating frame, the so-called libration points. Among them we are interested in the Lagrangian triangular points, corresponding to positions in the plane of motion of the two massive bodies, forming equilateral triangles with them.

It is known that for small mass ratios $\mu < \mu_1$ the Lagrangian triangular points are linearly stable. For the planar case nonlinear stability is proved except for a couple of values μ_2, μ_3, thanks to KAM theory (see [3, 9, 10]). In the spatial case it seems that there is no way to prevent from having Arnol'd diffusion [11]. Anyway, it is possible to prove some "practical or effective stability" in the sense that going away from the fixed point is extremely slow. Concretely, going from a distance $\delta_0 > 0$ from the fixed point (in the phase space) to a distance $\delta_1 > \delta_0$ requires a time $\mathcal{O}(\exp(a/\delta_1^b)), a, b > 0$. A big part of the dynamics occurs in tori of maximal

C. Simó (✉) · P. Sousa-Silva
Universitat de Barcelona, Gran Via 585, Barcelona, Spain
e-mail: carles@maia.ub.es; priandss@maia.ub.es

M. Terra
Instituto Tecnológico de Aeronáutica, São José dos Campos, SP, Brazil
e-mail: maisa@ita.br

S. Ibáñez et al. (eds.), *Progress and Challenges in Dynamical Systems*,
Springer Proceedings in Mathematics & Statistics 54,
DOI 10.1007/978-3-642-38830-9_23, © Springer-Verlag Berlin Heidelberg 2013

dimension and the diffusion between them is rather slow. See [5] and [14], where normal form methods and bounds on the remainder are used to obtain Nekhorosev-like estimates.

However, numerical evidence gives an indication that the domain of practical stability is large. Furthermore, in some parts, the boundaries of the domain are rather sharp. This is specially true for small mass ratios. This behaviour calls for an explanation.

In a real life problem, and even considering this simple model, we can ask: Why there exist Trojans so far away from the L_4, L_5 points of the Sun-Jupiter system?

The goal of this note is to present some preliminary facts addressed to solve the question. In Sect. 2 we consider the planar case. In Sect. 3 some properties of the 3D case are presented, while Sect. 4 is devoted to introduce the invariant manifolds which are responsible of the "quasi-confinement" of regions of non-negligible measure in the phase space. Section 5 ends with some conclusions and outlook.

Details on the many pending questions are the object of works in progress dealing with the planar case, the spatial case for small mass ratios and, finally, for larger mass ratios of astronomical/astrodynamical interest.

For concreteness we display here the equations and some basic things.

The RTBP studies the motion of a particle P_3 of negligible mass under the gravitational attraction of two massive bodies, P_1 and P_2, of respective masses m_1 and m_2, known as primaries or as primary and secondary. Without explicit mention in what follows (unless a different model is considered) we assume that the primaries move in a plane in circular orbits around the centre of masses. We can normalise $m_1 + m_2 = 1$ and $d(P_1, P_2) = 1$ and express the dynamics in a rotating frame (the so-called synodical frame) with unit angular velocity. The problem depends on a unique parameter $\mu = m_2$. Then the bodies P_1 and P_2 are kept fixed at $(\mu, 0, 0)$ and $(\mu - 1, 0, 0)$.

The equations of motion are

$$\ddot{x} - 2\dot{y} = \Omega_x, \quad \ddot{y} + 2\dot{x} = \Omega_y, \quad \ddot{z} = \Omega_z, \tag{1}$$

where $\Omega(x, y, z) = \frac{1}{2}(x^2+y^2)+\frac{1-\mu}{r_1}+\frac{\mu}{r_2}+\frac{\mu(1-\mu)}{2}$, being $r_1^2 = (x-\mu)^2+y^2+z^2$, $r_2^2 = (x+1-\mu)^2+y^2+z^2$. The function $J(x, y, z, \dot{x}, \dot{y}, \dot{z}) = 2\Omega(x, y, z) - (\dot{x}^2 + \dot{y}^2 + \dot{z}^2)$ is a first integral and its value is known as Jacobi constant. The related 5D energy manifolds are defined as

$$\mathcal{M}(\mu, C) = \left\{(x, y, z, \dot{x}, \dot{y}, \dot{z}) \in \mathbb{R}^6 | J(x, y, z, \dot{x}, \dot{y}, \dot{z}) = C\right\} \tag{2}$$

and their projections on the configuration space are known as Hill's regions, bounded by the zero velocity surfaces (ZVS) (the zero velocity curves, ZVC, in the planar case).

The problem has five equilibrium points:

- Three of them, collinear (or Eulerian) on the x-axis, $L_{1,2,3}$, of centre-centre-saddle type and, hence, they have a 4D centre manifold which contains the so-called horizontal and vertical Lyapunov orbits, halo orbits, invariant 2D tori and other periodic orbits, as well as chaotic regions.
- Two of them, triangular (or Lagrangian), $L_{4,5}$, at $x = \mu - 1/2$, $y = \pm\sqrt{3}/2$, $z = 0$. Let μ_j be the value of μ for which the ratio of frequencies in the plane, $\left[(1 \pm (1 - 27\mu(1-\mu))^{1/2})/2\right]^{1/2}$ is j. The points are totally elliptic for $0 < \mu < \mu_1 = (9 - \sqrt{69})/18$, while the 2:1, 3:1 resonances (leading to instability) show up for $\mu_2 = (45 - \sqrt{1833})/90$ and $\mu_3 = (15 - \sqrt{213})/30$. Associated to these frequencies there are short and long period periodic orbits. The vertical frequency, giving rise also to a vertical Lyapunov family of periodic orbits, is equal to 1.

2 The Planar Case

We consider first the planar case. Systematic simulations are done to try to identify the boundary of the domain of practical stability. To this end, we consider initial data with zero synodical velocity. Later on we shall discuss the reasons of this choice. We confine our attention to the domain around L_5, the one around L_4 being obtained from the reversibility of the RTBP. For preliminary results using rough methods we refer to [12].

The initial position of P_3 can be identified by two parameters, (α, ρ) as follows

$$x = \mu + (1 + \rho)\cos(2\pi\alpha), \quad y = (1 + \rho)\sin(2\pi\alpha). \tag{3}$$

The (α, ρ)-plane is discretised to a grid using steps 0.5×10^{-3} and 10^{-5}, respectively. Then we define a compact set K in the configuration space, typically excluding neighbourhoods of the primaries, points far away from the origin (e.g. at a distance > 1.5) and also points which come close to the domain that is related to L_4 (e.g., having $y < -0.6$ or $\alpha \in (3/5, 4/5)$).

To detect the practical stability domain we do:

(i) Every initial point in the grid is integrated at most up to a final time corresponding to a number of revolutions of the primaries, say 10^4, skipping it if it goes away from K before the final time. Pixels on the grid which subsist are marked with $+1$, otherwise with -1.

(ii) We introduce a new final time, e.g. 10^5 revolutions, and a "deepness index" d, e.g. $d = 5$. Let (i^*, j^*) be the indices of a pixel marked as $+1$. If there exist some point (i, j) in the grid marked as negative and such that

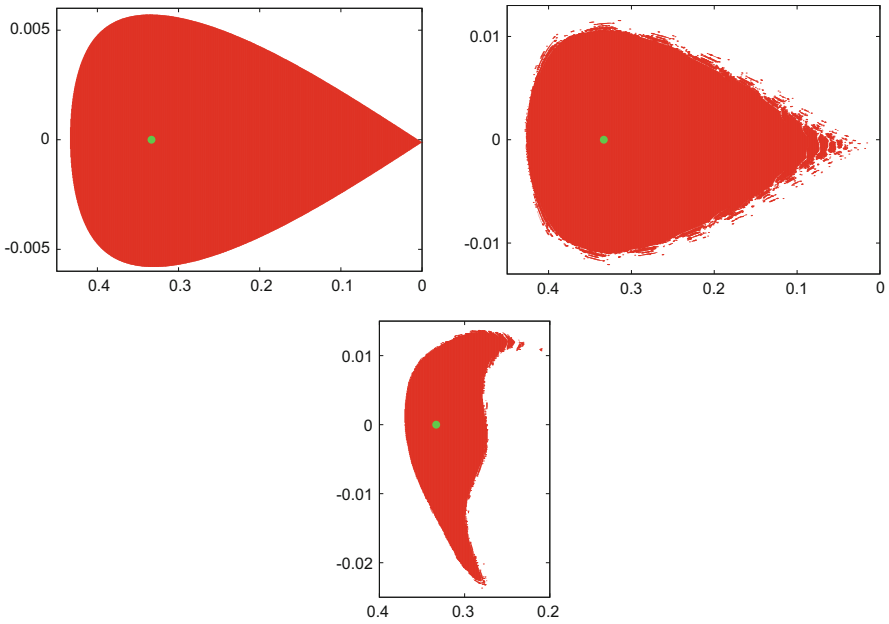

Fig. 1 Subsisting points around L_5 for $\mu = 0.0002$ and $\mu = \mu_{SJ}$ (*upper row*) and $\mu = \mu_{EM}$ (*lower row*) in the (α, ρ) coordinates. Plots in *red* online. See the text for details. The point marked inside the domain (in *green* online) shows the location of L_5

$\max\{|i - i^*|, |j - j^*|\} \leq d$, then the point is checked up to the new final time. If it remains in K up to the final time, it is marked as $+2$. Otherwise it is marked as -2. The grid is scanned once and again until no more changes are detected.

(iii) Again a new final time, e.g. 10^6 revolutions, is introduced and we proceed as in (ii), marking with $+3$ the subsisting points and -3 the escaping ones.

At the end, we consider the points with positive index as belonging to the domain of practical stability. This method combines a good determination of the domain with a reasonable CPU time using a cluster. In the spatial case, see Sect. 3, we proceed in a similar way for initial data in different levels of z, typically for values of z between 0 and 0.875 with step 0.005. The total number of "subsisting points" for different μ and different z computed up to now exceeds 10^9 and, among them, the ones checked up to 10^6 revolutions exceed 10^7.

Some results are shown in Fig. 1 for three different values of μ. The smallest one is 0.0002, close to the Titan-Saturn mass ratio, as representative of a small perturbation of the rotating two-body problem $\mu = 0$. The other two values correspond to the Sun-Jupiter and Earth-Moon cases, $\mu = \mu_{SJ} \approx 0.953881180363097 \times 10^{-3}$ and $\mu = \mu_{EM} \approx 0.0121506683$.

The changes from one case to another one are quite strong. For small μ, the boundary of the domain is quite sharp. For $\mu = \mu_{SJ}$, one can see many chains of

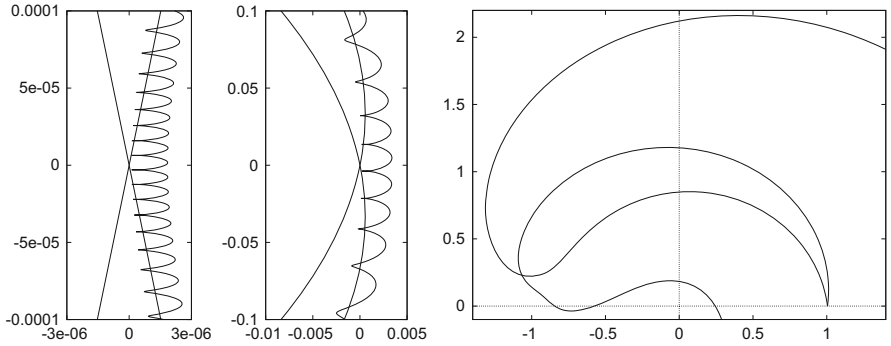

Fig. 2 *Left*: first return of the upper branch $W_{L_3}^{u,+}$ to the vicinity of L_3 for $\mu = 0.0002$. For completeness we also show the local branches of $W^{u,s}$. *Middle*: same for $\mu = \mu_{SJ}$. For better reference the plots have been done with respect to the location of L_3. Note the very different scales. *Right*: the case $\mu = \mu_{EM}$. The manifolds escape without returning near L_3

"islands" around the large central domain. In both cases the domain is reminiscent of the shape of the domain bounded by the ZVC of the L_3 point. The width of the domain in the ρ direction is also $\mathcal{O}(\mu^{1/2})$. Finally, in the $\mu = \mu_{EM}$ case, the situation is completely different: Even if it is large in the ρ direction, it is quite narrow in α and far away from L_3.

This suggests to have a look at the unstable/stable manifolds of L_3. We restrict our attention to the upper branches. For μ small and even in the μ_{SJ} case, they look similar to the ZVC on the level of $\Omega(L_3)$, but slightly outside the ZVC. One can see [1] and references therein for some plots. At a first sight it can seem that the upper branches $W_{L_3}^{u,+}$ and $W_{L_3}^{s,+}$ coincide (and the same for the lower ones $W_{L_3}^{u,-}$, $W_{L_3}^{s,-}$). This was the claim of an old conjecture by E. W. Brown, going back to 1911, disproved numerically by J. Henrard in [7]. The Fig. 2 shows a magnification of the first return of $W_{L_3}^{u,+}$ to the vicinity of L_3 for three values of μ. For $\mu = 0.0002$ and $\mu = \mu_{SJ}$, they are in some sense similar except for the scales. In contrast, in the Earth-Moon case the manifolds have a quite different behaviour.

A distinction between the μ small and the μ_{SJ} cases can be seen if the manifolds (e.g. $W_{L_3}^{u,+}$) are integrated for long time. In the μ_{SJ} case, assuming we set the time $t = 0$ at the first passage through $x = 0$, after a few millions of units of time the branch approaches the location of the secondary and after that, it shows a chaotic behaviour, with eventual escape. For μ up to a value near 0.0005, it seems that the manifold is confined to a narrow domain, slightly outside the ZVC on the level of $\Omega(L_3)$, both in the upper and lower parts, even for times up to $2\pi \times 10^9$. Of course, due to the lack of coincidence of the manifolds, in successive passages near L_3 coming, for instance, from the upper part, it can either return to the upper part or move to the lower one in a quasi-random way.

A natural way to clarify the situation is to look for some "splitting quantity", split(μ), to measure the distance between $W_{L_3}^{u,+}$ and $W_{L_3}^{s,+}$. It has been checked that

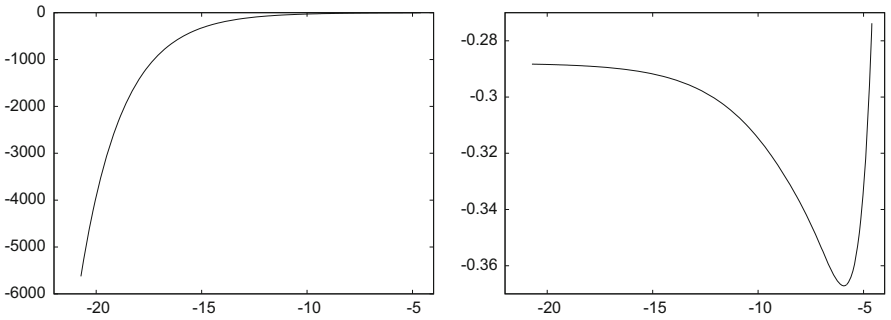

Fig. 3 Measures of the "splitting" between upper branches of the unstable and stable manifolds of L_3. *Left*: the logarithm of the splitting is plotted as a function of $\log(\mu)$. *Right*: a similar plot, but the logarithm of the splitting has been multiplied by $\lambda(\mu)$, the unstable eigenvalue at L_3. See the text for details

it is convenient to look at the distance in the phase space at the first passage through $r = (x^2 + y^2)^{1/2} = 1$ to the left of L_5. There it shows a smooth behaviour in μ. At other places, like passages through $\alpha = 1/4$ or $\alpha = 1/3$, inner parts, there is an oscillation superimposed to a smooth behaviour. The results can be seen in Fig. 3. On the left plot, $\log(\text{split}(\mu))$ is displayed as a function of $\log(\mu)$. As one could expect from averaging theory [13] or from upper bounds of splitting [4], the splitting has an exponential behaviour. Let $\lambda(\mu) = (21\mu/8)^{1/2} + \ldots$ be the unstable eigenvalue at L_3. Theoretical bounds of the splitting are of the form $\mathcal{O}(\exp(-c/\lambda))$ for some $c > 0$. The right part of Fig. 3 shows $\lambda(\mu) \times \log(\text{split}(\mu))$ as depending on $\log(\mu)$. One can clearly see the limit behaviour when $\mu \to 0$, which allows to guess (using different extrapolation tools) a value of $c \approx 0.2879793$.

Just to have a feeling of some values, we can mention that for $\mu = 10^{-k}, k = 5, \ldots, 9$ the values of $\text{split}(\mu)$ (showing only the first digits) are 1.923×10^{-26}, 1.393×10^{-73}, 7.692×10^{-247}, 5.267×10^{-775} and $1.797 \times 10^{-2,444}$, respectively. The computations have been done in a standard way: If the expected value of the splitting is of the order of 10^{-d} the computations have been done with $n = d + 100$ decimal digits (and with $d + 200$ as additional check). Then the local parametric expansions of the (analytical) invariant manifolds are obtained in a recurrent way to order n and some tests have been done on the value of the local parameter which gives a small enough remainder. To continue the manifold a Taylor method is used to integrate the equations in (1), also to order n and with local truncation error 10^{-n}. This gives a good combination of accuracy and CPU time. The implementation has been done using PARI [2].

From all the above considerations and checks we are allowed to assume that the reason leading to escape of an orbit of the domain K is the passage close to L_3 or, in fact, of its centre manifold $W^c_{L_3}$, following the "wrong side" of its unstable manifold $W^{u,-}(W^c_{L_3})$. Some preliminary results can already be found in [6]. As $W^c_{L_3}$ is foliated by planar Lyapunov periodic orbits (p.o.) around L_3, we have computed

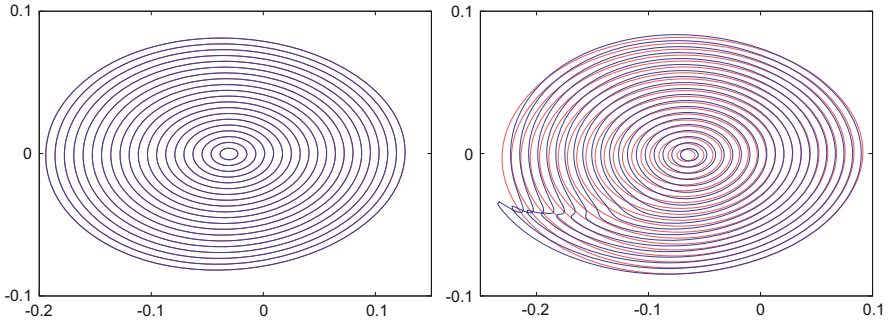

Fig. 4 Intersections of the upper branches of the unstable and stable manifolds of several periodic orbits in the *centre* manifold of L_3 with $x = 0$. *Left* and *right plots* show the cases $\mu = 0.0002$ and $\mu = \mu_{SJ}$ respectively. Intersections of the unstable (resp. stable) manifolds are shown in *light* (resp. *dark*) *grey*. They appear in *red* (resp. *blue*) online. See the text for details

these p.o. and its unstable/stable manifolds. These Lyapunov orbits can be indexed by the value of the Jacobi constant C or some equivalent parameter. As they are symmetric w.r.t. the x-axis, the initial conditions can be taken of the form $(x_0, y_0 = 0, \dot{x}_0 = 0, \dot{y}_0)$ with $\delta = x_0 - x_{L_3} > 0$. It has been found useful to use the value of δ as parameter.

Hence several planar Lyapunov p.o., po_δ, around L_3 have been computed, as well as the upper branches $W^{u,+}(\mathrm{po}_\delta)$ and $W^{s,+}(\mathrm{po}_\delta)$ of its manifolds. These are 2D manifolds in the 3D manifold $\mathscr{M}(\mu, C)$. They can be easily computed by integration of (1) starting in a fundamental domain of the manifold. A linear approximation of this one is obtained from the variational equations along the periodic orbit.

To see the relative position of these manifolds, it is useful to make a section. The section through $x = 0$ has been selected. Of course, when considering the unstable manifold one detects (in principle) the intersection with $x = 0$ going to the left, while for the stable one the intersection with $x = 0$ (integrating backwards in time) is detected going to the right, after passing to the left of L_5.

This approach has a difficulty: it is only valid for very small p.o., i.e. for δ small. The reason is simple: for the orbits in $W^{u,+}(\mathrm{po}_\delta)$ the behaviour of x as a function of t, when approaching $x = 0$ is not monotonous. The values of $x(t)$ oscillate left and right. This implies that, after crossing $x = 0$ for the first time going to the left, other crossings can occur for the same orbit. As limit cases, one finds quadratic and even cubic (i.e., on the ZVC) tangencies to $x = 0$. Taking into account all these passages until $x(t)$ moves definitely to the left, surrounding the ZVC on the C level, some results are shown in Fig. 4. Similar behaviour is observed for $W^{s,+}(\mathrm{po}_\delta)$, looking at the intersection with $x = 0$ which is closer to the origin than the ZVC (when this curve still exists, depending on C).

In Fig. 4 the intersections of the upper branches of both the unstable and stable manifolds of several p.o. are shown for $\mu = 0.0002$ (left) and $\mu = \mu_{SJ}$ (right).

Different colours have been used for the unstable and stable parts. The plots are displayed in the $(\dot{x}, \dot{y})$ variables. Given $x = 0, \dot{x}, \dot{y}$, it is possible to recover y from the Jacobi integral. Note that there are two solutions for y and one has to take the correct one.

One can see that while for small size p.o. the intersections are located on $\dot{x} < 0$, larger orbits intersect $x = 0$ both in $\dot{x} < 0$ and in $\dot{x} > 0$. In fact there are orbits in $W^{u,+}(\mathrm{po}_\delta)$ which intersect $x = 0$ at several places before going definitely to the left.

For $\mu = 0.0002$, the unstable and stable manifolds seem to be coincident. The property of having very small splitting for the manifolds of L_3 is inherited by the Lyapunov p.o. In contrast, for $\mu = \mu_{SJ}$ already for small p.o. the lack of coincidence can be detected visually, with two transversal homoclinic orbits. In the plot, the manifolds corresponding to the largest p.o. displayed in Fig. 4 in the μ_{SJ} case can be checked to have four transversal homoclinic orbits.

To put on evidence the lack of coincidence for $\mu = 0.0002$ and to illustrate the birth of new homoclinic points we proceed as follows:

1. Using as centre point the first intersection of $W^{u,+}_{L_3}$ with $x = 0$ we consider the points of $W^{u,+}(\mathrm{po}_\delta) \cap \{x = 0\}$ in polar coordinates. The values of the radius as a function of the angle is Fourier analyzed. Typically, using harmonics up to order 40, the maximal difference between the data and the fit is below 10^{-12}.
2. Then the points of $W^{s,+}(\mathrm{po}_\delta) \cap \{x = 0\}$ are expressed in terms of radius and angle with respect to the same centre. The splitting can be measured as the difference of radii (stable minus unstable) depending on the angle.

In Fig. 5 we show the results for small and large Lyapunov p.o. (i.e., small and large δ). The values of the Fourier approximation of the unstable manifold have been subtracted from the ones in that manifold (which hence become very close to zero) and also from the ones in the stable one. Increasing the size of the p.o. the number of homoclinic points increases. The typical behaviour consists in the apparition of a cubical tangency (eventually with a little shift because of the splitting of the manifolds of L_3), like the one seen on the right plot near the value -1.5 of the angle. Decreasing δ this intersection becomes transversal with positive slope. Increasing δ it becomes transversal but with negative slope, creating two more homoclinics. If we keep increasing δ these homoclinics move to left and right and more homoclinics are created by the same mechanism. The behaviour on the positive range of the angle is similar.

Finally we comment on the choice of initial data on the ZVC (and on the ZVS for the spatial case).

(a) Most of the initial conditions non-leading to escape are in 2D tori (3D in the spatial case). Hence starting with zero synodical velocity (a 2D set in the planar case, 3D in the spatial one) we scan a set of positive measure in the full phase space. Note that we do not consider the value of the Jacobi constant as fixed in the scanning.
(b) The results can be used as a "seed" to obtain the objects which act as "practical confiners" by looking at the transition from a point which is not escaping

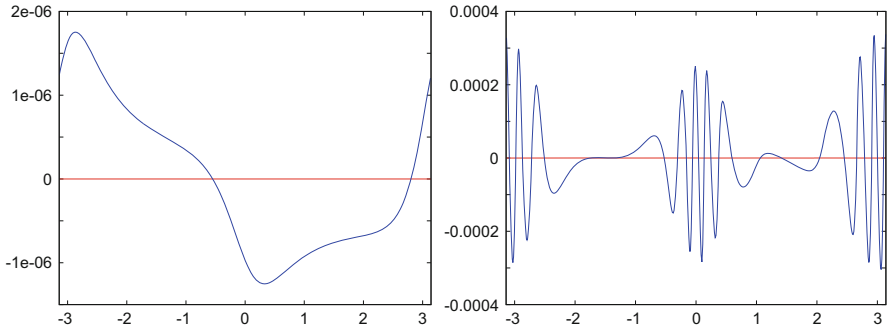

Fig. 5 In the plots we show the difference of radii between the intersections of the stable and unstable manifolds of small size (*left*) and large size (*right*) p.o. for $\mu = 0.0002$ as a function of the angle. Note the change in the number of homoclinic points in a fundamental domain

after a long time integration from another one with relatively fast escape, see [15]. Later on, these objects, mainly lower dimensional (partially) hyperbolic invariant tori, can be continued with respect to suitable parameters.

(c) Not all the points shown in Fig. 1 give rise to different tori. The reason is simple. If we consider a "standard torus" given, e.g., by the solutions of $u'' + u = 0$, $v'' + \omega^2 v = 0$, $\omega \notin \mathbb{Q}$, it has 4 points where the velocity is zero $u' = v' = 0$. The same has been observed with the points in Fig. 1 for $\mu = 0.0002$. In the other cases it can depend on the location. For instance, initial data in some of the islands can produce points with zero synodical velocity in several other islands.

In a similar way, for initial data in the ZVS having $z > 0$ one detects in the $\mu = 0.0002$ case, exactly 8 points in the same torus where the velocity is as close to zero as desired (four in the domain with $z > 0$ and four in the domain with $z < 0$).

3 The Spatial Case

First we compare the "abundance of subsisting points" in the planar and spatial cases, as a function of μ, see Fig. 6. In the planar (spatial) case we start on the ZVC (ZVS). This is the result of a rough computation: the spacings in α and ρ are larger than what was used in Fig. 1 and the final test time is shorter.

In the planar case the maximum is attained for $\mu \approx 0.0014$, while in the spatial case it occurs for $\mu \approx 0.0017$. Note the sharp decrease at the resonances in the planar case, leading to zero for μ_2 and μ_3, as we could expect. But the 4:1, 5:1, 6:1, etc. resonances are clearly visible. In the spatial case the decrease is milder and "delayed". The reasons are clear: Even if in the planar case the resonance decreases or even annihilates the region of stability, in the spatial one, many points subsist on $z \neq 0$. If we consider, for instance, the Lyapunov vertical family of p.o. born at L_5,

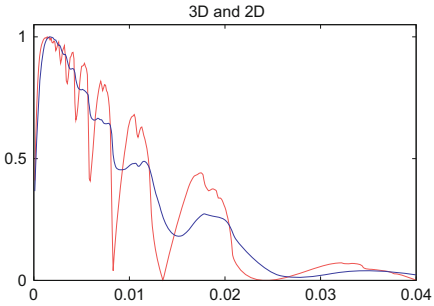

Fig. 6 Statistics on the measure of the subsisting set of points as a function of μ starting on the ZVC (ZVS) for the planar (spatial) case. The planar (spatial) case is shown in *light* (*dark*) *grey* (*red* and *blue*, respectively, online). The data are normalized so that in both cases the maximum equals 1. See the text for details

the nearby tori have rotation number (in the horizontal direction) which decreases when the size of the p.o. increases. Hence, for $\mu = \mu_3$ going up in z the rotation number is less than 1/3, avoiding the resonance. It is recovered for larger μ at some z, which produces the decrease on the abundance but delayed, see [16] for illustrations.

An interesting fact is that both in the planar and spatial case some set of points is confined to a vicinity of L_5 even for $\mu > \mu_1$, as it could be expected from a Hamiltonian-Hopf bifurcation with suitable coefficients in the normal form.

In what follows we sketch some facts for the spatial case. Preliminary results can be found in [6], not only for the circular RTBP but also for the elliptic one (the primaries in elliptic orbits). For the bicircular model, a simplified model for the model of a spacecraft in the Earth-Moon system perturbed by the Sun, see [17].

To prevent from too heavy and too many plots in this note we refer to [16] and [18] where many illustrations of the spatial case can be found for a variety of values of the masses and also data concerning initial conditions outside the ZVS.

To give an idea of the relevant facts which appear in the spatial case, we display a couple of examples in Fig. 7. Both of them are obtained for $\mu = 10^{-4}$. Very close initial data (same value of α and values of ρ differing in 10^{-10}) have been used. The top plot corresponds to initial data on $z = 0.3$ and the bottom one to initial data on $z = 0.6$. From the plots one can guess that what separates the confined and escaping tori in the upper case is an invariant curve (in the Poincaré section; a 2D torus in the phase space) in the centre manifold of L_3. In the lower plot the "separating" object is quite different. We shall describe in Sect. 4 which are the manifolds which contain these and similar invariant curves which have hyperbolic properties.

We return to $\mu = 0.0002$ to present more results in a systematic way. But while in the planar case the points starting on the ZVC and non-escaping were located close to the circle of radius 1, we can question where we should expect to have the non-escaping points in the spatial case.

To this end, we consider the case $\mu = 0$. A particle which moves in the domain K not too far from L_5 for all time must be in 1:1 resonance. Hence the semimajor

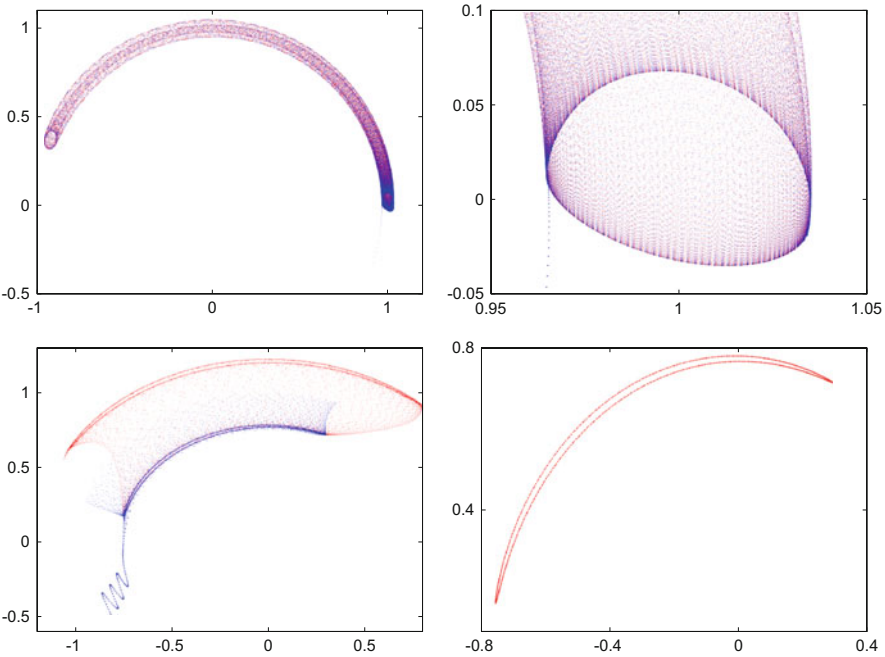

Fig. 7 *Top*: projections on (x, y) of the orbits, seen on a Poincaré section through $z = 0, \dot{z} > 0$ of two very close initial data in the ZVS for a small value of z. For one of the data the orbit (in the Poincaré section) seems to be in a 2D torus. For the other data, after moving for a while close to the previous torus, the orbit escapes. One can see some points going down on the *left* part of the magnification on the *right*. *Bottom*: similar but for very close initial data in the ZVS for a large value of z. One of the orbits remains confined while the other escapes (both orbits are shown in the *left plot*). On the *right bottom plot* one can see the (partially) hyperbolic invariant curve which separates both orbits

axis is $a = 1$. Assume the eccentricity is e. The initial data should correspond either to the passage through the pericentre or the apocentre. But the respective sidereal velocities are $v_p = \sqrt{(1+e)/(1-e)}$, $v_a = \sqrt{(1-e)/(1+e)}$. If we use cylindrical coordinates (R, z), where $R = \sqrt{x^2 + y^2} = 1 + \rho$, the velocity due to the rotating frame is R. To have the particle on the ZVS one must have $R = v_a$. And expressing the eccentricity as $e = \sqrt{R^2 + z^2} - 1$ one obtains the relation

$$z^2 = 4(1 + R^2)^{-2} - R^2 \tag{4}$$

which describes a paraboloid-like surface.

We can summarize the result as

Proposition 1. *In the limit case $\mu = 0$, the points non escaping from an extended vicinity of L_5, starting at the ZVS, must have initial cylindrical coordinates of the form (α, R, z) with R and z related by Eq. (4).*

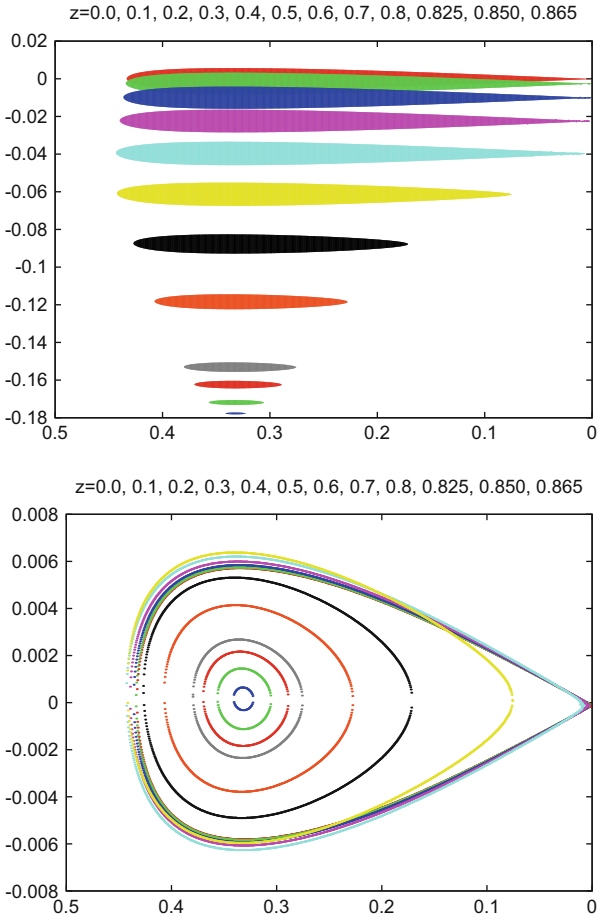

Fig. 8 *Top*: subsisting points for $\mu = 0.0002$ starting at the ZVS for different z values using the (α, ρ) coordinates. From the *upper* to the *lower* part in the plot the values of z are displayed on the plot. *Bottom*: boundaries of the previous domains for the different z values, after making the paraboloid-like correction, that is, using (α, γ) variables

Given a value of z, Eq. (4) can be solved for R. Introducing $w = z^2$ and $\psi = \psi(z) = R^2$ the first terms of the solution are

$$\psi = 1 - \frac{1}{2}w + \frac{3}{2^5}w^2 - \frac{1}{2^8}w^3 - \frac{25}{2^{13}}w^4 + \frac{33}{2^{16}}w^5 + \mathcal{O}(w^6).$$

This suggests to use the variables $(\alpha,\ \gamma = 1 + \rho - \sqrt{\psi(z)},\ z)$ instead of (α, ρ, z) to have the non-escaping points close to $\gamma = 0$.

Figure 8 shows, for initial data on the ZVS, the subsisting points for $\mu = 0.0002$ in the (α, ρ) coordinates. Different levels of z are plotted using

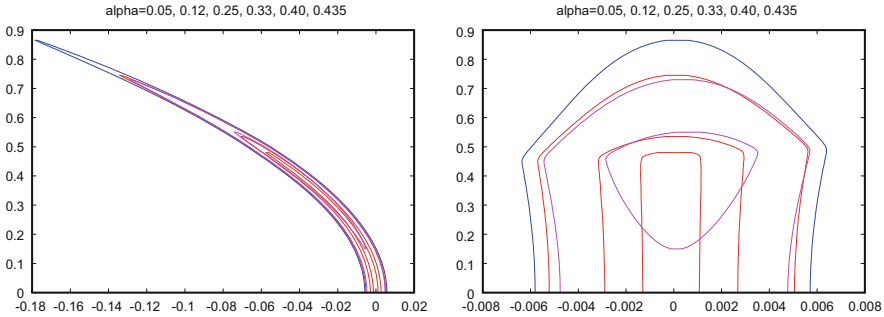

Fig. 9 Some sections of the boundary for $\mu = 0.0002$ starting at the ZVS for different α values. *Left*: in the (ρ, z) variables. *Right*: using the (γ, z) variables after the paraboloid-like correction

different colours. The range of z reaches values as large as 0.865. In the lower part of the Figure, the boundaries of the previous domains are shown in (α, γ) variables. They display a remarkable symmetry and simplicity.

In Fig. 9 we show a different view, which should be relevant for future work. Instead of showing the projections on the (x, y)-plane in polar or polar-corrected coordinates, we display the boundaries for a selected set of α values.

On the left one can clearly see the parabola-like shape of the domain in the (ρ, z) variables for all α. On the right part the variables used are (γ, z) which allow for a better interpretation of the results. Concretely, for $\alpha = 0.05$ one obtains a rectangle-like domain with basis on $z = 0$, while for $\alpha = 0.435$ one has a curved triangular domain not reaching $z = 0$. The other domains from small to large correspond, to $\alpha = 0.12$, 0.40, 0.25 and 0.33. Looking at the boundary of the larger domain, it is clear that there is a strong change around $z = 0.45$. We note that in any case, i.e., either if we fix z and look at the (α, ρ) variables or fixing α and looking at the (γ, z) variables, the boundaries are quite sharp.

To conclude this section on the spatial case we point out that the Sun-Jupiter case is rather similar to the small μ case. However, the boundaries are not so sharp and several "island-like" domains show up. On the other hand, the Earth-Moon case is quite different. Not only as seen in Fig. 1, but because the boundaries are rather fuzzy and resonances, specially the 4:1 one, play an extremely relevant role when z increases.

4 The Role of Invariant Manifolds

Even restricting to the $\mu = 0.0002$ case and with initial data on the ZVS, it is clear that there are different kinds of objects at the boundary. We look for normally hyperbolic invariant manifolds (NHIM) such that their manifolds play a role at the boundary of the non-escaping domain.

The method used to detect these objects is:

- Consider data which are close to the boundary of the non-escaping domain. Typically the orbit is in a 3D torus. Computing the Poincaré section through $z = 0, \dot{z} > 0$ one obtains a 2D torus. The dynamics "slows down" when approaching a curve or, in some cases, a couple of curves.

  We can try to look for this curve (or curves) as invariant under the Poincaré map. An example of the process can be found in [15]. There are different ways to obtain an invariant curve of a discrete map with quasi-periodic dynamics. Beyond the method presented in [15] one can look for a Fourier representation, invariant under the angle shift. See [8] and references therein.
- Next step is the do a continuation of the invariant curve, either with fixed Jacobi constant or with fixed rotation number. Standard tools of arc-parameter continuation can be used.
- The final step is to identify the origin of all these invariant curves.

Preliminary results in [18] and work in progress give a strong evidence that in the boundaries, there are two main kinds of objects: They are either in the centre manifold of L_3 or in the centre manifold of a family of periodic orbits. Each one of these orbits is of centre-saddle type, and the family is obtained by bifurcation of the Lyapunov vertical family of p.o. around L_5 when, for a size in z sufficiently large, it loses stability. In fact the loss of stability leads to two families of p.o. symmetric w.r.t. $z = 0$.

As both the centre manifold of L_3 and the centre manifold of the family of p.o. are 4D in the full phase space, the related $W^{u,s}$ of these NHIM have codimension 1, as it had to be expected.

Some difficulties show up when trying to identify invariant minimal objects in the NHIM, such as a 2D torus which separates stable/unstable orbits if this NHIM is in the centre manifold of L_3. Equivalently we can consider the invariant curve on the Poincaré section. Indeed:

- The rotational dynamics under the Poincaré map is very slow, because of the eigenvalues at L_3: both frequencies are rather close to 1. At the same time the instability is comparatively larger. An orbit approaching the NH curve can stay close to it for very few Poincaré iterates.
- After leaving a vicinity of the NH curve the Poincaré iterates move away to the left part of the Poincaré section ($x < 0$) and return near the centre manifold of L_3. The number of iterates between successive visits is of the order of hundreds.
- Given a level of C and two 2D tori on the centre manifold of L_3, they can have heteroclinic intersections (implying also tiny zones with Arnol'd diffusion, etc.). The returns can be close to different 2D tori.

This requires some effort to correctly identify the (different) 2D tori related to the escape boundary. It can be based on amplitude of the z component of the orbit in the suitable region.

For large z, the 2D NHIM can be continued. If the size shrinks they can lead to a periodic orbit. Equivalently, the invariant curves shrink to a fixed point. This is what has been observed, leading to the family of p.o. mentioned above.

Description of details on the methods used and final results are in progress and will appear elsewhere.

5 Conclusions and Outlook

We can draw several conclusions from the preliminary facts reported in this work.

- The role of some codimension-1 manifolds in problems of practical stability "boundaries" has been applied to the present problem.
- Similar tools work in other problems (some experiments done in the past) like: the elliptic 3D RTBP, bicircular coherent models. Applications to kinetics in chemistry: the transition state theory (TST). And in many other domains (e.g. in plasma physics).
- These manifolds explain the "sharp, too sharp, boundaries" mentioned by L. Exposito in his book about rings of planets and asteroids.

The work in progress deals with:

- To complete the computation of NHIM, around L_3 and around the vertical Lyapunov family of p.o. emerging from L_5, in narrow grids. Make identification checks: (z, α, ρ) vs C and rotation number. Carry out some additional checks with initial data not in ZVS. Complete the results on splitting available right now.
- To use perturbation methods for very small μ.
- Complete the Sun-Jupiter and Earth-Moon cases.

As a challenging question we can mention: Why no Trojan-like objects have been found in the Earth-Moon system? Some analysis in [6] suggests that the Sun is responsible for this. But some rocks could subsist in stable orbits not too close to the lunar plane.

Acknowledgements The first author has been supported by grants MTM2010-16425 (Spain) and 2009 SGR 67 (Catalonia). Part of the work was supported by grant MTM2006-05849/Consolider (Spain). The second author thanks the CNPq (Brazil) for the grant PDE-201932/2010-5. The third author thanks FAPESP (Brazil) for the grant 2010/18692-8. The computing facilities of the Dynamical Systems Group of the Universitat de Barcelona have been largely used in this work. The authors are warmly indebted to his colleague J. Timoneda for technical support.

References

1. Barrabés, E., Ollé, M.: Invariant manifolds of L_3 and horseshoe motion in the RTBP. Nonlinearity **19**, 2065–2089 (2006)
2. Batut, C., Belabas, K., Bernardi, D., Cohen, H., Olivier, M.: Users' guide to PARI/GP. Available at http://pari.math.u-bordeaux.fr/

3. Deprit, A., Deprit-Bartholomé, A.: Stability of the triangular Lagrangian points. Astron. J. **72**, 173–179 (1967)
4. Fontich, E., Simó, C.: The splitting of separatrices for analytic diffeomorphisms. Ergod. Theory Dyn. Syst. **10**, 295–318 (1990)
5. Giorgilli, A., Delshams, A., Fontich, E., Galgani, L., Simó, C.: Effective stability for a Hamiltonian system near an elliptic equilibrium point, with an application to the restricted three body problem. J. Differ. Equ. **77**, 167–198 (1989)
6. Gómez, G., Jorba, A., Masdemont, J., Simó, C.: Study of Poincaré maps for Orbits near Lagrangian points. ESA technical report, 1993. Reprinted as Dynamics and Mission Design Near Libration Points. Volume 4: Advanced Methods for Triangular Points. World Scientific Monograph Series in Mathematics, vol. 5. World Scientific Publisher, Singapore (2000)
7. Henrard, J.: On Brown's conjecture. Celest. Mech. **31**, 115–122 (1983)
8. Jorba, À., Olmedo, E.: On the computation of reducible invariant tori on a parallel computer. SIAM J. Appl. Dyn. Syst. **8**, 1382–1404 (2009)
9. Leontovich, A.M.: On the stability of the Lagrange periodic solutions of the restricted problem of three bodies. Sov. Math. Dokl. **3**, 425–428 (1962)
10. Markeev, A.P.: On the stability of the triangular libration points in the circular bounded three-body problem. Appl. Math. Mech. **33**, 105–110 (1969)
11. Markeev, A.P.: Stability of the triangular Lagrangian solutions of the restricted three-body problem in the three-dimensional circular case. Sov. Astron. **15**, 682–686 (1972)
12. McKenzie, R., Szebehely, V.: Nonlinear stability motion around the triangular libration points. Celest. Mech. **23**, 223–229 (1981)
13. Neishtadt, A.I.: The separation of motions in systems with rapidly rotating phase. Prikladnaja Matematika i Mekhanika **48**, 133–139 (1984)
14. Simó, C.: Estabilitat de sistemes hamiltonians. Memòries de la Reial Acad. de Ciències i Arts de Barcelona (in catalan). **XLVIII**, 303–336 (1989)
15. Simó, C.: Effective computations in celestial mechanics and astrodynamics. In: Rumyantsev, V.V., Karapetyan, A.V. (eds.) Modern Methods of Analytical Mechanics and Their Applications. CISM Courses and Lectures, vol. 387, pp. 55–102. Springer, Wien/New York (1998)
16. Simó, C.: Boundaries of stability. Slides available at http://www.maia.ub.es/dsg/2006/, number 2 (2006)
17. Simó, C., Gómez, G., Jorba, À., Masdemont, J.: The bicircular model near the triangular libration points if the RTBP. In: Roy, A.E. (ed.) From Newton to Chaos: Modern Techniques for Understanding and Coping with Chaos in N-Body Dynamical Systems, pp. 343–370. Plenum Press, New York (1995)
18. Simó, C., Sousa-Silva, P., Terra, M.: Domains of practical stability near $L_{4,5}$ in the RTBP. Slides available at http://www.maia.ub.es/dsg/2012/, number 8 (2012)
19. Szebehely, V.: Theory of Orbits: The Restricted Problem of Three Bodies. Academic Press, New York (1967)

A Physical Dissipative System with a Poincaré Homoclinic Figure-Eight

C. Simó and A. Vieiro

Abstract We consider 2D diffeomorphisms with a homoclinic figure-eight to a dissipative saddle under a periodic forcing. These systems are natural simplified models of phenomena with forcing and dissipation. As a physical example we study the dynamics of a parametrically driven dissipative pendulum with a magnetic kick forcing acting on it.

1 The Bifurcation Problem

Consider a family of analytic diffeomorphisms $T_{\boldsymbol{\mu},\epsilon} : \mathbb{R}^2 \to \mathbb{R}^2$ depending on the parameters $\boldsymbol{\mu} = (\mu_1, \mu_2) \in \mathbb{R}^2$ and $\epsilon \in \mathbb{R}$. We assume that $T_{\boldsymbol{\mu},\epsilon}$ verifies the following hypothesis:

(H1) The origin is a fixed point: $T_{\boldsymbol{\mu},\epsilon}(\mathbf{0}) = \mathbf{0}$.
(H2) The fixed point is of dissipative saddle type: if $\mathrm{Spec}(DT_{\boldsymbol{\mu},\epsilon}(\mathbf{p})) = \{\gamma, \lambda\}$, $0 < |\lambda| < 1 < |\gamma|$, then $|\gamma\,\lambda| < 1$.
(H3) For $\boldsymbol{\mu} = \mathbf{0}$ and $\epsilon = 0$ the invariant manifolds of the origin form a Poincaré homoclinic figure-eight Γ. In other words, the map $T_{\mathbf{0},0}$ has a double homoclinic loop to the dissipative saddle fixed point.
(H4) The homoclinic figure-eight Γ is (locally) an asymptotically stable invariant set of $T_{\mathbf{0},0}$.

Denote by W^{u+} and W^{u-} (resp. W^{s+} and W^{s-}) the two branches of the unstable (resp. stable) local invariant manifolds of the origin. For $\boldsymbol{\mu} = \mathbf{0}$, $\epsilon = 0$ we denote by $\Gamma^+ = W^{u+} = W^{s+}$ and $\Gamma^- = W^{u-} = W^{s-}$ the two homoclinic loops that form the figure-eight Γ (i.e., $\Gamma = \Gamma^- \cup \Gamma^+$), see Fig. 1 center. From (H4) it

C. Simó (✉) · A. Vieiro
Departament de Matemàtica Aplicada i Anàlisi, Universitat de Barcelona, Gran Via 585, 08007 Barcelona, Spain
e-mail: carles@maia.ub.es; vieiro@maia.ub.es

S. Ibáñez et al. (eds.), *Progress and Challenges in Dynamical Systems*,
Springer Proceedings in Mathematics & Statistics 54,
DOI 10.1007/978-3-642-38830-9_24,

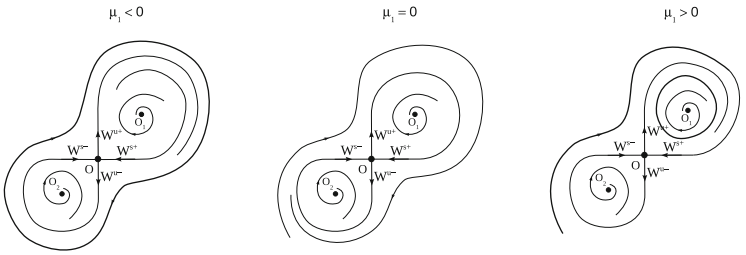

Fig. 1 Effect of the "autonomous" perturbation on the geometry of the invariant manifolds of the origin for the maps $T_{\boldsymbol{\mu},\epsilon}$. Note that the relative position of the invariant manifolds can be related to the birth of a new attractor of the system (in the figure we show invariant *curves* for $\mu_1 \neq 0$, assuming $\mu_2 = 0$ in the three cases, but for $\epsilon > 0$ these attractors can become periodic orbits and/or strange attractors (SA))

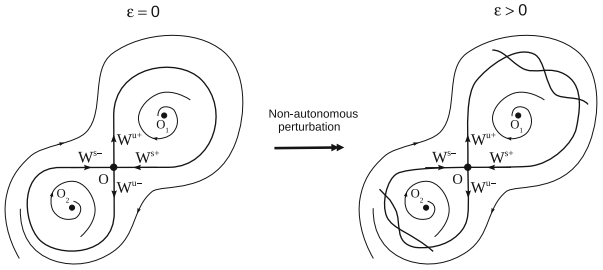

Fig. 2 Effect of the "non-autonomous" perturbation on the geometry of the invariant manifolds of the origin for the maps $T_{\boldsymbol{\mu},\epsilon}$. In this figure we assume $\boldsymbol{\mu} = 0$

follows that both inside Γ^+ and Γ^- there is a repulsive invariant set. To fix ideas we assume that two unstable equilibria O_1 and O_2 exist inside the loops (they can be foci, nodes,... in the illustrations we assume that they are repulsive foci).

It remains to explain the role of the parameters $\boldsymbol{\mu}$ and ϵ. They account for two different perturbation sources that change the geometry of $T_{\mathbf{0},0}$. More precisely,

(H5) The parameter $\boldsymbol{\mu} = (\mu_1, \mu_2)$ is related to an "autonomous" perturbation: μ_1 (resp. μ_2) is a splitting parameter accounting for the relative position of the invariant manifold W^{u+} (resp. W^{u-}) with respect to W^{s+} (resp. W^{s-}). See Fig. 1.

(H6) The parameter ϵ is related to a "non-autonomous" perturbation: for $\epsilon \neq 0$ the homoclinic loops of the figure-eight undulate. See Fig. 2.

A good framework to better understand the "autonomous" and "non-autonomous" perturbation effects is to assume that $T_{\boldsymbol{\mu},\epsilon}$ is obtained as the Poincaré (stroboscopic) map of a system of the form

$$\dot{\mathbf{x}} = X_{\boldsymbol{\mu},\epsilon}(\mathbf{x}, t), \tag{1}$$

where

$$X_{\boldsymbol{\mu},\epsilon}(\mathbf{x},t) = f_{\boldsymbol{\mu}}(\mathbf{x}) + \epsilon g_{\boldsymbol{\mu},\epsilon}(\mathbf{x},t),$$

with $g_{\boldsymbol{\mu},\epsilon}$ a 2π-periodic in $t \in \mathbb{R}$. Hence, the invariant manifolds of $T_{\boldsymbol{\mu},0}$ coincide with those of the autonomous vector field $f_{\boldsymbol{\mu}}$. The homoclinic loop Γ^+ splits for $\mu_1 \neq 0$ and the loop Γ^- splits for $\mu_2 \neq 0$. On the other hand, the non-autonomous perturbation $g_{\boldsymbol{\mu},\epsilon}$ is assumed to be "generic" in the sense that it undulates the invariant manifolds $T_{\mathbf{0},\epsilon}$ for $\epsilon \neq 0$ in such a way that a finite set of homoclinic trajectories to the origin survive. We consider both effects together: the invariant manifolds of $T_{\boldsymbol{\mu},\epsilon}$ are undulated and displaced according to both effects.

These kind of maps were already considered in detail in [4], where the following bifurcation problem was addressed:

Bifurcation problem
Consider ϵ fixed (and small enough), and study the bifurcations taking place as μ_1 and μ_2 change. Which is the main bifurcation diagram of $T_{\boldsymbol{\mu},\epsilon}$?

1.1 Comments on the Bifurcation Diagram

The first step to confront the bifurcation problem stated in Sect. 1 could be to analyse the bifurcation diagram when $\epsilon = 0$. This problem was addressed in [6, 7]. It is straightforward to sketch the (μ_1, μ_2)-bifurcation diagram in this case [4]. There are four bifurcation curves: B^-, B^+, $B^\pm$ and $B^\mp$. They are related to the homoclinic connection between the different branches of the saddle fixed point. Concretely, $B^- : \{\mu_2 = 0\}$, $B^+ : \{\mu_1 = 0\}$, $B^\pm : \{\mu_1 = -\hat{A}^- \mu_2^{\gamma/\lambda}(1 + \ldots), \quad \mu_2 > 0\}$ and $B^\mp : \{\mu_2 = -\hat{A}^+ \mu_1^{\gamma/\lambda}(1 + \ldots), \quad \mu_1 > 0\}$. These curves divide the $\boldsymbol{\mu}$-plane into six regions where the system shows different dynamics. Since in this case the dynamics of the map is "equivalent" to the dynamics of $f_{\boldsymbol{\mu}}$, it turns out that the only possible attractors that can appear either inside Γ^+ or Γ^- and/or surrounding Γ are simply invariant curves. They are created as a byproduct of an Andronov-Leontovich bifurcation where a limit cycle (for the autonomous flow) is created at the appropriate splitting of a homoclinic loop (see [5]). We denote these curves by C^+, C^- and C^* respectively.

Next step is to consider $\epsilon > 0$ fixed and small enough. The corresponding bifurcation problem was considered in [4]. For the reader's convenience we briefly summarize in this section the main results obtained.

Each of the bifurcation curves B^a (either with $a = +, -, \pm$ or $\mp$) where the separatrices of $f_{\boldsymbol{\mu}}$ coincide gives rise to a homoclinic zone HZ^a of size $\mathcal{O}(\epsilon)$. The corresponding curves L_1^a and L_2^a that bound the homoclinic zone HZ^a are related

to the so-called first and last, respectively, homoclinic quadratic tangencies between the invariant manifolds of the origin. Special attention deserves the structure of the boundaries of the homoclinic zones $HZ^{\pm}$ and $HZ^{\mp}$.

Theorem 1. *For systems verifying the hypothesis (H1),...,(H6), the curves $L_1^{\pm}$, $L_2^{\pm}$, $L_1^{\mp}$ and $L_2^{\mp}$ are $\mathscr{C}^0$ with infinitely many points of non-smoothness. These points where smoothness is lost accumulate to the vertices of the rectangle that the intersection of the homoclinic zones HZ^+ and HZ^- defines in the (μ_1, μ_2)-plane.*

This structure is related to the fact that these boundaries are formed by joining different arcs of quadratic tangency curves.

Theorem 2. *The quadratic tangency curves can be continued up to a primary cubic tangency. All the related cubic tangencies are of spring-area type (or "-" type) [2].*

We note that the bifurcation diagram close to a cubic tangency shows up a cascade of cusp points which accumulate to the cubic tangency as the period grows up. Around each cusp point of the cascade one expects a stability domain of spring-area type. However, if the period is not large enough other configurations show up (typically a cross-road scenario). We refer to [2] and references therein for details.

Taking into account the curves $L_{1,2}^a$, one obtains a total number of 17 different regions where different dynamics is expected. However, it is not true that these are all the possible dynamical scenarios. The reason is the following. Note that changing μ_1, μ_2 in such a way that the family of systems leaves the homoclinic zone HZ^a through the line L_1^a it turns out that the dynamics of $T_{\boldsymbol{\mu},\epsilon}$ becomes immediately "trivial" (it mimics the dynamics of a flow!). This is usually referred to as a Morse-Smale transition. However, when leaving HZ^a through a first tangency line L_2^a the dynamics remains "non-trivial": there is a region where SA (either made by a single piece or several pieces) might exist (and coexist) together with periodic sinks. In this regime the dynamics is difficult to describe, see [4]. The sinks create windows of stability and, thus, if the period is not very high, chaotic regimes can be seen (visually) to alternate with periodic ones. It can be hard to detect sinks of high period, probably preceded by a long transient, and even harder to show the existence of SA for concrete values of the parameters. Recall that even when sinks show up near a homoclinic tangency it can happen that a nearby SA subsists, see [2].

It turns out that one has to take into account the "boundaries" of the regions where the dynamics remains "non-trivial". Hence a total number of 11 curves are necessary to divide the $\boldsymbol{\mu}$-plane into different regions with different dynamics. This gives 35 open regions of the parameter plane, see [4]. By a simple sketch of the invariant manifolds of the saddle fixed point in each region one realizes that there are six main types of potential global strange attractors (SA): $A^{\pm}$, A^*, $AT^{\pm}$ and GA. Concretely, A^+, A^- and A^* are born under the breakdown of the closed invariant curves C^+, C^- and C^* of the autonomous case, respectively. On the other hand, AT^+, AT^- and GA are "homoclinic attractors" related to the homoclinic intersections of the invariant manifolds of the saddle O. The "global" attractor GA exists for $\boldsymbol{\mu}$-parameters when all the homoclinic zones intersect. The "tail"

attractor AT^- (resp. AT^+) exists for $\boldsymbol{\mu}$-parameters such that $W^{u+} \cap W^{s+} = \emptyset$ (resp. $W^{u-} \cap W^{s-} = \emptyset$).

At this point, several questions arise. What about the scenarios of the cascades of cusp points accumulating to a cubic tangency? Which is the size of the stability domains? How are these "boundaries" above described? Which is the size of the corresponding regions? Are relevant in concrete applications? To answer these questions in [4] it was proposed a quantitative approach to the bifurcation diagram. The idea is to derive a return map model (similar to the separatrix map [3, 8] but adapted to the dissipative setting [1]) to the union FD (which stands for Fundamental Domain) of two annular domains $FD_\pm$, each one referring to one of the loops (below labelled as $s = 1$ and $s = -1$) of the figure-eight. The simplest return model is

$$M_{a,b,\psi,A,\omega} : \begin{pmatrix} z \\ \eta \\ s \end{pmatrix} \mapsto \begin{pmatrix} z + \omega_j + A\log(|y|) \\ \text{sign}(y)|y|^\psi \\ \text{sign}(y)s \end{pmatrix}, \tag{2}$$

where $y = a_j + \eta + b_j \sin(2\pi z)$ and the index j takes the value 1 if $s = 1$ and the value 2 if $s = -1$. The piece of the unstable manifold inside each $FD_\pm$ is parametrized by $z \in [0, 1)$. The variable η measures the position with respect to the corresponding unstable branch of W^u, while y measures the distance with respect to W^s. The role of the exponent ψ is clear. It accounts for the passage near the dissipative saddle fixed point of $T_{\boldsymbol{\mu},\epsilon}$. If the eigenvalues at the origin are $0 < \lambda < 1 < \gamma$ then the linear flow near the saddle gives $\psi = \log(\lambda)/\log(\gamma)$.

Using (2) the authors illustrated in [4] the complicated shape of the "boundaries" above described and the different SA that can be obtained. On the other hand, the model reveals a nice trellis structure of stability domains related to the cascades of cusp points accumulating to the different cubic tangencies. The remainder of this note is devoted to show such phenomena in a concrete physical example.

2 A Physical Model

As a physical model we consider a mathematical pendulum, $x'' + \sin(x) = 0$, where $x \in (-\pi, \pi]$, but with several modifications.

2.1 The Flow Case

First, we perturb the pendulum adding dissipation but recovering the "figure-eight" discussed above by means of suitable kicks. The model is such that:

1. There is dissipation in an asymmetric way. The dissipation is proportional to the modulus of the velocity, but with a different coefficient if the velocity is either positive or negative. That is,

$$x'' + a_{\pm}x' + \sin(x) = 0,$$

where $a_+ > 0$ is used when $x' > 0$ and $a_- > 0$ is used when $x' < 0$.
This different dissipation coefficient can be accomplished physically with an asymmetric bulk, which has different aerodynamic coefficients in each side.

2. The dissipation, from one side, destroys the separatrices. From another side the elliptic fixed point of the pendulum becomes a stable focus. To recover the separatrices and to convert the stable focus into an unstable one we "kick" the pendulum everytime it passes through the minimum, at $x = 0$. The kick consists in a change of velocity, by adding a quantity which depends on the current velocity x' at the passage through $x = 0$. Concretely, the increment of velocity $\Delta x' = x'_{\text{new}} - x'$ is of the form

$$\Delta x' = J_{\pm}(|x'|),\ J_{\pm}(0) = 0,$$

where a suitable "jump" function $J_+(|x'|) \geq 0$ (resp. $J_-(|x'|) \leq 0$) is used in the case of crossing $x = 0$ with positive velocity (resp. with negative velocity).
This "kick" can be accomplished physically with a photoelectric cell system, which detects the passage through $x = 0$ and estimates the velocity. Then, a strong electric or magnetic field is excited (assuming the bulk to have some electric charge or magnet) and acts in a negligible amount of time to produce the kick.

Going near the saddle the ratio of eigenvalues, ψ, depends on the type of passage, due to the different values of $a_{\pm}$. Let us denote as ψ_{++} the ratio in the passage from the vicinity of W^s_+ to the vicinity of W^u_+, and as ψ_{+-} the one in the passage from the vicinity of W^s_+ to the vicinity of W^u_-. In a similar way we introduce the ratios ψ_{-+} and ψ_{--}. Let us introduce $\alpha_{\pm} = (1 + a^2_{\pm}/4)^{1/2} + a_{\pm}/2$. Then the corresponding values are $\psi_{++} = \alpha^2_+,\ \psi_{--} = \alpha^2_-,$ and $\psi_{+-} = \psi_{-+} = \alpha_+\alpha_-$.

Details on the Construction of the Model

The first step, once we fixed some dissipation coefficients a_+ and a_-, is to compute the jumps to be applied to recover the upper and lower separatrices. It should be noted that both $J_{\pm}(|x'|)$ should tend to a suitable constant $C_{\pm} < a_{\pm}2\pi$ when $|x'|$ is large. Indeed, assume for concreteness that x' is positive and of the order of $V \gg 1$. Then, the passage from $x = -\pi$ to $x = \pi$ takes place in a time of the order of $2\pi/V$ (the term in $\sin(x)$ is negligible in front of a_+V). Hence, the variation of the velocity in this passage is $\approx V(\exp(-a_+2\pi/V) - 1) \approx -a_+2\pi$. Any value of $J_+(V) > C_+ \approx a_+2\pi$ would produce, at the kick, an increase of the (unperturbed pendulum) energy larger than the loss due to dissipation. Another constraint on these functions $J_{\pm}(|x'|)$ is that they must be monotonous in $|x'|$.

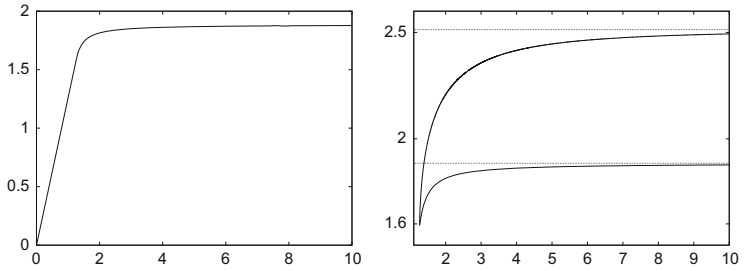

Fig. 3 In the plots the values $a_+ = 2/5$ and $a_- = 1/5$ have been chosen. *Left*: the jump function $J_+(|x'|)$ that we use in the simulations. *Right*: the *upper curve* shows the displacement produced by the dissipation as a function of x'. The *lower curve* corresponds to $J_+(|x'|)$, the upper one to $J_-(|x'|)$

It is a routine task to look for the analytical (in fact, entire) expansions of the manifolds expressing y as a graph on x. The invariance condition allows the recurrent computation of the coefficients. Evaluation of the different branches at $x = 0$ gives the values of $x' = y$ on the separatrices at $x = 0$. Let these values be $y^u_+ < 2 < y^s_+$ and $y^u_- > -2 > y^s_-$. Then we determine the function $z = J_+(y)$ as follows:

1. The "kick" in the upper part should send y^u_+ to y^s_+, i.e., $J_+(y^u_+) = y^s_+$.
2. On the interval $[0, y^u_+]$ we define $J_+(y) = my$ with $m = y^s_+/y^u_+$.
3. For $y > y^u_+$ let $h(y)$ be the branch of the hyperbola such that: (i) has $z = 3\pi a_+/2$ as horizontal asymptote, (ii) it passes through the point (y^u_+, y^s_+) and (iii) it has slope equals to m at this point. We define $J_+(y) = h(y)$.

We proceed in a similar way to determine $J_-(y)$. In particular, $J_\pm(y)$ are $\mathscr{C}^1$ functions. One can modify $J_\pm(y)$ so that they become $\mathscr{C}^r$ for any r (or even analytic using a function of the form $\beta_1 \tanh(\beta_2 x)$ for example) but this is not relevant for our purposes. Let us see that the functions $J_\pm(y)$ must necessarily be "similar" to the ones introduced here to fullfill the requirements of the flow case. The function $J_+(y)$ is shown in Fig. 3 left for $a_+ = 2/5$ and $a_- = 1/5$. In the right plot, we compare $J_+(y)$ with the displacement that the dissipation produces on a point on $x = 0$ above the separatrix (corresponding to $x' \approx 1.265832$) after the passage from $x = 0$ to $x = 2\pi$. In particular, on the separatrix a displacement of ≈ 2.857683 is produced. It should be compensated by the jump $J_+(|x'|)$ to recover the Γ^+ connection. We note that $J_+(|x'|)$ should be a monotonous function with a horizontal asymptote below the one that shows the dissipative displacement, which tends to $2\pi a_+$ as said. Hence, for $y > y^u_+$ the function $J_+(y)$ should be "similar" to the one we selected.

Up to this point we have shown how to recover the separatrix loops Γ^+ and Γ^- using the jump functions $J_\pm(y)$. The top left plot in Fig. 4 shows the related dynamics: the points outside and inside the separatrix loops tend to Γ. Next step is to unfold this double loop ("figure-eight") configuration. To split the loop Γ^+ (resp.

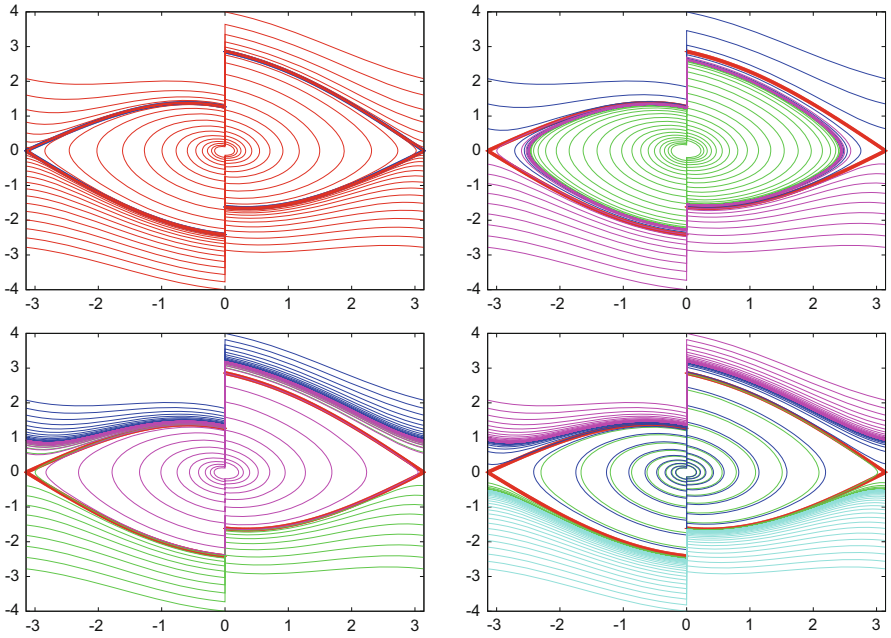

Fig. 4 The plots correspond to the model (flow case) for $a_+ = 0.4$ and $a_- = 0.2$. *Top left*: $\boldsymbol{\mu} = (0, 0)$. *Top right*: $\boldsymbol{\mu} = (-0.1, -0.05)$. *Bottom left*: $\boldsymbol{\mu} = (0.1, -0.05)$. *Bottom right*: $\boldsymbol{\mu} = (0.1, 0.05)$. Different invariant *curves* as global attractors are observed, see text for details (Colour online)

Γ^-) we modify the jump function $J_+(y)$ (resp. $J_-(y)$) by a multiplicative factor $f_+ = 1 + \mu_1$ (resp. $f_- = 1 + \mu_2$). The parameters $\boldsymbol{\mu} = (\mu_1, \mu_2)$ defined in this way are used below as coordinates in the parameter space. In the top right plot of Fig. 4 we represent the phase space dynamics for $\boldsymbol{\mu} = (-0.1, -0.05)$. A librational invariant curve C^* is observed. On the other hand, the bottom left plot of the same figure shows the dynamics for $\boldsymbol{\mu} = (0.1, -0.05)$. Here a rotational invariant curve C^+ above the separatrices is observed. Finally, in the bottom right plot of the same figure we observe two rotational invariant curves C^+ and C^- (above and below the separatrices respectively). It corresponds to $\boldsymbol{\mu} = (0.1, 0.05)$. In particular, we also show that the trajectories starting on $x = 0$ with $y = 0.5$ and $y = -0.3$ tend to the curves C^+ and C^- respectively.[1]

Clearly, the system described above reproduces the complete bifurcation diagram of the flow case summarized in Sect. 1.1. Hence, along the curve $B^+ : \{\mu_1 = 0\}$ (resp. $B^- : \{\mu_2 = 0\}$) the homoclinic loop Γ^+ (resp. Γ^-) is preserved. We also

[1] We note that for large negative values of $\mu_{1,2}$ (depending on a_+ and a_-) the origin becomes an stable focus and there is no longer a repellor inside the loops. In particular, the model does not verify the required assumptions (H1),. . . ,(H6).

note that for suitable parameters $\mu_1 < 0$ and $\mu_2 > 0$ along the curve $B^{\pm}$, there exits a homoclinic connection between W^u_+ and W^s_-. Similarly, there is a homoclinic connection between W^u_- and W^s_+ for suitable parameters $\mu_1 > 0$ and $\mu_2 < 0$ that define the curve $B^{\mp}$.

2.2 The Map $T_{\boldsymbol{\mu},\epsilon}$

Next we perturb the system in a non-autonomous way. For fixed dissipation values a_+, a_- and fixed $\boldsymbol{\mu}$ parameters we computed the jump function and derived a model for the flow case, essentially a kicked dissipative pendulum. To add the non-autonomous perturbation, we simply consider that the system of the flow-case is parametrically excited because it is attached to a periodic vertically oscillating support (i.e., a time-periodic forcing is added to the gravity field). That is, ignoring the kick force, the equation of motion is given by

$$x'' + a_{\pm}x' + (1 + \epsilon\cos(6\,t))\sin(x) = 0.$$

We define the map $T_{\boldsymbol{\mu},\epsilon}$ as the stroboscopic Poincaré map at a time $\tau = \pi/3$ obtained from the previous non-autonomous system (with the kick due to the jump function acting at $x = 0$). By construction $T_{\boldsymbol{\mu},\epsilon}$ fits within the framework defined in Sect. 1. Accordingly, in the following we perform a preliminary numerical analysis of this simple physical model to show that the different scenarios described in [4] can be directly observed from the simulations.

For the numerical explorations below we consider $\epsilon = 0.2$ and a_+ and a_- as in Figs. 3 and 4.[2] The value $\mu_1 \approx -0.003825$ corresponds to the inner (first) quadratic tangency between W^u_+ and W^s_+, while for $\mu_1 \approx 0.00351$ the outer (last) quadratic tangency takes place. Similarly, the invariant manifolds W^u_- and W^s_- have the inner (first) quadratic tangency for $\mu_2 \approx -0.005800$ and the outer (last) quadratic tangency takes place for $\mu_2 \approx 0.00555$.

To obtain a global picture of the dynamics for $\boldsymbol{\mu} \in [-0.2, 0.05]\times[-0.2, 0.05]$ we compute a *chaos indicator*, i.e., an indicator of the sign of the maximal Lyapunov exponent, taking the initial condition on $W^u_{+,\mathrm{loc}}$ at a distance 10^{-8} from the saddle point (Fig. 5 left) and also for the initial condition on W^u_- at a distance 10^{-8} from the saddle point (Fig. 5 right). Concretely, we iterate each of the initial conditions and we decide if it is chaotic or not (i.e., if the ω-limit of the orbit is chaotic or not). To decide chaoticity, after a transient of 10^4 iterates, we compute $N < 10^6$ iterates and look at the norm, `ntv`, of the tangent vector. The following criterion have been used. If the `ntv`$> 10^8$ we consider that the attractor is chaotic (in light grey –green in the electronic version (e.v.)– in Fig. 5), if `ntv`$< 10^{-8}$ we consider that the attractor is

[2]These values have been selected because the domains where the rich dynamics is expected are relatively large and the transient times to achieve the attractors not extremely long.

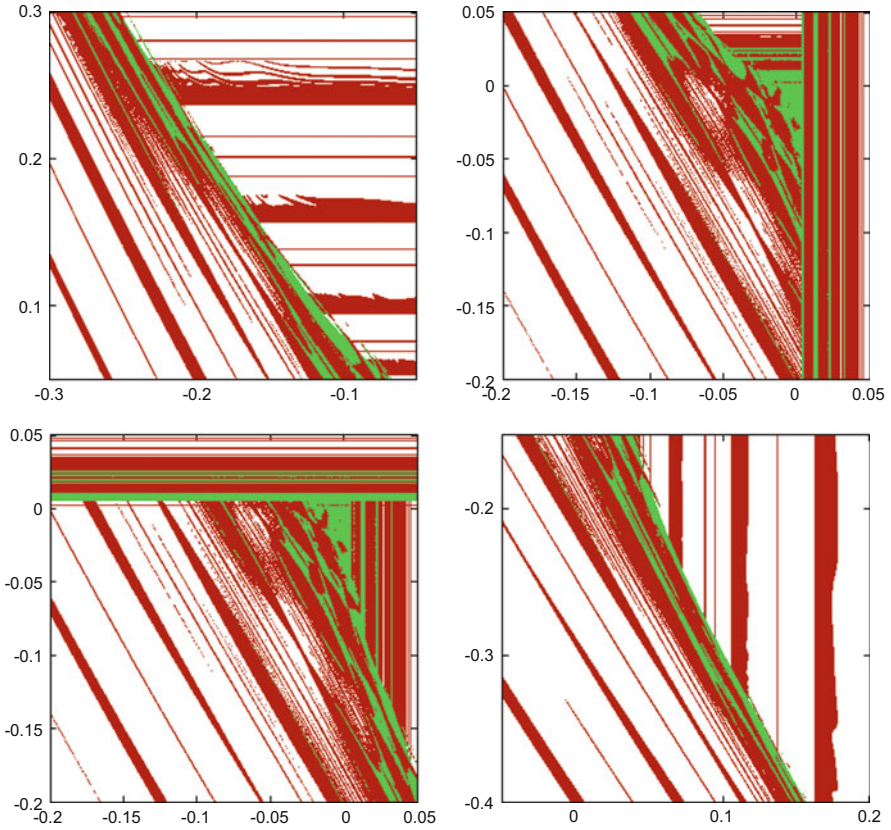

Fig. 5 Results of the chaos indicator computations (see text for details). We show in *light grey* those $\boldsymbol{\mu}$ parameters for which a chaotic attractor is found. In *dark grey* we display those $\boldsymbol{\mu}$ parameters for which the attractor is a periodic sink. The *white* domains parameters correspond to an invariant *curve* attractor. *Dark* (resp. *light*) *grey* appears in *red* (resp. *green*) in the e.v. The *top right* and *bottom left plots* show the structure close to $\boldsymbol{\mu} = \mathbf{0}$ for an initial condition taken on $W^u_{+,\mathrm{loc}}$ (*top right*) and on $W^u_{-,\mathrm{loc}}$ (*bottom left*). The regions where different attractors exist (and coexist) can be distinguished and the richness of the structure predicted in [4] is apparent. The *top left plot* shows the continuation of the "diagonal" structure observed in the *top right plot* for values of $\boldsymbol{\mu}$ above and to the *right* that those used in the *right plot*. Similarly the *bottom right plot* shows the continuation of the structure in the *bottom left plot* for values of $\boldsymbol{\mu}$ to the *bottom right part*

a periodic sink (in dark grey –red in the e.v.– in Fig. 5). Otherwise we consider that the attractor is an invariant curve (in white in Fig. 5).

The vertical lines in dark grey (red in the e.v.) to the right of 0 in the right upper plot correspond to the region where the dynamics becomes non-trivial at the crossing of the curve L_2^+ bounding HZ^+. Similarly, the horizontal lines in dark grey (red in the e.v.) above 0 in the left lower plot correspond to the region with non-trivial dynamics at the crossing of the boundary curve L_2^- of HZ^-. The non-trivial dynamics at the crossing of $L_2^\pm$ can be seen in both figures, where it can be

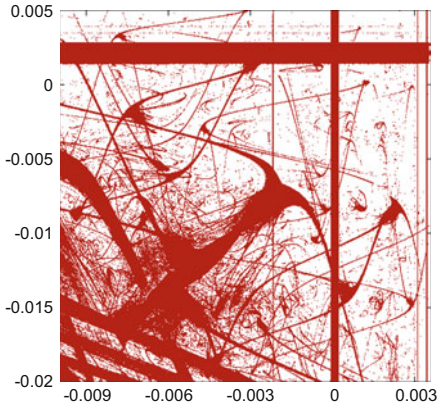

Fig. 6 Detail of the structure that form the stability domains related to the cascades of cusp points. We show the set of parameters for which the global attractor corresponds to periodic sinks. We can see the stability domains, related to different periods cusp points, accumulating to the cubic tangency points that are expected to exist within the $HZ^{\pm}$ and $HZ^{\mp}$ zones, see [4] for details

distinguished the structure of the set of parameters having SA. The "boundary" of this region shows up an amazing structure as was stated in [4]. Outside this complicated region, i.e., for $\boldsymbol{\mu}$ parameters closer to the bottom left part of the figures, we observe different regions corresponding to sinks that alternate with invariant curves.

We remark that, by examining the left and right plots in Fig. 5 one realizes that for many parameters there is a coexistence of attractors for the same $\boldsymbol{\mu}$ parameters, see [2, 4].

Moreover, following [4] one expects a rich structure related to stability domains of the cascades of cusp points accumulating to cubic tangency points. To observe this structure we repeat the previous computation for $\boldsymbol{\mu} \in [-0.01, 0.005] \times [-0.02, 0.005]$ and display only those $\boldsymbol{\mu}$ values for which the attractor (at least for one of the initial conditions considered) is a periodic sink. The results are shown in Fig. 6, where different configurations of stable domains (cross-road, spring-area and maybe other structures) interact. This structure was predicted in [4] using the return map (2). We refer to that previous work for further details and properties.

This is a preliminary analysis of the model. Further details on the bifurcation diagram (essentially the computation of the quadratic tangency curves) are needed to clarify the structures observed (for instance to determine the cubic tangency points and the cascades of cusp points). Also the different attractors observed deserve additional explanation. Details on the model and additional results will be given in a future work (in progress).

Acknowledgements This work has been supported by grants MTM2010-16425 (Spain) and 2009 SGR 67 (Catalonia). We thank J. Timoneda for the technical support on the computing facilities of the Dynamical Systems Group of the Universitat de Barcelona, largely used in this work.

References

1. Afraimovich, V.S., Shilnikov, L.P.: The annulus principle and problems on interaction of two self-oscillation systems. Prikladnaja Matematica i Mekhanika **41**, 618–627 (1977)
2. Broer, H., Simó, C., Tatjer J.C.: Towards global models near homoclinic tangencies of dissipative diffeomorphisms. Nonlinearity **11**, 667–770 (1998)
3. Chirikov, B.V.: A universal instability of many-dimensional oscillator system. Phys. Rep. **52**, 264–379 (1979)
4. Gonchenko, S.V., Simó, C., Vieiro, A.: A global study of 2D dissipative diffeomorphisms with a Poincaré homoclinic figure-eight. Nonlinearity **26**(3), 621–679 (2013)
5. Kuznetsov, Y.A.: Elements of applied bifurcation theory. In: Applied Mathematical Sciences, vol. 112, 3rd edn. Springer, New York (2004)
6. Turaev, D.V.: On a case of bifurcations of a contour composed by two homoclinic curves of a saddle. In: Methods of the Qualitative Theory of Differential Equations, pp. 162–175. Gorki State University Pub. (1984) (in Russian)
7. Turaev, D.V., Shilnikov, L.P.: On bifurcations of a homoclinic figure-eight for a saddle with a negative saddle value. Sov. Math. Dokl. **44**(2), 422–426 (1987)
8. Zaslavsky, G.M., Filonenko, N.N.: Stochastic instability of trapped particles and conditions of applicability of the quasi-linear approximation. Sov. Phys. JETP **27**, 851–857 (1968)

Generalizing the May-Leonard System to Any Number of Species

Genaro de la Vega and Santiago López de Medrano

Abstract We construct generalizations of the May-Leonard three species Lotka-Volterra system to any number of species, extending the property of cyclic dominance. First we recall the main properties of the May-Leonard system. Then we construct a Lotka-Volterra system for n species which has an invariant attracting polygon. We construct Lotka-Volterra-Kolmogorov deformations of higher degree of this system which have the same attracting polygon and all the properties of the May-Leonard one. We finish with the construction of Lotka-Volterra deformations of the same system which numerically show a curvilinear attracting polygon and the same properties, but the corresponding analytic results are still not complete.

1 Introduction

Warren Leonard and Robert May [8] constructed in 1975 a very interesting Lotka-Volterra system for three species with an attracting triangle and where each population in its turn is dominant while the two others almost disappear, but after a while the dominant population dwindles and the next one in cyclic order becomes the dominant one. The main feature of this system is its absence of any attracting fixed points and the robustness of that cyclic behaviour.

Many extensions of this system have been published (for example [3]) for systems with more than three species, but they feature the absence of attracting fixed points and the asymptotic tendency of most trajectories to the boundary of the unit simplex. None of the ones we have found seem to extend the cyclic behaviour

G. de la Vega (✉) · S. López de Medrano
Instituto de Matemáticas, UNAM, Universidad Nacional Autónoma de México, Area de la Investigación Científica, Circuito Exterior, Cd. Universitaria, 04510 México, D.F., México
e-mail: genarofis@matem.unam.mx; santiago@matem.unam.mx

S. Ibáñez et al. (eds.), *Progress and Challenges in Dynamical Systems*,
Springer Proceedings in Mathematics & Statistics 54,
DOI 10.1007/978-3-642-38830-9_25,

of the dominance of each species. In this article we present some systems which have this feature for any number of species.

In the first section we recall the definition and main properties of the May-Leonard system. In the second we construct an embedded polygon with n sides in $\mathbb{R}^n_+$, having one side in each of the coordinate hyperplanes. Although the existence of such a polygon follows from known facts in polytope theory we take care in giving a concrete construction and, for symmetry's sake, we produce a regular n-gon inside the unit simplex. We use a construction from [2] to give an explicit Lotka-Volterra field which has the polygon as an attracting invariant normally hyperbolic set and which in fact is point-wise fixed. The rest of the work consists in perturbing this vector field in such a way that we have the required cyclic property, using the fact that such a degenerate vector field can be deformed in many different ways. First we produce explicit Lotka-Volterra-Kolmogorov deformations of higher degree of the basic system that also leave this polygon invariant and have the cyclic property. In the third section we consider the more interesting question of finding Lotka-Volterra systems with the same cyclic property. For the moment we do not achieve completely this goal but obtain theoretically some of the required properties. First we show, using the theory of normal hyperbolicity of vector fields on invariant manifolds, that any small deformation of the basic field has an attracting invariant curvilinear n-gon near the unperturbed one. This means that the dynamics can be assumed to lie essentially on that deformed polygon. To prove the existence of cyclic behaviour we would have to:

1. Construct a deformation that contains fixed point in the interior of the deformed polygon which is a repelling focus and
2. Show that all trajectories stemming from the focus tend to the boundary of the polygon.

Since we have not yet been able to do this completely we illustrate the method in the case $n = 4$ where we construct the deformation (1) and obtain the cyclic behaviour but with a weaker conclusion than (2). This much works for other small values of n and numerical simulations suggest that (2) is true, even for not too small deformations.

This is a preliminary report of these results. A more detailed version will appear later.

2 The May-Leonard System

May and Leonard [8] proposed the following 2-parameter familiy of Lotka-Volterra vector fields:

$$ML = (x(1 - x - \alpha y - \beta z), y(1 - \beta x - y - \alpha z), z(1 - \alpha x - \beta y - z))$$

with $\alpha, \beta > 0$

The field *ML* has the origin as a repelling equilibrium point, 3 equilibrium points on the axes (the unit point in each) with eigenvalues -1 (along the axis) and $1-\alpha, 1-\beta$, and an interior equilibrium point

$$P = (\frac{1}{\alpha+\beta+1}, \frac{1}{\alpha+\beta+1}, \frac{1}{\alpha+\beta+1})$$

that lies in the invariant diagonal $\{x = y = z\}$. Depending on the values of α, β it may have 3 more equilibrium points on the coordinate planes.

The dynamic depends on the sign of the difference $\alpha+\beta-2$ and involves the function $H = \frac{xyz}{(x+y+z)^3}$. We now state our version of their result[1]:

Theorem 1. *The field ML has an invariant carrying*[2] *simplex Σ which is the unit simplex or a curvilinear deformation of it. Σ contains the interior equilibrium point P and also those on the axes.*

(A) If $\alpha+\beta = 2$, Σ is the unit simplex and has H as a first integral. Unless $\alpha = \beta = 1$, on the unit simplex P is a center whose closed trajectories fill the region between P and the boundary of the simplex. The rest of the trajectories in the open octant (but not in the the invariant diagonal) rotate on a level surface of H and approach a closed trajectory on Σ.[3] *If $\alpha+\beta \neq 2$ the field leaves invariant neither the unit simplex nor H.*

(B) If $\alpha+\beta > 2$, P is a saddle point in $\mathbb{R}^3$ and H is decreasing along the trajectories. On the carrying simplex, P is a repelling focus, unless $\alpha = \beta$, in which case it is a star point (both eigenvalues are equal). If one of α, β is less than 1, all the trajectories in the region of Σ between its boundary and P converge to the boundary. So do all the trajectories in the interior of the first octant and outside the invariant diagonal line.

(C) If $\alpha+\beta < 2$, P is an attractor and H grows along the trajectories. On the carrying simplex, P is an attracting focus, unless $\alpha = \beta$, in which case it is a star point. If one of α, β is greater than 1, all the trajectories in the region of Σ between P and its boundary converge to P. So do all the trajectories in the interior of the first octant.

The cyclic behaviour of the leading species thus has three possibilities:

In case (A) it is periodic. However, any small perturbation of the state of the system may affect the value of H and thus the period of rotation and the size of the

[1] All the statements in [8] are essentially correct, despite some imprecisions in the terminology and the reasoning. An even more detailed version of the theorem can be formulated, involving especially the character of the eigenvalues at the equilibrium points on the axes and coordinate planes. See [4]

[2] That is, it attracts all the orbits in the interior of the first octant.

[3] These closed trajectories are called *limit cycles* in [8], meaning that there are many other trajectories that approach them asymptotically. They are not limit cycles in the usual sense which requires that those approaching trajectories fill out a whole neighborhood of the cycle.

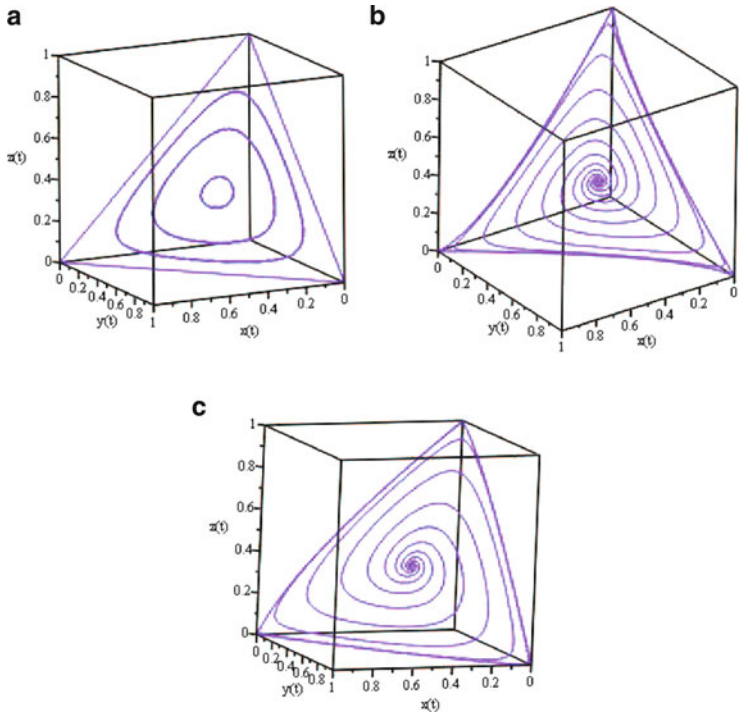

Fig. 1 Cases of the M-L system. (**a**) Case (A) $\alpha = 3/2, \beta = 1/2$. (**b**) Case (B) $\alpha = 2.5, \beta = 0.25$. (**c**) Case (C) $\alpha = 5/4, \beta = 2/5$

peak of the leading population. Also, a small structural perturbation may transform it into case (B) or (C).

In case (B) it is not periodic. The time between two peaks of the leading species grows with time without bound while the size of the peak keeps growing up to a finite value. This behaviour is not affected by small perturbations of the state or the parameters of the system.

In case (C) the size of the peaks decrease with time approaching a steady state of the three species and this behaviour is not affected by small perturbations of the state or the parameters of the system.

The first part of the theorem follows from the theorem of Hirsch in [5] on the existence of carrying simplices in competition systems. Parts (A), (B) and (C) follow from a computation of the variation of H along the trayectories and of the eigenvalues at equilibrium points (Fig. 1).

3 The Basic System in $\mathbb{R}^n_+$ with an Invariant Polygon and Some LVK Deformations

It is easy to see that any convex polytope of arbitrary dimension with n facets can be realized combinatorialy by one inside the unit simplex in $\mathbb{R}^n_+$ in such a way that each of its facets lies in one of the coordinate hyperplanes.[4] More interesting is the question of realizing it geometricaly (that is, isometricaly) in the same way. We now show how to embed linearly and isometrically a regular n-gon in $\mathbb{R}^n_+$ with all its sides on the boundary, which gives us a natural concrete way of realizing it for our purposes.

We start with some examples: For $n = 3$ it is the unit simplex. For $n = 4$ we can realize it by taking the product of two unit simplices in $\mathbb{R}^2$ and then normalizing to put it in the unit simplex: its equations become $x_1 + y_1 = \frac{1}{2}$, $x_2 + y_2 = \frac{1}{2}$, or, as we prefer to write it:

$$x_1 + y_1 - x_2 - y_2 = 0$$
$$x_1 + y_1 + x_2 + y_2 = 1$$

This gives a square with side $\frac{1}{\sqrt{2}}$.

A regular pentagon has been known for some time [7]: if ρ is a fifth root of unit then the equations

$$\Sigma_{i=1}^5 \rho^i x_i = 0$$
$$\Sigma_{i=1}^5 x_i = 1$$

give a polygon in $\mathbb{R}^5_+$ invariant under cyclic permutation of the coordinates. Therefore it is a regular pentagon in $\mathbb{R}^5$. Its vertices are

$$\left(\frac{1}{\sqrt{5}}, 0, \frac{1}{2} - \frac{1}{2\sqrt{5}}, \frac{1}{2} - \frac{1}{2\sqrt{5}}, 0\right)$$

and its cyclic permutations. The length of its side is $\frac{1}{2} - \frac{1}{2\sqrt{5}}$.

To do the general case, we assume that a vertex has the form

$$V_1 = (a_1, a_2, a_3, \ldots, a_{n-3}, a_{n-2}, 0, 0)$$

and the rest are its cyclic permutations V_i.

To have all the vertices in the same plane, we must have:

$$s(V_2 - V_1) + t(V_3 - V_2) = V_4 - V_3 \tag{1}$$

[4] This can be shown using the *Gale transform* or, directly by induction on n.

For a regular polygon of side 1 the values of s, t are: $t = 2\tau$ and $s = -1$, where $\tau = \cos(\frac{2\pi}{n})$, so to get such a polygon we must have:

$$V_2 - V_1 = 2\tau(V_3 - V_2) - (V_4 - V_3) \tag{2}$$

So we obtain

$$a_2 - a_1 = 2\tau a_1$$
$$a_3 - a_2 = 2\tau(a_2 - a_1) - a_1 = (4\tau^2 - 1)a_1$$
$$a_4 - a_3 = 2\tau(a_3 - a_2) - (a_2 - a_1) = (8\tau^3 - 4\tau)a_1$$
$$\cdots$$
$$a_{i+1} - a_i = 2\tau(a_i - a_{i-1}) - (a_{i-1} - a_{i-2})$$

It follows by induction that there exists a polynomial $c_i(x)$ such that

$$a_{i+1} - a_i = c_i(\tau)a_1$$

and

$$a_{i+1} = (\Sigma_0^i c_i(\tau))a_1.$$

c_i must satisfy:

$$c_{i+1}(\tau) = 2\tau c_i(\tau) - c_{i-1}(\tau)$$
$$c_0(\tau) = 1$$
$$c_1(\tau) = 2\tau$$

These are precisely the defining relations for the Chebyshev polynomials U_i of the *second kind* (see, for example, [1]). So $c_i = U_i$. Furthermore we have that

$$\Sigma_0^{n-2} U_i(\tau) = 0$$
$$U_{n-1}(\tau) = 0$$

which is consistent with $a_{n-1} = a_n = 0$.

So taking

$$a_{i+1} = (\Sigma_0^i U_i(\tau))a_1.$$

we get the vertices V_i defining a flat, regular n-gon inside a simplex, parallel to the unit one (since the sum of all the coordinates of each V_i is the same). We can assume it is the unit simplex by choosing the value of a_1.

Since $\sin(j\frac{2\pi}{n})$ is the imaginary part of the roots of unity, the vertices are of the form:

$$(a_1, a_2, a_3, \ldots, a_3, a_2, a_1, 0, 0)$$

So we have proved

Theorem 2. *There exists a regular n-gon in the unit simplex of* $\mathbb{R}^n$ *each of whose sides lies in one of the coordinate hyperplanes.*

Its equations are derived from those satisfied by the vertices:

$$x_j - (2\tau + 1)x_{j+1} + (2\tau + 1)x_{j+2} - x_{j+3} = 0 \tag{3}$$

for $j = 1, \ldots, n$. The first $n - 3$ are independient so, together with that of the unit simplex, define the n-gon.

From the equations we can get a Lotka-Volterra vector field whose solutions converge to the polygon as follows: making the change of coordinates: $x_i = y_i^2$ we get the equations for a manifold Z in $\mathbb{R}^n$ which is an intersection of quadrics:

$$y_j^2 - (2\tau + 1)y_{j+1}^2 + (2\tau + 1)y_{j+2}^2 - y_{j+3}^2 = 0, \quad j = 1 \ldots n - 3 \tag{4}$$

$$\Sigma_{i=1}^n y_i^2 - 1 = 0 \tag{5}$$

If f_j is the left hand side of the j-th of these equations, $j = 1 \ldots n - 2$, then, following a general construction in [2], we consider the potential function

$$V = -\Sigma_{j=1}^{n-2} f_j^2 \tag{6}$$

V takes its maximum 0 at Z and is negative elsewhere.

Therefore the gradient vector field $Y = \nabla(V)$, has Z as an invariant attracting manifold, actually point-wise fixed. It is shown in [2] that Z is a normally hyperbolic attracting invariant manifold of Y.

The components of Y are of the form

$$Y_i = y_i(b_i - \Sigma_{j=1}^n b_{ij} y_j^2) \tag{7}$$

Getting back to the coordinates x_i we get a vector field X in $\mathbb{R}_+^n$ with components[5]

[5]The field in the coordinates x_i would have a factor of 2 in each component, which we have removed to get X without changing its qualitative properties.

$$X_i = x_i(b_i - \Sigma_{j=1}^{n} b_{ij}x_j) \tag{8}$$

Clearly X has our polygon as an invariant point-wise fixed attractor. We will use the normal hyperbolicity property in the next section.

We refer to X as the *basic vector field* associated to the polygon. Since it is identically 0 in the polygon we can, in principle, perturb it to get any kind of dynamics on it. We will restrict to LVK and LV[6] deformations to obtain systems with the properties of the May-Leonard system.

We first construct a vector field with a center in the polygon, whose closed trajectories accumulate at the boundary. For this we start by considering the *vector product* W of the set of $n-1$ gradients of the product function $H = x_1x_2 \dots x_n$ and of the left-hand sides of the equations defining the polygon. W can be defined by the usual $n \times n$ determinant where the first row consists of the unit vectors in $\mathbb{R}^n$ and the other rows of the $n-1$ gradients. Then W is clearly a LVK vector field, is tangent to the plane of the polygon and has H as a first integral. It has also the property that the left hand sides of the defining equations of the polygon are constant along its trajectories.

The sum $X + W$ is then a vector field which has the polygon as an attractor, on which it has a center whose closed trajectories accumulate at the boundary.

Now we can consider the gradient of $-H^2$ along whose trajectories H decreases. It is a LVK vector field, not necessarily tangent to the polygon, but we can project it onto its plane to make it so. If we add to $X + W$ a small multiple of this projected field we obtain a LVK vector field which has all the properties, and we have proved:

Theorem 3. *There exist LVK vector fields on $\mathbb{R}^n_+$ which have an invariant n-gon as attractor and which have any of the following dynamics on it (Fig. 2):*

(a) A center whose closed trajectories accumulate at the boundary of the n-gon, or
(b) A repelling focus whose trajectories spiral asymptotically to the boundary of the n-gon.

Therefore, these vector fields reproduce, for n species, precisely the rotating properties of May-Leonard vector field for three species.

Observe that we have obtained also a LVK vector field for three species which has the unit simplex as an invariant attractor. Its properties are simpler to prove than in the May-Leonard example, but it has the disadvantage of being of higher degree.

[6] We follow the standard terminology: a Lotka-Volterra-Kolmogorov (LKV) vector field in $\mathbb{R}^n_+$ is one whose i-th component is of the form $x_iK_i(x)$ where the K_i are smooth enough functions in $\mathbb{R}^n_+$. A Lotka-Volterra (LK) vector field is a LVK field where all the K_i are degree 1 polynomials.

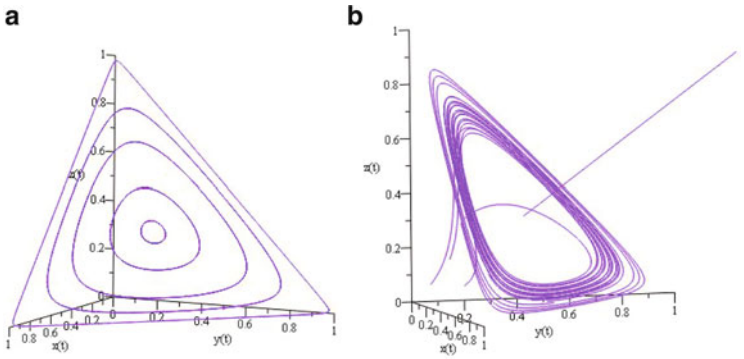

Fig. 2 LVK perturbations. (**a**) A center. (**b**) A repelling focus

4 The Search of LV Systems Generalizing the May-Leonard System for Any Number of Species

More interesting is the problem of constructing LV systems for more than three species with the circulating properties of the May-Leonard system.

It is easy to see that a vector field of degree 2 in the plane that leaves a polygon of four or more sides invariant and has a fixed point in its interior must be identically 0. Therefore, a LV system on $\mathbb{R}^n_+$ that leaves invariant a flat polygon cannot have any interesting dynamics on it. In other words, a deformation of the basic vector field X with an interesting dynamics cannot leave the flat polygon invariant. But we now show that for a small deformation it has an invariant attracting curvilinear polygon close to the flat one:

Consider the vector field Y in $\mathbb{R}^n$ related to X constructed in the previous section. To any small LV perturbation $\tilde{X}$ of X corresponds a small perturbation $\tilde{Y}$ of Y. Since the manifold Z is a normally hyperbolic attracting invariant manifold, if the deformation is small enough there will be a unique invariant, attracting invariant manifold $\tilde{Z}$ for $\tilde{Y}$ which is C^1-close and diffeomorphic to Z. Since $\tilde{Y}$ is symmetric with respect to reflections on the coordinate hyperplanes, each such reflected $\tilde{Z}$ is also invariant under $\tilde{Y}$, and due to uniqueness it follows that $\tilde{Z}$ coincides with its reflection. In other words, $\tilde{Z}$ is symmetric with respect to all coordinate hyperplanes, and its quotient under the group generated by those reflections coincides with its intersection with the first orthant, which we will denote by $\tilde{K}$.

Being Z transverse (actually orthogonal) to each coordinate hyperplane and to any codimension 2 intersection of two of them, so are $\tilde{Z}$ and $\tilde{K}$ if the deformation is small enough. Therefore, the intersections of Z and of $\tilde{Z}$ with any intersection of subsets of the form $\{x_i \geq 0\}$ are also diffeomorphic. In particular, the invariant

$\tilde{K}$ and the invariant one for Y are diffeomorphic and so are their intersections with each coordinate hyperplane.[7]

Going back to the coordinates x_i we obtain a (curvilinear) n-gon in $\mathbb{R}^n_+$ invariant and attracting for the vector field $\tilde{X}$ and we have proved:

Theorem 4. *Every small LV deformation of X has an invariant and attracting curvilinear n-gon close to the flat one invariant under X. Its sides and vertices sit in the same coordinate subspaces.*

Now begins the search for small deformations of X that have interesting dynamics on the deformed polygon. We illustrate with the case $n = 4$ what we have obtained so far:

The basic vector field X is as follows:

$$\begin{aligned} X_1 &= x_1(1 - 2x_1 - 2x_3) \\ X_2 &= x_2(1 - 2x_2 - 2x_4) \\ X_3 &= x_3(1 - 2x_1 - 2x_3) \\ X_4 &= x_4(1 - 2x_2 - 2x_4) \end{aligned}$$

We consider now the following deformation $\hat{X} = \hat{X}_{a,b}$:

$$\begin{aligned} \hat{X}_1 &= x_1(1 - 2x_1 - ax_2 - (2 + b)x_3) \\ \hat{X}_2 &= x_2(1 - 2x_2 - ax_3 - (2 + b)x_4) \\ \hat{X}_3 &= x_3(1 - 2x_3 - ax_4 - (2 + b)x_1) \\ \hat{X}_4 &= x_4(1 - 2x_4 - ax_1 - (2 + b)x_2) \end{aligned}$$

Then for small $(a, b) \neq (0, 0)$ the system has a unique fixed point outside the coordinate hyperplanes which is:

$$\left(\frac{1}{a + b + 4}, \frac{1}{a + b + 4}, \frac{1}{a + b + 4}, \frac{1}{a + b + 4}\right)$$

that must lie in the invariant quadrilateral. For symmetry reasons, the tangent space to the quadrilateral at the fixed point is parallel to the plane of the flat square.

[7] This proof works also works for a polytope of any dimension given by the same type of equations and inequalities.

The eigenvalues of the derivative of $\hat{X}$ at the fixed point are:

$$-1, -\frac{4+a-b}{4+a+b}, \frac{b \pm ai}{4+a+b}$$

where the first two correspond to the attracting nature of the quadrilateral and the last two to the restriction of the derivative to the tangent plane.

Therefore, for $a \neq 0$ and $b > 0$ the fixed point is a repelling focus on the quadrilateral.

Studying in the same way the eigenvalues at the vertices of the quadrilateral and other equilibrium points on the coordinate hyperplanes one sees that if $a > b$ there cannot be any trajectories in the quadrilateral converging to them.

This leaves us with two possibilities: Either the trajectories emanating from the focus tend to the boundary of the quadrilateral or they all tend to a closed orbit on its interior. So we end up with either a periodic behaviour where the four species alternate their peaks, partially recalling case (A)[8] of the May-Leonard system (see [Theorem 1]) or they alternate cyclically but with the periods of the cycles tending to infinity exactly as in case (B) because they cannot tend to equilibrium points. So we have proved:

Theorem 5. *For small enough $a \neq 0$ and $b > 0$ the LV vector field $\hat{X}$ has an invariant attracting curvilinear quadrilateral. On this quadrilateral the vector field has a unique equilibrium point which is a repelling focus. The trajectories emanating from the focus tend to a cyclic behaviour, which can be either*

(A) Strictly periodic in the interior of the quadrilateral, or
(B) Asymptotic to the boundary with a period tending to infinity.

In case A there could also be some behaviour of type B, since trajectories exterior to all closed orbits could approach the boundary asymptotically.

But we think that actually we have always only option B. To show that all trajectories on the quadrilateral tend to its boundary we would need to find a Lyapunov function that prevents any possible closed trajectories. The derivative along the flow of the function H considered in the previous section is negative on the flat square outside of its center, but this does not exclude possible positive values on the quadrilateral. Other candidates, like the ones in [3] or [6] do not seem to work, either (Fig. 3).

All the numerical evidence points to that conclusion. For many values of a, b, which need not be too small, we find precisely the behaviour in case B on a clearly defined curvilinear quadrilateral. For other small values of n we have made the same analysis of similar deformations, as well as numerical experiments giving always the attracting curvilinear polygon with an interior focus and trajectories spiralling asymptotically to their boundaries (Fig. 4).

[8] Partially, because we do not have a center whose closed orbits fill the interior of the quadrilateral.

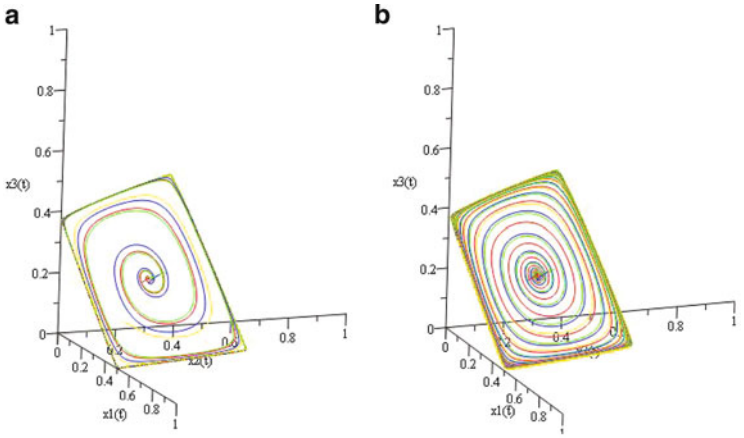

Fig. 3 LV perturbations (projections). (**a**) A perturbation with $a = \frac{1}{2}, b = \frac{1}{10}$. (**b**) A perturbation with $a = \frac{1}{2}, b = \frac{1}{20}$

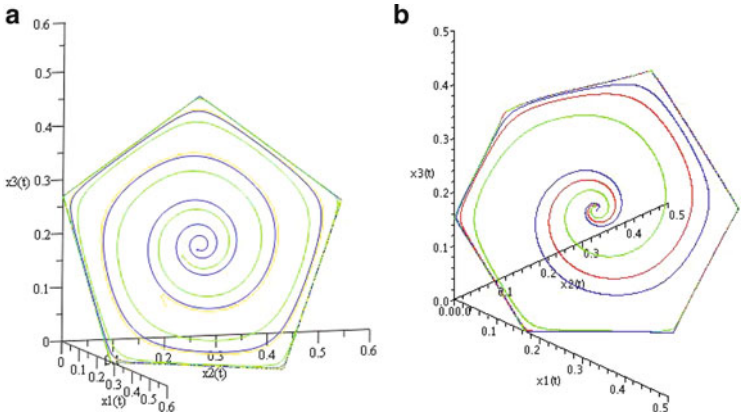

Fig. 4 LV perturbations. (**a**) A perturbation with invariant curvilinear pentagon (projection). (**b**) A perturbation with invariant curvilinear hexagon (projection)

We hope to obtain soon a more general and precise result.

Acknowledgements This work owes much to many years of joint work and long discussions of the second author with Marc Chaperon. The first author received a Conacyt grant for writing his Ph. D. Thesis, part of which is included in this article. The second author was partially supported by Conacyt-CNRS and by the UNAM-DGAPA-Papiit grants IN102009 and IN108112.

References

1. Arfken, G.: Mathematical Methods for Physicists, 3rd edn., p. 733. Academic, Orlando (1985)
2. Chaperon, M., López De Medrano, S.: Birth of attracting compact invariant submanifolds diffeomorphic to moment-angle manifolds in generic families of dynamics. C. R. Acad. Sci. París **346**(I), 1099–1102 (2008)
3. Chenciner, A.: Comportement asymptotique de systémes differentiels su type "compétition d'especes". C. R. Acad. Sci. París **284**, 313–315 (1977)
4. De la Vega, G.: Ecuaciones Lotka Volterra Kolmogorov y Sistemas Dinámicos. Ph. D. Dissertation, UNAM (2013)
5. Hirsch, M.W.: On existence and uniqueness of the carrying simplex for competitive dynamical systems. J. Biol. Dyn. **2**(2), 169–179 (2008)
6. Hofbauer, J., Sigmund, K.: The Theory of Evolution and Dynamical Systems: Mathematical Aspects of Selection. Cambridge University Press, Cambridge (1988)
7. López de Medrano, S.: The Topology of the Intersection of Quadrics in $\mathbb{R}^n$. Lecture Notes in Mathematics, vol. 1370, pp. 280–292. Springer, Berlin (1989)
8. May, R.M., Leonard, W.J.: Nonlinear aspects of competition between three species. SIAM J. Appl. Math. **29**, 243–253 (1975)

Index

S. Ibáñez et al. (eds.), *Progress and Challenges in Dynamical Systems*,
Springer Proceedings in Mathematics & Statistics 54, DOI 10.1007/978-3-642-38830-9,